Development of drug eluting biodegradable nanocomposite for use in coronary stents

A thesis presented for the degree of Doctor of Philosophy

By

Chaitra Venkatesh B.Eng.

Based on the research carried out under the supervision of

Dr Declan Devine

Co-supervisors- Dr Ian Major, Dr Sean Lyons

Material Research Institute

Athlone Institute of Technology

Athlone

Submitted to the Athlone Institute of Technology, July 2021

ABSTRACT

Development of drug eluting biodegradable nanocomposite for use in coronary stents

Chaitra Venkatesh

Coronary stents are the scaffolds placed inside the blocked arteries, which aids the restoration of the passage of blood to the heart. Coronary stenting has become a standard medical procedure to treat coronary heart disease (blockage or narrowing of the arteries), which is the no. 1 cause of death in the western world. Stents have been developed from the bare metallic stents to drug-eluting stents and then bioresorbable stents (BRS) to prevent various complications and improve their clinical efficacy. As the stent is indeed a foreign object within the vessel, fully biodegradable drug-eluting stents are currently used which will degrade after the required period of support. However, next-generation polymeric BRS still faces many challenges such as stent material (polymer type), mechanical support, and manufacturing process, strut thickness, stent design, under-expansion of the stents, and degradation rate.

To address these challenges, this study was designed to develop an innovative biodegradable polymer nanocomposite by using polylactic acid (PLA) as the polymer matrix reinforced with non-toxic nanoclay, halloysite nanotubes (HNT) and blended with poly e-caprolactone (PCL) to decrease brittleness, using an extrusion process. These materials were selected as they are widely used in the biomedical field due to their biodegradability, and high mechanical properties. The developed nanocomposite was characterized for mechanical, physiochemical, thermal, drug loading, drug release, and degradation properties to address the basic requirements of the stent material.

Primarily, the effect of screw speed during extrusion was examined to ensure homogenous dispersion of the HNT in the PLA matrix. It was found that an increase in screw speeds resulted in a significant increase in strength, and thermal properties by better dispersion of the nanoclay in the polymer matrix. The high strength PLA/HNT nanocomposite was further examined for drug delivery system which displayed sustained drug release. The PLA/HNT composite was fabricated into model stents by 3D printing which did not have the required flexibility for expansion during placement. Hence the composite was further blended with PCL to enhance its flexibility. The developed PLA/PCL/HNT nanocomposite presented improved toughness, strength and flexibility. Further, the degradation of drug-loaded PLA/HNT composite and PLA/PCL/HNT composites was studied for 8 months which indicated faster degradation of PLA/HNT composite loaded with an acidic drug (Aspirin) with no significant weight reduction of the PLA/PCL/HNT nanocomposite.

Results from this study indicate that the use of nanocomposite blends of materials may be suitable for the production of stents via 3D printing. Nevertheless, much work is needed prior to their use in areas such as coronary stents, but they may be suitable for other non-critical stents such as urinary stents, which may warrant further investigation.

Declaration

I hereby declare that this thesis submitted to the Athlone Institute of Technology for the Ph.D., is a result of my own work. This work has not been submitted either in the same or altered form, part or in whole, to this institute or any other institute or university in support for any degree other than for which I am now a candidate.

July 2021 Chaitra Venkatesh

Acknowledgement

I am extremely grateful to my mentor Dr Declan Devine for his invaluable guidance, unwavering support, and encouragement throughout the study and for giving me the opportunity to conduct this thesis. I would also like to express my gratitude to my co-supervisors Dr Sean Lyons and Dr Ian Major for their invaluable support and advice during the course.

My sincere gratitude extends to the AIT Presidents Doctoral Scholarship funding opportunity from Athlone Institute of Technology to undertake my studies. I would also like to thank all the members of Materials Research Institute (MRI), Applied Polymer Technology (APT), and Centre for Industrial Services Design (CISD), Graduate school and Research Office at Athlone Institute of Technology for their support.

Table of Contents

List of Tables

Chapter 2

Chapter 3

Chapter 4

Chapter 5

Chapter 6

Chapter 7

Chapter 8

List of Figures

Chapter 2 – Literature Review

Chapter 3 – Experimental Details

Chapter 4 – An investigation on the enhancement of mechanical properties of Polylactic Acid /Halloysite Nanotubes nanocomposites

Chapter 5 – Study of drug loading and drug release mechanism from the PLA/HNT nanocomposites

Chapter 6 – The effect of pKa values of the drug compound on the degradation and drug release mechanism of the PLA/HNT nanocomposite

Chapter 7 – Additive manufacturing of PLA/HNT nanocomposites for coronary stents

Chapter 8 – Inclusion of polycaprolactone (PCL) into high strength polylactic acid/halloysite nanotubes (PLA/HNT) nanocomposite for the enhancement of flexibility

Abbreviations

API	Active Pharmaceutical Ingredients
APAP	Acetaminophen
ASP	Aspirin
BMS	Bare Metal Stent
CAD	Coronary Artery disease
CNT	Carbon Nanotube
DES	Drug Eluting Stent
DSC	Differential scanning calorimetry
EDX	Energy Dispersive X-ray spectroscopy
FDA	Food and Drug Administration
FTIR	Fourier Transfer Infrared Spectroscopy
HME	Hot Melt Extrusion
HNT	Halloysite Nanotube
MMT	Montmorillonite
PCI	Percutaneous Coronary Intervention
PCL	Poly e-Caprolactone
PE	Polyethylene
PGA	Poly Glycolic Acid
PGLA	Poly Lactic Glycolic Acid
PLA	Poly Lactic Acid
PLLA	Poly L-Lactic Acid
POSS	Polyhedral Oligomeric SilSesquioxanes
PS	Polystyrene
PTCA	Percutaneous Transluminal Coronary Angioplasty
SEM	Scanning Electron Microscopy
TGA	Thermal Gravimetric Analysis

CHAPTER 1

Introduction

Preface

Coronary stenting has become a standard medical procedure to treat coronary stenosis (blockage or narrowing of the arteries), which is a frequent cause of myocardial infractions commonly known as heart attacks. Coronary stents are the tubular scaffolds placed inside the blocked arteries, which aids the restoration of the passage of blood to the heart (Conijn *et al.*, 2018). The risk of stent thrombosis (blood clotting) and restenosis (narrowing of arteries) has been the complications after stenting at every stage of stent evolution beginning from bare-metal stents followed by drug-eluting stent (DES) (Liu *et al.*, 2018; Sotoudehbagha *et al.*, 2018). These complications mainly depend on the response factor at the cellular level to a stent which is a foreign object which differs from person to person as is in most of all medical conditions. However, the essential demand for an immediate intervention leads to the continuous improvement of the stent material to facilitate its presence with maximum compatibility.

The presence of a stent in the vessel/arteries is associated with inflammatory reactions, progressive neointima development, and damaged endothelium and thrombosis risks (Gu, Zhao and Froemming, 2012; Hajiali, Dabagh and Jalali, 2014; Ng *et al.*, 2017). Hence, it is beneficial for the stent to be removed, after its job is done. Unlike the metal-mesh or drug-coated metals, the biodegradable drug-eluting stents are designed to be absorbed slowly by the coronary arteries in a two-year timeframe. The incomplete repair of the endothelium at the site of vascular wall injury aided by drug coatings and hypersensitivity to the permanent presence of the metal facilitated the complications (Sakamoto *et al.*, 2018; Tabraiz Alam *et al.*, 2019). There has therefore been significant interest and development in recent years in the field of biodegradable stents. This led to the development of biodegradable stents which are degraded in the body, once their job is done leaving behind healed vessels (Borhani *et al.*, 2018).

Fully biodegradable drug-eluting stents (BDS) are currently researched and used with an emphasis on polymeric BDS which will degrade after healing the vessel by drug elution (Wang *et al.*, 2018). However, next-generation polymeric BDSs still face many challenges. For instance, Abbott's FDA-approved Absorb bioresorbable

vascular scaffold (BVS) was removed from the market, owing to a higher risk of adverse heart events such as myocardial infraction and scaffold thrombosis when compared to a metallic drug-coated stent (Virmani, Jinnouchi and Finn, 2017). Factors such as stent material (polymer type), mechanical support, and manufacturing process, under-expansion of the stents, strut thickness, stent design, and degradation rate are the primary causes of complications (Qiu and Zhao, 2018).

1.1 The Research Problem

Coronary heart disease has been a major cause of mortality across the world (McDowell, Slevin and Krupinski, 2011; Ramadugu and Latha Alikatte, 2016). It is a disease in which a waxy substance called plaque is built up inside the coronary arteries over many years. This plaque can harden which narrows the coronary arteries and reduces the flow of the blood to the heart which can lead to cardiac arrest. Coronary stenting is one of the corrective methods which is used for coronary heart disease and is one of the biggest achievements in medical history (Wu *et al.*, 2012).

Coronary stents are tubular scaffolds. The coronary stent is placed inside the blocked arteries, which aids to restore the passage of blood through the arteries (Moore, O'Sullivan and Verdecchia, 2016). The first-generation coronary stent which was introduced in the early 1990s was made of bare metal (Wilson and Cruden, 2013). Early development of metallic stents emphasized mainly the research of stent design and assessment of the different types of materials (O'Brien and Carroll, 2009). Clinical trial results proved that thinner stent struts would lead to reduced restenosis rates (O'Brien and Carroll, 2009; Jaganathan *et al.*, 2014). In recent years, research took place in testing metallic stents coated with drugs that interrupted the re-narrowing of the arteries, as the drug coating the stent is released gradually during healing. These are called Drug-Eluting Stents (Jaganathan *et al.*, 2014). There are concerns of a blood clot being formed in the stent in one or more years after it is implanted, which is called late stent thrombosis (Shimura *et al.*, 2016). To overcome this, polymers loaded with drugs were coated onto the metallic stents.

Evolution of such DES ranged from using novel drugs combination with non-biodegradable polymers and biodegradable polymers for coatings with thin metallic strut over the years is currently the first choice for the treatment of coronary artery

disease (CAD) (Ang *et al.*, 2018; Kobo *et al.*, 2020; Rykowska and Nowak, 2020). Although these solutions improved the potency of the stents, potentially the non-biodegradable polymer coating could accumulate and would require to be removed surgically. Along with this, the presence of a metal scaffold in the artery after the degradation of polymer coating could lead to restenosis (Englert *et al.*, 2018; Rykowska and Nowak, 2020). Thus, much attention is given to the development of fully biodegradable drug-eluting stents also referred to as bioresorbable scaffold (BRS). Most of these are either investigated clinically or are undergoing clinical trials with very few approved for commercial use in coronary patients (Englert *et al.*, 2018).

For instance, in 2016, the FDA (Food and Drug Administration) approved a new type of stent Absorb Bioresorbable Vascular Scaffold (BVS) system made of polymer poly L-lactic acid (PLLA), which eventually dissolves into the body developed by Abbott Vascular. However, the analysis of phase three clinical trial data reveals the limitations of the scaffold such as recoiling of stents, little expansion without breaking the stent, and thicker struts which caused hindrances to delivery (Virmani, Jinnouchi and Finn, 2017). Hence, the FDA directed Abbott Vascular to recall the Absorb Bioresorbable Vascular Scaffold (BVS) system due to studies showing elevated rates of major adverse events, specifically, myocardial infraction and scaffold thrombosis, when compared to patients treated with the Xience metallic drug-eluting stent, (U. S. Food and Drug Administration, 2017). Boston Scientific terminated their Renuvia scaffold development program as the devices showed a high risk of myocardial infarction and thrombosis. This was due to the non-uniform structure of the polymer used in the stents that makes the device susceptible to large deformation and causes flow disruption (*Bioabsorbable Stents Global Market Report 2020-30: Covid 19 Growth and Change*, 2020).

Currently, the clinical trials of BRS from Asian countries show consistently better results compared to the Western countries. Thus far, six BRS device companies have obtained Conformitè Europëenne (CE) mark. However, it has been concluded by the 'The European Society of Cardiology-European Association of Percutaneous Cardiovascular Interventions (ESC-EAPCI) Task Force' that the current generation DES should be preferred over BRS in everyday clinical practice (Kawashima *et al.*, 2020). Nevertheless, BRS still holds the advantage over first-generation metallic

stents, as a first-generation metallic stent could lead to long-term complications due to its permanent presence (Bezrouk *et al.*, 2020).

The currently investigated BRS for clinical trials attempts to improve the efficacy and long-term safety compared to the Absorb BVS's (PLLA) trial results. The most common materials used as a stent body/platform in BRS currently investigated for clinical trials are PLLA and magnesium (Englert *et al.*, 2018; Sakamoto *et al.*, 2018).

Following the stent placement, endothelialization and the healing process begins within 1-3 months of stent placement and after 3 months, the stent is fully covered by vascular tissue. Hence, it would be ideal for the scaffold to degrade within 4-6 months. And the risk of thrombosis and restenosis due to material-tissue interactions can be prevented by drug delivery during the healing process (Borhani *et al.*, 2018). One of the issues relating to the use of BRS is the degradation rate is too long (Onuma and Serruys, 2011; Collet *et al.*, 2016; McMahon *et al.*, 2018). For instance, the Absorb BVS made of PLLA had a biodegradation duration of 3 years, and experts suggest the use of materials such as magnesium-based BRS to circumvent this shortcoming as the resorption rate is less than 12 months (Kawashima *et al.*, 2020; Wee *et al.*, 2020). However, the resorption process of the magnesium alloy used in the magnesium-based scaffold left behind chemical by-products forming complications such as calcification in the surrounding tissue. Also, further clinical evidence and long-term follow-up data of the magnesium-based BRS would be required to confirm the safety and efficiency (Sakamoto *et al.*, 2018; Kobo *et al.*, 2020). The thickness of stent struts plays an essential role in stent recoil. Thicker struts lead to increased incidence of in-stent restenosis (reoccurrence of the blockage) (Hoare *et al.*, 2019). The polymeric PLLA stent requires thicker struts to achieve good radial strength. Hence careful consideration has to be given in material selection to bring balance between the radial strength and in-stent restenosis (Wu *et al.*, 2012; McMahon *et al.*, 2018).

Although polymeric BRS is not expected to possess the mechanical properties of a metallic stent, however, improvement of the polymeric properties certainly has the possibility of addressing some of the shortcomings. Innovative processing methods and stent designs or novel polymer composites could be used to improve the BRS properties (Wee *et al.*, 2020). Thus, the characteristics of an ideal BRS would require

a stronger and thinner strut, faster bioresorption, improved stent design, faster and proper enclosure of struts within the vessel wall (Kawashima *et al.*, 2020; Wee *et al.*, 2020). They would also require to be biocompatible, non-toxic, and possess drug delivery function (Beshchasna *et al.*, 2020).

1.2 Proposed Solution

The proposed solution aims to overcome the shortcomings of the currently used coronary stents such as toughening of the material and longer resorption time by improving its strength and elongation and to achieve faster resorption of the material post once its function has been fulfilled.

The objective of this study was to develop an innovative biodegradable polymer nanocomposite focusing on factors such as material requirements for the stent production, mechanical support, manufacturing process, and degradation rate which can be used to manufacture drug-eluting biodegradable stents. Poly lactic acid (PLA) was used as the base polymer, which is biodegradable and was reinforced with a non-toxic nanoclay, halloysite nanotubes (HNT) dispersed in the PLA matrix using an extrusion process. These materials are selected as they are widely used in the biomedical field due to their biodegradability, natural origin, and high mechanical properties.

This PLA/HNT composite was developed by examining the effect of changes in processing parameters such as extruder screw speed on the dispersion of the nanoclay, HNT in the PLA matrix. The resultant composite films were characterized to determine their mechanical and thermal properties matching the requirements for the stent material capable to withstand pressures observed in the coronary artery.

Antiproliferative drugs are routinely coated onto the outer surface of the stents to prevent restenosis. To examine the potential of the PLA/HNT nanocomposite as a drug carrier, a model API, Aspirin (ASP) was encapsulated into the composite and tested for drug elution. The composites were also fabricated into model stents by 3D printing. Degradability tests were conducted to determine the rate at which the stent will be degraded in a simulated environment of pH 7.4 at 37±1 °C.

Thus, a novel composite material was developed and tested for key requirements of a fully biodegradable drug-eluting stent such as mechanical properties

of toughening of the material for both radial strength and expansion of the stent during deployment, drug encapsulation, drug release kinetics, and faster degradability.

1.3 Significance

The medical device section is a major contributor to the Irish economy. As 80% of global stent production is carried out in Ireland. With the move to polymeric stents, there is an urgent need to develop associated technologies nationally. The global stent industry has a preference to move to the use of biodegradable stents, while the current stent materials are not sufficiently suitable and the current processes are designed for manufacturing metal stents, for instance, laser cutting. In the currently used commercial polymeric stents for clinical trials, PLLA dominates the market and despite the issues during and after the stent placement, it remains the material of choice for such applications (McMahon *et al.*, 2018).

The significance of this study was to show that the mechanical properties of the polymeric materials were enhanced using nanotechnology reinforcement and in principle, the stents could be 3D printed which was a polymer-based system. As current commercial stents mostly use polymer coating to incorporate drugs, in this study the drug loading and sustained release capacity were demonstrated from the stent body/platform itself. These were obtained with the aid of HNT's presence with made a significant change.

The study also attempted to manufacture a prototype of the stent via 3D printing for easy process ability and customization. Thus, the 3D printing method could be revolutionary in the medical field and has been researched extensively in various fields of the medical industry. Polymer composite stents manufactured with 3D printing processes could be highly effective for future applications for stents. Ease of maintenance, low cost, and flexibility make the FFF the most commonly preferred process of 3D printing (Berretta *et al.*, 2017). The 3D printing process has a minimum effect on the material's structure and eliminates the need for post-processing methods for material's property recovery which is commonly required by laser cutting, makes it feasible for the manufacturing of the medical devices (Guerra and Ciurana, 2018; Wang *et al.*, 2020).

Thus, the proposed research is significant in terms of material development for the toughness of stents, addressing the requirement of drug loading and drug release and customization of stent manufacturing via 3D printing.

1.4 Value of the study

The global stent market is worth $7.98 billion and coronary stents solely contribute 67.3% of it. The American Heart Association predicts $1.1 trillion of direct and indirect costs of CVD in 2035 (Hoare *et al.*, 2019). Europe following North America was projected as the second-largest market for biodegradable stents. However, in 2019 Europe was the largest region in the bioabsorbable market (*Bioabsorbable Stents Global Market Report 2020-30: Covid 19 Growth and Change*, 2020). As 80% of the global stent production is carried out in Ireland, there are extensive opportunities for industrial collaborations in this area (Innovation, 2013).

However, Abbott's FDA approved Absorb bioresorbable vascular scaffold (BVS) was removed from the market, Boston Scientific terminated their Renuvia scaffold development program as the devices showed a high risk of myocardial infarction and thrombosis owing to a higher risk of adverse heart events such as myocardial infraction and scaffold thrombosis when compared to a metallic drug-coated stent (U. S. Food and Drug Administration, 2017; Virmani, Jinnouchi and Finn, 2017). If these limitations can be overcome, there is massive potential for bioresorbable stents.

CHAPTER 2

Literature Review

2.1 Coronary Artery Disease

Coronary artery disease (CAD) has been a major cause of mortality across the world (McDowell, Slevin and Krupinski, 2011; Ramadugu and Latha Alikatte, 2016). In 2016, CAD accounted for approximately 9.43 million deaths worldwide (Hoare *et al.*, 2019). According to World Health Organisation (WHO), by 2030, the estimated number of cardiovascular deaths will be approximately 23.4 million and one of the four primary causes of death in the world will be coronary artery disease (Yin, Yang and Wu, 2014; Hu *et al.*, 2015). The medical diagnosis of this condition is mostly limited, as the signs and symptoms are generally nonspecific (McDowell, Slevin and Krupinski, 2011). Despite many study reports, there are various questions to establish the factors for such events (Ramadugu and Latha Alikatte, 2016). A major cause of coronary artery disease is atherosclerosis (Ma, Wu and Robich, 2012). In atherosclerosis organic and inorganic materials such as calcium, fat, cholesterol-containing deposit (plaque) are build-up and narrow the coronary arteries which are referred to as stenosis, decreasing blood flow to the heart (Roy and Chanda, 2014; Zhang *et al.*, 2014; Tabraiz Alam *et al.*, 2019). Eventually, the decreased blood flow may cause chest pain (angina), shortness of breath, or other coronary artery disease signs and symptoms. A complete blockage can cause a heart attack (Bhatia, 2010a; Zhang *et al.*, 2014; Naseem *et al.*, 2017).

2.2 Treatment of Coronary Artery Disease

In some cases, medications and lifestyle changes may be the treatment of choice. In other cases, open heart bypass surgery or percutaneous coronary intervention such as balloon angioplasty or coronary stenting may be recommended to open the clogged arteries depending on the degree of occlusion (Nidhi *et al.*, 2011). Usually, bypass surgery is performed in cases with more than 70% of the artery occluded (De Mel, Cousins and Seifalian, 2012).

2.2.1 Bypass surgery

During bypass surgery, surgeons take a section of a healthy blood vessel often from inside the chest wall or the lower leg, and attach it above and below the blocked

artery. This allows blood to bypass the blocked area and flow to the heart muscle (Bhatia, 2010b). Some studies show coronary bypass surgery may also be an appropriate treatment if you have multiple blocked or narrowed arteries and diabetes (Klein, 2006). Bypass surgery is highly invasive where the chest wall is required to open for surgery which may lead to complications such as chest wound infections and graft infections. Besides, it is technically difficult and expensive for the patients to access the procedure (Bhatia, 2010b). Although bypass surgery is an effective approach for coronary artery disease, a lot of research and development was done to bring in new methods to treat the condition mainly to avoid the costly surgery which has prolonged recovery times (Ma, Wu and Robich, 2012).

2.2.2 Percutaneous coronary intervention

Percutaneous coronary intervention (PCI) is the most frequently used treatment for coronary artery disease at present (Strohbach and Busch, 2015; McKittrick *et al.*, 2020). In the U.S. alone, around 600,000 people per year receive PCI treatment without going through coronary artery bypass surgery (Holman, Kavarana and Rajab, 2020). PCI is used to mechanically improve the artery condition without surgery. Procedures regularly used for percutaneous coronary intervention are balloon angioplasty and balloon angioplasty with stent implantation (Zhang *et al.*, 2014).

2.2.2.1 Balloon Angioplasty

Balloon Angioplasty for coronary artery disease was first conducted by Andreas Gruntzig in 1977 and was a beginning process of percutaneous intervention in cardiovascular medicine (Naseem *et al.*, 2017; Raleigh *et al.*, 2018). Angioplasty may especially be recommended if there is chest discomfort (angina) due to reduced blood flow that has not responded to medication and lifestyle changes. During angioplasty, the doctor inserts a tiny balloon at the site of the blockage and expands it to widen the narrowed artery. This procedure may cause injury to blood vessels leading to vascular elastic recoil and restenosis. Thus, sometimes emergency coronary bypass surgery is necessary (Ma, Wu and Robich, 2012). Recoiling or relapse of the stenosis which is the narrowing of the artery is usually referred to as restenosis as shown in Figure 2.1 (Yin, Yang and Wu, 2014; Tabraiz Alam *et al.*, 2019).

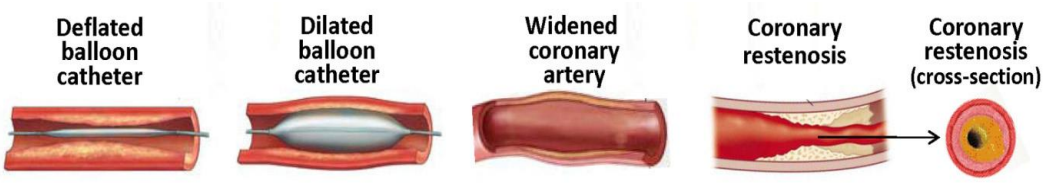

Figure 2.1. *Percutaneous transluminal coronary angioplasty and coronary restenosis* (Yin, Yang and Wu, 2014).

2.2.2.2 Coronary Stenting

Balloon angioplasty was a revolutionary treatment for CAD, however, its success was hindered by the problems such as restenosis or acute vessel closure. It is now sparingly selected as a treatment (Raleigh *et al.*, 2018). This led to the development of further advances in the treatment of CAD termed coronary stenting by percutaneous intervention. This procedure was first performed by Sigwart et. al. in 1986 (Garg and Serruys, 2010a). Currently, percutaneous coronary intervention is most commonly performed by coronary stenting (Giacchi *et al.*, 2016). Coronary stenting is considered a breakthrough in cardiology provided a solution to vessel occlusion by preventing recoil in comparison with balloon angioplasty (Foerst *et al.*, 2013). This reduced the rate of occlusion by 1.5% which in turn reduced the necessity of emergency bypass surgery (Onuma and Serruys, 2011). Hence, it has improved the treatment procedures concerning safety and efficiency (Zhang *et al.*, 2014).

In this procedure, an expandable balloon catheter is inserted into the diseased artery via arm or leg along with the stent. The stent mounted on the balloon is expanded by inflating the balloon and positioned where the plaque is formed. This expansion pushes the stent outwards, expanding the arterial wall and compresses the plaque against the wall. The stent stays in that position when the balloon is deflated (Moravej and Mantovani, 2011; Roy and Chanda, 2014). Thus, the stent remains in that position and keeps the artery open for the easy flow of blood as shown in Figure 2.2. This reduces the chances of restenosis, which would occur in most cases after balloon angioplasty. Evidence from clinical results has shown that in comparison to plain balloon angioplasty, the restenosis rate is significantly reduced to 20-30% by coronary stenting (Ma, Wu and Robich, 2012; Filipovic *et al.*, 2018).

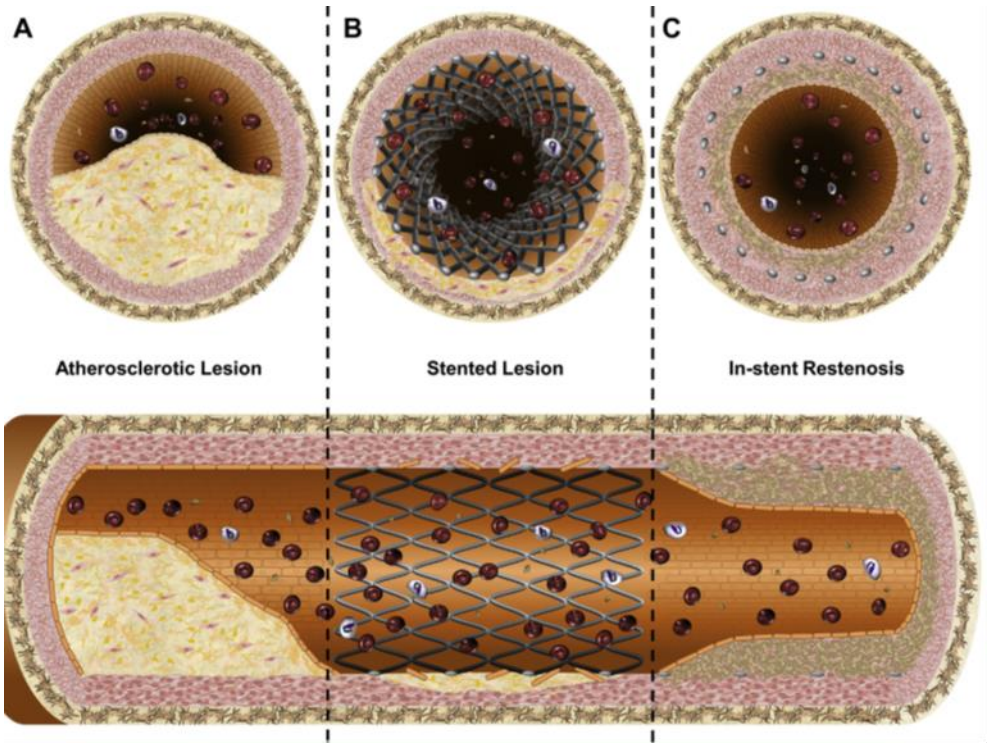

Figure 2.2. *Progression of in-stent restenosis. Cross-sectional and longitudinal views of arteries depicting the chronological progression of in-stent restenosis. (A) Obstructive atheromatous plaque-causing flow-limiting stenosis of the arterial lumen with reduced luminal diameter. (B) After percutaneous stenting restores the native vessel diameter by compressing the atheromatous plaque into the vessel wall with resultant denudation of the endothelial layer. (C) In-stent restenosis after inappropriate neointimal hyperplasia in response to percutaneous stent insertion resulting in recurrence of flow-limiting stenosis*

(Simard et al., 2014).

2.3 Coronary Stent Evolution

2.3.1 Bare metal stents

The stents are tubular mesh-like scaffolds and first-generation stents were made of bare metal (Wilson and Cruden, 2013; Moore, O'Sullivan and Verdecchia, 2016). In the beginning, a bare-metal stent (BMS) was chosen in the event of artery closure post balloon angioplasty (Raleigh *et al.*, 2018). The Belgium Netherlands Stent Arterial Revascularisation Therapies Study (BENESTENT) and the North American Stent Restenosis Study (STRESS) was a milestone in widely spreading coronary stenting technique, establishing the advantage of BMS over the balloon angioplasty (Dave, 2016; Wee *et al.*, 2020). There has been the development of stronger alloys,

improvement in delivery and deployment systems along augmentation in strut design, with reduction of strut size to <120 micrometers (Raleigh *et al.*, 2018; Omar and Kumbhani, 2019). The strut thickness plays a significant role as the studies indicate higher inflammation and neointimal hyperplasia with thicker strut compared to thin strut design. At one year, ISAR-STEREO randomized clinical trial, the rate of restenosis was 25.8% for the thick strut group and 15% for the thin strut group (Sakamoto *et al.*, 2018).

While most of the BMS were made from stainless steel, some were alloys such as nitinol composed of nickel and titanium, cobalt-chromium (Co-Cr) alloy with iron and nickel, platinum chromium alloy (Pt-Cr) with iron, nickel, and molybdenum (Kobo *et al.*, 2020). Stainless steel is considered a standard material for BMS due to its mechanical strength. Currently, cobalt-based alloys such as Co-Cr stents are preferred as they have high strength and helps obtain thinner struts (Jaganathan *et al.*, 2014). Although no particular metallic stent has clinical evidence for precedence over the others for safety and biocompatibility, the presently used stent metal such as chromium, cobalt, tungsten, and nickel have been reported to induce immune reactions with some scarce reports of hypersensitivity to metallic stents (Sakamoto *et al.*, 2018).

Studies from autopsies showed that vascular healing following the BMS implantation was very similar to a wound healing response. Two-four weeks of the early vascular healing process is followed by smooth muscle cell migration and matrix formation. Complete vascular healing occurs within 3-4 months of implantation. However, in 30-40% of these cases, resulted in in-stent restenosis (ISR) where the stented artery lumen narrows (Figure 1.2), from smooth muscle proliferation developing neointimal hyperplasia (Foerst *et al.*, 2013; Yin, Yang and Wu, 2014; Rebagay and Bangalore, 2019). Additionally, there were risks of inflammatory reaction due to the permanent presence of the stent and late or very late stent thrombosis (clotting of blood) within the stent lumen with eventual occlusion of the vessel (Braunersreuther, Mach and Montecucco, 2012; Bezrouk *et al.*, 2020) as shown in Figure 2.3. This prompted the development of drug-eluting stents to tackle the issues (Jaganathan *et al.*, 2014).

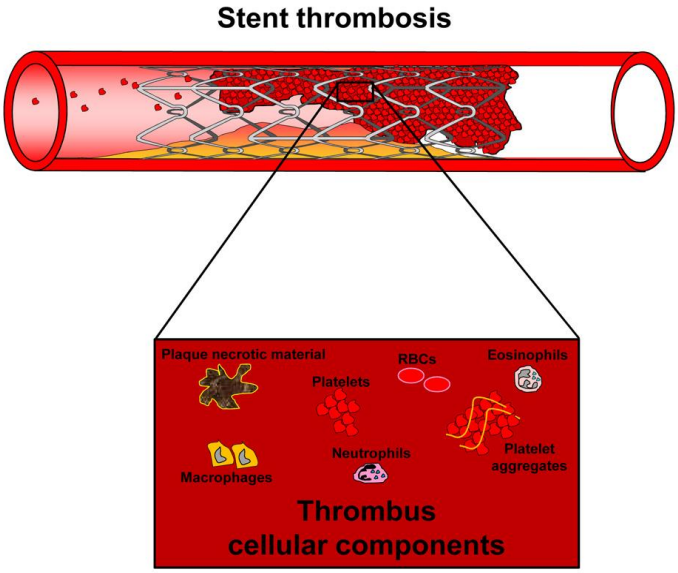

Figure 2.3 *In-stent thrombosis with constituents of a thrombus (Braunersreuther, Mach and Montecucco, 2012)*

2.3.2 Drug-Eluting Stents

The objective of manufacturing a drug-eluting stent (DES) was to prevent ISR by coating anti-proliferative drugs which would be released in a sustained manner to the surroundings of the stent (Rebagay and Bangalore, 2019). The occurrence of ISR was reduced to 5% with the use of DES when compared to 30-40% with BMS (McKittrick *et al.*, 2020). A permanent metallic scaffold, a coating, and an active pharmaceutical ingredient are the three main constituents of a DES (Jaganathan *et al.*, 2014; Moore, O'Sullivan and Verdecchia, 2016). The first-generation DES were made of stainless steel scaffold coated with durable yet non-biodegradable polymers loaded with drugs (Rebagay and Bangalore, 2019; Wee *et al.*, 2020). The polymers were either poly(n-butyl methyl acrylate) (PBMA), poly(ethylene-co-vinyl acetate) (PEVA), poly(styrene-b-isobutylene-b-styrene) (PSIBS), polyvinylidene fluoride (PVDF), or hexafluoropropylene (HFP) and the drugs used were sirolimus, everolimus or paclitaxel (Hu *et al.*, 2015; Lee *et al.*, 2018; Kobo *et al.*, 2020; Rykowska and Nowak, 2020). DES with non-biodegradable polymer coatings available on the market or during clinical trials is shown in Table 2.1.

Table 2.1*: Drug-eluting stents (DES) with non-biodegradable polymer coatings available on the market or during clinical trials (Rykowska and Nowak, 2020).*

Trade Name	Stent Platform	Polymer System	Drug	Drug Release (Days)	Company	Approval
Cypher®	SS	PEVA, PBMA	Sirolimus	40% (5) 85% (30) 100% (90)	Cordis Corporation	FDA, CE
Taxus®	SS	PSIBS	Paclitaxel	<10% (28)	Boston Scientific	FDA, CE
Promus PREMIER™	Pt-Cr	PBMA,PVDF -HFP	Everolimus	71% (28) 100% (120)	Boston Scientific	FDA, CE
Xience V®	Co-Cr	PBMA,PVDF -HFP	Everolimus	80% (28) 100% (120)	Abbot Vascular	FDA, CE
Firebird 2®	Co-Cr	PSIBS	Sirolimus	50% (7) 90% (30)	Essen Technology	Phase IV

The safety concerns of the first-generation DES raised the probability of late-stent thrombosis due to the delayed healing of the endothelial layer and this led to the advancement towards second-generation DES (Rykowska and Nowak, 2020; Wee *et al.*, 2020). Although dual antiplatelet therapy (DAPT) was advised for patients to reduce the rate of thrombosis, the improvements in second-generation DES were made to use the more effective drug in the polymer coating and thinner struts were produced for more rapid endothelialization and to prevent restenosis (Kobo *et al.*, 2020; McKittrick *et al.*, 2020). The drugs used were everolimus and zotarolimus (Lee *et al.*, 2018). Similar to first-generation DES, the polymers used for coating were non-biodegradable and the stent platform was metallic such as Co-Cr, Pt-Cr to achieve a thinner strut of 60–90 μm compared to 130–140 μm in first-generation DES (Rebagay and Bangalore, 2019; Rykowska and Nowak, 2020; Wee *et al.*, 2020). The thinner struts were introduced as they could assist in the reduction in blood flow disturbances and turn thrombogenicity (Caiazzo *et al.*, 2015). However, the safety concerns continued with second-generation DES as it had a non-biodegradable polymer coating similar to first-generation DES, which remains on the stent after the drug release and could accumulate in the body or instigate inflammation, delayed healing, and late stent

thrombosis. Some of the currently used drug-eluting stents are listed in Table 2.2 with details of the material and drug used along with drug-eluting time.

Table 2.2: *Drug-eluting stents (DES) with biodegradable polymer coatings available on the market or during clinical trials (Rykowska and Nowak, 2020).*

Trade Name	Stent Platform	Polymer System	Drug	Drug Release (Days)	Manufacturer	Approval
Synergy™	Pt-Cr	PLGA	Everolimus	(60) 50% (90) 100%	Boston Scientific	FDA, CE
Axxess™	Nitinol	PLA	Biolimus A9	(30) 45%	Biosensors	CE
BioMatrix Flex™	SS	PLA	Biolimus A9	(30) 45%	Biosensors	CE
Nobori®	SS	PLA	Biolimus A9	(30) 45%	Terumo	CE
BioMime™	Co-Cr	PLLA + PLGA	Sirolimus	(30) 100%	Meril	CE
Firehawk®	Co-Cr	PDLLA	Sirolimus	(90) 90%	MicroPort Medica	CE
DESyne® BD	Co-Cr	PLA	Novolimus	(90) 90%	Elixir®	CE
MiStent SES®	Co-Cr	PLGA	Sirolimus	(270) 100%	Micell Technologies	CE
Tivoli®	Co-Cr	PLGA	Sirolimus	(7) 50% (28) 80%	Essen Technology	Phase III NCT02448524

The third-generation DES thus introduced fully biodegradable polymers as drug-eluting coatings on metallic stents such as everolimus-eluting PLGA copolymer coated on Pt-Cr stent platform. The polymers used were polycaprolactone (PCL), polylactic acid (PLA), poly-lactic-co glycolide (PLGA), poly-L-lactic acid (PLLA), poly-DL-lactic acid (PDLLA) (Lee *et al.*, 2018). These DES showed reduced late stent thrombosis in a clinical setting compared to second-generation DES (Matsuhiro *et al.*, 2020) An international randomized study compared the clinical outcomes of patients with ultrathin (60 μm) strut having sirolimus-eluting biodegradable polymer coating and patients having stent of the thin strut (81 μm) with everolimus-eluting durable-polymer coating. With revascularisation and no very late stent thrombosis, the 3-year

follow-up displayed the precedence of the ultrathin stent with biodegradable polymer coating compared to the stent with a durable polymer coating (Kandzari *et al.*, 2020). Despite clinical studies follow-up up to 10 years, further studies and longer-term follow-up are required to ascertain promising results of ultra-thin DES with biodegradable polymer coating (Rebagay and Bangalore, 2019).

Thus, DES being more effective than the BMS, to restrain the occurrence of restenosis, the issue of in-stent thrombosis has prevailed at both short and long-term follow-up. To counter, DAPT is recommended for a longer period after stenting (Ang, Bulluck, *et al.*, 2017a; Ng *et al.*, 2017). Numerous cases of late thrombosis, hypersensitivity, and delayed healing have been reported for the long-term use of DES. The presence of a permanent metal scaffold in the artery after the healing could lead to complications like the prevention of late lumen expansion hindering the return of natural vasomotion (Moore, O'Sullivan and Verdecchia, 2016; McMahon *et al.*, 2018; Wee *et al.*, 2020). Another key issue is the ion leaching from metallic stents which could be toxic to cells. For instance, the presence of nickel in 316L stainless steel and nitinol stents could be toxic as nickel has been reported to be potentially carcinogenic (Y. Chen *et al.*, 2016). Thus, recently, fourth-generation DES is focusing on the stent body to be made of biodegradable polymeric or metallic material loaded with a drug (Moore, O'Sullivan and Verdecchia, 2016; Rykowska and Nowak, 2020). These are called biodegradable or bioresorbable stents which have been used in the treatment of CAD (Bezrouk *et al.*, 2020).

2.3.3 Bioresorbable Stents (BRS)

A fully bioresorbable stent provides the scaffolding of the vessel preventing the closure or recoil and a sustained release of the drug. Gradually the stent struts are tissue covered, degrading into non-toxic by-products and resorbed (Onuma and Serruys, 2011; Kokot *et al.*, 2018). Hence, the lifecycle of a BRS can be divided into three phases: revascularisation, restoration, and resorption. Bioresorbable is the total elimination of the material (Brie *et al.*, 2016).

There are several advantages of the BRS over BMS or DES. The BRS responds positively to factors released by endothelium and allows the vessel to react normally for remodeling (Wu *et al.*, 2012). As these stents are biodegradable, the vessel

scaffolding and drug elution are provided for 3-6 months until the vessels are healed. This reduces the occurrence of stent thrombosis and the requirement for dual anti platelet therapy which reduces the risk of bleed complications. As the stent biodegrades, it facilitates the late luminal enlargement, remodeling of the vessel, and restoration of endothelial coverage with no residual material (Garg and Serruys, 2010b; Ang, Bulluck, *et al.*, 2017a; Lee *et al.*, 2018). Some of the bioresorbable stents developed are shown in Figure 2.2. Various materials are currently used for the manufacturing of the bioresorbable stent. Bioresorbable stents are commonly made of polymers, magnesium alloy, or iron alloy.

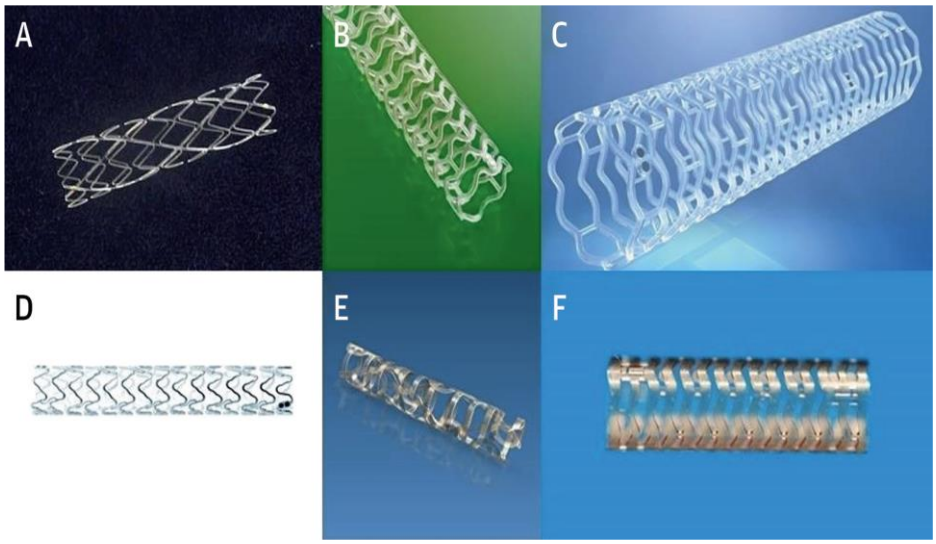

Figure 2.4 *Various materials are currently used for bioresorbable scaffolds (BRS). The Igaki-Tamai stent (Kyoto Medical Planning Co., Ltd., Kyoto, Japan) (A), the ABSORB Bioresorbable Vascular Scaffold (Abbott Vascular, Santa Clara, California) (B), and the DESolve bioresorbable scaffold (Elixir Medical Corporation, Sunnyvale, California) (C) are all manufactured from poly-L-lactic acid. The DREAMS magnesium alloy (Biotronik, Berlin, Germany) (D) is a metal bioresorbable vascular scaffold. The ReZolve 2 BRS (Reva Medical Inc., San Diego, California) (E) is produced on a desaminotyrosine polycarbonate basis, and the Ideal BioStent (Xenogenics Corp., Canton, Massachusetts) (F) is composed of a salicylate polymer and linker (Wiebe, Nef and Hamm, 2014).*

Table 2.3. *Drug-eluting stents (DES) with fully biodegradable scaffolds and coatings* (Rykowska and Nowak, 2020).

Trade Name	Stent Platform	Polymer System	Drug	Drug Release (DAYS)	Manufacturer	APPROVAL
Absorb™	PLLA	PDLLA	Everolimus	(28) 80%	Abbot Vascular	FDA approval
DESolve®	PLLA	PLLA	Novolimus™	(180–270) 100%	Elixir®	CE approval
Dreams I	Mg	PLGA	Paclitaxel	(90) 100%	Biotronik	Phase 0 NCT01168830
Dreams II	Mg	PLLA	Sirolimus	n.a.	Biotronik	Phase 0 NCT01960504

Mg: magnesium, n.a.: not applicable.

The material for the biodegradable stent, should match the basic criteria of biocompatibility, have enough radial strength for scaffolding, provide scaffolding for several months before it degrades, and finally, its degradation products should be biocompatible (Jaganathan *et al.*, 2014). The materials should be deformable with minimum elasticity, strong enough to maintain an open artery, and flexible to allow stent deformation. They must be cell compatible at least on the surface and should be non-toxic (Bhatia, 2010b; Beshchasna *et al.*, 2020). Based on these requirements, biodegradable metallic alloys such as iron alloys, magnesium alloys, or biodegradable polymers have been explored (Onuma and Serruys, 2011; Borhani *et al.*, 2018).

2.3.3.1 Magnesium based alloys:

Magnesium (Mg) been a principal element in the body, makes it an excellent choice for using it in the manufacture of stents. Mg alloy stents were the first metallic BRS implemented in humans (Jaganathan *et al.*, 2014; Tabraiz Alam *et al.*, 2019). The outcome of the first clinical studies for the Mg alloy stent showed that struts healed the inner walls of the vessel with no inflammatory reactions, increased endothelial cell proliferation, decreased smooth muscle cell proliferation without any systemic toxicity (Alexy and Levi, 2013; Jaganathan *et al.*, 2014). However, the early loss of radial strength, vessel recoil, and predominantly, fast degradation (corrosion) were still the associated issues to be addressed (Borhani *et al.*, 2018; Sakamoto *et al.*, 2018).

Several research studies focus on improving the composition of Mg alloy or surface coatings that could improve corrosion resistance. In most cases, improvised surface coatings demonstrated better corrosion resistance, and particularly polymer coatings have been proposed for the same. However, the commercialization of these

proposals for new Mg stents is yet to be reached (Borhani *et al.*, 2018; Beshchasna *et al.*, 2020). Besides, during degradation, the chemical by-products were found left in the surrounding tissue which could lead to calcification as a barrier. The hydrogen released during the degradation process of Mg could lead to inflammation and systemic toxicity (Beshchasna *et al.*, 2020).

Currently, Mg-based BRS are undergoing clinical and pre-clinical tests. Recently, a 12-month follow-up of 184 patients and 189 lesions from BIOSOLVE II and BIOSOLVE III (magnesium stents from BIOTRONIK) trials reveal safety profiles (Kobo *et al.*, 2020). Recent clinical studies of Biotronik AG's Mg-based BRS (Magmaris) revealed higher thromboresistance and complete resorption within 12 months compared to the present-day polymeric BRS (Sakamoto *et al.*, 2018; Wee *et al.*, 2020). However, longer-term, larger group follow-up and real-world clinical evidence are warranted for safety and efficacy. (Sakamoto *et al.*, 2018; Kobo *et al.*, 2020).

2.3.3.2 Iron-based biodegradable stent

The biodegradable stents made of iron are biocompatible and iron is a natural element present in the body (Boland *et al.*, 2016). They have good mechanical properties matching stainless steel BMS and are radio-opaque eliminating the use of markers to make the stent visible by fluoroscopy (Zivic *et al.*, 2018). Iron stents tested in animal models have shown endothelialization of the stents as positive remodeling and show decreased proliferation of smooth muscle cells inhibiting neointimal hyperplasia in *in-vitro* conditions (Im, Jung and Kim, 2017). However, preliminary animal studies have also reported slow *in-vivo* degradation rates as the iron stents are mechanically similar to permanent stents (Boland *et al.*, 2016; Ang, Bulluck, *et al.*, 2017a).

The ferromagnetic property of iron could also obstruct magnetic resonance imaging (MRI). Thus, modifications such as iron-manganese alloy were developed with good mechanical properties and anti-ferromagnetic properties (Alexy and Levi, 2013; Ramadugu and Latha Alikatte, 2016; Zivic *et al.*, 2018). Several other alloying elements such as cobalt, sulfur, carbon also showed improvement in the yield and ultimate strength (Yang *et al.*, 2018). Based on corrosion tests and cytotoxicity the elements cobalt, carbon, tungsten was considered suitable with high mechanical

properties, good biocompatibility, and corrosion rate. However, manganese was considered as a promising alloying element for the overall required properties of the stent (Sotoudehbagha *et al.*, 2018; Zivic *et al.*, 2018; Hoare *et al.*, 2019). The efficiency of the corrodible iron stent needs to be analyzed with long-term follow-up studies as its corrosion products, oxides are not metabolized at a reasonable rate hindering the integrity of the arterial wall (Beshchasna *et al.*, 2020; Rykowska and Nowak, 2020).

2.3.3.3 Polymeric stent:

Biodegradable polymeric stents have been the main focus of research in recent years as they are promising materials for providing temporary support to blood vessels followed by full disintegration without long term limitations of the metallic stents (Debusschere *et al.*, 2015; Dreher, Nagaraja and Batchelor, 2016; Guerra, Roca and de Ciurana, 2017; Chen *et al.*, 2018; Qiu and Zhao, 2018). The Igaki Tamai stent (Kyoto Medical Planning, Japan) made from poly (L-lactic acid) (PLLA) was the first BRS used in humans. Neither stent thrombosis nor stent recoil occurred within 30 days. A six months follow-up showed acceptable revascularisation and restenosis rates with no deaths (Tamai *et al.*, 2000; Gu *et al.*, 2016). The cumulative revascularisation rates per patient were 16% after 1 and 3 years, 18% after 5 years, and 28% after 10 years (Wiebe, Nef and Hamm, 2014).

Another BRS worth mentioning is ABSORB BVS developed by Abbott USA made of PLLA (Gu *et al.*, 2016). The evaluation of the stent over time showed inferior performance compared to DES. A three-year trial result revealed target vessel myocardial infraction in 6% of ABSORB group whereas 1% in the DES group of patients. The rates of thrombosis were significant at a 4-year trial. In addition to the reported safety issues, five-year follow-up data indicated no difference in the restoration of normal endothelial function compared to DES. Thus, in regards to the safety concerns, ABSORB BVS was removed from the European market in 2017 (Charpentier *et al.*, 2015; Omar and Kumbhani, 2019). Currently, further safety assessment studies for ABSORB BVS are ongoing.

The mechanical strength of the polymers is lower than those of the metals. Thus, in turn, polymeric BRS requires a larger strut thickness to provide the required radial strength. This could lead to the incomplete expansion or disruption in blood flow

causing coagulation of platelets (Hoare *et al.*, 2019; Beshchasna *et al.*, 2020; Wee *et al.*, 2020). However, considering the benefits, the development of BRS continues with intensive research to improvise the functionality, particularly, strut size reduction to decrease thrombogenicity and faster reabsorption (Omar and Kumbhani, 2019; Beshchasna *et al.*, 2020; Ni *et al.*, 2020).

2.4 Biodegradable polymers

Polymers having good mechanical properties, biodegradability and biocompatibility are an ideal choice when compared to metallic biomaterials (Jaganathan *et al.*, 2014). Polymers such as poly (L-lactic acid) (PLLA), polyglycolic acid (PGA), poly(lactic-co-glycolic acid) (PLGA), Poly(anhydride), Poly(urethane) and polycaprolactone (PCL) have been researched for BRS (Moore, O'Sullivan and Verdecchia, 2016; Wee *et al.*, 2020). The main polymers used for the BRS are the polyesters which have aliphatic ester bonds as the backbone. They are degraded and absorbed by the process of hydrolysis where the molecular weight and mechanical strength decrease resulting in mass loss. Finally, it is dissolved by converting into carbon-di-oxide and water resulting in the complete bioabsorption of the polymer (Ang, Bulluck, *et al.*, 2017b).

PGA is a highly crystalline polymer with excellent strength and degradation profile, yet it is limited for use as the by-products of PGA during the degradation are acidic and could cause inflammation in the surrounding tissues. PLGA is a co-polymer of PLA and PGA. It is biodegradable and its physical properties depend on the composition of PLA and PGA which can be modified accordingly. PCL is semicrystalline and hydrophobic which has a very long degradation period ranging from months to years depending upon its molecular weight (Rykowska and Nowak, 2020).

Table 2.4. *Mechanical and thermal properties of the most commonly used medical biodegradable polymers* (Rykowska and Nowak, 2020).

Material	E (GPa)	σ (MPa)	ε (%)	Tg (°C)	Tmelt (°C)	Loss of Mech. Prop. (Months)	Degradation (Months)
PLLA	3.4–4.8	10–100	2–6	60–65	170–180	6	24–67
PGA	6.8–12.5	70–647	min	35–40	180–230	1–2	6–12
PLGA (D/L/PLG) 85/15-50/50	2	20–50	3–10	45–55	-	1–4	2–6
PCL	0.3–0.4	16–23	300–700	⁻60	59–64	0.8	>34

The most commonly chosen polymer for polymeric BRS is Poly-l-lactic acid (PLLA) (Wu *et al.*, 2012; Wang *et al.*, 2018). It is a semicrystalline polymer where some molecules are aligned and packed in the crystalline region and some molecules are randomly arranged in the amorphous region. Such structural arrangement distributed throughout the polymer determines the strength and degradation properties of the polymer (Wang *et al.*, 2018). Thus, PLA-based polymers such as PLLA are promising due to their mechanical properties and biocompatibility. (Strohbach and Busch, 2015).

2.4.1 Poly Lactic Acid (PLA)

PLA is an aliphatic polyester, as the monomer units are connected through ester bonds (Casalini *et al.*, 2019). The basic building block for PLA is lactic acid, which was first isolated in 1780 from sour milk by the Swedish chemist Scheele (Garlotta, 2002; Tyler *et al.*, 2016). Lactic acid is also produced by fermenting the sugars obtained from biomass such as beet sugar, sugarcane, corn, potato, or rice (Farah, Anderson and Langer, 2016; Puchalski *et al.*, 2017). At present, the fermentation of sugars from renewable resources is the most employed method for lactic acid production (Casalini *et al.*, 2019). It is later synthesized into PLA by direct polycondensation of the lactic acid to obtain low molecular weight PLA or by ring-opening polymerization for high molecular weight PLA (Ramot *et al.*, 2016; Saini, Arora and Kumar, 2016; Dillon *et al.*, 2019). It is easily processed for use in various industrial and biomedical applications and since it is derived from renewable resources it is biodegradable (Castro-Aguirre *et al.*, 2016; Farah, Anderson and Langer, 2016). The lifecycle of PLA is shown in Figure 1.4.

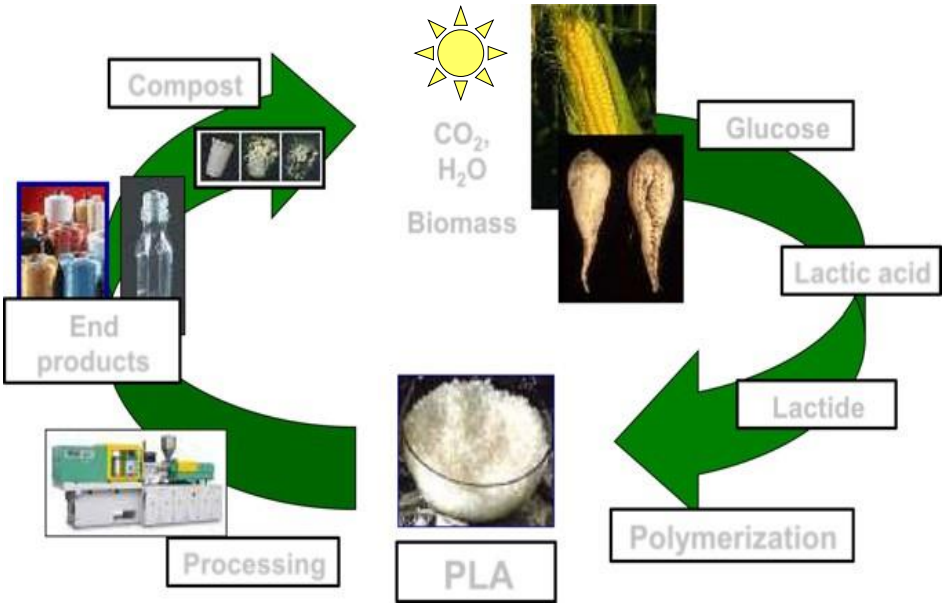

Figure 2.5 *The lifecycle of PLA (Murariu and Dubois, 2016)*

2.4.1.1 Characteristics of PLA

The monomer unit of PLA, lactic acid has two enantiomeric forms, L and D-lactic acid isomer. The lactic acid is predominantly L-type as most of the fermentation processes generate L-isomer. In certain conditions, lactic acid can racemize and convert to D-lactic acid and the chemical synthesis of lactic acid produces an equal amount of L-lactide and D-lactide called meso-lactic acid (Murariu and Dubois, 2016; Pretula, Slomkowski and Penczek, 2016). PLA when entirely composed of L-lactide is called PLLA, whereas PLA which is entirely composed of D-lactide is called PDLA which is semicrystalline. While, PLA with meso-lactide is called PDLLA and is amorphous with very low tensile strength (Bergström and Hayman, 2016; Casalini *et al.*, 2019). The commercial PLA is a copolymer of PLLA and PDLLA with a significant proportion of L-lactide and a negligible percent of D-lactide (Basu *et al.*, 2016; Pretula, Slomkowski and Penczek, 2016; Tyler *et al.*, 2016; Y. Chen *et al.*, 2016).

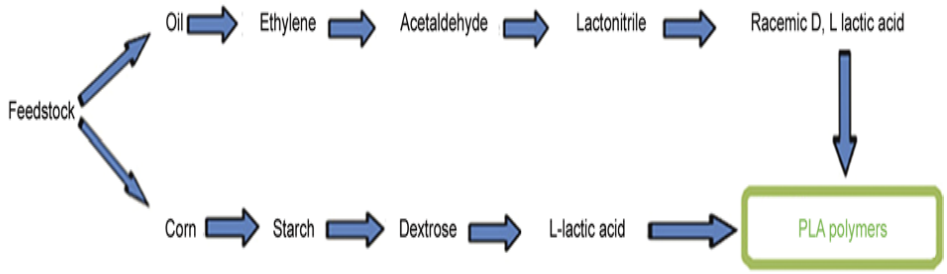

Figure 2.6. *Lactic acid preparation methods (Hamad et al., 2015)*

Over the past decade, PLA has attracted attention due to its characteristics such as biodegradability, renewability, high mechanical properties, biocompatibility, easy availability, and processability (Garlotta, 2002; Y. Chen *et al.*, 2016). These unique properties led the researchers to study the PLA alone or combined with other polymers or blend for various applications such as packaging, consumer goods, biomedical products (Castro-Aguirre *et al.*, 2016; Saini, Arora and Kumar, 2016). PLA has a glass transition T_g of about 60-65˚C and melt temperature of 175˚C and requires processing temperatures over 185- 190˚ C (Pawar *et al.*, 2014). It can easily be processed in applications such as injection molding, blow molding, thermoforming, and extrusion to yield films or fibers as it possesses adequate thermal processability when compared to other biopolymers such as poly(hydroxyl alkanoates) (PHAs), poly(ethylene glycol) (PEG), poly(caprolactone) (PCL) (Farah, Anderson and Langer, 2016; Sangeetha *et al.*, 2018).

PLA degrades by simple hydrolysis of the ester bond and has a degradation time in order of six months to two years (Bergström and Hayman, 2016). The Food and Drug Administration (FDA) has approved the use of PLA for implantation in the human body as they are tested to be biocompatible and degrades to non-toxic components, lactic acid which naturally occurs in metabolism (Farah, Anderson and Langer, 2016; Elsawy *et al.*, 2017). PLA has been researched and used for various medical applications such as resorbable sutures, tissue engineering, drug delivery systems, and dental, ophthalmic, fracture fixation, orthopedic applications, coating over stents, fully biodegradable stents (Ramot *et al.*, 2016; Y. Chen *et al.*, 2016).

However, there is a limitation of the use of PLA in many applications due to slow degradation rate, slow crystallization, and extreme brittleness (Hamad *et al.*, 2015; Dillon *et al.*, 2019). PLA is fairly hydrophobic which could lead to low cell

affinity and inflammation (Farah, Anderson and Langer, 2016; Sangeetha *et al.*, 2018). It also has poor thermal stability as it undergoes thermal degradation at 200°C (Hamad *et al.*, 2015; Y. Chen *et al.*, 2016). PLA is commonly blended with clay-based nanofillers to improve mechanical and thermal properties as the clay nanofiller has good strength on its own with a large aspect ratio (Basu *et al.*, 2016; Jia *et al.*, 2017; Sangeetha *et al.*, 2018).

2.4.2 Poly caprolactone (PCL)

Polycaprolactone (PCL) is a biodegradable, biocompatible polymer known to have good ductility and a degradation time of 2-3 years. It has been considered for medical applications and has been used as microspheres, nanospheres, and implants (Qiu *et al.*, 2020). It is hydrophobic with a glass transition temperature of around 60 °C and melting temperatures ranging between 50 -60 °C with a low viscosity. The molecular weight of the PCL determines the physical and mechanical properties (Fortelny *et al.*, 2019; Moura *et al.*, 2019).

It is a synthetic aliphatic polyester with high ductility and compared to other polymers it has slow biodegradability. Although initially, it was used in slow degrading suture materials, it was soon replaced by other resorbable polymers. Due to its lack of high mechanical strength, it was not considered for high load-bearing applications such as biodegradable implants (Woodruff and Hutmacher, 2010). Also, its low melting temperature of about 60 °C limits its use in a wide range of applications (Quiles-Carrillo, , Nestor Montanes, Fede Pineiro and Torres-Giner, 2018).

2.4.3 PLA/PCL blends

To improve the properties of a polymer as a biomaterial, the preparation of polymer blends is one of the methods used as the combination of two polymers blends the characteristics of each to enhance the performance of the blended material (Quiles-Carrillo, , Nestor Montanes, Fede Pineiro and Torres-Giner, 2018). One such commonly blended polymers are PLA and PCL. PLA/PCL blends have been studied extensively for improvement in mechanical performance especially with PLA as a major component, to enhance the toughness of PLA with minimum reduction in stiffness. Both binary and ternary blends have been researched depending on the

individual properties of the PLA and PCL to obtain the required miscibility or toughness of the material (Ferri *et al.*, 2016).

PLA/PCL binary blend has been studied with approximately 70/30 ratio for improvement in the properties (Urquijo, Guerrica-Echevarría and Eguiazábal, 2015; Ferri *et al.*, 2016; Ostafinska *et al.*, 2017). It has been shown that the toughness of the PLA/PCL blend can be 15 times greater than neat PLA (Fortelny *et al.*, 2019). The immiscibility of the polymers is generally addressed by the addition of compatibilizers so that the interaction between the polymer phases is increased (Carvalho *et al.*, 2020). PLA/PCL samples containing graphite nanoplatelets were analyzed by Luyt et.al. and observed the nanoplatelets had a catalyzing role in the crystallization and degradation process (Stephanus and Ivan, 2018). Huang et.al. studied the hydrolytic degradation of various blends of PLA, PCL, PEG and demonstrated the improvement of degradability of PCL by co-polymerization with PEG and PLA (Huang *et al.*, 2006). Carvalho et.al. studied the biocompatibility and biodegradability of PLA and PLA/PCL with low molecular weight, non-toxic compatibilizer derived from e-caprolactone, and tetrahydrofuran, and found the PLA and the blend to be biocompatible and biodegradable (Carvalho *et al.*, 2020).

Ternary blends of PLA/PCL using nanoparticles have been a recent area of research anticipating multifunctional enabling properties of the blend. There are nanoparticles used to develop ternary blends of PLA/PCL, such as silk fibroin nanoparticles (Dadras *et al.*, 2020), graphite nanoplatelets (Kelnar *et al.*, 2017; Stephanus and Ivan, 2018), multiwalled carbon nanotubes (Wu *et al.*, 2009), Octadecylamine Modified montmorillonites (ODAMMT) (Hairaldin *et al.*, 2012), poly(e-caprolac-tone)-b-poly(L-lactide) diblock copolymer (POSS-PCL-b-PLLA) a synthesized nanohybrid by ring-opening polymerization (Monticelli *et al.*, 2014). Thermal degradation behavior and kinetics of HNT in microfibrillated PLA/PCL were studied by Luyt et al. and showed the presence of nanotubes on the interface catalyzed the PLA and PCL degradation (Luyt and Kelnar, 2017).

2.5 Biodegradable Polymer nanocomposite

A nanocomposite is a two-phase solid material where one of the phases has one, two, or three dimensions of less than 100 nanometres. Polymer nanocomposites consist of a polymer matrix with inorganic or organic fillers, commonly a nanofiller

distributed evenly (Bari, Chatterjee and Mishra, 2016)(Raquez *et al.*, 2013). A broad selection of the basic components allows synergetic properties of the produced nanocomposites. Mechanical properties, like, yield stress, tensile strength, and Young's modulus generally increase in a nanocomposite when compared to pure polymers (Oliveira and Machado, 2013). Biodegradable polymers have been extensively used to prepare biodegradable polymer nanocomposites with improved properties for biomedical applications (Bari, Chatterjee and Mishra, 2016). The incorporation of nanofillers as a reinforcing agent in the polymer has been of significant interest as it enhances the properties of the biopolymer with low content (typically ≤5 wt%) when compared to 40-50 wt% of common fillers in conventional composites. Thus producing a polymer nanocomposite with mechanical and thermal stability, flame retardance, improved abrasion resistance, reduced shrinkage, and residual stress (Mousa, Dong and Davies, 2016)(Liu *et al.*, 2014; Anand Narayanan, Babu and Vasanthakumari, 2016; Pollack *et al.*, 2019). The size of the nanofillers does not produce stress points in the polymer matrix and in turn, does not lead to material failure when dispersed uniformly without agglomeration.

2.6 Nanofiller

Nanofillers can be characterized as follows:

- Clay-based nano fillers include Layered silicates, Sepiolite, Montmorillonite, and Halloysite.
- Nanocellulose based nanofillers include Cellulose Nanocrystals, Nano fibrillated cellulose and Bacterial cellulose.
- Carbonaceous-based nano fillers include Carbon nanotubes and Graphene derivatives.
- Metal-based nanofillers include Silver nanoparticles, Zinc oxide nanoparticles, Titanium oxide nanoparticles, and layered double hydroxide nanoparticles.
- Silicon-based nanofillers include Silica and Polyhedral oligomeric silsesquioxanes (POSS)(Raquez *et al.*, 2013).

Although most of the above-mentioned nanofillers can enhance the mechanical properties of the polymer, some materials such as carbon nanotubes on which numerous investigations have been focused are technologically demanding to produce in bulk, making them expensive (Liu *et al.*, 2014). There are concerns that nanofillers can enter the inner layers of the blood vessel wall. The nanoparticles tend to affect the dispersion in the polymer matrix as they could agglomerate (McDowell, Slevin and Krupinski, 2011; Atif and Inam, 2016). Studies have shown that nano fillers such as Montmorillonite, nanocellulose which is hydrophilic and multi-layered graphene and carbon nanotubes, cannot be readily dispersed within the polymer matrix causing filler aggregation and increased water uptake due to weak bonding between the polymer matrix and the nanofiller (Atif and Inam, 2016; Mousa, Dong and Davies, 2016).

It is also shown that the silicate layers and polymeric matrix affinity are relatively low with no proper intercalation between the polymer and the layered silicates, resulting in rarely improved materials and even diminished after the addition of layered silicates. Even though layered silicates are organomodified with various techniques such as in situ intercalacative polymerization, solvent intercalation, and melt-intercalation, it is reported that in comparison to both carbon nanotubes and organomodified layered silicates, HNT represents a good alternative as nanofiller (Raquez *et al.*, 2013).

HNT has been studied extensively and has been shown to enhance the mechanical properties of biodegradable polymers. HNT is a non-toxic, biocompatible, much cheaper material and naturally available when compared to synthetic carbon nanotubes. They also have a higher intrinsic stiffness compared to montmorillonite nanoplatelets (Yang, Zhang and Ouyang, 2016). HNT has an advantage over other clay nano fillers with strongly stacked layers which require an expensive process of exfoliation before the dispersion into the polymer matrix (Abdullayev and Lvov, 2013).

2.7 Halloysite Nanotubes

Halloysite is a type of clay mineral formed naturally in the earth over millions of years (Kamble *et al.*, 2012). In many geographic areas, HNT deposits have been found in different states of hydration and a variety of particle conformations (Deepak

and Agrawal, 2012). The occurrences of Halloysite are widely distributed worldwide and are generally derived from weathering or hydrothermal alteration of rocks and soils (Yuan, Tan and Annabi-Bergaya, 2015). The name 'Halloysite' was coined by Berthier in 1826 in honor of Omalius d'Halloy who first identified the mineral from a sample taken from Belgium. In the 1930s the name Halloysite was reserved for the fully hydrated mineral. Later endellite was suggested after one of the discoverers for the hydrated Halloysite. The dehydrated phase was named 'meta halloysite' or halloysite (Joussein *et al.*, 2005).

2.7.1 Morphology

HNT is a clay mineral that belongs to the group of Kaolin (Lun, Ouyang and Yang, 2014). The structure of HNT is similar to that of kaolinite, dickite, or nacrite. The separation of unit layers in HNT by the monolayers of water molecules makes it different from the other minerals of the Kaolin group. HNT has morphological variability due to various factors such as the degree of alteration, chemical composition, crystal structure, and the effect of dehydration (Zhang, Zhang and Zhu, 2019).

The three main morphologies of HNT are tubular, spheroidal, and platy. The most common morphology of HNT particles is the elongated tubule (Yuan, Tan and Annabi-Bergaya, 2015). The tubular HNT is commonly derived from crystalline minerals such as feldspar and mica. The tubules can be short and stubby or long and thin. Juossein et. al. in 2005 have neatly collated from various literature for various morphologies of the HNT from different occurrences around the world. The typical dimensions of tubular forms of HNT range from 100 nm – 4000 nm in length, 20 nm – 100 nm in outer diameter, and 5 nm – 30 nm for inner diameter and high concentration of small pores (Joussein *et al.*, 2005).

2.7.2 Chemical Composition

HNT has a chemical formula of $Al_2Si_2O_5(OH)_{4}.{}_nH_2O$ (Joussein *et al.*, 2005; Liu *et al.*, 2009; Dong *et al.*, 2015a; Yuan, Tan and Annabi-Bergaya, 2015) where it can intercalate up to two molecules of H_2O in a unit cell, which makes it different from kaolinite (Jock Churchman *et al.*, 2016). HNT is made up of two different interlayer surfaces. The external surface is mainly composed of siloxane (Si-O-Si) groups and

has two types of hydroxyl groups, silanol (Si-OH) and aluminol (Al-OH) groups are exposed at the edges of the tube, whereas aluminol (Al-OH) are located on the internal surface (Alberton *et al.*, 2014; Yuan, Tan and Annabi-Bergaya, 2015).

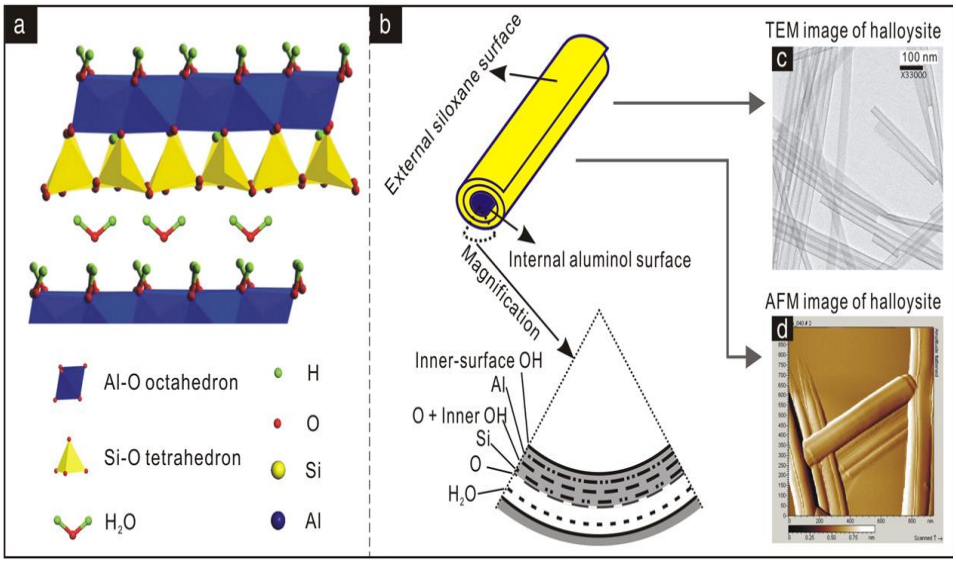

Figure 2.7. *Structure of halloysite nanotubes (Yuan, Tan and Annabi-Bergaya, 2015)*

2.7.3 HNT as nanofillers

HNT has been used as nano fillers for various polymer nanocomposites due to its high aspect ratio, good dispersion, and excellent mechanical properties (Deepak and Agrawal, 2012; Yuan, Tan and Annabi-Bergaya, 2015; Pasbakhsh *et al.*, 2016). HNT has been studied for being durable in high shear mixing and is easily dispersed in aqueous and organic solvents (Guo, Qiao and Zhang, 2016). The performance of HNT polymer nanocomposites is usually determined by two major factors. One is the good dispersion of the HNT in the polymer matrix and the other is an interfacial affinity between the HNT and the polymer (Liu *et al.*, 2014; Yuan, Tan and Annabi-Bergaya, 2015). Compared to other nanofillers, HNT has a large amount of filler-polymer interactions due to its high aspect ratio (Anand Narayanan, Babu and Vasanthakumari, 2016). Little surface charges of HNT are a distinct characteristic of nanomaterials which require no intercalation and exfoliation when compared to other nanofillers like MMT. Due to the composition of HNT which has several siloxane groups and only a few hydroxyl groups, HNT gets the ability to form hydrogen bonds that have the potential for better dispersion. HNT has a large luminal diameter which can provide a chance to accommodate different polymer molecules (Deepak and Agrawal, 2012).

2.7.4 Properties of HNT-Polymer nanocomposites

HNT loading increases the tensile strength and Young's modulus of polymer nanocomposites such as PA6, epoxy, vinyl ester nanocomposite, chitosan, PVA, PCL, PLGA nanofibers, and EPDM (Chen *et al.*, 2017). In comparison to other natural silicates like MMT and Kaolinite or CNT, HNT disperses better within the polymer, usually when the HNT loading is low. It has been shown to improve the mechanical properties of the polymer nanocomposite without the need for surface treatment (Jock Churchman, Pasbakhsh and Hillier, 2016; Therias, Murariu and Dubois, 2017). It has been studied for easy and uniform dispersion in the polymer matrix such as polyamide, polypropylene by direct melt blending without the need for surface modification of HNT (Du, Guo and Jia, 2010; Deepak and Agrawal, 2012).

The structural characteristics of the HNT and the interfacial interactions in the nanocomposites change the crystallization behavior of the polymer by the addition of the HNT (Liu *et al.*, 2014). HNT-polymer nanocomposite can also be used as promising drug containers for various applications as the drug release rate could be controlled by coating the polymers onto the drug-loaded HNT (Liu *et al.*, 2014). When the HNT are capped with polymers, the loading of the drug can be increased to 10-30% and there will be sustained drug release even for months (Leporatti, 2017). Hence it has been researched for biomedical applications such as dental fillers, drug delivery, cosmetics, cancer cell isolation, etc. (Lvov and Abdullayev, 2013).

2.8 PLA/HNT nanocomposites

PLA/HNT nanocomposites are of great interest in the biomedical field owing to the relatively high strength of PLA compared to other biodegradable polymers and the naturally available and biocompatible HNT (Chen *et al.*, 2017). The hydroxide groups in the hollow structure of HNT resist the harmful degradation of the PLA products to local tissues. Besides, the drawbacks of the PLA such as limited toughness, low thermal stability are addressed by the addition of HNT into the PLA matrix (Dong *et al.*, 2015a).

Studies have shown that the major challenge in the incorporation of HNT in PLA-based composites is the agglomeration of HNT into clusters. To address these issues, surface treatment of HNT can be used to improve dispersion of the

nanoparticles in the PLA matrix (Prashantha *et al.*, 2013; Gorrasi *et al.*, 2014; Dong *et al.*, 2015b; Guo, Qiao and Zhang, 2016; Krishnaiah, Ratnam and Manickam, 2017). Also, to further enhance the mechanical properties of the nanocomposite, HNT has been modified organically or grafted before blending with PLA. The overall effect of the HNT on the PLA matrix has been reported previously (Liu, Zhang and Zhou, 2013; Liu *et al.*, 2014; Dong *et al.*, 2015a; Chen *et al.*, 2018). It has been shown in earlier studies that 10wt% HNT loadings result in increases in the mechanical, thermal properties (Dong, Bickford and Haroosh, 2012; De Silva *et al.*, 2014; Liu *et al.*, 2014; Chen *et al.*, 2017), flame retardant properties (Liu *et al.*, 2014; Stoclet *et al.*, 2014) of PLA.

However, little research has been done on the influence of screw speeds during extrusion for the PLA/HNT composites. Increases in screw speed during compounding have been shown to increase melt shear and it is hypothesized that this increase in shear will lead to better dispersion of the HNT in the polymer matrix.

2.9 Hot Melt Extrusion (HME)

The Hot Melt Extrusion (HME) has emerged to be a robust processing technology for developing dispersions of Active Pharmaceutical Ingredients (API) or nanofillers into the polymer matrices (Maniruzzaman *et al.*, 2012). Extrusion is a process of feeding raw materials at an elevated controlled temperature and pressure through the heated barrel into a product of uniform shape and density (Breitenbach, 2002). Polymer nanocomposites can be prepared by the method of extrusion for better dispersion which in turn enhances the properties of the polymer. (Abeykoon *et al.*, 2014). Extruders are mainly classified as single-screw which is widely used for general polymer processing or twin-screw extruder utilized for compounding various polymer blends, fillers, or fibers (Hyvärinen, Jabeen and Kärki, 2020). The twin-screw extrusion is a high shear process where the material melts under high temperature in the barrel and continues to move towards the die with a homogenous melt which helps for better dispersion of the filler in the polymer matrix (Gamon, Evon and Rigal, 2013; Stanković, Frijlink and Hinrichs, 2015).

For an appropriate degree of filler dispersion, co-rotating twin-screw extruders are used for the fabrication of the polymer nanocomposites as they exhibit very high mixing efficiency (Sasimowski and Majewski, 2019). Besides, the extruder can be

configured as required. For instance, the addition of kneading elements in the screw profile for the augmentation of the blending (Hornsby, 2017) The factors influencing filler dispersion during melt compounding with thermoplastics are shown in Figure 2.8. The processing conditions such as shear force due to screw speed, temperature, etc. also plays a vital role in an effective clay dispersion (Oliveira and Machado, 2013). Dispersion mechanism occurs during extrusion when the polymer melts while blending with the nanofiller, it penetrates the primary agglomerates breaking them into individual nanotubes. This mechanism is susceptible to the individual characteristics of the polymer and the nanofiller used, in addition to the processing parameters (Gs, Al and Youseffi, 2019).

The HME technology has been used effectively for drug delivery systems in various applications such as sustained release, implants, and films (Maniruzzaman and Nokhodchi, 2017). Parameters such as the use of plasticizers, reduction in the processing temperatures and residence time could be used while processing to potentially reduce the thermal degradation of the APIs and recrystallization of APIs during the storage of the product (Repka *et al.*, 2018). It has been used to melt or solubilize APIs inside polymer matrix to generate amorphous systems that can effectively improve solubility, modulate controlled release, and have improved bioavailability (Fule, Paithankar and Amin, 2016; Martinez-Marcos *et al.*, 2016; Patil, Tiwari and Repka, 2016) (Maniruzzaman *et al.*, 2012; Saerens *et al.*, 2014; Martinez-Marcos *et al.*, 2016; Patil, Tiwari and Repka, 2016).

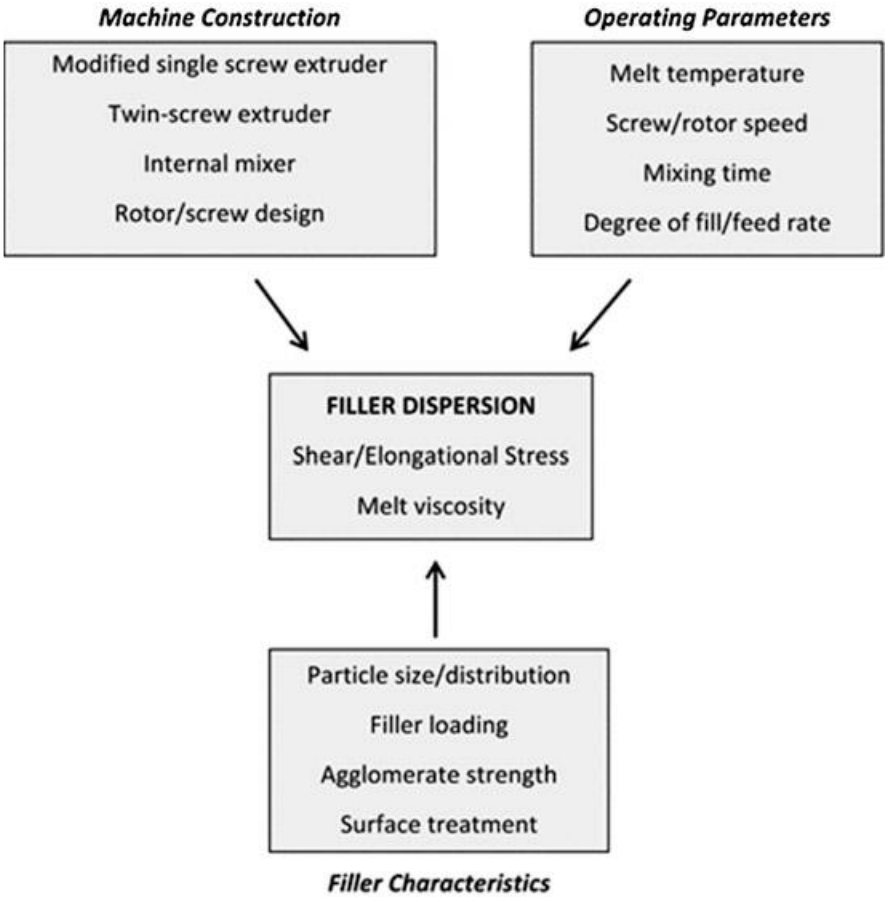

***Figure 2.8**. Key factors influencing filler dispersion during melt compounding with thermoplastics (Hornsby, 2017).*

2.10 Three-dimensional (3D) Printing

Three-dimensional (3D) printing is an additive process used to fabricate 3D structures and geometries whereby material is built up layer by layer using a computer-created design (Okolie *et al.*, 2020). Charles Hull developed this process initially as stereo lithography (SLA) in 1986. Following this, several processes were developed such as fused deposition modeling (FDM), Polyjet, and selective laser sintering (SLS), direct ink writing (DIW), and digital light processing (DLP). However, FDM is the most commonly used process of 3D printing (Matias and Rao, 2015; Tuan D. Ngo *et al.*, 2018; Wu *et al.*, 2019). FDM is an extrusion-based additive manufacturing developed by S.Scott Crump who commercialized it through his company, Stratasys. Generally, FDM is referred to as fused filament fabrication (FFF) due to the copyright of the FDM term. FFF is a printer that has a spool to hold the filament which is unrolled towards the extrusion head which can move horizontally or vertically (X, Y) with bed

movements typically enabling printing in the Z direction to fabricate a 3D structure. The head contains a nozzle that is heated to melt the filament according to the path instructed by software (Miguel *et al.*, 2017; Fuenmayor *et al.*, 2018; Pranzo *et al.*, 2018). The schematic representation of the FFF is shown in Figure 1.9.

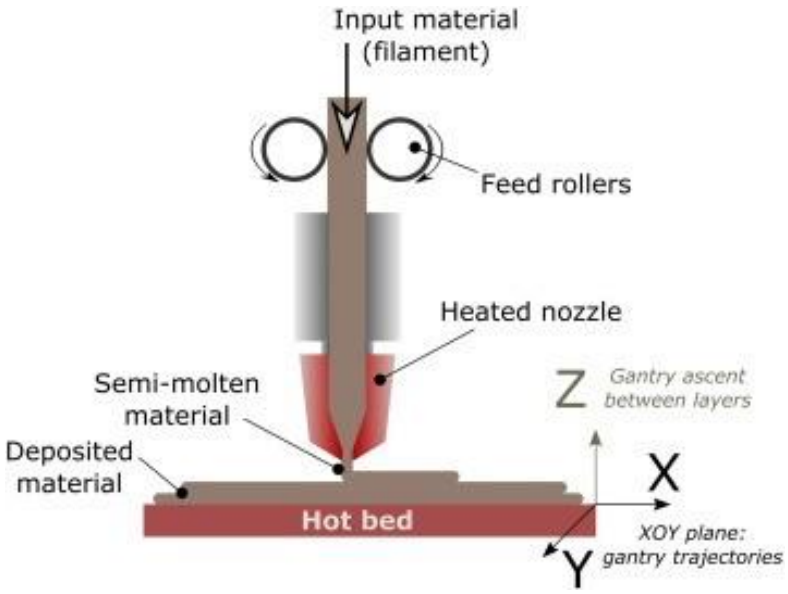

***Figure 2.9**. Fused filament fabrication (FFF) process (Pranzo et al., 2018).*

FFF has displayed ease of use, developing objects from complex shapes, low cost, and the use of common thermoplastic polymers such as PLA, Nylon, ABS, PET. Several studies have investigated various polymer nanocomposites for FFF (Berretta *et al.*, 2017; Gnanasekaran *et al.*, 2017; Coppola *et al.*, 2018; Lamberti *et al.*, 2018). The nanomaterial can be reinforced into the host matrices by 3D printing to produce nanocomposite signifies numerous advantages due to its properties and also improves the homogeneity of the product (Tuan D Ngo *et al.*, 2018). The high viscosity of the thermoplastics can be further increased by the addition of nanofillers which affects the printability of the nanocomposite filament. This can be addressed by opting for suitable mixing strategies while compounding to enhance the dispersion of the nanomaterial into the polymer matrix. Various other methods such as solution mixing by sonication and high shear mixing by extrusion can be employed to reinforce the nanomaterial into the polymer matrix before 3D printing (Dermanaki Farahani and Dubé, 2017).

3D printing has been emerging widely as an application to various fields of biomedical science. It is rapidly developing and is preferred in the area of tissue

engineering as models of heterogeneous properties can be achieved close to those of native tissues as it can be fabricated into multicellular tissues with intrinsic structures (Wenger and Giraud, 2018). Pharmaceutical drugs can be personalized with specific doses, immediate and sustained release of multi-layered drugs. It has been researched and developed prostheses and organs for surgical planning or medical training. For instance, a 3D printed model of congenital heart defect was used to preoperatively plan a heart surgery (Paul *et al.*, 2018; Khanesar, 2019). Similarly in the area of stents, although the real application of 3D fabricated stents is limited because of material and machine constraints, much research is ongoing in the areas such as 3D printed PLA/PCL cardiovascular stent (Guerra *et al.*, 2018), 3D printed ureteric stent (Youssef *et al.*, 2015), a nasal stent (Mills *et al.*, 2017) for potential future application.

2.11 Drug loading and drug release

In a drug-eluting stent, the sustained release behavior of the drug is very important. Ideally, the drug should be released quickly in the first week and gradually the release must be consistent for at least a month. The drug release mechanism is characterized into the physical mechanism where the drug released by the polymer layer, via degradation of the polymer is advantageous than the chemical mechanism which is based on the breakage of the covalent bonds that connect the drug molecule to the polymer chains by chemical or enzymatic degradation (Naseem *et al.*, 2017; Beshchasna *et al.*, 2020).

The drug release mechanism is classified into three primary controlled systems depending upon the properties of the polymer. In the first system, the drug is eluted from the non-degraded polymer and is called a diffusion-controlled system. In the second system, the drug elution is enhanced as the polymer swells and is called, swelling controlled system. In the third controlled system, the drug is released due to polymer degradation or erosion and is called an erosion control system. However, in all these systems diffusion is involved (Hu *et al.*, 2015).

Nanocomposite-based drug delivery system with controlled release property is of great interest in biomedical applications. Physical properties of the material have to be considered for the drug delivery system as they influence the rate and time of release (Fuenmayor *et al.*, 2018). To improve the bioavailability, solubility, and sustained

release of drugs, the polymeric nanoparticles are prepared from the polymers such as PLA. In such cases, the drug molecules are confined inside the polymer membrane or uniformly dispersed on the surface of the polymer (Nagavarma *et al.*, 2012; Sha *et al.*, 2016). PLA has been studied as a drug release membrane and the results have achieved sustained drug release for a long duration due to diffusion and degradation (Mhlanga and Ray, 2015).

HNT has been widely used as drug delivery systems as they are known to have a high aspect ratio, high surface area, non-toxicity, process ability, fine particle size, and biocompatibility (Gaaz *et al.*, 2017). The HNT can be loaded with the drug due to its large outer surface and inner lumen (Lvov, DeVilliers and Fakhrullin, 2016). The loading of various molecules into HNT may be realized in two approaches: 1) selective loading in the inner tubular lumen, and 2) drug linkage to the outer surface (Santos Ana *et al.*, 2018). Recent researches have demonstrated the feasibility of loading different drugs on the HNT (Abdullayev and Lvov, 2011; Lun, Ouyang and Yang, 2014; Patel *et al.*, 2015; Fu *et al.*, 2017; Leporatti, 2017).

The drug release from biodegradable polymers depends not only on the properties of the polymer but the type of drug used also plays an important role. Siegel et al. studied 6 different types of drugs on PLGA pellets which varied the drug release rate and pellet degradation mechanism by the functions of different drug types (Siegel *et al.*, 2006). Frank et al. compare the drug release rate of different drugs in base and salt forms from biodegradable polymers and demonstrate that the drug chemistry affects the matrix degradation dominating the release pattern (Frank, Rath and Venkatraman, 2005). In few other studies by Miyajima et al., the drug release properties from PLGA and PLLA were reported for the effects of the physiochemical properties of a drug-using basic and acidic drugs (Miyajima, Koshika, Jun Okada, *et al.*, 1998; Miyajima *et al.*, 1999a, 1999b).

One of the most fundamental properties of drug action is the acidity and basicity of the drug molecule in medicinal chemistry. Although there is a lack of a clear definition for acids and bases, the compounds that can donate a proton are classified as acids and the compounds that can accept a proton are classified as bases. Both the compounds have to be at least 50% ionized at pH 7.4 (Charifson and Walters, 2014). However, to determine the acidity and basicity of the drug in a solution we need

to understand the functional groups that confer the acidity and basicity on a molecule. For the reaction or equation of accepting or donating a proton, the equilibrium constant is the acidity constant K_a which is a simple ratio determining the acidity. The negative logarithm of K_a is pK_a (pKa = −log Ka) and the acid is stronger as the value of pK_a is lower. The functional group carboxyl confers acidity on drug molecules such as aspirin (ASP) (pKa 3.5). Conversely, phenol groups have pKa values ~ 10 and a common phenol drug is acetaminophen (APAP) which has a pKa of 9.5. Thus pKa value of a drug helps to predict the ionization of the drug at the pH of the human blood (7.4) (Cairns, 2003).

The pKa values are significant for determining the absorption and permeation of the drug. Literature also identifies how the risk factors were previously faced by medical chemists when pKa values of acids and bases were not given importance and how it affected when the values were far from 7 which is the neutral value (Manallack *et al.*, 2013).

2.12 Aspirin

Aspirin (ASP) is one of the oldest and most commonly used anti-inflammatory drugs in the world (Trabert *et al.*, 2014; Mollace *et al.*, 2017). It is a derivative of salicylic acid in which acetyl replaces one hydroxyl group to form acetyl salicylic acid. It has the potential to stop the production of hormones which aids the process of inflammation or increased body temperature (A, 2003). To improve the solubility of the ASP the drug AsproClear was made with the addition of sodium bi-carbonate and citric acid improves the pH condition. The drug was also reported faster relief of pain compared to regular ASP tablets (Kalepu and Nekkanti, 2015).

However, due to the poor oral availability (Khadka *et al.*, 2014) and gastrointestinal side effects (Semalty *et al.*, 2010; Ng and Yeomans, 2018) by long term oral administration of the ASP, parenteral administration is required (Tang and Singh, 2008; Zhang, Ma and Gene, 2017). The acidic nature of ASP can cause damage to the mucous membrane of the digestive system (A, 2003). Recently, ASP was tested as soluble ASP-$_{D,\ L}$-lysine salt for intravenous injection (IV) for migraine and the results revealed that ASP was more effective in relieving migraine attacks by intravenous administration (Kalepu and Nekkanti, 2015).

ASP is also commonly prescribed to patients after coronary interventions (Ellis *et al.*, 2015; Kimura *et al.*, 2015; Cassese *et al.*, 2016; von Birgelen *et al.*, 2016). Patients are maintained on dual anti platelet therapy with both ASP and P2Y12 inhibitors (Ali *et al.*, 2017; Ang, Bulluck, *et al.*, 2017a; King and Gogas, 2017). The risk of early stent thrombosis was most certainly removed by the dual therapy of ASP and an inhibitor of platelet aggregation after placing the stent (Surgery and College, 2017). To provide anti-inflammatory and anti-proliferative effects, fully absorbable stent IDEAL BDS releases ASP and sirolimus and is made up of polyanhydride ester and salicylic acid (Jabara *et al.*, 2009; Wilson and Cruden, 2013).

It is a hydrophilic, acidic drug (Tang and Singh, 2008) and has been studied for loading in polymers. Zhang and researchers demonstrated the controlled drug delivery by loading ASP on chitosan nanoparticles for bone regeneration study (Zhang, Ma and Gene, 2017). The *in-vitro* drug release of ASP and degradation of PLGA matrix was studied by adding ASP to PLGA solution along with a plasticizer. There was sustained drug release and the degradation of the PLGA matrix was faster. It also increases the water absorption of the polymer matrix affecting the rate of drug release and polymer degradation (Tang and Singh, 2008). Various characterizations including loading and encapsulation efficiency were studied by Shi and researchers on various concentrations of ASP in the drug-polymer delivery system of ASP-chitosan nanoparticles (Shi *et al.*, 2014). Chitosan/HNT/ASP nanocomposite was studied for effective ASP concentration in the body and had a fast rate and high amount of release from simulated intestinal fluid compared to the simulated gastric fluid which had a low release amount (Li *et al.*, 2016).

2.13 Acetaminophen (APAP)

4-Acetamidophenol is commonly known as acetaminophen or paracetamol (Oliveira and Peter, 2003; Fujisawa, Eda and Hanaya, 2017). It is the second most frequently used API after ASP (Lawson, Ogwu and Tanna, 2018). It is an acylated aromatic amide and is widely prescribed for headaches, cold, cough, fevers, arthritis, and postoperative pain as it is safe and effective in recommended doses (Tertis *et al.*, 2013; Fujisawa, Eda and Hanaya, 2017; Montaseri and Forbes, 2018; Wei *et al.*, 2019). In comparison with most of the nonsteroidal anti-inflammatory drugs (NSAIDs) has less severe side effects of long-term administration with no gastrotoxicity. It is also a

weak inhibitor of aggregation of human platelets and is preferred over ASP for hemophiliac patients in the likelihood of bleeding (Mielke *et al.*, 1976; Pearson, 1981; Botting, 2000). Thus, post-operative or post-traumatic welling and bleeding can be reduced or prevented with paracetamol unlike ASP (Skjelbred, Album and Løkken, 1977)

The drug is commonly incorporated into a hydrophilic polymeric matrix for sustained release of oral dosage. APAP release from hydroxypropyl methylcellulose (HPMC) and hydroxypropyl cellulose (HPC) matrices was studied with and without the effect of pseudoephedrine (PE) as a co-active and found the drug release was slower in a formulation containing both APAP and PE than only APAP (Ebube and Jones, 2004). The amount of APAP release from hydroxypropyl methyl cellulose (HPMC)/polyvinylpyrrolidone (PVP) matrices was linearly related to the weight loss percentage of the prepared tablet (Ebube *et al.*, 1997). Orally dissolving filmstrips with APAP, polymers, and plasticizers were evaluated to show faster release from the dissolution of filmstrips compared to the chewable tablets (Dave, Shah and Patel, 2014).

Paracetamol-loaded polymer composites with layered silicate nanoclay have been prepared by hot-melt extrusion and the drug release was significantly slowed on the addition of nanoclays (Campbell, Craig and Mcnally, 2008). The PDLLA and organically modified MMT were encapsulated with paracetamol and the presence of nanoclay MMT increased the drug loading efficiency and extended the drug release (GaRea, 2017). Controlled release of paracetamol from MMT modified with PEG was obtained by hot-melt extrusion (Cavallaro, Lazzara and Fakhrullin, 2018). Profound initial burst release of paracetamol was observed from PDLLA electrospun fibers (Cui *et al.*, 2006).

2.14 Scope of the research

The scope of the research is mainly focused on the material development for the polymeric drug-eluting biodegradable stent by addressing current challenges during and after its placement in the narrowed artery. The current study aimed to develop a polymer nanocomposite that focused on factors such as stent material, mechanical support, manufacturing process, and degradation rate.

The research gap from the literature review addressed in this study are as listed below:

1. Material selection

Currently used polymeric BRSs, as the latest generation of a stent, are mostly made of biodegradable polymer PLLA. PLLA has low mechanical strength and poor elongation compared to metal. Hence in this study, polylactic acid (PLA) is used as the base polymer which is reinforced with non-toxic nanoclay, halloysite nanotubes (HNT) via extrusion as they are widely used in the biomedical field due to their biodegradability, natural availability, and high mechanical properties.

2. Mechanical support

PLA/HNT nanocomposite was developed via twin-screw extrusion by studying different screw speeds to evaluate the properties of the nanocomposite.

3. Drug elution:

The PLA/HNT nanocomposite was studied for dug loading and drug release characteristics.

4. Comparative study of acidic and basic drug loading and release:

The PLA/HNT nanocomposite was encapsulated with ASP and APAP as model acidic and basic drugs which have similar molecular weights.

5. Manufacturing process:

PLA/HNT nanocomposite developed via extrusion was pelletized and was extruded successfully into filaments of 1.75±0.10 mm diameter using twin-screw extruder with specialized die fixed to the extruder for the manufacture of production-grade 3D printing filament. This resultant filament was utilized for Fused Filament Fabrication (FFF) into 25mm medical implants.

6. Stent ductility:

Due to the brittle nature of PLA, the blending of PLA with PCL was performed to increase the ductility of the final construct.

7. Degradation study:

Degradation studies were conducted to determine the mechanical properties of the composite during degradation for 32 weeks which considers reports that the stents should retain their mechanical properties for six months.

CHAPTER 3

Experimental Details

3.1 Materials

PLA was obtained from Corbion PLA LX 175 in pellet form. It has a density of 1.24 g/cm^2, min. 99% L-isomer, melting temperature of 175°C, the glass transition temperature of 55°C, the tensile modulus of 3500 MPa, and strength of 45 MPa.

HNT was supplied by Applied Minerals; DRAGONITE-HP and Sigma-Aldrich Ireland Ltd. in powder form. It is a tubular shape with a length of 0.2-2µm, an outer diameter of 50-70 nm, an inner diameter of 15-45 nm, and an aspect ratio (L/D) of 10-20.

Aspirin (ASP) was obtained from Sigma-Aldrich Ireland Ltd in crystal form white in color. The chemical name of ASP is acetyl salicylic acid with molecular formula $C_9H_8O_4$ and molecular weight 180.16.

Acetaminophen (APAP) was obtained from Alfa Aesar, Thermo Fisher Scientific Chemicals, Inc. The chemical name is 4-Acetamidophenol and is also referred to as p-Hydroxyacetanilide; Paracetamol; Acetaminophen; with molecular formula $C_8\ H_9\ N\ O_2$, molecular weight 151.16.

PCL was obtained from CAPA^{TM}, CAPA 6500 with a molecular weight of 50000 g/mol in powder form. It has a melting point of 58-60 °C and percentage elongation at a break of 800. All the materials were used as received unless otherwise stated.

3.2 Methods

3.2.1 Melt extrusion

Extrusion is a process of feeding raw materials at an elevated controlled temperature and pressure through the heated barrel into a product of uniform shape and density. The HME has emerged to be a robust processing technology for developing dispersions of API or nano fillers into the polymer matrices to develop numerous drug delivery systems (Maniruzzaman *et al.*, 2012).

A schematic representation of the melt extrusion process is shown in Figure 3.1 below. The twin-screw extruder contains two rotating screws inside the heated barrel which is either co rotated or counter-rotated (Maniruzzaman *et al.*, 2012)(Jani and Patel, 2014). The screw along with the barrel is usually divided into 3 sections. a) Feeding section, where the materials are fed from the hopper to the barrel. b) Compression or melting section, where the entrapped air is removed, and the polymer begins to soften and melt. c) Metering zone, where the pulsating flow is reduced to prevent the uneven material flow to the die, as the polymer is already in the molten state in this zone as shown in Figure 3.1 (Jani and Patel, 2014).

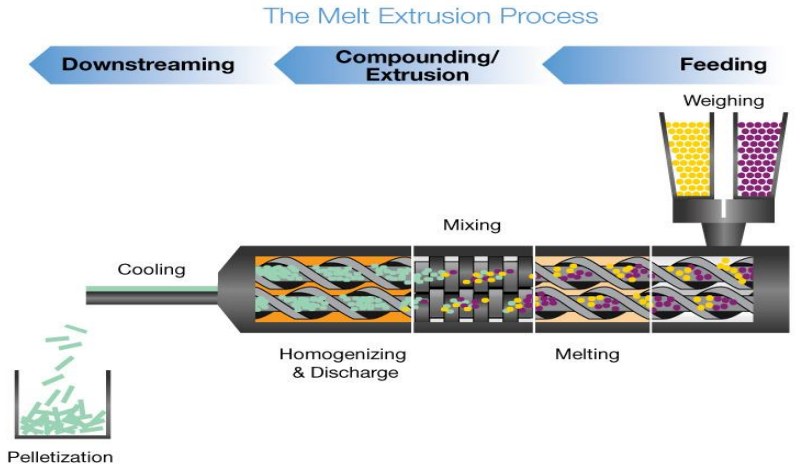

Figure 3.1 *Melt Extrusion process*

The compounding of the materials in this study was carried out using an APV Extruder (Model MP19TC) which is a twin-screw compounder with a 19 mm screw diameter and 35:1 length and diameter ratio. For the preparation of the nanocomposites in chapter 4, the virgin PLA is again fed into the hopper and extruded with the above temperature profiles and with the screw speed of 40 RPM, 80 RPM, and 140 RPM. The extruded PLA was passed through 3 cylinders rolling machine to compress into thin sheets as shown in Figure 3.2.

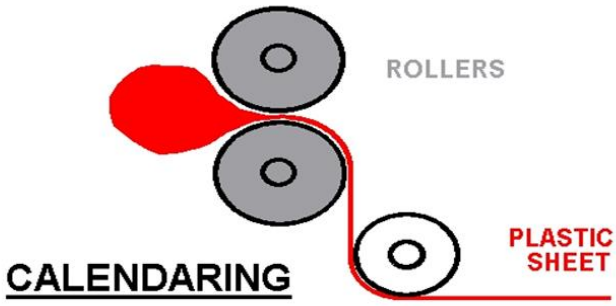

Figure 3.2. *Schematic representation of 3 roll calendar*

The dried HNT powder and the dried PLA were weighed with mass fractions of 100/0, 95/5, 90/10, and 80/20 accordingly with the PLA. The weighed HNT powder is mixed with the PLA and fed into the hopper and extruded with the temperature profile maintained at (from feeder to the die) 200/190/180/170/160/110/50°C, with the screw speeds of 40 RPM, 80 RPM, and 140 RPM. The extruded composites are passed through the 3-cylinder calendaring machine with mains water-cooled to compress the composites into thin sheets. These thin sheets are cut into long strips and labeled as per their respective weight fractions and respective screw speeds as mentioned above. The thin composite strips of various mass fractions and screw speeds are then prepared into test specimens for tensile testing, using a physical punching process to punch out standard tensile test samples as shown in Figure 3.3.

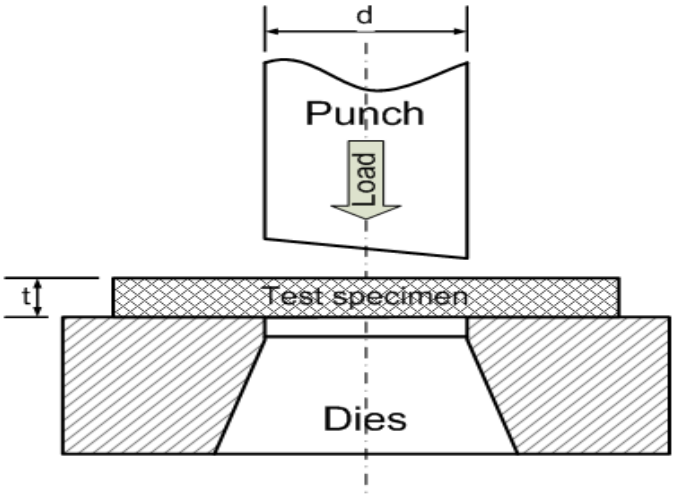

Figure 3.3. *Punching process (Edy Pramono, Rebet and Zulfia, 2015)*

In chapter 5, extrusion was performed by using APV (Model MP19TC (25:1)) (APV Baker, Newcastle-under-Lyme, UK) twin-screw compounder at a screw speed of 140 rpm. The mass fractions of PLA: HNT were 100:0 and 95:5 for both preloaded and matrix loading samples. The preloaded HNT/ASP for both 1:1 and 2:1 ratio was tumble mixed with PLA and extruded. These samples are referred to here as lumen loaded. As a control, HNT, ASP, and the PLA were hand-mixed and extruded at the same ratios. These samples are referred to here as matrix loading.

The extruded film was drawn through the three-roll calendar as shown in Figure 3.2 to form a continuous film. Finally, ASTM standard tensile test specimens were punched out of the film for testing as shown in Figure 3.3. The nomenclature of each batch by the method of preparation and composition is described below in Table 3.1.

Table 3.1. *Description of the prepared sample batches, method of processing, composition, and the ratio of each component for each batch.*

Batch	Type of Loading	Composition	HNT: ASP ratio
B1	Lumen loaded	95% PLA, 5% (HNT+ASP)	1:1
B5	Lumen loaded	95% PLA, 5% (HNT+ASP)	2:1
B2	Matrix loaded	95% PLA, 5% (HNT+ASP)	1:1
B3	Matrix loaded	95% PLA, 5% (HNT+ASP)	2:1
B4	Matrix loaded	95% PLA, 5% HNT	-
B6	Matrix loaded	100% PLA	-

In chapter 6, Extrusion was performed by using a Prism^{TM} twin-screw extruder with 16mm diameter screws and a 25/1 length to diameter ratio. The temperature profile was maintained at (die to the feeder) 210/190/180/170/160 and screw speed was kept at 140 rpm. The composition details of the prepared nanocomposites are listed below in Table 3.2.

Table 3.2. *Description of the prepared polymer nanocomposites with PLA, HNT, ASP, and APAP. The corresponding compositions for each category are in percentages*

BATCH	PLA	HNT	ASP	APAP
P	100	0	0	0
P+H	95	5	0	0
P+ASP+H	95	2.5	2.5	0
P+APAP+H	95	2.5	0	2.5
P+ASP	95	0	5	0
P+APAP	95	0	0	5

In chapter 7, Compounding was performed by using APV (Model MP19TC (25:1)) (APV Baker, Newcastle-under-Lyme, UK) twin-screw compounder with 19 mm diameter screws. The temperature profile was maintained at (from feeder to the die) 190/180/170/170/160/140/120/50°C. The extrusion was performed at a screw speed of 140 rpm with the mass fractions of 100:0, 97:3, and 95:5 for PLA: HNT.

In chapter 8, Extrusion was performed by using a Prism^{TM} twin-screw extruder with 16mm diameter screws and a 25/1 length to diameter ratio. The mass fractions of PLA: HNT were 100:0 and 95:5. A master batch of PCL: HNT was prepared into films in the ratio of 90:10. The prepared master batch was pelletized. The nomenclature is illustrated in Table 3.3. The pelletized PCL/HNT nanocomposites were then extruded with PLA in 95:5 and 90:10 compositions as shown in Table 3.4. For the extrusion of PLA and PLA composites the temperature profile was maintained at (die to the feeder) 210/190/180/170/160 and for PCL and PCL related composites, the temperature profile was (die to the feeder) 70/70/60/60/50. The screw speed was set at 140 rpm. The extruded film was drawn through the three-roll calendar to form a continuous film. All the samples had a thickness of approximately 1 mm, length of 2 cm, and width of 20 mm. Finally, the films were punched into ASTM standard tensile test specimens for testing. Each specimen had a gage length of 20 mm, gage width of 4 mm, and shoulder width of 10 mm with a thickness of approximately 1 mm.

Table 3.3. *Description of the prepared PCL/HNT master batches.*

Batch	PCL	PCL	HNT
A	50000 g/mol (powder)	90%	10%

Table 3.4. *Description of the prepared polymer nanocomposites with PLA, PCL, and HNT. The corresponding compositions for each category are in percentages.*

Number	PLA	PCL	A	HNT
1	100	0	0	0
2	95	0	0	5
3	95	0	5	0
4	90	0	10	0
5	95	5	0	0
6	0	100	0	0
7	0	0	100	0

3.2.2 3D printing – Fused Filament Fabrication

Compounding of the PLA/HNT nanocomposites was performed as described in section 3.2.1 above. The extrudate was drawn through a cooler belt as shown in Figure 3.4 and pelletized. These pellets were reprocessed using the same machine into a 3D printing filament of PLA and PLA/HNT.

Figure 3.4. *In-house high precision filament production line*

The metal die used to produce filament had a bore diameter of 1.75 mm. The extrusion temperature was adjusted through a control panel and the melt temperature used for PLA pellets was 170 °C. This filament extrudate was passed through a cooler belt and finally wound onto a spool for 3D printing as seen in Figure 3.5.

Figure 3.5. *Photograph of the 3D printable filaments*

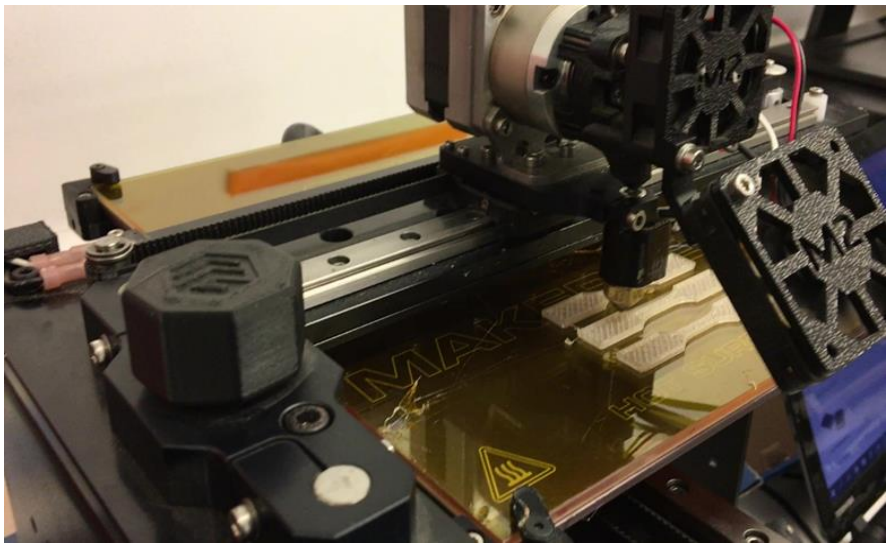

Figure 3.6. *MakerGear M2 3D printer*

Once the filaments were extruded, they were printed into tensile test specimens and model medical implant using a FFF 3D printer (MakerGear M2 3D printer, US) as seen in Figure 3.6. The filament is extruded from movable head on the FFF machine and deposited in ultra-thin layers onto a substrate, translating the dimensions of digital data into an actual printed parts (Wang *et al.*, 2017). The material is heated slightly above its melting point; this is to ensure it will quickly solidify after being deposited

and welds to the former layer or printing bed. A chamber before the nozzle melts the material and the filament pushed into this cavity forces out the necessary amount of molten material. FFF printer (MakerGear M2 3D printer, US) has a spool to hold the filament which is unrolled towards the extrusion head which can move horizontally or vertically (X, Y) with bed movements typically enabling printing in the Z direction to fabricate a 3D structure. The head contains a nozzle that is heated to melt the filament according to the path instructed by software. The nozzle temperature was fixed at 200°C, bed temperature at 70°C with 25% infill for all the filaments. The STL files were generated from SolidWorks designs.

3.2.3 Differential Scanning Calorimetry

Calorimetry was used as a primary technique to measure the thermal properties of materials and to establish a connection between the temperature and physical properties of the materials. Differential scanning calorimetry is the thermoanalytical technique in which the difference in heat flow to the sample and the reference was monitored against time or temperature, while the temperature of the sample, in a specified atmosphere, was programmed. The quantity of the heat flow in and out of the DSC sensor was dependent on the applied temperature, properties of the sample, thermal resistance, and capacitance of both the reference and the sample cell (Gill, Moghadam and Ranjbar, 2010).

In a DSC experiment as shown in the schematic representation in Figure 3.7, the energy is introduced into a reference cell and a sample cell simultaneously and the temperatures are raised over time for both the cells. The amount of excess heat absorbed or released by the molecule of the sample would require a difference in the input energy to match the temperature of the sample to that of the reference. The concept of heat excess is needed as more energy is required to bring the temperature of the sample to the same temperature as the reference because of the presence of a molecule of interest (Gill, Moghadam and Ranjbar, 2010).

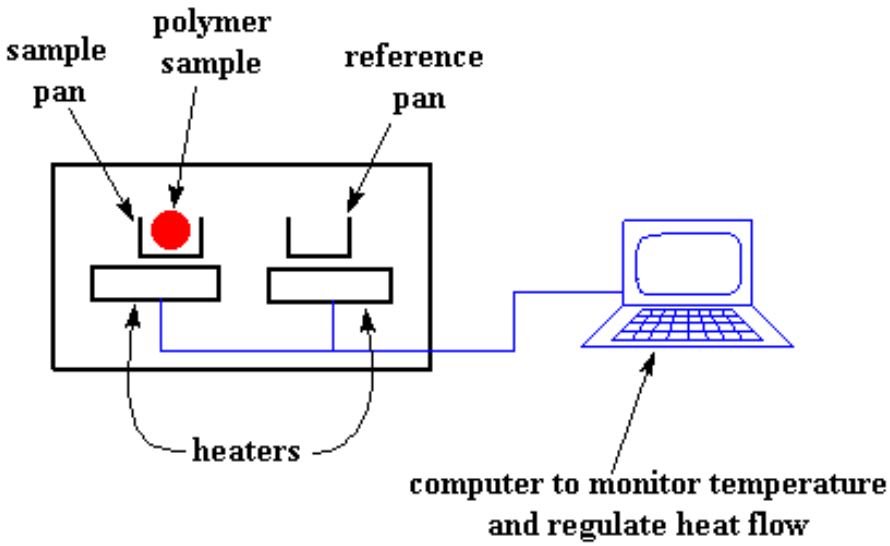

Figure 3.7. *Schematic representation of differential scanning calorimetry*

(Freire, 1995)

The resulting DSC scans with the reference subtracted from the sample show how this excess heat changes as a function of temperature (Gill, Moghadam and Ranjbar, 2010). This is illustrated in Figure 3.8 which shows the features of the typical DSC curve. The Glass transition temperature, Crystallinity, and melting temperature are considered from the curve.

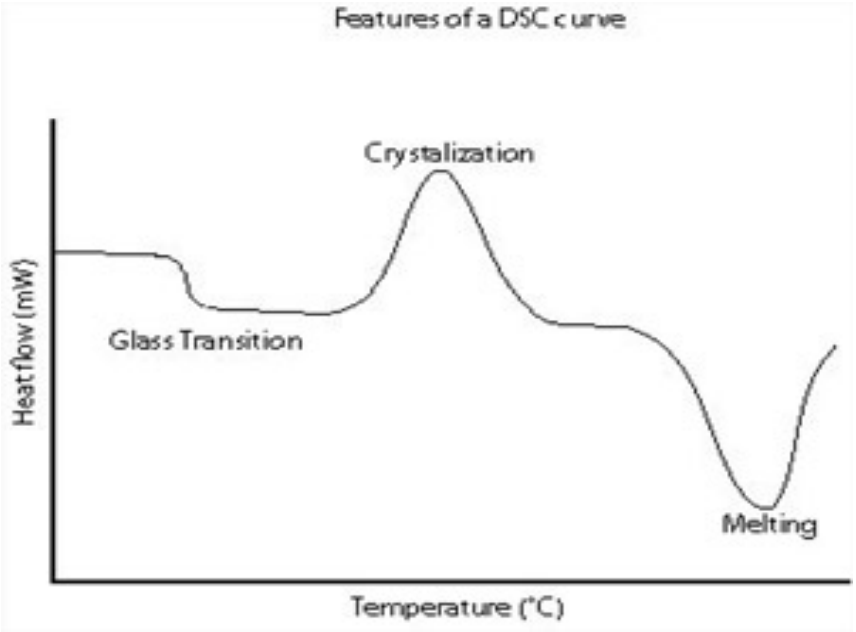

Figure 3.8. *Typical DSC curve (Calorimetry and Analysis, 2010)*

In this project, The Differential scanning calorimetry (DSC) was carried out in triplicate using a DSC 2920 Modulated DSC (TA Instruments) with a nitrogen flow rate of 20 ml/min to prevent oxidation. Calibration of the instrument was performed using indium as standard. The test specimens weighing between 8 and 12 mg were measured on a Sartorius scale (MC 210P), capable of being read to five decimal places. Samples were crimped in non-perforated aluminum pans, with an empty crimped aluminum pan used as a reference.

The thermal history was removed by heating samples from 20°C to 220°C at the rate of 30°C/min and held isothermally at 220°C for 10 mins. The sample was then cooled from 220°C to 20°C at 30°C/min. Finally, the thermal properties of the samples were recorded by heating the samples from 20°C to 220°C at the rate of 10°C/min. Crystallinity, glass transition temperature, and the melting temperature of each sample were recorded on the graphs.

3.2.4 Mechanical properties

The primary concern of the newly processed material is its strength. Usually, the tensile properties are measured to compare the strength of the materials before and after processing. The results show the maximum stress the material can withstand or its ductility to see how much it deforms before fracture (ASM International 2004).

The standard tensile specimen is dumbbell shape with length and cross-sectional area as shown in Figure 3.9. The specimen is placed on the tensile equipment as shown in Figure 3.10. The specimen is held at both the end of the clamps and subjected to tension which acts along the length of the specimen. The function of the increase in gauge length is recorded as the tensile force (ASM International, 2004).

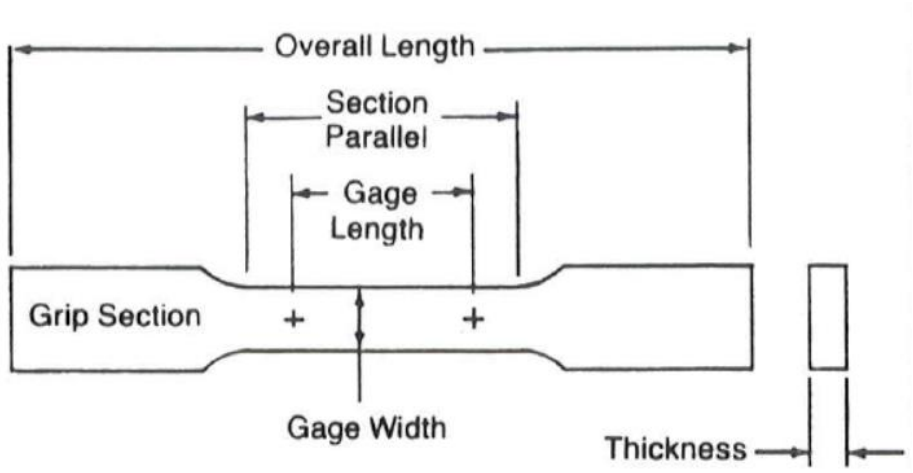

Figure 3.9. *Standard tensile specimen (ASM International 2004)*

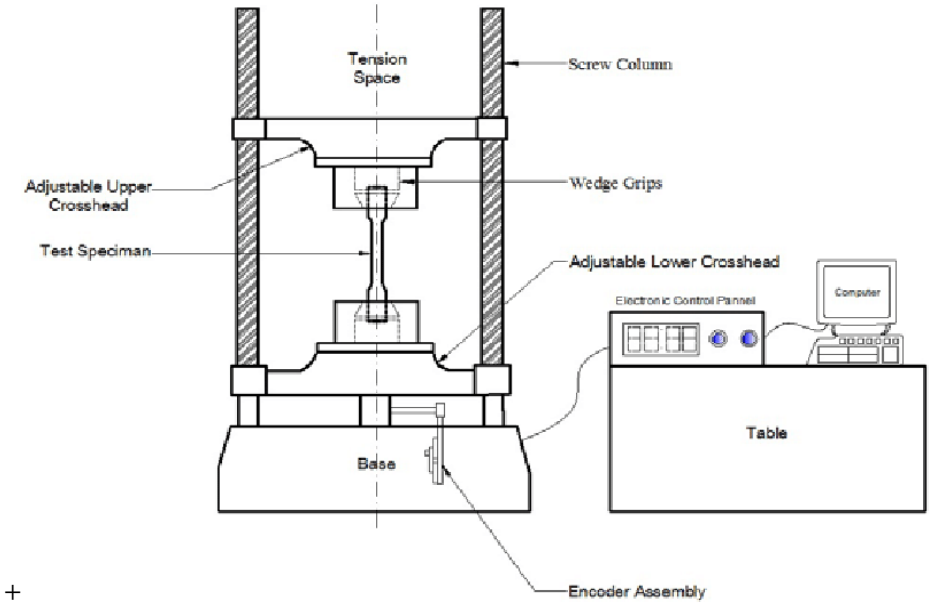

Figure 3.10*. Schematic representation of the tensile equipment (Chellamuthu, Sabarinathan & Muthu, S & Naushad Ali, 2012)*

Mechanical properties of the PLA/HNT composites were characterized by tensile testing each different blend. Tensile testing was carried out on a Lloyd Lr10k tensometer using a 2.5 kN load cell. It was carried on ASTM standard test specimens at a strain rate of 50 mm/min. Data was recorded using NexygenTM software. The tensile tests were carried out in adherence to ASTM D 882. Ten individual test specimens were analyzed per group and before testing, the thickness of each sample was measured. The percentage strain at maximum load, stress at maximum load, stiffness, and Young's Modulus of each sample were obtained.

3.2.5 Scanning Electron Microscopy (SEM)/Energy Dispersive X-ray (EDX)

Scanning Electron Microscopy (SEM) was used to obtain the details of the surface and the composition of a specimen. The electromagnetic lenses focus on an electron beam that scans the surface of the specimen line by line. The scanning movement and the display device are synchronized to obtain the image (Schmitt, 2014). Energy Dispersive X-ray (EDX) analyses the elemental composition of the solid material or the composite. The electrons transiting to a high energy level results in the emission of characteristic X-rays. As the characteristic X-rays have specific energy corresponding to each element, the element can be identified from the peak energy; and the content of the element in the compound can be analyzed from the integrated intensity of the peak (Shindo and Oikawa, 2002).

Scanning Electron Microscopy (SEM) was performed using a Mira XMU SEM (TESCAN Brno, Czech Republic) in a backscattered electron mode to determine the shape and distribution of HNT in the PLA matrix. Energy Dispersive X-ray (EDX) was performed using an Oxford Instruments detector to determine the elemental composition of HNT and the composites of PLA and HNT. The accelerating voltage utilized was 10 kV for raw HNT and 20 kV for composite materials. Before analysis, test samples were placed on an aluminum stub and the samples were sputtered with gold using Baltec SCD 005 for 110 seconds at 0.1 mbar vacuum before testing.

3.2.6 Fourier transform infrared spectroscopy (FTIR)

Fourier Transform Infrared (FTIR) Spectroscopy is conducted to identify new materials and determine the components of a mixture or the quality of a sample. In this method, the infrared radiation is transmitted through the sample, out of which, some are absorbed by the sample and some are transmitted. These absorption peaks correspond to the frequency of the vibration between the atoms making up the composite. The size of the peak is directly related to the amount of material present (Ganzoury et al. 2015).

Fourier transform infrared spectroscopy (FTIR) for this project was carried out on a Perkin Elmer Spectrum One fitted with a universal ATR sampling accessory. All data were recorded at 218 °C in the spectral range of 4,000–650 cm^{-1}, utilizing a four

scan per sample cycle and a fixed universal compression force of 70–80 N. Subsequent analysis was carried out using Spectrum software.

3.2.7 Surface wettability

The surface wettability was conducted to examine the relative hydrophilicity or hydrophobicity of the composites. If the composite is hydrophobic, the water droplet is nearly spherical when placed on the surface. This can be determined by drawing a tangential line between the water droplet and the surface of the composites and recording the advancing and receding contact angle between the droplet and the surface (Manoudis and Karapanagiotis, 2014).

The surface wettability of the composites was assessed using the First ten angstroms, FTA32 goniometer as shown in Figure 3.11. In this test, the Sessile Drop contact angle technique was utilized with distilled water as the probe liquid. Five contact angle readings (n=5) were recorded for each sample. Water droplets were delivered to five different points of each specimen and from a height sufficiently close to the sub-strata so that the needle remained in contact with the liquid droplet. Then, the delivery needle was withdrawn, and the image of the drop was captured immediately to measure the static contact angle.

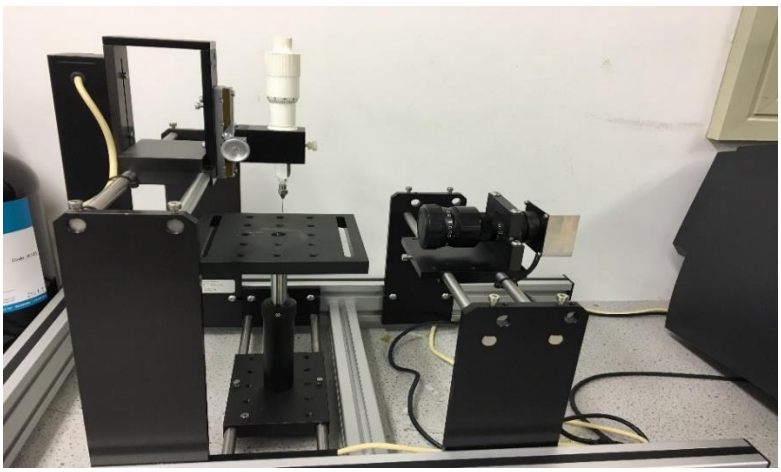

***Figure 3.11**. Photograph of the Goniometer equipment*

The capillary force is recorded and the image is captured at every step after the 15 s waiting for relaxation. The contact angle hysteresis was calculated by the dynamic sessile drop method. The advancing/receding contact angle was the maximum/minimum angle measured while the volume of the droplet was increased/decreased without increasing/decreasing the solid-liquid interfacial area. The reported contact angles (static, advancing, and receding) are averages of five measurements and varied within ±2◦. The same, narrow variation was recorded for different samples prepared using the same coating composition.

3.2.8 Drug loading on HNT

ASP was encapsulated into the HNT at two ratios of 1:1 and 2:1. For the preparation of the 1:1 ratio, 12 grams of ASP was dissolved in 120 ml of ethanol by stirring. Once the solution became transparent, 12 grams of HNT were added and stirred for 4 hours at 700 rpm. The solution was then centrifuged to separate the solid part and dried overnight at 40°C with a vacuum. Similarly, the 2:1 ratio is prepared using 12 grams of HNT and 6 grams of ASP.

3.2.9 In vitro drug release

Simulated body fluid (SBF) was prepared according to the method described by Kokubo and Takadama (Kokubo and Takadama, 2006) with a pH of 7.4. All samples had a thickness of approximately 1 mm, length of 2 cm, and width of 20 mm. The samples were placed in a dissolution apparatus. Each vessel of the dissolution apparatus contained 500 mL of SBF at 37±1 °C with a rotation speed of the stirring element shaft at 50 rpm for three weeks. At selected time intervals, 5 mL of the release buffer was removed for UV analysis and replaced with an equal volume of fresh buffer. The amount of released ASP was measured by UV Spectrophotometer at 298 nm and APAP at 243 nm. This experiment was carried out in triplicate to obtain the release profile of the ASP with time.

3.2.10 In vitro degradation

Simulated body fluid (SBF) was prepared according to the method described by Kokubo and Takadama (Kokubo and Takadama, 2006) with a pH of 7.4. All the samples for the weight measurement had a thickness of approximately 1 mm, length

of 2 cm, and width of 20 mm. Ten ASTM standard tensile test specimens for each week had a gage length of 20 mm, gage width of 4 mm, and shoulder width of 10 mm with a thickness of approximately 1 mm for each specimen. The samples were placed in falcon tubes containing 50 mL simulated body fluid (SBF) and kept in a water bath at 37°C to mimic the human body environment. The SBF solution was replaced every two days. The samples were weighed at weeks 2, 4, 6, 8, 14, 20, 26, and 32. The characterization of the samples was performed using DSC, FTIR, and tensile testing as previously outlined. The weight loss ratio was calculated by the formula below:

$$m = \frac{(mo - md)}{mo} \times 100$$

where m_o refers to original mass and m_d refers to mass after degradation.

3.2.11 Statistical analysis

Statistical analysis of the tensile test results, surface wettability, and the DSC measurements was carried out using Minitab 17 Statistical Software. All the values were considered at a 95% confidence interval and p-values are considered for <0.05. The results in chapter 4 were analyzed using General Linear Model (GLM) of two-way ANOVA considering:

Null hypothesis	All means are equal
Alternative hypothesis	At least one mean is different
Significance level	$\alpha = 0.05$

Equal variances were assumed for the analysis.

The above method considers the hypothesis with one mean as different and the p-value is considered significant when p-value <0.05. In this test, the effect of both the loading of HNT and the screw speed on the PLA and PLA/HNT composites is compared

The results in chapters 5-8 were analyzed using a one-way ANOVA to determine the global differences with a Tukey posthoc test employed to detect differences between individual groups.

CHAPTER 4

An investigation on the enhancement of mechanical properties of Polylactic Acid /Halloysite Nanotubes nanocomposites

4.1 Introduction

Poly lactic Acid (PLA) is a thermoplastic polyester derived from renewable sources such as corn and sugarcane. It has been utilized in medical applications due to its good biocompatibility, biodegradability, good mechanical properties, processability, and availability. (Liu *et al.*, 2014)(Anand Narayanan, Babu and Vasanthakumari, 2016). Halloysite nanotubes (HNT) are a type of clay mineral formed naturally in the earth over millions of years (Kamble *et al.*, 2012). HNT has been used as nanofillers for various polymer nanocomposites due to their high aspect ratio, good dispersion, and excellent mechanical properties (Deepak and Agrawal, 2012; Yuan, Tan and Annabi-Bergaya, 2015; Pasbakhsh *et al.*, 2016). The extraordinary reinforcing effect of HNT has been reported without surface treatment (Therias, Murariu and Dubois, 2017).

HNT within the PLA matrix is reported to improve mechanical, thermal and flame retardant properties (Dong, Bickford and Haroosh, 2012; De Silva *et al.*, 2014; Liu *et al.*, 2014; Chen *et al.*, 2017). Various surface modifications of HNT to further improve dispersion and adhesion in a polymer matrix have also been investigated (Prashantha *et al.*, 2013; Gorrasi *et al.*, 2014; Dong *et al.*, 2015b; Guo, Qiao and Zhang, 2016; Krishnaiah, Ratnam and Manickam, 2017). However, the effect of melt compounding conditions on HNT dispersion and adhesion in the polymer matrix has been rarely studied.

Twin-screw extrusion is a type of hot melt extrusion process where the material melts under high temperature in the barrel and continues to move towards the die with a homogenous melt or dispersion (Stanković, Frijlink and Hinrichs, 2015). It has been extensively used for various applications such as plastic, food, and pharmaceutical industries (Lyons, Holehonnur, *et al.*, 2007; Healy *et al.*, 2018).

Other research works suggest that the shear force from high screw speed during melt blending improves the dispersion of the nanoclay in the polymer matrix. The screw profile of the extruder has a feeding zone followed by a melting zone consisting of kneading elements, which melt the polymer pellets. Homogeneous dispersion of the filler is obtained by the kneading and the mixing element of the following metering zone (Villmow, Kretzschmar and Pötschke, 2010). Li et.al. postulated that an increase

in shear force during melt blending enhances the dispersion of the clay when they investigated polymer/clay nanocomposites (Li *et al.*, 2014). High shear of twin-screw by increasing the screw speed facilitated the dispersion of nanoclay in polyamide which in turn improved the mechanical properties (Anwar, Halim and Florida, 2012). Sasimowski et. al. investigated the extrusion process and showed that the screw speed had a great impact on the efficiency of the extrusion process, the pressure of the processed material, polymer mass flow rate, and the energy consumption of the extruder (Sasimowski and Majewski, 2019). Albareeki et. al. studied the effect of screw speed on the melt temperature, drive torque, and residence time in the extruder and found that increasing the screw speed increases the melt temperature and there is a decrease in the residence time with better dispersion of the filler in the polymer matrix (Albareeki, Driscoll and Barry, 2019). Mixing of thermoplastic pellets with carbon nanotube (CNT) in a twin-screw extruder had good dispersion by shear flow created at high screw speed (Atif and Inam, 2016). Thus, to eliminate the need for surface treatment of HNT, in the current study, the processing of PLA/HNT was examined by varying the screw speed keeping other parameters of extrusion constant throughout.

The present work mainly evaluates the mechanical and thermal properties of the nanocomposites with two mass fractions of 5 wt. % and 10 wt. % of the nanoclay HNT blended into the PLA matrix using a twin-screw extruder with three different screw speeds of 40 rpm, 80 rpm, and 140 rpm based on findings in previous work where a low screw speed resulted in poor HNT dispersion without surface modification (Chen *et al.*, 2017). The nanocomposite produced is characterized by tensile testing, differential scanning calorimetry, dynamic mechanical analysis, scanning electron microscopy, Fourier transform infrared microscopy and surface wettability.

4.2 Results

4.2.1 Processing of the nanocomposite

The PLA/HNT composite was melt-extruded followed by calendaring into films without difficulty. The extruded composite changed in color from transparent for virgin PLA to opaque with the blending of halloysite as seen in Fig 4.1. This color change could be attributed to the nucleating effect of HNT in the PLA matrix which

was similarly observed by De Silva et al. (De Silva *et al.*, 2014) This was also observed by Liu et al. with injection moulded composite of PLA and HNT (Liu, Zhang and Zhou, 2013) and by Chen et al. with extruded PLA/HNT composite (Chen *et al.*, 2017).

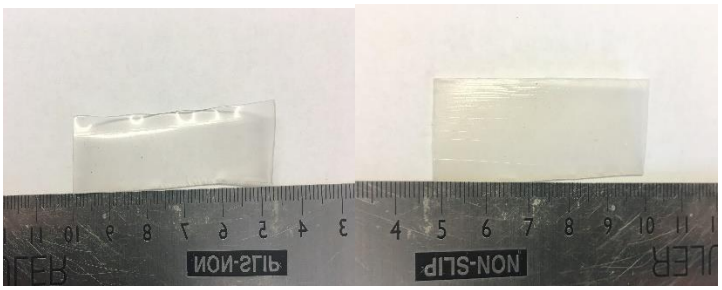

(a) (b)

Figure 4.1: *Photograph of (a) virgin PLA films are transparent (b) PLA/HNT nanocomposite films are opaque*

The screw configuration used is illustrated in Figure 4.2. It had a feeding zone followed by a mixing section comprising two sets of kneading block elements. The first kneading set had ten paddles, four of which had a forwarding angle of 30°, 60° for the next six, and the remaining paddle at 90°. The second block near the discharge end had six paddles with a 60° forwarding angle. The end of the screw had a metering zone of conveying elements. Processing parameters were varied only in terms of screw speed, which in turn reduces the residence time in general which was in the range of 1-3 mins.

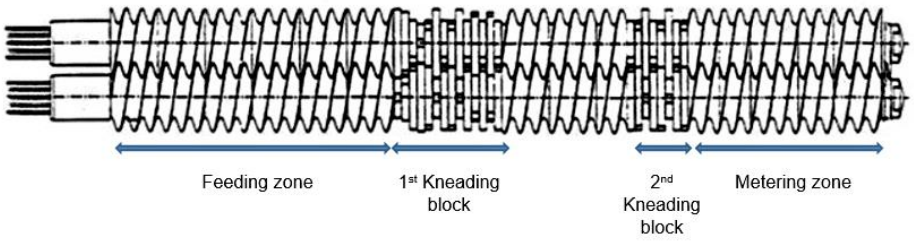

Figure 4.2. *Schematic representation of the screw profile geometry*

4.2.2 Mechanical Properties

Mechanical testing was performed to assess the effect of HNT incorporation at different screw speeds on percent strain at maximum load (elongation at break), stress

at maximum load (Tensile strength), Young's modulus, and stiffness of PLA. The results found that the Young's Modulus increased significantly with the increase in screw speed for both virgin PLA and the nanocomposites as shown in Figure 4.3. The Young's Modulus of PLA is 1707.03 for 40 rpm, 1718.3 for 80 rpm, and is 1927.04 for 140 rpm screw speed. Thus, there is an increase in Young's modulus for the virgin PLA at 140 rpm screw speed when compared to 40 rpm and with no significant changes at 80 rpm screw speed. Similarly, Young's modulus for the composite increases with an increase in screw speed as well. The Young's Modulus for PLA/HNT wt. 5% is 1911.72 for 40 rpm, 1923.56 for 80 rpm, and was increased to 2193.18 for 140 rpm. And Young's Modulus for PLA/HNT wt. 10% is 1960.8 for 40 rpm, 1949.75 for 80 rpm, and was increased to 2234.34 for 140 rpm. Similar to PLA, the nanocomposites exhibited an increase in Young's Modulus at the highest screw speed.

The statistical analysis of variance compared the effect of screw speed and the effect of HNT loading for the above results. Considering the p-value < 0.05, the effect of screw speed had p=0.00 and the effect of loading had p=0.00. However, when the effect of speed and loading are considered together, the p-value was 0.08. Hence the screw speed and the percentage loadings of the HNT separately have a significant effect on Young's modulus. As shown, the increase in screw speed increased the Young's Modulus of PLA and the nanocomposites. The effect of percentage loading of the HNT can be seen for all screw speeds. At 40 rpm, the Young's Modulus of PLA at 1707.03 was increased to 1911.72 for wt. 5% HNT addition and further increased to 1960.8 for wt. 10% HNT loading. At 80 rpm, the Young's Modulus of PLA was 1718.3 and increased to 1923.56 for wt. 5% HNT loading which further increased to 1949.75 for wt. 10% HNT loading. Similarly, at 140 rpm, the PLA's Young's Modulus of 1927.04 increased to 2193.18 for wt. 5% HNT loading and further increased to 2234.34 for wt. 10% HNT loading.

Thus, the Young's Modulus of the PLA/HNT nanocomposites for both wt. 5% and wt. 10% were higher at high screw speed.

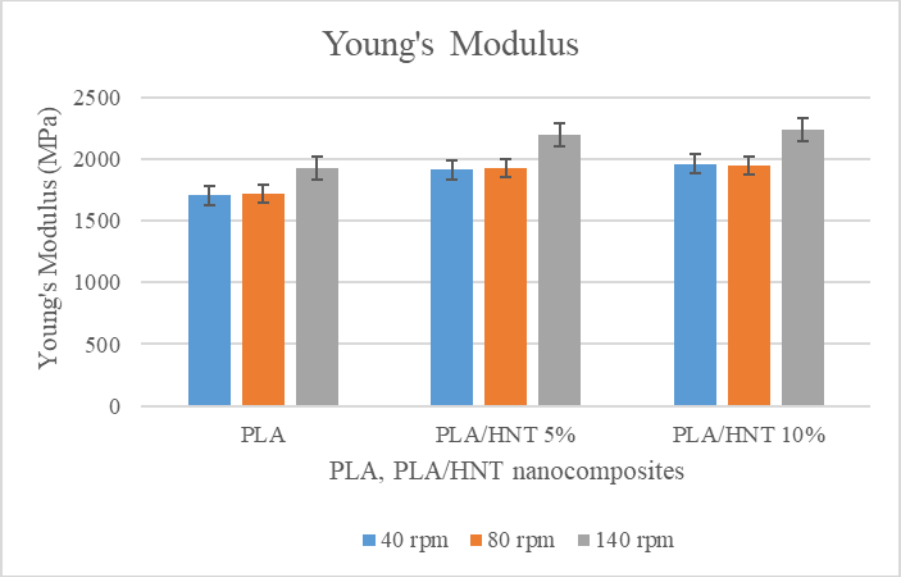

***Figure 4.3**: Graphical representation for the effect of Young's Modulus on the composite. Increased SS and HNT loadings had a significantly increased Young's modulus of PLA and PLA/HNT composites (p=0.02)*

The tensile strength of PLA was 51.52 for 40 rpm, 52.49 for 80 rpm, and 54.49 for 140 rpm. In the case of PLA/HNT wt. 5% the tensile strength was 50.85 for 40 rpm, 53.42 for 80 rpm, and 59.26 for 140 rpm. And for PLA/HNT wt. 10% the tensile strength was 50.13 for 40 rpm, 48.5 for 80 rpm, and 50.84 for 140 rpm. Thus, the tensile strength of the material compounded at 80 rpm screw speed shows no significant changes for PLA and composites as seen in Figure 4.4. However, for 140 rpm, there is an increase in tensile strength for PLA and composite with 5% loading.

The statistical analysis of variance also confirmed the effect of screw speed on the tensile results. The effect of screw speed had p=0.04 and the effect of HNT loading had p=0.09. Together the effect of screw speed and HNT loading had p=0.089. Thus, considering the $p<0.05$, the screw speed had a significant effect on the increase in tensile strength. The screw speed had a significant effect on the increase of tensile strength of PLA/HNT wt. 5% and PLA with p=0.04. However, the effect of HNT loading was not seen when we compare the results for each screw speed. For 40 rpm, the tensile strength of PLA at 51.52 was 50.85 and 50.13 for wt. 5% and wt. 10% HNT loading respectively with no significant change. Similarly, for 80 rpm, the tensile strength of PLA at 52.49 was 53.42 for wt. 5% and 48.5 for wt. 10% with no increase with HNT loading. However, for 140 rpm, the tensile strength of PLA was 54.75 which

increased to 59.26 for wt. 5% HNT loading and decreased to 50.84 for wt. 10% HNT loading.

Thus, the increase of tensile strength of PLA/HNT wt. 5% at 140 rpm could be attributed to the higher screw speed.

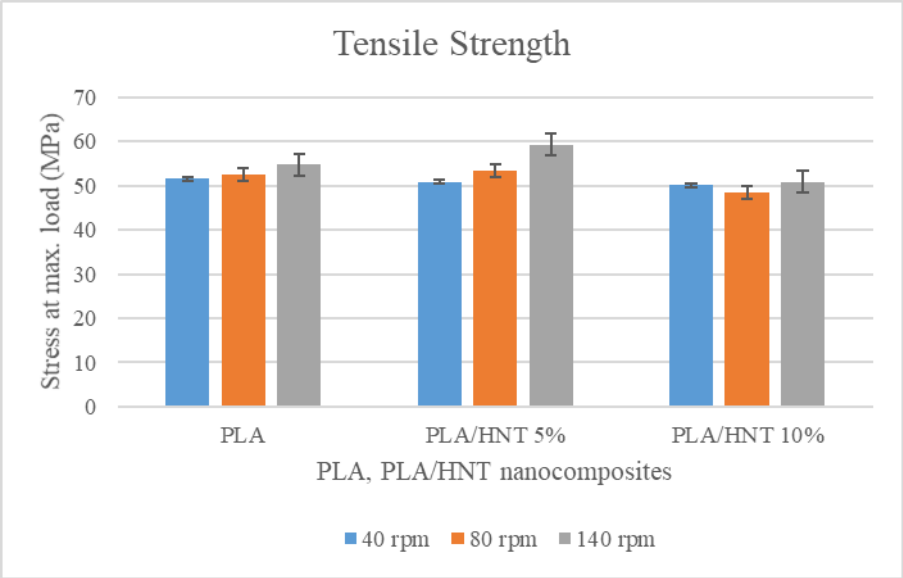

***Figure 4.4**. Graphical representation for the effect of tensile strength. Increased screw speed increased the tensile strength of PLA and 5%.*

The stiffness of the PLA and PLA/HNT composites are shown in Figure 4.5. The stiffness of the virgin PLA was 235.83 for 40 rpm and increased to 362.37 for 140 rpm can be seen to have the highest increase for 140 rpm. In the case of PLA/HNT wt. 5% nanocomposites, the stiffness was 235.64 for 40 rpm, 205 for 80 rpm, and 250 for 140 rpm. For PLA/HNT wt. 10% nanocomposites, the stiffness was 240.17 for 40 rpm, 224.69 for 80 rpm, and 284.3 for 140 rpm. There is an increase in stiffness for 140 rpm with a statistically significant increase for PLA/HNT wt. 10% nanocomposites.

The statistical analysis of variance had a p-value ≤ 0.05 for the effect of screw speed, the effect of HNT loading, and for the effect of screw speed and the HNT loading. This indicates the screw speed and the HNT loading together and individually affected the increase in stiffness as we see the increase in virgin PLA which only had the effect of screw speed. As there is a slight increase in stiffness for wt. 5% HNT loading, the significant increase in PLA/HNT wt. 10% had the effect of both screw speed and the HNT loading.

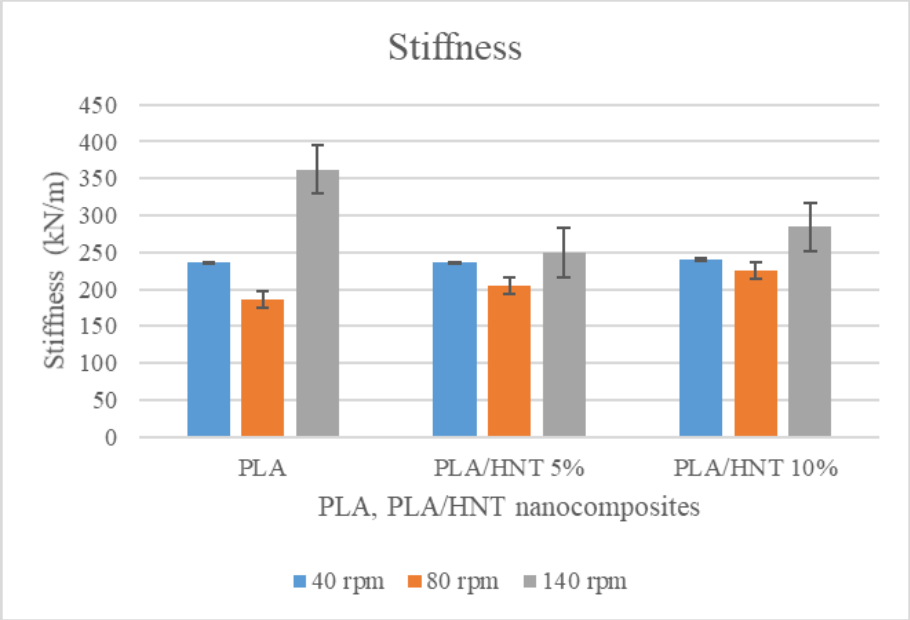

***Figure 4**.5: Graphical representation for the effect of Stiffness on the composite. Increased SS and HNT loadings had a significantly increased stiffness for virgin PLA and the 10% nanocomposites (p=0.01).*

The elongation at break for PLA was 4.85 for 40 rpm, 4.94 for 80 rpm, and with a significant increase to 5.23 for 140 rpm. In the case of PLA/HNT wt. 5% nanocomposites the elongation at break was 4.95 for 40 rpm, 4.9 for 80 rpm and showed a significant increase to 5.25 for 140 rpm. Thus, the elongation at break does not show any difference for PLA and PLA/HNT composites for 40 and 80 rpm as shown in Figure 4.6. In the case of 140 rpm, there is an increase in percentage strain for PLA and PLA/HNT wt. 5% which is also confirmed by the statistical analysis.

The analysis of variance shows that screw speed alone had a p-value of 0.000 and HNT loading had a p-value of 0.25. The effect of screw speed and the HNT loading had a p-value of 0.425. With a p-value of 0.25, there was no effect of the HNT loading as there is no increase in the elongation at break for PLA/HNT wt. 10%.

Thus, considering the p-value for <0.05 statistically, only the screw speed had a significant effect on the increase of elongation at break for both PLA and PLA/HNT wt. 5%.

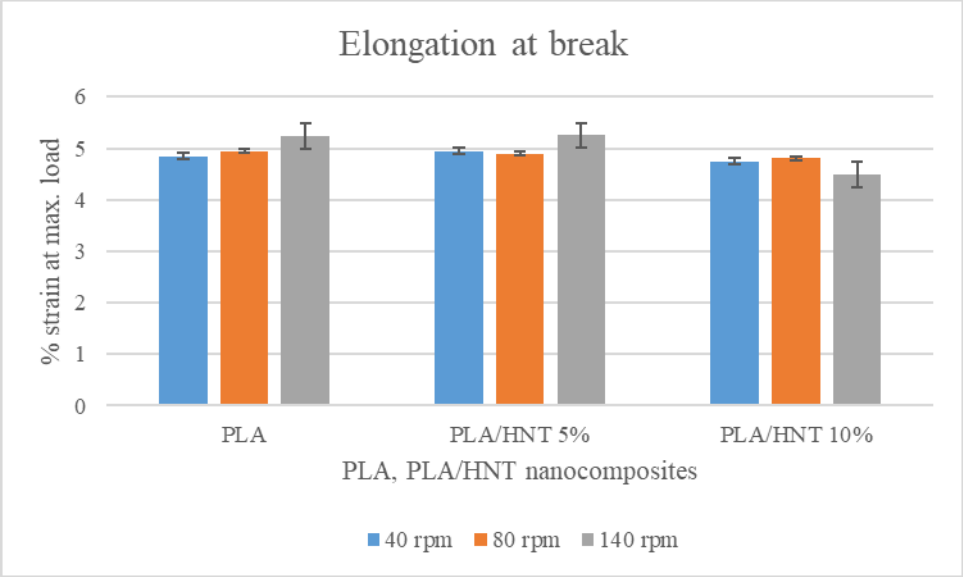

***Figure 4.6**: Graphical representation for the effect of percentage strain at max load. Increased screw speed had an increased elongation for PLA and PLA/HNT wt. 5% while decreasing it for PLA/HNT wt. 10% composites (p=0.01).*

4.2.3 Differential Scanning Calorimetry

The secondary heating curves of DSC are shown in Figure 4.7. The DSC curves for PLA and PLA/HNT composites extruded at 40 rpm as shown in Figure 4.7 (a) depicts no significant change in the glass transition temperature (T_g). The cold crystallization temperature (T_{cc}) of PLA at 128.82 °C significantly decreases to 117.04 °C when HNT is added to the PLA in 5 wt. % and to 118.19 °C for 10 wt. % of HNT. The melting temperature (T_m) of the PLA/HNT composites is doubled with two peaks when compared to PLA and shifts to lower melting temperature.

A similar trend of the peaks for T_g, T_{cc}, and T_m of PLA and PLA/HNT composites at 80 rpm and 140 rpm can be seen in Figure 4.7 (b) and (c) respectively. There is no significant decrease in T_g and a significant decrease in T_{cc} for PLA/HNT composites with 129.92 °C for PLA, 117.55 °C for PLA/HNT wt. 5% and 116.20 °C for PLA/HNT wt. 10% in case of 80 rpm and 125.68 °C for PLA, 118.14 °C for PLA/HNT wt. 5% and 116.2 °C for PLA/HNT wt. 10% for 140 rpm when compared with PLA. The T_m of PLA was similar to 157 °C for all screw speeds and the twin melting peaks were evident for the nanocomposites for 40, 80, and 140 rpm.

Statistical analysis confirmed the above results. The statistical analysis of variance compared the effect of screw speed and the effect of HNT loading for the above results. Statistical analysis of $T_{g.}$ has a p-value of 0.104 for speed and 0.034 for percentage loading. The effect of speed and loading had a p-value of 0.476. This shows both screw speed and the percentage loading did not have any effect on the T_g considering the p-value as <0.05. T_{cc} has a p-value of 0.000 for speed and 0.000 for percentage loading. The effect of speed and loading also has a p-value of 0.000. This shows that the percentage loading of the HNT and the speed has a significant effect on the decrease of T_{cc} considering the p-value as <0.005. In the case of T_m the p-value for speed is 0.062 and 0.003 for HNT loading. The effect of speed and loading has a p-value of 0.074. This also shows that the screw speed did not have a significant effect on melting temperature with a p-value of 0.062, but the percentage loading had a significant effect on the melting temperature considering the p-value as <0.05.

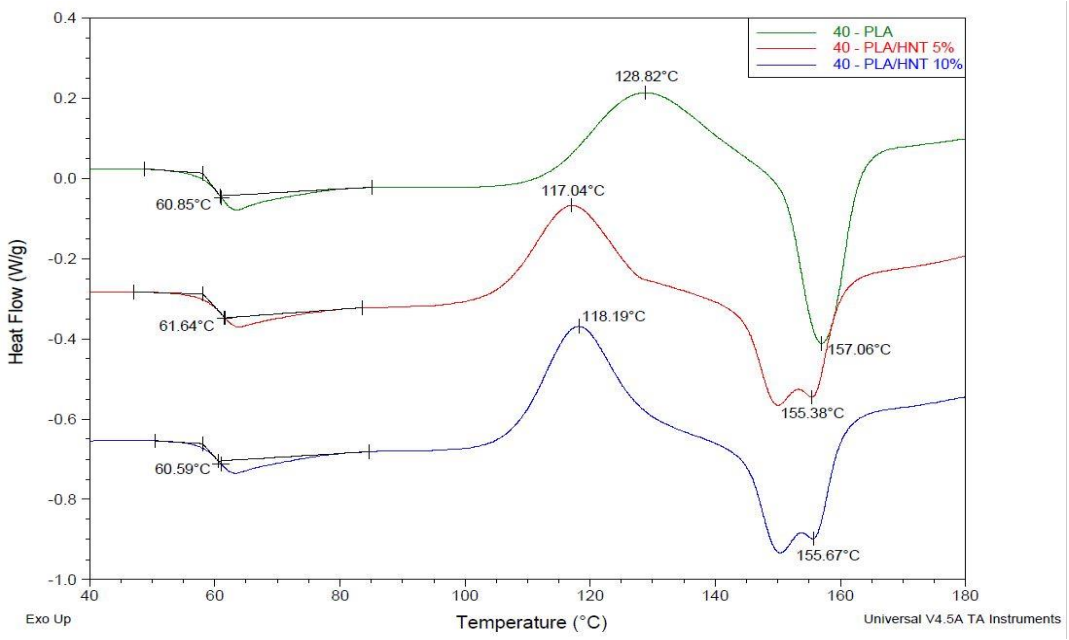

(a)

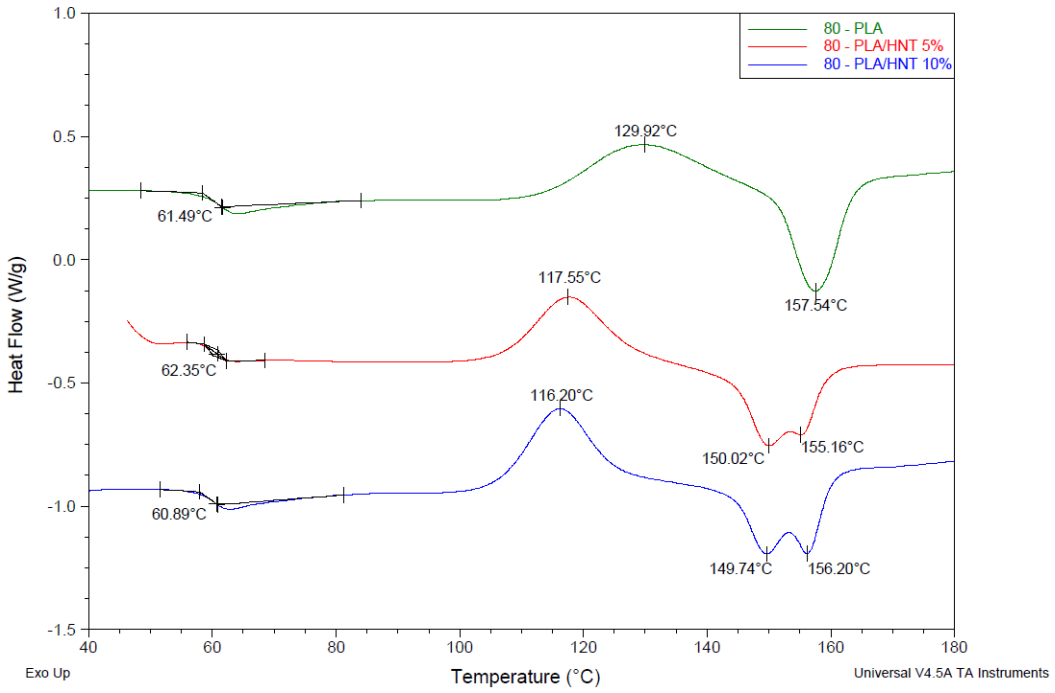

(b)

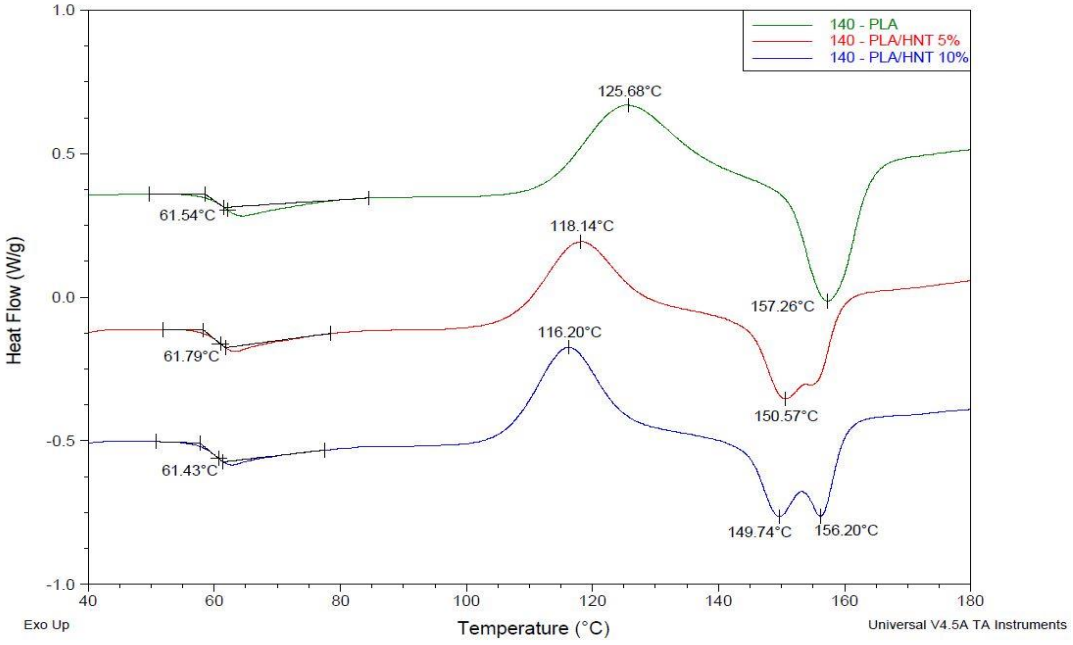

(c)

Figure 4.7: *Secondary heating DSC curves for the PLA/HNT Nanocomposites at (a) 40 rpm (b) 80 rpm (c) 140 rpm. The peak maximum for the glass transition, cold crystallization, and melting temperature are shown.*

***Table 4.1**: Values corresponding to the glass transition (T_g), cold crystallization temperature (T_{cc}), melting temperature (T_m) of the secondary heating DSC curves, and the tan **δ** peaks of the dynamic mechanical analysis for the PLA/HNT Nanocomposites.*

RPM	Loading	T_g	T_{cc}	T_m (1st peak)	T_m (2nd peak)	Tan δ
40	PLA0	60.85	128.82	157.06	0	66.61
40	PLA/HNT5	61.64	117.04	150.15	155.38	64.58
40	PLA/HNT10	60.59	118.19	150.5	155.67	65.56
80	PLA0	61.49	129.92	157.57	0	63.59
80	PLA/HNT5	62.35	117.55	150.02	155.16	63.87
80	PLA/HNT10	60.89	116.20	149.74	156.20	65.02
140	PLA0	61.54	125.68	157.26	0	62.73
140	PLA/HNT5	61.79	118.14	150.57	155.11	67.47
140	PLA/HNT10	61.43	116.20	149.74	156.20	63.46

The DSC curves show that the addition of HNT into the PLA matrix with different loadings and compounding at different screw speeds showed no significant difference in the glass transition temperature (T_g) with p=0.42 as shown in Table 4.1and Figure 4.7. A similar result has been reported previously (Stoclet *et al.*, 2014). As seen in Table 4.1 and Figure 4.7, the cold crystallization temperature (T_{cc}) at peak gradually shifts to lower temperature regions. The melting temperature of the composite was also lower than that of virgin PLA. A similar decrease in cold crystallization temperature and the melting temperature was observed by Prashanta et.al. Chen et.al, Wu et al. and Guo et al. in their study using surface-treated HNT (Prashantha *et al.*, 2013; Wu *et al.*, 2013; Guo, Qiao and Zhang, 2016; Chen *et al.*, 2018). A single melting peak was observed for virgin PLA. However, a secondary melting peak was observed for 5 wt. % and becomes clearer for 10 wt. % loading of the HNT. This was observed in other studies by Chen et. al. (Chen *et al.*, 2018), Prashantha et. al. (Prashantha *et al.*, 2013).

4.3.3 Dynamic Mechanical Analysis

Dynamic mechanical analysis was used to evaluate the viscoelastic properties of the PLA/HNT nanocomposite below and above the glass transition. The temperature at the peak of the Tan δ curve was considered as the T_g of the material. The tan δ peaks as listed in Table 4.1. show no significant difference in T_g.

4.3.4 Energy Dispersive X-ray spectroscopy

Scanning electron microscopy photomicrographs indicated that the structure of the PLA was uniform as seen in Figure 4.8(a), and its elemental composition as measured by EDX was recorded with only carbon and oxygen. The incorporation of HNT resulted in the presence of microscale particles, which exhibited an elemental composition consisting of aluminum and silicon which is indicative of the presence of HNT. Heterogeneous structures are observed for 10 wt. % loadings of HNT for all screw speeds. This was due to the presence of agglomerates of HNT, with the magnitude of the agglomerates being larger in the 10 wt. % composites. The magnified image of the agglomerate site on the 10 wt. % composite in Figure 4.8(d) indicates the cluster of HNT. Furthermore, very few agglomerations of small sizes were apparent in 5 wt. % composites compounded at 140 rpm as seen in Figure 4.8(c) indicating a better distribution of HNT in the matrix.

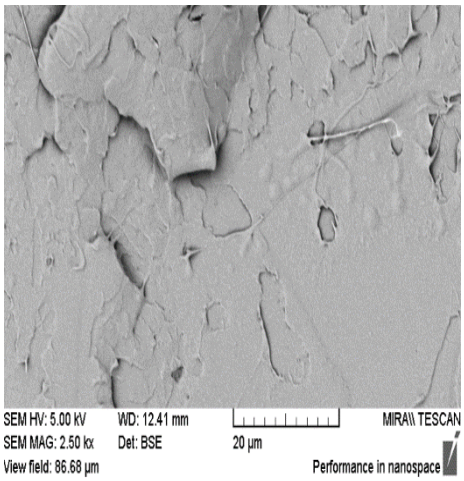

(**a**)

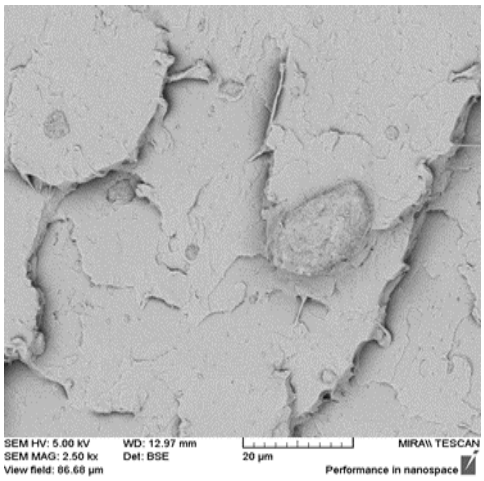

(b)

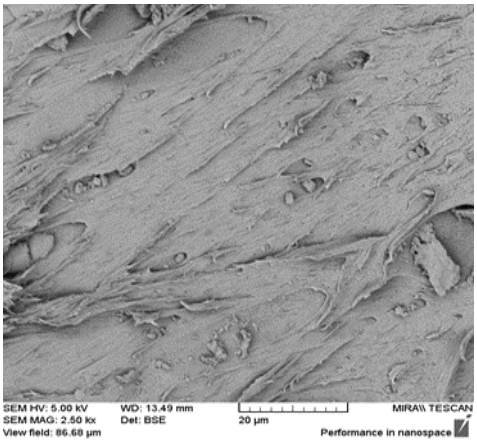

(C)

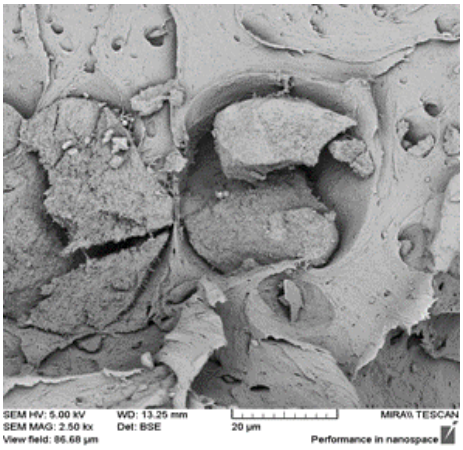

(d)

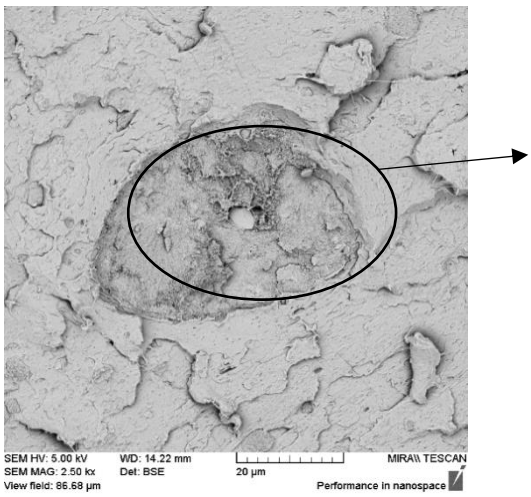

(e)

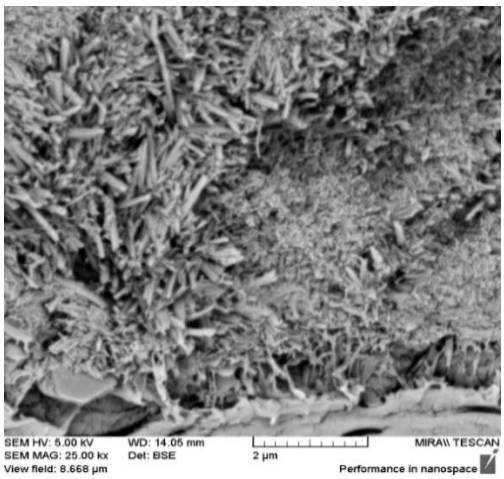

(f)

***Figure 4.8**. Photomicrograph of the cross section of the samples PLA and PLA/HNT nanocomposite (a) PLA (b) 5 wt. % composite at 40 rpm (c) 5 wt. % composite at 140 rpm (d) 10 wt. % composite at 40 rpm (e) 10 wt. % composite at 140 rpm (f) Magnified image of the agglomerate site of the 10 wt. % composite where the HNT tubular structure was observed.*

The elemental composition of the composite is seen in Table 4.2. indicated the presence of aluminum and silicone from the composition of the HNT, which confirmed the presence of HNT in the polymer matrix. Elemental data indicated that the dispersion of HNT (evidenced by aluminum and silicone) into polymer matrix

increases with the increase in screw speed. This was also seen by Liu et al. in their study (Liu *et al.*, 2014).

Table 4.2 *Values corresponding to the elemental composition of aluminum and silicone in the composite by EDX.*

Sample Screw speed	Aluminum	Silicon	Sample screw speed	Aluminum	Silicon
PLA/HNT5_40	0.43	0.43	**PLA/HNT10_40**	1.32	1.33
PLA/HNT5_80	0.64	0.66	**PLA/HNT10_80**	1.82	1.95
PLA/HNT5_140	0.87	0.70	**PLA/HNT10_140**	1.92	1.98

4.3.5 Fourier Transfer Infrared (FTIR) Spectroscopy

FTIR spectra for PLA, HNT, and PLA/HNT composites are shown in Figure 4.9. Virgin PLA exhibited a characteristic peak at 3571 cm^{-1} corresponding to –OH stretch and peaks at 2996 cm^{-1} and 2948.34 cm^{-1} are attributed to CH stretch and the peak at 1750 cm^{-1} corresponding to –C=O carbonyl group (Garlotta, 2002). The characteristic absorption band at 1450 cm^{-1} is attributed to the bending vibrations of CH3 and absorption bands at 1384 cm^{-1} and 1364 cm^{-1} are the CH deformation and asymmetric/symmetric bending (Liu, Zhang and Zhou, 2013). The spectra of PLA extruded at 40 and 80 rpm were similar to140 rpm spectra with all the characteristic peaks as described above and as we see in Figure 4.9 for spectra PLA_140.

The spectrum of HNT as seen in Figure 4.9 displayed peaks at 3693.26 cm^{-1} and 3623.39 cm^{-1} which can be assigned to the O-H group and peak at 906.81 cm^{-1} to Al-OH group. The spectra of PLA/HNT wt. 5% nanocomposite extruded at 40, 80, and 140 rpm and PLA/HNT wt. 10% nanocomposite extruded at 140 rpm are also shown in Figure 4.9 for significant comparison. They all revealed the absorption bands of both PLA and HNT. However, only PLA/HNT wt. 5% nanocomposite displays a gradual increase in the intensity of the peaks which overlaps with characteristic peaks of PLA and HNT when we compare PLA/HNT5_40, PLA/HNT5_80 and PLA/HNT5_140. PLA/HNT wt.10% did not show any significant changes and at all screw speeds the spectra were similar to PLA/HNT10_140 as seen in Figure 4.9.

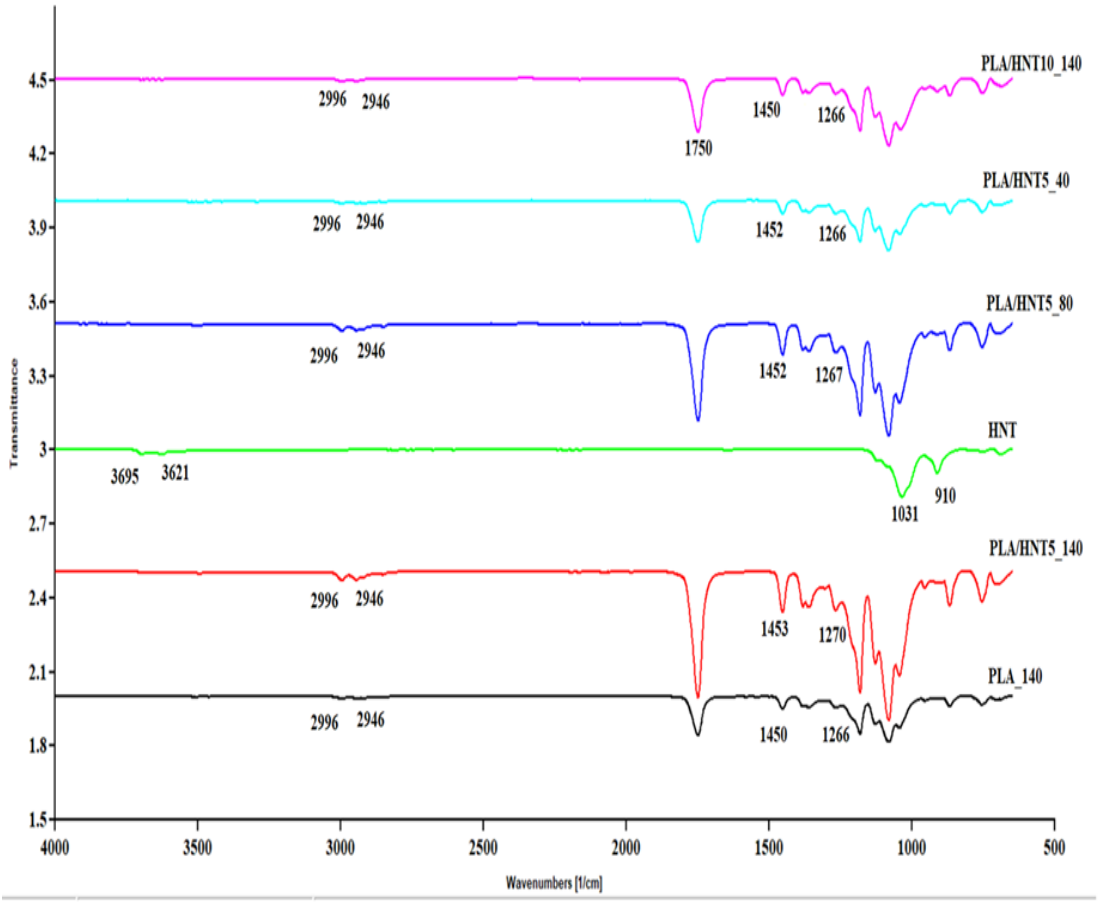

***Figure 4.9**: FTIR Spectra of HNT, PLA, and PLA/HNT composites*

The spectra of PLA/HNT wt. 5% composites revealed the absorption bands of both PLA and HNT. The overlapping of HNT absorption bands increases the intensity of the PLA absorption band as the screw speed increases in the region between 1300 cm^{-1} - 500 cm^{-1}. For instance, the overlapping of the HNT absorption band 1031 cm^{-1} increases the intensity of the 1043 cm^{-1} absorption band of PLA. This observation is also seen in other studies as well (Liu, Zhang and Zhou, 2013; De Silva *et al.*, 2014; Guo, Qiao and Zhang, 2016). The absorption band 1266 cm^{-1} of PLA shifts to 1270 cm^{-1} for 5 wt. % composites and is more intense and sharpens as the screw speed increases. This kind of shift is also seen in the study by Dong et. al. in which the HNT was modified (Dong *et al.*, 2015b).

4.3.6 Surface Wettability

The surface wettability of PLA and PLA/HNT composites was studied by contact angle measurement. The contact angle for PLA was within a range of 60°–65°

at all screw speeds. The nanocomposite produced by the incorporation of 5 wt. % HNT compounded at different screw speeds did not have a statistically significant effect on the surface wettability for p=0.245 for different screw speeds and the contact angle remained within the same range as virgin PLA as seen in Figure 4.10. Hence, they are hydrophilic. The addition of 5wt% loading HNT to PLA resulted in the composite being hydrophilic, regardless of the screw speed analyzed, with a slight decrease in contact angle between the distilled water and the composite surface, which was similarly reported by De Silva et al. (De Silva *et al.*, 2014).

However, for 10 wt. % composites the contact angle increased to 99° indicating its hydrophobic nature at least on the surface. This was similar for all screw speeds. Thus, screw speed did not have any effect on the surface wettability which is also confirmed from statistical analysis with a p-value of 0.245 calculated from the means of 5 readings per sample for all the screw speeds individually. The contact angle of the distilled water on the surface of the samples for 140 rpm is as shown in Figure 4.10 which depicts the angle of water formed on the surface of PLA, PLA/HNT wt. 5% and PLA/HNT wt. 10% composites.

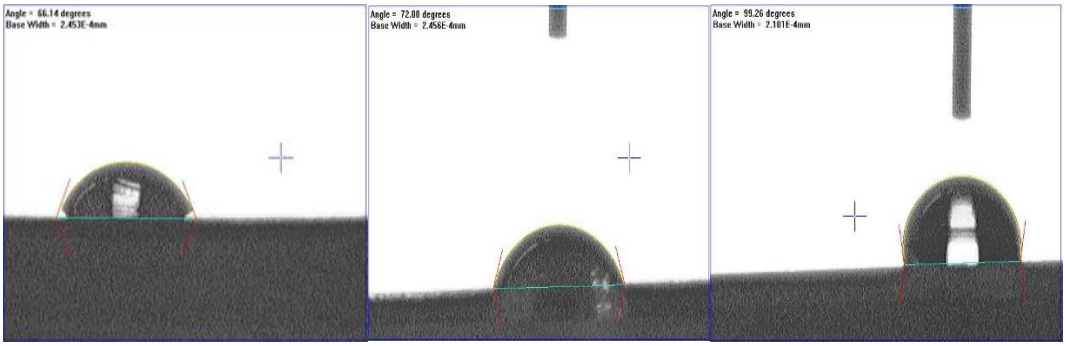

(a) (b) (c)

***Figure 4.10**: The contact angle of the distilled water on the (a) PLA (angle is <90°) (b) 5% PLA/HNT nanocomposite (angle is <90°) and (b) 10% PLA/HNT nanocomposite (angle is >90°) compounded at 140 rpm screw speed. The PLA and 5% composite is hydrophilic and 10% composite is hydrophobic*

4.4 Discussion

Twin-screw extrusion is a high shear process, which aids the dispersion of different components during melt processing. The main focus of this study was to assess the effect of screw speeds, as increases in screw speed during compounding

have been shown to increase melt shear and as such homogeneity of the final compounded material. Gamon et. al. hypothesized that a screw speed of 150 rpm was ideal to obtain homogenous properties of fiber-reinforced PLA composites (Gamon, Evon and Rigal, 2013). Normand et.al. demonstrated that when the screw speed is increased from 100 to 600 rpm while compounding polypropylene/clay nanocomposites, the number of the aggregates decreases and screw speeds higher than 600 rpm did not improve the state of the microscopic dispersion nor had better exfoliation which could be due to the thermal degradation of the clay modifier, mechanical breakage of the clay sheets or degradation of the matrix (Normand *et al.*, 2017). Similarly, Domenech et.al. found a reduction in the size of the clay agglomerate as the screw speed increases principally between 100-500 rpm. And more than 500 rpm did not show any changes (Domenech, Peuvrel-Disdier and Vergnes, 2012). Conversely, previous work by Chen et.al. showed that screw speeds of 35 rpm did not give sufficient mixing and necessitated the surface treatment of HNT to improve dispersion (Chen *et al.*, 2018). The above literature review reveals that screw speed less than 40 rpm and higher than 500 rpm, did not show much difference in dispersion of nanoparticles in polymer matrix. In addition, extrusion at higher screw speeds could lead to thermal degradation of the nanocomposite at very high screw speed. Hence, in this study, the polymer PLA and the PLA/HNT nanocomposites were compounded at three screw speeds of 40, 80, and 140 rpm for comparison. However, the selected screw speeds were not exhaustive and the effects of dispersion at higher screw speeds cannot be assumed based on these findings.

The filler dispersion and melt blending are augmented and intensified by the kneading elements of the screw configuration (Villmow, Kretzschmar and Pötschke, 2010). Thus using the above-described screw configuration with two kneading elements in the mixing section, three different screw speeds were investigated. The primary concern of the newly processed material is its strength. Compounding at 140 rpm screw speed improved the mechanical properties of the composites. It is noteworthy that the mechanical properties improve significantly for virgin PLA itself as the screw speed increases. This could be attributed to the high shear force at higher screw speed when the polymer structure rearranges during the extrusion process or possibly due to low-level crosslinking. It is noticed that Young's modulus increases for 5 and 10 wt. % HNT loaded composites. Additionally, the tensile strength and the

elongation at break increases by 5 wt. % HNT loaded composites for 140 rpm screw speed.

The improvement in the tensile strength usually indicates good interfacial bonding resulting in effective stress transfer from the PLA matrix to the reinforcing nanoclay (Dong *et al.*, 2015b). Hou et.al. showed that tensile behavior is significantly impacted by an increase in screw speed and loading of Multiwalled Carbon Nanotubes (MWCNTs) (Hou *et al.*, 2008). Guo et.al. also reported similar improvements when processed by a mini extruder at 50 rpm when utilizing surface-modified HNT (Guo, Qiao and Zhang, 2016). Hence, we can say that melt compounding at 140 rpm or higher screw speed had equivalent results without the modification of HNT.

The DSC analysis observed a twin melting peak which could be due to the melting of the crystals formed in the cold crystallization stage during heating and followed by recrystallization and further melting processes at higher temperatures (Prashantha *et al.*, 2013). The melting temperature (T_m) also decreases with an increase in screw speed and HNT loading. The decrease in the T_{cc} indicated that HNT had a nucleating effect on the PLA and crystallizes the PLA/HNT composite more quickly than virgin PLA (Liu, Zhang and Zhou, 2013; Wu *et al.*, 2013) and that heterogeneous nucleation was likely to occur where thinner crystalline lamella was formed compared to that of virgin PLA (Dong *et al.*, 2015b). Hence, the melting temperature of the composite was also lower than that of virgin PLA.

The glass transition temperature T_g is a measure of rigidity (D.M. Devine *et al.*, 2017) and the T_g does not show any considerable difference from the DSC results. However, the analysis of T_g is more accurately determined by DMA (Liu, Zhang and Zhou, 2013). Hence, the results from the DMA were statistically analyzed to confirm that there is no significant difference in T_g with an increase in screw speed. The T_g from DMA can be analyzed from the storage modulus (E´) onset temperature, by using the graphical intersection of two tangent lines, one drawn before the curve transition and the other from the modulus drop midpoint to the inflection point of the curve. However, it is preferred to use the peak maximum of the tan δ plot for T_g as the precise positioning of the tangents in E´ is more uncertain than defining the maximum points of the peak in tan δ plot (Debra Dunson, Ph.D., 2017).

Elemental data from EDX indicated that the dispersion of HNT (evidenced by aluminum and silicone) into polymer matrix increases with the increase in screw speed. This indicates that HNT could interact better with PLA with increasing screw speeds via hydrogen bonding interactions. The orientation of HNT in the matrix under the shear force of increasing screw speed during processing was individually separated and could bear the load. As a result of which, the nanocomposite has higher strength. This was also seen by Liu et al. in their study (Liu *et al.*, 2014).

The observed sharpening, increase in the intensity of the peaks, and shifting to higher frequencies in FTIR results, as the screw speed increases are the most for PLA/HNT 5 wt. % nanocomposites at 140 rpm. This can be attributed to the interactions between the PLA and HNT via hydrogen bonding which could have contributed to the increased thermal and mechanical properties of the PLA/HNT composite, which were also confirmed by FTIR in other studies (Liu, Zhang and Zhou, 2013)

The contact angle measuring less than 90° corresponds to high wettability and the contact angle of more than 90° corresponds to low wettability (Bracco and Holst, 2013). Hence from the results of this study indicated that virgin PLA and the 5% composites are relatively hydrophilic with contact angle <90°. The OH group in the HNT increases the number of polar groups within the composite as a result of which, the surface energy is increased which makes the contact angle ɵ decrease slightly for the 5% of HNT loading (De Silva *et al.*, 2014). However, the 10% composites are hydrophobic as the contact angle increases to >90° when compounded at 140 rpm. Similar findings have been reported by De Silva et.al. which can be attributed to the increase in the surface roughness at higher concentrations. This in turn reduces the surface energy which makes the material hydrophobic (De Silva *et al.*, 2014).

4.5 Summary

The HNT was reinforced into the PLA matrix using three different screw speeds (40, 80, and 140 rpm). The formation of HNT networks within the PLA matrix when compounded at 140 rpm screw speed for 5% loading, as evidenced by HNT dispersion in SEM images and absorption peak of FTIR contributed to the increase in the glass transition temperature, tensile strength, Young's Modulus and hydrophilicity

of the composite. The could be due to the nucleating effect of HNT and good interfacial bonding with PLA for higher screw speeds with high melt shear during the compounding. The mechanical characteristics of a stent material require a high value of Young's Modulus to reduce stent recoil and a combination of high tensile strength and Young's Modulus to increase the stent's radial strength. Thus, the functionality of the nanocomposite was improved, despite the decrease in stiffness, making it a potential material for use in the manufacture of the resorbable stents, as it eliminates the need for organomodification of HNT. Hence, it can be concluded that the high melt shear during compounding enhances the dispersion of the HNT into the polymer matrix which in turn improved the overall properties of the composites without the need for surface treatment of the HNT.

As such this study will further explore the feasibility of loading the drug and its controlled release from PLA/HNT composites. Two methods will be employed for loading the drug. Firstly, the HNT will be encapsulated with the drug and this drug-loaded HNT will be reinforced into the PLA matrix through extrusion. For comparison, in the second method, the PLA, HNT, and the drug will be tumble mixed and extruded into drug-loaded nanocomposite films. These two types of drug-loaded nanocomposite films will be characterized for mechanical, thermal, morphological, and drug release.

CHAPTER 5

Study of drug loading and drug release mechanism from the PLA/HNT nanocomposites

5.1 Introduction

Hot-melt extrusion (HME) is widely used in the manufacture of drug delivery systems for the controlled release of pharmaceuticals, as the mixing process of the drug and the polymer is efficient at controlled temperatures and pressures. This process can be used to melt or solubilize active pharmaceutical ingredients (APIs) in a polymer matrix to generate amorphous systems that effectively can improve solubility, modulate controlled release, and have improved bioavailability (Lyons, Hallinan, *et al.*, 2007; Saerens *et al.*, 2014; Fule, Paithankar and Amin, 2016; Martinez-Marcos *et al.*, 2016; Patil, Tiwari and Repka, 2016).

PLA is approved by the FDA for direct contact with biological fluids as it is biocompatible and its degradation products are nontoxic (Farah, Anderson and Langer, 2016; Y. Chen *et al.*, 2016). PLA and PLA blends are used for and various drug delivery strategies such as nanosystems, films and fibrous matrices (Saini, Arora and Kumar, 2016). PLA has been studied as a drug release membrane, and the results have achieved sustained drug release for a long duration due to diffusion of the API from the metrics and bulk degradation (Mhlanga and Ray, 2015).

PLA has been used to prepare biodegradable polymeric nanoparticles to improve their bioavailability, solubility, and sustained release of APIs. In such cases, the APIs are confined inside the polymer membrane or uniformly dispersed on the surface of the polymer (Nagavarma *et al.*, 2012; Sha *et al.*, 2016). However, PLA on its own does not have all the mechanical properties required. The addition of nanoclays, specifically halloysite nanotubes (HNT), has shown to improve the properties such as tensile strength, storage modulus, flexural properties, and Young's Modulus (Murariu *et al.*, 2012; Prashantha *et al.*, 2013; Wu *et al.*, 2013; Castro-aguirre *et al.*, 2017; Chen *et al.*, 2017). The HNT can be loaded with drugs due to its large outer surface and inner lumen (Lvov, DeVilliers and Fakhrullin, 2016). Recent research has demonstrated the feasibility of loading of different drugs into the HNT (Lun, Ouyang and Yang, 2014; Patel *et al.*, 2015; Fu *et al.*, 2017; Leporatti, 2017). HNT has also been studied for drug delivery in various polymer composites. Patel and researchers demonstrated the successful loading and sustained release of various drugs including antibiotics, antiseptics and disinfectants on electrospun HNT/PCL nanocomposites (Patel *et al.*, 2015). Qi and researchers successfully studied the double

drug loading on HNT and electrospinning with Poly (lactic-co-glycolic acid) (PLGA) (Qi *et al.*, 2010). To our knowledge, this is the first report for loading the HNT with API and compounding with PLA by hot-melt extrusion (HME). We can hypothesise that the loading of the APIs into HNT has better drug encapsulation and sustained drug release than when the APIs are compounded together with PLA and HNT. This drug-loaded nanocomposite can be employed for various medical applications requiring drug delivery such as scaffolds. Aspirin (ASP) is a well-known pharmaceutical product used for various medical treatments.

ASP is known to minimize inflammation, reduce body temperature, and decrease the process of adhesion of platelets by blocking the production of hormones that participate in the process of inflammation, increasing body temperature and platelet fusion (A, 2003). Several studies have characterized drug loading and release profiles of ASP from polymer matrices. Devine et al. studied the encapsulation of ASP in hydrophilic polymer coatings and copolymer hydrogels along with its associated release characteristics (Devine, Geever and Higginbotham, 2005; Devine *et al.*, 2006). Shi et al. studied the loading of ASP in different molecular weights of chitosan to analyze the release kinetics (Shi *et al.*, 2014), and Zhang et al. recently demonstrated sustained drug release from ASP-loaded chitosan nanoparticles (Zhang, Ma and Gene, 2017).

In the current study, ASP was used as a model drug to study the effect of loading the API into the lumen of the HNT before forming an HNT/PLA nanocomposite. This was compared to directly loading the API into the polymer matrix during the compounding of the PLA/HNT nanocomposite. The objective of this study was to evaluate the release of ASP from the PLA/HNT nanocomposite matrix and the effect of preloading the drug into the lumen of the HNT on its release profile. For this, ASP was encapsulated into the HNT. The ASP-loaded HNT was compounded into the PLA matrix by twin-screw extrusion. This was compared to directly loading the API (ASP) into the polymer matrix during the compounding of the PLA/HNT nanocomposite. Regarding the previous chapter, the HME processing parameters were improved in terms of enhanced mechanical properties of the final nanocomposite. Hence, these production settings were utilized in this study to examine drug loading into the PLA/HNT nanocomposite structure to investigate the controlled release of drugs from these structures.

5.2 Method

5.2.1. Drug loading on HNT

ASP was encapsulated into the HNT in two batches of 1:1 and 2:1 ratio (HNT: ASP). For the preparation of the 1:1 ratio, 12 grams of ASP was dissolved in 120 ml of ethanol by stirring. Once the solution became transparent, 12 grams of HNT were added and stirred for 4 hours at 700 rpm. The solution was then centrifuged to separate the solid part and dried overnight at 40°C with a vacuum. Similarly, the 2:1 ratio is prepared using 12 grams of HNT and 6 grams of ASP. These are referred to here as lumen loading. 1:1 ratio batch are referred to here as B1 and 2:1 ratio is referred to as B5.

5.2.2 Preparation of PLA/HNT/ASP nanocomposites

Extrusion was performed by using APV (Model MP19TC (25:1)) (APV Baker, Newcastle-under-Lyme, UK) twin-screw compounder at a screw speed of 140 rpm. The mass fractions of PLA: HNT were 100:0 and 95:5 for both lumen-loaded and matrix-loaded samples. The lumen-loaded HNT/ASP for both 1:1 and 2:1 ratio was tumble mixed with PLA and extruded. These samples are referred to here as lumen loaded. As a control, HNT, ASP, and the PLA were hand-mixed and extruded at the same ratios. These samples are referred to here as matrix loading. Schematic illustration of these methods is shown in Figures 5.1 and 5.2. In the matrix loaded batch, the 1:1 ratio is referred to as B2, and the 2:1 ratio is referred to as B3.

The extruded film was drawn through the three-roll calendar to form a continuous film. Finally, ASTM standard tensile test specimens were punched out of the film for testing. The nomenclature of each batch by the method of preparation and composition is described below in Table 5.1.

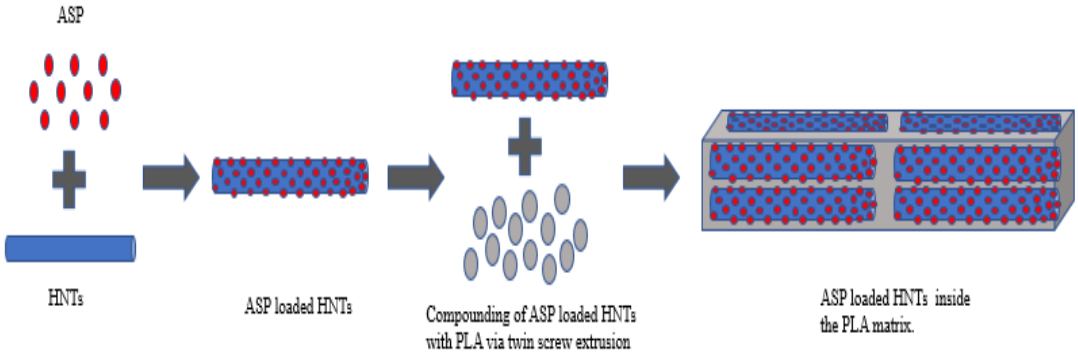

Figure 5.1. *Schematic illustration PLA/(HNT/ASP) nanocomposite by Preloading method.*

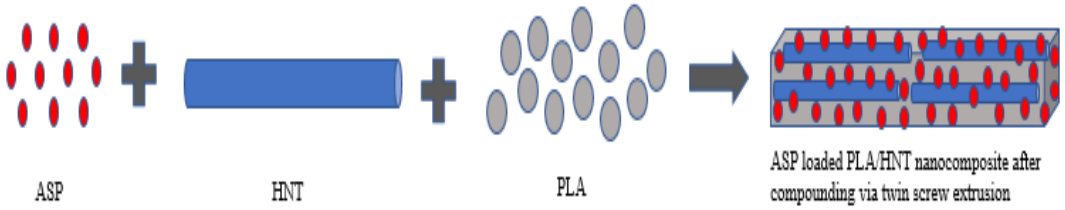

Figure 5.2. *Schematic illustration of PLA/HNT/ASP nanocomposite by Matrix loading method.*

Table 5.1. *Description of the prepared sample batches, method of processing, composition, and the ratio of each component for each batch.*

Batch	Type of Loading	Composition	HNT: ASP ratio
B1	Lumen loaded	95% PLA, 5% (HNT+ASP)	1:1
B5	Lumen loaded	95% PLA, 5% (HNT+ASP)	2:1
B2	Matrix loaded	95% PLA, 5% (HNT+ASP)	1:1
B3	Matrix loaded	95% PLA, 5% (HNT+ASP)	2:1
B4	Matrix loaded	95% PLA, 5% HNT	-
B6	Matrix loaded	100% PLA	-

5.3 Results

5.3.1 Drug loading on HNT

ASP loading into HNT was performed without any difficulty. Before the loading, the ASP and HNT were in white powder form as shown in Figures 5.3 (a) and (b). The ASP-loaded HNT turned pale (mild pink colored) powder as shown in Figure 5.3 (c).

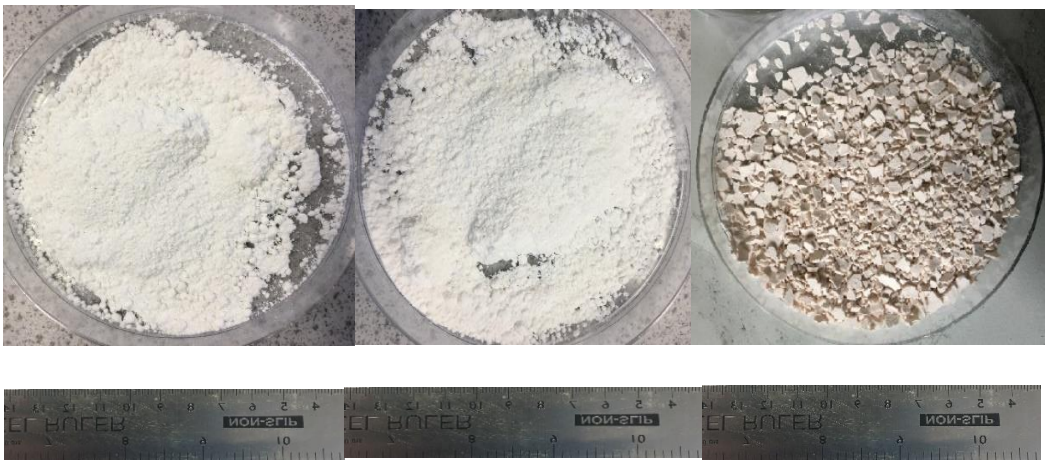

(a) (b) (c)

Figure 5.3*. Photograph of (a) ASP (b) HNT (c) ASP loaded HNT after drying it in the oven at 40°C overnight. The resultant blend had a pale pink color as compared to the white color of the ASP and HNT individually.*

5.3.2 Evaluation of drug-loaded efficiency

ASP encapsulation and loading efficiency were studied by separating the ASP-loaded HNT from the aqueous medium containing free drug by centrifugation at 700 rpm at room temperature for 30 minutes. The amount of free ASP was determined by a UV spectrophotometer at 276 nm. A standard calibration curve of concentration versus absorbance was plotted for this curve. The ASP encapsulation efficiency (EE) and the ASP loading capacity (LC) of the process were calculated from the equations below:

$$EE = \frac{(total\ amount\ of\ ASP - free\ ASP)}{total\ amount\ of\ ASP * 100\%} \qquad (1)$$

$LC = \frac{total\ amount\ of\ ASP - free\ ASP}{nanoparticles\ weight * 100\%}$ (2) (Das, Banerjee and Bellare, 2005; Qi *et al.*, 2010; Shi *et al.*, 2014)

The ASP encapsulation efficiency (EE) for the 2:1 and 1:1 ratio was calculated to be 45.3% and 66.66% respectively. The ASP loading capacity (LC) for the 2:1 and 1:1 ratio was 22.6% and 66.6% respectively. The ASP encapsulation efficiency (EE) and the loading capacity (LC) were better for the 1:1 ratio of loading (B1). A similar result was found by Qi et. al. in their drug release study from electrospun PLGA/HNT nanofiber composites (Qi *et al.*, 2010).

5.3.3 Extruded nanocomposites

Virgin PLA, PLA/HNT, PLA/(HNT-ASP), and PLA/HNT/ASP nanocomposites were melt compounded at screw speeds of 140 rpm followed by calendaring without difficulty. The extruded PLA remained transparent (Figure 5.4 (a)), however, the nanocomposites changed in color from transparent to opaque (Figure 5.4 (b)). The drug-loaded nanocomposites were opaque with mild pink color as shown in Figure 5.4 (c).

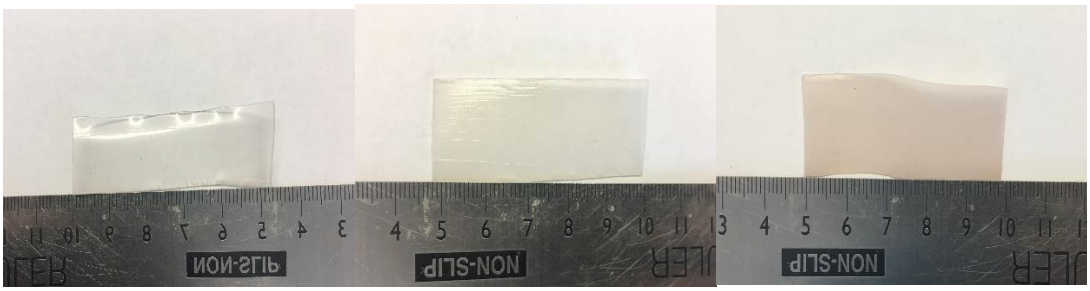

(a) (b) (c)

Figure 5.4. *Photographs of (a) virgin PLA films are transparent (b) PLA/HNT nanocomposite films are opaque (c) ASP loaded PLA/HNT nanocomposite are mild pink in color.*

5.3.4 Mechanical analysis

Mechanical testing was conducted to analyze and compare the effect of the drug on the mechanical properties of the nanocomposite. Mechanical properties of the PLA/HNT composites were characterized by Young's Modulus, tensile strength, stiffness, and elongation at break.

Young's Modulus of the API-loaded nanocomposites as shown in Figure 5.5 was not inferior to the PLA or PLA/HNT nanocomposites. The Young's Modulus of lumen loaded (2:1) B5 was significantly higher with a value of 1599.4 MPa ($p = 0.001$) when compared to matrix loaded (2:1) B3 nanocomposite which had a value of 1326.2 MPa and PLA/HNT nanocomposite B4 with a value of 1194.6 MPa which can be seen in Figure 5.5.

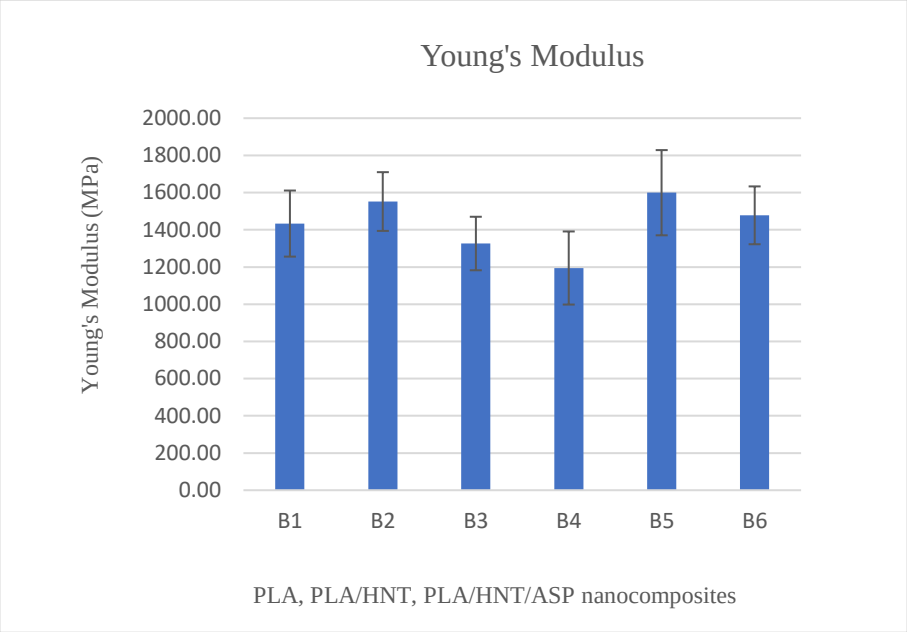

Figure 5.5. *Graphical representation for the effect of Young's Modulus*.

The elongation at break as seen in Figure 5.6 doesn't show any significant difference between the nanocomposites B2, B3, B4, B5, and B6 ($p \geq 0.07$). However, there was a significant decrease in the elongation at break for lumen loaded 1:1 ratio nanocomposite, B1 compared to all other batches ($p = 0.001$).

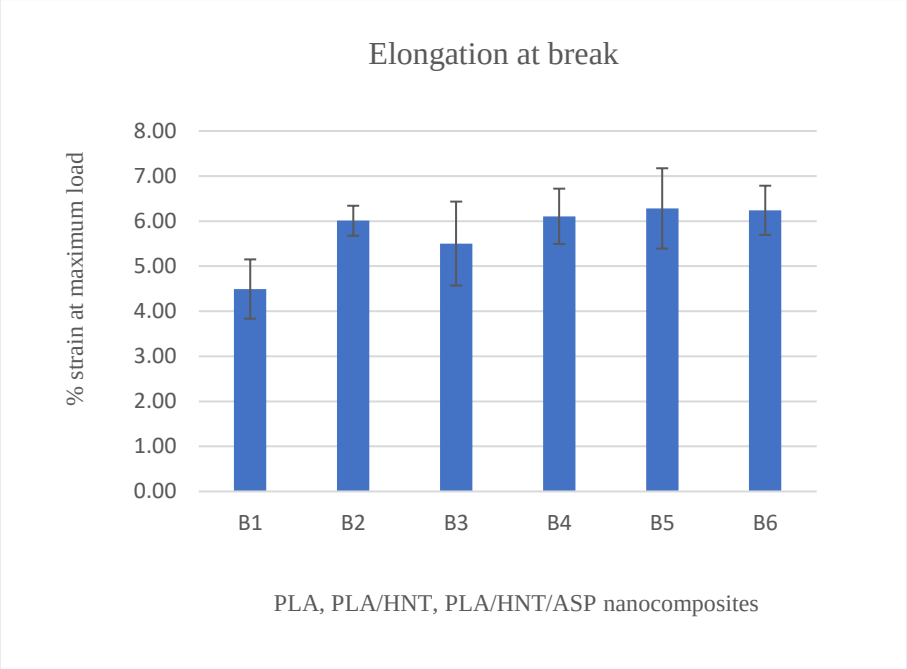

***Figure 5.6**. Graphical representation for the effect of the elongation at break*

The stiffness of the nanocomposite B3 was significantly higher than other nanocomposites as shown in Figure 5.7 ($p = 0.001$). With a mean value of 229.6 kN/m, the stiffness increases for the B3 batch which was matrix loaded with a 2:1 ratio.

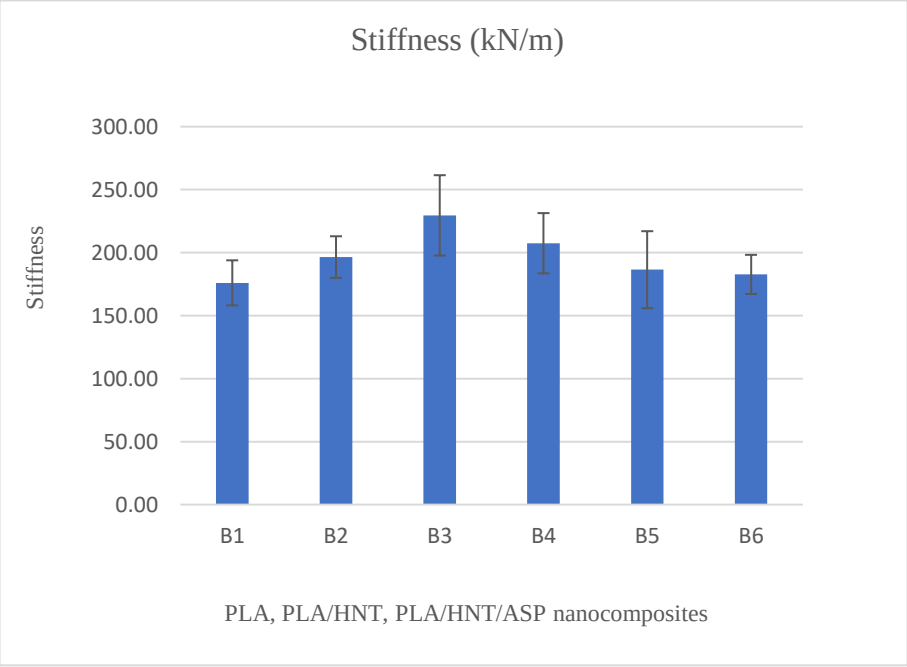

***Figure 5.7.** Graphical representation for the effect on the stiffness*

The tensile strength of the lumen-loaded nanocomposite B5 with 2:1 ratio loading was significantly higher than the PLA/HNT nanocomposite B4 as shown in Figure 5.8 ($p = 0.001$). With a mean value of 56.21 MPa, the tensile strength was significantly increased for B5 when compared to the mean value of 45.74 MPa for B4 PLA/HNT nanocomposite, 45.98 MPa for lumen loaded nanocomposite B1 with 1:1 ratio, and 46.11 MPa for matrix loaded nanocomposite B3 with 1:1 ratio loading.

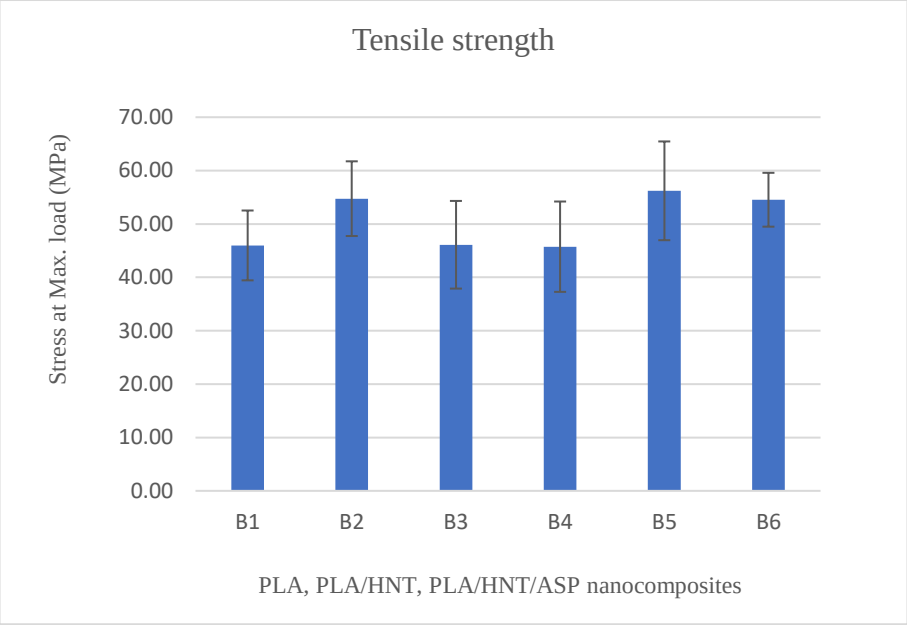

***Figure 5.8**. Graphical representation for the effect on the tensile strength*

In comparison to the virgin PLA (B6) and PLA/HNT nanocomposite (B4), Young's modulus and the tensile strength significantly increases for the lumen-loaded 2:1 nanocomposite (B5) with $p=0.001$. Whereas stiffness significantly increases for matrix loaded 2:1 nanocomposite (B3) ($p=0.001$), with no significant change in the elongation at break for any batch ($p=0.07$).

5.3.5 Differential Scanning Calorimetry (DSC)

The thermal properties of the nanocomposites following drug encapsulation were analyzed using DSC. Fig. 5.9 shows the thermograms of all the batches including ASP and HNT for comparison. ASP shows its characteristic melting peak at 142.45°C as expected. However, this peak is not evident in the ASP-loaded HNT curve.

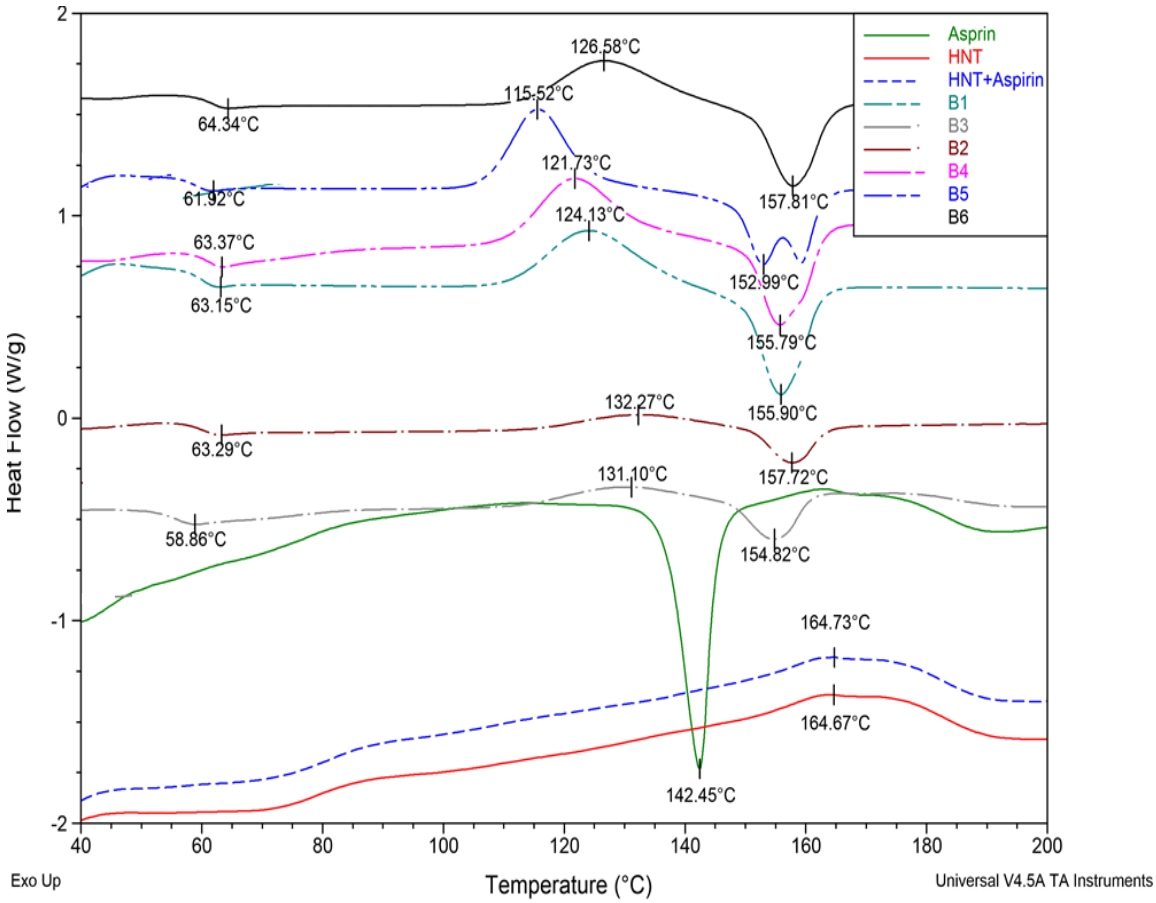

Figure 5.9. *Thermograms of B1, B2, B3, B4, B5, B6, HNT, ASP and HNT+ASP. There is no change in T_g due to ASP loading when compared to the virgin PLA and PLA/HNT nanocomposite.*

The analysis of the thermograms of the nanocomposites indicates that the glass transition temperature (T_g) doesn't show any significant change by the addition of API in the nanocomposite. The cold crystallization temperature has a significant decrease when the ASP is lumen loaded in a 2:1 ratio when compared to other batches of the nanocomposites. It is interesting to note the very small or almost no curve for the cold crystallization of 1:1 and 2:1 matrix-loaded nanocomposites (B2 and B3). The melting temperature slightly decreases for only 2:1 lumen-loaded nanocomposite (B5).

5.3.6 Morphological characteristics

SEM was conducted for HNT, ASP-loaded HNT, 2:1 matrix loaded nanocomposite and 2:1 lumen loaded nanocomposite films. The SEM photomicrographs are as shown in Figure 5.10. In Figure 5.10 (b) the ASP-loaded HNT sample does not indicate the presence of the ASP from the photomicrograph. Figure

5.10 (c) and (d) indicate the presence of the filler in the nanocomposite. However, the presence of ASP cannot be distinguished. Hence, the photomicrographs did not show any visual evidence indicating ASP encapsulation, however, the HNT was evident as bright particles in the images.

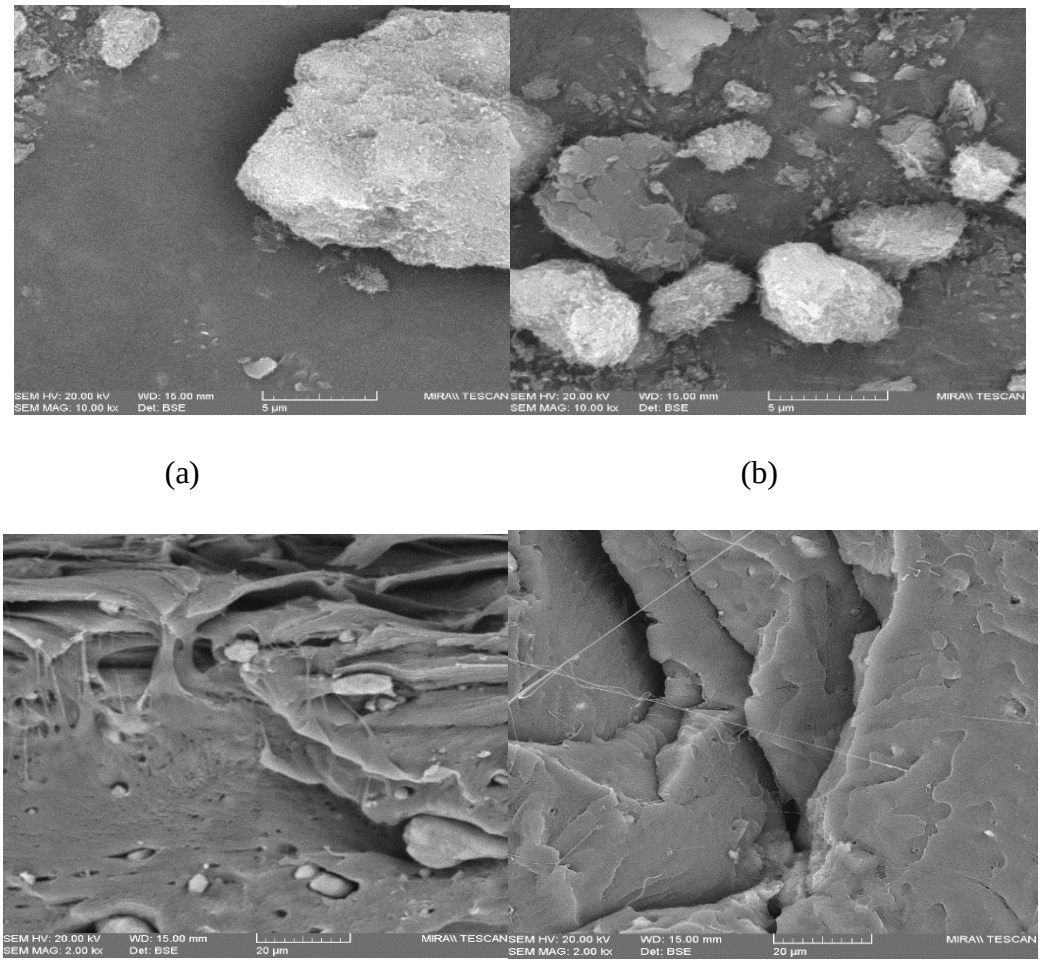

***Figure.5.10**. Photomicrograph of (a) HNT (b) ASP loaded HNT (c) preloaded 2:1 nanocomposite (d) matrix loaded 2:1 nanocomposite*

5.3.7 Fourier Transform Infrared (FTIR) Spectroscopy

FTIR was performed to study the chemical reaction in PLA/HNT composites. Virgin PLA exhibited characteristic peaks at 3571 cm^{-1} corresponding to –OH stretch, peaks at 2995 cm^{-1} and 2946.34 cm^{-1} were attributed to CH stretch and the peaks at

1750 cm^{-1} indicated –C=O carbonyl group (Garlotta, 2002). The spectrum of HNT displayed peaks at 3693.26 cm^{-1} and 3623.39 cm^{-1} which can be assigned to the O-H group and peak at 906.81 cm^{-1} to the Al-OH group (Chen *et al.*, 2018).

The spectra of PLA/HNT composites displayed characteristic peaks of both PLA and HNT. The functional groups of HNT such as the O-H stretching of the hydroxyl group are displayed by the characteristic peak located at 3696.39 cm^{-1} and 3626.39 cm^{-1}. However, the spectra API loaded (matrix and lumen) nanocomposites did not display any characteristic peaks of ASP and were very similar to PLA/HNT nanocomposites with characteristic peaks of PLA and HNT.

The analysis of the spectra of HNT, ASP, and the ASP lumen-loaded HNT are shown in Figure 5.11. The spectrum indicate the characteristic peaks of ASP at 1751 cm^{-1} corresponding to C=O stretching, 1697 cm-^{1} corresponding to –COO stretch and 1486 cm^{-1} from antisymmetric stretching vibration of a carboxylate form of ASP (Semalty *et al.*, 2010; Lun, Ouyang and Yang, 2014) These peaks were observed in the lumen loaded HNT at 1751 cm^{-1}, 1697 cm^{-1} and 1486 cm^{-1} which can be seen in the higher magnification of the ASP pre-loaded HNT spectrum in Figure 5.11 (b). Similar analyses and findings were reported by Lun and researchers (Lun, Ouyang and Yang, 2014). This indicates the ASP molecules had been attached to the HNT after API loading.

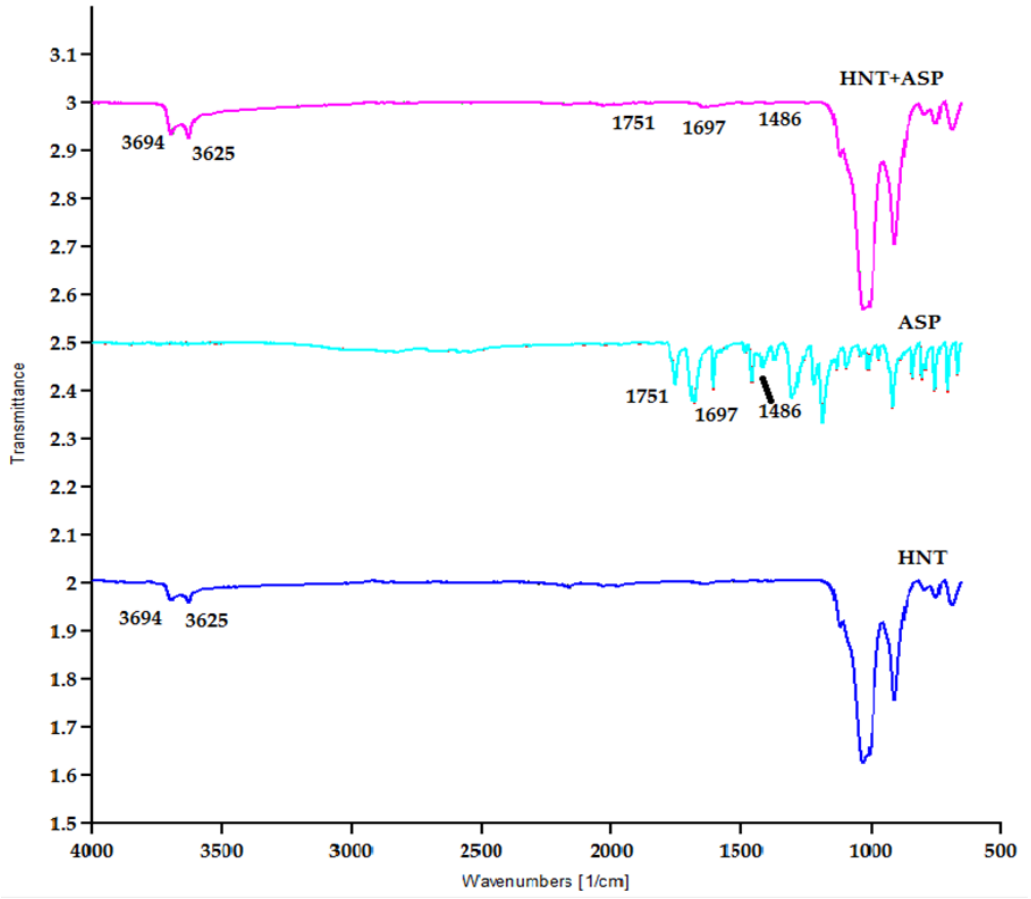
HNT+ASP
3694
3625
1751
1697
1486
ASP
1751
1697
1486
HNT
3694
3625
Transmittance
Wavenumbers [1/cm]

(a)

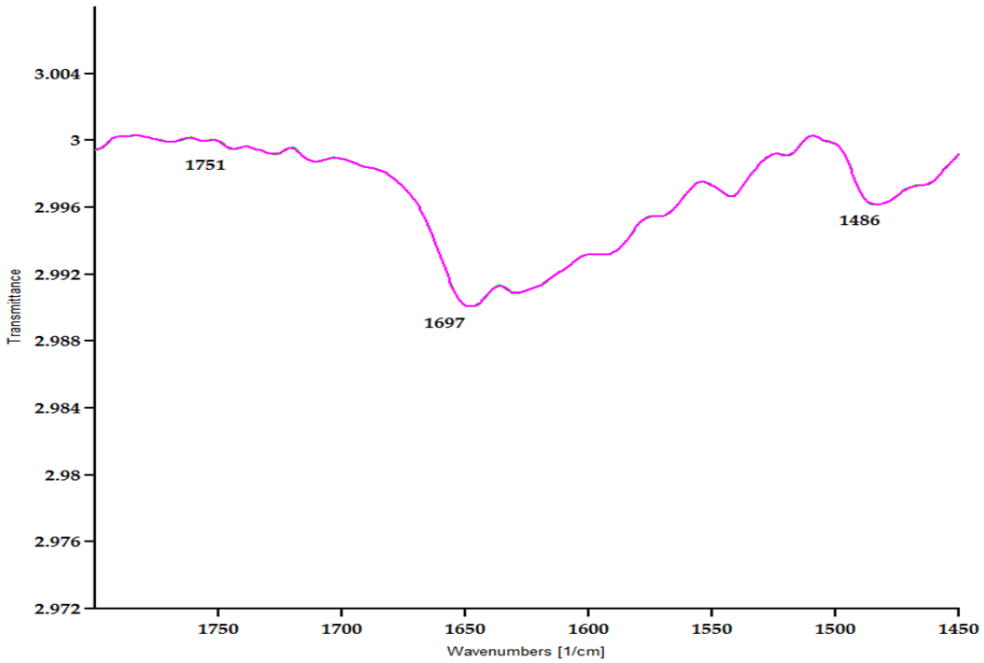
1751
1697
1486
Transmittance
Wavenumbers [1/cm]

(b)

***Figure 5.11**. a) FTIR spectra of HNT, ASP, and ASP-loaded HNT samples. The peaks of ASP at 1751 cm^{-1}, 1697 $cm^{-1,}$ and 1486 cm^{-1} correspond with the peaks of ASP-loaded HNT at 1751 cm^{-1}, 1697 $cm^{-1,}$ and 1486 cm^{-1}. This indicates the drug is loaded in the HNT. (b) Higher magnification of HNT + ASP spectrum.*

5.3.8 Goniometry (Surface Wettability)

The surface wettability of all the composites was assessed. The contact angle measurements as shown in Figure 5.12, indicating that the contact angle of PLA (B6) and PLA/HNT (B4) displayed between the ranges of 60-65°. The contact angle of the lumen-loaded nanocomposite with ratio 2:1 (B5) and matrix-loaded nanocomposite with ratio 2:1 (B3) significantly decreases with $p \leq 0.04$. Thus, B5 and B3 are hydrophilic with a mean contact angle of 62.77° and 68.22° respectively. However, the contact angle measurement significantly increases for lumen-loaded nanocomposite with 1:1 ratio B1 and matrix loaded nanocomposite with 1:1 ratio B2 with $p \leq 0.035$. Thus, B1 and B2 had increased hydrophobicity with a mean contact angle of 84.89° and 88.90° respectively.

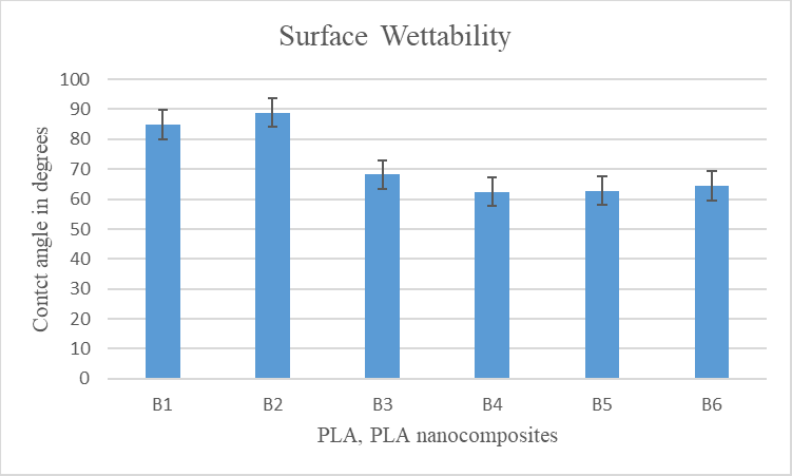

***Figure 5.12.** Graphical representation of contact angle measurements for all batches indicates the hydrophilicity in B5 and B3 batch of 2:1 ratio of both preloading and matrix loading. The B1 and B2 of 1:1 ratio tends to be hydrophobic*

.

5.3.9 In-vitro drug release study

The amount of API released from the lowest to the highest concentration is plotted against the time of release as seen in Figure 5.13. The graphical representation of the amount of API release (Q%) versus time (t) shows linearity. Thus, the API release rate is independent of the concentration of the API. In this study, the release kinetics of ASP showed the best fit for the zero-order model (R^2 = 0.9995) which represents a slow release of drug and is expressed by the equation $Q_t = Q_0 + K_0 t$ where Q_t is the amount of drug dissolved at time t, Q_0 is the initial amount of API in the solution and K_0 is the zero-order release constant expressed in units of concentration/time. The data obtained from in vitro drug release studies were plotted as the cumulative amount of drug released versus time.

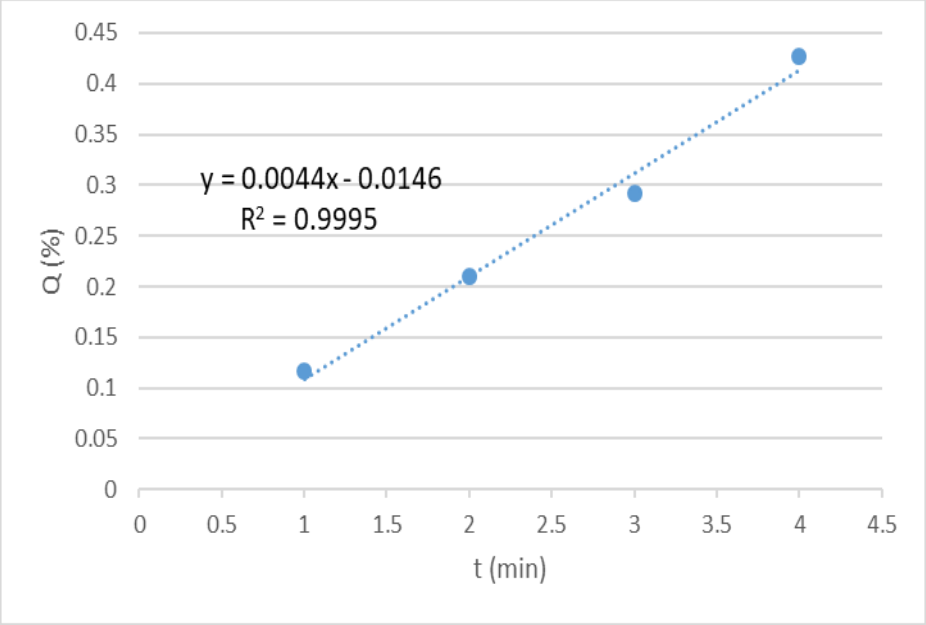

Figure 5.13. *Standard curve of API release for the lowest to the highest concentration of API*

The *in vitro* release kinetics for the lumen-loaded nanocomposite in 1:1 ratio (B1) is shown in Figure 5.14. From drug release studies it was found that lumen-loaded B1 samples exhibited a burst release of 26% in 8 hours. This was followed by a slow release of 33% up to 72 hours and 55% at 144 hours. On the ninth day, there was a gradual decrease to 51% release. The *in vitro* release kinetics for the matrix-loaded nanocomposite in 1:1 ratio (B2) is shown in Figure 5.15. The drug release study for the B2 exhibit release of 6% after 2 hours, with no further release, observed until 9

days when 33% release was detected which was reduced to 20% release on the ninth day.

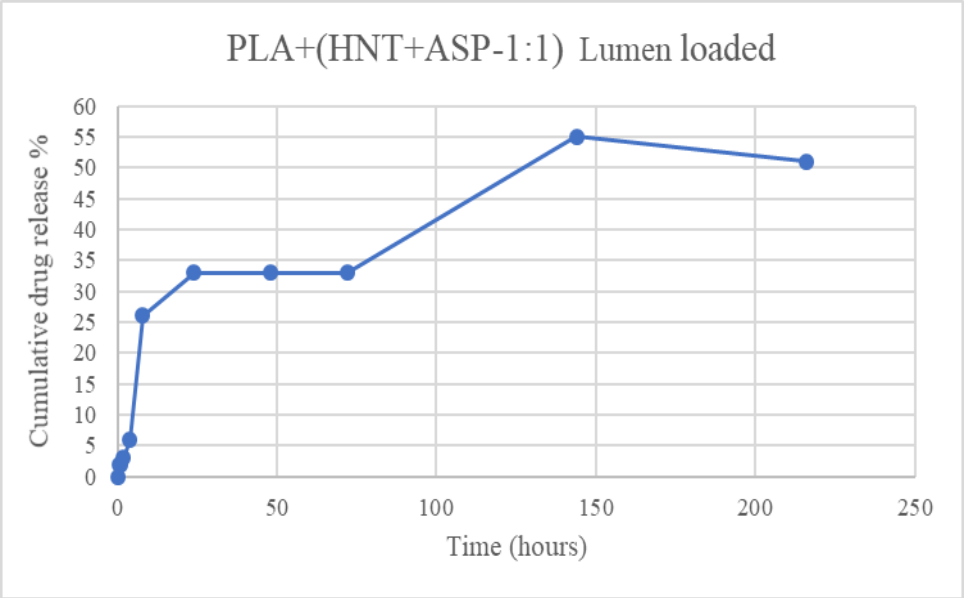

Figure 5.14. *In vitro release kinetics for lumen loaded 1:1 nanocomposite (B1)*

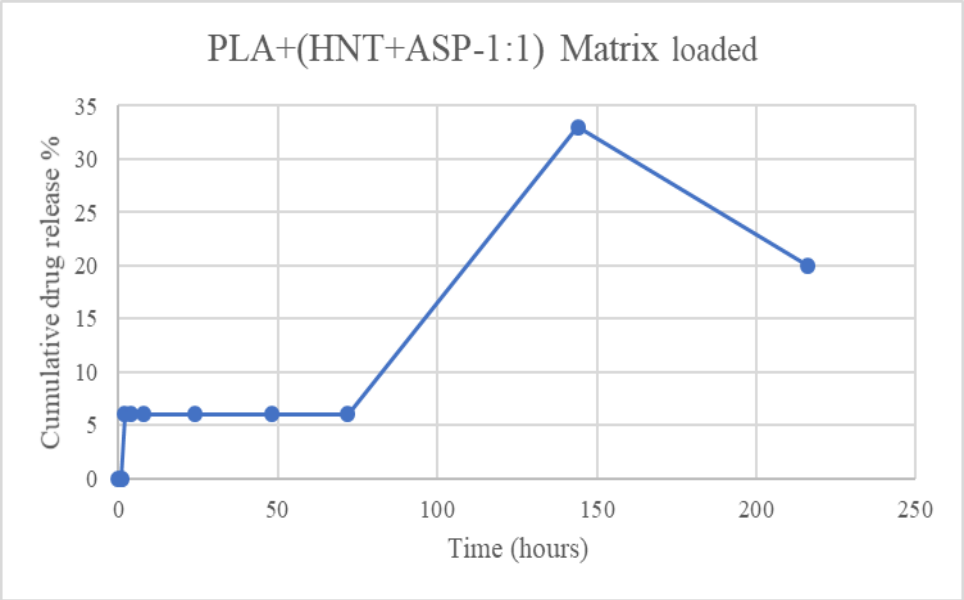

Figure 5.15. *In vitro release kinetics for matrix loaded 1:1 nanocomposite (B2)*

The *in vitro* release kinetics for the matrix-loaded nanocomposite in 2:1 ratio (B3) is shown in Figure 5.16. The matrix-loaded B3 samples exhibited a burst release of 14% after 4 hours which again did not increase until 6 days when 17% drug release

was detected. The *in vitro* release kinetics for the lumen-loaded nanocomposite in 2:1 ratio (B5) is shown in Figure 5.17. The lumen-loaded B5 samples exhibited a burst release of 21% within 1 hour with no further drug release detected until after nine days when 32% drug release was recorded which decreased to a release of 23% on the ninth day.

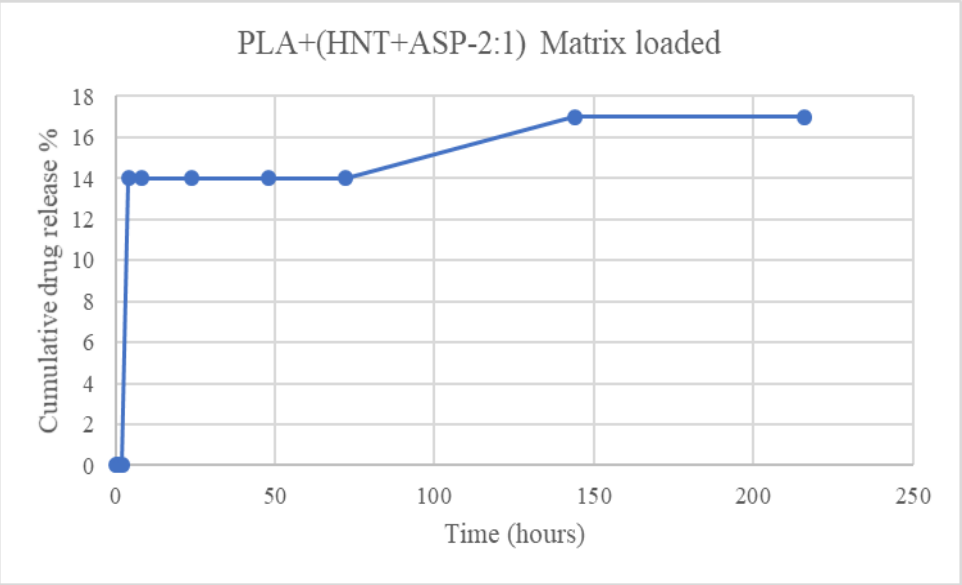

Figure 5.16. *In vitro release kinetics for matrix loaded 2:1 nanocomposite (B3)*

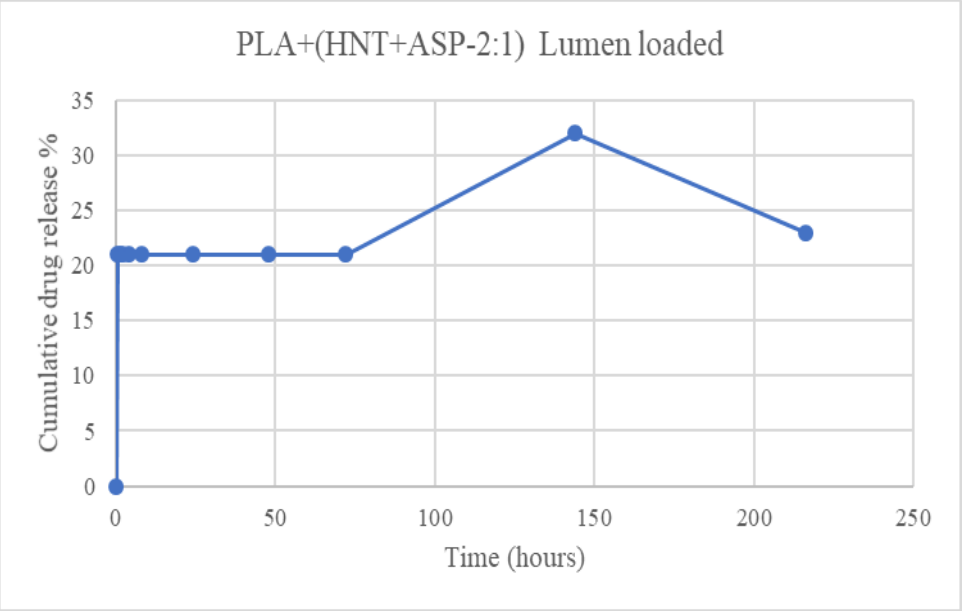

Figure 5.17. *In vitro release kinetics for lumen loaded 2:1 nanocomposite (B5)*

The drug release profiles for all batches tested are presented in Figure 5.18. Batches B1 and B2 had a drug loading ratio of 1:1; HNT: ASP. Batch numbers B3 and B5 had a drug loading ratio of 2:1; HNT: ASP.

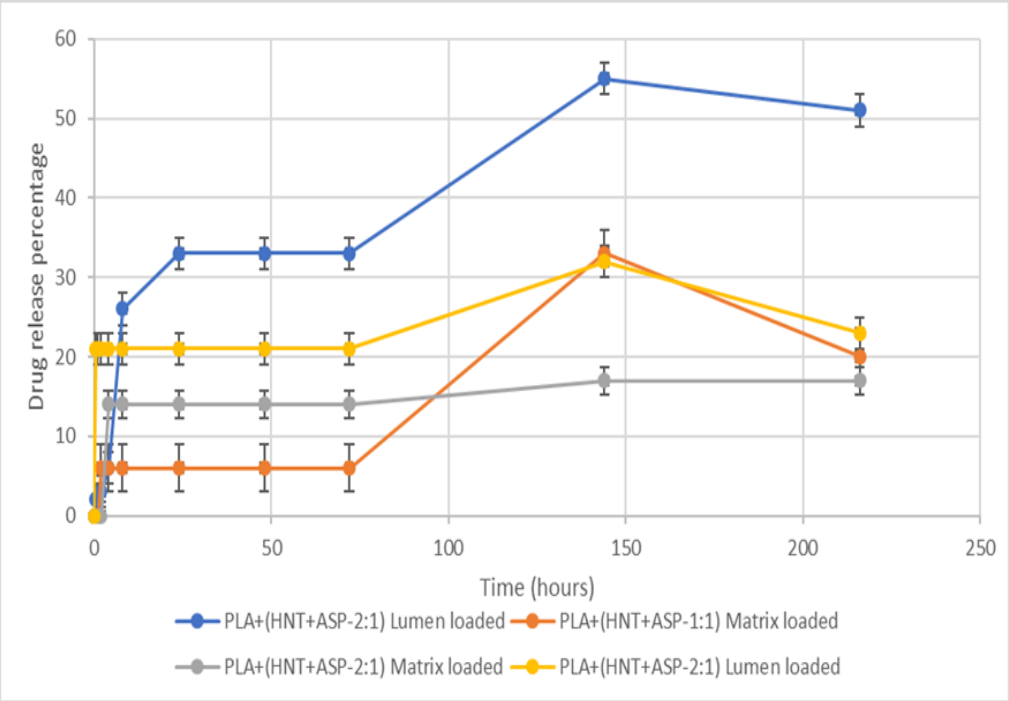

***Figure 5.18**. In vitro release kinetics show the sustained drug release over 9 days (216 hours). Total release at the end of 72 hours is 5%, 15%, 22%, and 33% for B2, B3, B5, and B1 respectively. At 144 hours, 18%, 31%, 32% and 54% are released for B3, B5, B2 and B1 respectively.*

5.4 Discussion

The present study explored the feasibility of the controlled release of API from PLA/HNT composites. The PLA has a glass transition temperature of 60 °C. This is important as the polymer selected for the HME must have deformation potential and the glass transition temperature must be less than the melting point of the drug, which in the case of ASP is 135 °C (Fule, Paithankar and Amin, 2016). HNT was utilized as a drug carrier as, structurally, the large surface area and the inner lumen of HNT make it suitable for drug loading and sustained release. It has also been shown to increase drug effectiveness without increasing the concentration of the drug as it is slowly released from the HNT (Lvov, DeVilliers and Fakhrullin, 2016). The HNT is normally mixed with a saturated solution of chosen active agent in ethanol, water, or other solvents to entrap hydrophilic drugs (Qi *et al.*, 2013). However, the low dissolution

rate of the ASP in water reduces the drug absorption rate and also toughens the maintenance of its concentration inside the body (Lun, Ouyang and Yang, 2014). Hence, in this study, the ASP was dissolved in ethanol, and HNT are added to the solution for the drug loading.

The API loading on the HNT is either the API is encapsulated in the inner lumen, or it may be bound to the outer surface. The negatively charged outer surface of the HNT could encapsulate the ASP through hydrogen bonding between the carbonyl group of the ASP and the hydroxyl or the siloxane group of the HNT. When the vacuum is applied during the API loading, the positively charged inner lumen of the HNT could entrap the ASP (Qi *et al.*, 2013; Lun, Ouyang and Yang, 2014). Most likely, the drug molecules are distributed both in the inner lumen and in the outer surfaces but with a possibility of the drug on the outer surface could be washed out (Lvov, DeVilliers and Fakhrullin, 2016). The outer diameter of the HNT is 50-70 nm and the inner diameter is 15-30 nm. The molecular size of the ASP being 0.8 nm x 0.6 nm, can be attributed to the presence of ASP in the lumen of HNT (Lun, Ouyang and Yang, 2014). This is confirmed by FTIR spectroscopy and thermal analysis.

The lumen loading method where ASP is loaded onto HNT, displayed better encapsulation efficiency (EE) and the loading capacity (LC) for a 1:1 ratio of loading. In this work, it was hypothesized that the fast deposition and aggregation of HNT at higher concentrations lead to relatively less surface area being exposed to the drug which resulted in lower EE and LCs for 2:1 ratio of loading (Qi *et al.*, 2010). A similar 1:1 ratio of the mixture of PDLLA and drug sirolimus is used in the currently used biodegradable coronary scaffold NeoVas from Lepu Medical Technology, Beijing, China (Kawashima *et al.*, 2020). The bioabsorbable vascular solutions (BVS) everolimus-eluting stent from Abbott Vascular, Santa Clara, CA also used a mixture of 1:1 of the drug to PLA coated on PLA stent which released 80% of the drug within 30 days (Ramadugu and Latha Alikatte, 2016).

It is interesting to note the API inclusion in the nanocomposite does not deteriorate the strength unlike the study conducted by Patel and researchers where the tensile strength is reduced when the drug-loaded HNT was loaded in the PLA matrix (Patel *et al.*, 2015). However, in their study, the method of processing was electrospinning. Here, the process of extrusion would have induced HNT dispersion

through melt shearing. Similarly, there was a significant increase in stiffness for matrix loaded 2:1 nanocomposite (B3) when compared to the other batches. The results indicating an increase in Young's Modulus and the tensile strength of the 2:1 lumen loaded nanocomposite (B5) compared to the PLA/HNT may be due to the good hydrogen bonding interaction between the ASP molecules and the HNT during pre-loading which later blends well in the PLA matrix. This could also be related to the plasticizing effect of ASP on the system as observed in DSC data which allowed molecular chains to slide over each other more easily under tension. When the drug-loaded nanocomposites are compared to the PLA/HNT nanocomposites (B4), the improvement of the mechanical properties could be due to the interactions of the ASP molecules with the HNT which enhances the interfacial adhesion and good dispersion (Shi *et al.*, 2015).

The absence of the characteristic melting peak of ASP in the DSC thermograms of ASP-loaded HNT could indicate the loading of the ASP inside the cavity of the HNT (Gao *et al.*, 2017). This could also indicate the amorphous state of the drug (Balogh *et al.*, 2018). The glass transition temperature is the measure of rigidity (Declan M. Devine *et al.*, 2017). The addition of HNT or the ASP has a minimal effect on the rigidity of the polymer PLA backbone chain. The cold crystallization temperature exhibited a significant decrease when the ASP is preloaded in the HNT at a 2:1 ratio when compared to other batches of the nanocomposites. A reduction in T_{cc} of PLA/ASP-HNT composites has been reported to be indicative of heterogeneous nucleation, where thinner or less perfect crystalline lamella are formed (Dong *et al.*, 2015b; Chen *et al.*, 2018). This is further supported by the twin melting peak of the nanocomposite which is indicative of the melting of imperfect crystalline segments.

Conversely, the matrix-loaded nanocomposites show a negligible or nearly no cold crystallization curve for both 2:1 and 1:1 ratios. This may be due to the plasticizing effect of the ASP when processed together with PLA and HNT. In a previous study by Shi et al., the addition of plasticizer into the PLA composites has shown very small or no cold crystallization peak indicating the mobility of PLA chains and advanced crystallization of the nucleating agents before cooling (Shi *et al.*, 2015).

The FTIR peaks of ASP are not intense and very similar to HNT peaks, this could indicate the loading of the ASP in the HNT cavity which is relatable to the

thermal analysis of the same. This also could indicate the surface of HNT free of residual ASP (Gao *et al.*, 2017). The spectra of all the drug-loaded PLA/HNT nanocomposite films were very similar to the PLA spectrum with no peaks of ASP were observed. This could be due to the insensitivity of the FTIR technique or factually, the vibration bands of ASP or HNT could be overlapping with PLA bands (Qi *et al.*, 2010).

ASP is a hydrophilic drug (Tang and Singh, 2008). The hydrophilicity of B5 and B3 indicates that the loading ratio of 2:1 of HNT: ASP irrespective of the type of processing decreases the contact angle of the nanocomposites. This could result in a higher amount of ASP in the matrix system for 2:1 ratio as 1:1 samples had better API loading efficiency in HNT, which had a plasticizing effect and rendered the composite more hydrophilic compared to the 1:1 samples. Similar findings were seen by Patel and researchers in their study with PCL/HNT nanocomposites with antibacterial drugs (Patel *et al.*, 2015).

The API release mechanism for the PLA/HNT/ASP nanocomposite was through diffusion and swelling of the nanocomposite as shown in Figure 5.19.

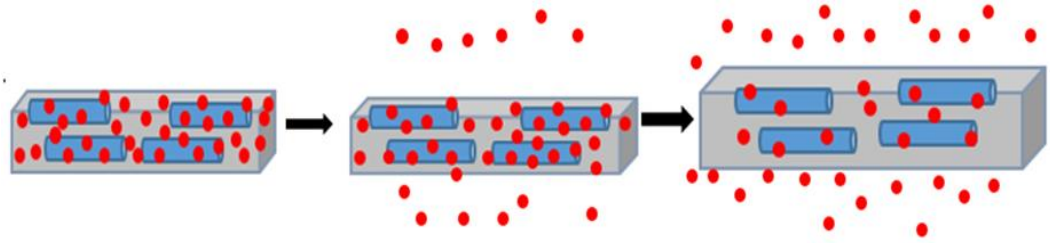

Figure 5.19. *Schematic representation of API release mechanism for PLA/HNT/ASP nanocomposite through diffusion and swelling*

The ASP release from the nanocomposite systems indicates that both the HNT: ASP ratio and entrapment method had a large effect on ASP release. From ASP data it was shown that the matrix loaded samples did not have any burst release and that the release began following 8 hours incubation which would indicate that the drug had started to diffuse through the hydrophilic PLA matrix. Conversely, the lumen-loaded samples did have a burst release of 21-28% in the first 1-8 hours. This may be attributed to the ASP washing out of the outer lumen of the HNT which was close to the surface of the PLA. In terms of HNT: ASP ratio, and in agreement with drug loading findings, the 1:1 samples yielded a higher total drug release at the end of the nine-day experiment.

Literature review reports the reduction in initial burst release due to the plasticizing effect of the plasticizer, poly(ethylene glycol)400 in the polymer matrix (Tang and Singh, 2008). The slow drug release suggests the presence of a major amount of ASP in the HNT or PLA/HNT nanocomposite film at that time point (Qi *et al.*, 2010). The thermal properties of this study show that the matrix-loaded ASP for both 2:1 and 1:1 ratio nanocomposite had negligible cold crystallization curves which could be due to the plasticizing effect of the ASP when loaded directly into the PLA matrix. Plasticizers that are capable of increasing the flexibility of the polymers can reduce the degradation of the thermolabile drugs (Patil, Tiwari and Repka, 2016). The higher percentage of drug release after 140 hours can be attributed to the gradual degradation of the PLA which had extended the retention time of the API (Sha *et al.*, 2016).

It is interesting to note the reduction in the percentage release of the API from the nanocomposites on the ninth day except for the 1:1 matrix loaded nanocomposite (B2). This could be due to the presence of the ASP in the inner lumen of the HNT, which gradually diffused to the PLA matrix during the nine days. Thus the loading of the ASP onto the HNT potentially on the inner lumen reduces the bust release and aids for sustained release over some time.

5.5 Summary

In this study, the API loading and release characteristics of the PLA/HNT nanocomposite were examined to establish its drug-eluting capacity as a potential stent material. FTIR characterization revealed the presence of ASP in the ASP-loaded HNT. The addition of ASP in the nanocomposite did not deteriorate the mechanical properties of the nanocomposites and could have displayed plasticizing effect on the nanocomposites which could be seen with an increase in the mechanical properties of the lumen loaded samples and with negligible cold crystallization curve for matrix loaded samples from DSC. Lumen-loaded samples had burst release and overall higher release of the ASP when compared to the matrix-loaded samples. Whereas in terms of ratios, 1:1 for HNT: ASP, a higher total of API was released at the end of the nine-day experiment. The encapsulation efficiency and the loading capacity were better for the 1:1 ratio loading of HNT: ASP. From all the results and analyses, the 1:1 ratio of HNT: ASP matrix loaded was better for improved properties of the composite and sustained

release with no initial burst release. The significant reduction in burst release is desirable as higher initial burst release could lead to initial toxicity associated with a high dose (Nazila *et al.*, 2016), and in coronary artery disease, it could have unfavorable effects such as arterial aneurysms and delayed endothelialization (F. Li *et al.*, 2018).

Further to this study, following the 1:1 ratio for HNT: API composition and the matrix loading method, the PLA/HNT nanocomposites will be evaluated for the behavior of two types of drugs with a different functional group, in particular the pKa value of the drug molecule inside the PLA/HNT nanocomposite. For this aspirin (ASP) will be used as the model drug with a lower pKa value of 3.5 and for comparison with a higher pKa value of the drug, acetaminophen (APAP) will be used which has a pKa value of 9.96. The prepared nanocomposites will be characterized for mechanical, thermal, and physicochemical properties along with drug release kinetics. The drug-loaded nanocomposites will also be investigated for 32-week degradation tests followed by mechanical, thermal, and physicochemical properties of the degradation samples.

CHAPTER 6

The effect of pKa values of the drug compound on the degradation and drug release mechanism of the PLA/HNT nanocomposite

6.1 Introduction

The drug release from biodegradable polymers depends not only on the properties of the polymer but the type of drug used also plays an important role. It has been reported that the chemistry of the drug effect the release pattern and the rate of degradation (Alexis, 2005; Devine *et al.*, 2006; Siegel *et al.*, 2006). In medicinal chemistry, drugs are most commonly classified as weak acids or bases and sometimes neutral. The acidic or basic properties of the drug molecule are one of the essentials for the behavior or action of the drug (Charifson and Walters, 2014). These properties affect the ability of the compound to dissolve in the fats, lipids, oils (lipophilicity) which is a key requirement for intestinal absorption, membrane permeability, and protein binding (Waterbeemd and Rose, 2008) is mainly controlled by the pKa values (ionization constants) of the functional group (Manallack *et al.*, 2013). This inherent property of the compound also impacts various drug attributes such as physical properties, safety, tissue distribution, and formulatability (Manallack *et al.*, 2013; Charifson and Walters, 2014).

This study aims to investigate the behavior of two types of API with different functional groups, in particular, the pKa value of the drug molecule inside the PLA/HNT nanocomposite. For a lower pKa value, aspirin (ASP) with a pKa value of 3.5 was selected as a model drug as it is prescribed to patients for dual antiplatelet therapy after a coronary intervention to reduce the risk of early stent thrombosis (Ang, Bulluck, *et al.*, 2017b; King and Gogas, 2017; Surgery and College, 2017). The model drug with a higher pKa value was acetaminophen (APAP) which has a pKa value of 9.5 (Cairns, 2003). APAP was selected as a model drug, as several drugs currently used in commercial drug-eluting stents have pKa value similar to APAP or in the same range, such as sirolimus (pKa – 9.96) (Wishart DS, 2017), paclitaxel (pKa – 10.9) (Shah, Wyandt and Stodghill, 2013; Wishart DS, 2017), zotarolimus (pKa - 10.40 ± 0.74) (Book, 2017) to name a few (Majewska, Oledzka and Sobczak, 2019). It is also an analgesic and antipyretic drug commonly used for the treatment of post-operative pain (Wei *et al.*, 2019; Zhang *et al.*, 2019) and has a similar molecular weight to ASP (Devine *et al.*, 2006).

The drug loading and release profile of the PLA/HNT nanocomposite was successfully characterized as studied previously in chapter 5. For the coronary stent application, 1:1 ratio loading of ASP: HNT in PLA matrix via extrusion was particularly ideal as the burst release was minimum which is desirable for stents, as higher initial burst release could have unfavorable effects such as arterial aneurysms and delayed endothelialization (F. Li *et al.*, 2018). Hence, in this study, we go forward with the 1:1 ratio via the matrix loading method for the comparative study of both drugs. The two drugs ASP and APAP were incorporated individually as two batches into the PLA matrix along with HNT via extrusion. As control samples, PLA was incorporated with these drugs separately without HNT. The composition details of the prepared nanocomposites are listed below in Table 6.1.

Table 6.1. *Description of the prepared polymer nanocomposites with PLA, HNT, ASP and APAP. The corresponding compositions for each category are in percentages*

BATCH	PLA	HNT	ASP	APAP
PLA	100	0	0	0
PLA+HNT	95	5	0	0
P+ASP+H	95	2.5	2.5	0
P+APAP+H	95	2.5	0	2.5
PLA+ASP	95	0	5	0
PLA+APAP	95	0	0	5

6.2. Results

6.2.1. Processing of PLA, PLA/HNT, and PLA/HNT/API nanocomposite

PLA and PLA nanocomposites were processed without difficulty. The extrudate was transparent for PLA films. The nanocomposite films were opaque.

6.2.2. Mechanical properties

The mechanical properties of the PLA and PLA nanocomposites prepared are as shown in Figure 6.1. The tensile strength of the PLA/HNT nanocomposites with the addition of ASP and APAP as shown in Figure 6.1 (a) exhibits a decrease in the tensile strength for all the drug-loaded nanocomposites P+ASP+H, P+APAP+H, PLA+ASP, and PLA+APAP when compared to the PLA and PLA/HNT nanocomposite. There was no difference in the tensile strength with the addition of ASP and APAP to the control samples or the PLA/HNT nanocomposite. The statistical analysis also confirmed the above results with a p-value > 0.05 for all the samples.

On the contrary, the elongation at break of the nanocomposites as shown in Figure 6.1 (b) shows a significant increase for the drug-loaded nanocomposite when compared to PLA and PLA/HNT nanocomposite. The addition of ASP showed a higher increase for PLA/HNT composite when compared to the control sample PLA+ASP. However, the addition of APAP in PLA/HNT nanocomposite and the control samples had no significant difference. The statistical analysis also confirmed the above results with a p-value > 0.05 for all the samples.

The stiffness of the nanocomposites as seen in Figure 6.1(c) displayed no significant changes for the API-loaded nanocomposites when compared to PLA and PLA/HNT composites. Thus, the addition of ASP and APAP to both control samples and PLA/HNT composites did not change the stiffness of the composite when compared to PLA and PLA/HNT composite. With a p-value<0.05 for all samples, the results were confirmed statistically.

The Young's Modulus of the API-loaded nanocomposites had a similar trend of tensile strength as shown in Figure 6.1 (d). The Young's Modulus of the API-loaded nanocomposite significantly reduced when compared to PLA and PLA/HNT nanocomposites. However, the addition of ASP or APAP did not show any significant changes in PLA/HNT nanocomposite when compared to the control samples PLA+ASP or PLA+APAP. This was confirmed by the statistical analysis with the p-value<0.05 for all the samples.

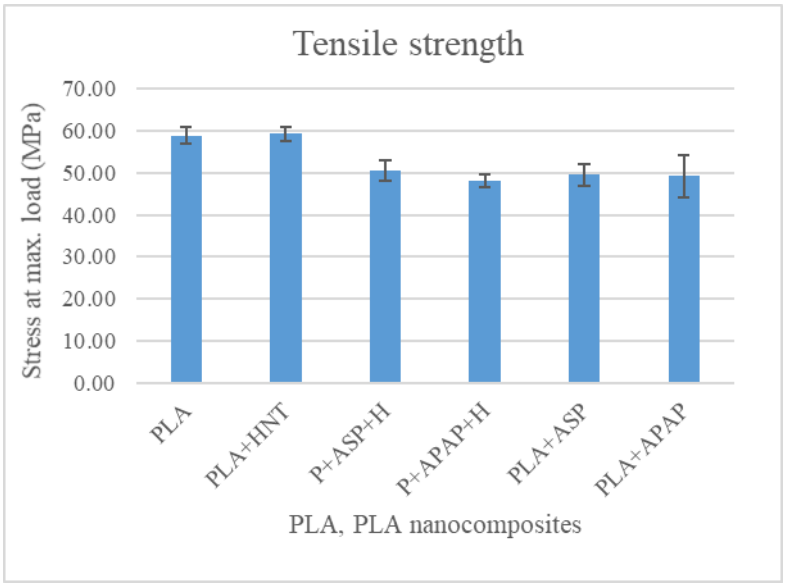
Tensile strength
Stress at max. load (MPa)
70.00
60.00
50.00
40.00
30.00
20.00
10.00
0.00
PLA
PLA+HNT
P+ASP+H
P+APAP+H
PLA+ASP
PLA+APAP
PLA, PLA nanocomposites

(a)

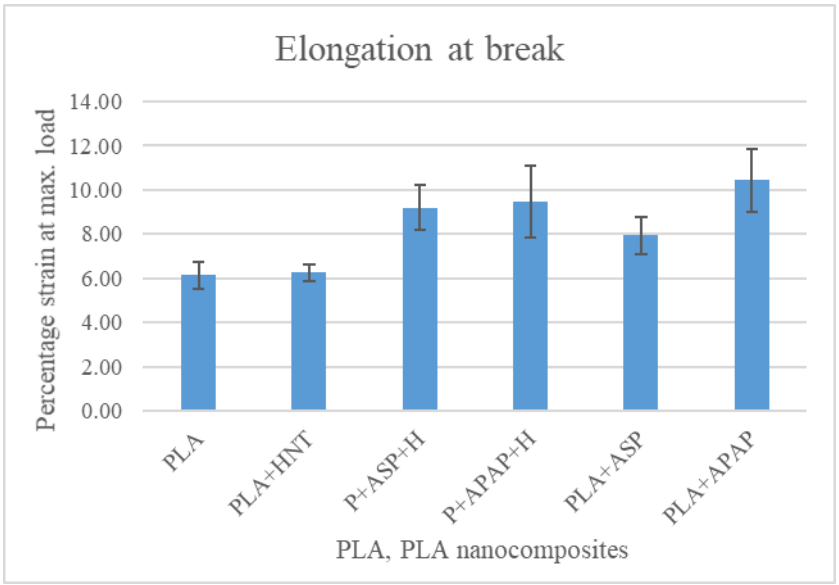
Elongation at break
Percentage strain at max. load
14.00
12.00
10.00
8.00
6.00
4.00
2.00
0.00
PLA
PLA+HNT
P+ASP+H
P+APAP+H
PLA+ASP
PLA+APAP
PLA, PLA nanocomposites

(b)

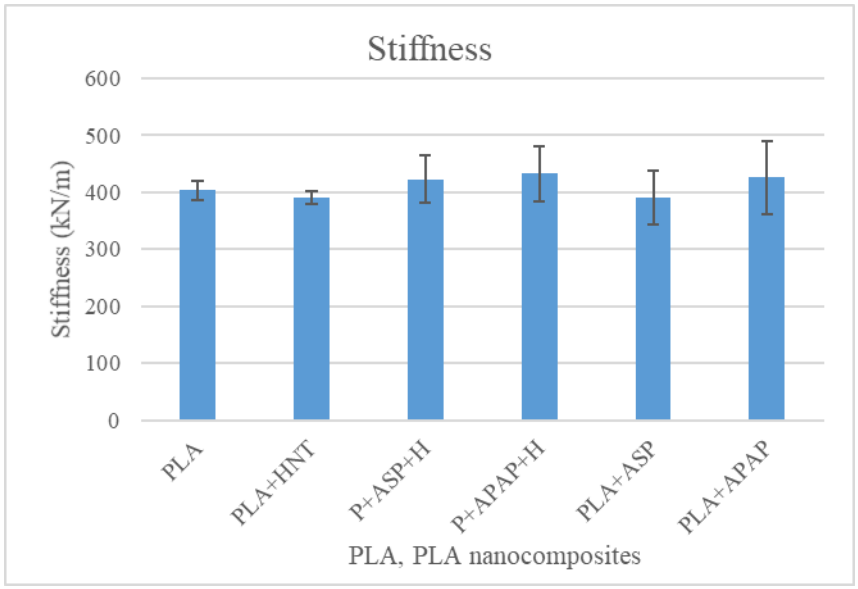

(c)

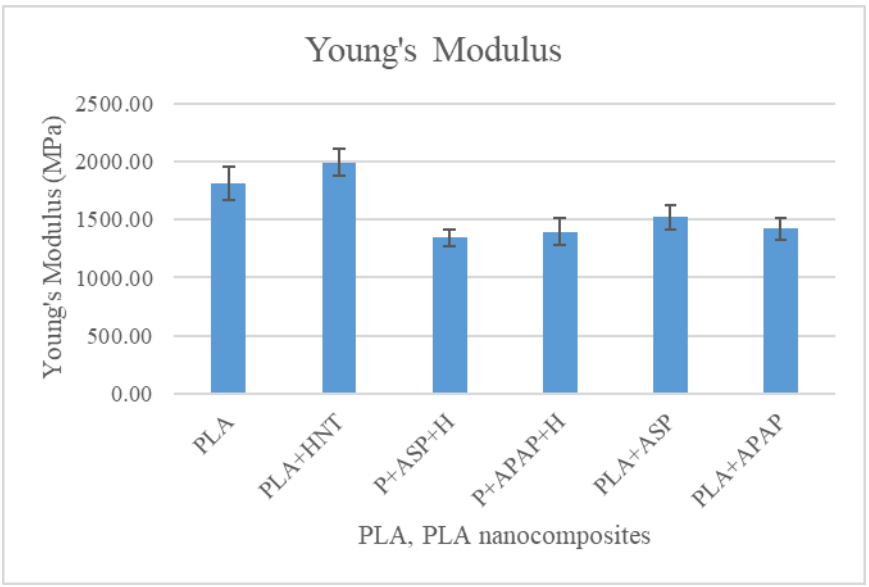

(d)

Figure 6.1. *Mechanical properties of the PLA and PLA-API-loaded nanocomposites. There were no significant changes ($p>0.05$) in (a) tensile strength (b) elongation at break (c) stiffness (d) Young's Modulus for the API-loaded nanocomposites*

Thus, the addition of API irrespective of their pKa values, into the PLA and PLA/HNT matrix does not show any significant difference ($p<0.05$) in the tensile strength, stiffness, and the Young's Modulus of the API-loaded nanocomposites. Patel et.al. reported a significant reduction in tensile strength with API-loaded HNT in PLA

matrix via electrospinning (Patel *et al.*, 2015). On contrary, the results from this study demonstrate that the addition of API with different pKa values retains the mechanical strength of the PLA and the PLA/HNT nanocomposites.

6.2.3. Differential Scanning Calorimetry

The secondary heating thermograms of the nanocomposites are shown in Fig 6.2 (a) and the thermograms of ASP and APAP are shown in Fig 6.2 (b). The glass transition temperature (T_g) of the nanocomposites was similar to the PLA and there was no significant change ($p>0.05$) with the addition of APIs as seen in Figure 6.2 (a). In comparison to PLA, the cold crystallization temperature (T_{cc}) significantly decreased ($p=0.03$) in PLA/HNT nanocomposites The APAP-loaded nanocomposites (P+APAP+H) displayed no significant change in the T_{cc} compared to PLA. Whereas, ASP-loaded nanocomposite (P+ASP+H) had a significant increase in the T_{cc} with very small or no peak. A similar result was found by Shi et.al. in their study by the addition of plasticizer into PLA matrix (Shi *et al.*, 2015). The control samples PLA+ASP and PLA+APAP did not show any changes in the T_g and T_{cc}.

There was a slight decrease of approximately 3 °C of the T_m of both PLA+ASP and PLA+APAP composites compared to PLA which was also seen by Lyons et. al. Othman et.al. and Campbell et. al. in their study (Lyons *et al.*, 2006; Campbell, Craig and Mcnally, 2008; Othman *et al.*, 2016). There was no significant change ($p>0.05$) in the melting temperature (T_m) with the addition of ASP or APAP in the PLA/HNT nanocomposite. The PLA/HNT nanocomposite displayed a twin melting peak which could be due to the heterogeneous nucleation by melting of imperfect crystals at a lower temperature (T_{m1}) followed by rearranging for an ordered structure at heating and melting at higher temperature (T_{m2}) (Dadras *et al.*, 2020). However, this was not displayed with the addition of either ASP or APAP to PLA/HNT nanocomposite.

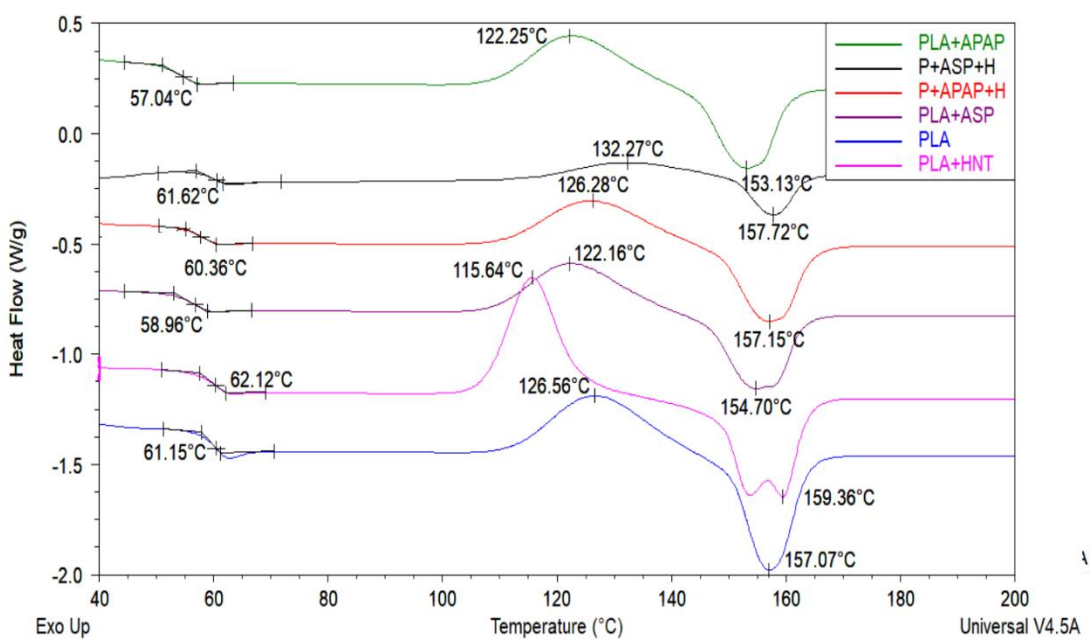

(a)

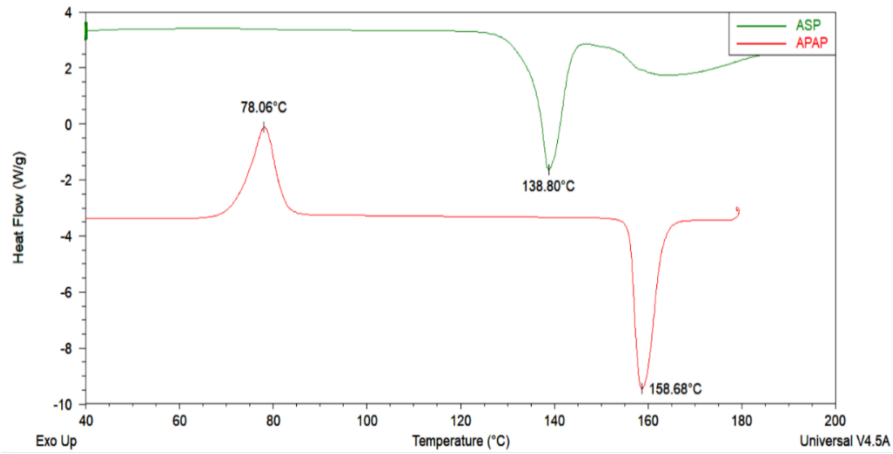

(b)

Figure 6.2. *DSC thermograms of (a) PLA, PLA-API loaded nanocomposites. The addition of APAP did not change the Tg and Tm of the polymer. The Tcc of the P+ASP+H had significantly increased due to the plasticizing effect of ASP in the system (b) ASP and APAP. The distinct peaks of ASP and APAP are evident.*

6.2.4. Fourier Transform Infrared (FTIR) Spectroscopy

The spectrum of PLA, PLA/HNT, and ASP-loaded PLA blends obtained from the FTIR are as shown in Fig. 6.3 (a). The characteristic peaks of PLA at 2995 cm^{-1}

attributing to CH stretch and 1750 cm^{-1} indicating –C=O carbonyl group, ASP at 1625 cm^{-1} attributing to the carboxyl group, 1751 cm^{-1} for C=O stretching vibration and –OH bending at 1454 cm^{-1} (Semalty *et al.*, 2010; Lun, Ouyang and Yang, 2014; Shahi *et al.*, 2018) and HNT at 3694 cm^{-1}, 3625 cm^{-1} (OH) are evident. The spectra of all the ASP-loaded PLA/HNT nanocomposite films were very similar to the PLA spectrum with no peaks of ASP observed.

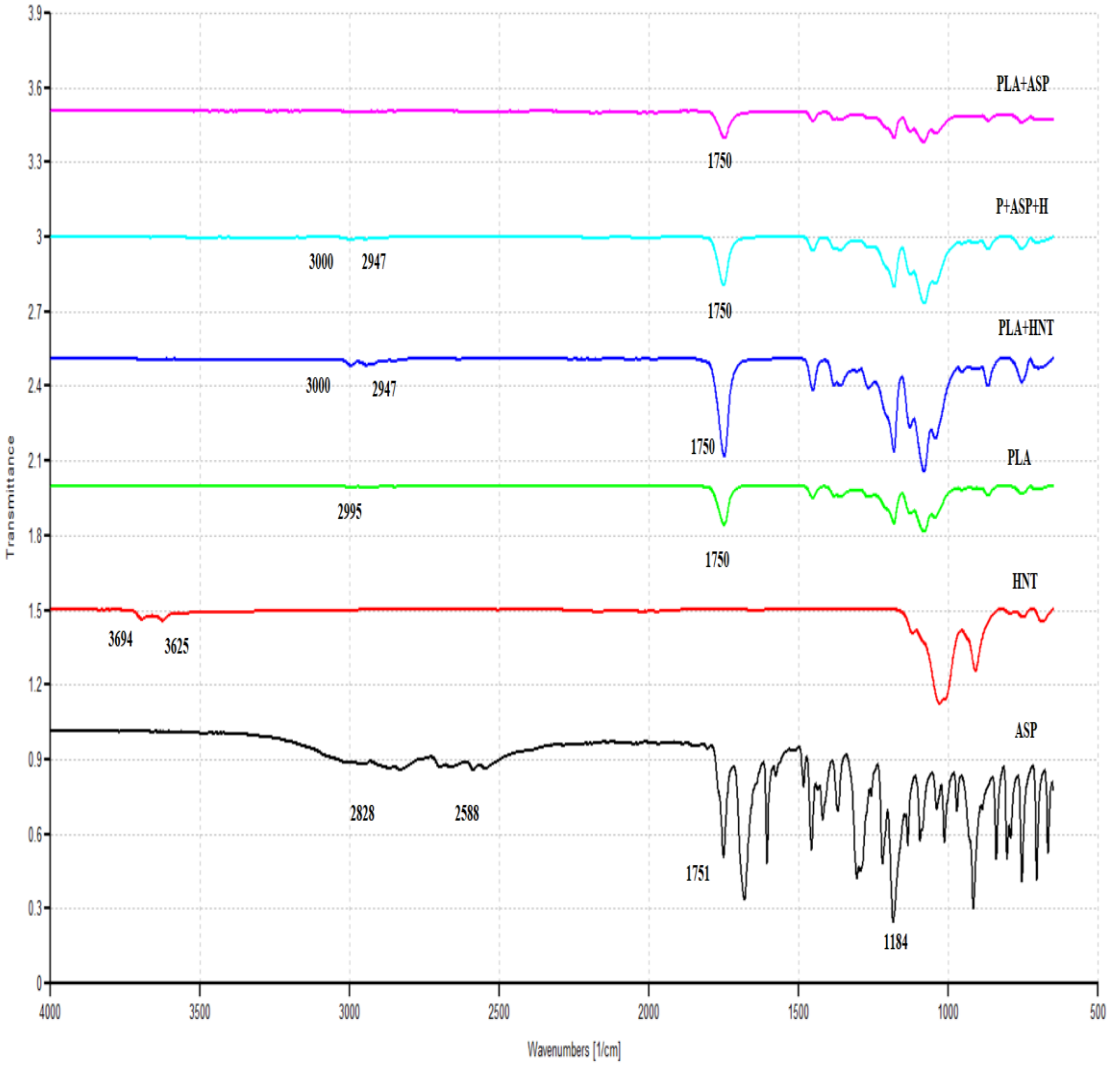

(a)

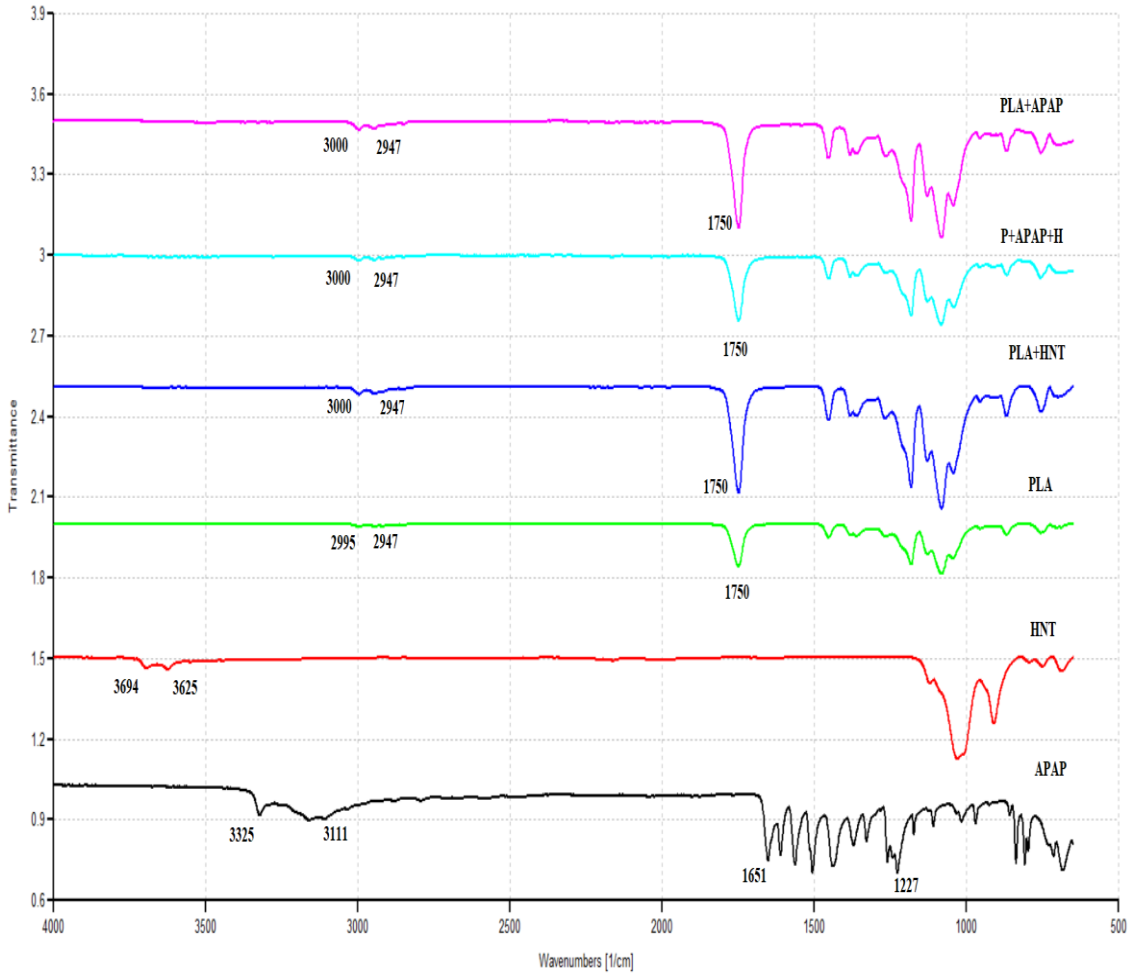

(b)

Figure 6.3. *FTIR spectra of (a) PLA, PLA/HNT, and PLA-ASP-loaded nanocomposites. (b) PLA, PLA/HNT, and PLA-APAP-loaded nanocomposites. There were no observed changes in the peaks of the nanocomposites and the peaks of ASP and APAP were not evident in the PLA nanocomposites.*

The spectrum of PLA, PLA/HNT, and APAP-loaded PLA blends obtained from the FTIR are as shown in Fig. 6.3 (b). The spectra of the APAP have the peak at 1227 cm^{-1} corresponds to the –OH plane and 1505 cm^{-1} correspond to $–CH_3$ vibration (Lawson, Ogwu and Tanna, 2018). The 3325 cm^{-1} and 3162 cm^{-1} in APAP spectra were due to the N-H amide group and the C-OH stretching group. The C-N stretching band was detected at 1220 cm^{-1} and the methyl (CH_3) group of APAP was characterized by vibration at 1432 cm^{-1} (Zaki, 2011). The addition of APAP in PLA and PLA/HNT sharpens and intensifies the characteristic peaks of PLA in both the composites, however, the intensity of the peaks is more evident in the PLA+APAP

composite. Similar results are seen in other studies (Zaki, 2011; Liu, Zhang and Zhou, 2013; Dong *et al.*, 2015b).

6.2.5 In-vitro drug release

The amount of API released from the lowest to the highest concentration is plotted against the time of release. The graphical representation of the amount of API release (Q%) versus time (t) shows linearity for both the drugs as seen in Figure 6.4. Thus, the drug release rate is independent of the concentration of the API. In this study, the release kinetics of ASP (aspirin) (Fig 6.4. (a)) and APAP (paracetamol) (Fig 6.4. (b)) showed the best fit for the zero-order model ($R^2 = 0.9995$) which represents a slow release of drug and is expressed by the equation $Q_t = Q_0 + K_0 t$ where Q_t is the amount of drug dissolved at time t, Q_0 is the initial amount of drug in the solution and K_0 is the zero-order release constant expressed in units of concentration/time. The data obtained from in vitro drug release studies were plotted as the cumulative amount of drug released versus time.

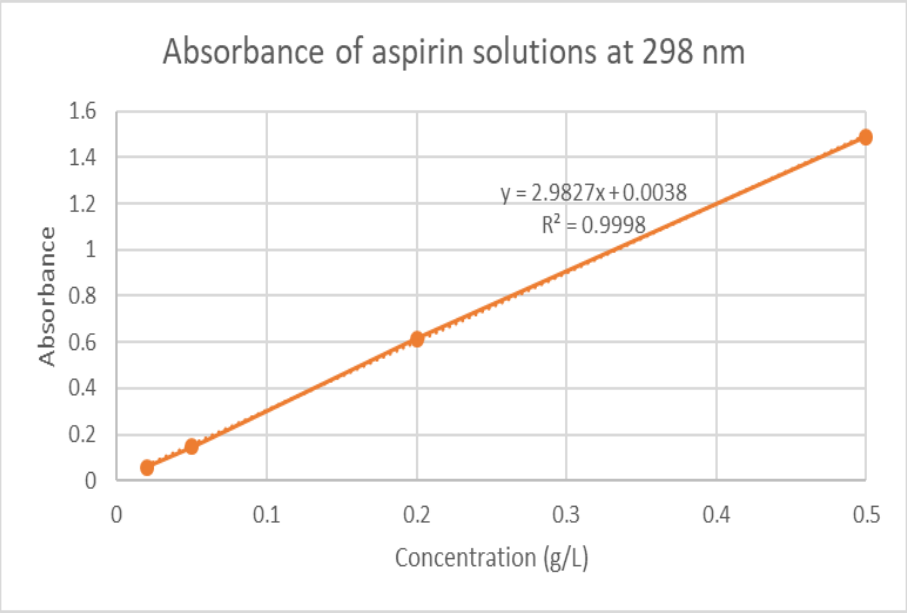

(a)

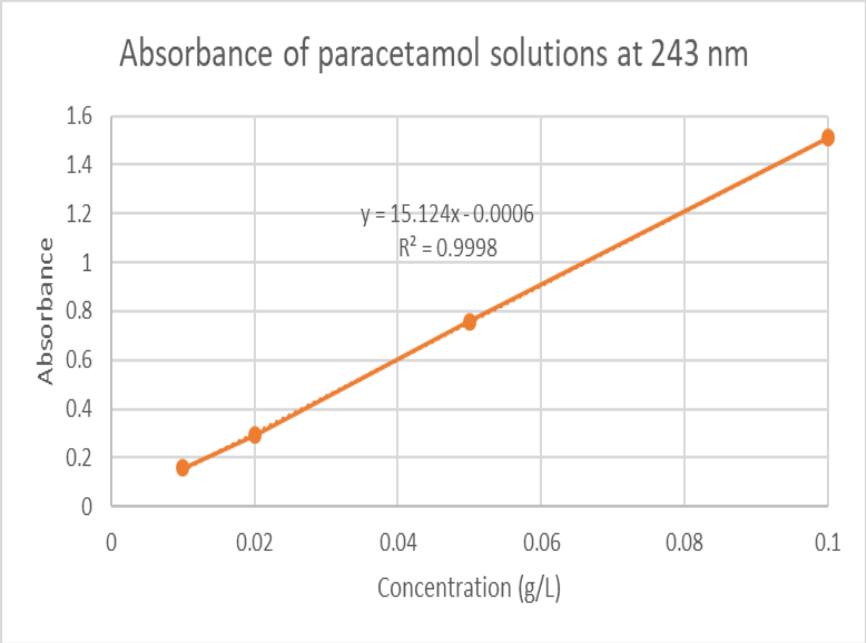

(b)

Figure 6.4. *Standard curve of API release for the lowest to the highest concentration of API (a) ASP (b) APAP.*

The cumulative drug release profiles of the P+ASP+H and P+APAP+H samples along with control samples PLA+ASP and PLA+APAP for 6 weeks are shown in Fig 6.5. Figure 6.5 (a) depicts the cumulative drug release percentage from the ASP-loaded control sample PLA and the nanocomposite PLA/HNT. The P+ASP+H exhibited a burst release of 6% in one day. This was followed by a slow release of 15% up to 2 weeks. There was a gradual increase to 36.9% by 3 weeks, 49.2% for 4 weeks, and showed a total release of 78.1% by 6 weeks. In the case of the control sample PLA+ASP, there was a significantly higher burst release of 42.2% on day one. This was followed by a slow release of 51.2% up to 2 weeks. There was a gradual increase to 65.4% by 3 weeks, 76.8% by 4 weeks, and had a total release of 89.4% by 6 weeks.

The cumulative drug release profile of APAP-loaded nanocomposites is shown in Figure 6.5 (b). The P+APAP+H exhibited a burst release of 4% within day one. This was followed by a lag phase up to 1 week with a gradual increase to 10.4% up to 2 weeks. Further, it had 16% release by 3 weeks, 21.5% release by 4 weeks with a total of 36.5% release by 6 weeks. For PLA+APAP samples, there was a higher burst release of 20.1% within day one which was followed by a lag phase up to 2 weeks with

a cumulative release of 26.8%. Further, it had 32.5% release by 3 weeks, 36.8% release by 4 weeks with a total of 45.8% release by 6 weeks.

The cumulative drug release of all the samples is shown together for comparison in Figure 6.5 (c). The control sample PLA+ASP and PLA+APAP exhibited a higher percentage of initial burst release. Around 42.2% and 20.1% of ASP and APAP respectively were released from the PLA matrix within the first day. There was a lag phase up to 2 weeks and by 6 weeks, a total of 89.4% and 45.8% of the ASP and APAP respectively was released from the control samples. Conversely, the API-loaded PLA/HNT nanocomposite exhibited only 6% and 4% of ASP and APAP release respectively on day one. A plateau was reached until 2 weeks followed by a gradual increase in release, with a total release of 78.1% and 36.4% for P+ASP+H and P+APAP+H respectively.

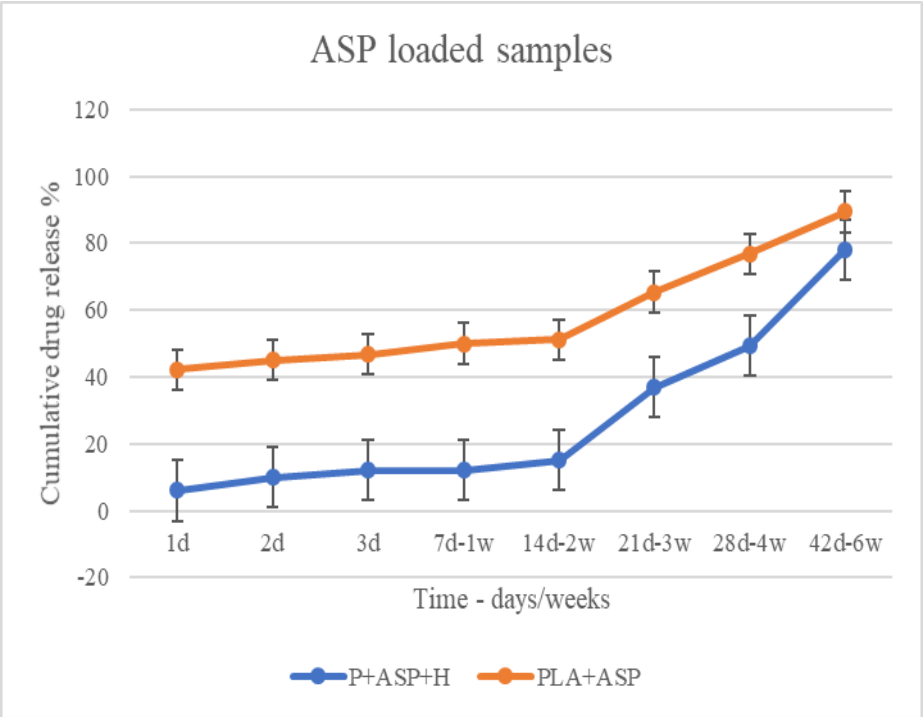

(a)

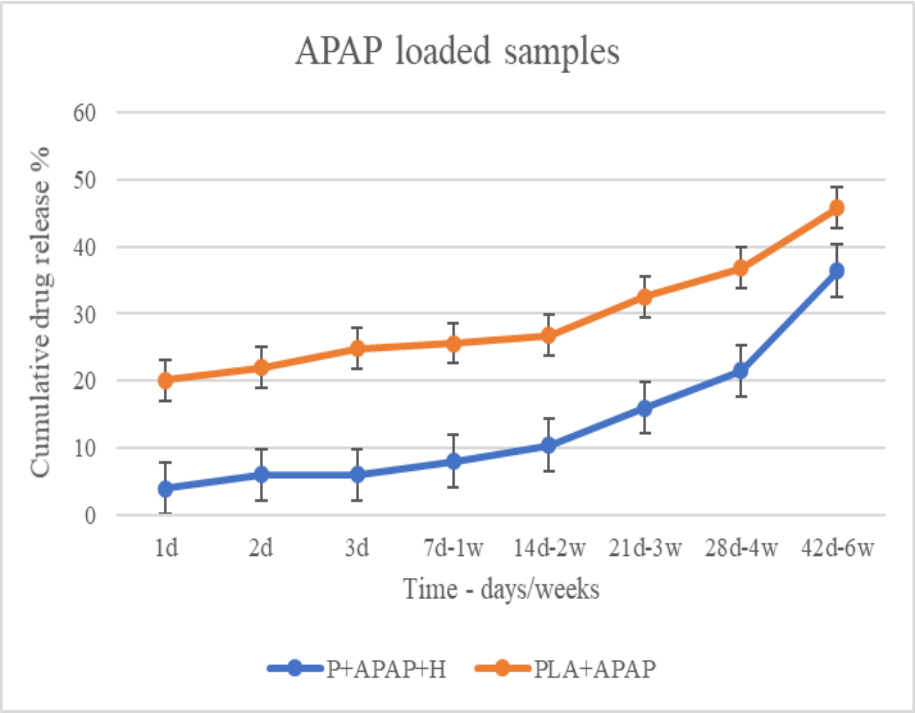

(b)

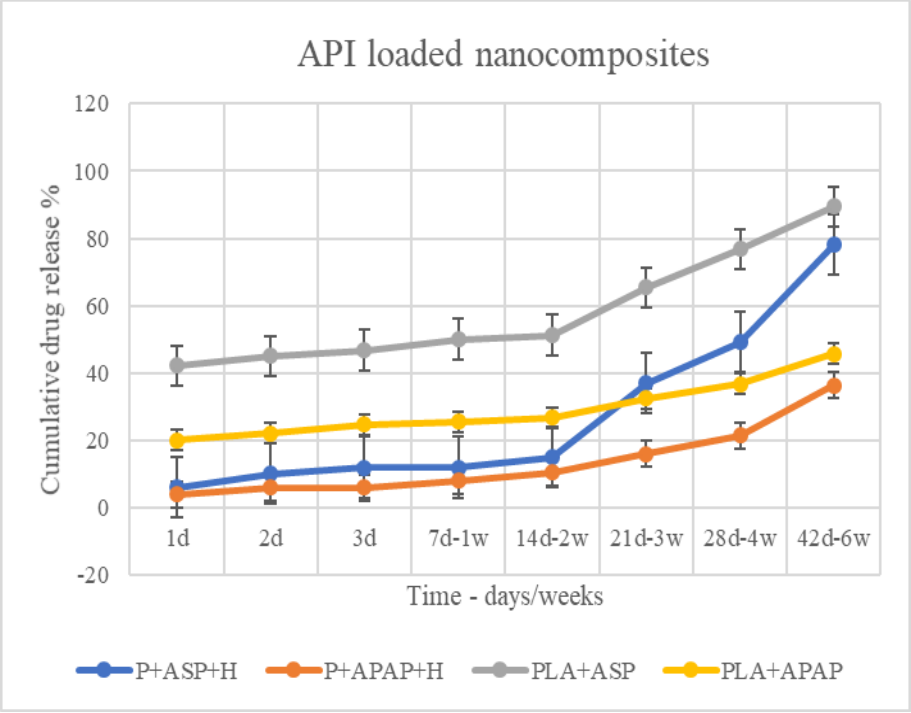

(c)

Figure 6.5. *The cumulative drug release of the API-loaded nanocomposites for 6 weeks.*

6.2.7 In-vitro degradation study

The mass reduction of the samples was studied for 32 weeks duration. The weight loss profiles for the ASP-loaded composites along with PLA and PLA/HNT composites are as shown in Figure. 6.6. No significant weight reduction was observed until 8 weeks for all samples. By the 14th week, the gradual reduction began, and by the end of the 14th, 20^{th,} and 32nd week

- 1.2, 1.5, and 4.7% for PLA and 0.83, 1.62, and 8.1% for PLA/HNT composites respectively reduced in weight.
- The ASP-loaded samples P+ASP+H had 10.2, 25.6, and 85.9% and PLA+ASP had 18.6, 34.06, and 94.1% reduction.

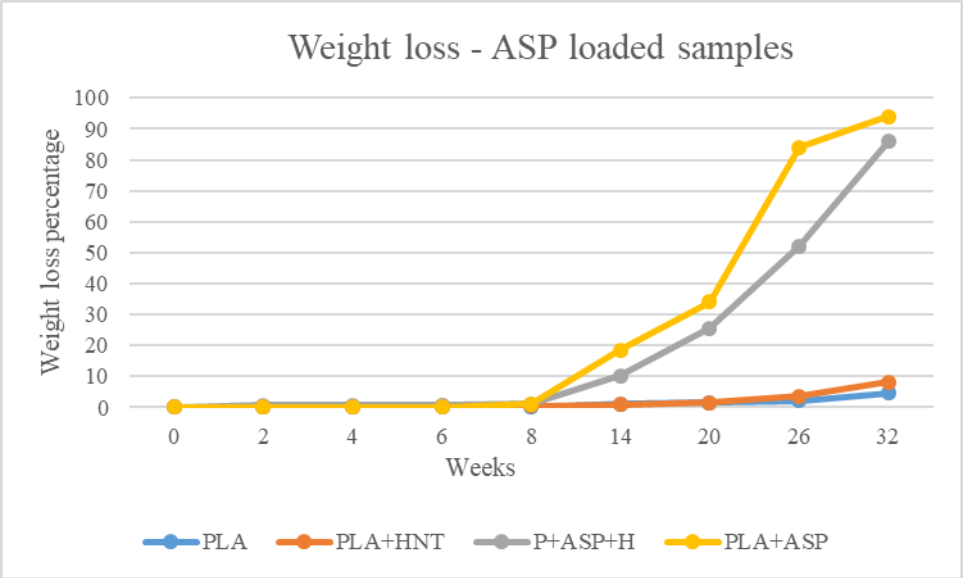

***Figure 6.6**. Weight loss percentage of PLA, PLA-API loaded nanocomposites for 32 weeks*

Thus, the weight loss of all the samples began only after 8 weeks. However, the weight loss for the PLA and PLA/HNT was not significant when compared to the ASP-loaded samples. Gradual reduction of the weight loss could be seen for all the samples after the 14th week, however, the weight loss was significantly higher for P+ASP+H and PLA+ASP with a total of 85.9% and 94.1% reduction respectively by the 32nd week.

The weight loss profiles for the APAP-loaded composites along with PLA and PLA/HNT composites are as shown in Figure. 6.7. No significant weight reduction

was observed until 8 weeks for all samples. By the 14th week, the gradual reduction began, and by the end of the 14th, 20^{th,} and 32nd week

- 1.2, 1.5, and 4.7% for PLA and 0.83, 1.62, and 8.1% for PLA/HNT composites respectively reduced in weight.
- The APAP loaded samples had 2.1, 12.5, and 32.5% weight reduction for P+APAP+H and 0.76, 7.57, and 39.4% reduction for PLA+APAP.

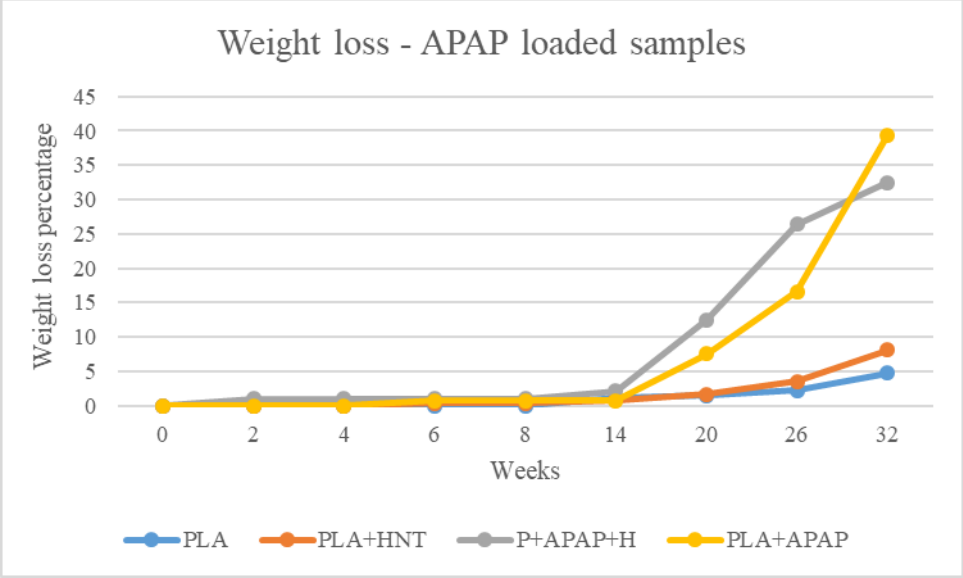

Figure 6.7*. Weight loss percentage of PLA, PLA-API loaded nanocomposites for 32 weeks.*

Thus, the weight loss of all the samples began only after 8 weeks. However, the weight loss for the PLA and PLA/HNT was not significant when compared to the APAP-loaded samples. Gradual reduction of the weight loss could be seen for all the samples after the 14th week, however, the weight loss was significantly higher for P+APAP+H and PLA+APAP with a total of 32.5% and 39.4% reduction respectively by the 32nd week.

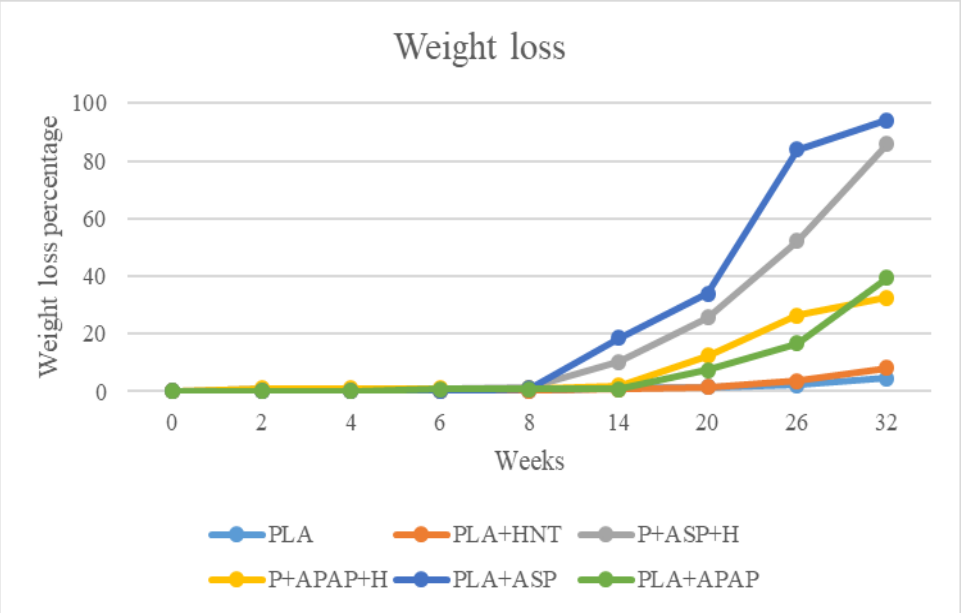

***Figure 6.8**. Weight loss percentage of PLA, PLA-API loaded nanocomposites for 32 weeks.*

The API-loaded samples together along with PLA and PLA/HNT composites are compared together in Figure 6.8. All the ASP and the APAP-loaded PLA/HNT composites and the control samples of PLA+ASP and PLA+APAP had the highest weight loss percentage compared to PLA and PLA/HNT nanocomposites.

The mechanical properties of the PLA, PLA+HNT, and PLA+API loaded samples during the degradation study are shown in Fig. 6.9. The tensile strength of the nanocomposites is as shown in Figure 6.8 (a). There is a gradual decrease in the tensile strength of 63.07% for PLA, 25.27% for PLA/HNT, 61.45% for P+ASP+H, and 42.09% for P+APAP+H from 0 to 20th week. Whereas, PLA+ASP and PLA+APAP had 78.7% and 80.7% reduction in tensile strength by the 20th week. By the 32nd week, the PLA+ASP and PLA+APAP were degraded with a 99.9% reduction. In the case of P+ASP+H and P+APAP+H, there was a 99% and 82.87% reduction respectively.

The elongation at break for the samples is as shown in Figure 6.9 (b). The percentage strain for PLA and PLA/HNT reduces from 6.15% and 6.25% respectively at 0 weeks to 2.36% and 4.4% by the 20th week and further reduces to 0.9% and 2.7% respectively by the 32nd week. In the case of P+ASP+H and P+APAP+H composites, the percentage strain reduces from 9.19% and 8.38% respectively for 0 weeks to 4.62% and 5.64% by the 20th week and further to 0.24% and 3.78% at the end of the 32nd week. However, the control samples, PLA+ASP and PLA+APAP show a drastic

reduction from 7.94% and 10.44% respectively at 0 weeks to 2.1% and 3.56% by the 20th week and further to 0.4% indicating degradation.

The stiffness of the composites is shown in Figure 6.9 (c). The stiffness for PLA is reduced to 302.27 kN/m from 403.25 kN/m by the 20th week and to 163.78 kN/m by the 32nd week. PLA/HNT reduces from 390.1 kN/m to 330 kN/m for 0 to 20th week respectively and further to 274.98 kN/m. The control samples PLA+ASP and PLA+APAP reduce in stiffness from 390.48 kN/m and 426.05 kN/m for 0 weeks to 243.56 kN/m and 199.5 kN/m for 20th week respectively and significant further decrease to 10 kN/m and 56.77 kN/m respectively. In the case of P+ASP+H and P+APAP+H, the stiffness of 423 kN/m and 417 kN/m respectively for 0 weeks reduces to 254.2 kN/m and 330.5 kN/m for 20th week and 10 kN/m, 210 kN/m respectively for the 32nd week.

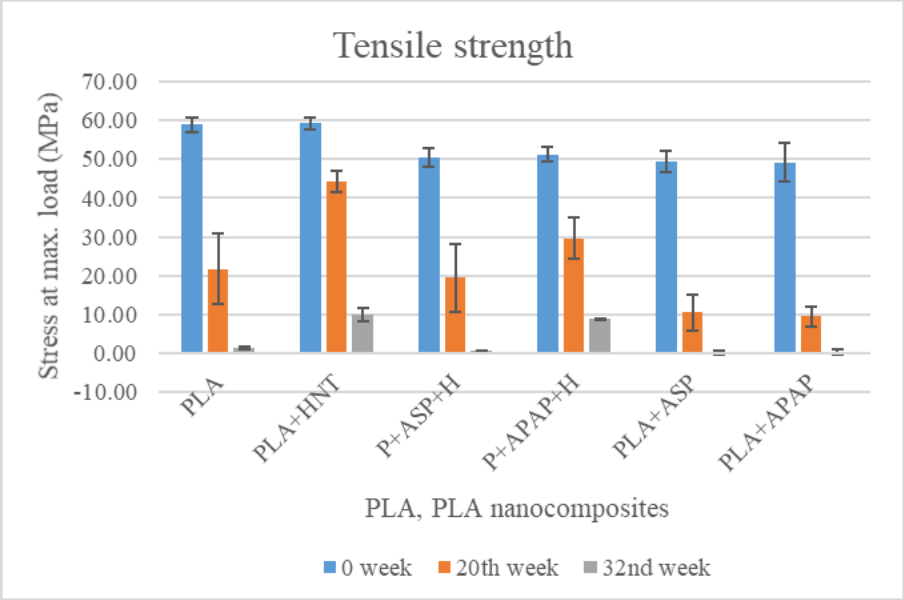

(a)

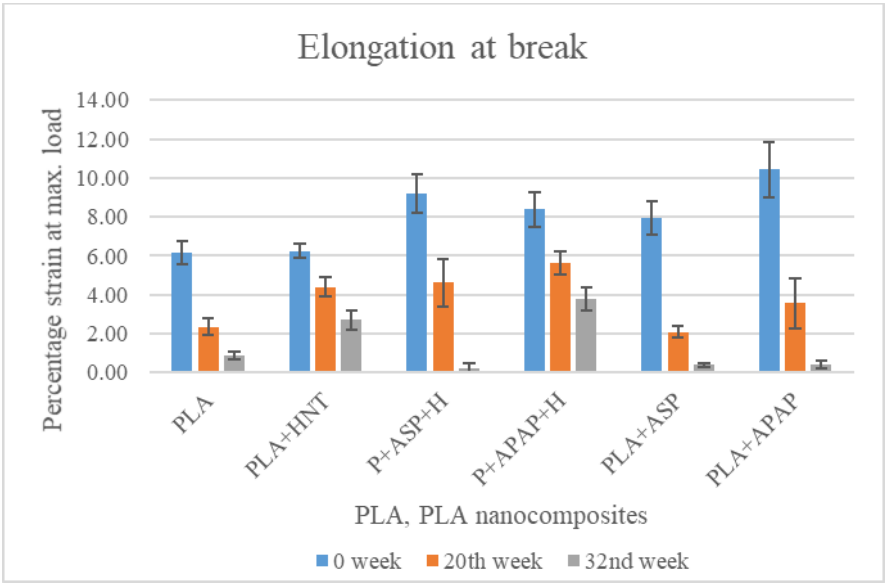
Elongation at break
Percentage strain at max. load
14.00
12.00
10.00
8.00
6.00
4.00
2.00
0.00
PLA
PLA+HNT
P+ASP+H
P+APAP+H
PLA+ASP
PLA+APAP
PLA, PLA nanocomposites
0 week
20th week
32nd week

(b)

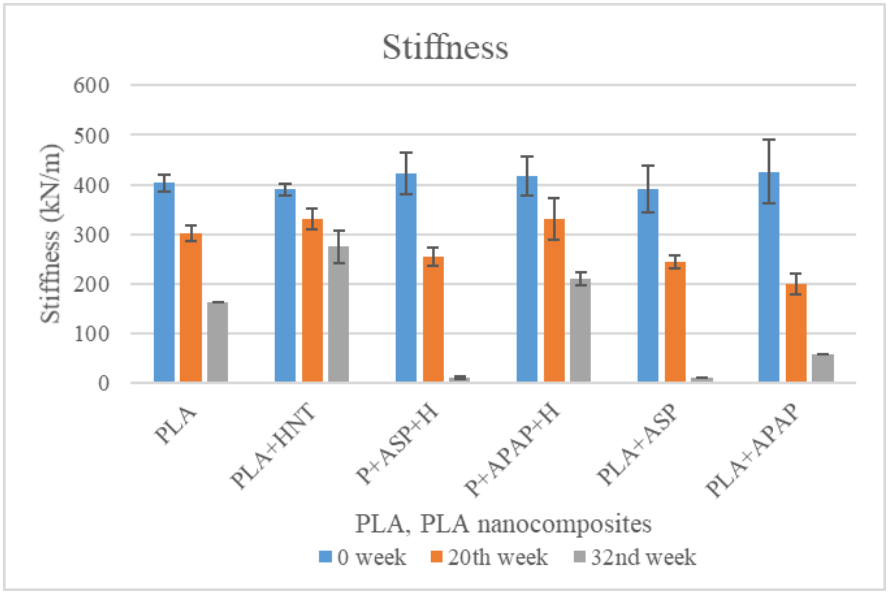
Stiffness
Stiffness (kN/m)
600
500
400
300
200
100
0
PLA
PLA+HNT
P+ASP+H
P+APAP+H
PLA+ASP
PLA+APAP
PLA, PLA nanocomposites
0 week
20th week
32nd week

(c)

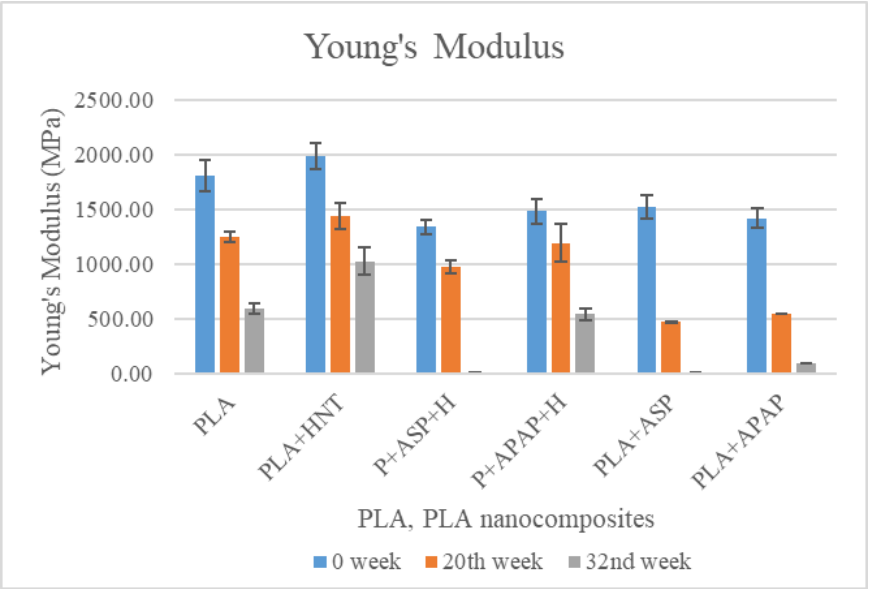

(d)

Figure 6.9. *Graphical representation of mechanical properties during the in-vitro degradation study of PLA, PLA+HNT, and PLA+API loaded nanocomposites for (a) tensile strength (b) elongation at break (c) stiffness (d) Young's modulus*

In terms of Young's Modulus as shown in Figure 6.9 (d), there is a 30.99% and 27.52% reduction from 0 to 20th week for PLA and PLA/HNT respectively. This further reduces to 67.09% and 48.5% by 32nd week respectively. In the case of P+ASP+H and P+APAP+H, there was a 27.26% and 19.3% reduction by the 20th week respectively and by the 32nd week, 99.25% and 63.37% respectively. In the case of control samples, there was a 69.04% and 61.25% reduction for PLA+ASP and PLA+APAP respectively by the 20th week and a 99.9% reduction for both by the 32nd week.

The control samples PLA+ASP and PLA+APAP displayed a drastic reduction in tensile strength, elongation at break, and Young's Modulus by 20th week and up to 99% reduction by 32nd week. Comparatively, the API-loaded samples P+ASP+H and P+APAP+H had a gradual degradation, however, by the 32nd week, there was a significant reduction for P+ASP+H. The P+APAP+H had 17.13% of tensile strength and 36.63% of Young's Modulus retained by the end of the 32nd week. Thus, the P+APAP+H samples retained the tensile strength, elongation at break, and Young's Modulus significantly higher than P+ASP+H samples.

The degradation profile in terms of ASP and APAP influence, the ASP-loaded samples had faster degradation both in PLA/HNT composites and in control sample PLA. The samples were hard to handle after the 20th week. The acidic nature of ASP could have led to faster degradation through bulk erosion of the core of the PLA matrix. Similar results were seen in other studies as well (Siegel *et al.*, 2006)

The DSC results from the degradation study are as shown in Fig. 6.10 and Table 6.2 for the PLA, PLA/HNT, and PLA-API-loaded nanocomposites. In Fig. 6.10 (a) which displays the thermograms of the samples in the 20th week, there is a gradual and consistent reduction in the T_g, $T_{cc,}$ and the T_m of PLA and PLA/HNT nanocomposites from 0 weeks as also seen in Table 6.2. By the 32nd week, there was a further reduction. The T_m of PLA displayed two melting peaks for 20th and 32nd week during degradation. The PLA/HNT continued to display two melting peaks with a reduction of temperature for the first melting peak for the 20th and 32nd weeks.

The ASP-loaded composites displayed a significant reduction in T_g, $T_{cc,}$ and the T_m by the 20th week for both control samples PLA+ASP and P+ASP+H. By the 32nd week, they were degraded as seen in Figure 6.10 (b) with no curve. The faster degradation of P+ASP+H and PLA+ASP samples evident in weight loss and mechanical results correlates to the DSC results as well with no curve for T_g, $T_{cc,}$ and the T_m. Whereas in the case of APAP loaded samples, P+APAP+H samples had a gradual decrease trend in T_g, $T_{cc,}$ and the T_m from 0 to 20th and 32nd week. However, for PLA+APAP, there was a significant reduction in T_g, $T_{cc,}$ and the T_m for the 20th week and further reduction for the 32nd week which is in equivalence with mechanical and weight loss results.

Table 6.2. *Tabulated data for glass transition temperature (T_g), cold crystallization temperature (T_{cc}), and melting temperature (T_{m1} and T_{m2}) of the PLA and PLA nanocomposites for 0, 20^{th,} and 32nd week.*

Batch	T_g			T_{cc}			T_m		
	0 week	20th week	32nd week	0 week	20th week	32nd week	0 week	20th week	32nd week
PLA	61.15	58.07	53.3	126.56	111.07	103.14	157.07	150.76, 159.05	145.17, 155.23
P+H	62.12	60.62	58.67	115.64	108.66	105.36	153.13, 159.36	151.57, 160.47	149.39, 158.48
P+ASP+H	61.62	54.96	0	132.27	102.96	0	157.72	146.74, 156.50	0
P+APAP+H	60.36	57.26	55.34	126.28	109.76	106.23	157.15	149.12, 157.80	146.83, 156.43
P+ASP	58.96	54.87	0	122.16	102.3	0	154.7	155.09	0
P+APAP	57.04	0	49.97	122.25	85.66	107.7	153.13	140.79	126.8, 137.48

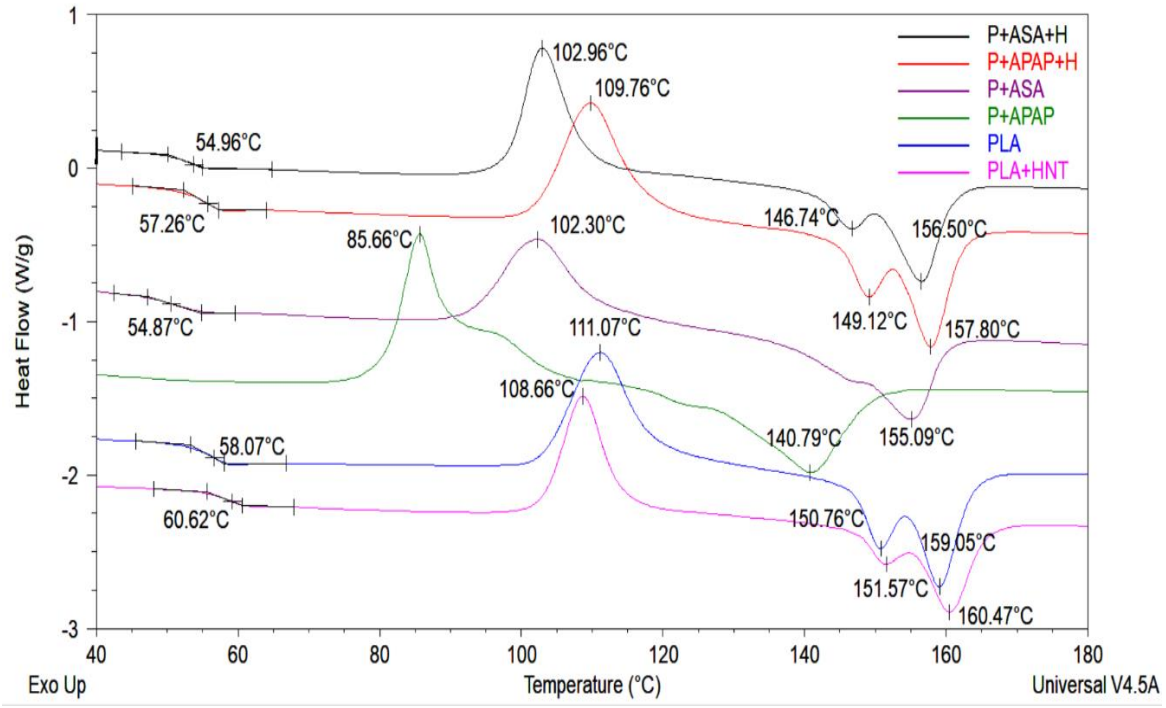

(a)

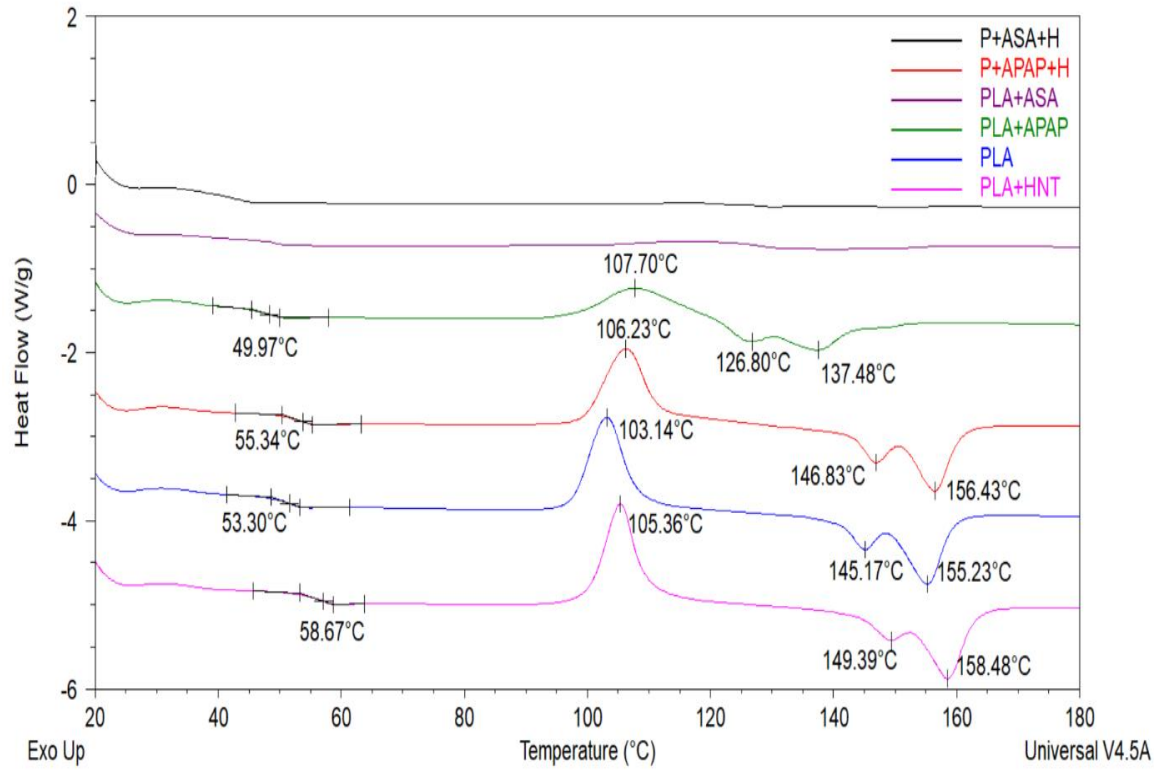

(b)

Figure 6.10. *DSC thermograms of (a) 20th week (b) 32nd week during the in-vitro degradation study*

The FTIR spectra for the PLA, PLA/HNT, and PLA+API composites during the degradation are shown in Fig 6.11. The FTIR spectra for the 20th week degradation of the composites are as shown in Figure 6.11 (a). The characteristic peaks of PLA were seen in all the samples. There was a shift in the peaks during the degradation for PLA+ASP and P+APAP+H from 1750 cm^{-1} to 1752 cm^{-1}and 1755 cm^{-1} in the 20th week. The intensity of the peaks is increased for P+ASP+H samples.

The FTIR spectra for the 32nd week are as shown in Figure 6.11 (b). The samples displayed the characteristic peaks of PLA with interesting shifts in several peaks and some with higher intensity. The 1750 cm^{-1} peak of PLA showed a shift to 1760 cm^{-1}, 1452 cm^{-1} of PLA shifts to 1454 cm^{-1} and 1457 cm^{-1} for the control samples PLA+ASP and PLA+APAP respectively.

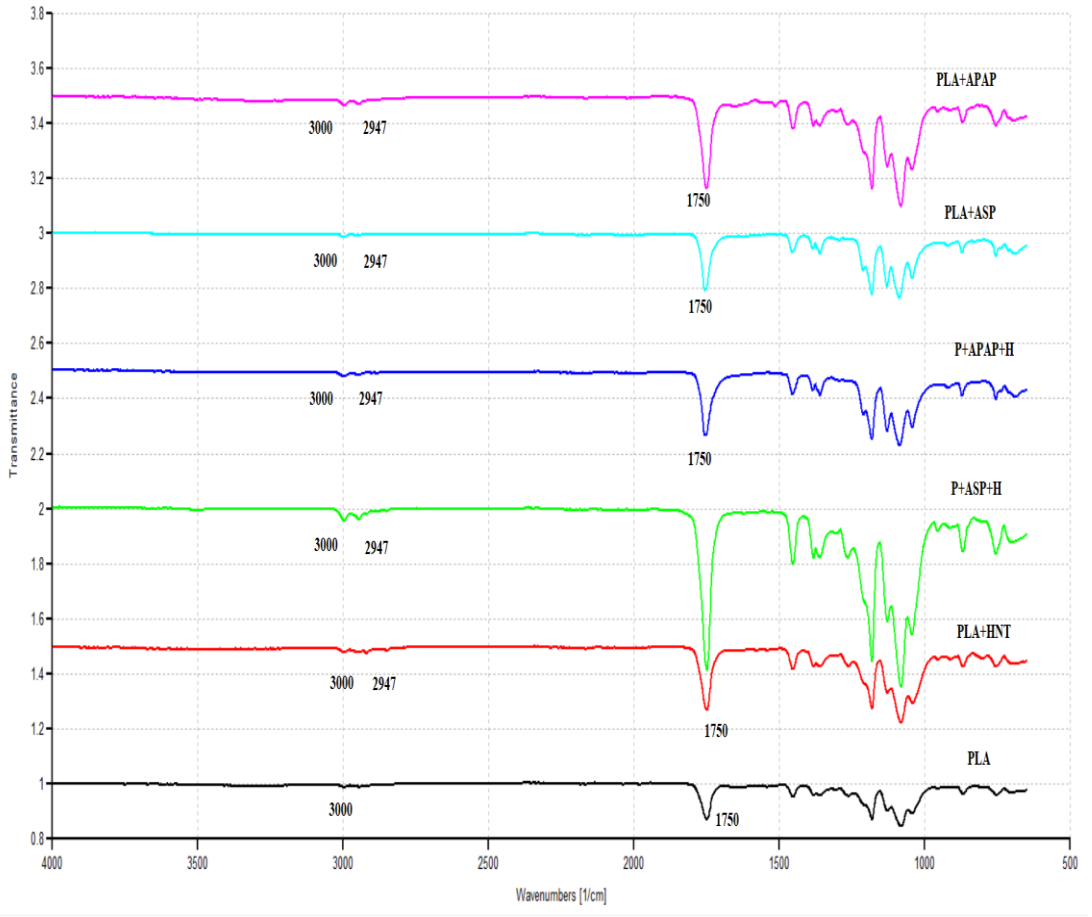

(a)

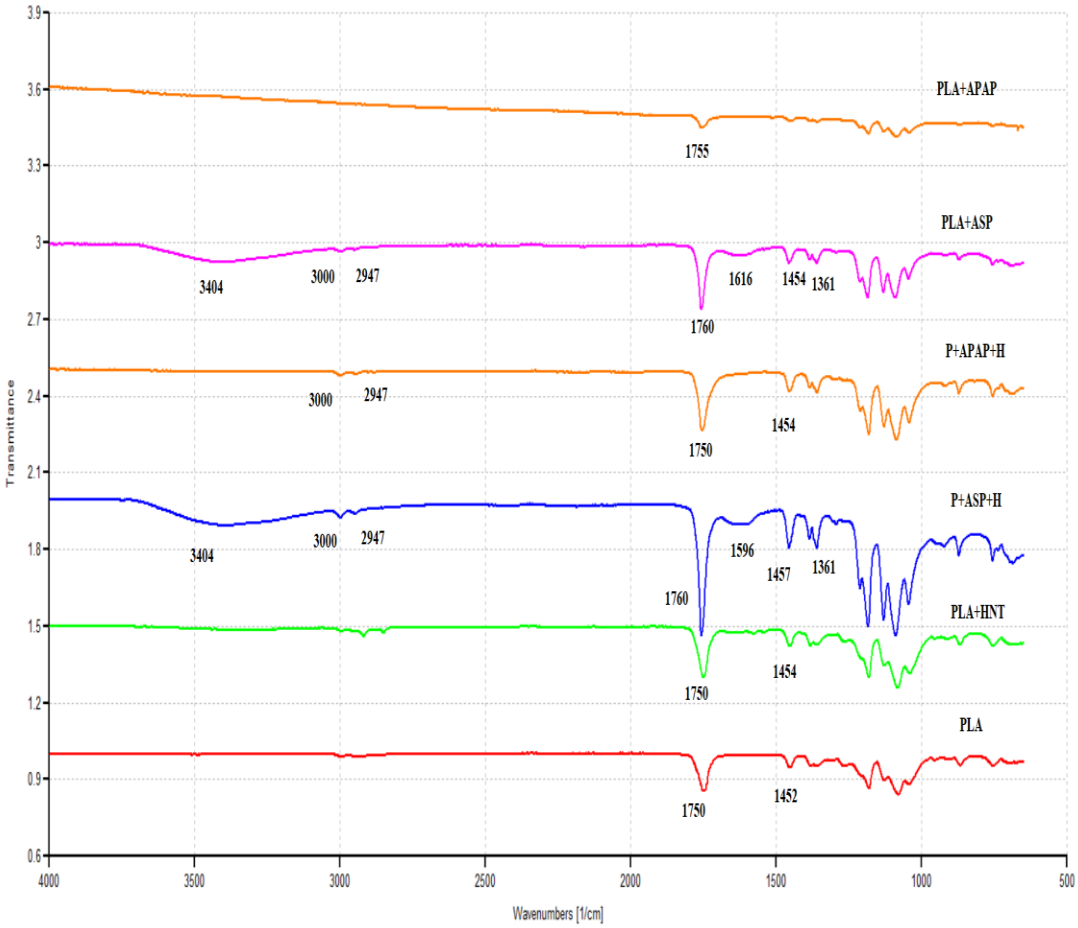

(b)

Figure 6.11. *FTIR spectra of PLA, PLA/HNT, and PLA-API loaded samples for (a) 20th week, (b) 32nd week during the in-vitro degradation study*

Correlating to the mechanical and DSC results, the degradation of ASP loaded samples displayed new peaks at 3404 cm^{-1} which can be attributed to the absorbed water and 1616 cm^{-1} (for PLA+ASP)/1596 cm^{-1} (for P+ASP+H) corresponding to the OH deformation (water), the characteristic peaks of water (Prete and Arnaldo, 2016). The ester bond of PLA did not change during the degradation process for APAP-loaded samples, evidenced by the unchanged carbonyl group C=O band at 1750 cm^{-1} and C-O band at 1000–1300 cm^{-1}. As ester group cleavage is the primary degradation mechanism of PLA (Chen *et al.*, 2018). However, the ASP-loaded samples had a higher intensity of C=O band along with a shift to 1760 cm^{-1} which indicates the degradation of PLA.

6.3 Discussion

The addition of API with different pKa values retains the mechanical strength of the PLA and the PLA/HNT nanocomposites. This could be due to the process of extrusion which would have induced HNT dispersion through melt shearing. The high value of Young's modulus and tensile strength are the key requirement of stent material to reduce the stent recoil and to increase radial strength (Beshchasna *et al.*, 2020). Even though there is a reduction in tensile strength of the API-loaded nanocomposite to ~50 MPa for all the API-loaded nanocomposites from ~ 60 MPa of PLA and PLA/HNT composites, and Young's Modulus of ~ 1500 MPa of API-loaded nanocomposites from ~ 2000 MPa of PLA and PLA/HNT composites, the tensile strength and Young's Modulus of the API-loaded nanocomposites are still in the similar range of the biodegradable polymers used as stent materials as per the literature (Ang, Huang, *et al.*, 2017; Lee *et al.*, 2018).

The addition of HNT, ASP, or APAP has a minimal effect on the rigidity of the PLA backbone chain as glass transition temperature is the measure of rigidity (Declan M. Devine *et al.*, 2017). This is in correlation with the mechanical analysis which shows no significant change in the stiffness. The negligible or no cold crystallization peak for ASP-loaded nanocomposite (P+ASP+H) indicates the increased mobility of the PLA chains and the advanced crystallization of the nucleating agents before cooling which correlates to the increase in elongation at break and decrease in the tensile strength (Shi *et al.*, 2015). A drop in approximately 3 °C of the T_m of both PLA+ASP and PLA+APAP composites compared to PLA could indicate the plasticizing effect of both ASP and APAP in PLA matrix as also seen by Lyons et. al. and Campbell et. al. in their study (Lyons *et al.*, 2006; Campbell, Craig and Mcnally, 2008). This shift to lower temperature could also indicate that APAP was in an amorphous or disordered crystalline phase in the PLA matrix as observed in a study by Othman et.al. (Othman *et al.*, 2016). This observation was not seen in PLA/HNT API loaded samples and this could be due to the presence of HNT. The characteristic melting peak of ASP or APAP as shown in Figure 6.2 (b) did not appear in the DSC thermograms of drug-loaded nanocomposites. This could indicate the loading of the APIs inside the cavity of the HNT (Gao *et al.*, 2017) or the dispersion of the drug as

the amorphous state due to the drug-clay or drug –polymer interactions (Bounabi *et al.*, 2016).

The spectra of all the ASP-loaded PLA/HNT nanocomposite films were very similar to the PLA spectrum with no peaks of ASP observed. This could be due to the insensitivity of the FTIR technique or factually, the vibration bands of ASP or HNT could be overlapping with PLA bands (Qi *et al.*, 2010). The addition of APAP in PLA and PLA/HNT sharpens and intensifies the characteristic peaks of PLA in both the composites, however, the intensity of the peaks is more evident in the PLA+APAP composite. The intensity confirms the presence of APAP in the matrix with no evidence of hydrogen bonding as there is no shift in the peaks. Similar results are seen in other studies (Zaki, 2011; Dong *et al.*, 2015b).

A typical drug release profile was observed for all the samples with an initial burst release followed by a plateau or a lag phase and a gradual increase of release after the lag phase. The control sample PLA+ASP and PLA+APAP exhibited a higher percentage of initial burst release. This could be due to the higher concentration of the drug or the dispersion of drug molecules closer to the surface without even loose bonding to the surface (Devine, Geever and Higginbotham, 2005; Pierchala *et al.*, 2018). A plateau was reached until 2 weeks with a gradual increase in release thereafter. By 6 weeks, ASP exhibited a higher total release and higher initial burst release. Balogh et. al. also found an ultrafast ASP release from Polyvinylpyrrolidone-ASP (PVPK30-ASP) nanofibers and they attributed it to the increased solubility of the amorphous form of ASP which was per their DSC result which did not find the melting peak of the ASP in the PVPK30-ASP nanofiber evidencing the amorphous state of the drug (Balogh *et al.*, 2018). This correlates to our study where the melting peaks of ASP were absent in the PLA and PLA/HNT composites and the release rate was fast.

According to literature, the drug substances with pKa above 11 or acidic with pKa below 1 are known for better dissolution as they remain ionized throughout the physiological pH range. However, when the pH values are higher than the pKa of a weak acid and lower than the pKa of a weak base (4.5-9.5), the solubility of the API significantly increases via the ionization process (Manallack *et al.*, 2013; Acharya *et al.*, 2018). Devine et. al. observed that at pH 9, the ASP released faster than at pH 2 due to the ionization of carboxylic acid groups of ASP at a pH value higher than the

pKa of ASP. They observed with the addition of acrylic acid, the hydrogen bonding was obtainable at pH below the pKa of ASP, and at pH above the pKa of ASP, the carboxylic acid groups were ionized (Devine *et al.*, 2006).

Miyajima et. al. studied the effect of the drug properties on PLGA and PLLA in separate studies and reported that acidic drugs released faster than basic drugs attributing it to the higher solubility of the acidic drug (Miyajima, Koshika, Jun Okada, *et al.*, 1998; Miyajima, Koshika, Jun'Ichi Okada, *et al.*, 1998; Miyajima *et al.*, 1999a, 1999b). Similarly in this study too, ASP could be ionized and increased solubility which led to the faster release from the control samples of PLA matrix as well from PLA/HNT composite. The ASP located in the hydrated amorphous regions on the polymer could have ionized speedily in turn increases the acidity inside the matrix which could have led to the faster release (Tang and Singh, 2008). Whereas, the APAP had a high burst release only from the control sample of PLA matrix due to the dispersion of drug molecules closer to the surface without even loosely bound to the surface. And the total amount released was lesser than ASP as they might be unionized compared to the extent of ASP. Cui et al. also found an initial burst release and a plateau for 2 weeks of paracetamol from casting polymer films similar to our results with APAP-loaded PLA (Cui *et al.*, 2006).

Conversely, the API-loaded PLA/HNT nanocomposite exhibited only 6% and 4% of ASP and APAP release respectively on day one. A plateau was reached until 2 weeks followed by a gradual increase in the release, with a total release of 78.1% and 36.4% for P+ASP+H and P+APAP+H respectively. Thus, the API-loaded PLA/HNT composites demonstrated a sustained release. A similar release profile of high burst release of model drug tetracycline hydrochloride (TCH) from control sample TCH/PLGA of around 83.8% release within day one and a sustained release from HNT/PLGA composite in PBS (pH-7.4) was found in a study by Qi et.al. (Qi *et al.*, 2013). They found about 77.6% and 68.5% of total release from PLGA/HNT composites at the end of 6 weeks. Lyons et al. studied the release rate of API with the incorporation of agar as a filler in the polymer matrix and found a reduction in the release rate of API in an acidic dissolution medium of pH 1.2. The increase in dissolution time was in proportion to the amount of filler (Lyons *et al.*, 2006). Campbell et al. also observed similar sustained-release of paracetamol loading into PEG/modified MMT by hot-melt extrusion compared to the release from PEG in

dissolution medium of distilled water. They observed the retardance of liquid penetration and dissolution of paracetamol with the presence of nanoclays and the time to release paracetamol increased as the nanoclay content increased (Campbell, Craig and Mcnally, 2008). Othman et. al. report the initial fast and higher total release of paracetamol from PLA nanoparticles (NPs) compared to the reduced rate of drug release from nanoclay-loaded PLA NPs. They attribute it to the hindrances in the path of drug molecules by the non-permeable clay molecules dispersed in the PLA matrix (Othman *et al.*, 2016). Thus, the reduced burst release of both ASP and APAP from PLA/HNT matrix could be due to relatively more uniform drug mixing and the dispersion of HNT in the matrix which could have led to the loading of some of the drug onto HNT and the movement of the rest could be hindered by the presence of HNT (Siegel *et al.*, 2006; Othman *et al.*, 2016).

In our results, APAP-loaded PLA/HNT nanocomposites displayed a better-sustained release. This could be because APAP may be loaded onto HNT in the PLA matrix and has to be released from the HNT firstly to the PLA matrix and later from the PLA (Qi *et al.*, 2013). Whereas, the ASP-loaded nanocomposites displayed a higher release amount. A similar result was obtained by Li et. al. from the prepared HNT-chitosan microsphere where, the model drug ASP had a faster release rate and higher release from a dissolution medium of higher pH (6.6) when compared to its lower release amount from the medium of low pH (1.2) (Li *et al.*, 2016). It is also evaluated that, in acidic conditions, HNT leaches out exchangeable cations and there is weak interactions with the drug leading to the faster drug release (Wang *et al.*, 2014; Carazo *et al.*, 2019) which could be the case with ASP in this study due to the acetic acid in ASP couldn't interact or load onto HNT during diffusion. This could in turn indicate the APAP molecules were able to interact with the outer negative siloxane group of HNT or were loaded in the inner lumen.

Thus, in comparison to the control samples, the presence of HNT aids the significant advantageous reduction in burst release after day one as higher initial burst release could lead to initial toxicity associated with a high dose (Nazila *et al.*, 2016) and in coronary artery disease, it could have unfavorable effects such as arterial aneurysms and delayed endothelialization (F. Li *et al.*, 2018). In terms of the drug release profile of the commercial stents, we see most of them use drug-eluting polymeric coating (Beshchasna *et al.*, 2020). Here, we have evaluated the stent

material itself as the drug carrier. XINSORB (HuaAn Biotechnology, China) is a PLLA scaffold coated with sirolimus-eluting PDLLA which releases 80% of sirolimus within 28 days (Kawashima *et al.*, 2020), and several others elute 100% of the drug within 4 weeks (Beshchasna *et al.*, 2020).

In a study by Zhao et al., sirolimus-loaded PDLLA nanoparticles were studied as a coating on PLLA stents. They reported a drug release of 20% within a day and reached 40% by 20 days for 5% Sirolimus in PDLLA (Zhao *et al.*, 2016). With pKa values of sirolimus (9.96) similar to APAP (9.6), APAP had a similar release from the PLA matrix in our study. However, from P+APAP+H, APAP released only 4% within one day and had 36% total release, which could be due to the presence of HNT and the possibility of APAP loading onto HNT's inner lumen. The remaining amount must have been released through the degradation mechanism.

The degradation rate of polymers depends on several factors. One such factor would be the addition of drugs or plasticizers. Thus, the faster degradation of ASP loaded nanocomposite could be due to the acidic compound of the ASP or it could have acted as a plasticizer elevating the degradation process as we see from the above DSC results as well, as plasticizer helps water diffusion or water uptake faster for faster degradation (Casalini *et al.*, 2019). The ASP release rate and the polymer degradation could be due to the hydrophilicity of the ASP which increases the water absorption into the polymer matrix as also seen by Siegel et. al. who saw the highest rate of diffusion and degradation for hydrophilic drugs, ASP from PLGA matrix in their study (Siegel *et al.*, 2006). Tang et.al. also found similar results in their PLGA based phase-sensitive in situ gel-forming delivery system using ASP. The acidic property of the ASP could also be the reason for the degradation of the polymer as the ASP located in the hydrated amorphous regions on the polymer could have ionized speedily in turn increases the acidity inside the matrix which could have led to the faster degradation (Tang and Singh, 2008).

The degradation of APAP-loaded samples had a gradual increase in weight loss comparatively lower than ASP-loaded samples, which could be due to neutralization of the basic compound in APAP by carboxyl end groups and progressed the degradation through base catalysis (Alexis, 2005; Casalini *et al.*, 2019). In comparison to PLA and PLA/HNT nanocomposite, faster degradation is evident in API-loaded

samples. As seen in Figure 6.12 the changes on the surface and scaling on the surface of the samples is profound for PLA+ASP and PLA+APAP in Figure 6.12 (f) and (e) respectively. Whereas the samples P+ASP+H and P+APAP+H in Figure 6.12 (c) and (d) show slight changes and chipping of the surface when compared to PLA and PLA/HNT samples in Figure 6.12 (a) and (b).

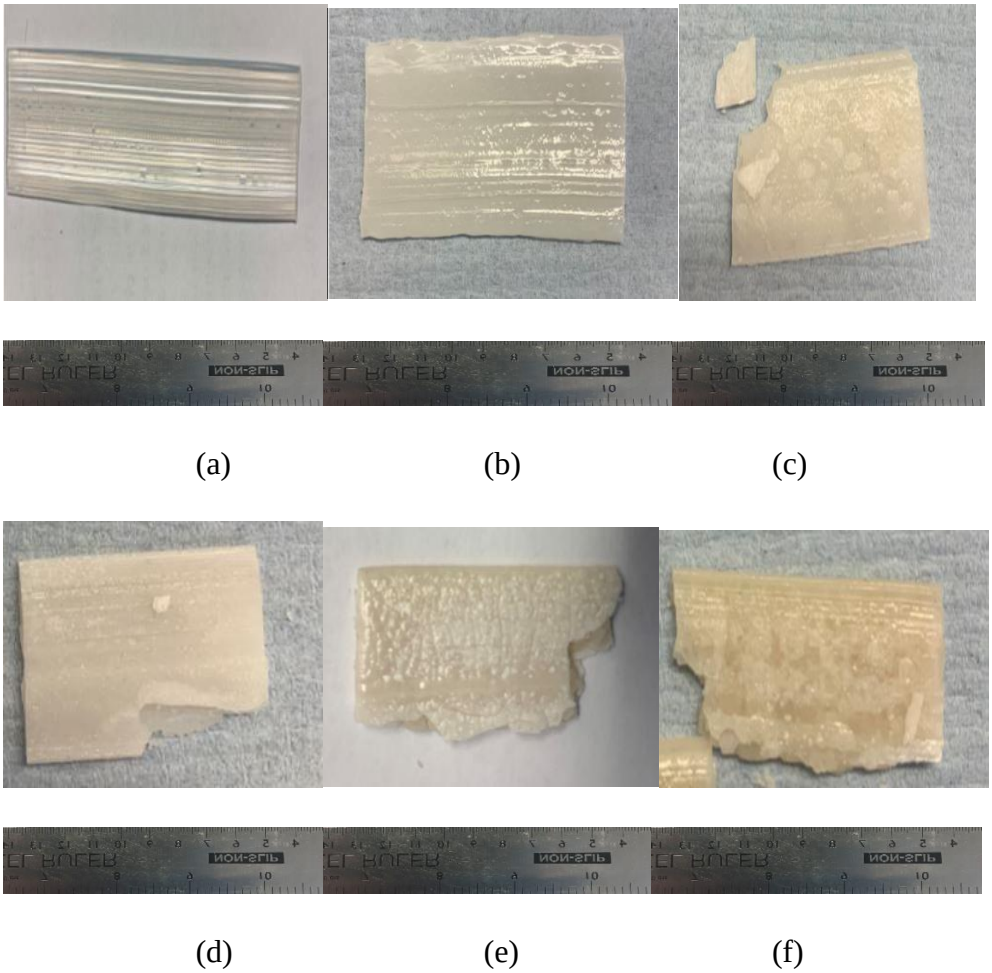

(a) (b) (c)

(d) (e) (f)

Figure 6.12. *Images of the degradation samples (a) PLA (b) PLA/HNT (c) P+ASP+H (d) P+APAP+H (e) PLA+APAP (f) PLA+ASP at 32nd week during the in-vitro degradation study*

The decrease in the glass transition temperature of the composites signifies less rigidity or stiffness after degradation for 32 weeks as T_g is the measure of rigidity (Declan M. Devine *et al.*, 2017). The P+APAP+H retains the T_g corresponding to its mechanical properties with a gradual reduction from 0 to 32nd week. The shift of T_{cc} to lower temperature with an increasing degradation period indicates faster crystallization (Beslikas *et al.*, 2011). The hydrolytic degradation process could have aided the cold crystallization process because of the formation of less intensified and

loose chain PLA entanglement during the degradation providing greater mobility leading to the crystallinity of PLA. Similar results were reported by Valapa et.al. and Chen et.al. (Valapa, Pugazhenthi and Katiyar, 2016; Chen *et al.*, 2018). This also reveals the initial degradation of amorphous domains than the crystalline domain. By the end of the degradation period, the crystalline parts could have started to hydrolyze as molecular weights of the samples are decreased (Beslikas *et al.*, 2011). The decrease in the melting peak during degradation could also be due to the depletion in the molecular weight of the samples (Valapa, Pugazhenthi and Katiyar, 2016). The two peaks of T_m could indicate the alpha form of PLA melts at higher temperature and the beta form could melt at a lower temperature (Chavalitpanya and Phattanarudee, 2013). This could also be due to the growth of small crystals which could melt at low heating rates and recrystallize before melting again (Finotti *et al.*, 2017).

The FTIR spectra for the 32nd week displayed the characteristic peaks of PLA with interesting shifts in several peaks to a higher frequency and some with higher intensity. This could indicate less intermolecular bonding within the matrix (Coates, 2000). Correlating to the mechanical and DSC results, the complete degradation of ASP loaded samples displayed new peaks at 3404 cm^{-1} which can be attributed to the absorbed water and 1616 cm^{-1} (for PLA+ASP)/1596 cm^{-1} (for P+ASP+H) corresponding to the OH deformation (water), the characteristic peaks of water (Prete and Arnaldo, 2016). The ester bond of PLA did not change during the degradation process for APAP-loaded samples, evidenced by the unchanged carbonyl group C=O band at 1750 cm^{-1} and C-O band at 1000–1300 cm^{-1}. As ester group cleavage is the primary degradation mechanism of PLA (Chen *et al.*, 2018). However, the ASP-loaded samples had a higher intensity of C=O band along with a shift to 1760 cm^{-1} which indicates the degradation of PLA due to less intermolecular bonding.

The ASP-loaded samples PLA+ASP and P+ASP+H were hard to handle by the end of the 32nd week which correlates to the deteriorated mechanical properties and the significant weight loss as seen above. Thus, the ASP-loaded samples had the highest rate of drug release profile (diffusion) and higher degradation rate. The acidic nature of ASP could have led to faster degradation through bulk erosion of the core of the PLA matrix Similar results were seen in other studies as well (Siegel *et al.*, 2006; Tang and Singh, 2008). The ASP being acidic increases the water absorption of the

polymer matrix affecting the polymer degradation and the drug release rate (Tang and Singh, 2008) which can be seen in the above results for ASP-loaded samples.

To improve the patient's compliance, the sustained release of the drug is important as it is released slowly over an extended period to prolong the therapeutic effect (Pierchala *et al.*, 2018). Thus, in this study, the APAP-loaded PLA/HNT nanocomposite suits the requirement as it displays a sustained release profile with gradual degradation. This could be due to the presence of HNT where the APAP could have been loaded onto the inner lumen of HNT. Because the interaction/bonding between the clay and the polymer enhances the solubility of the active ingredients and properties of the composite promoting stable controlled drug release generally prolonged (Maria, Meirelles and Raffin, 2017). This could be seen in APAP-loaded composites.

The currently used APIs in the coronary stents are 'limus family' drugs with anti-inflammatory, anti-thrombogenic, immuno-suppressive, and anti-proliferative mechanisms (Beshchasna *et al.*, 2020) have pKa values approximately between 9.6 – 10.40 ± 0.74 (Shah, Wyandt and Stodghill, 2013; Book, 2017; Wishart DS, 2017) which is similar to the pKa value of the model drug APAP used in this study. Thus, the PLA/HNT nanocomposite could be suitable for the currently used API types with pKa of ~9.6 for coronary stents.

The incomplete repair of the endothelium at the site of vascular wall injury due to the drug coatings and hypersensitivity to the presence of the stent facilitated the complications (Sakamoto *et al.*, 2018; Tabraiz Alam *et al.*, 2019). The APAP-loaded PLA/HNT nanocomposite displayed a sustained drug release from the stent body itself without the need for drug coating and its gradual degradation also suits the requirement of the stent for faster degradation.

6.4 Summary

The PLA/HNT nanocomposites were successfully extruded with two model APIs with different pKa values as separate batches. The prepared batches displayed no significant changes in the mechanical, thermal, and physicochemical properties. However, the drug release and the degradation profiles demonstrated significant differences for the APIs used. The high burst release from the PLA/HNT

nanocomposite was remarkably weakened due to the presence of HNT in the matrix. The results demonstrated that the API with a lower pKa value (3.6) had a higher initial burst release and overall release followed by a complete degradation by the end of the 32nd week in both PLA and PLA/HNT nanocomposites which according to the literature is due to the acidic property of the ASP. The ASP located in the hydrated amorphous regions on the polymer ionizes speedily in turn increases the acidity inside the matrix which led to faster drug release and degradation.

The drug with a higher pKa value (9.5) had a high initial burst release from only the control sample PLA, however, had a sustained release for both PLA and PLA/HNT nanocomposites and considerably gradual degradation with 36.33% of Young's Modulus retention by the end of 32nd week. This indicates the significance of the presence of HNT which aided the nominal burst release, a sustained release of APAP, and a gradual degradation for P+APAP+H as the APAP molecules were able to bond with the outer negative siloxane group of HNT or were loaded in the inner lumen. As the higher pKa value used here is equivalent to the pKa values of the currently used drugs in drug-eluting coronary stents, the PLA/HNT nanocomposite is suitable for drug-eluting stents as the stents are supposed to be designed as such they dissolve after the arterial remodeling obtains a stable phase at 6 months. In the following chapter, the PLA/HNT nanocomposite will be examined for the processing of the stent by 3D printing.

CHAPTER 7

Additive manufacturing of PLA/HNT nanocomposites for coronary stents

7.1. Introduction

Additive manufacturing (AM) also known as three-dimensional (3D) printing has increased in research interest particularly in various medical applications due to its transformative nature and ability of customization. Recent research has explored the areas such as 3D printing of tablets for more precise controlled drug delivery, patient-specific prostheses, tissue structures, and organ printing which are in the early stage of development for potential deployment in the future (Paul *et al.*, 2018).

One such area of interest is 3D printed implantable medical devices. Although the real application of 3D fabricated stents is limited because of material and machine constraints, much research is ongoing in the areas such as 3D printed PLA/PCL cardiovascular stent (Guerra *et al.*, 2018), 3D printed ureteric stent (Youssef *et al.*, 2015), a nasal stent (Mills *et al.*, 2017) for potential future application. The 3DP process has a minimum effect on the material's structure and eliminates the need for post-processing methods for material's property recovery which is commonly required by laser cutting, makes it feasible for the manufacturing of medical devices. It also has the advantage of design personalization and hence it has been considered as an alternative for the manufacturing of the stents (Guerra *et al.*, 2018; Qiu *et al.*, 2020; Wang *et al.*, 2020).

Fused Filament Fabrication (FFF) is one of the most widespread technologies of extrusion-based AM (Pranzo *et al.*, 2018). In this method, the thermoplastic filament is extruded onto a surface to fabricate a 3D structure as designed from software and the process is controlled by the computer (Miguel *et al.*, 2017; Fuenmayor *et al.*, 2018). Several studies have investigated various polymer nanocomposites for FFF (Berretta *et al.*, 2017; Gnanasekaran *et al.*, 2017; Coppola *et al.*, 2018; Lamberti *et al.*, 2018).

Nanocomposites have enormous potential in 3D printing applications. As shrinking the scale size to the nanoscale can change the properties of the materials, a variety of nanomaterials such as carbon nanotubes, graphene, metal nanoparticles are used in 3D printing for various applications (Ivanova, Williams and Campbell, 2013). Several research has been conducted to study the physical properties of the final printed part when they are blended with nanomaterials. Recent studies show that in

FFF the mechanical properties of the filament can be increased by the addition of the nanofillers.

In this study, the PLA/HNT nanocomposite is evaluated for the development of model stents by the method of FFF. For, this first the polymer PLA with a nanoclay HNT is processed by the method of Hot Melt Extrusion (HME). The resultant PLA/HNT nanocomposite was pelletized and was extruded by HME to produce 3D printable filaments of diameter size 1.75±0.10 mm. These filaments were 3D printed by the method of FFF to make standard tensile bars for mechanical characterization and the PLA/HNT nanocomposite is studied for the 3D printability by varying the percentages of HNT nanoclay for comparison but keeping the 3D printing parameters the same for all the PLA and PLA/HNT nanocomposite samples. Model implants are also developed by the method of which can potentially be adapted specifically for the 3D printing of stents.

7.2 Method

Compounding was performed by using APV (Model MP19TC (25:1)) (APV Baker, Newcastle-under-Lyme, UK) twin-screw compounder with 16 mm diameter screws. The temperature profile was maintained at (from feeder to the die) 190/180/170/170/160/140/120/50°C. The extrusion was performed at a screw speed of 140 rpm with the mass fractions of 100:0, 97:3, and 95:5 for PLA: HNT and are referred to here as PLA, PLA/HNT3%, and PLA/HNT5% respectively. The extrudate was drawn through a cooler belt and pelletized. These pellets were reprocessed using the same machine into a 3D printing filament of PLA and PLA/HNT.

The metal die used for the extrusion point had a bore diameter of 1.75 mm. The extrusion temperature was adjusted through a control panel and the melt temperature used for PLA pellets was 170 °C. This filament extrude was passed through the cooler belt and finally wound onto a spool for 3D printing. Once the filaments were extruded, they were printed into a tensile test specimen and implant using a FFF 3D printer (MakerGear M2 3D printer, US). The nozzle temperature was fixed at 200°C, bed temperature at 70°C with 25% infill for all the filaments. The STL file generated from the designing of the implant and the tensile bars from SolidWorks software was used to dictate the construct dimensions to the printer through MakerGear.

7.3 Results

7.3.1 Preparation of the nanocomposite into filaments

Virgin PLA and PLA/HNT nanocomposites were melt compounded, pelletized, and extrude into filaments at screw speeds of 140 rpm without difficulty. The extruded PLA filaments had small bubble-like structures as shown in Figure 7.1. However, the PLA/HNT nanocomposites filaments changed in color from transparent to opaque in particular the 5% nanocomposite as we compare Figure 7.1 (a) of PLA to the Figure 7.1 (b) of PLA/HNT 3% and Figure 7.1 (c) of PLA/HNT 5%. The resultant filaments of PLA and PLA/HNT nanocomposites had a diameter size of 1.75±0.10 mm.

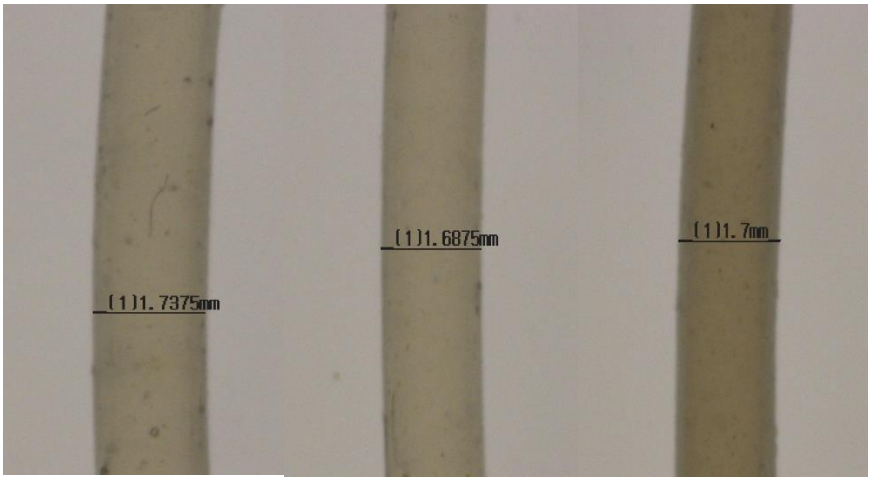

(a) *(b)* *(c)*

Figure 7.1. *Photographs of the filaments produced by twin-screw extrusion (a) PLA (b) PLA/HNT 3% (c) PLA/HNT 5%.*

7.3.2 Fabrication of tensile test bars

The PLA and PLA/HNT nanocomposite filaments were used for the 3D printing of tensile test bars. The morphology of the 3D printed samples was investigated using an optical microscope is shown in Figure 7.2 (a) and a detailed picture of a sample corner is reported in Figure 7.2 (b-d). The 3D printing of tensile test bars of PLA was processed without difficulty. However, the 3D printing of the PLA/HNT 3% and 5% nanocomposites was difficult to process and the 3D printed

bars had denser infill as the percentage of the HNT increased along with a change in color as shown in Figure 7.2. The gradual increase in the infill density can be carefully observed in Figure 7.2 (b) of PLA which has clear lines when compared to Fig 7.2 (c) of PLA/HNT 3% which little denser than PLA and Figure 7.2 (d) of PLA/HNT 5% shows a change in color similar to the filament and denser infill.

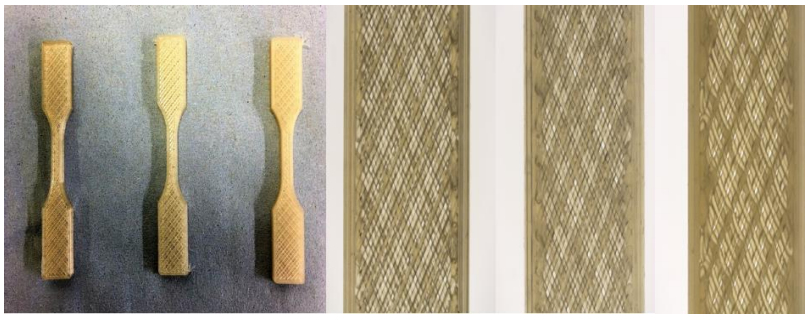

(a) (b) (c) (d)

***Figure 7.2**. Photographs from the optical microscope of 3D printed tensile bars (a) (L-R) PLA, PLA/HNT 3%, and PLA/HNT 5% nanocomposites. (b) Zoomed-in photograph of PLA (c) zoomed-in photograph of PLA/HNT 3% and (d) zoomed-in photograph of PLA/HNT 5% nanocomposite indicates the infill pattern becomes denser with the increase in the nanoclay percentage along with the color change*

.

7.3.3 Mechanical properties

The 3D printed tensile test bars were characterized for mechanical properties by uniaxial tensile testing and the tensile test results of PLA and PLA/HNT nanocomposite 3D printed tensile bars are as shown in Table 7.1.

***Table 7.1**. Mechanical properties of PLA and PLA/HNT nanocomposites*

Batch	Young's Modulus	Stiffness	Tensile Strength	Elongation at break
PLA	391.22±32.02	240.61±19.86	33.37±1.9	14.71±4.52
PLA/HNT3%	443.58±41.11	269.11±12.22	37.44±5.11	14.7±2.55
PLA/HNT5%	357.10±69.24	224.3±43.49	29.97±4.54	12.75±0.31

The mechanical properties of the 3D printed PLA is significantly lower than the usual values of PLA films extruded and the mechanical properties did not show any significant difference between the PLA and PLA/HNT nanocomposites 3D printed tensile samples. Previously in chapter 4, we have established in correlation to various literature that the mechanical properties of the PLA significantly improve by the addition of HNT into the PLA matrix up to 5% loading. In contrast, the results in this study show that the Young's Modulus of PLA of 391.22 to 357.10 MPa for PLA/HNT 5% nanocomposite.

Figure 7.3. Shows the photographs of the tensile bars after the tensile testing. The break point of the tensile test bars was mostly near the neck and in line with the infill of the tensile bars which indicates that 3D printing parameters have to be optimized and the printing pattern needs to be changed which had a significant influence on the mechanical properties. Torrado et al. found a similar decrease in mechanical property for samples of ABS/styrene ethylene butadiene styrene compared to ABS as they studied the samples by printing in XYZ and ZYX directions (Torrado *et al.*, 2015). On the contrary, a study by Yun et al. demonstrated that as the infill density increases, Young's Modulus and stiffness increase due to the formation of bonding between the printed layers (Yun *et al.*, 2018). Coppola et al. studied different printing parameters for PLA/layered silicates and found changes in elastic modulus for different fillers as printing temperature increases (Coppola *et al.*, 2018).

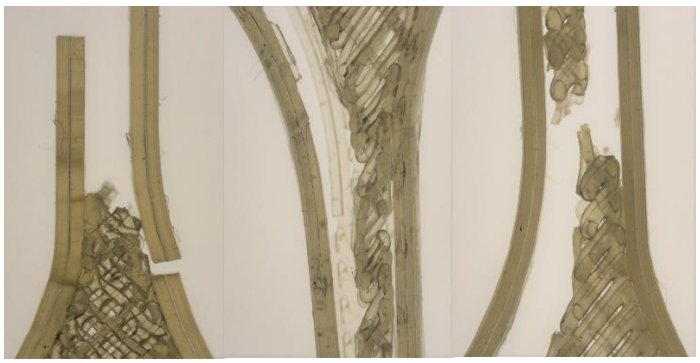

(a) *(b)* *(c)*

Figure 7.3. *Photographs of 3D printed tensile bars after testing (a) PLA (b) PLA/HNT 3% (c) PLA/HNT 5% indicate the breaking point of the bars during testing is influenced by the 3D printing processing.*

7.3.4 Differential Scanning Calorimetry

Thermal properties of the 3D printed nanocomposites were analyzed by the method of DSC and the results are as shown in Figure 7.4. There is no significant difference in the glass transition temperature (T_g) by the addition of HNT into the PLA matrix. However, the cold crystallization temperature (T_{cc}) significantly decreases with an increase in HNT percentage which indicates the nucleating effect of the HNT with the PLA. Two melting peaks are evident from the nanocomposites of 3% and 5% as indicated in previous studies that the peak at the lower temperature relates to the melting of the disordered α form (α´), while the second peak corresponds to the melting of the α form (Coppola *et al.*, 2018).

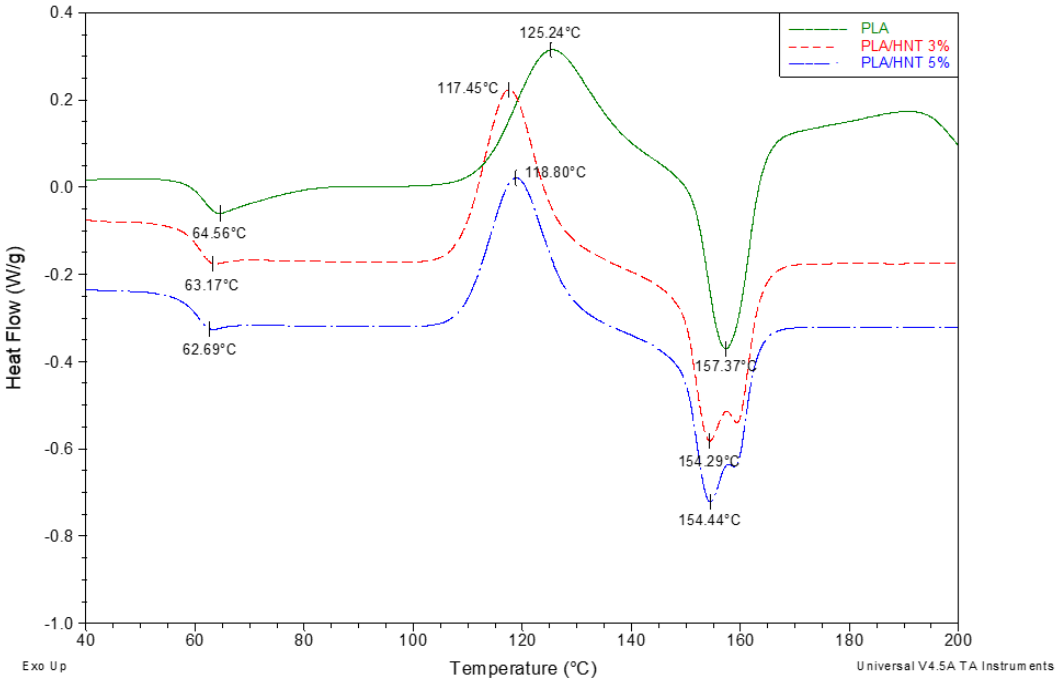

***Figure 7.4**. DSC thermographs of PLA, PLA/HNT 3%, and PLA/HNT 5% nanocomposites.*

The glass transition temperature T_g is a measure of rigidity (Declan M. Devine *et al.*, 2017). There is no significant difference in the glass transition temperature. However, the decrease in the cold crystallization temperature indicated that nanocomposites are more likely crystallized which could be due to the nucleating effect of HNT on the PLA (Liu, Zhang and Zhou, 2013; Wu *et al.*, 2013; Coppola *et al.*, 2018) and that heterogeneous nucleation was likely to occur where thinner crystalline lamella was formed compared to that of virgin PLA (Dong *et al.*, 2015b).

Hence the melting temperature of the composite is also lower than that of virgin PLA. Based on the above result, the composite appears to have an amorphous (low crystalline) structure. HNT acting as the nucleating agent in the PLA crystallizes the PLA/HNT composite more quickly than the virgin PLA (Liu, Zhang and Zhou, 2013; Wu *et al.*, 2013; Chen *et al.*, 2018).

7.3.5 Fabrication of the model stent

The filaments were 3D printed as 25 mm model medical implants as shown in Fig 7.5. The printing of the implants for PLA filament was easy when compared to the nanocomposites. However, all the stents had rough finishing as seen in the optical microscope images in Fig 7.6. which is due to the nozzle speed between the points. Besides, the 3D printed stents for nanocomposites had bubble-like structures at some points which may be due to the influence of the percentage of clay along with the processing temperatures.

(a) *(b)* *(c)*

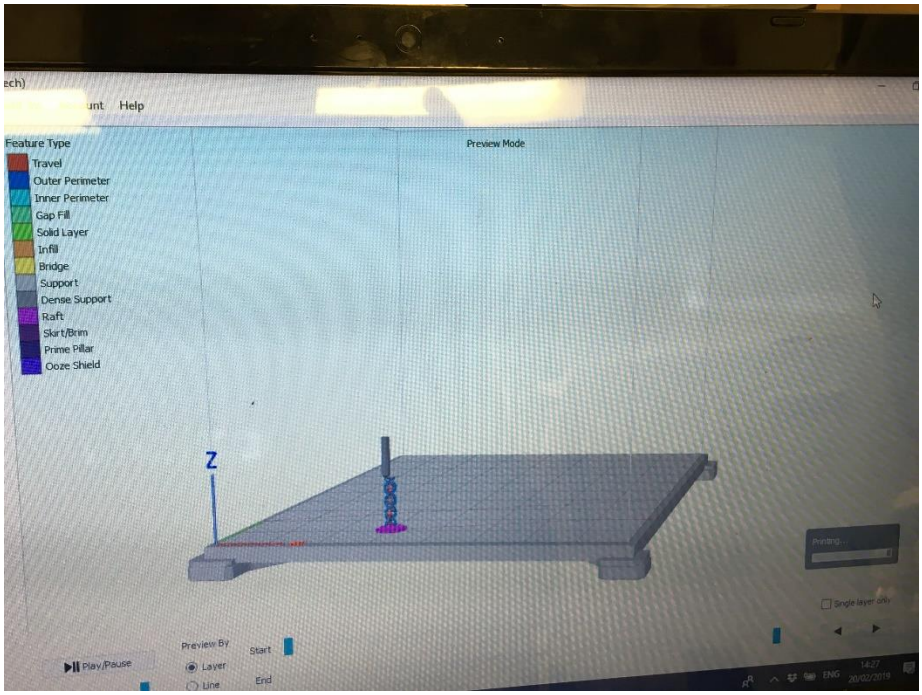

(d)

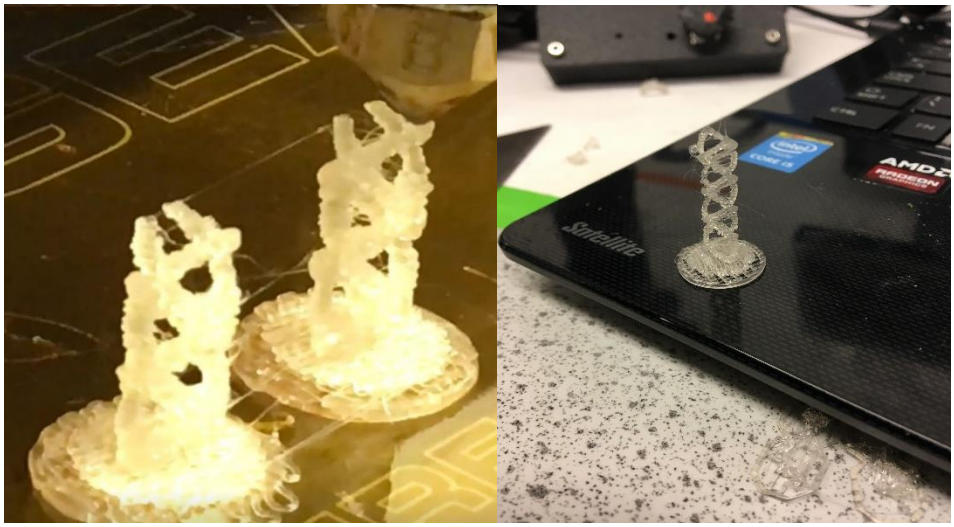

(e) *(f)*

Figure 7.5. *3D printed implants of (a) PLA, (b) PLA/HNT 3% and (c) PLA/HNT 5% nanocomposites (d) 3D printing imaging in solidworks software (e) screenshot of 3d printing the implant (f) 3D pritnted implant*

(a) *(b)* *(c)*

***Figure 7.6**. Photographs from optical microscope of 3D printed implants of (a) PLA, (b) PLA/HNT 3% and (c) PLA/HNT 5% nanocomposites*

In addition to the rough finishing and surface imperfections, the prepared model stents were very stiff and had no flexibility for expansion. A similar result of insufficient flexibility was obtained by Wang et al. in their study of designing and 3D printing of cardiovascular PLLA/PCL stents (Wang *et al.*, 2020) and by Guerra et al. on their 3D printed control sample PLA stent which had an unacceptable radial expansion compared to their PCL stents and PLA/PCL stents. However, PLA/PCL stents exhibited the characteristics of both PLA and PCL as the PLA layer was unbroken during expansion and by removal of the force, there was no recoil of PCL due to the rigidity of PLA (Guerra *et al.*, 2018). Another study displays the flexibility and strength of the developed PCL stents by Guerra et al. which had uniform radial expansion due to the flexibility of PCL (Guerra and Ciurana, 2018).

Thus, the PLA and PLA/HNT model stents in this study displayed rigidity of PLA and as the addition of HNT tends to crystallize the PLA matrix by increasing the stiffness and Young's modulus, as we see from the DSC results, model PLA/HNT stents were as well rigid.

7.4 Discussion

This research work outlines the possibility of firstly developing nanocomposite filament using biodegradable thermoplastic polymer PLA and nanoclay HNT. This

developed PLA/HNT nanocomposite filament could further be 3D printed by the method of FFF into standard tensile test bars and model medical implants. The printability, morphology, thermal and mechanical properties were evaluated. Analysis showed that the ease of printing and the morphology of the printed tensile bars and model implants varied with the clay compositions as the printing parameters were maintained the same for all the PLA and PLA/HNT nanocomposite batches for comparison.

Ease of maintenance, low cost, and flexibility make the FFF the most commonly preferred process of 3D printing (Berretta *et al.,* 2017). However, some disadvantages such as surface roughness, need for support material and support removal and mainly imperfect sealing between layers and toolpaths (Pranzo *et al.*, 2018) have to be considered while the FFF process. In this study as the printing parameters were the same for all the batches, the mechanical properties of the 3D printed tensile bars were not in correlation with the mechanical properties of the PLA/HNT nanocomposite. As illustrated in Fig. 7.3, the breaking point of the tensile bars was mostly at the neck and in line with the printing pattern of the bars. This suggests that delamination between layers occurred. This effect can be reduced by adjusting the 3D printing parameters such as infill pattern, temperature, and nozzle speed. Similar breakage at the neck was shown by the study of mechanical properties by the influence of FFF printing parameters by Kalinowski et. al. Minor discontinuities in filament extrusion, uncontrolled shrink during the cooling process, weakness between the layers could lead to the decrease in the mechanical properties of the 3D printed parts (Ćwikła *et al.*, 2017). It is also reported that FFF reduces the properties of the 3D printed parts as may create void spaces between the material deposition lines (Ferreira *et al.*, 2017).

The thermal analysis of the 3D printed PLA/HNT nanocomposites is in correlation with the thermal analysis of the PLA/HNT as a nanocomposite. During the 3D printing process, the nozzle movement in the X-Y direction induces uniform heat transfer allowing crystallization (Gnanasekaran *et al.*, 2017). However, in our study, the results differ, which could be due to the nucleating effect of HNT on the PLA matrix decreasing the cold crystallization temperature. Similar results are obtained in the study of CNT-Graphene-based polymer nanocomposite for 3D printing by FFF (Gnanasekaran *et al.*, 2017).

3D printed implants were successfully fabricated into mesh forms using FFF's layer-by-layer approach composed of PLA/HNT nanocomposite. Coronary stents are commonly manufactured as stent tubes and laser cutting is used to cut the stent. However, due to the thermal sensibility of the polymers, the conventional laser cutting manufacturing process is difficult to make stents from composites or nanocomposites (Guerra, San and Ciurana, 2017; Qiu *et al.*, 2020). The 3DP process has a minimum effect on the material's structure and eliminates the need for post-processing methods for material's property recovery which is commonly required by laser cutting, makes it feasible for the manufacturing of the medical devices (Guerra and Ciurana, 2018; Wang *et al.*, 2020). Thus, polymer composite stents manufactured with 3D printing processes is highly effective for future applications for stents.

7.5 Summary

In this study, it was possible to develop a 3D printing filament using biodegradable PLA and reinforcing with biocompatible filler HNT. The filament had a diameter of 1.75±0.10 mm for use in FFF 3D printing. The 3D printed model implants were successfully fabricated into mesh forms whose mechanical properties can be enhanced by optimizing the printing parameters. Along with surface imperfections of the produced stents, the stents were rigid and no flexibility was required for the expansion of the stent during and after the placement in the artery. As per previous results, it is due to the enhancement of strength and stiffness of the nanocomposite with the addition of HNT. The insufficiency of stent flexibility indicates a need for material improvement. Thus, in the next chapter, the PLA/HNT nanocomposite is examined with the addition of PCL to improve flexibility while maintaining the required strength for the coronary stents.

CHAPTER 8

Inclusion of polycaprolactone (PCL) into high strength polylactic acid/halloysite nanotubes (PLA/HNT) nanocomposite for the enhancement of flexibility

8.1 Introduction

The primary function of a stent is to provide radial support to the vessel which is a mechanical role of the stent material (Dreher, Nagaraja and Batchelor, 2016). Thus, mechanical properties such as tensile strength, strain and modulus of the biodegradable polymers are considered for the fabrication of stents (Jenjob *et al.*, 2015). During the stent placement, the stent is mounted on a catheter and inserted into the blood vessel to the site of blockage where the stent expands exerting a radial force on the blood vessel to keep it open (Azaouzi, Makradi and Belouettar, 2012). Stent under expansion has been often related to early stent thrombosis as there could be a higher shear rate (concentration of platelets or adhesion proteins) in that segment and shear concentration on the strut edges leading to thrombosis (Ng *et al.*, 2017). Thus, the expansion of the polymer also plays an important role after insertion (Kokot *et al.*, 2018). According to the European Society of Cardiology guidelines, the stent after implantation must not move, however, it must cooperate with the contraction and dilation of the vessel (Majewska, Oledzka and Sobczak, 2019).

The latest generation of polymeric biodegradable stents is mostly made of poly L-lactic acid (PLLA) which has low mechanical strength and elongation in comparison with metallic stents. Due to the limit of expansion PLLA devices can fracture due to over-dilation, thus making it a criterion of BRS to improve the expandability and also maintain radial strength (Ang, Huang, *et al.*, 2017). Several studies have investigated the mechanical behavior and its improvement of poly-lactic acid (PLA), poly(D-lactic acid) (PDLA), poly(lactide-co-glycolide) (PLGA), and polycaprolactone (PCL) for potential consideration as stent material (Ang, Bulluck, *et al.*, 2017a; Qiu and Zhao, 2018).

The properties of the PLA such as brittleness can be tuned by co-polymerization, the addition of plasticizers, or compatibilizers for more flexibility and ductility. PLA blending with other flexible polymers such as PCL also presents a way of toughening the material (Sangeetha *et al.*, 2018; Casalini *et al.*, 2019). PCL which is known to be biocompatible along with properties such as ductility, low stiffness, and high toughness appears to be a good selection for blending with PLA and has been studied intensively (Ferri *et al.*, 2016; Wachirahuttapong, Thongpin and

Sombatsompop, 2016; Finotti *et al.*, 2017; Ostafinska *et al.*, 2017; Carvalho *et al.*, 2020). Guerra et.al. studied the PLA/PCL composite as a potential material for cardiovascular stents via 3D printing. They also fabricated PLA/PCL tubes for stents with results relatable to the dynamic modulus and degradation rate of the stent requirements (Guerra, San and Ciurana, 2017; Guerra *et al.*, 2018).

Modified HNT in PCL has been shown to improve the thermal properties of the PCL/HNT nanocomposite films (Çakman, 2016). PLA/PCL composite embedded with HNT has been researched by Haroosh et.al. via electrospinning which displayed good dispersion of HNT with a decrease in crystallinity of the composite (Haroosh, Chaudhary, Deeptangshu Dong and Hawkins, 2011; Haroosh *et al.*, 2013). Kelnar et.al. studied the behavior of PLA/PCL microfibrillar composite with the effect of 3 phr HNT content indicating a favorable increase in crystallinity of PLA and enhanced mechanical performance (Kelnar *et al.*, 2016).

In this study, the PLA/PCL/HNT nanocomposite was studied as a potential material for biodegradable coronary stents with high strength of PLA and the flexibility of PCL in turn increasing the toughness of the material. A masterbatch of PCL/HNT was prepared via twin-screw extrusion with 10% of HNT in the PCL matrix. This was followed by the extrusion of PLA with 5% and 10% of the pre-blends of PCL/HNT composite. For comparison, PLA, PLA/HNT, PLA/PCL 5% composites were prepared. The prepared nanocomposites were studied for mechanical, thermal, physiochemical properties. The PLA, PLA/HNT, and PLA/PCL-HNT composites were also tested for *in-vitro* degradation for 32 weeks. Weight loss percentage was reported for every 4 weeks, mechanical, thermal, and physiochemical properties were reported for the 8^{th}, $20^{th,}$ and 32^{nd} week.

8.2 Methods

8.2.1. Preparation of PLA/PCL/HNT Nanocomposites

Extrusion was performed by using Prism^{TM} twin-screw extruder with 16mm diameter screws and a 25/1 length to diameter ratio. The mass fractions of PLA: HNT were 100:0 and 95:5. A master batch of PCL: HNT was prepared into films in the ratio of 90:10. The prepared master batch was pelletized. The nomenclature is illustrated in Table 8.1. The pelletized PCL/HNT nanocomposites were then extruded with PLA in

95:5 and 90:10 compositions as shown in Table 8.2. For the extrusion of PLA and PLA composites the temperature profile was maintained at (die to the feeder) 210/190/180/170/160 and for PCL and PCL related composites, the temperature profile was (die to the feeder) 70/70/60/60/50. The screw speed was set at 140 rpm. The extruded film was drawn through the three-roll calendar to form a continuous film. Finally, the films were punched into ASTM standard tensile test specimens for testing.

Table 8.1. *Description of the prepared PCL/HNT master batches.*

Batch	PCL	PCL	HNT
A	50000 g/mol (powder)	90%	10%

Table 8.2. *Description of the prepared polymer nanocomposites with PLA, PCL, and HNT. The corresponding compositions for each category are in percentages.*

Number	PLA	PCL	A	HNT
1	100	0	0	0
2	95	0	0	5
3	95	0	5	0
4	90	0	10	0
5	95	5	0	0
6	0	100	0	0
7	0	0	100	0

8.3 Results

8.3.1 Processing of PLA/PCL/HNT nanocomposite

PLA, PCL, and nanocomposites were processed without difficulty. The extrudate was transparent for PLA films. The PCL films and the composite films changed to opaque in color.

8.3.2 Mechanical properties

The primary concern of the processed material is its strength. The results show the maximum stress the material can withstand or its ductility to see how much it deforms before fracture (ASM International 2004). Mechanical testing was performed to assess the percent strain at maximum load (elongation at break), stress at maximum load (Tensile strength), Young's modulus, and stiffness of PLA/PCL/HNT nanocomposites.

The mechanical properties of the nanocomposites prepared are as shown in Fig 8.1 and Table 8.3. The tensile strength of the PLA and PLA nanocomposites is as shown in Figure 8.1 (a). The PLA and PLA/HNT were 58.88 MPa and 59.26 MPa respectively. PCL on the other hand had a tensile strength of 24 MPa and increased to 26.92 MPa with the addition of HNT. However, PCL blended with PLA had a tensile strength of 51.53±8.23 MPa. The 5% addition of PCL+HNT into PLA (PLA+A 5%) had a tensile strength of 51.37±3.63 MPa and 10% of PCL+HNT into PLA (PLA+A 10%) had a tensile strength of 49.61±3.58 MPa. Thus, the addition of HNT to PCL significantly increases the tensile strength of the PCL with a p-value of 0.04. With $p<0.05$, there was a slight decrease in the tensile strength of the PLA+PCL5%, PLA+A5%, and PLA+A10% when compared to PLA.

The stiffness of the nanocomposites is as shown in Figure 8.1 (b). The stiffness of PLA and PLA/HNT was displayed at 403.25 kN/m and 390.1 kN/m respectively. Whereas the stiffness of PCL was 110.2 kN/m and PCL+HNT was 131.34 kN/m. In the case of PLA+PCL and PLA+A10%, the stiffness was 381.84 kN/m and 428.25 kN/m respectively. However, the stiffness of PLA+A5% decreases to 234.19 kN/m. Thus, PCL+HNT did not show any significant difference with the addition of HNT to PCL with a p-value of 0.089. Similarly, PLA+PCL and PLA+A10% do not show any significant difference in stiffness with the addition of PCL to PLA and 10% PCL+HNT addition respectively ($P>0.05$). However, the stiffness of PLA significantly decreases with the addition of PCL+HNT 5% with a p-value of 0.002 for PLA+A5% nanocomposite.

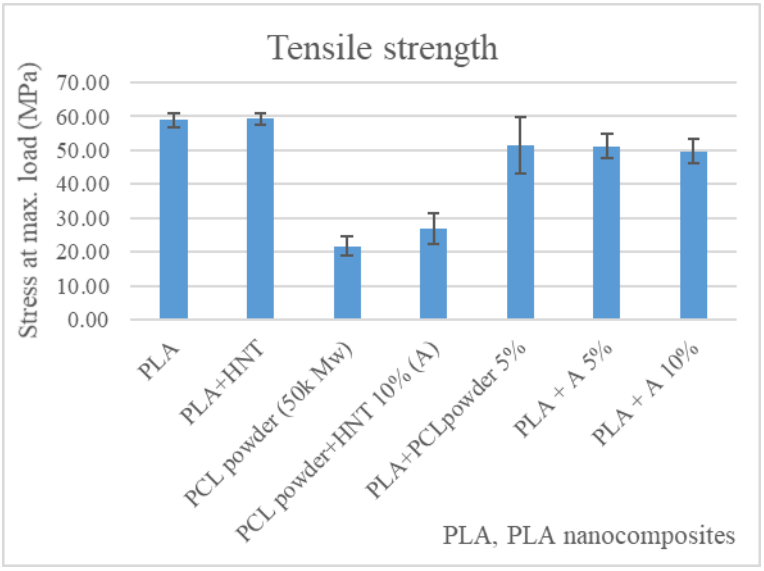

(a)

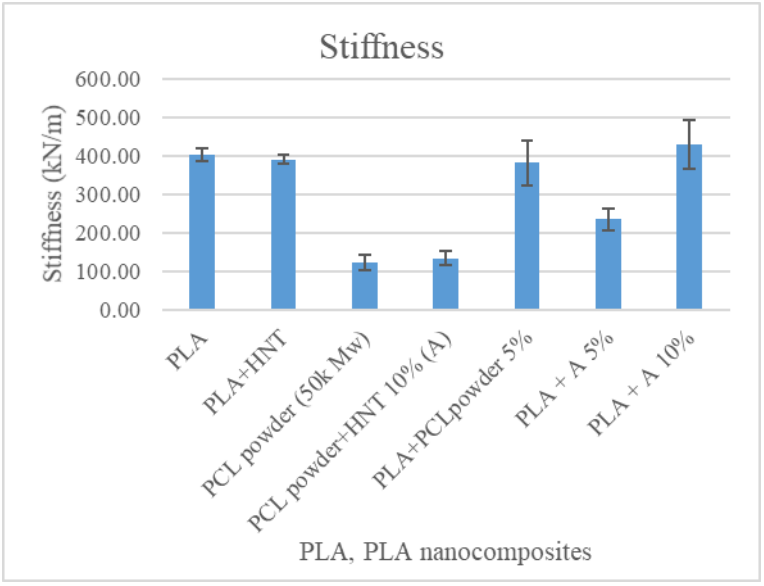

(b)

Figure 8.1. *Graphical representation of the mechanical properties of the PCL-related nanocomposites. (a) Effect of tensile strength on the PLA, PCL, PLA/PCL, and the nanocomposites. (b) Effect of stiffness on the PLA, PCL, PLA/PCL, and the nanocomposites*

.

The elongation at break and the Young's Modulus differs significantly for PLA and PCL in general due to the brittleness of PLA and flexibility of PCL. Thus, the results of elongation at break and the Young's Modulus could not be illustrated graphically and are tabulated in Table 8.3. The elongation at break was displayed at 6.15% and 6.25% for PLA and PLA/HNT respectively and for PCL, the elongation at break was 853.67%. This increased to 943.45% with the addition of HNT. In the case of PLA+PCL, the elongation at break was 7.4% and for PLA+A5% and PLA+A10%, it was 8.06% and 6.62% respectively. Thus, the addition of HNT to PCL significantly increases the percentage elongation with a p-value of 0.01. Similarly, the addition of PCL+HNT 5% to PLA (PLA+A5%) significantly improves the elongation at break (p=0.02) when compared to PLA.

The Young's Modulus of the composites as shown in Table 8.3, was 1812 MPa and 1992 MPa for PLA and PLA/HNT respectively. Whereas for PCL it was 256.6 MPa and increased to 384.7 MPa with the addition of HNT for PCL+HNT. In the case of PLA+PCL, Young's Modulus was 1338.4 MPa and 1781.4 MPa, 1287.3 MPa for PLA+A5% and PLA+A10% respectively. Thus the addition of HNT displayed an improvement in the Young's Modulus of PCL significantly (p=0.03). The Young's Modulus significantly reduces for PLA+PCL and PLA+A 10% with p>0.05 which indicates a higher influence of PCL in the composites. Whereas, PLA+A5% shows Young's Modulus which correlates to that of PLA.

Table 8.3. *Mechanical properties of the PCL-related nanocomposites for elongation at break and Young's modulus.*

Sample	**Elongation at break (%)**	**Young's Modulus (MPa)**
PLA	6.15 ± 0.61	1812 ± 118.37
PLA/HNT	6.25 ± 0.37	1992 ± 145.33
PCL	853.67 ± 167.25	256.6 ± 14.37
PCL+HNT 10% (A)	943.45 ± 210.15	384.7 ± 18.63
PLA+PCL 5%	7.4 ± 0.64	1338.4 ± 193.36
PLA+A 5%	8.06 ± 0.73	1781.4 ± 194.69
PLA+A 10%	6.62 ± 0.39	1287.3 ± 95.82

8.3.3. Differential Scanning Calorimetry

The secondary heating thermograms of the nanocomposites for PCL are shown in Figure 8.2. The melting temperature of PCL corresponds to 58.03°C as shown in Figure 8.2 (a). The addition of HNT did not show any significant difference in T_m of PCL and corresponds to 57.61 °C. The thermograms of the PLA had the T_g of 61.1 °C, T_{cc} of 126.56 °C, and T_m of 157.07 °C. The thermograms of PLA+HNT had a similar T_g of PLA, however, the T_{cc} decreases to 115.64 °C and had twin melting peaks of 154.31 °C and 159.36 °C for T_{m1} and T_{m2} of PLA respectively. Similar twin melting peaks of 154.31 °C and 159.36 °C for T_{m1} and T_{m2} respectively and a decrease in T_{cc} to 116.51 °C was seen for the PLA+PCL composite. Besides, the distinction of the T_g of PLA and T_m of PCL could be depicted at 62.55 °C and 58.03 °C with no significant changes.

The thermograms of PLA+A5% are shown in Figure 8.2 (b). It displays the T_g of PLA at 62.71 °C and T_m of PCL at 56.97 °C. The T_{cc} was 117.61 °C and T_m of PLA at 155.51 °C. The thermograms of PLA+A10% as shown in Figure 8.2 (c) displays the T_g of PLA at 62.15 °C and T_m of PCL at 54.51 °C which has a more significantly intense peak than the T_g of PLA which is overlapped. The T_{cc} was at 115.41 °C and T_m of PLA displayed distinct two peaks at 159.56 °C and 155 °C for T_{m2} and T_{m1} respectively

The PCL/HNT pre-blend addition to the PLA the nanocomposite shows two distinct peaks with a lower temperature peak corresponding to the T_m of PCL and a higher temperature peak corresponding to the T_g of PLA. A similar distinction was reported by Finotti et.al. with PLA/PCL blends with triblock ε-caprolactone-tetrahydrofuran-ε-caprolactone (CT) copolymer which demonstrated the separate peaks of PLA T_g and PCL T_m (Finotti *et al.*, 2017). The T_m of PCL overlaps with the T_g of PLA in the PLA/PCL blend in most of the literature data (Ferri *et al.*, 2016; Wachirahuttapong, Thongpin and Sombatsompop, 2016; Kelnar *et al.*, 2017; Dadras *et al.*, 2020). However, in this study, they could be distinguished through modulated DSC and it shows no significant difference in the T_g of PLA in the blends compared

to the virgin PLA. However, there is a significant decrease in the T_m of the PCL for the PLA+A5% and PLA+A10% blends ($p<0.05$).

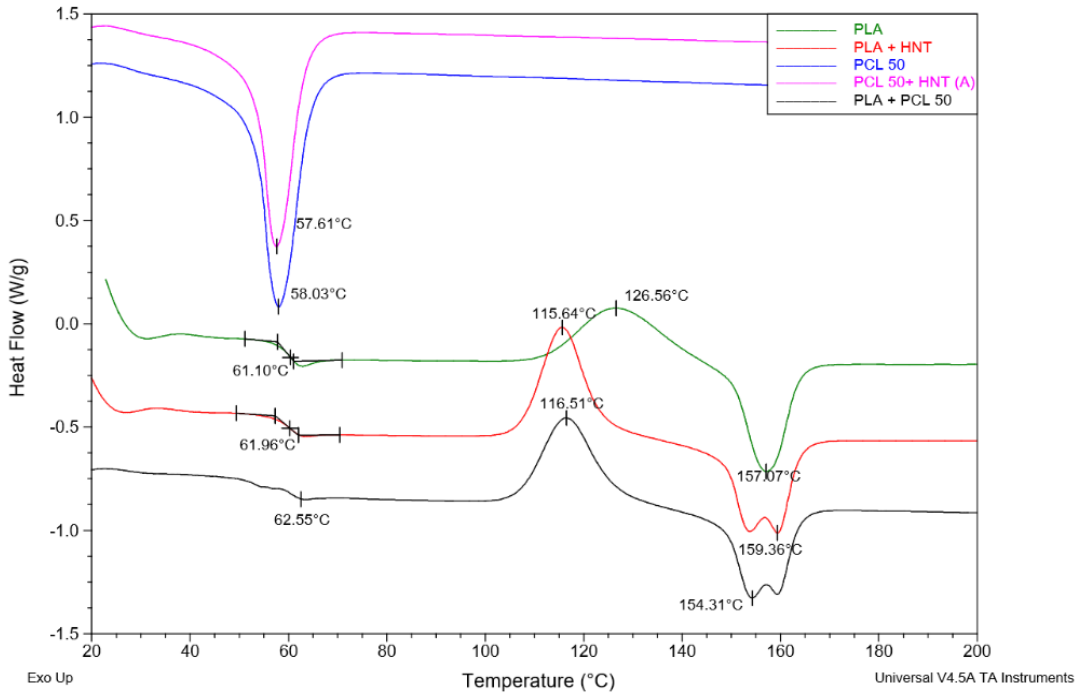

(a)

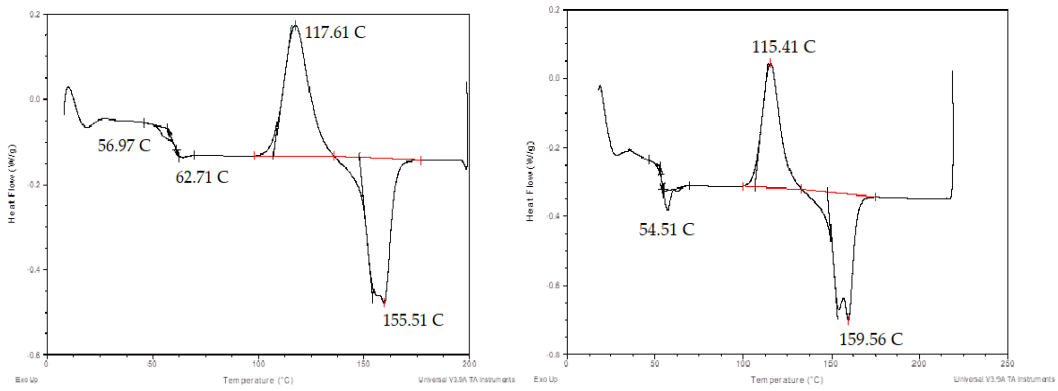

(b) *(c)*

Figure 8.2. *DSC thermograms of PCL 50k Mw related nanocomposites (a) PLA, PLA/HNT, PCL, PCL/HNT, PLA/PCL (b) PLA+A5% (c) PLA+A10%.*

In comparison to PLA, the cold crystallization temperature (T_{cc}) significantly decreases for all the nanocomposites which are similar to several previous literature data. The double melting peak with no significant difference in T_m of PLA is observed here as well in all the blends indicating heterogeneous nucleation by melting of imperfect crystals at a lower temperature (T_{m1}) followed by rearranging for an ordered

structure at heating and melting at higher temperature (T_{m2}) (Dadras *et al.*, 2020). It could also indicate the melting of the alpha form of PLA at higher temperatures and the melting of beta form at a lower temperature (Chavalitpanya and Phattanarudee, 2013).

8.3.4. Fourier Transform Infrared (FTIR) Spectroscopy

The spectrum of PLA, PCL, HNT, PLA/PCL, and PLA/PCL/HNT blends obtained from the FTIR are as shown in Fig. 8.3. The characteristic peaks of PLA at 2995 cm^{-1} attributing to CH stretch and 1750 cm^{-1} indicating –C=O carbonyl group (Dadras *et al.*, 2020), PCL at 2942 cm^{-1}, 2865 cm^{-1} (CH stretch), and 1721 cm^{-1} (C=O stretch) (Shoja *et al.*, 2015; Dadras *et al.*, 2020) and HNT at 3694 cm^{-1}, 3625 cm^{-1} (OH) (Haroosh *et al.*, 2013) are evident.

From the spectrum of PCL/HNT pre-blend, the characteristic peaks of HNT corresponding to OH stretch is apparent in blend along with the peaks of PCL also being more intense than neat PCL. A similar finding was reported by Haroosh et.al. where the characteristic peak of HNT in PLA/PCL blend prepared by electrospinning was shown for modified HNT (Haroosh *et al.*, 2013) and in a study by Cakman et.al. where modified HNT displayed successful interaction with PCL with blends prepared by solvent casting (Çakman, 2016).

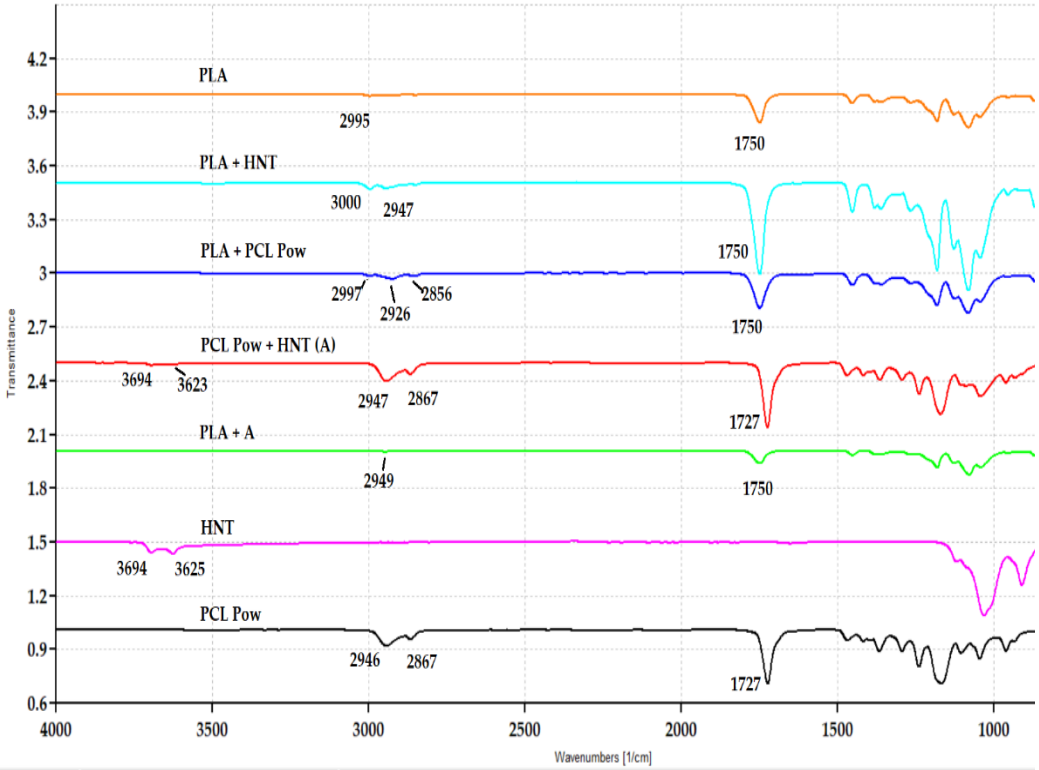

Figure 8.3. *FTIR spectra of PLA, PCL, PLA/PCL, and nanocomposites*

The peaks of PCL were more evident along with the characteristic peaks of PLA with slight shifting to lower wave numbers for PCL peaks at 2926 cm^{-1} and 2856 cm^{-1} in PLA/PCL composite when compared to PLA/PCL/HNT blend. Chen et.al. studied the PLA/PCL blends with 10-40% of PCL range and found no significant shift or new peaks in the blends indicating little or no interaction between PLA and PCL (Chen *et al.*, 2014). Dadras et.al. investigated the PLA/PCL blends with silk fibroin nanoparticles and the results revealed an increase in the intensity of PCL peak in PLA/PCL blend with the increase in the PCL content and no new peak or shift when nanoparticles are added in a small amount (Dadras *et al.*, 2020).

8.3.5 In-vitro degradation study

In this study, PCL/HNT addition to PLA increased ductility of PLA by an increase in percentage elongation with no significant change in the tensile strength and Young's Modulus which makes the PLA+A5% (PLA/PCL-HNT) nanocomposite desirable for biodegradable stents which require flexibility for expansion of the stent during placement and good mechanical strength for adequate radial support until 6

months. Thus, PLA+A5% was taken forward for *in-vitro* degradation tests along with PLA and PLA/HNT for comparison.

The mass reduction of the samples was studied for 32 weeks duration. As shown in Fig. 8.5 no significant weight reduction was observed until 8 weeks for all samples. PLA+A5% nanocomposite displayed weight loss of 6.8, 9.9, and 18.56% by the end of 14th, 20^{th,} and 32nd week when compared to 1.2, 1.5, and 4.7% for PLA and 0.83, 1.62, and 8.1% for PLA/HNT composites respectively as seen in Fig. 8.4. Similar weight loss of 7% by 15 weeks was reported by Huang et.al. for PEG-PCL-PLA composite with a burst loss of nearly 49% from 15 – 25th week of their degradation study (Huang *et al.*, 2006). 20% mass loss of PLA/PCL fibers by the end of the 28th week was reported by Vieira et.al (Vieira *et al.*, 2010, 2011).

Figure 8.4. *Graphical representation of weight loss percentage of PLA, PLA+HNT, and PLA+A5% nanocomposite*

The mechanical properties of the PLA, PLA+HNT, and PLA+A5% samples during the degradation study are shown in Figure 8.5. The tensile strength of the composites as shown in Figure 8.5 (a) displayed no significant change for all samples until the 8th week and gradual reduction was displayed by the 20th week as seen for PLA/HNT and PLA+A5% samples with 22.28% and 25.54% reduction respectively. Whereas PLA showed a sudden reduction to 66.25% by the 20th week. By the 32nd week, a drastic reduction was seen for all samples with 97.8, 83.5, and 95.6% for PLA, PLA/HNT, and PLA+A5% composites.

The elongation at break as shown in Fig. 8.5 (b) displayed a consistent reduction during the degradation process for all the samples. The PLA which had an elongation at a break of 6.15% at 0 weeks reduced to 5.7% by the 8th week, 2.36% by the 20th week, and 0.9% by the 32nd week. PLA/HNT, on the other hand, was reduced to 5.27% by the 8th week from 6.35 at 0 weeks, further to 4.4% by 20th week and 2.7% by 32nd week. PLA+A5% which had an elongation at break of 8.06% at 0 weeks, reduced to 4.91% by 8th week, 2.98% by 20th week, and 0.89% by 32nd week.

The stiffness of the composites displayed a gradual reduction with significant retention by the 32nd week for all samples as seen in Figure 8.5 (c). The 403.25 kN/m of stiffness for PLA at 0 weeks was reduced only to 396.62 kN/m by the 8th week, 302.27 kN/m by 20th week, and further reduced to 163.78 kN/m by the 32nd week. Similarly, the PLA/HNT composites also reduced from 390.1 kN/m at 0 weeks to 388.1 kN/m by the 8th week 330 kN/m by the 20th week, and 275 kN/m by the 32nd week. The PLA+A 5% also displayed a similar decrease to 228 kN/m by the 8th week from 234.1 kN/m at 0 weeks. It was further reduced to 200.8 kN/m by the 20th week and 133.36 kN/m by the 32nd week.

The Young's modulus in Figure 8.5 (d) shows no significant reduction by the 8th week. There is a 13.2, 15.17, and 3.19% reduction by the 20th week for PLA, PLA/HNT, and PLA+A5% which continues to reduce by 58.65, 40.1, and 72% respectively at the end of the 32nd week.

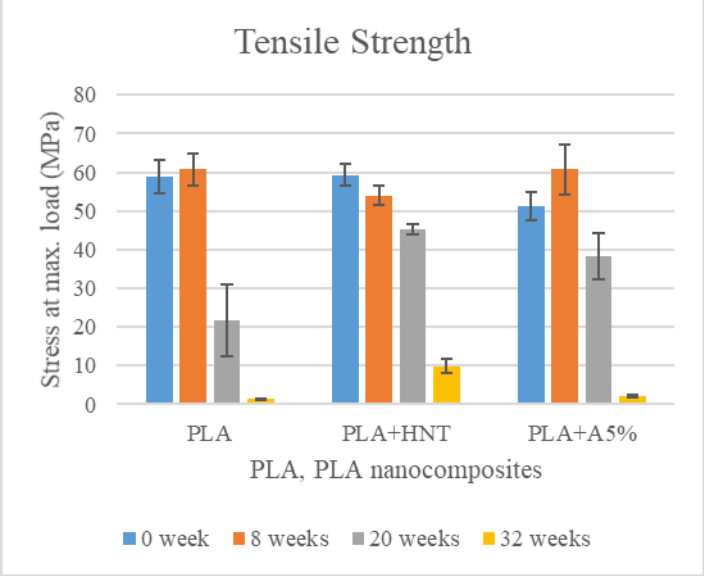

(a)

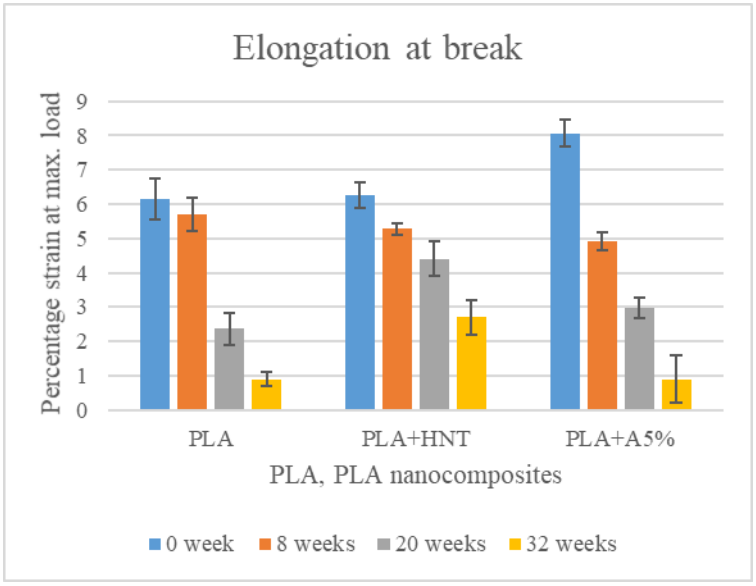
Elongation at break
Percentage strain at max. load
9
8
7
6
5
4
3
2
1
0
PLA
PLA+HNT
PLA+A5%
PLA, PLA nanocomposites
0 week
8 weeks
20 weeks
32 weeks

(b)

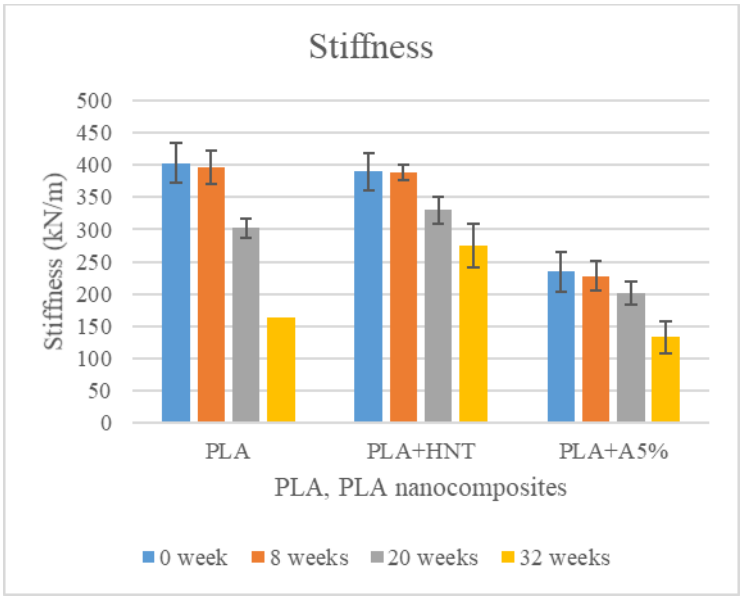
Stiffness
Stiffness (kN/m)
500
450
400
350
300
250
200
150
100
50
0
PLA
PLA+HNT
PLA+A5%
PLA, PLA nanocomposites
0 week
8 weeks
20 weeks
32 weeks

(c)

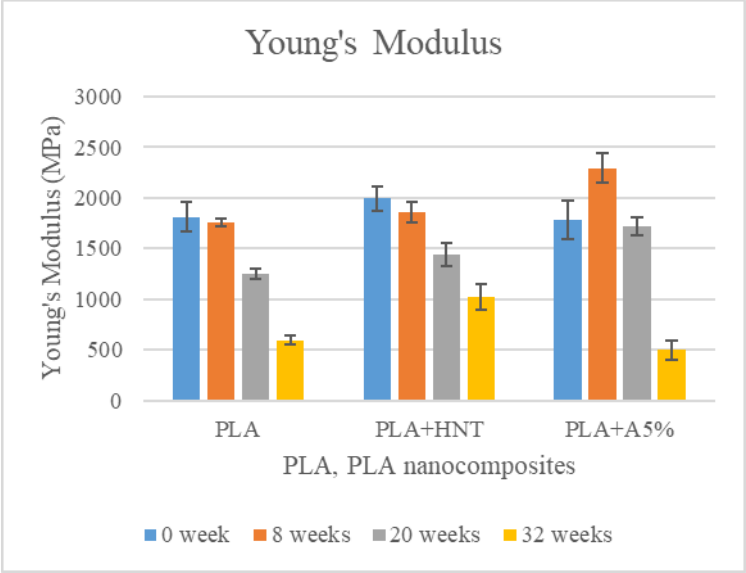

(d)

Figure 8.5. *Graphical representation of mechanical properties during the in-vitro degradation study of PLA, PLA+HNT and PLA+A5% for (a) tensile strength (b) elongation at break (c) stiffness (d) Young's modulus*

The Young's Modulus and stiffness show small retention by the 32nd week. On the contrary, Vieira et.al. reported 80% strength loss in 16 weeks degradation of PLA/PCL fibers (Vieira *et al.*, 2011) and Chen et.al. reported 33.7, 27.6% modulus loss at the end of the 24th week for PLA and PLA/HNT composites (Chen *et al.*, 2018).

The DSC results from the degradation study are as shown in Fig. 8.6, which shows that the PLA, PLA/HNT, and PLA+A5% composite. The thermograms of PLA as shown in Fig. 8.7 (a) has a gradual and consistent reduction in the T_g, $T_{cc,}$ and T_m. The T_g of PLA at 61°C before the degradation is significantly reduced to 53.25°C by the 32nd week. The cold crystallization temperature of PLA noticeably decreases by the 8th week compared to the PLA before degradation at 126.56°C and continues to decrease gradually to 103.14°C by the 32nd week. The melting temperature is bimodal from the 8th week onwards of degradation with a reduction in temperature from 157.07°C at 0 weeks to 145.17°C considering the first peak T_{m1} at 32nd week.

The thermograms of PLA/HNT composites as shown in Fig 8.7(b) has a slight reduction in T_g and a significant reduction in T_{cc} and T_m during the degradation. The T_g shifts from 62.15°C to 58.73°C by the 32nd week. A gradual reduction in T_{cc} with 115.64°C, 112.35°C, 108.66°C and 105.36°C for 0, 8, 20, and 32nd week respectively.

The two peaks of T_m for PLA/HNT before degradation continues during degradation with a reduction in temperature for the T_{m1} of 149.39°C and the T_{m2} is more intense with no significant change in temperature.

The thermograms of PLA+A composites shown in Fig 8.7 (c) continue to display the distinctive peaks for T_m of PCL and T_g of PLA until 8 weeks and gradually overlap by the 20th week and continue the trend for the 32nd week with a decrease in temperature. However, it is difficult to distinguish the temperature of T_m of PCL and T_g of PLA due to the overlapping. The T_{cc} significantly reduces from 118.46°C to 95.28°C during degradation. Two peaks of T_m are observed for the 8th week and 20th week with a decrease in temperature for T_{m1}. However, for the 32nd week, the T_m is a single peak.

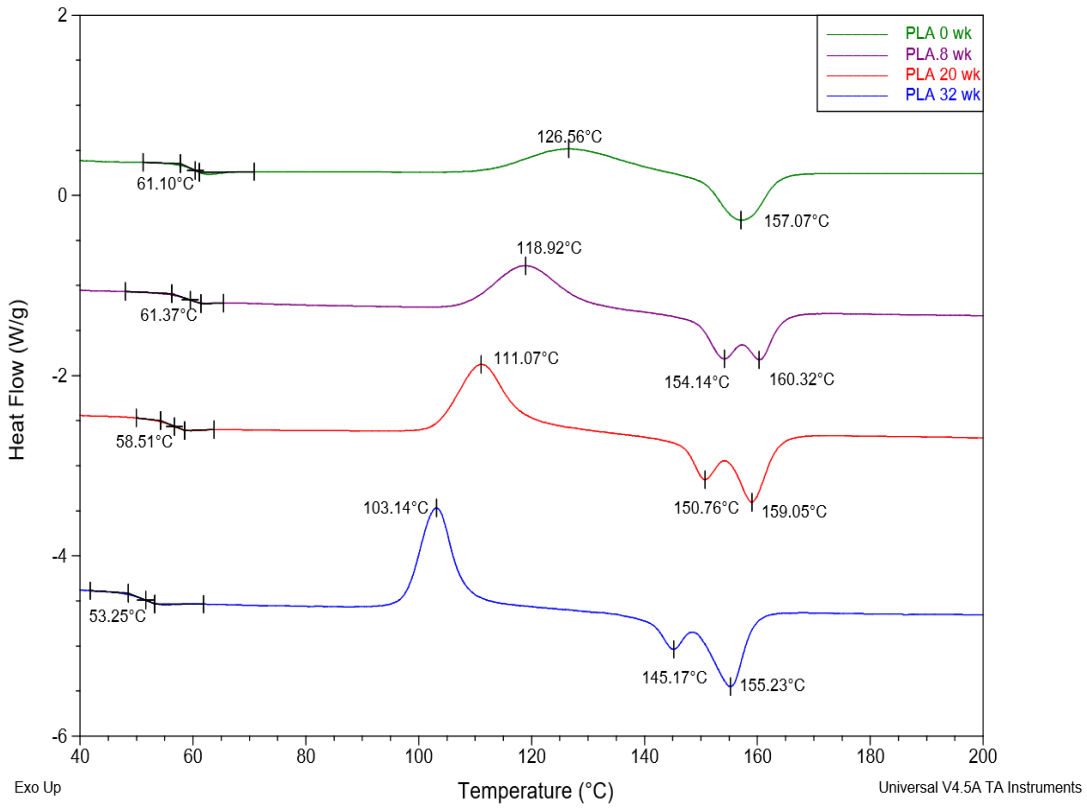

(a)

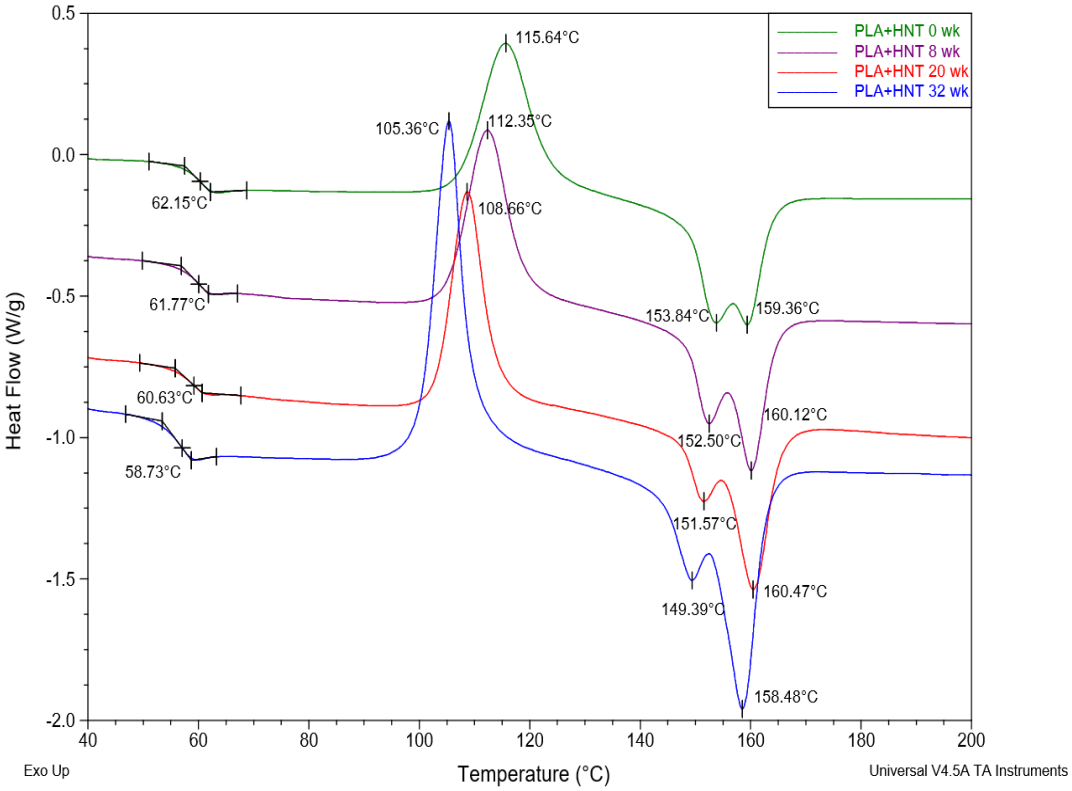
PLA+HNT 0 wk
PLA+HNT 8 wk
PLA+HNT 20 wk
PLA+HNT 32 wk
115.64°C
105.36°C
112.35°C
108.66°C
62.15°C
61.77°C
153.84°C
159.36°C
60.63°C
160.12°C
152.50°C
58.73°C
151.57°C
160.47°C
149.39°C
158.48°C
Heat Flow (W/g)
Temperature (°C)
Exo Up
Universal V4.5A TA Instruments

(b)

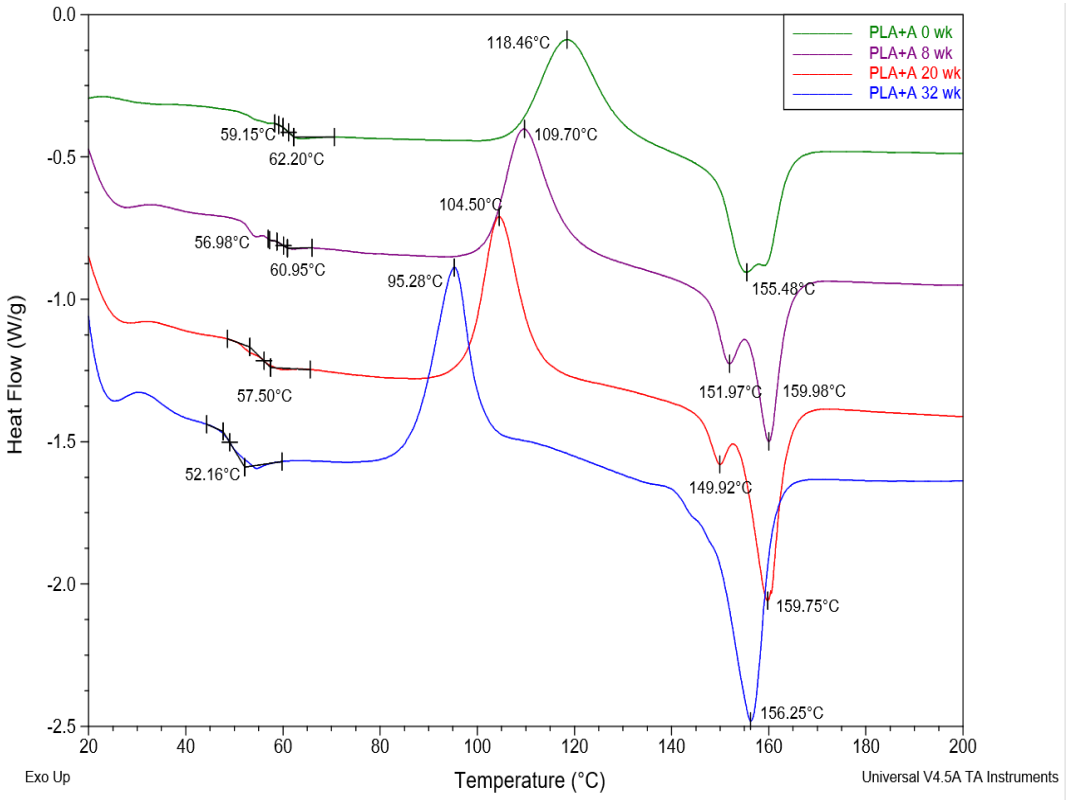
PLA+A 0 wk
PLA+A 8 wk
PLA+A 20 wk
PLA+A 32 wk
118.46°C
59.15°C
62.20°C
109.70°C
104.50°C
56.98°C
60.95°C
95.28°C
155.48°C
57.50°C
151.97°C
159.98°C
52.16°C
149.92°C
159.75°C
156.25°C
Heat Flow (W/g)
Temperature (°C)
Exo Up
Universal V4.5A TA Instruments

(c)

Figure 8.6. *DSC thermograms of (a) PLA, (b) PLA+HNT, and (c) PLA+A5% during the in-vitro degradation study*

The FTIR spectra for the PLA, PLA/HNT, and PLA+A composites during the degradation are shown in Fig 8.7. There are no significant shifts in the peaks during the degradation for all the samples however, only the intensity of the peaks are reduced for 32nd-week samples which could imply no bulk degradation occurred. The ester bond of PLA did not change during the degradation process, evidenced by the unchanged carbonyl group C=O band at 1750 cm^{-1} and C-O band at 1000–1300 cm^{-1}.

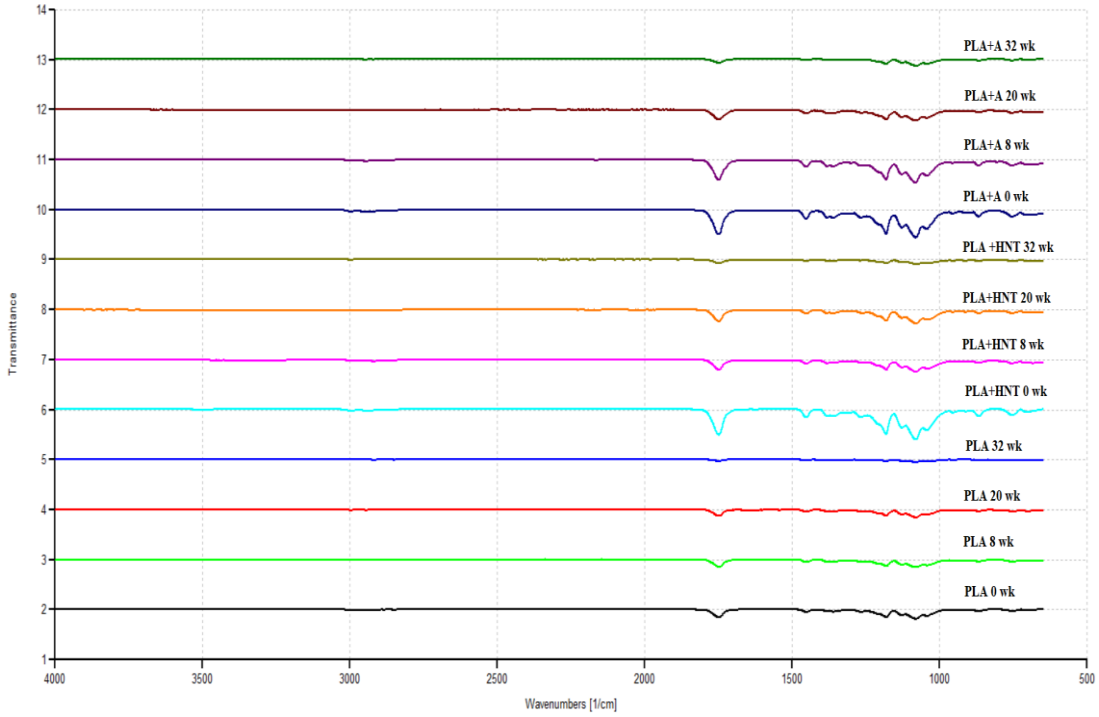

Figure 8.7. *FTIR spectra of (a) PLA, (b) PLA+HNT and (c) PLA+A5% during the in-vitro degradation study for 0, 8, 20 and 32 weeks*

8.4 Discussion

PLA is well known to be a glassy polymer at room temperature, showing a relatively high modulus and maximum strength associated with a low deformation at the break. On the other hand, PCL has significantly lower stiffness and resistance but exhibits a very high elongation at break. With the addition of HNT almost certainly a compatible blend of PLA/PCL/HNT was obtained. Unlike most studies, a

compatibilizer was not used for making the blend. This could be attributed to the presence of HNT in the nanocomposite. Various studies have reported improved ductility of PLA with the addition of PCL either because of the presence of a compatibilizer or if the amount of PCL was high, nearly 22.5% or 30% and in some studies, 50/50 composition of PLA and PCL was required to achieve improved ductility (Urquijo, Guerrica-Echevarría and Eguiazábal, 2015; Ferri *et al.*, 2016; Quiles-Carrillo, , Nestor Montanes, Fede Pineiro and Torres-Giner, 2018; Dadras *et al.*, 2020). In this study, the addition of HNT could be the reason for the increased elongation percentage with only 5% of PCL/HNT addition to the dominant PLA content where 10% HNT was pre-blended with PCL. The addition of HNT to PCL significantly increases the percentage elongation. Similarly, the addition of PCL+HNT 5% to PLA (PLA+A5%) significantly improves the elongation at break when compared to PLA. The improvement in percentage elongation could be due to the compatibility of PLA, PCL phases (Monticelli *et al.*, 2014) and this could also indicate the HNT acting as a compatibilizer between PLA and PCL.

The increase in elongation at break and retention of Young's Modulus for PLA+A5% is significant. A similar trend is observed in the study of PLA/PCL/POSS by Monticelli et.al. (Monticelli *et al.*, 2014). Wachirahuttapong et.al. studied the PLA/PCL with pluronic loading and found a decrease in tensile strength and Young's Modulus (Wachirahuttapong, Thongpin and Sombatsompop, 2016). However, in this study, the tensile strength remained within the significant range of the tensile strength of the PLA. This could be the effect of HNT interaction within the polymer interface or because of the high molecular weight of PCL (50k Mw) which gives strength as chains become large and entangle (Kantesh Balani, Vivek Verma, Arvind Agarwal, 2015).

In comparison to PLA, the cold crystallization temperature (T_{cc}) significantly decreases for all the nanocomposites which are similar to several previous literature data. As reported earlier, this could be due to the nucleating effect of HNT, PCL, and PCL/HNT pre-blend with the PLA (Chen *et al.*, 2017; Finotti *et al.*, 2017). It also indicates the promotion of the crystallization behavior of PLA (A. Hou, 2019). The double melting peak with no significant difference in T_m of PLA is observed here as well in all the blends indicating heterogeneous nucleation by melting of imperfect crystals at a lower temperature (T_{m1}) followed by rearranging for an ordered structure

at heating and melting at higher temperature (T_{m2}) (Dadras *et al.*, 2020). It could also indicate the melting of the alpha form of PLA at higher temperatures and the melting of beta form at a lower temperature (Chavalitpanya and Phattanarudee, 2013). The presence of two independent melting peaks corresponding to PCL and PLA or no significant change in T_g of the nanocomposites when compared to neat PLA implies the immiscibility of the PLA and PCL as seen in previous studies (Patrício and Bártolo, 2013; Chen *et al.*, 2014; Urquijo, Guerrica-Echevarría and Eguiazábal, 2015; Ferri *et al.*, 2016; Kelnar *et al.*, 2016).

The interaction of HNT with PCL was evident from the FTIR spectrum and this could be achieved without modifying via twin-screw extrusion. It could be due to the better interaction of HNT with PCL with high molecular weight which was also in powder form as HNT which could have led to efficient dispersion of HNT in the PCL matrix. The hydrogen bonding interaction between the HNT and PCL was displayed in the blend along with the good interaction of PCL with PLA in the PLA/PCL blend. This indicates the high melt shear and high melt temperature during the extrusion led to the bonding and reaction between the carboxyl and hydroxyl end groups of the PLA, PCL, and HNT as analyzed (A. Hou, 2019). Thus, the influence of high molecular weight PCL and PCL/HNT with good bonding could have led to the improvement in the mechanical properties of PLA/PCL/HNT (PLA+A).

To obtain good mechanical properties, effectual interaction between the matrices of the polymer is required in the case of composites (Akos *et al.*, 2013) and along with this uniform dispersion of nanoclay is necessary in the case of polymer nanocomposites. In this study, PLA+A5% demonstrates toughness with good tensile strength and ductility which could be due to hydrogen bonding which is seen in FTIR results. A similar toughening effect was seen by Shi et al. in their study with a balance of the stiffness and toughness was obtained by combining both nanofillers and plasticizers (Shi *et al.*, 2015). Thus, through FTIR and mechanical testing, the interfacial adhesion between the dispersed phases in the PLA matrix could be seen. However, from DSC results immiscibility of the polymers was seen. A well-dispersed phase with a high degree of load transfer is required for the augmentation of mechanical properties (Bugatti, 2017). It is reported that if polymers are immiscible, there is a clear phase separation for continuous phase of dominant polymer with development of minority polymer domains and this phase separation leads to

suspension of elongation (Ferri *et al.*, 2016). Contrary to this, the results from this study present good compatibility, which could be due to the good interfacial adhesion between the polymer phases due to selective interface localization of well-dispersed HNT (Wu *et al.*, 2009). The effect of HNT as a compatibilizer could have improved the interfacial bonding of the PLA matrix and PCL (Dadras *et al.*, 2020).

A similar result was obtained by Ferri et. al. in their study for 20-30% of PCL addition which revealed immiscibility of polymers from DSC without deterioration in mechanical resistance along with better ductile properties (Ferri *et al.*, 2016). In their study, the effect of miscibility on the thermal and mechanical properties of PLA/PCL blend using ~50K Mw PCL via twin-screw extrusion followed by injection molding was investigated. Though their results revealed the immiscibility of polymers from DSC, the composites had better ductile properties without concession of mechanical resistance properties for 20-30% of PCL addition to the composite (Ferri *et al.*, 2016). Similar results were obtained in our study for PCL-based composite where PCL was pre-blended with 10% HNT and this pre-blend PCL/HNT composite of 5% was added to PLA. We too find the immiscibility of the polymers from the DSC results, however, the mechanical properties are improved in terms of toughness which correlates to the FTIR results as well similar to the results of Ferri et.al. This improvement in overall mechanical properties could be due to the higher molecular weight of PCL (Chen *et al.*, 2003).

The *in-vitro* degradation images of the samples are as shown in Figure 8.8. The images depicts the surface changes is higher in PLA+A5% when compared to the PLA and PLA/HNT samples.

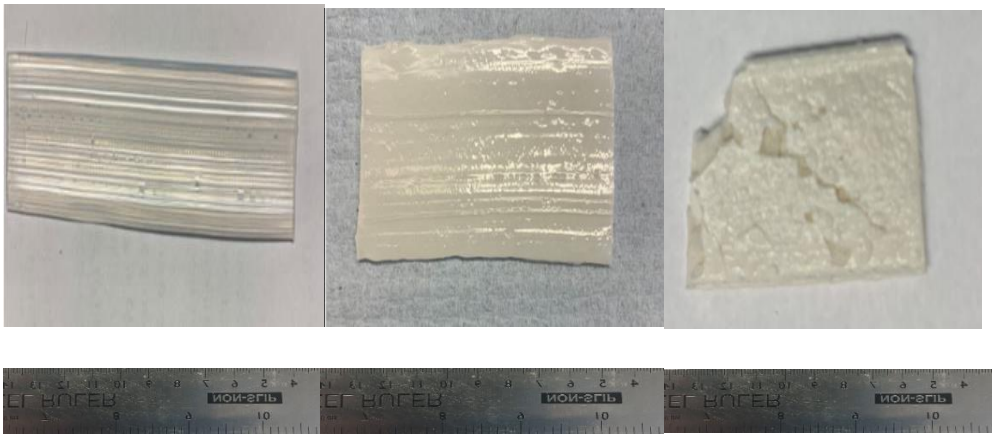

(a) (b) (c)

Figure 8.8. *Images of the degradation samples (a) PLA (b) PLA/HNT (c) PLA+A5% at 32nd week during the in-vitro degradation study*

The results depict the slight reduction of the mass of PLA, PLA/HNT compared to PLA+A5% which had the highest reduction of 18.56% by the end of the 32nd week. This could be due to the heterogeneous nature of the composite which allowed easier permeation of water. The results for the mechanical and thermal properties also suggest the hydrolytic degradation process. The Young's Modulus and stiffness show small retention by the 32nd week. On the contrary, Vieira et.al. reported 80% strength loss in 16 weeks degradation of PLA/PCL fibers (Vieira *et al.*, 2011) and Chen et.al. reported 33.7, 27.6% modulus loss at the end of the 24th week for PLA and PLA/HNT composites (Chen *et al.*, 2018). The intermolecular bonding is more in the crystalline phase which leads to oriented chains during polymer deformation for good strength (Kantesh Balani, Vivek Verma, Arvind Agarwal, 2015).

The decrease in the glass transition temperature of the PLA, PLA/HNT composites signifies less rigidity or stiffness after degradation for 32 weeks as T_g is the measure of rigidity (Declan M. Devine *et al.*, 2017). The hydrolytic degradation process could have aided the cold crystallization process because of the formation of less intensified and loose chain PLA entanglement during the degradation providing greater mobility leading to the crystallinity of PLA. Similar results were reported by Valapa et.al. and Chen et.al. (Valapa, Pugazhenthi and Katiyar, 2016; Chen *et al.*, 2018). The two peaks of T_m could indicate the alpha form of PLA melts at higher temperature and the beta form could melt at a lower temperature (Chavalitpanya and Phattanarudee, 2013). This could also be due to the growth of small crystals which could melt at low heating rates and recrystallize before melting again (Finotti *et al.*, 2017).

The cold crystallization temperature tends to decrease for all samples indicating greater mobility of loose chain of a polymer leading to crystallinity (Valapa, Pugazhenthi and Katiyar, 2016). The intermolecular bonding is more in the crystalline phase which leads to oriented chains during polymer deformation for good strength (Kantesh Balani, Vivek Verma, Arvind Agarwal, 2015). This could have in turn led to the sustainability of tensile strength, stiffness, and modulus at the 8th week for all

samples and continues to retain until the 20th week for PLA/HNT and PLA+A5% samples. On contrary, the elongation at break notably reduces by the 8th, 20th, and 32nd week. This would be ideal for the stent material as the stent has to maintain good strength until the vessel heals without stent recoil. As the stent is not required after the vessel healing normally after 6 months, the decrease in mechanical properties by the 32nd week suggests the hydrolytic degradation of the samples.

There was no significant shifts in the peaks during the degradation for all the samples however, only the intensity of the peaks are reduced for 32nd-week samples which could imply no bulk degradation occurred. The ester bond of PLA did not change during the degradation process, evidenced by the unchanged carbonyl group C=O band at 1750 cm^{-1} and C-O band at 1000–1300 cm^{-1}. As ester group cleavage is the primary degradation mechanism of PLA (Chen *et al.*, 2018).

It has been reported that matrix yielding could be delayed if the interfacial adhesion is very strong and thus not preferred for toughness (A. Hou, 2019). Hence, in our study, PLA+A 5% composite displayed a suitable interfacial adhesion necessary for the toughening of the blend. The mechanical properties required for the stent are rather contradictory. Generally high tensile strength and Young's Modulus are needed for the stent's radial strength and to reduce recoil. However, low yield strength is required for the expansion of the stent during deployment (McMahon *et al.*, 2018; Beshchasna *et al.*, 2020). Thus, PLA+A 5% matches the requirement with good strength, modulus, and elongation which correlates to biodegradable polymers used for the manufacture of stents (Ang, Huang, *et al.*, 2017; Lee *et al.*, 2018).

In terms of resorption time of the stent, it is suggested for a faster resorption post the scaffolding period. The idea is to remove the material presence once the vessel is healed (McMahon *et al.*, 2018). The incomplete repair of the endothelium at the site of vascular wall injury due to the drug coatings and hypersensitivity to the presence of the stent facilitated the complications (Sakamoto *et al.*, 2018; Tabraiz Alam *et al.*, 2019). For faster resorption, currently, Magmaris (Biotronik, Berlin) has demonstrated the potential of magnesium-based BRS with high mechanical property and faster resorption within 4 months (Beshchasna *et al.*, 2020; Wee *et al.*, 2020).

Thus, in this study, the sustainability of tensile strength, stiffness, and modulus at 8th week, retention until 20th week, and decrease in mechanical properties of the

PLA+A5% composite by 32nd week suggest the hydrolytic degradation of the samples which could be seen from DSC results as well would be ideal as the stent is not required after the vessel healing normally after 6 months.

8.5 Summary

The prepared ternary blend with higher molecular weight PCL 50k Mw pre-blended with 10% HNT and extruded with PLA with 5%, displayed toughness with good mechanical strength and ductility, on contrary to other literature on PLA/PCL where large amounts of PCL is required to improve the ductility. Additionally, heterogeneous nucleation was seen in DSC results with good hydrogen bonding interaction was displayed in FTIR results. Thus, the pre-blending of HNT with PCL played a significant role in the improvement of the composite properties without increasing the PCL content which would be ideal for biodegradable coronary stents. It has been reported that after 6 months when the artery remodels to a fairly stable phase, the mechanical support of the stent is no longer required. The *in-vitro* degradation results demonstrate heterogeneous degradation of the samples gradually over 32 weeks with consistent weight loss and maximum mechanical degradation after the 20th week.

CHAPTER 9

Conclusion

The research and development of biodegradable drug-eluting coronary stents (BDS) aim to overcome the key limitations of the stents namely in-stent restenosis and stent thrombosis by improving the primary requirements such as biocompatibility, biodegradability, and mechanical behavior. The scope of this research was to address the research gap of material consideration, the flexibility of the stent during deployment, and degradation of the material.

1. Material selection

The most widely used polymer in currently used polymeric BDSs by more than 15 companies is PLLA (McMahon *et al.*, 2018; Wee *et al.*, 2020). Although it is highly difficult to match the mechanical properties of the polymeric stents to a metallic stent, improvement in the properties could aid in addressing the limitations (Wee *et al.*, 2020). Hence in this study, polylactic acid (PLA) is used as the base polymer which is reinforced with non-toxic nanoclay, halloysite nanotubes (HNT) via extrusion as they are widely used in the biomedical field due to their biodegradability, natural availability, and high mechanical properties.

The mechanical characteristics of a stent material require a high value of Young's Modulus to reduce stent recoil and a combination of high tensile strength and Young's Modulus to increase the stent's radial strength (Beshchasna *et al.*, 2020). In this study, the addition of 5% HNT to PLA matches the above requirement with an increase in Young's Modulus and tensile strength. It also matches the mechanical and physical properties of the biodegradable polymer PLLA currently used for commercial stents. To retain the biocompatibility of the composite, the HNT was extruded into the PLA matrix without any surface modification. The high melt shear during compounding assisted the better dispersion of the HNT into the polymer matrix which in turn improved the overall properties of the composites without the need for surface treatment of the HNT as desired for coronary stent material.

It was possible to develop a 3D printing filament using biodegradable PLA and reinforcing with biocompatible filler HNT. The filament had a diameter of 1.75±0.10 mm for use in FFF 3D printing. The 3D printed model stents were successfully fabricated into mesh forms whose mechanical properties can be enhanced by optimizing the printing parameters.

In terms of the drug release profile of the commercial stents, most of them use drug-eluting polymeric coating (Lee *et al.*, 2018). Here, we have evaluated the stent material itself as the drug carrier. To improve the patient's compliance, the sustained release of the drug is important as it is released slowly over an extended period to prolong the therapeutic effect (Pierchala *et al.*, 2018). The incomplete repair of the endothelium at the site of vascular wall injury due to the drug coatings and hypersensitivity to the permanent presence of the metal facilitated the complications (Sakamoto *et al.*, 2018; Tabraiz Alam *et al.*, 2019). Thus, in this study, the APAP-loaded PLA/HNT nanocomposite suits the requirement as it displays a sustained release profile with gradual degradation. This could be due to the presence of HNT where the APAP could have been loaded onto the inner lumen of HNT. Because the interaction between the clay and the polymer enhances the properties of the composite promoting stable controlled drug release generally prolonged (Maria, Meirelles and Raffin, 2017). This could be seen in APAP-loaded composites.

The currently used APIs in the coronary stents are 'limus family' drugs with anti-inflammatory, anti-thrombogenic, immuno-suppressive, and anti-proliferative mechanisms (Beshchasna *et al.*, 2020) have pKa values approximately between 9.6 – 10.40 ± 0.74 (Shah, Wyandt and Stodghill, 2013; Book, 2017; Wishart DS, 2017) which is similar to the pKa value of the model drug APAP used in this study. Thus, the PLA/HNT nanocomposite could be suitable for the currently used API types with pKa of ~9.6 for coronary stents.

2. Stent ductility:

The developed model stent via 3D printing was not flexible for expansion of the stent during placement. Hence, PCL was reinforced with HNT and pelletized. The pelletized PCL/HNT composite was extruded with PLA. Generally high tensile strength and Young's Modulus are needed for the stent's radial strength and to reduce recoil. However, low yield strength is required for the expansion of the stent during deployment (McMahon *et al.*, 2018; Beshchasna *et al.*, 2020). Thus, PLA loaded with PCL/HNT composite of 5% matches the requirement with good strength, modulus, and elongation which correlates to biodegradable polymers used for the manufacture of stents (Ang, Huang, *et al.*, 2017; Lee *et al.*, 2018).

3. Degradation study:

The in vitro degradation study was conducted for 8 months on PLA/PCL/HNT nanocomposites and drug-loaded nanocomposites.

In terms of resorption time of the stent, it is suggested for a faster resorption post the scaffolding period. The idea is to remove the material presence once the vessel is healed (McMahon *et al.*, 2018). For faster resorption, currently, Magmaris (Biotronik, Berlin) has demonstrated the potential of magnesium-based BRS with high mechanical property and faster resorption within 4 months (Beshchasna *et al.*, 2020; Wee *et al.*, 2020). The presence of HNT aided the nominal burst release, a sustained release of APAP and a gradual degradation for the APAP loaded PLA/HNT nanocomposite. As the higher pKa value used here is equivalent to the pKa values of the currently used drugs in drug-eluting coronary stents, the PLA/HNT nanocomposite is suitable for drug-eluting stents.

The *in-vitro* degradation results for PLA blended with 5% of PCL/HNT composite demonstrate heterogeneous degradation of the samples gradually over 32 weeks with consistent weight loss and mechanical degradation after the 20^{th} week.

Thus, the research gap of material consideration, toughening of the material for both radial strength and expansion of the stent during deployment, faster degradation of the material are addressed in this study. The key highlight of this study was the introduction of HNT and its assistance in meeting the requirements of the stent such as

- Material property enhancement
- Sustained drug release capacity from the stent body
- Improvement in the toughness of the material to address the ductility of the stent
- Faster yet gradual degradation of the APAP-loaded nanocomposites and PLA/PCL/HNT nanocomposite.

Thus, an innovative polymer nanocomposite developed could be proposed as a stent material. Further research of developing the PLA/PCL/HNT nanocomposite with drug-eluting capacity into 3D printed stents with a detailed study of designing the stent with ideal strut thickness, followed by the study of degradation mechanism of the stent will be able to provide detailed stages of stent degradation along with drug elution

mechanism from the produced stent would be beneficial for a new prospect of stent technology.

REFERENCES

A. Hou (2019) ‘Super-Toughened Poly (lactic Acid) with’, *Polymers*. doi: 10.3390/polym11050771.

A, S. Z. O. (2003) ‘Секція : Matsyutsya Katerina Kiev National University of Technology and Design ASPIRIN – FRIEND OR FOE ? Ahtyamova D . PARAMETERS AFFECTING THE PERFORMANCE OF IMMOBILIZED ENZYME Supervisor : Zvonok O .’ ТНТУ, pp. 150–151.

Abdullayev, E. and Lvov, Y. (2011) ‘Halloysite Clay Nanotubes for Controlled Release of Protective Agents’, *Journal of Nanoscience and Nanotechnology*, 11(5), pp. 10007–10026. doi: 10.1166/jnn.2011.5724.

Abdullayev, E. and Lvov, Y. (2013) ‘Halloysite clay nanotubes as a ceramic “skeleton” for functional biopolymer composites with sustained drug release’, *Journal of Materials Chemistry B*, 1(23), pp. 2894–2903. doi: 10.1039/C3TB20059K.

Abeykoon, C. *et al.* (2014) ‘Investigation of the process energy demand in polymer extrusion: A brief review and an experimental study’, *Applied Energy*. Elsevier Ltd, 136, pp. 726–737. doi: 10.1016/j.apenergy.2014.09.024.

Acharya, P. C. *et al.* (2018) *Discovery and Development, Dosage Form Design Considerations*. Elsevier Inc. doi: 10.1016/B978-0-12-814423-7.00013-7.

Akos, N. I. *et al.* (2013) ‘Preparation , Characterization , and Mechanical Properties of Poly (e -caprolactone)/ Polylactic Acid Blend Composites’, pp. 2–7. doi: 10.1002/pc.

Albareeki, M. M., Driscoll, S. B. and Barry, C. F. (2019) ‘Compounding of polyethylene composites using high speed twin and quad screw extruders’, *AIP Conference Proceedings*, 2139(August). doi: 10.1063/1.5121653.

Alberton, J. *et al.* (2014) ‘Mechanical and moisture barrier properties of titanium dioxide nanoparticles and halloysite nanotubes reinforced polylactic acid (PLA)’, *IOP Conference Series: Materials Science and Engineering*, 64, p. 012010. doi: 10.1088/1757-899X/64/1/012010.

Alexis, F. (2005) ‘Factors affecting the degradation and drug-release mechanism of poly (lactic acid) and poly [(lactic acid) - co - (glycolic acid)]’, 46(June 2004), pp. 36–46. doi: 10.1002/pi.1697.

Alexy, R. D. and Levi, D. S. (2013) ‘Materials and manufacturing technologies available for production of a pediatric bioabsorbable stent’, *BioMed Research International*, 2013. doi: 10.1155/2013/137985.

Ali, Z. A. *et al.* (2017) ‘2-year outcomes with the Absorb bioresorbable scaffold for treatment of coronary artery disease: a systematic review and meta-analysis of seven randomised trials with an individual patient data substudy’, *The Lancet*. Elsevier Ltd, 390(10096), pp. 760–772. doi: 10.1016/S0140-6736(17)31470-8.

Amato, S. and Ezzell, Jr, R. (2015) *Regulatory Affairs for Biomaterials and Medical Devices*. Elsevier. doi: 10.1016/C2013-0-16313-1.

Anand Narayanan, A. G., Babu, R. and Vasanthakumari, R. (2016) ‘Studies on Halloysite Nanotubes (HNT) Natural Rubber Nanocomposites for Mechanical Thermal and Wear Properties’, *International Journal of Engineering Research & Technology*, 5(03), pp. 152–156. doi: 10.17577/IJERTV5IS030167.

Andre, J.-C., Le Mehaute, A. and De Witte, O. (1984) ‘Dispositif pour réaliser un modèle de pièce industrialle (Device for fabrcating an industrial part model)’.

Ang, H. Y., Bulluck, H., *et al.* (2017a) ‘Bioresorbable stents: Current and upcoming bioresorbable technologies’, *International Journal of Cardiology*. Elsevier B.V., 228, pp. 931–939. doi: 10.1016/j.ijcard.2016.11.258.

Ang, H. Y., Bulluck, H., *et al.* (2017b) ‘Bioresorbable stents: Current and upcoming bioresorbable technologies’, *International Journal of Cardiology*. Elsevier B.V., 228, pp. 931–939. doi: 10.1016/j.ijcard.2016.11.258.

Ang, H. Y., Huang, Y. Y., *et al.* (2017) ‘Mechanical behavior of polymer-based vs. metallic-based bioresorbable stents’, *Journal of Thoracic Disease*, 9(Suppl 9), pp. S923–S934. doi: 10.21037/jtd.2017.06.30.

Ang, H. Y. *et al.* (2018) ‘Radiopaque Fully Degradable Nanocomposites for

Coronary Stents', *Scientific Reports*, 8(1), pp. 1–14. doi: 10.1038/s41598-018-35663-2.

Anwar, K., Halim, A. and Florida, S. (2012) 'Optimisation of a Twin Screw Extrusion Process for Enhanced Short-term Mechanical Properties of Polyamide 11 nanocompo ....', (June 2014).

ASM International (2004) 'Introduction to Tensile Testing', *Tensile testing*, pp. 1–13. doi: 10.1017/CBO9781107415324.004.

Atif, R. and Inam, F. (2016) 'Reasons and remedies for the agglomeration of multilayered graphene and carbon nanotubes in polymers', *Beilstein Journal of Nanotechnology*, 7(1), pp. 1174–1196. doi: 10.3762/bjnano.7.109.

Azaouzi, M., Makradi, A. and Belouettar, S. (2012) 'Deployment of a self-expanding stent inside an artery: A finite element analysis', *Materials and Design*. Elsevier Ltd, 41, pp. 410–420. doi: 10.1016/j.matdes.2012.05.019.

Balogh, A. *et al.* (2018) 'Supporting Information Continuous End-to-End Production of Solid Drug Dosage Forms : Coupling Flow Synthesis and Formulation by Electrospinning', *Chemical Engineering Journal*. Elsevier, 350(March), pp. 1–23. doi: 10.1016/j.cej.2018.05.188.

Bari, S. S., Chatterjee, A. and Mishra, S. (2016) 'Biodegradable polymer nanocomposites: An overview', *Polymer Reviews*, 56(2), pp. 287–328. doi: 10.1080/15583724.2015.1118123.

Basu, A. *et al.* (2016) 'Poly(lactic acid)-based nanocomposites', *Polymers for Advanced Technologies*, (November). doi: 10.1002/pat.3985.

Bellini, A. and Guceri, S. (2003) 'Mechanical characterization of parts fabricated using fused deposition modeling', *Rapid Prototyping Journal*, 9(4), pp. 252–264. doi: Doi 10.1108/13552540310489631.

Bergström, J. S. and Hayman, D. (2016) 'An Overview of Mechanical Properties and Material Modeling of Polylactide (PLA) for Medical Applications', *Annals of Biomedical Engineering*, 44(2), pp. 330–340. doi: 10.1007/s10439-015-1455-8.

Berretta, S. *et al.* (2017) 'Fused Deposition Modelling of high temperature polymers: Exploring CNT PEEK composites', *Polymer Testing*. Elsevier Ltd, 63, pp. 251–262. doi: 10.1016/j.polymertesting.2017.08.024.

Beshchasna, N. *et al.* (2020) 'Recent Advances in Manufacturing Innovative Stents', *Pharmaceutics*, 12(349), pp. 1–37. doi: 10.3390/pharmaceutics12040349.

Beslikas, T. *et al.* (2011) 'Crystallization Study and Comparative in Vitro – in Vivo Hydrolysis of PLA Reinforcement Ligament', pp. 6597–6618. doi: 10.3390/ijms12106597.

Bezrouk, A. *et al.* (2020) 'Mechanical properties of a biodegradable self-expandable polydioxanone monofilament stent: In vitro force relaxation and its clinical relevance', *PLoS ONE*, 15(7 July), pp. 1–16. doi: 10.1371/journal.pone.0235842.

Bhatia, S. K. (2010a) 'Biomaterials for clinical applications', *Biomaterials for Clinical Applications*, pp. 1–283. doi: 10.1007/978-1-4419-6920-0.

Bhatia, S. K. (2010b) 'Biomaterials for clinical applications', *Biomaterials for Clinical Applications*, pp. 1–283. doi: 10.1007/978-1-4419-6920-0.

Bhatt, A. and Anbarasu, A. (2017) 'Nanoscale Biomaterials for 3D printing', *IOSR Journal of Pharmacy and Biological Sciences*, 12(03), pp. 80–86. doi: 10.9790/3008-1203068086.

Bioabsorbable Stents Global Market Report 2020-30: Covid 19 Growth and Change (2020). Available at: https://www.reportlinker.com/p05948405/Bioabsorbable-Stents-Global-Market-Report-30-Covid-19-Growth-and-Change.html?utm_source=GNW#backAction=2.

von Birgelen, C. *et al.* (2016) 'Very thin strut biodegradable polymer everolimus-eluting and sirolimus-eluting stents versus durable polymer zotarolimus-eluting stents in allcomers with coronary artery disease (BIO-RESORT): a three-arm, randomised, non-inferiority trial', *The Lancet*, 388(10060), pp. 2607–2617. doi: 10.1016/S0140-6736(16)31920-1.

Boland, E. L. *et al.* (2016) 'A Review of Material Degradation Modelling for the

Analysis and Design of Bioabsorbable Stents', *Annals of Biomedical Engineering*, 44(2), pp. 341–356. doi: 10.1007/s10439-015-1413-5.

Book, C. (2017) *Zotarolimus properties*. Available at: https://www.chemicalbook.com/ChemicalProductProperty_EN_CB21011766.htm (Accessed: 10 October 2020).

Borhani, S. *et al.* (2018) *Cardiovascular stents: overview, evolution, and next generation, Progress in Biomaterials*. Springer Berlin Heidelberg. doi: 10.1007/s40204-018-0097-y.

Botting, R. M. (2000) 'Mechanism of action of acetaminophen: Is there a cyclooxygenase 3?', *Clinical Infectious Diseases*, 31(SUPPL. 5), pp. 202–210. doi: 10.1086/317520.

Bounabi, L. *et al.* (2016) 'Journal of Drug Delivery Science and Technology Development of poly (2-hydroxyethyl methacrylate)/ clay composites as drug delivery systems of paracetamol', *Journal of Drug Delivery Science and Technology*. Elsevier Ltd, 33, pp. 58–65. doi: 10.1016/j.jddst.2016.03.010.

Bracco, G. and Holst, B. (2013) *Surface science techniques, Springer Series in Surface Sciences*. doi: 10.1007/978-3-642-34243-1.

Braunersreuther, V., Mach, F. and Montecucco, F. (2012) 'Statins and stent thrombosis', (February), pp. 1–9. doi: 10.4414/smw.2012.13525.

Breitenbach, J. (2002) 'Melt extrusion: from process to drug delivery technology', *European Journal of Pharmaceutics and Biopharmaceutics*, 54(2), pp. 107–117. doi: 10.1016/S0939-6411(02)00061-9.

Brie, D. *et al.* (2016) 'Bioresorbable scaffold — A magic bullet for the treatment of coronary artery disease?', *International Journal of Cardiology*. Elsevier Ireland Ltd, 215(April), pp. 47–59. doi: 10.1016/j.ijcard.2016.04.027.

Bugatti, V. V. G. N. C. G. G. (2017) 'Nanocomposites Based on PCL and Halloysite Nanotubes Filled with Lysozyme: Effect of Draw Ratio on the Physical Properties and Release Analysis', *Nanomaterials*, 7(8), p. 213. doi: 10.3390/nano7080213.

Caiazzo, G. *et al.* (2015) ‘Absorb bioresorbable vascular scaffold: What have we learned after 5 years of clinical experience?’, *International Journal of Cardiology*, 201, pp. 129–136. doi: 10.1016/j.ijcard.2015.07.101.

Cairns, D. (2003) ‘Essentials of Pharmaceutical Chemistry.’

Çakman, G. (2016) ‘Preparation and Physical , Thermal Properties of Polycaprolactone / m-Halloysite Nanocomposite’, 2(9), pp. 842–848.

Calorimetry, D. S. and Analysis, T. (2010) ‘Differential Scanning Calorimetry & Thermo-Gravimetric Analysis , Fleming PTC Differential Scanning Calorimetry & Thermo-Gravimetric Analysis , Fleming PTC’, *Scanning*, pp. 1–2.

Campbell, K., Craig, D. Q. M. and Mcnally, T. (2008) ‘Poly (ethylene glycol) layered silicate nanocomposites for retarded drug release prepared by hot-melt extrusion’, 363, pp. 126–131. doi: 10.1016/j.ijpharm.2008.06.027.

Carazo, E. *et al.* (2019) *Clay minerals in drug delivery systems 6 ´*. doi: 10.1016/B978-0-12-814617-0.00010-4.

Carvalho, J. R. G. *et al.* (2020) ‘Biocompatibility and biodegradation of poly (lactic acid) (PLA) and an immiscible PLA / poly (ε -caprolactone) (PCL) blend compatibilized by poly (ε -caprolactone- b -tetrahydrofuran) implanted in horses’, *Polymer Journal*. Springer US. doi: 10.1038/s41428-020-0308-y.

Casalini, T. *et al.* (2019) ‘A Perspective on Polylactic Acid-Based Polymers Use for Nanoparticles Synthesis and Applications’, *Frontiers in Bioengineering and Biotechnology*, 7(October), pp. 1–16. doi: 10.3389/fbioe.2019.00259.

Cassese, S. *et al.* (2016) ‘Everolimus-eluting bioresorbable vascular scaffolds versus everolimus-eluting metallic stents: A meta-analysis of randomised controlled trials’, *The Lancet*. Elsevier Ltd, 387(10018), pp. 537–544. doi: 10.1016/S0140-6736(15)00979-4.

Castro-aguirre, E. *et al.* (2017) ‘Impact of Nanoclays on the Biodegradation of Poly (lactic acid) Nanocomposites’, 2, pp. 1–24. doi: 10.3390/polym10020202.

Castro-Aguirre, E. *et al.* (2016) ‘Poly(lactic acid)—Mass production, processing,

industrial applications, and end of life', *Advanced Drug Delivery Reviews*. Elsevier B.V., 107, pp. 333–366. doi: 10.1016/j.addr.2016.03.010.

Cavallaro, G., Lazzara, G. and Fakhrullin, R. (2018) 'Mesoporous inorganic nanoscale particles for drug adsorption and controlled release'.

'Cerezen device provides treatment for temporomandibular joint disorders day and night' (2016) *Bdj*. Nature Publishing Group, 220, p. 666.

Charifson, P. S. and Walters, W. P. (2014) 'Acidic and basic drugs in medicinal chemistry: A perspective', *Journal of Medicinal Chemistry*, 57(23), pp. 9701–9717. doi: 10.1021/jm501000a.

Charpentier, E. *et al.* (2015) 'Fully bioresorbable drug-eluting coronary scaffolds: A review', *Archives of Cardiovascular Diseases*. Elsevier Masson SAS, 108(6–7), pp. 385–397. doi: 10.1016/j.acvd.2015.03.009.

Chavalitpanya, K. and Phattanarudee, S. (2013) 'Poly (lactic acid)/ Polycaprolactone Blends Compatibilized with Block Copolymer', *Energy Procedia*. Elsevier B.V., 34, pp. 542–548. doi: 10.1016/j.egypro.2013.06.783.

Chellamuthu, Sabarinathan & Muthu, S & Naushad Ali, M. (2012) 'Experimental study on tensile behavior of multi wall carbon nanotube reinforced epoxy composites', (November). doi: 8. 3253-3259.

Chen, C. C. *et al.* (2003) 'Preparation and characterization of biodegradable PLA polymeric blends', *Biomaterials*. Elsevier Ltd, 24(7), pp. 1167–1173. doi: 10.1016/S0142-9612(02)00466-0.

Chen, Y. *et al.* (2014) 'Analysis of the Mechanical Properties of Solvent Cast Blends of PLA/PCL', *https://www.scientific.net/AMM*, 679, pp. 50–56. doi: https://doi.org/10.4028/www.scientific.net/AMM.679.50.

Chen, Y. *et al.* (2016) 'A Review of Multifarious Applications of Poly (Lactic Acid)', *Polymer-Plastics Technology and Engineering*, 2559(March), pp. 1057–1075. doi: 10.1080/03602559.2015.1132465.

Chen, Y. *et al.* (2016) 'Review of Multifarious Applications of Poly (Lactic Acid)',

Polymer - Plastics Technology and Engineering, 55(10). doi: 10.1080/03602559.2015.1132465.

Chen, Y. *et al.* (2017) 'Halloysite nanotube reinforced polylactic acid composite', *Polymer Composites*, 38(10). doi: 10.1002/pc.23794.

Chen, Y. *et al.* (2018) 'Surface-modified halloysite nanotubes reinforced poly(lactic acid) for use in biodegradable coronary stents', *Journal of Applied Polymer Science*, 135(30), p. 46521. doi: 10.1002/app.46521.

Chia, H. N. and Wu, B. M. (2015) 'Recent advances in 3D printing of biomaterials', *Journal of Biological Engineering*. BioMed Central, 9(1), p. 4. doi: 10.1186/s13036-015-0001-4.

Coates, J. (2000) 'Interpretation of Infrared Spectra , A Practical Approach Interpretation of Infrared Spectra , A Practical Approach', *Encyclopedia of Analytical Chemistry*, pp. 10815–10837. doi: DOI: 10.1002/9780470027318.

Collet, C. *et al.* (2016) 'The Absorb Bioresorbable Vascular Scaffold for the treatment of coronary artery disease', 5247(August). doi: 10.1080/17425247.2016.1227788.

Conijn, M. *et al.* (2018) 'The Y-stenting technique for pulmonary artery bifurcation stenosis: Initial results and mid-term outcomes', *International Journal of Cardiology*. Elsevier B.V., 268, pp. 202–207. doi: 10.1016/j.ijcard.2018.03.100.

Conner, B. P. *et al.* (2014) 'Making sense of 3-D printing: Creating a map of additive manufacturing products and services', *Additive Manufacturing*. Elsevier B.V., 1, pp. 64–76. doi: 10.1016/j.addma.2014.08.005.

Coppola, B. *et al.* (2018) '3D printing of PLA/clay nanocomposites: Influence of printing temperature on printed samples properties', *Materials*, 11(10), pp. 1–17. doi: 10.3390/ma11101947.

Corea, J. R. (2016) *Screen Printed MRI Receive Coils*.

Cui, W. *et al.* (2006) 'Investigation of Drug Release and Matrix Degradation of Electrospun Poly (DL -lactide) Fibers with Paracetanol Inoculation', pp. 1623–

1629.

Ćwikła, G. *et al.* (2017) ‘The influence of printing parameters on selected mechanical properties of FDM/FFF 3D-printed parts’, *IOP Conference Series: Materials Science and Engineering*, 227(1). doi: 10.1088/1757-899X/227/1/012033.

Dadbakhsh, S. *et al.* (2016) ‘Effect of powder size and shape on the SLS processability and mechanical properties of a TPU elastomer’, *Physics Procedia*, 83, pp. 971–980. doi: 10.1016/j.phpro.2016.08.102.

Dadras, M. *et al.* (2020) ‘Biodegradable Nanocomposites Developed from PLA / PCL Blends and Silk Fibroin Nanoparticles : Study on the Microstructure , Thermal Behavior , Crystallinity and Performance’, *Journal of Polymers and the Environment*. Springer US, (0123456789). doi: 10.1007/s10924-020-01684-0.

Das, S., Banerjee, R. and Bellare, J. (2005) ‘Aspirin loaded albumin nanoparticles by coacervation: Implications in drug delivery’, *Trends in Biomaterials and Artificial Organs*, 18(2), pp. 203–212.

Dave, B. (2016) ‘Bioresorbable scaffolds: Current evidences in the treatment of coronary artery disease’, *Journal of Clinical and Diagnostic Research*, 10(10), pp. 1–7. doi: 10.7860/JCDR/2016/21915.8429.

Dave, R. H., Shah, D. A. and Patel, P. G. (2014) ‘Development and Evaluation of High Loading Oral Dissolving Film of Aspirin and Acetaminophen’, pp. 112–122. doi: 10.1166/jpsp.2014.1014.

Debra Dunson, Ph.D., E. L. (2017) ‘Characterization of Polymers using Dynamic Mechanical Analysis (DMA)’.

Debusschere, N. *et al.* (2015) ‘A finite element strategy to investigate the free expansion behaviour of a biodegradable polymeric stent’, *Journal of Biomechanics*. Elsevier, 48(10), pp. 2012–2018. doi: 10.1016/j.jbiomech.2015.03.024.

Deepak, R. and Agrawal, Y. K. (2012) ‘Study of nanocomposites with emphasis to halloysite nanotubes’, *Reviews on Advanced Materials Science*, 32(2), pp. 149–157.

Dermanaki Farahani, R. and Dubé, M. (2017) ‘Printing Polymer Nanocomposites

and Composites in Three Dimensions', *Advanced Engineering Materials*, 1700539, pp. 1–9. doi: 10.1002/adem.201700539.

DeSimone, J. *et al.* (2015) 'Continuous liquid interphase printing'.

Devine, D. M. *et al.* (2006) 'Multifunctional polyvinylpyrrolidinone-polyacrylic acid copolymer hydrogels for biomedical applications', *International Journal of Pharmaceutics*, 326(1–2), pp. 50–59. doi: 10.1016/j.ijpharm.2006.07.008.

Devine, D. M. *et al.* (2017) 'Extended release of proteins following encapsulation in hydroxyapatite/chitosan composite scaffolds for bone tissue engineering applications', *Materials Science and Engineering C*. doi: 10.1016/j.msec.2017.11.001.

Devine, D. M. *et al.* (2017) 'Extended release of proteins following encapsulation in hydroxyapatite/chitosan composite scaffolds for bone tissue engineering applications', *Materials Science and Engineering C*. Elsevier, 84(November 2016), pp. 281–289. doi: 10.1016/j.msec.2017.11.001.

Devine, D. M., Geever, L. M. and Higginbotham, C. L. (2005) 'Drug release from a N-vinylpyrrolidinone / acrylic acid lubricious hydrophilic coating', 0, pp. 3429–3436.

Dillon, B. *et al.* (2019) 'The influence of low shear microbore extrusion on the properties of high molecular weight poly(l-lactic acid) for medical tubing applications', *Polymers*, 11(4). doi: 10.3390/polym11040710.

Dizon, J. R. C. *et al.* (2018) 'Mechanical characterization of 3D-printed polymers', *Additive Manufacturing*. Elsevier B.V., 20(January), pp. 44–67. doi: 10.1016/j.addma.2017.12.002.

Domenech, T., Peuvrel-Disdier, E. and Vergnes, B. (2012) 'Influence of twin-screw processing conditions on structure and properties of polypropylene - Organoclay nanocomposites', *International Polymer Processing*, 27(5), pp. 517–526. doi: 10.3139/217.2591.

Dong, Y. *et al.* (2015a) 'Polylactic acid (PLA)/halloysite nanotube (HNT) composite

mats: Influence of HNT content and modification', *Composites Part A: Applied Science and Manufacturing*, 76(October), pp. 28–36. doi: 10.1016/j.compositesa.2015.05.011.

Dong, Y. *et al.* (2015b) 'Polylactic acid (PLA)/halloysite nanotube (HNT) composite mats: Influence of HNT content and modification', *Composites Part A: Applied Science and Manufacturing*. doi: 10.1016/j.compositesa.2015.05.011.

Dong, Y., Bickford, T. and Haroosh, H. J. (2012) 'Statistical Design of Experiments for Electrospun Poly (lactic acid) (PLA)/ Halloysite Nanotube (HNT) Composites in Response to Fibre Diameter and Thermal Properties', (November), pp. 6–8.

Dorigato, A. *et al.* (2017) 'Electrically conductive nanocomposites for fused deposition modelling', *Synthetic Metals*. Elsevier B.V., 226, pp. 7–14. doi: 10.1016/j.synthmet.2017.01.009.

Dreher, M. L., Nagaraja, S. and Batchelor, B. (2016) 'Effects of fatigue on the chemical and mechanical degradation of model stent sub-units', *Journal of the Mechanical Behavior of Biomedical Materials*. Elsevier, 59, pp. 139–145. doi: 10.1016/j.jmbbm.2015.12.020.

Du, M., Guo, B. and Jia, D. (2010) 'Newly emerging applications of halloysite nanotubes: A review', *Polymer International*, 59(5), pp. 574–582. doi: 10.1002/pi.2754.

Dul, S., Fambri, L. and Pegoretti, A. (2016) 'Fused deposition modelling with ABS-graphene nanocomposites', *Composites Part A: Applied Science and Manufacturing*. Elsevier Ltd, 85, pp. 181–191. doi: 10.1016/j.compositesa.2016.03.013.

Ebube, N. K. *et al.* (1997) 'Sustained Release of Acetaminophen from Heterogeneous Matrix Tablets : Influence of Polymer Ratio , Polymer Loading , and Co-active on Drug Release', 2(2), pp. 161–170.

Ebube, N. K. and Jones, A. B. (2004) 'Sustained release of acetaminophen from a heterogeneous mixture of two hydrophilic non-ionic cellulose ether polymers', 272, pp. 19–27. doi: 10.1016/j.ijpharm.2003.11.020.

Edy Pramono, A., Rebet, I. and Zulfia, A. (2015) 'Tensile and Shear Punch Properties of Bamboo Fibers Reinforced Polymer Composites', *International Journal of Composite Materials*, 5(1), pp. 9–17. doi: 10.5923/j.cmaterials.20150501.02.

Ellis, S. G. *et al.* (2015) 'Everolimus-Eluting Bioresorbable Scaffolds for Coronary Artery Disease', *New England Journal of Medicine*, 373(20), pp. 1905–1915. doi: 10.1056/NEJMoa1509038.

Elsawy, M. A. *et al.* (2017) 'Hydrolytic degradation of polylactic acid (PLA) and its composites', *Renewable and Sustainable Energy Reviews*. Elsevier Ltd, 79(May), pp. 1346–1352. doi: 10.1016/j.rser.2017.05.143.

Englert, C. *et al.* (2018) 'Pharmapolymers in the 21st century: Synthetic polymers in drug delivery applications', *Progress in Polymer Science*. Elsevier B.V., 87, pp. 107–164. doi: 10.1016/j.progpolymsci.2018.07.005.

Farah, S., Anderson, D. G. and Langer, R. (2016) 'Physical and mechanical properties of PLA, and their functions in widespread applications - A comprehensive review', *Advanced Drug Delivery Reviews*, pp. 367–392. doi: 10.1016/j.addr.2016.06.012.

FDA's Role in 3D Printing (no date).

Ferreira, R. T. L. *et al.* (2017) 'Experimental characterization and micrography of 3D printed PLA and PLA reinforced with short carbon fibers', *Composites Part B: Engineering*. Elsevier Ltd, 124, pp. 88–100. doi: 10.1016/j.compositesb.2017.05.013.

Ferri, J. M. *et al.* (2016) 'Effect of miscibility on mechanical and thermal properties of poly(lactic acid)/ polycaprolactone blends', *Polymer International*, 65(4), pp. 453–463. doi: 10.1002/pi.5079.

Filipovic, N. *et al.* (2018) *Computer Modeling of Stent Deployment in the Coronary Artery Coupled with Plaque Progression, Biomaterials in Clinical Practice: Advances in Clinical Research and Medical Devices*. doi: 10.1007/978-3-319-68025-5.

Finotti, P. F. M. *et al.* (2017) 'Journal of the Mechanical Behavior of Biomedical Materials Immiscible poly (lactic acid)/ poly (ε -caprolactone) for temporary implants : Compatibility and cytotoxicity', *Journal of the Mechanical Behavior of Biomedical Materials*. Elsevier Ltd, 68(October 2016), pp. 155–162. doi: 10.1016/j.jmbbm.2017.01.050.

Foerst, J. *et al.* (2013) 'Evolution of Coronary Stents: From Bare-Metal Stents to Fully Biodegradable, Drug-Eluting Stents', *Comb Prod Ther*, (3), pp. 9–24. doi: 10.1007/s13556-013-0005-7.

Fortelny, I. *et al.* (2019) 'Phase Structure, Compatibility, and Toughness of PLA/PCL Blends: A Review', *Frontiers in Materials*, 6(August), pp. 1–13. doi: 10.3389/fmats.2019.00206.

Frank, A., Rath, S. K. and Venkatraman, S. S. (2005) 'Controlled release from bioerodible polymers : effect of drug type and polymer composition', 102, pp. 333–344. doi: 10.1016/j.jconrel.2004.10.019.

Freire, E. (1995) 'Differential Scanning Calorimetry', *Methods in Molecular Biology*, pp. 191–218. doi: 10.1385/0-89603-232-9:125.

Fu, L. *et al.* (2017) 'Engineering a tubular mesoporous silica nanocontainer with well-preserved clay shell from natural halloysite', *Nano Research*, 10(8), pp. 2782–2799. doi: 10.1007/s12274-017-1482-x.

Fuenmayor, E. *et al.* (2018) 'Material considerations for fused-filament fabrication of solid dosage forms', *Pharmaceutics*, 10(2), pp. 1–27. doi: 10.3390/pharmaceutics10020044.

Fujisawa, J. ichi, Eda, T. and Hanaya, M. (2017) 'Facile, quick and selective visible-light sensing of phenol-containing drug molecules acetaminophen and biosol by use of interfacial charge-transfer transitions with TiO2 nanoparticles', *Chemical Physics Letters*. Elsevier B.V., 684, pp. 328–332. doi: 10.1016/j.cplett.2017.07.019.

Fule, R., Paithankar, V. and Amin, P. (2016) 'Hot melt extrusion based solid solution approach: Exploring polymer comparison, physicochemical characterization and in-vivo evaluation', *International Journal of Pharmaceutics*. Elsevier B.V.,

499(1–2), pp. 280–294. doi: 10.1016/j.ijpharm.2015.12.062.

Gaaz, T. *et al.* (2017) 'The Impact of Halloysite on the Thermo-Mechanical Properties of Polymer Composites', *Molecules*, 22(6), p. 838. doi: 10.3390/molecules22050838.

Gamon, G., Evon, P. and Rigal, L. (2013) 'Twin-screw extrusion impact on natural fibre morphology and material properties in poly(lactic acid) based biocomposites', *Industrial Crops and Products*. Elsevier B.V., 46, pp. 173–185. doi: 10.1016/j.indcrop.2013.01.026.

Gao, M. *et al.* (2017) 'Preparation of a novel breviscapine-loaded halloysite nanotubes complex for controlled release of breviscapine Preparation of a novel breviscapine-loaded halloysite nanotubes complex for controlled release of breviscapine', *Material Science and Engineering*, 265, pp. 1–8. doi: 10.1088/1757-899X/265/1/012011.

Gao, W. *et al.* (2015) 'The status, challenges, and future of additive manufacturing in engineering', *Computer-Aided Design*. Elsevier Ltd, 69, pp. 65–89. doi: 10.1016/j.cad.2015.04.001.

GaRea, S. A. (2017) *List of Abbreviations*. doi: 10.1016/B978-0-323-46153-5.00014-8.

Garg, S. and Serruys, P. W. (2010a) 'Coronary stents: Current status', *Journal of the American College of Cardiology*. Elsevier Masson SAS, 56(10 SUPPL.), pp. S1–S42. doi: 10.1016/j.jacc.2010.06.007.

Garg, S. and Serruys, P. W. (2010b) 'Coronary stents: Looking forward', *Journal of the American College of Cardiology*. Elsevier Masson SAS, 56(10 SUPPL.), pp. S43–S78. doi: 10.1016/j.jacc.2010.06.008.

Garlotta, D. (2002) 'A Literature Review of Poly (Lactic Acid)', *Journal of Polymers and the Environment*, 9(2), pp. 63–84. doi: 10.1023/A:1020200822435.

Giacchi, G. *et al.* (2016) 'Bioresorbable vascular scaffolds technology: current use and future developments.', *Medical devices (Auckland, N.Z.)*, 9, pp. 185–98. doi:

10.2147/MDER.S90461.

Gill, P., Moghadam, T. T. and Ranjbar, B. (2010) ‘Differential scanning calorimetry techniques: applications in biology and nanoscience.’, *Journal of biomolecular techniques : JBT*, 21(4), pp. 167–93. Available at: /pmc/articles/PMC2977967/?report=abstract.

Gnanasekaran, K. *et al.* (2017) ‘3D printing of CNT- and graphene-based conductive polymer nanocomposites by fused deposition modeling’, *Applied Materials Today*. Elsevier Ltd, 9, pp. 21–28. doi: 10.1016/j.apmt.2017.04.003.

Gorrasi, G. *et al.* (2014) ‘PLA/halloysite nanocomposite films: Water vapor barrier properties and specific key characteristics’, *Macromolecular Materials and Engineering*, 299(1), pp. 104–115. doi: 10.1002/mame.201200424.

Gross, B. C. *et al.* (2014) ‘Evaluation of 3D printing and its potential impact on biotechnology and the chemical sciences’, *Analytical Chemistry*, 86(7), pp. 3240–3253. doi: 10.1021/ac403397r.

Gs, E., Al, K. and Youseffi, M. (2019) ‘Effect of screw configuration on the dispersion and properties of polypropylene / multiwalled carbon nanotube composite’.

Gu, L., Zhao, S. and Froemming, S. R. (2012) ‘Arterial wall mechanics and clinical implications after coronary stenting: Comparisons of three stent designs’, *International Journal of Applied Mechanics*, 4(2). doi: 10.1142/S1758825112500135.

Gu, X. *et al.* (2016) ‘Biodegradable, elastomeric coatings with controlled anti-proliferative agent release for magnesium-based cardiovascular stents’, *Colloids and Surfaces B: Biointerfaces*. Elsevier B.V., 144, pp. 170–179. doi: 10.1016/j.colsurfb.2016.03.086.

Guerra, A. and Ciurana, J. (2018) ‘3D-printed bioabsordable polycaprolactone stent: The effect of process parameters on its physical features’, *Materials & Design*. Elsevier Ltd, 137, pp. 430–437. doi: 10.1016/J.MATDES.2017.10.045.

Guerra, A. J. *et al.* (2018) '3D-printed PCL/PLA composite stents: Towards a new solution to cardiovascular problems', *Materials*, 11(9), pp. 1–13. doi: 10.3390/ma11091679.

Guerra, A. J., San, J. and Ciurana, J. (2017) 'Fabrication of PCL/PLA Composite Tube for Stent Manufacturing', *Procedia CIRP*. The Author(s), 65, pp. 231–235. doi: 10.1016/j.procir.2017.03.339.

Guerra, A., Roca, A. and de Ciurana, J. (2017) 'A novel 3D additive manufacturing machine to biodegradable stents', *Procedia Manufacturing*. Elsevier B.V., 13, pp. 718–723. doi: 10.1016/j.promfg.2017.09.118.

Guo, J., Qiao, J. and Zhang, X. (2016) 'Effect of an alkalized-modified halloysite on PLA crystallization, morphology, mechanical, and thermal properties of PLA/halloysite nanocomposites', *Journal of Applied Polymer Science*, 133(48), pp. 1–9. doi: 10.1002/app.44272.

Hairaldin, S. Z. *et al.* (2012) 'Effect Addition of Octadecylamine Modified Clay (ODA-MMT) to Polylactide / Polycaprolactone (PLA / PCL) blend', 364, pp. 317–321. doi: 10.4028/www.scientific.net/AMR.364.317.

Hajiali, Z., Dabagh, M. and Jalali, P. (2014) 'A Computational Model to Assess Poststenting Wall Stresses Dependence on Plaque Structure and Stenosis Severity in Coronary Artery', *Mathematical Problems in Engineering*, 2014. doi: 10.1155/2014/937039.

Hamad, K. *et al.* (2015) 'Properties and medical applications of polylactic acid: A review', *Express Polymer Letters*, 9(5), pp. 435–455. doi: 10.3144/expresspolymlett.2015.42.

Haroosh, H., Chaudhary, Deeptangshu Dong, Y. and Hawkins, B. (2011) 'Electrospun PLA : PCL / halloysite nanotube nanocomposites fibers for drug delivery', *Nineteenth International Conference on Processing and Fabrication of Advanced Materials*, (Pfam Xix), pp. 847–858.

Haroosh, H. J. *et al.* (2013) 'Electrospun PLA: PCL composites embedded with unmodified and 3-aminopropyltriethoxysilane (ASP) modified halloysite nanotubes

(HNT)', *Applied Physics A: Materials Science and Processing*, 110(2), pp. 433–442. doi: 10.1007/s00339-012-7233-7.

Healy, A. V *et al.* (2018) 'Degradable Nanocomposites for Fused Filament Fabrication Applications'. doi: 10.3390/jmmp2020029.

Hiemenz, J. (2011) '3D printing jigs , fixtures and other manufacturing tools', *Stratasys,Inc*.

Hoare, D. *et al.* (2019) 'The Future of Cardiovascular Stents : Bioresorbable and Integrated Biosensor Technology', 1900856. doi: 10.1002/advs.201900856.

Holman, H., Kavarana, M. and Rajab, T. K. (2020) 'Smart Materials in Cardiovascular Implants: Shape Memory Alloys and Shape Memory Polymers', *Artificial Organs*, pp. 0–2. doi: 10.1111/aor.13851.

Hornbeck, L. J. (1997) 'Digital Light Processing for high-brightness high-resolution applications', in Wu, M. H. (ed.). International Society for Optics and Photonics, pp. 27–40. doi: 10.1117/12.273880.

Hornsby, P. (2017) 'Compounding of Particulate-Filled Thermoplastics', pp. 95–110. doi: 10.1007/978-3-319-28117-9.

Hou, Z. *et al.* (2008) 'Structural orientation and tensile behavior in the extrusion-stretched sheets of polypropylene/multi-walled carbon nanotubes' composite', *Polymer*, 49(16), pp. 3582–3589. doi: 10.1016/j.polymer.2008.06.008.

Hu, T. *et al.* (2015) 'Controlled Slow-Release Drug-Eluting Stents for the Prevention of Coronary Restenosis: Recent Progress and Future Prospects', *ACS Applied Materials and Interfaces*, 7(22), pp. 11695–11712. doi: 10.1021/acsami.5b01993.

Huang, M. *et al.* (2006) 'Degradation Characteristics of Poly (□ -caprolactone) -Based Copolymers and Blends', pp. 1–7. doi: 10.1002/app.24196.

Hull, C. W. and Arcadia, C. (1986) 'Apparatus for production of three-dimensional objects by stereolithography', *Apparatus for Production of Three-Dimensional Objects by Stereolithography*. doi: 10.1145/634067.634234.

Hwa, L. C. *et al.* (2017) 'Recent advances in 3D printing of porous ceramics: a review', *Current Opinion in Solid State and Materials Science*. Elsevier, pp. 323–347. doi: 10.1016/j.cossms.2017.08.002.

Hyvärinen, M., Jabeen, R. and Kärki, T. (2020) 'The Modelling of Extrusion Processes for'.

Im, S. H., Jung, Y. and Kim, S. H. (2017) 'Current status and future direction of biodegradable metallic and polymeric vascular scaffolds for next-generation stents', *Acta Biomaterialia*, 60, pp. 3–22. doi: 10.1016/j.actbio.2017.07.019.

Innovation, R. (2013) 'MedIcal devIces'.

ISO 10993 - Biological Evaluataion of Medical Devices (no date).

Ivanova, O., Williams, C. and Campbell, T. (2013) 'Additive manufacturing (AM) and nanotechnology: promises and challenges', *Rapid Prototyping Journal*, 19(5), pp. 353–364. doi: 10.1108/RPJ-12-2011-0127.

Jabara, R. *et al.* (2009) 'Bioabsorbable Stents: The Future Is Near, A review of the breakthroughs and challenges of bioabsorbable stents as a potential solution to the risks associated with available drug-eluting stents', *Cardiac Interventions Today*, June/July(July), pp. 50–53. Available at: http://bmctoday.net/citoday/2009/07/article.asp?f=CIT0709_07.php.

Jaganathan, S. K. *et al.* (2014) 'Biomaterials in Cardiovascular Research: Applications and Clinical Implications', *Biomed Research International*, 2014, p. 11. doi: 10.1155/2014/459465.

Jani, R. and Patel, D. (2014) 'Hot melt extrusion: An industrially feasible approach for casting orodispersible film', *Asian Journal of Pharmaceutical Sciences*. Elsevier Ltd, 10(4), pp. 292–305. doi: 10.1016/j.ajps.2015.03.002.

Jenjob, R. *et al.* (2015) 'Recent trend in applications of polymer materials to stents', pp. 83–88. doi: 10.18528/gii150022.

Jia, S. *et al.* (2017) 'Morphology, crystallization and thermal behaviors of PLA-based composites: Wonderful effects of hybrid GO/PEG via dynamic impregnating',

Polymers, 9(10). doi: 10.3390/polym9100528.

Jock Churchman, G. *et al.* (2016) 'Unique but diverse: some observations on the formation, structure and morphology of halloysite', *Clay Minerals*, 51(3), pp. 395–416. doi: 10.1180/claymin.2016.051.3.14.

Jock Churchman, G., Pasbakhsh, P. and Hillier, S. (2016) 'The rise and rise of halloysite', *Clay Minerals*, 51(3), pp. 303–308. doi: 10.1180/claymin.2016.051.3.00.

Joussein, E. *et al.* (2005) 'Halloysite clay minerals – a review', *Clay Minerals*, 40(4), pp. 383–426. doi: 10.1180/0009855054040180.

Kalepu, S. and Nekkanti, V. (2015) 'Insoluble drug delivery strategies: Review of recent advances and business prospects', *Acta Pharmaceutica Sinica B*. Elsevier, 5(5), pp. 442–453. doi: 10.1016/j.apsb.2015.07.003.

Kamble, R. *et al.* (2012) 'Review article halloysite nanotubes and applications : A review', *Journal of Advanced Scientific Research*, 3(2), pp. 25–29.

Kandzari, D. E. *et al.* (2020) 'Ultrathin Bioresorbable-Polymer Sirolimus-Eluting Stents Versus Thin Durable-Polymer Everolimus-Eluting Stents for Coronary Revascularization', 13(11). doi: 10.1016/j.jcin.2020.02.019.

Kantesh Balani, Vivek Verma, Arvind Agarwal, R. N. (2015) 'Physical, thermal, and mechanical properties of polymers', in *Biosurfaces: A Materials Science and Engineering Perspective*. First. John Wiley & Sons, Inc, pp. 329–344.

Kawashima, H. *et al.* (2020) 'Expert Opinion on Drug Delivery Drug-eluting bioresorbable scaffolds in cardiovascular disease , peripheral artery and gastrointestinal fields : a clinical update', *Expert Opinion on Drug Delivery*. Taylor & Francis, 00(00), pp. 1–15. doi: 10.1080/17425247.2020.1764932.

Kelnar, I. *et al.* (2016) 'Effect of halloysite on structure and properties of melt-drawn PCL/PLA microfibrillar composites', *Express Polymer Letters*, 10(5), pp. 381–393. doi: 10.3144/expresspolymlett.2016.36.

Kelnar, I. *et al.* (2017) 'Graphite nanoplatelets-modified PLA/PCL: Effect of blend ratio and nanofiller localization on structure and properties', *Journal of the*

Mechanical Behavior of Biomedical Materials, 71(March), pp. 271–278. doi: 10.1016/j.jmbbm.2017.03.028.

Khadka, P. *et al.* (2014) 'Pharmaceutical particle technologies: An approach to improve drug solubility, dissolution and bioavailability', *Asian Journal of Pharmaceutical Sciences*. Elsevier Ltd, 9(6), pp. 304–316. doi: 10.1016/j.ajps.2014.05.005.

Khanesar, M. A. (2019) 'Medical Applications of 3D Printing', pp. 3–5. doi: 10.33552/ABEB.2019.02.000531.

Kim, H. *et al.* (2018) 'Enhanced dielectric properties of three phase dielectric MWCNTs/BaTiO 3 /PVDF nanocomposites for energy storage using fused deposition modeling 3D printing', *Ceramics International*. Elsevier Ltd and Techna Group S.r.l. doi: 10.1016/j.ceramint.2018.02.107.

Kimura, T. *et al.* (2015) 'A randomized trial evaluating everolimus-eluting Absorb bioresorbable scaffolds vs. everolimus-eluting metallic stents in patients with coronary artery disease: ABSORB Japan', *European Heart Journal*, 36(47), pp. 3332–3342. doi: 10.1093/eurheartj/ehv435.

King, S. B. and Gogas, B. D. (2017) 'Can the Vanishing Stent Reappear?', *Journal of the American College of Cardiology*, (4), pp. 3–5. doi: 10.1016/j.jacc.2017.10.009.

Klein, L. W. (2006) 'Are drug-eluting stents the preferred treatment for multivessel coronary artery disease?', *Journal of the American College of Cardiology*. Elsevier Masson SAS, 47(1), pp. 22–26. doi: 10.1016/j.jacc.2005.08.057.

Kobo, O. *et al.* (2020) 'Modern stents: Where are we going?', *Rambam Maimonides Medical Journal*, 11(2), pp. 1–9. doi: 10.5041/RMMJ.10403.

Kodama, H. (1981) 'Automatic method for fabricating a three-dimensional plastic model with photo-hardening polymer', *Review of Scientific Instruments*, 52(11), pp. 1770–1773. doi: 10.1063/1.1136492.

Kokkinis, D., Schaffner, M. and Studart, A. R. (2015) 'Multimaterial magnetically

assisted 3D printing of composite materials', *Nature Communications*. Nature Publishing Group, 6(1), p. 8643. doi: 10.1038/ncomms9643.

Kokot, G. *et al.* (2018) 'A project of bioresorbable self-expanding vascular stents. the crimping process numerical simulation', *AIP Conference Proceedings*, 1922, pp. 1–7. doi: 10.1063/1.5019071.

Kokubo, T. and Takadama, H. (2006) 'How useful is SBF in predicting in vivo bone bioactivity?', *Biomaterials*, 27(15), pp. 2907–2915. doi: 10.1016/j.biomaterials.2006.01.017.

Krishnaiah, P., Ratnam, C. T. and Manickam, S. (2017) 'Development of silane grafted halloysite nanotube reinforced polylactide nanocomposites for the enhancement of mechanical, thermal and dynamic-mechanical properties', *Applied Clay Science*. Elsevier B.V., 135, pp. 583–595. doi: 10.1016/j.clay.2016.10.046.

Kruth, J.-P., Leu, M. C. and Nakagawa, T. (1998) 'Progress in Additive Manufacturing and Rapid Prototyping', *CIRP Annals - Manufacturing Technology*, 47(2), pp. 525–540. doi: 10.1016/S0007-8506(07)63240-5.

Lamberti, P. *et al.* (2018) 'Evaluation of thermal and electrical conductivity of carbon-based PLA nanocomposites for 3D printing', 020158, p. 020158. doi: 10.1063/1.5046020.

Lawson, G., Ogwu, J. and Tanna, S. (2018) 'Quantitative screening of the pharmaceutical ingredient for the rapid identification of substandard and falsified medicines using reflectance infrared spectroscopy', pp. 1–17.

Lee, J. H. *et al.* (2018) 'Analysis of trends and prospects regarding stents for human blood vessels', *Biomaterials Research*. Biomaterials Research, 22(1), p. 8. doi: 10.1186/s40824-018-0114-1.

Leporatti, S. (2017) 'Halloysite clay nanotubes as nano-bazookas for drug delivery', *Polymer International*, 66(8), pp. 1111–1118. doi: 10.1002/pi.5347.

Li, F. *et al.* (2018) 'Journal of Drug Delivery Science and Technology In vitro release study of sirolimus from a PDLLA matrix on a bioresorbable drug-eluting

stent', *Journal of Drug Delivery Science and Technology*. Elsevier, 48(August), pp. 88–95. doi: 10.1016/j.jddst.2018.08.026.

Li, G. *et al.* (2018) 'Effect of ultrasonic vibration on mechanical properties of 3D printing non-crystalline and semi-crystalline polymers', *Materials*, 11(5). doi: 10.3390/ma11050826.

Li, X. *et al.* (2016) 'Chitosan modified halloysite nanotubes as emerging porous microspheres for drug carrier', *Applied Clay Science*. Elsevier B.V., 126, pp. 306–312. doi: 10.1016/j.clay.2016.03.035.

Li, Y. *et al.* (2014) 'Poly(L-lactide)/Poly(D-lactide)/clay nanocomposites: Enhanced dispersion, crystallization, mechanical properties, and hydrolytic degradation', *Polymer Engineering & Science*, 54(4), pp. 914–924. doi: 10.1002/pen.23620.

Ligon, S. C. *et al.* (2017) 'Polymers for 3D Printing and Customized Additive Manufacturing', *Chemical Reviews*, 117(15), pp. 10212–10290. doi: 10.1021/acs.chemrev.7b00074.

van Lith, R. *et al.* (2016) '3D-Printing Strong High-Resolution Antioxidant Bioresorbable Vascular Stents', *Advanced Materials Technologies*, 1(9), pp. 1–7. doi: 10.1002/admt.201600138.

Liu, L. *et al.* (2018) 'Comparison of drug-eluting balloon versus drug-eluting stent for treatment of coronary artery disease : a meta-analysis of randomized controlled trials'. BMC Cardiovascular Disorders, pp. 1–16.

Liu, M. *et al.* (2009) 'Halloysite nanotubes as a novel ??-nucleating agent for isotactic polypropylene', *Polymer*. Elsevier Ltd, 50(13), pp. 3022–3030. doi: 10.1016/j.polymer.2009.04.052.

Liu, M. *et al.* (2014) 'Recent advance in research on halloysite nanotubes-polymer nanocomposite', *Progress in Polymer Science*. Elsevier Ltd, 39(8), pp. 1498–1525. doi: 10.1016/j.progpolymsci.2014.04.004.

Liu, M., Zhang, Y. and Zhou, C. (2013) 'Nanocomposites of halloysite and polylactide', *Applied Clay Science*. Elsevier B.V., 75–76, pp. 52–59. doi:

10.1016/j.clay.2013.02.019.

Lun, H., Ouyang, J. and Yang, H. (2014) ‘Natural halloysite nanotubes modified as an aspirin carrier’, *RSC Adv.* Royal Society of Chemistry, 4(83), pp. 44197–44202. doi: 10.1039/C4RA09006C.

Luo, Y. *et al.* (2016) ‘Synthesis and Biological Evaluation of Well-Defined Poly(propylene fumarate) Oligomers and Their Use in 3D Printed Scaffolds’, *Biomacromolecules*, 17(2), pp. 690–697. doi: 10.1021/acs.biomac.6b00014.

Luyt, A. S. and Kelnar, I. (2017) ‘Effect of halloysite nanotubes on the thermal degradation behaviour of poly(ε-caprolactone)/poly(lactic acid) microfibrillar composites’, *Polymer Testing*. Elsevier Ltd, 60, pp. 166–172. doi: 10.1016/j.polymertesting.2017.03.027.

Lvov, Y. and Abdullayev, E. (2013) ‘Functional polymer-clay nanotube composites with sustained release of chemical agents’, *Progress in Polymer Science*. Elsevier Ltd, 38(10–11), pp. 1690–1719. doi: 10.1016/j.progpolymsci.2013.05.009.

Lvov, Y. M., DeVilliers, M. M. and Fakhrullin, R. F. (2016) ‘The application of halloysite tubule nanoclay in drug delivery’, *Expert Opinion on Drug Delivery*, 13(7), pp. 977–986. doi: 10.1517/17425247.2016.1169271.

Lyons, J. G. *et al.* (2006) ‘The use of Agar as a novel filler for monolithic matrices produced using hot melt extrusion’, 64, pp. 75–81. doi: 10.1016/j.ejpb.2006.03.008.

Lyons, J. G., Hallinan, M., *et al.* (2007) ‘Preparation of monolithic matrices for oral drug delivery using a supercritical fluid assisted hot melt extrusion process’, *International Journal of Pharmaceutics*. Elsevier, 329(1–2), pp. 62–71. doi: 10.1016/J.IJPHARM.2006.08.028.

Lyons, J. G., Holehonnur, H., *et al.* (2007) ‘The incorporation of an organically modified layered silicate in monolithic polymeric matrices produced using hot melt extrusion’, *Materials Chemistry and Physics*, 103(2–3), pp. 419–426. doi: 10.1016/j.matchemphys.2007.02.080.

Ma, X., Wu, T. and Robich, M. P. (2012) ‘Drug-eluting stent coatings’,

Interventional Cardiology, 4(1), pp. 73–83. doi: 10.2217/ica.11.88.

Macdonald, N. P. *et al.* (2017) 'Comparing microfluidic performance of three-dimensional (3D) printing platforms', *Analytical Chemistry*. American Chemical Society, 89(7), pp. 3858–3866. doi: 10.1021/acs.analchem.7b00136.

Majewska, P., Oledzka, E. and Sobczak, M. (2019) 'Biomaterials Science drug-eluting stent technology'. Royal Society of Chemistry. doi: 10.1039/c9bm00468h.

Manallack, D. T. *et al.* (2013) 'The significance of acid/base properties in drug discovery', *Chemical Society Reviews*, 42(2), pp. 485–496. doi: 10.1039/c2cs35348b.

Maniruzzaman, M. *et al.* (2012) 'A review of hot-melt extrusion: process technology to pharmaceutical products.', *ISRN pharmaceutics*, 2012(2), pp. 436763–436769. doi: 10.5402/2012/436763.

Maniruzzaman, M. and Nokhodchi, A. (2017) 'Continuous manufacturing via hot-melt extrusion and scale up: regulatory matters', *Drug Discovery Today*. Elsevier Ltd, 22(2), pp. 340–351. doi: 10.1016/j.drudis.2016.11.007.

Manoudis, P. N. and Karapanagiotis, I. (2014) 'Modification of the wettability of polymer surfaces using nanoparticles', *Progress in Organic Coatings*. Elsevier B.V., 77(2), pp. 331–338. doi: 10.1016/j.porgcoat.2013.10.007.

Maria, L., Meirelles, A. and Raffin, F. N. (2017) 'Clay and Polymer-Based Composites Applied to Drug Release : A Scientific and Technological Prospection .', 1(10), pp. 115–134.

Martinez-Marcos, L. *et al.* (2016) 'A novel hot-melt extrusion formulation of albendazole for increasing dissolution properties', *International Journal of Pharmaceutics*. Elsevier B.V., 499(1–2), pp. 175–185. doi: 10.1016/j.ijpharm.2016.01.006.

Masood, S. H. and Song, W. Q. (2004) 'Development of new metal/polymer materials for rapid tooling using fused deposition modelling', *Materials and Design*. Elsevier, 25(7), pp. 587–594. doi: 10.1016/j.matdes.2004.02.009.

Matias, E. and Rao, B. (2015) '3D printing: On its historical evolution and the implications for business', *Portland International Conference on Management of Engineering and Technology*. Portland International Conference on Management of, 2015–Septe, pp. 551–558. doi: 10.1109/PICMET.2015.7273052.

Matsuhiro, Y. *et al.* (2020) 'Difference of vascular healing between bioabsorbable-polymer and durable-polymer new generation drug-eluting stents: an optical coherence tomographic analysis', *International Journal of Cardiovascular Imaging*. Springer Netherlands, (0123456789). doi: 10.1007/s10554-020-02094-y.

McDowell, G., Slevin, M. and Krupinski, J. (2011) 'Nanotechnology for the treatment of coronary in stent restenosis: a clinical perspective.', *Vascular cell*. BioMed Central Ltd, 3(1), p. 8. doi: 10.1186/2045-824X-3-8.

McKittrick, C. M. *et al.* (2020) 'Development of a Bioactive Polymeric Drug Eluting Coronary Stent Coating Using Electrospraying', *Annals of Biomedical Engineering*, 48(1), pp. 271–281. doi: 10.1007/s10439-019-02346-6.

McLouth, T. D. *et al.* (2017) 'The impact of print orientation and raster pattern on fracture toughness in additively manufactured ABS', *Additive Manufacturing*. Elsevier, 18, pp. 103–109. doi: 10.1016/j.addma.2017.09.003.

McLure, T. (2017) *3D Printing Moves Align Technology Toward $1.3 Billion In Sales, Forbes*.

McMahon, S. *et al.* (2018) 'Bio-resorbable polymer stents: a review of material progress and prospects', *Progress in Polymer Science*. Elsevier Ltd, 83, pp. 79–96. doi: 10.1016/j.progpolymsci.2018.05.002.

De Mel, A., Cousins, B. G. and Seifalian, A. M. (2012) 'Surface modification of biomaterials: A quest for blood compatibility', *International Journal of Biomaterials*, 2012. doi: 10.1155/2012/707863.

Melchels, F. P. W., Feijen, J. and Grijpma, D. W. (2010) 'A review on stereolithography and its applications in biomedical engineering', *Biomaterials*. Elsevier Ltd, 31(24), pp. 6121–6130. doi: 10.1016/j.biomaterials.2010.04.050.

Mhlanga, N. and Ray, S. S. (2015) ‘Kinetic models for the release of the anticancer drug doxorubicin from biodegradable polylactide/metal oxide-based hybrids’, *International Journal of Biological Macromolecules*. Elsevier B.V., 72, pp. 1301–1307. doi: 10.1016/j.ijbiomac.2014.10.038.

Mielke, C. H. *et al.* (1976) ‘Hemostasis, Antipyretics, and Mild Analgesics: Acetaminophen vs Aspirin’, *JAMA: The Journal of the American Medical Association*, 235(6), pp. 613–616. doi: 10.1001/jama.1976.03260320021016.

Miguel, C. *et al.* (2017) ‘3D Printing for Biomedical Applications: Where Are We Now?’, *European Medical Journal*, 2(1), pp. 16–22. Available at: http://emjreviews.com/wp-content/uploads/Editor.s-Pick-3D-Printing-for-Biomedical-Applications-Where-Are-We-Now...pdf.

Mills, D. *et al.* (2017) ‘The Use of 3D Printing in the Fabrication of Nasal Stents’, *Inventions*, 3(1), p. 1. doi: 10.3390/inventions3010001.

Miyajima, M., Koshika, A., Okada, J., *et al.* (1998) ‘Factors influencing the diffusion-controlled release of papaverine from poly (L -lactic acid) matrix’, 56, pp. 85–94.

Miyajima, M., Koshika, A., Okada, J., *et al.* (1998) ‘The effects of drug physico-chemical properties on release from copoly (lactic/glycolic acid) matrix’, *International Journal of Pharmaceutics*, 169(2), pp. 255–263. doi: 10.1016/S0378-5173(98)00133-1.

Miyajima, M. *et al.* (1999a) ‘Effect of polymer / basic drug interactions on the two-stage diffusion-controlled release from a poly (L -lactic acid) matrix’, 61, pp. 295–304.

Miyajima, M. *et al.* (1999b) ‘Mechanism of drug release from poly (L -lactic acid) matrix containing acidic or neutral drugs’, 60, pp. 199–209.

Mohamed, O. A., Masood, S. H. and Bhowmik, J. L. (2016) ‘Optimization of fused deposition modeling process parameters for dimensional accuracy using I-optimality criterion’, *Measurement: Journal of the International Measurement Confederation*. Elsevier Ltd, 81, pp. 174–196. doi: 10.1016/j.measurement.2015.12.011.

Mollace, V. *et al.* (2017) ‘Aspirin wears smart’, *European Heart Journal - Cardiovascular Pharmacotherapy*, 3(4), pp. 185–188. doi: 10.1093/ehjcvp/pvx017.

Montaseri, H. and Forbes, P. B. C. (2018) ‘Trends in Analytical Chemistry Analytical techniques for the determination of acetaminophen : A review’, *Trends in Analytical Chemistry*. Elsevier Ltd, 108, pp. 122–134. doi: 10.1016/j.trac.2018.08.023.

Monticelli, O. *et al.* (2014) ‘Silsesquioxanes: Novel compatibilizing agents for tuning the microstructure and properties of PLA/PCL immiscible blends’, *European Polymer Journal*. Elsevier Ltd, 58, pp. 69–78. doi: 10.1016/j.eurpolymj.2014.06.021.

Moore, S. S., O’Sullivan, K. J. and Verdecchia, F. (2016) ‘Shrinking the Supply Chain for Implantable Coronary Stent Devices’, *Annals of Biomedical Engineering*, 44(2), pp. 497–507. doi: 10.1007/s10439-015-1471-8.

Moravej, M. and Mantovani, D. (2011) ‘Biodegradable metals for cardiovascular stent application: Interests and new opportunities’, *International Journal of Molecular Sciences*, 12(7), pp. 4250–4270. doi: 10.3390/ijms12074250.

Moura, N. K. de *et al.* (2019) ‘Production and Characterization of Porous Polymeric Membranes of PLA/PCL Blends with the Addition of Hydroxyapatite’, *Journal of Composites Science*, 3(2), p. 45. doi: 10.3390/jcs3020045.

Mousa, M. H., Dong, Y. and Davies, I. J. (2016) ‘Recent advances in bionanocomposites: Preparation, properties, and applications’, *International Journal of Polymeric Materials and Polymeric Biomaterials*, 65(5), pp. 225–254. doi: 10.1080/00914037.2015.1103240.

Mueller, J., Shea, K. and Daraio, C. (2015) ‘Mechanical properties of parts fabricated with inkjet 3D printing through efficient experimental design’, *Materials and Design*. Elsevier Ltd, 86, pp. 902–912. doi: 10.1016/j.matdes.2015.07.129.

Munz, O. J. (1956) ‘Photo-Glyph Recording’.

Murariu, M. *et al.* (2012) ‘Polylactide (PLA)-Halloysite Nanocomposites: Production, Morphology and Key-Properties’, *Journal of Polymers and the*

Environment, 20(4), pp. 932–943. doi: 10.1007/s10924-012-0488-4.

Murariu, M. and Dubois, P. (2016) 'PLA composites: From production to properties', *Advanced Drug Delivery Reviews*. Elsevier B.V., 107, pp. 17–46. doi: 10.1016/j.addr.2016.04.003.

Nagavarma, B. V. N. *et al.* (2012) 'Different Techniques for', *Asian Journal of Pharmaceutical and Clinical Research*, 5, pp. 16–23.

Naseem, R. *et al.* (2017) 'Experimental and computational studies of poly-L-lactic acid for cardiovascular applications: recent progress', *Mechanics of Advanced Materials and Modern Processes*. Mechanics of Advanced Materials and Modern Processes, 3(1), p. 13. doi: 10.1186/s40759-017-0028-y.

Nazila, K. *et al.* (2016) 'Nanoparticles: Mechanisms of Controlling Drug Release', *Chem Rev.*, 116(4), pp. 2602–2663. doi: 10.1021/acs.chemrev.5b00346.Degradable.

Ng, J. *et al.* (2017) 'Local hemodynamic forces after stenting: Implications on restenosis and thrombosis', *Arteriosclerosis, Thrombosis, and Vascular Biology*, 37(12), pp. 2231–2242. doi: 10.1161/ATVBAHA.117.309728.

Ng, J. C. and Yeomans, N. D. (2018) 'Helicobacter pylori infection and the risk of upper gastrointestinal bleeding in low dose aspirin users: systematic review and meta-analysis', *The Medical Journal of Australia*, 209(7), pp. 306–311. doi: 10.5694/mja17.01274.

Ngo, T. D. *et al.* (2018) 'Additive manufacturing (3D printing): A review of materials , methods , applications and challenges', *Composites Part B*. Elsevier, 143(December 2017), pp. 172–196. doi: 10.1016/j.compositesb.2018.02.012.

Ngo, T. D. *et al.* (2018) 'Additive manufacturing (3D printing): A review of materials, methods, applications and challenges', *Composites Part B: Engineering*. Elsevier Ltd. doi: 10.1016/j.compositesb.2018.02.012.

Ni, L. *et al.* (2020) 'Bioresorbable vascular stents and drug- eluting stents in treatment of coronary heart disease : a meta-analysis', 5, pp. 1–7.

Nidhi, K. *et al.* (2011) 'Hydrotropy: A promising tool for solubility enhancement: A

review', *International Journal of Drug Development and Research*, 3(2), pp. 26–33. doi: 10.1002/jps.

Norman, J. *et al.* (2016) 'A new chapter in pharmaceutical manufacturing: 3D-printed drug products', *Advanced Drug Delivery Reviews*. Elsevier B.V. doi: 10.1016/j.addr.2016.03.001.

Normand, G. *et al.* (2017) 'Matrix Degradation during High Speed Extrusion of Polypropylene / Clay Nanocomposites – Influence on Filler Dispersion To cite this version : polypropylene / clay nanocomposites – influence on filler dispersion'.

O'Brien, B. and Carroll, W. (2009) 'The evolution of cardiovascular stent materials and surfaces in response to clinical drivers: A review', *Acta Biomaterialia*. Acta Materialia Inc., 5(4), pp. 945–958. doi: 10.1016/j.actbio.2008.11.012.

Okolie, O. *et al.* (2020) '3d printing for hip implant applications: A review', *Polymers*, 12(11), pp. 1–29. doi: 10.3390/polym12112682.

Oliveira, M. and Machado, A. V (2013) 'Preparation of polymer-based nanocomposites by different routes', *Nanocomposites: synthesis, characterization and applications*, pp. 1–22. Available at: http://repositorium.sdum.uminho.pt/handle/1822/26120.

Oliveira, M. and Peter, J. (2003) 'Crystallization and Transformation of Acetaminophen 2003', *Growth (Lakeland)*, pp. 0–4.

Omar, W. A. and Kumbhani, D. J. (2019) 'The Current Literature on Bioabsorbable Stents : a Review'. Current Atherosclerosis Reports.

Onuma, Y. and Serruys, P. W. (2011) 'Bioresorbable scaffold: The advent of a new era in percutaneous coronary and peripheral revascularization?', *Circulation*, 123(7), pp. 779–797. doi: 10.1161/CIRCULATIONAHA.110.971606.

Ostafinska, A. *et al.* (2017) 'Strong synergistic effects in PLA/PCL blends: Impact of PLA matrix viscosity', *Journal of the Mechanical Behavior of Biomedical Materials*, 69(January), pp. 229–241. doi: 10.1016/j.jmbbm.2017.01.015.

Othman, R. *et al.* (2016) 'Fabrication of composite poly (D , L -lactide)/

montmorillonite nanoparticles for controlled delivery of acetaminophen by solvent-displacement method using glass capillary microfluidics', *Colloids and Surfaces B: Biointerfaces*. Elsevier B.V. doi: 10.1016/j.colsurfb.2016.01.042.

Parry, J. A. *et al.* (2017) 'Three-Dimension-Printed Porous Poly(Propylene Fumarate) Scaffolds with Delayed rhBMP-2 Release for Anterior Cruciate Ligament Graft Fixation', *Tissue Engineering Part A*, 23(7–8), pp. 359–365. doi: 10.1089/ten.tea.2016.0343.

Pasbakhsh, P. *et al.* (2016) 'Halloysite nanotubes : Prospects and challenges of their use as additives and carriers – A focussed review', *Clay Minerals*, 51(June), pp. 479–487. doi: 10.1180/claymin.2016.051.3.15.

Patel, S. *et al.* (2015) 'Sustained Release of Antibacterial Agents from Doped Halloysite Nanotubes', *Bioengineering*, 3(1), p. 1. doi: 10.3390/bioengineering3010001.

Patil, H., Tiwari, R. V. and Repka, M. A. (2016) 'Hot-Melt Extrusion: from Theory to Application in Pharmaceutical Formulation', *AAPS PharmSciTech*, 17(1), pp. 20–42. doi: 10.1208/s12249-015-0360-7.

Patrício, T. and Bártolo, P. (2013) 'Thermal stability of PCL/PLA blends produced by physical blending process', *Procedia Engineering*. Elsevier B.V., 59, pp. 292–297. doi: 10.1016/j.proeng.2013.05.124.

Paul, G. M. *et al.* (2018) 'Medical Applications for 3D Printing: Recent Developments.', *Missouri medicine*, 115(1), pp. 75–81. Available at: http://www.ncbi.nlm.nih.gov/pubmed/30228688%0Ahttp://www.pubmedcentral.nih.gov/articlerender.fcgi?artid=PMC6139809.

Pawar, R. P. *et al.* (2014) 'Biomedical Applications of Poly(Lactic Acid)', *PLA Applications*, 4, pp. 40–51. doi: 10.2174/2210296504666140402235024.

Pearson, H. (1981) 'Comparative Effects of Aspirin and Acetaminophen on Hemostasis', *Archives of Internal Medicine*, 141(3), pp. 305–310. doi: 10.1001/archinte.1981.00340030037008.

Pierchala, M. K. *et al.* (2018) 'Nanotubes in nanofibers: Antibacterial multilayered polylactic acid/halloysite/gentamicin membranes for bone regeneration application', *Applied Clay Science*. Elsevier, 160(November 2017), pp. 95–105. doi: 10.1016/j.clay.2017.12.016.

Pollack, S. *et al.* (2019) 'Polymer-Based Additive Manufacturing: Historical Developments, Process Types and Material Considerations', in Devine, D. (ed.) *Polymer-Based Additive Manufacturing*. file:///C: © Springer Nature Switzerland AG 2019, pp. 1–22. doi: https://doi.org/10.1007/978-3-030-24532-0_1.

Pranzo, D. *et al.* (2018) 'Extrusion-Based 3D Printing of Microfluidic Devices for Chemical and Biomedical Applications: A Topical Review', *Micromachines*, 9(8), p. 374. doi: 10.3390/mi9080374.

Prasad, L. K. and Smyth, H. (2016) '3D Printing technologies for drug delivery: a review', *Drug Development and Industrial Pharmacy*, 42(7), pp. 1019–1031. doi: 10.3109/03639045.2015.1120743.

Prashantha, K. *et al.* (2013) 'Poly(lactic acid)/halloysite nanotubes nanocomposites: Structure, thermal, and mechanical properties as a function of halloysite treatment', *Journal of Applied Polymer Science*, 128(3), pp. 1895–1903. doi: 10.1002/app.38358.

Prete, M. C. and Arnaldo, C. (2016) 'RSC Advances A nanocomposite based on multi-walled carbon nanotubes grafted by molecularly imprinted', pp. 28751–28760. doi: 10.1039/C6RA02150F.

Pretula, J., Slomkowski, S. and Penczek, S. (2016) 'Polylactides—Methods of synthesis and characterization', *Advanced Drug Delivery Reviews*. Elsevier B.V., 107, pp. 3–16. doi: 10.1016/j.addr.2016.05.002.

Puchalski, M. *et al.* (2017) 'Investigation of the influence of PLA molecular structure on the crystalline forms (α'' and α) and Mechanical Properties ofWet Spinning Fibres', *Polymers*, 9(1). doi: 10.3390/polym9010018.

Qi, R. *et al.* (2010) 'Electrospun poly(lactic-co-glycolic acid)/halloysite nanotube composite nanofibers for drug encapsulation and sustained release', *Journal of*

Materials Chemistry, 20(47), p. 10622. doi: 10.1039/c0jm01328e.

Qi, R. *et al.* (2013) 'Controlled release and antibacterial activity of antibiotic-loaded electrospun halloysite/poly(lactic-co-glycolic acid) composite nanofibers', *Colloids and Surfaces B: Biointerfaces*. Elsevier B.V., 110, pp. 148–155. doi: 10.1016/j.colsurfb.2013.04.036.

Qiu, T. *et al.* (2020) 'Development of 3D-Printed Sulfated Chitosan Modified Bioresorbable Stents for Coronary Artery Disease', 8(May), pp. 1–12. doi: 10.3389/fbioe.2020.00462.

Qiu, T. and Zhao, L. (2018) 'Research into biodegradable polymeric stents: a review of experimental and modelling work', *Vessel Plus*, 2(6), p. 12. doi: 10.20517/2574-1209.2018.13.

Quiles-Carrillo, L., , Nestor Montanes, Fede Pineiro, A. J.-V. and and Torres-Giner, S. (2018) 'Ductility and Toughness Improvement of Injection-moulded compostable pieces of Polylactide by melt blending with poly(e-caprolactone) and thermoplastic starch', pp. 1–20. doi: 10.3390/ma11112138.

Raleigh, J. V. *et al.* (2018) 'Restenosis, Stent Thrombosis, and Bleeding Complications', 71(15). doi: 10.1016/j.jacc.2018.02.023.

Ramadugu, P. and Latha Alikatte, K. (2016) 'A Review on Biodegradable and Bioabsorbable Stents for Coronary Artery Disease', *Journal of Bioequivalence & Bioavailability*, 08(02), pp. 64–67. doi: 10.4172/jbb.1000269.

Ramot, Y. *et al.* (2016) 'Biocompatibility and safety of PLA and its copolymers', *Advanced Drug Delivery Reviews*. Elsevier B.V., 107, pp. 153–162. doi: 10.1016/j.addr.2016.03.012.

Raquez, J. M. *et al.* (2013) 'Polylactide (PLA)-based nanocomposites', *Progress in Polymer Science*. Elsevier Ltd, 38(10–11), pp. 1504–1542. doi: 10.1016/j.progpolymsci.2013.05.014.

Rebagay, G. and Bangalore, S. (2019) 'Biodegradable Polymers and Stents: the Next Generation?', *Current Cardiovascular Risk Reports*. Current Cardiovascular Risk

Reports, 13(8), pp. 2–7. doi: 10.1007/s12170-019-0617-x.

Repka, M. A. *et al.* (2018) 'Melt extrusion with poorly soluble drugs – An integrated review', *International Journal of Pharmaceutics*. Elsevier, 535(1–2), pp. 68–85. doi: 10.1016/j.ijpharm.2017.10.056.

Rolland, J., Chen, K. and Poelma, J. (2016) 'Methods of Producing Polyurethane Three-Dimensional Objects From Materials Having Multiple Mechanisms of Hardening', *US Patent*.

Roy, T. and Chanda, A. (2014) 'Computational Modelling and Analysis of Latest Commercially Available Coronary Stents During Deployment', *Procedia Materials Science*, 5, pp. 2310–2319. doi: 10.1016/j.mspro.2014.07.474.

Rykowska, I. and Nowak, I. (2020) 'Drug-Eluting Stents and Balloons—Materials, Structure Designs, and Coating Techniques: A Review'.

Sachs, E., Cima, M. and Cornie, J. (1990) 'Three-Dimensional Printing: Rapid Tooling and Prototypes Directly from a CAD Model', *CIRP Annals - Manufacturing Technology*. American Society of Mechanical Engineers, 39(1), pp. 201–204. doi: 10.1016/S0007-8506(07)61035-X.

Saerens, L. *et al.* (2014) 'Process monitoring and visualization solutions for hot-melt extrusion: A review', *Journal of Pharmacy and Pharmacology*, 66(2), pp. 180–203. doi: 10.1111/jphp.12123.

Saini, P., Arora, M. and Kumar, M. N. V. R. (2016) 'Poly(lactic acid) blends in biomedical applications', *Advanced Drug Delivery Reviews*. Elsevier B.V., 107, pp. 47–59. doi: 10.1016/j.addr.2016.06.014.

Sakamoto, A. *et al.* (2018) 'Understanding the Impact of Stent and Scaffold Material and Strut Design on Coronary Artery Thrombosis from the Basic and Clinical Points of View', *Bioengineering*, 5(3), p. 71. doi: 10.3390/bioengineering5030071.

Sangeetha, V. H. *et al.* (2018) 'State of the art and future prospectives of poly(lactic acid) based blends and composites', *Polymer Composites*, 39(1), pp. 81–101. doi: 10.1002/pc.23906.

Santos Ana, C. *et al.* (2018) ‘Halloysite clay nanotubes for life sciences applications: From drug encapsulation to bioscaffold’, *Advances in Colloid and Interface Science*. Elsevier B.V., 257, pp. 58–70. doi: 10.1016/j.cis.2018.05.007.

Sasimowski, E. and Majewski, Ł. (2019) ‘Effect of the intensive plasticizing zone design on the effectiveness of corotating twin-screw extrusion’, *Advances in Polymer Technology*, 2019, pp. 15–17. doi: 10.1155/2019/8518341.

Schmitt, R. (2014) *Scanning Electron Microscope*. doi: 10.1007/978-3-642-20617-7.

Semalty, a *et al.* (2010) ‘Development and Characterization of Aspirin-Phospholipid Complex for Improved Drug Delivery ABSTRACT ’:, *Journal of Pharmaceutical Sciences*, 3(2), pp. 940–947.

Sha, L. *et al.* (2016) ‘Polylactic acid based nanocomposites: Promising safe and biodegradable materials in biomedical field’, *International Journal of Polymer Science*, 2016. doi: 10.1155/2016/6869154.

Shah, A. K., Wyandt, C. M. and Stodghill, S. P. (2013) ‘Physico chemical characterization of a novel anti-cancer agent and its comparison to Taxol ®’, 39(July 2011), pp. 89–101. doi: 10.3109/03639045.2012.659187.

Shahi, P. K. *et al.* (2018) ‘Silver nanoparticles embedded hybrid organometallic complexes : Structural interactions , photo-induced energy transfer , plasmonic effect and optical thermometry Silver nanoparticles embedded hybrid organometallic complexes : Structural interactions , ph’, 065117. doi: 10.1063/1.5020812.

Sharma, R. (2013) ‘The 3D Printing Revolution You Have Not Heard About’, *Forbes*.

Shi, X. *et al.* (2015) ‘Synergistic effects of nucleating agents and plasticizers on the crystallization behavior of Poly(lactic acid)’, *Molecules*, 20(1), pp. 1579–1593. doi: 10.3390/molecules20011579.

Shi, Y. *et al.* (2014) ‘Experimental and mathematical studies on the drug release properties of aspirin loaded chitosan nanoparticles’, *BioMed Research International*, 2014. doi: 10.1155/2014/613619.

Shimura, T. *et al.* (2016) ‘Extreme late-phase observation using coronary angioscopy until 7 years after sirolimus-eluting stent implantation’, *Coronary Artery Disease*, 27(1), pp. 29–33. doi: 10.1097/MCA.0000000000000315.

Shindo, D. and Oikawa, T. (2002) ‘Energy dispersive X-ray spectroscopy’, *Analytical electron microscopy for materials science*, pp. 81–102. doi: 10.1007/978-4-431-66988-3.

Shirazi, S. F. S. *et al.* (2015) ‘A review on powder-based additive manufacturing for tissue engineering: Selective laser sintering and inkjet 3D printing’, *Science and Technology of Advanced Materials*. IOP Publishing, 16(3), pp. 1–20. doi: 10.1088/1468-6996/16/3/033502.

Shoja, M. *et al.* (2015) ‘PREPARATION AND CHARACTERIZATION OF POLY (ε -’, 10(2), pp. 471–477.

Siegel, S. J. *et al.* (2006) ‘Effect of drug type on the degradation rate of PLGA matrices’, *European Journal of Pharmaceutics and Biopharmaceutics*, 64(3), pp. 287–293. doi: 10.1016/j.ejpb.2006.06.009.

De Silva, R. T. *et al.* (2014) ‘Synthesis and characterisation of poly (lactic acid)/halloysite bionanocomposite films’, *Journal of Composite Materials* , 48(30), pp. 3705–3717. doi: 10.1177/0021998313513046.

Simard, T. *et al.* (2014) ‘The Evolution of Coronary Stents: A Brief Review’, *Canadian Journal of Cardiology*. Canadian Cardiovascular Society, 30(1), pp. 35–45. doi: 10.1016/j.cjca.2013.09.012.

Skjelbred, P., Album, B. and Løkken, P. (1977) ‘Acetylsalicylic acid vs paracetamol: Effects on post-operative course’, *European Journal of Clinical Pharmacology*, 12(4), pp. 257–264. doi: 10.1007/BF00607424.

Skowyra, J., Pietrzak, K. and Alhnan, M. A. (2015) ‘Fabrication of extended-release patient-tailored prednisolone tablets via fused deposition modelling (FDM) 3D printing’, *European Journal of Pharmaceutical Sciences*. Elsevier, 68, pp. 11–17. doi: 10.1016/J.EJPS.2014.11.009.

Sood, A. K., Ohdar, R. K. and Mahapatra, S. S. (2010) 'Parametric appraisal of mechanical property of fused deposition modelling processed parts', *Materials and Design*. Elsevier, 31(1), pp. 287–295. doi: 10.1016/j.matdes.2009.06.016.

Sotoudehbagha, P. *et al.* (2018) 'Novel antibacterial biodegradable Fe-Mn-Ag alloys produced by mechanical alloying', *Materials Science and Engineering: C*. Elsevier B.V, p. #pagerange#. doi: 10.1016/j.msec.2018.03.005.

Stanković, M., Frijlink, H. W. and Hinrichs, W. L. J. (2015) 'Polymeric formulations for drug release prepared by hot melt extrusion: application and characterization', *Drug Discovery Today*, 20(7), pp. 812–823. doi: 10.1016/j.drudis.2015.01.012.

Stephanus, A. and Ivan, L. (2018) 'Effect of blend ratio and nanofiller localization on the thermal degradation of graphite nanoplatelets-modified PLA / PCL', *Journal of Thermal Analysis and Calorimetry*. Springer International Publishing, 0123456789. doi: 10.1007/s10973-018-7870-y.

Stoclet, G. *et al.* (2014) 'Elaboration of poly(lactic acid)/halloysite nanocomposites by means of water assisted extrusion: structure, mechanical properties and fire performance', *RSC Adv.* Royal Society of Chemistry, 4(101), pp. 57553–57563. doi: 10.1039/C4RA06845A.

Strohbach, A. and Busch, R. (2015) 'Polymers for Cardiovascular Stent Coatings', *International Journal of Polymer Science*, 2015. doi: 10.1155/2015/782653.

Surgery, D. and College, S. D. (2017) 'INTERNATIONAL JOURNAL OF SCIENTIFIC RESEARCH DRUG DELIVERY THROUGH DRUG ELUTING STENTS -A REVIEW Pharmacology Bhawani Gupta', (9), pp. 20–22.

Tabraiz Alam, M. S. *et al.* (2019) 'A review based on biodegradable and bioabsorbable stents for coronary artery disease', *Procedia Computer Science*. Elsevier B.V., 152, pp. 354–359. doi: 10.1016/j.procs.2019.05.006.

Tamai, H. *et al.* (2000) 'Initial and 6-month results of biodegradable poly-l-lactic acid coronary stents in humans.', *Circulation*, 102(4), pp. 399–404. doi: 10.1161/01.CIR.102.4.399.

Tang, Y. and Singh, J. (2008) ‘Controlled delivery of aspirin: Effect of aspirin on polymer degradation and in vitro release from PLGA based phase sensitive systems’, *International Journal of Pharmaceutics*, 357(1–2), pp. 119–125. doi: 10.1016/j.ijpharm.2008.01.053.

Tertis, M. *et al.* (2013) ‘Carbon Based Electrodes Modified with Horseradish Peroxidase Immobilized in Conducting Polymers for Acetaminophen Analysis’, pp. 4841–4854. doi: 10.3390/s130404841.

Therias, S., Murariu, M. and Dubois, P. (2017) ‘Bionanocomposites based on PLA and halloysite nanotubes: From key properties to photooxidative degradation’, *Polymer Degradation and Stability*. Elsevier Ltd, pp. 1–10. doi: 10.1016/j.polymdegradstab.2017.06.008.

Tian, X. *et al.* (2016) ‘Interface and performance of 3D printed continuous carbon fiber reinforced PLA composites’, *Composites Part A: Applied Science and Manufacturing*. Elsevier Ltd, 88, pp. 198–205. doi: 10.1016/j.compositesa.2016.05.032.

Tian, X. *et al.* (2017) ‘Recycling and remanufacturing of 3D printed continuous carbon fiber reinforced PLA composites’, *Journal of Cleaner Production*. Elsevier Ltd, 142, pp. 1609–1618. doi: 10.1016/j.jclepro.2016.11.139.

Tiwari, R. V., Patil, H. and Repka, M. A. (2016) ‘Contribution of hot-melt extrusion technology to advance drug delivery in the 21st century’, *Expert Opinion on Drug Delivery*. doi: 10.1517/17425247.2016.1126246.

Torrado, A. R. *et al.* (2015) ‘Characterizing the effect of additives to ABS on the mechanical property anisotropy of specimens fabricated by material extrusion 3D printing’, *Additive Manufacturing*. Elsevier B.V., 6, pp. 16–29. doi: 10.1016/j.addma.2015.02.001.

Trabert, B. *et al.* (2014) ‘Aspirin, Nonaspirin Nonsteroidal Anti-inflammatory Drug, and Acetaminophen Use and Risk of Invasive Epithelial Ovarian Cancer: A Pooled Analysis in the Ovarian Cancer Association Consortium’, *JNCI Journal of the National Cancer Institute*, 106(2), pp. djt431-djt431. doi: 10.1093/jnci/djt431.

Tumbleston, J. R. *et al.* (2015) ‘Additive manufacturing. Continuous liquid interface production of 3D objects.’, *Science (New York, N.Y.)*. American Association for the Advancement of Science, 347(6228), pp. 1349–52. doi: 10.1126/science.aaa2397.

Tyler, B. *et al.* (2016) ‘Polylactic acid (PLA) controlled delivery carriers for biomedical applications’, *Advanced Drug Delivery Reviews*. Elsevier B.V., 107, pp. 163–175. doi: 10.1016/j.addr.2016.06.018.

U. S. Food and Drug Administration (2017) ‘Class 1 Device Recall Absorb Bioresorbable Vascular Scaffold (BVS) System’. Available at: https://www.accessdata.fda.gov.

Urquijo, J., Guerrica-Echevarría, G. and Eguiazábal, J. I. (2015) ‘Melt processed PLA/PCL blends: Effect of processing method on phase structure, morphology, and mechanical properties’, *Journal of Applied Polymer Science*, 132(41), pp. 1–9. doi: 10.1002/app.42641.

Valapa, R., Pugazhenthi, G. and Katiyar, V. (2016) *Hydrolytic Degradation Behaviour of Sucrose Palmitate Reinforced Poly(lactic acid) Nanocomposites, International Journal of Biological Macromolecules*. Elsevier B.V. doi: 10.1016/j.ijbiomac.2016.04.040.

Vasquez, G.M, Majewski, C.E, Haworth, B. & Hopkinson, N. (2014) ‘2014_A targeted material selection process for polymers in laser sintering’, 1–4(2014), pp. 127–138. doi: http://dx.doi.org/10.1016/j.addma.2014.09.003.

Verbelen, L. *et al.* (2016) ‘Characterization of polyamide powders for determination of laser sintering processability’, *European Polymer Journal*. doi: 10.1016/j.eurpolymj.2015.12.014.

Vieira, A. C. *et al.* (2010) ‘Degradation and Viscoelastic Properties of PLA-PCL, PGA-PCL, PDO and PGA Fibres’, *Materials Science Forum*, 636–637(January 2014), pp. 825–832. doi: 10.4028/www.scientific.net/msf.636-637.825.

Vieira, A. C. *et al.* (2011) ‘Mechanical study of PLA-PCL fibers during in vitro degradation’, *Journal of the Mechanical Behavior of Biomedical Materials*. Elsevier Ltd, 4(3), pp. 451–460. doi: 10.1016/j.jmbbm.2010.12.006.

Villmow, T., Kretzschmar, B. and Pötschke, P. (2010) ‘Influence of screw configuration, residence time, and specific mechanical energy in twin-screw extrusion of polycaprolactone/multi-walled carbon nanotube composites’, *Composites Science and Technology*. Elsevier Ltd, 70(14), pp. 2045–2055. doi: 10.1016/j.compscitech.2010.07.021.

Virmani, R., Jinnouchi, H. and Finn, A. V. (2017) ‘Discontinuity’, *Journal of the American College of Cardiology*, 70(19), pp. 2345–2348. doi: 10.1016/j.jacc.2017.09.029.

Voit, W. *et al.* (2016) ‘Cartridge-Based 3D Printing System’.

Wachirahuttapong, S., Thongpin, C. and Sombatsompop, N. (2016) ‘Effect of PCL and Compatibility Contents on the Morphology, Crystallization and Mechanical Properties of PLA/PCL Blends’, *Energy Procedia*. The Author(s), 89, pp. 198–206. doi: 10.1016/j.egypro.2016.05.026.

Wang, C. *et al.* (2020) ‘Design , Characterization , and 3D Printing of Cardiovascular Stents with Zero Poisson ’ s Ratio in Longitudinal Deformation’, *Engineering*. THE AUTHORS, (xxxx), pp. 0–11. doi: 10.1016/j.eng.2020.02.013.

Wang, P.-J. *et al.* (2018) ‘Strain-induced accelerated asymmetric spatial degradation of polymeric vascular scaffolds’, *Proceedings of the National Academy of Sciences*, p. 201716420. doi: 10.1073/pnas.1716420115.

Wang, Q. *et al.* (2014) ‘Colloids and Surfaces B : Biointerfaces Adsorption and release of ofloxacin from acid- and heat-treated halloysite’, *Colloids and Surfaces B: Biointerfaces*. Elsevier B.V., 113, pp. 51–58. doi: 10.1016/j.colsurfb.2013.08.036.

Wang, X. *et al.* (2017) ‘3D printing of polymer matrix composites: A review and prospective’, *Composites Part B: Engineering*. Elsevier Ltd, 110, pp. 442–458. doi: 10.1016/j.compositesb.2016.11.034.

Waterbeemd, H. Van De and Rose, S. (2008) ‘Quantitative Approaches to Structure – Activity Relationships’, pp. 491–513.

Wee, D. *et al.* (2020) ‘Bioresorbable Polymeric Sca ff old in Cardiovascular

Applications', *Int. J. Mol. Sci*, (Cvd), pp. 1–35. doi: doi:10.3390/ijms21103444.

Wei, Z. *et al.* (2019) 'Simultaneous Determination of Acetaminophen and Tyrosine Using Screen-printed Electrochemical Sensor Based on MWCNTs-doped Poly (glycine)/ Poly (acrylic acid) Conducting Polymers', 14, pp. 6748–6758. doi: 10.20964/2019.07.26.

Wenger, R. and Giraud, M.-N. (2018) '3D Printing Applied to Tissue Engineered Vascular Grafts', *Applied Sciences*, 8(12), p. 2631. doi: 10.3390/app8122631.

Wiebe, J., Nef, H. M. and Hamm, C. W. (2014) 'Current status of bioresorbable scaffolds in the treatment of coronary artery disease', *Journal of the American College of Cardiology*, 64(23), pp. 2541–2551. doi: 10.1016/j.jacc.2014.09.041.

Wilson, W. M. and Cruden, N. L. M. (2013) 'Advances in coronary stent technology: current expectations and new developments', *Research Reports in Clinical Cardiology*, 4, pp. 85–96. doi: 10.2147/RRCC.S34408.

Wishart DS, E. a. (2017) *DrugBank 5.0: a major update to the DrugBank database for 2018.* doi: doi: 10.1093/nar/gkx1037.

Wohlers, T. T. (2005) *Early Research & Development, Wohlers Report 2005: rapid prototyping, tooling and manufacturing state of the industry worldwide progress report*.

Woodruff, M. A. and Hutmacher, D. W. (2010) 'The return of a forgotten polymer - Polycaprolactone in the 21st century', *Progress in Polymer Science (Oxford)*, 35(10), pp. 1217–1256. doi: 10.1016/j.progpolymsci.2010.04.002.

Wu, D. *et al.* (2009) 'Selective Localization of Multiwalled Carbon Nanotubes in Poly (ε -caprolactone)/ Polylactide Blend', pp. 417–424.

Wu, F. *et al.* (2019) 'Halloysite nanotubes coated 3D printed PLA pattern for guiding human mesenchymal stem cells (hMSCs) orientation', *Chemical Engineering Journal*. Elsevier, 359(October 2018), pp. 672–683. doi: 10.1016/j.cej.2018.11.145.

Wu, W. *et al.* (2013) 'Polylactide/halloysite nanotube nanocomposites: Thermal,

mechanical properties, and foam processing', *Journal of Applied Polymer Science*, 130(1), pp. 443–452. doi: 10.1002/app.39179.

Wu, Y. *et al.* (2012) 'Comparison of acute recoil between bioabsorbable poly-L-lactic acid XINSORB stent and metallic stent in porcine model', *Journal of Biomedicine and Biotechnology*, 2012. doi: 10.1155/2012/413956.

Wudy, K., Drummer, D. and Drexler, M. (2014) 'Characterization of polymer materials and powders for selective laser melting', *AIP Conference Proceedings*, 1593(May), pp. 702–707. doi: 10.1063/1.4873875.

Yang, H., Zhang, Y. and Ouyang, J. (2016) *Physicochemical Properties of Halloysite*. 1st edn, *Developments in Clay Science*. 1st edn. Elsevier Ltd. doi: 10.1016/B978-0-08-100293-3.00004-2.

Yang, K. *et al.* (2018) 'Bio-functional design, application and trends in metallic biomaterials', *International Journal of Molecular Sciences*, 19(1). doi: 10.3390/ijms19010024.

Yao, X. *et al.* (2017) 'Evaluation of carbon fiber-embedded 3D printed structures for strengthening and structural-health monitoring', *Materials and Design*. Elsevier Ltd, 114, pp. 424–432. doi: 10.1016/j.matdes.2016.10.078.

Yin, R., Yang, D. and Wu, J. (2014) 'T h e r a n o s t i c s Nanoparticle Drug- and Gene-eluting Stents for the Prevention and Treatment of Coronary Restenosis', 4(2). doi: 10.7150/thno.7210.

Youssef, R. F. *et al.* (2015) 'Applications of three-dimensional printing technology in urological practice', *BJU International*, 116(5), pp. 697–702. doi: 10.1111/bju.13183.

Yuan, P., Tan, D. and Annabi-Bergaya, F. (2015) 'Properties and applications of halloysite nanotubes: recent research advances and future prospects', *Applied Clay Science*. Elsevier B.V., 112–113, pp. 75–93. doi: 10.1016/j.clay.2015.05.001.

Yun, Y. *et al.* (2018) 'Effect of Printing Parameters on Tensile, Dynamic Mechanical, and Thermoelectric Properties of FDM 3D Printed CABS/ZnO

Composites', *Materials*, 11(4), p. 466. doi: 10.3390/ma11040466.

Zaharin, H. A. *et al.* (2018) 'Additive Manufacturing Technology for Biomedical Components: A review', *IOP Conference Series: Materials Science and Engineering*, 328, p. 012003. doi: 10.1088/1757-899X/328/1/012003.

Zaki, H. (2011) 'Spectroscopy Surface Analysis of Paracetamol and Paracetamol and Excipient Systems', pp. 1–256.

Zamarayeva, A. (EECS/UC B. *et al.* (2018) 'Custom, 3D Sprayed MRI receive coils', in *International Society for Magnetic Resonance in Medicine*. Paris.

Zhang, A., Zhang, Y. and Zhu, Z. (2019) 'Thermal properties of Halloysite nanotubes (HNTs) intercalation complexes-A review', 01055.

Zhang, J., Ma, S. and Gene, H. (2017) 'Guided bone regeneration with asymmetric collagen-chitosan membranes containing aspirin- loaded chitosan nanoparticles', *International Journal of Nanomedicine*, 12, pp. 8855–8866.

Zhang, K. *et al.* (2014) 'Surface modification of implanted cardiovascular metal stents: From antithrombosis and antirestenosis to endothelialization', *Journal of Biomedical Materials Research - Part A*, 102(2), pp. 588–609. doi: 10.1002/jbm.a.34714.

Zhang, P. *et al.* (2015) 'Placement suitability criteria of composite tape for mould surface in automated tape placement', *Chinese Journal of Aeronautics*, 28(5), pp. 1574–1581. doi: 10.1016/j.cja.2015.06.002.

Zhang, W. *et al.* (2019) 'Biosensors and Bioelectronics An electrochemical sensor based on electro-polymerization of ca ff eic acid and Zn / Ni-ZIF-8 – 800 on glassy carbon electrode for the sensitive detection of acetaminophen', *Biosensors and Bioelectronic*. Elsevier B.V., 131(February), pp. 200–206. doi: 10.1016/j.bios.2019.01.069.

Zhao, J. *et al.* (2016) 'Drug loaded nanoparticle coating on totally bioresorbable PLLA stents to prevent in-stent restenosis', pp. 1–8. doi: 10.1002/jbm.b.33794.

Zivic, F. *et al.* (2018) *Biodegradable Metals as Biomaterials for Clinical Practice :*

Iron-Based Materials.

PUBLICATIONS

materials

MDPI

Article

Faster Release of Lumen-Loaded Drugs than Matrix-Loaded Equivalent in Polylactic Acid/Halloysite Nanotubes

Chaitra Venkatesh [1], Oran Clear [2], Ian Major [1], John G. Lyons [2] and Declan M. Devine [1,*]

[1] Material Research Institute, Athlone Institute of Technology, Athlone N37 FK59, Ireland; c.venkatesh@research.ait.ie (C.V.); imajor@ait.ie (I.M.)

[2] Faculty of Engineering and Informatics, Athlone Institute of Technology, Athlone N37 FK59, Ireland; A00251270@student.ait.ie (O.C.); slyons@ait.ie (J.G.L.)

* Correspondence: ddevine@ait.ie

Received: 8 May 2019; Accepted: 3 June 2019; Published: 5 June 2019

Abstract: Nanocomposite-based drug delivery systems with intrinsic controlled release properties are ofgreatinterestinbiomedicalapplications. Wereportanovelpolylacticacid(PLA)/halloysitenanotube (HNT) nanocomposite-based drug delivery system. PLA/HNT nanocomposites have shown immense potential for use in biomedical applications due to their favorable cyto- and hemo-compatibility. The objective of this study was to evaluate the release of active pharmaceutical ingredients (API) from PLA/HNT composites matrix and the effect of preloading the API into the lumen of the HNT on its release profile. Aspirin was used in this study as a model drug as it is a common nonsteroidal anti-inflammatory and antiplatelet agent widely used for various medical conditions. These two types of drug-loaded PLA/HNT nanocomposites were characterised by scanning electron microscopy (SEM), differential scanning calorimetry (DSC), Fourier transform infrared spectroscopy (FT-IR), surface wettability and mechanical testing. Statistical analysis was conducted on numerical data. Drug entrapment and in vitro drug release studies were conducted using UV spectrophotometry. Results indicate that aspirin was successfully loaded into the lumen of HNT, which resulted in the sustained release of aspirin from the nanocomposites. Furthermore, the addition of HNT into the polymer matrix increased the mechanical properties, indicating its suitability as a drug-eluting reinforcing agent.

Keywords: Aspirin; polylactic acid; halloysite nanotubes; nanocomposites; active pharmaceutical ingredients; melt extrusion; drug loading; drug delivery

1. Introduction

Hot-melt extrusion (HME) is widely used in the manufacture drug delivery systems for the controlled release of pharmaceuticals, as the mixing process of the drug and the polymer is efficient at controlled temperatures and pressures. This process can be used to melt or solubilize active pharmaceutical ingredients (APIs) in a polymer matrix to generate amorphous systems that effectively can improve solubility, modulate controlled release and have improved bioavailability [1–6].

Polylactic acid (PLA) is the most widely used biodegradable aliphatic polymer as it is obtained from renewable resources such as corn and rice starch [7,8]. PLA is approved by the FDA for direct contact with biological fluids as it is biocompatible and its degradation products are nontoxic [9,10]. PLA and PLA blends are most commonly used for medical applications such as stents, sutures, dermal fillers [11] and various drug delivery strategies such as nanosystems, films and fibrous matrices [12]. PLA has been studied as a drug release membrane, and the results have achieved sustained drug release for a long duration due to diffusion of the API from the metrics and bulk degradation [13].

PLA has been used to prepare biodegradable polymeric nanoparticles to improve their bioavailability, solubility and sustained release of APIs. In such cases, the APIs are confined inside the polymer membrane or uniformly dispersed on the surface of the polymer [14,15]. However, PLA on its own does not have all the mechanical properties required. The addition of nanoclays, specifically halloysite nanotubes (HNTs), has shown to improve the properties such as tensile strength, storage modulus, flexural properties and Young's Modulus [16–20].

HNTs are a naturally occurring clay mineral which has been widely used in drug delivery systems as they are known to have a high aspect ratio, high surface area, nontoxicity, processability, fine particle size and biocompatibility [21]. The HNTs can be loaded with drugs due to its large outer surface and inner lumen [22]. Recent research has demonstrated the feasibility of loading of different drugs into the HNTs [23–27].

HNTs have also been studied for drug delivery in various polymer composites. Patel and researchers demonstrated the successful loading and sustained release of various drugs including antibiotics, antiseptics and disinfectants on electrospun HNT/PCL nanocomposites [27]. Qi and researchers successfully studied the double drug loading on HNTs and electrospinning with Poly (lactic-*co*-glycolic acid) (PLGA) [28]. To our knowledge, this is the first report for loading the HNTs with API and compounding with PLA by hot-melt extrusion (HME). We can hypothesise that the loading of the APIs into HNTs has better drug encapsulation and sustained drug release than when the APIs are compounded together with PLA and HNT. This drug-loaded nanocomposite can be employed for various medical applications requiring drug delivery such as scaffolds.

Aspirin (ASP) is a well-known pharmaceutical product used for various medical treatments. ASP is known to minimise inflammation, reduce body temperature and decrease the process of adhesion of platelets by blocking the production of hormones that participate in the process of inflammation, increasing body temperature and platelet fusion [29]. Due to the poor oral availability [30] and gastrointestinal side effects [31] of long-term oral administration of the aspirin, parenteral administration is required [32,33]. Also, ASP is an acidic drug which increases the water absorption of the polymer matrix, thereby affecting the rate of drug release and polymer degradation [32].

A number of studies have characterised drug loading and release profiles of ASP from polymer matrices. Devine et al. studied the encapsulation of aspirin in hydrophilic polymer coatings and copolymer hydrogels along with its associated release characteristics [34,35]. Shi et al. studied the loading of aspirin in different molecular weights of chitosan to analyse the release kinetics [36] and Zhang et al. recently demonstrated sustained drug release from aspirin-loaded chitosan nanoparticles [33].

In the current study, ASP was used as a model drug to study the effect of loading the API into the lumen of the HNTs prior to forming an HNT/PLA nanocomposite. This was compared to directly loading the API into the polymer matrix during compounding of the PLA/HNT nanocomposite. In previous work, the HME processing parameters were optimised in terms of enhanced mechanical properties of the final nanocomposite. In the current study, these optimised production settings were utilised to examine drug loading into the PLA/HNT nanocomposite structure to investigate the controlled release of API from these structures. We hypothesise that the loading of the ASP into the lumen of HNTs will result in enhanced sustained API release compared to direct loading of the API into the matrix. This drug-loaded nanocomposite may be employed for various medical applications requiring sustained drug delivery such as polymeric stents.

2. Experimental Details

2.1. Materials

PLA was obtained from Corbion, PLA LX 175 (Total Corbian, Gorinchem, The Netherlands). The density of the PLA was 1.24 g/cm^3. HNT was obtained from Applied Minerals, DRAGONITE-HP (APPLIED MINERALS INC, Brooklyn. NY, USA) and had a density of 2.56 g/cm^3. Acetyl salicylic acid (aspirin) was obtained from Sigma-Aldrich Ireland Ltd. (Wicklow, Ireland). The PLA and HNT were dried for 4 h in the oven at 80 °C. The moisture content of the PLA was measured before processing and 100 ppm moisture was utilised as an upper process limit.

2.2. Methods

2.2.1. Drug Loading of HNTs

Aspirin was encapsulated into the lumen of the HNTs in two batches at ratios of 1:1 and 2:1. For the preparation of 1:1 ratio, 12 g of ASP were dissolved in 120 mL of ethanol under continuous stirring. Once the solution became transparent, 12 g of HNTs were added and stirred for 4 h at 700 rpm. The solution was then centrifuged to separate the solid part and dried overnight at 40 °C. Similarly, the 2:1 ratio was prepared using 12 g of HNTs and 6 g of ASP.

2.2.2. Preparation of PLA/HNT/ASP Nanocomposites

Extrusion was performed by using APV (Model MP19TC (25:1), APV Baker, Newcastle-under- Lyme, UK) twin-screw compounder with 16 mm diameter screws. The temperature profile was maintained at (from die to the feeder) 140/135/130/125/120/115/110/50 °C. During extrusion, the screw speed was set at 140 rpm based on previous work. The mass fractions of PLA: HNTs were 100:0 and 95:5 for both lumen-loaded and matrix-loaded samples. The lumen-loaded HNT/ASP for both 1:1 and 2:1 ratios was tumble-mixed with PLA and extruded. These samples are referred to here as lumen-loaded. As a control, HNTs, ASP and the PLA were tumble-mixed and extruded at the same ratios. These samples are referred to here as matrix-loaded. The methods are illustrated in Figures 1 and 2.

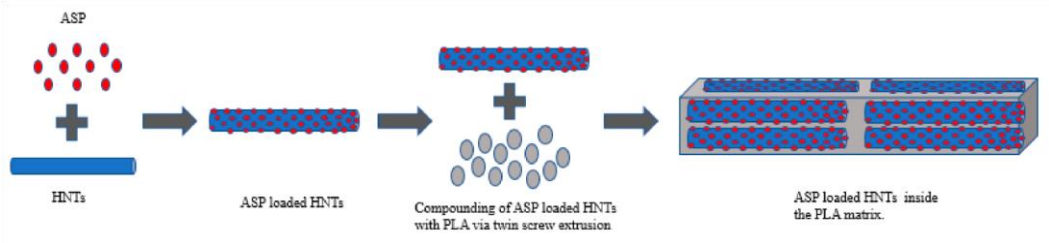

Figure 1. Schematic illustration PLA/(HNTs/ASP) nanocomposite by lumen-loading method for batch B1 and B5.

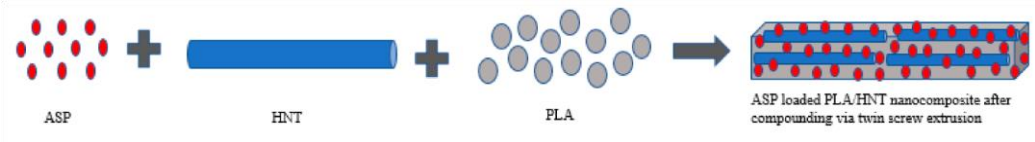

Figure 2. Schematic illustration of PLA/HNTs/ASP nanocomposite by matrix-loading method for batch B2 and B3.

The extruded film was drawn through the three-roll calendar to form a continuous film. Finally, the films were punched into ASTM standard tensile test specimens for testing. The nomenclature are described below in Table 1.

Table 1. Description of the prepared sample batches, the method of processing, composition and ratio of each component for each batch.

Batch	Type of Loading	Composition	HNTs:ASP Ratio

B1	Lumen-loaded	95% PLA, (HNT+ASP)	5%	1:1
B5	Lumen-loaded	95% PLA, (HNT+ASP)	5%	2:1
B2	Matrix-loaded	95% PLA, (HNT+ASP)	5%	1:1
B3	Matrix-loaded	95% PLA, (HNT+ASP)	5%	2:1
B4	Matrix-loaded	95% PLA, 5% HNT		-
B6	Matrix-loaded	100%PLA		-

2.2.3. Characterisation of the Drug-Loaded Nanocomposite

Differential Scanning Calorimetry (DSC)

DSC analysis was carried out in triplicate using a DSC 2920 Modulated DSC (TA Instruments, New Castle, DE, USA). The nitrogen flow rate was maintained at 20 mL/min to prevent oxidation. Using indium as standard, the instrument was calibrated. Tests were conducted on samples weighing between 8 and 12 mg, while a sample weight of 2.0 ± 0.5 mg was used for ASP due to the bulk volume of the drug. Samples were measured on a Sartorius scale (MC 210 P, Sartorius Lab Instruments GmbH & Co. KG, Goettingen, Germany), which could read up to five decimal places. Samples were placed into non-perforated aluminum pans with an empty crimped aluminum pan used as a reference.

To remove the thermal history, the samples were heated from 20 °C to 220 °C at the rate of 30 °C/min where they were held isothermally for 10 min. Later, they were cooled from 220 °C to 20 °C at 30 °C/min. To record the thermal properties the samples were heated from 20 °C to 220 °C at the rate of 10 °C/min. Thus glass transition temperature, cold crystallisation temperature and melting temperature of each sample were recorded.

Mechanical Testing

Mechanical properties of the PLA/HNTs composites were characterised by tensile testing, using Lloyd Lr10k tensometer (Ametek ltd, West Sussex, UK). A 2.5 kN load cell was used on ASTM standard test specimens. The strain rate was maintained at 50 mm/min (n = 12). Data was recorded using NexygenTM software (Ametek ltd). The tensile tests were carried out in adherence to ASTM D 882. Twelve test specimens were analysed per group. Dimensional measurements were completed on each sample prior to testing. For each tested sample Young's Modulus, stiffness, percentage strain at maximum load and stress at maximum load were recorded

Fourier Transform Infrared (FTIR) Spectroscopy

FTIR was carried out on a Perkin Elmer Spectrum One fitted with a universal ATR sampling accessory (Perkin Elmer, Waltham, MA, USA). The recordings of all the data were in the spectral range of 4000–650 cm^{-1} at 21 °C. A resolution of 1 cm^{-1} was employed, a fixed universal compression force of

70–80 N with four scans per sample was recorded. Spectrum software was used for subsequent analysis.

Goniometry (Surface Wettability)

The assessment of surface wettability of the composites was done using First Ten Angstroms

FTA32 goniometer (FTA Europe, Cambridge, UK). In this test, the Sessile Drop contact angle technique was utilised using distilled water as the probe liquid. Five measurements at various places on the films were taken for each composite sample.

Evaluation of Drug-Loaded Efficiency

Aspirin encapsulation and loading efficiency were studied by separating the ASP-loaded HNTs from the free drug present in the aqueous medium by method of centrifugation. Centrifugation was carried out at room temperature for 30 min at 700 rpm. A UV spectrophotometer was used to determine the amount of free aspirin at 276 nm. A standard calibration curve of concentration versus absorbance was plotted. The ASP encapsulation efficiency (EE) and the ASP loading capacity (LC) of the process were calculated from the equations below [28,36,37]

$$EE = \frac{(total\ amount\ of\ ASP - free\ ASP)}{total\ amount\ of\ ASP} \times 100 \quad (1)$$

$$LC = \frac{total\ amount\ of\ ASP - free\ ASP}{nanoparticles\ weight} \times 100 \quad (2)$$

In Vitro Drug Release Properties

The drug release mechanism was studied by placing the samples in simulated body fluid (SBF) pH 7.4 in DISTEK 2100 dissolution apparatus (Distek, Inc. North Brunswick, NJ, USA). Each vessel of the dissolution apparatus contained 500 mL of SBF at 36.7 °C with rotation speed of the stirring element shaft at 50 rpm for three weeks. At selected time intervals, 5 mL of the release buffer was removed for UV analysis and replaced with an equal volume of fresh buffer. The amount of released aspirin was measured by UV Spectrophotometer (Shimadzu Europa GmbH, Duisburg, Germany) at 298 nm. This experiment was carried out in triplicate to obtain the release profile of the ASP in relation to time.

Statistical Analysis

Statistical analysis of the tensile test results, DSC measurements and the surface wettability measurements were carried out by analysis of variance (one-way ANOVA) with a Tukey Post hoc test for multiple comparisons using Minitab 17 Statistical Software (Minitab Ltd., Coventry, UK). All the values were considered at a 95% confidence interval, and differences were considered significant when $p \leq 0.05$.

3. Results

3.1. Preparation of Drug-Loaded HNTs

Aspirin loading into HNTs was performed without any difficulty. Prior to loading, the ASP and HNTs were received in white powder form. The ASP-loaded HNTs underwent a subtle colour change to a pale (mild pink-colored) powder as seen in Figure 3.

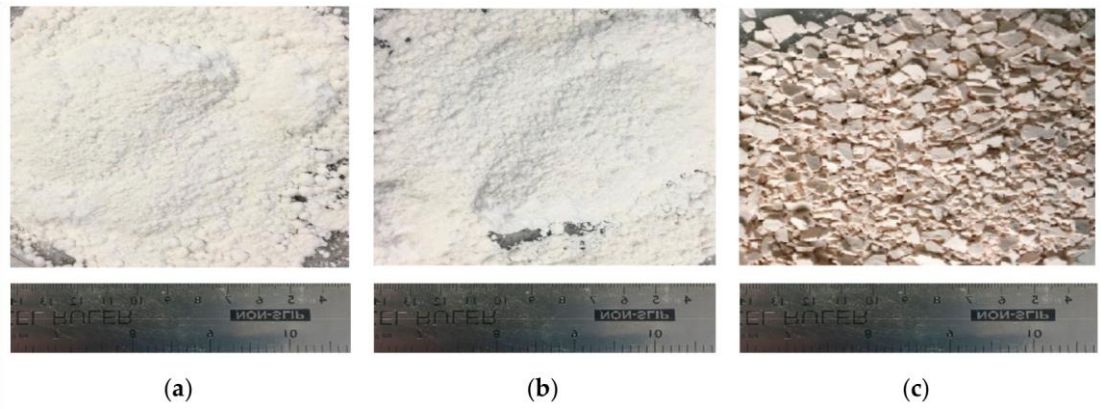

Figure 3. Photograph of (a) ASP, (b) HNTs, (c) ASP-loaded HNTs after drying in the oven at 40 °C overnight. The resultant blend had a pale pink colour as compared to the white colour of the ASP and HNTs individually.

The ASP encapsulation efficiency (EE) for 2:1 and 1:1 ratios was calculated to be 45.3% and 66.6%, respectively. The ASP loading capacity (LC) for 2:1 and 1:1 ratios was 22.6% and 66.6%, respectively.

3.2. Processing of PLA and HNT through Melt Extrusion

Virgin PLA, PLA/HNTs, PLA/(HNT-ASP) and PLA/HNT/ASP nanocomposites were melt-compounded followed by calendaring at screw speeds of 140 rpm without difficulty. The extruded PLA remained transparent. However, the PLA/HNTs nanocomposites changed in colour from transparent to opaque. The PLA/(HNT-ASP) and PLA/HNT/ASP nanocomposites were opaque with mild pink colour as shown in Figure 4.

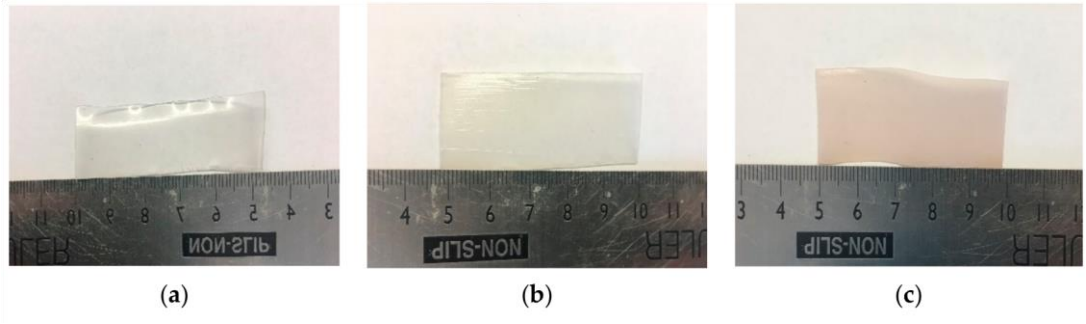

Figure 4. Photographs showing (a) virgin PLA films are transparent, (b) PLA/HNT nanocomposite films are opaque, (c) ASP-loaded PLA/HNT nanocomposite are mild pink in colour.

3.3. Differential Scanning Calorimetry (DSC)

The thermal properties of the nanocomposites following drug encapsulation were analysed using DSC. Figure 5 shows the thermograms of all the batches including the ASP and HNTs for comparison. Aspirin shows its characteristic melting peak at 142.45 °C as expected. However, this peak is not evident in the ASP-loaded HNTs curve.

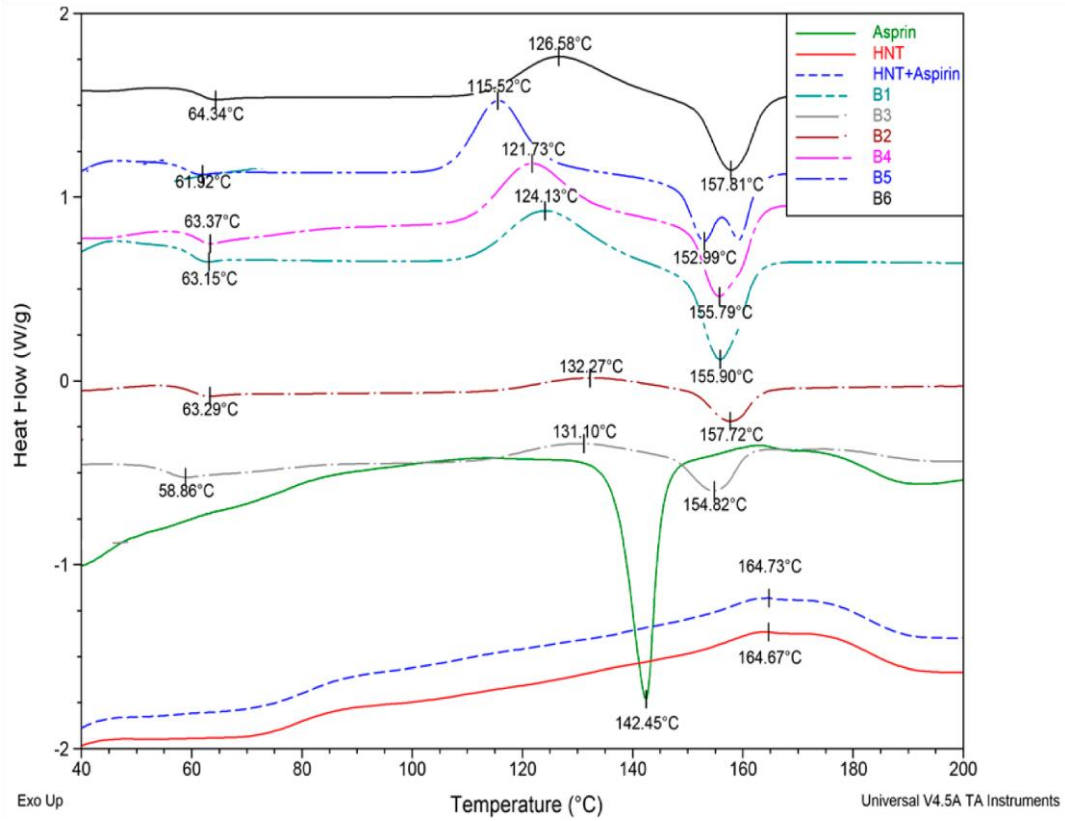

Figure 5. Thermograms of B1, B2, B3, B4, B5, B6, HNT, ASP and HNT+ASP. There is no change in T_g due to ASP loading when compared to the virgin PLA and PLA/HNT nanocomposite.

From analysis of the thermograms of the nanocomposites, the results indicate that the glass transition temperature (T_g) does not show any significant change due to the addition of ASP in the nanocomposite. However, the cold crystallisation temperature exhibits a significant decrease when the ASP is lumen-loaded at a 2:1 ratio when compared to other nanocomposite batches. It is interesting to note that the cold crystallization temperature increases and there is little or no curve for the cold crystallization observable in the matrix-loaded batches B2 and B3 of both 1:1 and 2:1 ratios. The melting temperature of the PLA (B6) is 157 °C, which decreases only for the lumen-loaded 2:1 nanocomposite (B5) and there is no significant difference in the melting temperature for other samples.

3.4. Mechanical Testing

Mechanical testing was conducted to analyse and compare the effect of the drug on the mechanical properties of the nanocomposite. The analysis of the mechanical properties of all the batches produced is depicted in Figure 6.

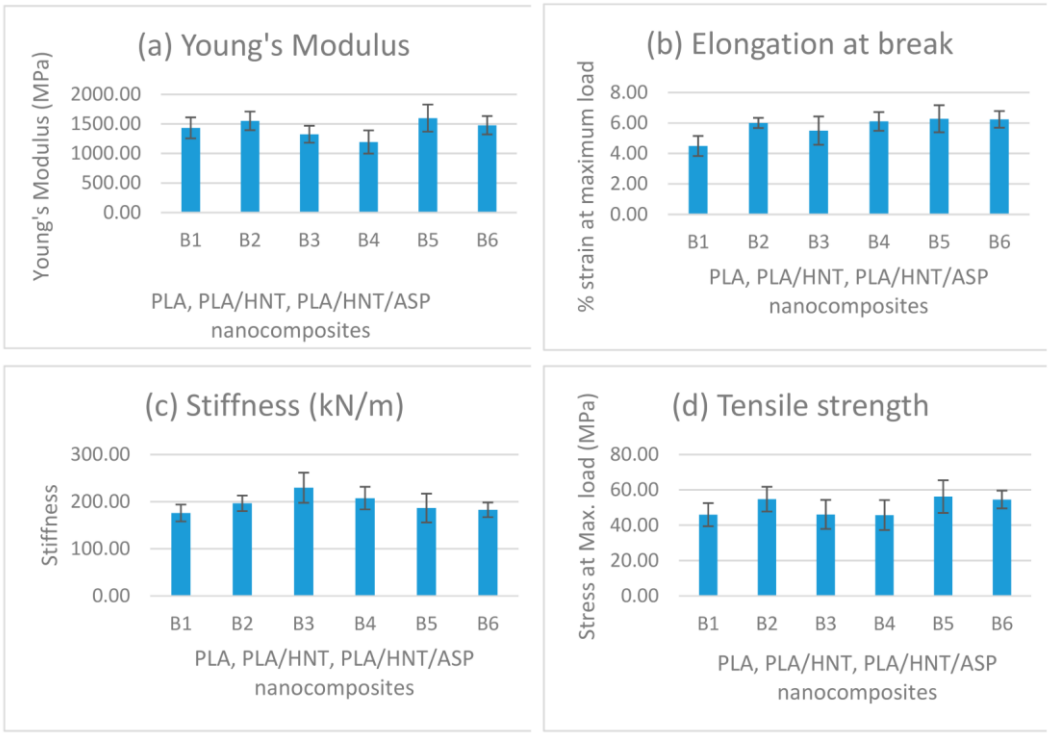

Figure 6. Mechanical properties of the nanocomposites are shown in the above graph. (a) Young's modulus of the preloaded 2:1 nanocomposite (B5) is significantly higher with *p*-value of 0.001. (b) Elongation at break does not show any significant change. (c) Stiffness significantly increases for 2:1 matrix-loaded nanocomposite (B3) with a *p*-value of 0.001. (d) Tensile strength significantly increases for preloaded 2:1 nanocomposite (B5) batch with *p*-value of 0.001.

In comparison to the virgin PLA (B6) and PLA/HNT nanocomposite (B4), Young's modulus and the tensile strength significantly increased for the preloaded 2:1 nanocomposite (B5), whereas stiffness significantly increased for matrix-loaded 2:1

nanocomposite (B3), with no significant change in the elongation at break for any batch. It is interesting to note that 2:1 ratio of ASP loading changed the mechanical properties of the nanocomposite when compared to the 1:1 loading of the ASP.

3.5. Fourier Transfer Infrared Spectroscopy (FTIR)

The chemical structure of PLA is $(C_3H_4O_2)_n$, HNT is $Al_2Si_2O_5(OH)_{4.2}(H_2O)$ and ASP is $C_9H_8O_4$. FTIR analysis was performed to study the chemical reaction in PLA/HNTs composites. Virgin PLA exhibited characteristic peaks at 3571 cm^{-1} corresponding to –OH stretch, peaks at 2995 cm^{-1} and 2946.34 cm^{-1} were attributed to CH stretch, and the peaks at 1750 cm^{-1} indicated –C=O carbonyl group [38]. The spectrum of HNTs displayed peaks at 3693.26 cm^{-1} and 3623.39 cm^{-1} which can be assigned to O–H group and peak at 906.81 cm^{-1} to Al–OH group.

The spectra of PLA/HNTs composites displayed characteristic peaks of both PLA and HNTs. The functional groups of HNT such as O–H stretching of the hydroxyl group are displayed by the characteristic peak located at 3696.39 cm^{-1} and 3626.39 cm^{-1}.

The analysis of the spectra of HNTs, ASP and the ASP lumen-loaded HNTs is shown in Figure 7. The spectra indicate the characteristic peaks of ASP at 1751 cm^{-1} corresponding to C=O stretching, 1697 cm^{-1} corresponding to –COO stretch and 1486 cm^{-1} from antisymmetric stretching vibration of a carboxylate form of aspirin [26,39]. These peaks were observed in the lumen-loaded HNT at 1751 cm^{-1}, 1697 cm^{-1} and 1486 cm^{-1}. This indicates the ASP molecules had been attached on the HNTs after drug loading.

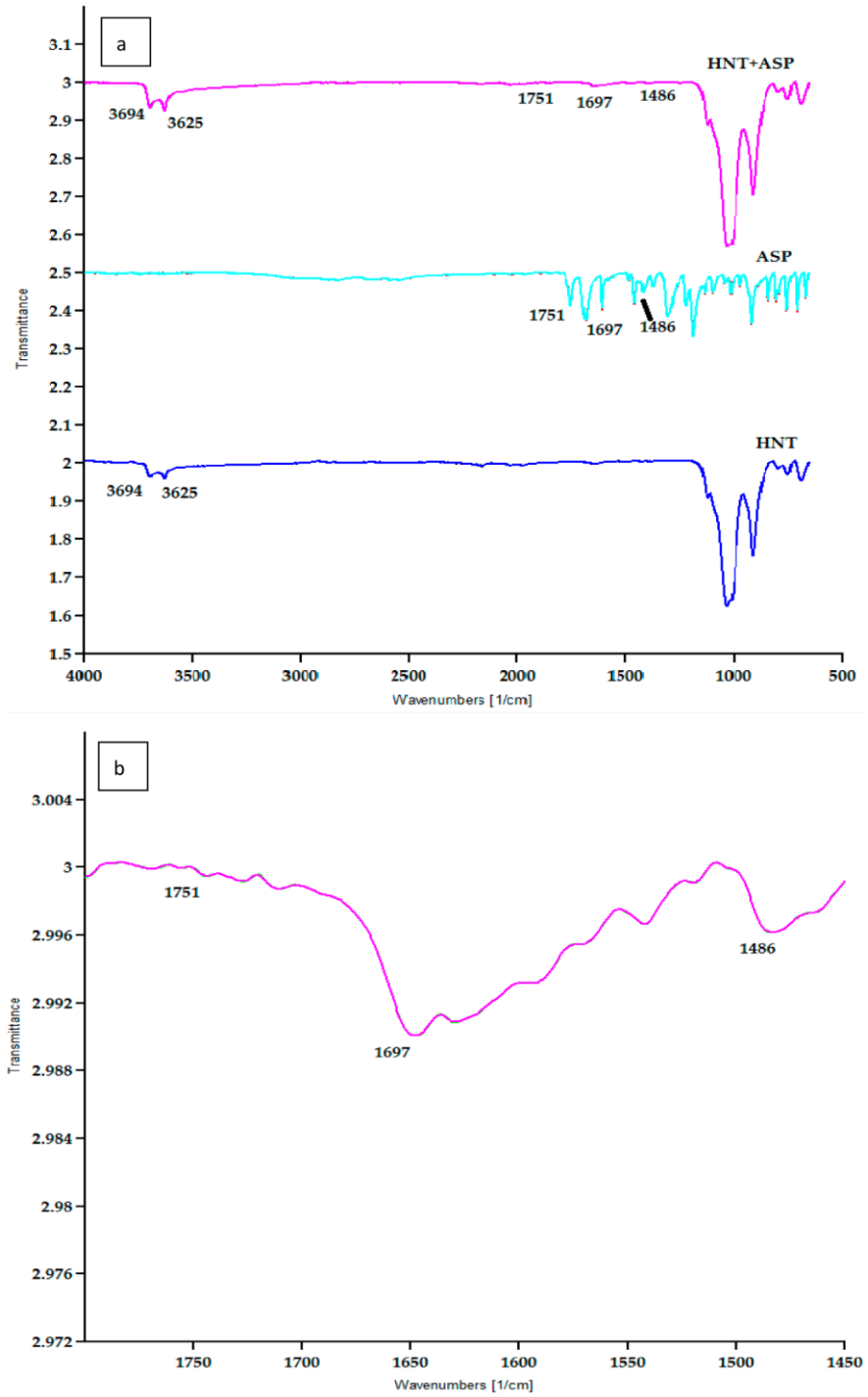

Figure 7. (a) FTIR spectra of HNT, ASP and ASP-loaded HNTs samples. The peaks of ASP at 1751 cm^{-1}, 1697 cm^{-1} and 1486 cm^{-1} correspond with the peaks of ASP-loaded HNTs at 1751 cm^{-1}, 1697 cm^{-1} and 1486 cm^{-1}. This indicates the drug is loaded in the HNT. (b) Higher magnification of HNT + ASP spectrum.

3.6. Surface Wettability

As showen in Figure 8, the contact angle of the B5 and B3 significantly decreases when compared to B1 and B2 (with $p \leq 0.04$, for all comparisons), whereas the contact

angle measurement significantly increases for B1 and B2 when compared to B6 with $p \leq 0.035$ (for both comparisons).

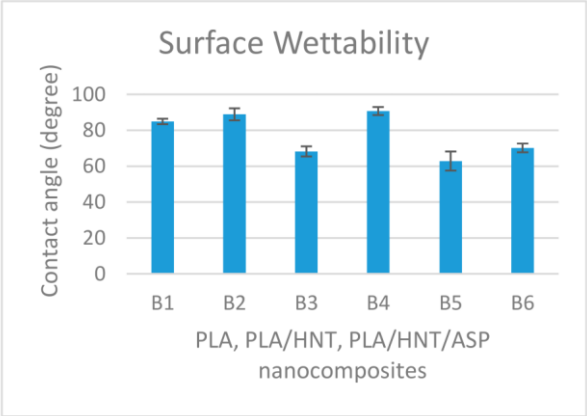

Figure 8. Graphical representation of contact angle measurements for all batches indicates the hydrophilicity nature of B5 and B3 batch of 2:1 ratio of both preloading and matrix-loading which is comparable to native PLA which has a contact angle of 70°. The B1 and B2 samples with a 1:1 ratio tend to be hydrophobic, exhibiting a contact angle of ca. 90°.

3.7. Drug Release

The amount of API released from the lowest to the highest concentration is plotted against the time of release. The graphical representation of the amount of API release (Q%) versus time (t) shows linearity as seen in Figure 9. Thus, the drug release rate is independent of the concentration of the API. In this study, the release kinetics of aspirin showed the best fit for zero-order model ($R^2 = 0.9995$) which represents slow release of drug and is expressed by the equation $Q_t = Q_0 + K_0 t$ where Q_t is the amount of drug dissolved at time t, Q_0 is the initial amount of drug in the solution and K_0 is the zero-order release constant expressed in units of concentration/time. The data obtained from in vitro drug release studies were plotted as cumulative amount of drug released versus time.

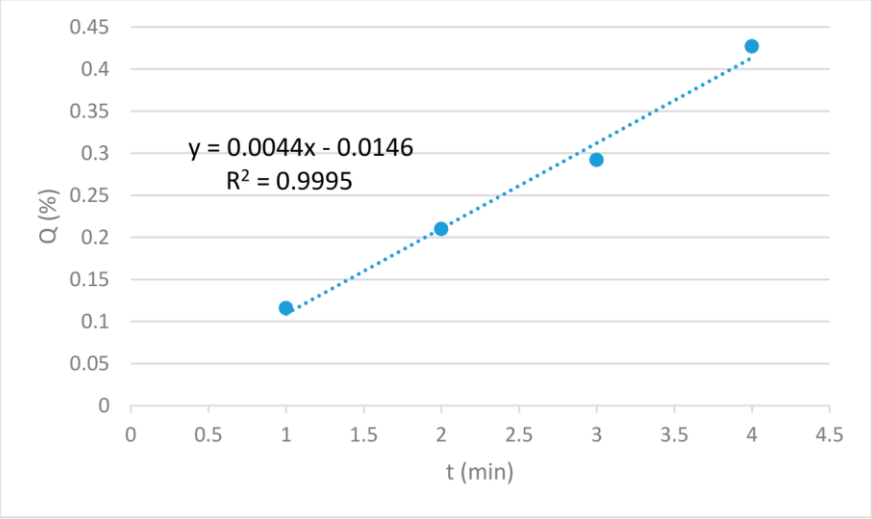

Figure 9. Standard curve of API release for the lowest to the highest concentration of API.

The API release profiles for all batches tested are presented in Figure 10. Batches B1 and B2 had an API loading ratio of 1:1, HNT:API. From API release studies, it was found that lumen-loaded B1 samples of 1:1 ratio exhibited a burst release of 26% in 8 h. This was followed by a slow release of 33% up to 72 h and 55% at 144 h. On the ninth day, there was a gradual decrease to 51% release. Conversely, the release from the matrix-loaded B2 was recorded at 6% after 2 h, with no further release observed until the sixth day when 33% release was detected, which was reduced to 20% release on the ninth day.

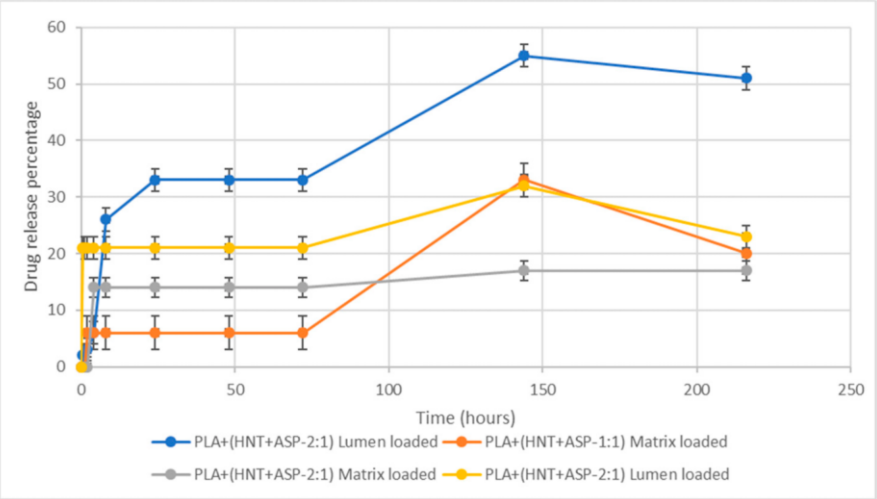

Figure 10. In vitro release kinetics show a general burst release of API followed by no further release until at least 72 h. The lumen samples exhibited a higher release rate compared to the matrix-loaded counterparts.

Batches B3 and B5 had an API loading ratio of 2:1, HNT:API. The matrix-loaded B3 samples exhibited a burst release of 14% after 4 h, which again did not increase until the ninth day when 17% API release was detected. The lumen-loaded B5 samples exhibited a burst release of 21% within 1 h with no further API release detected until after six days when 32% API release was recorded, which

decreased to a release of 23% on the ninth day.

4. Discussion

The present study explored the feasibility of controlled release of API from PLA/HNT composites. It also compared the release of API preloaded into the lumen of the HNT component of the nanocomposite compared to API loaded directly into the matrix of the nanocomposite.

The polymer matrix utilized in this study was PLA. This polymer was selected as it is a commonly used biomedical polymer [9] which has a glass transition temperature of 60 °C. This is important as the polymer selected for the HME must have

deformation potential and the glass transition temperature must be less than the melting point of the drug, which in the case of aspirin is 135 °C [1]. Aspirin was selected to molecularly disperse inside the polymer matrix by the generation of pressure during HME and melting the various components within the mixture (drug, polymer and nanoparticle) at a set temperature [1].

HNTs were selected as they have shown great potential as a reinforcing agent in a PLA nanocomposite system [40], and structurally, the large surface area and the inner lumen of HNTs make it suitable for the drug loading and sustained release. HNTs have been shown to increase drug effectiveness without increasing the concentration of the drug as it is slowly released from the HNTs [22].

4.1. Drug Loading

The HNTs are normally mixed with a saturated solution of a chosen API in ethanol, water or other solvents to entrap hydrophilic drugs [41]. However, the low dissolution rate of the ASP in water reduces the drug absorption rate and also toughens the maintenance of its concentration inside the body [26]. Hence, in this study, the ASP was dissolved in ethanol and HNTs were added to the solution for the drug loading.

The API loading on the HNT is either the API is encapsulated in the inner lumen, or it may be bound to the outer surface. The negatively charged outer surface of the HNT could encapsulate the ASP through hydrogen bonding between the carbonyl group of the ASP and the hydroxyl or the siloxane group of the HNT. When the vacuum is applied during the API loading, the positively charged inner lumen of the HNT could entrap the ASP [26,41]. Most likely, the ASP is distributed in both inner and outer lumen which could lead to initial burst release from the outer surface and gradual and slow release of the API from the inner lumen [22].

The ASP encapsulation efficiency (EE) and the loading capacity (LC) were better for 1:1 loading ratio. Similar results were reported by Qi et al. in their API release study from electrospun PLGA/HNT nanofiber composites. In this work, it was hypothesised that the fast deposition and aggregation of HNTs at higher concentrations lead to relatively less surface area being exposed to the API, which resulted in lower EE and LCs [28].

4.2. Melt Extrusion

Twin-screw extrusion is a high-shear process and it has been shown that increases in screw speed during compounding increase melt shear and aid HNT distribution in the PLA matrix. As such, a screw speed of 140 rpm was utilised in this study based on previous findings [42].

The temperature profile set for melting the PLA during extrusion was between 140 and 200 °C. The temperature profiles for the extrusion process should be 20–40 °C above the T_g of the polymer [43]. However, since the melting temperature of the ASP is 135 °C, the extrusion was performed above 140 °C. This enabled ASP to disperse molecularly inside the polymer matrix [1].

4.3. Thermal Characteristics

The characteristic melting peak of ASP did not appear in the DSC thermograms of ASP-loaded HNTs. This could indicate the loading of the ASP inside the cavity of the HNTs [44]. This could also be indicative of the amorphous state of the drug [45].

The glass transition temperature is the measure of rigidity [46]. The addition of HNTs or the ASP has a minimal effect on the rigidity of the PLA backbone chain. The cold crystallisation temperature exhibited a significant decrease when the ASP was preloaded into the lumen of the HNT at a 2:1 ratio when compared to other batches of the nanocomposites. A reduction in Tcc of PLA/ASP-HNTs composites has been reported to be indicative of heterogeneous nucleation, where thinner or less perfect crystalline lamella are formed [8,47]. This is further supported by the twin melting peak of the nanocomposite, which is indicative of the melting of imperfect crystalline segments.

Conversely, the matrix loaded nanocomposites showed a negligible or nearly no cold crystallisation curve for both 2:1 and 1:1 ratios. In a previous study by Shi et al., the addition of plasticizer into the PLA composites has been shown to result in very small or no cold crystallisation peak indicating the increased mobility of PLA chains and advanced crystallisation of the nucleating agents prior to cooling [48]. Hence, a negligible or nearly no cold crystallisation curve for both 2:1 and 1:1 ratio ASP-loaded nanocomposite may be due to the plasticizing effect of the ASP when processed together with PLA and HNT.

4.4. Mechanical Properties

The mechanical properties of the nanocomposites varied with HNT:ASP loading and encapsulation method. The coaxial alignment of HNTs in the PLA matrix enables the efficient load transfer from PLA to HNTs, which improves the mechanical properties.

Results from the current study indicate that the 2:1 lumen-loaded nanocomposite (B5) exhibited an increase in Young's Modulus and the tensile strength compared to the PLA/HNT. This is likely related to the plasticising effect of ASP on the system as observed in DSC data which allowed molecular chains to slide over each other more easily under tension. It is interesting to note the drug inclusion in the nanocomposite does not deteriorate the strength, unlike the study conducted by Patel and researchers where the tensile strength was reduced when the drug-loaded HNTs were loaded

into the PLA matrix [27]. However, in their study, the method of processing was electrospinning. Here, the process of extrusion would have induced HNT dispersion through melt shearing [42]. Similarly, there was a significant increase in stiffness for matrix-loaded 2:1 nanocomposite (B3) when compared to the other batches.

When the drug-loaded nanocomposites are compared to the PLA/HNT nanocomposites (B4), the observed increases in mechanical properties could be due to the interactions of the ASP molecules with the HNTs, which enhance their interfacial adhesion and dispersion within the matrix [48].

4.5. Fourier Transform Infrared (FTIR) Spectroscopy

The spectrum of ASP-loaded HNTs shows similarities to the HNT spectrum. However, the characteristic peaks of ASP are evident at low intensities as indicated by peaks at 1751 cm^{-1}, 1486 cm^{-1} and 1697 cm^{-1} which are characteristic of C=O stretch, –COO stretch and antisymmetric stretching vibration of a carboxylate form of aspirin in ASP. Similar analyses and findings were reported by Lun and researchers [26]. As the peaks of ASP are not intense and very similar to HNT peaks, this could indicate the loading of the ASP in the HNT cavity, which is relatable to the thermal analysis of the same. This also could indicate the surface of HNTs are free of residual ASP [44].

The spectra of all the drug-loaded PLA/HNT nanocomposite films were very similar to the PLA spectrum with no peaks of ASP observed. This could be due to the insensitivity of the FTIR technique or factually, the vibration bands of ASP or HNTs could be overlapping with PLA bands [28].

4.6. Surface Wettability

PLA exhibited a hydrophilic nature, whereas HNTs were relatively hydrophobic in agreement with previous work [20,49]. ASP is a hydrophilic drug [32]. The hydrophilicity of B5 and B3 indicate that the loading ratio of 2:1 of HNTs:ASP irrespective of the type of processing decreases the contact angle of the nanocomposites. This could be attributed to the higher agglomeration of HNT which resulted in a lower drug uptake. This could result in a higher amount of ASP in the matrix system which had a plasticising effect and rendered the composite more hydrophilic compared to the 1:1 samples. Similar findings were seen by Patel and researchers in their study with PCL/HNT nanocomposites with antibacterial drugs [27].

4.7. Drug Release

ASP release from the nanocomposite systems indicate that both the HNT:ASP ratio and entrapment method had a large effect on ASP release. The API release

mechanism for the PLA/HNT/ASP nanocomposite was through diffusion and swelling of the nanocomposite as shown in Figure 11.

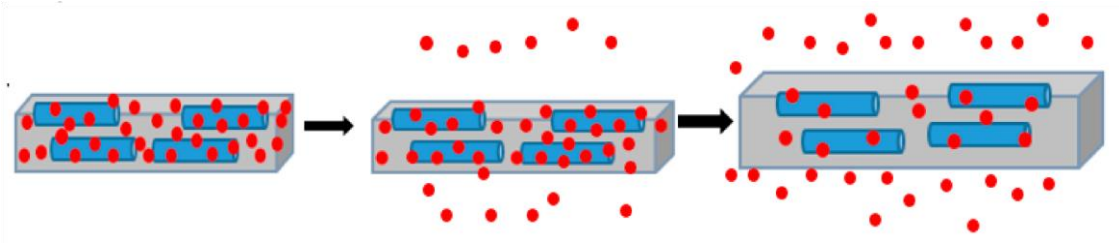

Figure 11. Schematic representation of API release mechanism for PLA/HNT/ASP nanocomposite through diffusion and swelling.

From ASP data, it was shown that the matrix-loaded samples did not have any burst release and that the release began following 8 h incubation, which would indicate that the drug had started to diffuse through the hydrophilic PLA matrix. Conversely, the lumen-loaded samples did have a burst release of 21–28% in the first 1–8 h. This may be attributed to the ASP washing from the outer lumen of the HNT, which were close to the surface of the PLA. In terms of HNT:ASP ratio, and in agreement with drug-loading findings, the 1:1 samples yielded a higher total API release at the end of the nine-day experiment. From the literature, it has been reported that the reduction in initial burst release may be due to the effect of the plasticizer in the polymer matrix [32]. The slow drug release suggests the presence of major amounts of ASP in the lumen of the HNTs at that time point [28]. The thermal properties of test samples in this study show that the matrix-loaded ASP for both 2:1 and 1:1 ratio nanocomposite had negligible cold crystallisation curves, which could be due to the plasticizing effect of the ASP when loaded directly into the PLA matrix. Plasticizers, which are capable of increasing flexibility of the polymers and can reduce the degradation of the thermolabile drugs [4]. The higher percentage of drug release after 140 h can be attributed to the gradual degradation of the PLA which had extended the retention time of the API [15].

It is interesting to note the reduction in the percentage release of the API from the nanocomposites on the ninth day except for the 1:1 matrix-loaded nanocomposite (B3). This could be due to the presence of the ASP in the inner lumen of the HNT, which gradually diffused to the PLA matrix during the nine days. Thus the loading of the ASP onto the HNT potentially on the inner lumen reduces the burst release and aids sustained release over a period of time. In this study, the matrix-loaded samples did not have a burst release and were followed by a sustained release, which could be due to the better dispersion and loading of the ASP on the HNT during extrusion.

5. Conclusions

The drug–polymer nanocomposite delivery system of ASP-PLA/HNT nanocomposite exhibits a sustained release performance. The encapsulation efficiency and the loading capacity were better for 1:1 ratio loading of HNT:ASP. FTIR

characterisation revealed the presence of ASP in the ASP-loaded HNTs. DSC data demonstrated the API–polymer interaction between aspirin and PLA/HNTs. The API–polymer interaction affected the release of aspirin, resulting in a sustained release action. Lumen-loaded samples had burst release and overall higher release of the API when compared to the matrix-loaded samples, which did not have initial burst release. In terms of ratios, 1:1 for HNT:ASP resulted in a higher total of API released at the end of the nine-day experiment. Hence, we have shown that the release of API can be controlled using different nanocomposite compositions.

Author Contributions: Conceptualization, D.M.D.; methodology, C.V.; experimentation, C.V. and O.C.; Characterisation, C.V. and O.C.; writing—original draft preparation, C.V.; writing—review and editing, C.V., D.M.D., I.M. and J.G.L.; supervision, D.M.D.; funding acquisition, D.M.D., I.M. and J.G.L.

Funding: This publication has emanated from research conducted with the financial support of Athlone Institute of Technology under the Presidents Seed Fund, Enterprise Ireland funding under the Technology Gateway program, grant number TG-2017-0114 and Science Foundation Ireland (SFI) under Grant Number 16/RC/3918.

Conflicts of Interest: The authors declare no conflict of interest.

Nomenclature

HME	Hot-melt extrusion
API	Active pharmaceutical ingredients
PLA	Polylactic acid
HNTs	Halloysite nanotubes
ASP	Aspirin (acetyl salicylic acid)
Lumen loading	ASP loading on HNTs and processing with PLA
Matrix loading	ASP, HNTs and PLA are mixed and processed
B1	1:1 ratio of lumen loading
B2	1:1 ratio of matrix loading
B3	2:1 ratio of matrix loading
B4	Processed PLA/HNT nanocomposite (matrix loading)
B5	2:1 ratio of lumen loading
B6	Processed virgin PLA (matrix loading)
DSC	Differential scanning calorimetry
Tg	Glass transition temperature
Tcc	Cold crystallisation temperature
Tm	Melting temperature
FTIR	Fourier transfer infrared spectroscopy
SEM	Scanning electron microscopy

References

Fule, R.; Paithankar, V.; Amin, P. Hot melt extrusion based solid solution approach: Exploring polymer comparison, physicochemical characterization and in-vivo evaluation. *Inter. J. Pharm.* 2016, *499*, 280–294. [CrossRef]

Lyons, J.G.; Holehonnur, H.; Devine, D.M.; Kennedy, J.E.; Geever, L.M.; Blackie, P.; Higginbotham, C.L. The incorporation of an organically modified layered silicate in monolithic polymeric matrices produced using hot melt extrusion. *Mater. Chem. Phys.* 2007, *103*, 419–426. [CrossRef]

Martinez-Marcos, L.; Lamprou, D.A.; McBurney, R.T.; Halbert, G.W. A novel hot-melt extrusion formulation of albendazole for increasing dissolution properties. *Inter. J. Pharm.* 2016, *499*, 175–185. [CrossRef] [PubMed]

Patil, H.; Tiwari, R.V.; Repka, M.A. Hot-Melt Extrusion: From Theory to Application in Pharmaceutical Formulation. *AAPS PharmSciTech* 2016, *17*, 20–42. [CrossRef] [PubMed]

Maniruzzaman, M.; Boateng, J.S.; Snowden, M.J.; Douroumis, D. A review of hot-melt extrusion: Process technology to pharmaceutical products. *ISRN Pharm.* 2012, *2012*, 436763–436769. [CrossRef] [PubMed]

Saerens, L.; Vervaet, C.; Remon, J.P.; De Beer, T. Process monitoring and visualization solutions for hot-melt extrusion: A review. *J. Pharm. Pharmacol.* 2014, *66*, 180–203. [CrossRef]

Healy, A.V.; Waldron, C.; Geever, L.M.; Devine, D.M.; Lyons, J.G. Degradable Nanocomposites for Fused Filament Fabrication Applications. *J. Manuf. Mater. Process.* 2018, *2*, 29. [CrossRef]

Chen, Y.; Murphy, A.; Scholz, D.; Geever, L.M.; Lyons, J.G.; Devine, D.M. Surface-modified halloysite nanotubes reinforced poly(lactic acid) for use in biodegradable coronary stents. *J. Appl. Polym. Sci.* 2018a, *135*, 46521. [CrossRef]

Chen, Y.; Geever, L.M.; Killion, J.A.; Lyons, J.G.; Higginbotham, C.L.; Devine, D.M. Review of Multifarious Applications of Poly (Lactic Acid). *Polym. Plastics Technol. Eng.* 2016, *55*. [CrossRef]

Farah, S.; Anderson, D.G.; Langer, R. Physical and mechanical properties of PLA, and their functions in widespread applications — A comprehensive review. *Adv. Drug Deliv. Rev.* 2016, *107*, 367–392. [CrossRef]

Tyler, B.; Gullotti, D.; Mangraviti, A.; Utsuki, T.; Brem, H. Polylactic acid (PLA) controlled delivery carriers for biomedical applications. *Adv. Drug Deliv. Rev.* 2016, *107*, 163–175. [CrossRef] [PubMed]

Saini, P.; Arora, M.; Kumar, M.N.V.R. Poly(lactic acid) blends in biomedical applications. *Adv. Drug Deliv. Rev.* 2016, *107*, 47–59. [CrossRef] [PubMed]

Mhlanga, N.; Ray, S.S. Kinetic models for the release of the anticancer drug doxorubicin from biodegradable polylactide/metal oxide-based hybrids. *Inter. J. Biol. Macromol.* 2015, *72*, 1301–1307. [CrossRef] [PubMed]

Nagavarma, B.V.N.; Yadav, H.K.S.; Ayaz, A.; Vasudha, L.S.; Shivakumar, H.G. Different Techniques for preparation of polymeric nanoparticles—A review. *Asian J. Pharm. Clinical Res.* 2012, *5*, 16–23.

Sha, L.; Chen, Z.; Chen, Z.; Zhang, A.; Yang, Z. Polylactic acid based nanocomposites: Promising safe and biodegradable materials in biomedical field. *Inter. J. Polym. Sci.* 2016. [CrossRef]

Laboratory of Polymeric and Composite Materials. Available online: http://morris.umh.ac.be/smpc/poster. aspx (accessed on 27 May 2019).

Prashantha, K.; Lacrampe, M.-F.; Krawczak, P. Halloysite Nanotubes-Polymer Nano composites:A New Class of Multifaceted Materials. *Advan. Mater. Manuf. Charact.* 2013, *3*, 11–14. [CrossRef]

Wu, W.; Cao, X.; Zhang, Y.; He, G. Polylactide/halloysite nanotube nanocomposites: Thermal, mechanical properties, and foam processing. *J. Appl. Polym. Sci.* 2013, *130*, 443–452. [CrossRef]

Castro-aguirre, E.; Auras, R.; Selke, S.; Rubino, M.; Marsh, T. Impact of Nanoclays on the Biodegradation of Poly (lactic acid) Nanocomposites. *Polymers* 2018, *10*, 202. [CrossRef]

Chen, Y.; Geever, L.M.; Killion, J.A.; Lyons, J.G.; Higginbotham, C.L.; Devine, D.M. Halloysite nanotube reinforced polylactic acid composite. *Polym. Compos.* 2017, *38*. [CrossRef]

Gaaz, T.; Sulong, A.; Kadhum, A.; Al-Amiery, A.; Nassir, M.; Jaaz, A. The Impact of Halloysite on the Thermo-Mechanical Properties of Polymer Composites. *Molecules* 2017, *22*, 838. [CrossRef] [PubMed]

Lvov, Y.M.; DeVilliers, M.M.; Fakhrullin, R.F. The application of halloysite tubule nanoclay in drug delivery. *Expert Opin. Drug Deliv.* 2016, *13*, 977–986. [CrossRef] [PubMed]

Abdullayev, E.; Lvov, Y. Halloysite Clay Nanotubes for Controlled Release of Protective Agents. *J. Nanosci. Nanotechnol.* 2011, *11*, 10007–10026. [CrossRef] [PubMed]

Fu, L.; Yang, H.; Tang, A.; Hu, Y. Engineering a tubular mesoporous silica nanocontainer with well-preserved clay shell from natural halloysite. *Nano Res.* 2017, *10*, 2782–2799. [CrossRef]

Leporatti, S. Halloysite clay nanotubes as nano-bazookas for drug delivery. *Polym. Inter.* 2017, *66*, 1111–1118. [CrossRef]

Lun, H.; Ouyang, J.; Yang, H. Natural halloysite nanotubes modified as an aspirin carrier. *RSC Adv.* 2014, *4*, 44197–44202. [CrossRef]

Patel, S.; Jammalamadaka, U.; Sun, L.; Tappa, K.; Mills, D. Sustained Release of Antibacterial Agents from Doped Halloysite Nanotubes. *Bioengineering* 2015, *3*, 1. [CrossRef]

Qi, R.; Guo, R.; Shen, M.; Cao, X.; Zhang, L.; Xu, J.; Yu, J.; Shi, X. Electrospun poly(lactic-co-glycolic acid)/halloysite nanotube composite nanofibers for drug encapsulation and sustained release. *J. Mater. Chem.* 2010, *20*, 10622. [CrossRef]

Katerina, M. Aspirin–friend or foe? *THTY* 2008, *1*, 150–151.

Khadka, P.; Ro, J.; Kim, H.; Kim, I.; Kim, J.T.; Kim, H.; Cao, J.M.; Yun, G.; Lee, J. Pharmaceutical particle technologies: An approach to improve drug solubility, dissolution and bioavailability. *Asian J. Pharm. Sci.* 2014, *9*, 304–316. [CrossRef]

Ng, J.C.; Yeomans, N.D. Infection and the risk of upper gastrointestinal bleeding in low dose aspirin users: Systematic review and meta-analysis. *Med. J. Aust.* 2018, *209*, 306–311. [CrossRef] [PubMed]

Tang, Y.; Singh, J. Controlled delivery of aspirin: Effect of aspirin on polymer degradation and in vitro release from PLGA based phase sensitive systems. *Inter. J. Pharm.* 2008, *357*, 119–125. [CrossRef] [PubMed]

Zhang, J.; Ma, S.; Gene, H. Guided bone regeneration with asymmetric collagen-chitosan membranes containing aspirin- loaded chitosan nanoparticles. *Inter. J. Nanomed.* 2017, *12*, 8855–8866. [CrossRef] [PubMed]

Devine, D.M.; Geever, L.M.; Higginbotham, C.L. Drug release from a N-vinylpyrrolidinone/acrylic acid lubricious hydrophilic coatin. *J. Mater. Sci.* 2005, *40*, 3429–3436. [CrossRef]

Devine, D.M.; Devery, S.M.; Lyons, J.G.; Geever, L.M.; Kennedy, J.E.; Higginbotham, C.L. Multifunctional polyvinylpyrrolidinone-polyacrylic acid copolymer hydrogels for biomedical applications. *Inter. J. Pharm.* 2006, *326*, 50–59. [CrossRef] [PubMed]

Shi, Y.; Wan, A.; Shi, Y.; Zhang, Y.; Chen, Y. Experimental and mathematical studies on the drug release properties of aspirin loaded chitosan nanoparticles. *BioMed. Res. Inter.* 2014, *2014*. [CrossRef]

Das, S.; Banerjee, R.; Bellare, J. Aspirin loaded albumin nanoparticles by coacervation: Implications in drug delivery. *Trends Biomater. Artif. Org.* 2005, *18*, 203–212.

Garlotta, D. A Literature Review of Poly (Lactic Acid). *J. Polym. Environ.* 2002, *9*, 63–84. [CrossRef]

Semalty, A.; Semalty, M.; Singh, D.; Rawat, M.S.M. Development and Characterization of Aspirin-Phospholipid Complex for Improved Drug Delivery. *J. Pharm. Sci.* 2010, *3*, 940–947.

Višnjic´, D.; Lalic´, H.; Dembitz, V.; Banfic´, H. Metabolism and differentiation. *Period. Biol.* 2014, *116*, 37–43. [CrossRef]

Qi, R.; Guo, R.; Zheng, F.; Liu, H.; Yu, J.; Shi, X. Controlled release and antibacterial activity of antibiotic-loaded electrospun halloysite/poly(lactic-co-glycolic acid) composite nanofibers. *Coll. Surf. B Biointerfaces* 2013, *110*, 148–155. [CrossRef] [PubMed]

Venkatesh, C.; Chen, Y.; Cao, Z.; Brennan, S.; Major, I.; Lyons, J.; Devine, D. Increased screw speed has positive effect on Polylactic Acid-Halloysite Nanotubes nanocomposite. In submission.

Jani, R.; Patel, D. Hot melt extrusion: An industrially feasible approach for casting orodispersible film. *Asian J. Pharm. Sci.* 2014, *10*, 292–305. [CrossRef]

Gao, M.; Lu, L.; Wang, X.; Lin, H.; Zhou, Q. Preparation of a novel breviscapine-loaded halloysite nanotubes complexforcontrolledreleaseofbreviscapinePreparationofanovelbreviscapine-loadedhalloysitenanotubes complex for controlled release of breviscapine. *Mater. Sci. Eng.* 2017, *265*, 1–8. [CrossRef]

Balogh, A.; Domokos, A.; Farkas, B.; Farkas, A.; Rapi, Z.; Kiss, D. Supporting Information Continuous End-to-End Production of Solid Drug Dosage Forms: Coupling Flow Synthesis and Formulation by Electrospinning. *Chem. Eng. J.* 2018, *350*, 1–23. [CrossRef]

Devine, D.M.; Hoctor, E.; Hayes, J.S.; Sheehan, E.; Evans, C.H. Extended release of proteins following encapsulation in hydroxyapatite/chitosan composite scaffolds for bone tissue engineering applications. *Mater. Sci. Eng. C* 2017, *84*, 281–289. [CrossRef]

Dong, Y.; Marshall, J.; Haroosh, H.J.; Mohammadzadehmoghadam, S.; Liu, D.; Qi, X.; Lau, K.T. Polylactic acid

(PLA)/halloysite nanotube (HNT) composite mats: Influence of HNT content and modification. *Compos. Part A Appl. Sci. Manuf.* 2015, *76*, 28–36. [CrossRef]

Shi, X.; Zhang, G.; Phuong, T.V.; Lazzeri, A. Synergistic effects of nucleating agents and plasticizers on the crystallization behavior of Poly(lactic acid). *Molecules* 2015, *20*, 1579–1593. [CrossRef]

Lazzara, G.; Massaro, M.; Milioto, S.; Riela, S. Halloysite-based bionanocomposites. *Handb. Compos.Renew. Mater.* 2017, *1–8*, 557–584. [CrossRef]

Available online at www.sciencedirect.com

ScienceDirect

Procedia Manufacturing 00 (2019) 000–000

Procedia MANUFACTURING

www.elsevier.com/locate/procedia

29th International Conference on Flexible Automation and Intelligent Manufacturing (FAIM2019), June 24-28, 2019, Limerick, Ireland.

Additive manufacturing of PLA/HNT nanocomposites for biomedical applications

Chaitra Venkatesh[a], Evert Fuenmayor[a], Patrick Doran[a], Ian Major[a], John G Lyons[b], Declan M Devine[a1]

[a]*Material Research Institute, Athlone Institute of Technology, Athlone, N37 HD68, Ireland*
[b]*Faculty of Engineering and Informatics, Athlone Institute of Technology, Athlone, N37 HD68, Ireland*

Abstract

Additive manufacturing has been of great interest of research in various applications due to their ease in processability, cost effectiveness and adaptability. In this study Poly Lactic Acid (PLA) was used as the base polymer which was reinforced with Halloysite Nanotubes (HNT) powder as they are known to be biodegradable and has high mechanical properties individually.
HNT loadings with 3% and 5% were added to PLA by the method of twin screw extrusion and pelletized. For comparison, the PLA on its own was also extruded and pelletized. The resultant homogeneous pellets was extruded successfully into filaments of 1.75±0.10 mm diameter using twin screw extruder with specialized die fixed to the extruder for the manufacture of production grade 3D printing filament. This resultant filament was utilized for Fused Filament Fabrication (FFF) into standard tensile test bars and 25mm medical implants using a standard FFF printing machine.
The 3D printed samples were characterized for mechanical properties by uniaxial tensile test and thermal stability by Differential scanning calorimetry. Interestingly there was no significant change in the mechanical properties of the 3D printed tensile bars due to the processing parameters during FFF. However, the decrease in cold crystallization temperature by DSC indicates the nucleating effect of the HNT on the PLA matrix which in turn increases the mechanical properties. We could successfully 3D print medical implants.

Peer review under the responsibility of the scientific committee of the Flexible Automation and Intelligent Manufacturing 2019

Keywords: Additive manufacturing; Fused Filament Fabrication; biodegradable stents; polylactic acid; halloysite nanotubes

1. Introduction

Additive manufacturing (AM) also known as three-dimensional (3D) printing has increase in research interest particularly in various medical applications due to its transformative nature and ability of customization. Recent research has explored the areas such as 3D printing of tablets for more precise controlled drug delivery, patient specific prostheses, tissue structures which are in the early stage of development for potential deployment in future [1].

One such area of interest is 3D printed implantable medical devices. Although the real application of 3D fabricated stents are limited because of material and machine constraints, much research is ongoing on in the areas such as 3D printed PLA/PCL cardiovascular stent [2], 3D printed ureteric stent

* Corresponding author. Tel.: +353 (0)90 64 68291; fax: +0-000-000-0000 .
E-mail address: ddevine@ait.ie

[3], nasal stent [4] for potential future application. Fused Deposition Modeling (FDM) often referred as Fused Filament Fabrication (FFF) is one of the most widespread technology of extrusion based AM [5]. In this method, the thermoplastic filament is extruded on to a surface in X, Y and Z co-ordinates to fabricate a 3D structure as designed from as software and the process is controlled by the computer [6], [7]. Several studies have investigated various polymer nanocomposites for FFF [8]–[11].

Nanocomposites are emerging potentially in various industries due to excellent mechanical, electrical and thermal properties. The nanomaterial can be reinforced into the host matrices by 3D printing to produce nanocomposite signifies numerous advantages due to its properties and also improves the homogeneity of the product. [12] The high viscosity of the thermoplastics can be further increased by the addition of nanofillers which effects the printability of the nanocomposite filament. This can be addressed by opting for suitable mixing strategies while compounding to enhance dispersion of the nanomaterial into the polymer matrix. Various other methods such as solution mixing by sonication and high shear mixing by extrusion can be employed to reinforce the nanomaterial into the polymer matrix before 3D printing [13].

Nanocomposites have enormous potential in 3D printing applications. As shrinking the scale size to nanoscale can change the properties of the materials, a variety of nanomaterials such as carbon nanotubes, graphene, metal nanoparticles are used in 3D printing for various applications [14]. Several research has been conducted to study the physical properties of the final printed part when they are blended with nanomaterials. Recent studies show that in FFF the mechanical properties of the filament can be increased by addition of the nanofillers.

In this study we process the polymer PLA with a nanoclay HNT by the method of Hot Melt Extrusion (HME). The resultant PLA/HNT nanocomposite was pelletized and was extruded by HME to produce 3D printable filaments of diameter size 1.75±0.10 mm. These filaments were 3D printed by the method of FFF to make standard tensile bars for mechanical characterization and we aim to see if the PLA/HNT nanocomposite is 3D printable by varying the percentages of HNT nanoclay for comparison but keeping the 3D printing parameters the same for all the PLA and PLA/HNT nanocomposite samples. We also developed implants for medical applications by the method of which can potentially be adapted specifically for 3D printing of stents for various anatomical applications.

Nomenclature

AM	Additive manufacturing
FFF	Fused Filament Fabrication
HME	Hot melt Extrusion
HNT	Halloysite nanotubes
PLA	Poly Lactic Acid

2. Experimental Details

2.1. Materials

PLA was obtained from Corbion, PLA LX 175. The density of the PLA is 1.24 g/cm³. HNT was supplied by Applied Minerals; DRAGONITE-HP and has a density of 2.56 g/cm³. The PLA and HNT were dried in the oven at 80°C for 4 hours. The moisture content of the PLA was measured before processing for less than 100 ppm.

2.2. Methods

Compounding was performed by using APV (Model MP19TC (25:1)) (APV Baker, Newcastle-under-Lyme, UK) twin-screw compounder with 16 mm diameter screws. The temperature profile was maintained at (from feeder to the die) 190/180/170/170/160/140/120/50°C. The extrusion was performed at a screw speed of 140 rpm with the mass fractions of 100:0, 97:3 and 95:5 for PLA: HNT and are referred here as PLA, PLA/HNT3% and PLA/HNT5% respectively. The extrudate was drawn through a cooler belt and pelletized.

These pellets were reprocessed using the same machine into 3D printing filament of PLA and PLA/HNT. The metal die used for extrusion point had a bore diameter of 1.75 mm. The extrusion temperature was adjusted through a control panel and the melt temperature used for PLA pellets was

170 °C. This filament extrude was passed through cooler belt and finally wound onto a spool for 3D printing.

Once the filaments were extruded, they were printed into tensile test specimen and implant using a FFF 3D printer (MakerGear M2 3D printer, US). The nozzle temperature was fixed at 200°C, bed temperature at 70°C with 25% infill for all the filaments. The STL file generated from the designing of the implant and the tensile bars from SolidWorks software was used to dictate the construct dimensions to the printer through MakerGear.

Mechanical properties of the PLA/HNTs composites were characterized by tensile testing, which was carried out on a Lloyd Lr10k tensometer (Lloyd Instruments Ltd, West Sussex, UK) using a 2.5 kN load cell on ASTM standard test specimens at a strain rate of 10 mm/min (n = 5). Data was recorded using NexygenTM software. The tensile tests were carried out in adherence to ASTM D 882. Five test specimens were analyzed per group, and before testing, the thickness of each sample was measured. The percentage strain at maximum load, stress at maximum load, stiffness, and Young's Modulus of each sample was recorded.

DSC analysis was carried out in triplicate using a DSC 2920 Modulated DSC (TA Instruments, New Castle, DE, USA) with a nitrogen flow rate of 20ml/min to prevent oxidation. Calibration of the instrument was performed using indium as standard. Tests were conducted on samples weighing between 8 and 12 mg. Samples were measured on a Sartorius scales (MC 210 P), capable of being read to five decimal places. Samples were crimped in non-perforated aluminum pans, with an empty crimped aluminum pan used as the reference. The thermal history was removed by heating samples from 20°C to 220°C at the rate of 30°C/min and then held isothermally at 220°C for 10 min. The samples were cooled from 220°C to 20°C at 30°C/min. Finally, the thermal properties of the samples were recorded by heating the samples from 20°C to 220°C at the rate of 10°C/min, glass transition temperature, cold crystallization temperature and melting temperature of each sample were recorded.

3. Results

Virgin PLA and PLA/HNTs nanocomposites were melt compounded, pelletized and melt compounded to filaments at screw speeds of 140 rpm without difficulty. The extruded PLA filaments had small bubble like structures as shown in Fig 1. However, the PLA/HNTs nanocomposites filaments changed in color from transparent to opaque in particular the 5% nanocomposite. The resultant filaments of PLA and PLA/HNT nanocomposites had diameter size of 1.75±0.10 mm.

a b c

Fig. 1. Photographs of the filaments produced by twin screw extrusion (a) PLA (b) PLA/HNT 3% (c) PLA/HNT 5%.

The PLA and PLA/HNT nanocomposite filaments were used for 3D printing of tensile test bars. The morphology of the 3D printed samples was investigated using an optical microscope and a detail picture of a sample corner is reported in Fig 2. The 3D printing of tensile test bars of PLA was processed without difficulty. However, the 3D printing of the nanocomposites were difficult to process and the 3D printed bars had denser infill as the percentage of the HNT increased along with change in color as shown in Fig 2.

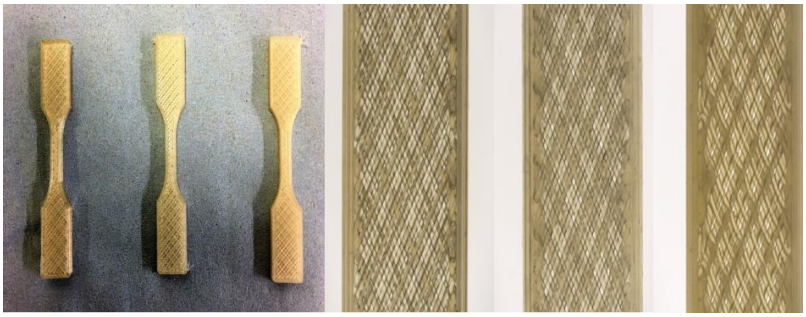

a b c d

Fig. 2. Photographs from optical microscope of 3D printed tensile bars (a) (L-R) PLA, PLA/HNT 3% and PLA/HNT 5% nanocomposites. (b) Zoomed in photograph of PLA (c) zoomed in photograph of PLA/HNT 3% and (d) zoomed in photograph of PLA/HNT 5% nanocomposite indicates the infill pattern becomes denser with increase in the nanoclay percentage along with change in color.

The 3D printed tensile test bars were characterized for mechanical properties by uniaxial tensile testing and the tensile test results of PLA and PLA/HNT nanocomposite 3D printed tensile bars are as shown in Table 1.

Table 1. Mechanical properties of PLA and PLA/HNT nanocomposites

Batch	Young's Modulus	Stiffness	Tensile Strength	Elongation at break
PLA	391.22±32.02	240.61±19.86	33.37±1.9	14.71±4.52
PLA/HNT3%	443.58±41.11	269.11±12.22	37.44±5.11	14.7±2.55
PLA/HNT5%	357.10±69.24	224.3±43.49	29.97±4.54	12.75±0.31

The mechanical properties did not show any significant difference between the PLA and PLA/HNT nanocomposites 3D printed tensile samples. This result is in contrast with other research work and our previous research which indicates increase in mechanical properties by the addition of HNT into the PLA matrix up to 5% loading. The results obtained in this study could be due to the effect of 3D printing parameters which did not increase the mechanical properties. The break point of the tensile test bars as shown in Fig. 3 is mostly near the neck and in line with the infill of the tensile bars which indicates that 3D printing parameters have to be optimized which had significant influence on the mechanical properties.

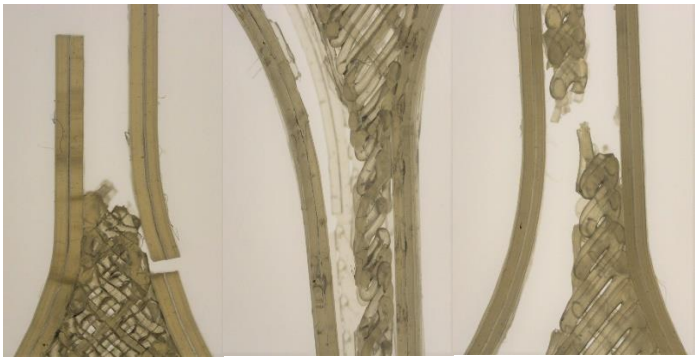

a b c

Fig. 3. Photographs of 3D printed tensile bars after testing (a) PLA (b) PLA/HNT 3% (c) PLA/HNT 5% indicates the breaking point of the bars during testing is influenced by the 3D printing processing.

Thermal properties of the 3D printed nanocomposites were analysed by the method of DSC and the results are as shown in the Fig 4. There is no significant difference in the glass transition temperature (T_g) by the addition of HNT into the PLA matrix. However, the cold crystallisation temperature (T_{cc}) significantly decreases with increase in HNT percentage which indicates the nucleating effect of the HNT with the PLA.

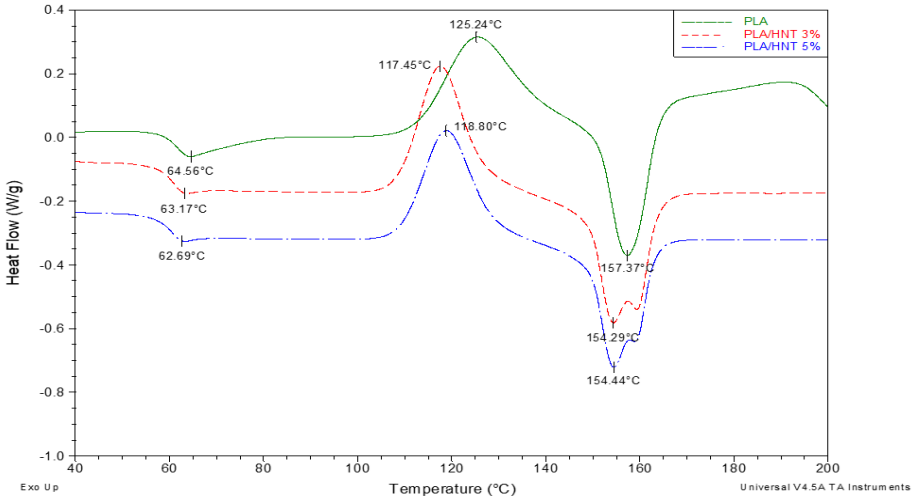

Fig. 4. DSC thermographs of PLA, PLA/HNT 3% and PLA/HNT 5% nanocomposites.

The filaments were 3D printed as 25 mm medical implants as shown in Fig 5. The printing of the implants for PLA filament was easy when compared to the nanocomposites. However, all the stents had rough finishing as seen in the optical microscope images in Fig 6. which could be due to the nozzle speed between the points. In addition, the 3D printed stents for nanocomposites had bubble like structures at some points which could be due to the influence of percentage of clay along with the processing temperatures.

a b c

Fig. 5. 3D printed implants of (a) PLA, (b) PLA/HNT 3% and (c) PLA/HNT 5% nanocomposites

a b c

Fig. 6. Photographs from optical microscope of 3D printed implants of (a) PLA, (b) PLA/HNT 3% and (c) PLA/HNT 5% nanocomposites

4. Discussion

This research work outlines the possibility of firstly developing nanocomposite filament using biodegradable thermoplastic polymer PLA and nanoclay HNT. This developed PLA/HNT nanocomposite filament could further be 3D printed by the method of FFF into standard tensile test bars and model medical implants. The printability, morphology, thermal and mechanical properties were evaluated. Analysis showed that the ease of printing and the morphology of the printed tensile bars and implants varied with the clay compositions as the printing parameters were maintained the same for all the PLA and PLA/HNT nanocomposite batches for comparison.

Ease of maintenance, low cost and flexibility make the FFF the most commonly preferred process of 3D printing (Berretta *et al.*, 2017). However, some disadvantages such as surface roughness, need for support material and support removal and mainly imperfect sealing between layers and toolpaths (Pranzo *et al.*, 2018) have to be considered while FFF process. In this study as the printing parameters were same for all the batches, the mechanical properties of the 3D printed tensile bars were not in correlation with the mechanical properties of the PLA/HNT nanocomposite. As illustrated in Fig. 3, the breaking point of the tensile bars was mostly at the neck and in line with the printing pattern of the bars. This suggests that delamination between layer occurred. This effect can be reduced by adjusting the 3D printing parameters such as infill pattern, temperature and nozzle speed. Similar breakage at the neck was shown by the study of mechanical properties by the influence of FFF printing parameters by Kalinowski et. al. Minor discontinuities in filament extrusion, uncontrolled shrink during the cooling process, weakness between the layers could lead to the decrease in the mechanical properties of the 3D printed parts (Ćwikła *et al.*, 2017). It is also reported that FFF reduces the properties of the 3D printed parts as may create void spaces between the material deposition lines (Ferreira *et al.*, 2017).

However, thermal analysis of the 3D printed PLA/HNT nanocomposites is in correlation with the thermal analysis of the PLA/HNT as a nanocomposite. Thermal analysis suggest a significant decrease in cold crystallisation temperature and negligible decrease in melting temperature. The glass transition temperature T_g is a measure of rigidity (Declan M. Devine *et al.*, 2017). There is no significant difference in the glass transition temperature. However, the decrease in the cold crystallisation temperature indicated that nanocomposites are more likely crystallized which could be due to the nucleating effect of HNTs on the PLA (Liu, Zhang and Zhou, 2013; Wu *et al.*, 2013) and that heterogeneous nucleation was likely to occur where thinner crystalline lamella was formed compared to that of virgin PLA (Dong *et al.*, 2015b). Hence the melting temperature of the composite is also lower than that of virgin PLA. Based on the above result, the composite appears to have an amorphous (low crystalline) structure. HNTs acting as the nucleating agent in the PLA crystallises the PLA/HNT

composite more quickly than the virgin PLA (Liu, Zhang and Zhou, 2013; Wu *et al.*, 2013; Chen *et al.*, 2018).

During the 3D printing process, the nozzle movement in X-Y direction induces uniform heat transfer allowing crystallization (Gnanasekaran *et al.*, 2017). However, in our study the results differ, which could be due to the nucleating effect of HNT on the PLA matrix decreasing the cold crystallisation temperature. Similar results are obtained in the study of CNT-Graphene based polymer nanocomposite for 3D printing by FFF (Gnanasekaran *et al.*, 2017).

3D printed implants were successfully fabricated into mesh forms using FFF's layer-by-layer approach composed of PLA/HNT nanocomposite.

4. Conclusion

In this study, it was possible to develop 3D printing filament using biodegradable PLA and reinforcing with biocompatible filler HNT. The filament had a diameter 1.75±0.10 mm for use in FFF 3D printing. The 3D printed model implants were successfully fabricated into mesh forms whose mechanical properties can be enhanced by optimizing the printing parameters. In future work, the properties of the nanocomposites such as melt flow and viscosity will be studied in order to optimize printing parameters for higher mechanical properties and good finishing of the 3D printed model implants.

Acknowledgements

This work was supported in part by financial support from Athlone Institute of Technology under the Presidents Seed Fund, Enterprise Ireland funding under the Technology Gateway program, grant number TG-2017-0114 and Science Foundation Ireland (SFI) under Grant Number 16/RC/3918, co-funded by the European Regional Development Fund.

References

[1] [1] G. M. Paul et al., "Medical Applications for 3D Printing: Recent Developments." Mo. Med., vol. 115, no. 1, pp. 75–81, 2018. [2] A. J. Guerra, P. Cano, M. Rabionet, T. Puig, and J. Ciurana, "3D-printed PCL/PLA composite stents: Towards a new solution to cardiovascular problems," Materials (Basel)., vol. 11, no. 9, pp. 1–13, 2018.

[3] R. F. Youssef et al., "Applications of three-dimensional printing technology in urological practice," BJU Int., vol. 116, no. 5, pp. 697–702, 2015.

[4] D. Mills, K. Tappa, U. Jammalamadaka, J. Weisman, and J. Woerner, "The Use of 3D Printing in the Fabrication of Nasal Stents," Inventions, vol. 3, no. 1, p. 1, 2017.

[5] D. Pranzo, P. Larizza, D. Filippini, and G. Percoco, "Extrusion-Based 3D Printing of Microfluidic Devices for Chemical and Biomedical Applications: A Topical Review," Micromachines, vol. 9, no. 8, p. 374, 2018.

[6] C. Miguel, C. Estomba, I. González Fernández, M. Ángel, and I. Otero, "3D Printing for Biomedical Applications: Where Are We Now?," Eur. Med. J., vol. 2, no. 1, pp. 16–22, 2017.

[7] E. Fuenmayor et al., "Material considerations for fused-filament fabrication of solid dosage forms," Pharmaceutics, vol. 10, no. 2, pp. 1–27, 2018.

[8] P. Lamberti et al., "Evaluation of thermal and electrical conductivity of carbon-based PLA nanocomposites for 3D printing," vol. 020158, p. 020158, 2018.

[9] S. Berretta, R. Davies, Y. T. Shyng, Y. Wang, and O. Ghita, "Fused Deposition Modelling of high temperature polymers: Exploring CNT PEEK composites," Polym. Test., vol. 63, pp. 251–262, 2017.

[10] B. Coppola, N. Cappetti, L. Di Maio, P. Scarfato, and L. Incarnato, "3D printing of PLA/clay nanocomposites: Influence of printing temperature on printed samples properties," Materials (Basel)., vol. 11, no. 10, pp. 1–17, 2018.

[11] K. Gnanasekaran et al., "3D printing of CNT- and graphene-based conductive polymer nanocomposites by fused deposition modeling," Appl. Mater. Today, vol. 9, pp. 21–28, 2017.

[12] T. D. Ngo, A. Kashani, G. Imbalzano, K. T. Q. Nguyen, and D. Hui, "Additive manufacturing (3D printing): A review of materials , methods , applications and challenges," Compos. Part B, vol. 143, no. December 2017, pp. 172–196, 2018.

[13] R. Dermanaki Farahani and M. Dubé, "Printing Polymer Nanocomposites and Composites in Three Dimensions," Adv. Eng. Mater., vol. 1700539, pp. 1–9, 2017.

[14] O. Ivanova, C. Williams, and T. Campbell, "Additive manufacturing (AM) and nanotechnology: promises and challenges," Rapid Prototyp. J., vol. 19, no. 5, pp. 353–364, 2013.

[15] G. Ćwikła, C. Grabowik, K. Kalinowski, I. Paprocka, and P. Ociepka, "The influence of printing parameters on selected

mechanical properties of FDM/FFF 3D-printed parts," IOP Conf. Ser. Mater. Sci. Eng., vol. 227, no. 1, 2017.
[16] R. T. L. Ferreira, I. C. Amatte, T. A. Dutra, and D. Bürger, "Experimental characterization and micrography of 3D printed PLA and PLA reinforced with short carbon fibers," Compos. Part B Eng., vol. 124, pp. 88–100, 2017.
[17] D. M. Devine, E. Hoctor, J. S. Hayes, E. Sheehan, and C. H. Evans, "Extended release of proteins following encapsulation in hydroxyapatite/chitosan composite scaffolds for bone tissue engineering applications," Mater. Sci. Eng. C, vol. 84, no. November 2016, pp. 281–289, 2017.
[18] W. Wu, X. Cao, Y. Zhang, and G. He, "Polylactide/halloysite nanotube nanocomposites: Thermal, mechanical properties, and foam processing," J. Appl. Polym. Sci., vol. 130, no. 1, pp. 443–452, 2013.
[19] M. Liu, Y. Zhang, and C. Zhou, "Nanocomposites of halloysite and polylactide," Appl. Clay Sci., vol. 75–76, pp. 52–59, 2013. [20] Y. Dong et al., "Polylactic acid (PLA)/halloysite nanotube (HNT) composite mats: Influence of HNT content and modification," Compos. Part A Appl. Sci. Manuf., 2015.
[21] Y. Chen, A. Murphy, D. Scholz, L. M. Geever, J. G. Lyons, and D. M. Devine, "Surface-modified halloysite nanotubes reinforced poly(lactic acid) for use in biodegradable coronary stents," J. Appl. Polym. Sci., vol. 135, no. 30, p. 46521, Aug. 2018.

Influence of extrusion screw speed on the properties of halloysite nanotube impregnated polylactic acid nanocomposites

Chaitra Venkatesh [1], Yuanyuan Chen [1], Zhi Cao [1], Shane Brennan [1], Ian Major [1], John G. Lyons [2] and Declan M. Devine [1,*]

[1] Materials Research Institute, Athlone Institute of Technology, Dublin Road, Athlone, Co. Westmeath, Ireland;
[2] Faculty of Engineering and Informatics, Athlone Institute of Technology, Dublin Road, Athlone, Co. Westmeath, Ireland
* Correspondence: ddevine@ait.ie;

Abstract

Poly (lactic acid)/halloysite nanotube (PLA/HNT) nanocomposites have been studied extensively over the past few years owing to the interesting properties of the polymer, PLA, and the nanoclay, HNT, individually and as composites. In this paper, the influence of the screw speed during extrusion was investigated and was found to have a significant impact on the mechanical and thermal performance of the extruded PLA/HNT nanocomposite. To determine the effect of screw speed on PLA/HNT nanocomposites, 5 wt. % and 10 wt. % of HNTs were blended into the PLA matrix through compounding at screw speeds of 40, 80, and 140 rpm. Virgin PLA was compounded for comparison. The resultant polymer melt was quench cooled onto a calendar system to produce composite films which were assessed for mechanical, thermal, chemical and surface properties. Results illustrate that in comparison to 40 and 80 rpm, the virgin PLA when compounded at 140 rpm, indicated a significant increase in mechanical properties. The PLA/HNT 5 wt. % nanocomposite compounded at 140 rpm showed significant improvement in the dispersion of HNTs in the PLA matrix which in turn enhanced the mechanical and thermal properties. This can be attributed to the increased melt shear at higher screw speeds.

Keywords: Biodegradable; Poly (lactic acid); Halloysite nanotubes; nanocomposites; twin-screw extrusion;

1. Introduction

Biodegradable polymers derived from renewable sources have been of great research interest over the past decade as they solve the problems of waste disposal of petroleum-based thermoplastics [1–4]. Biodegradable polymers have been used in various biomedical applications such as sutures, tissue engineering, etc. [5]. However, on its own, it cannot meet all the required properties for some biomedical applications. Therefore, consideration for selection of polymer, incorporation of nanofillers, processing methods aids to prepare biodegradable polymer nanocomposites with improved properties for biomedical applications [6]. Biodegradable polymer nanocomposites, in which the nanofillers act as a reinforcing agent in the polymer when added in small quantities have been of significant interest because of nanoparticle properties such as high surface reactivity, large surface area, and relatively low cost. Nanofillers improve various polymer properties producing high mechanical strength, thermal resistance in a polymer nanocomposite. The

nanomaterial can be reinforced into polymer via solution mixing or extrusion [7–10]. Also, the size of the nanofillers does not produce stress points in the polymer matrix and in turn, does not lead to material failure when dispersed uniformly without agglomeration.

Polylactic acid (PLA) polymer has characteristics such as biodegradability, high mechanical properties, easy availability, and processability. [11,12]. PLA has been researched and used for various medical applications such as resorbable sutures, tissue engineering, drug delivery systems, and dental, ophthalmic, fracture fixation [13,14]. However, there is a limitation of the use of PLA in many applications due to low crystallinity and extreme brittleness [15]. PLA is commonly blended with clay-based nanofillers to improve mechanical and thermal properties as the clay nanofiller has good strength on its own with a large aspect ratio [14,16, 17].

Halloysite nanotubes (HNT) is a type of clay mineral formed naturally in the earth and has a high aspect ratio (length/diameter), biocompatibility, non-toxicity, and easy availability at low cost [14,18–20]. Because of these characteristics, they have been researched for biomedical applications such as dental fillers, drug delivery, cosmetics, cancer cell isolation, etc. [21]. HNT has been used as nanofillers for various polymer nanocomposites has been shown to improve the mechanical properties of the composite without the need for surface treatment [22,23]They have been studied for easy and uniform dispersion in the polymer matrix such as polyamide, polypropylene by direct melt blending without the need for surface modification of HNT [24,25,26].

PLA/HNT nanocomposites are of great interest in the biomedical field owing to the relatively high strength of PLA compared to other biodegradable polymers and the natural, original, and biocompatibility of HNT. It has been shown in earlier studies that 10wt% HNT loadings result in increases in the mechanical, thermal properties [7, 26-28] and flame retardant properties [7,29] of PLA. It has further been shown that surface treatment of HNT can be used to improve dispersion of the nanoparticles in the PLA matrix [26,28,30]. However, very little research has been done on the influence of screw speeds during extrusion for the PLA/HNT composites.

Melt blending is a method of amalgamating two or more polymers into a single material with blended properties [31] or combining clay and polymer as a nanocomposite for better dispersion with enhanced properties [32]. Twin-screw extrusion is a type of hot melt extrusion process where the material melts under high temperature in the barrel and continues to move towards the die with a homogenous melt or dispersion [33]. It has been extensively used for various applications such as plastic, food, and pharmaceutical industries [14,34,35].

Other research works suggest that the shear force from high screw speed during melt blending improves the dispersion of the nanoclay in the polymer matrix. Li et.al. postulated that an increase in shear force during melt blending enhances the dispersion of the clay when they investigated polymer/clay nanocomposites [37]. Sasimowski et. al. investigated the extrusion process and showed that the screw speed had a great impact on the efficiency of the extrusion process, the pressure of the processed material, polymer mass flow rate, and the energy consumption of the extruder [38]. Albareeki et. al. studied the effect of screw speed on the melt temperature, drive torque, and residence time in the extruder and found that increasing the screw speed increases the melt temperature and there is a decrease in the residence time with better dispersion of the filler in the polymer matrix [39].

Mixing of thermoplastic pellets with carbon nanotube (CNT) in a twin-screw extruder had good dispersion by shear flow created at high screw speed [40]. Thus, to eliminate the need for surface treatment of HNT, in the current study, the processing of PLA/HNT was examined by varying the screw speed keeping other parameters of extrusion constant throughout.

The present work mainly evaluates the mechanical and thermal properties of the nanocomposites with two mass fractions of 5 wt. % and 10 wt. % of the nanoclay HNT blended into the PLA matrix using a twin-screw extruder with three different screw speeds of 40 rpm, 80 rpm, and 140 rpm based on findings in previous work where a low screw speed resulted in poor HNT dispersion without surface modification [28]. The nanocomposite produced is characterized by tensile testing, differential scanning calorimetry, dynamic mechanical analysis, scanning electron microscopy, Fourier transform infrared microscopy, surface wettability

2. Materials and Methods

2.1. Materials

PLA was obtained from Corbion, PLA LX 175 (Total Corbian, Gorinchem, The Netherlands). The density of the PLA is 1.24 g/cm^3, melting temperature of 155 °C, Glass transition temperature of 55-60 °C. HNT was supplied by Applied Minerals; DRAGONITE-HP (APPLIED MINERALS INC, Brooklyn, NY, USA) and had a density of 2.56 g/cm^3, length of 0.2 – 2.0 µm and aspect ratio (L/D) of 10-20. All materials were dried before use. PLA was dried at 80 °C for 4 hrs and HNT was dried at 100 °C for 3 hrs.

2.2. Processing

Extrusion was performed by using APV (Model MP19TC (25:1), APV Baker, Newcastle-under-

Lyme, UK) twin-screw compounder with 19 mm diameter screws and length-diameter ratio *L/D* of 25/1. The temperature profile was maintained at (from die to the feeder) 200/190/180/170/160/110/50 °C. The feed rate, barrel temperature were kept constant throughout. Three different screw speeds were selected for the study: 40 rpm, 80 rpm, and 140 rpm. The different mass fractions of 100:0, 95:5, and 90:10 for PLA: HNT were prepared for extrusion by tumble mixing of the dried PLA pellets with the dried HNT powder in a container and fed into the hopper of the extruder.

Extruded films of the molten composite were then drawn through a three-roll calendar. Cooling of the calendar rolls and extruder barrel was provided by a constant flow of tap water temperature (ca. 12° C). Similarly, the virgin PLA was processed by melt compounding under similar conditions for comparison. These samples were punched out from the center of the film into ASTM standard tensile test specimen with a sample cutter using a physical punching process.

2.3. Differential Scanning Calorimetry

Differential scanning Calorimetry (DSC) was conducted out using a DSC 2920 Modulated DSC (TA Instruments, New Castle, DE, USA). To prevent oxidation, a nitrogen flow rate of 20ml/min was applied. Indium was used as a standard to calibrate the instrument. Test specimens were weighed on a Sartorius scale (MC 210 P, Sartorius Lab Instruments GmbH & Co. KG, Goettingen, Germany) measuring between 8 mg and 12 mg. Samples were crimped in non-perforated aluminum pans,

with an empty crimped aluminum pan used as the reference. The thermal history was removed by heating samples from 20 °C to 220 °C at the rate of 30 °C/min and then held isothermally at 220 °C for 10 min. The samples were then cooled down from 220 °C to 20 °C at 30 °C/min. Finally, the thermal properties of the samples were recorded by heating the samples from 20 °C to 220 °C at the rate of 10 °C/min, glass transition temperature, and melting temperature of each sample was recorded.

2.4. Tensile Testing

Mechanical properties of the PLA/HNT composites were characterized by tensile testing each different blend. Tensile testing was carried out on a Lloyd Lr10k tensometer (Ametek Ltd, West Sussex, UK) using a 2.5 kN load cell on ASTM standard test specimens at a strain rate of 50 mm/min. Data was recorded using Nexygen™ software (Ametek ltd). The tensile tests were carried out in adherence to ASTM D 882. Ten individual test specimens were analyzed per batch and the thickness of each sample was measured before testing. The percentage strain at maximum load, stress at maximum load, stiffness, and Young's Modulus of each tested sample were recorded.

2.5. Scanning Electron Microscopy

Scanning Electron Microscopy (SEM) was performed using a Mira XMU SEM (TESCAN Brno, Czech Republic) in a backscattered electron mode to determine the shape and distribution of HNTs in the PLA matrix. Energy Dispersive X-ray (EDX) was performed using an Oxford Instruments detector to determine the elemental composition of HNT and the composites of PLA and HNT. The accelerating voltage utilized was 10 kV for raw HNT and 20 kV for composite materials. Before analysis, test samples were placed on an aluminum stub and the samples were sputtered with gold using Baltec SCD 005 for 110 seconds at 0.1 mbar vacuum before testing.

2.6. Fourier Transform Infrared Spectrometry

Fourier transform infrared spectroscopy (FTIR) was carried out on a Perkin Elmer Spectrum One fitted with a universal ATR sampling accessory (Perkin Elmer, Waltham, MA, USA). All data were recorded in the spectral range of 4,000–650 cm^{-1} and at 21 °C. A fixed universal compression force of 70–80 N was utilized and each sample was recorded with four scans. Following analysis of the recordings was carried out using Spectrum software.

2.7. Contact Angle (Goniometry)

The prepared nanocomposites were assessed for the surface wettability properties by using First Ten Angstrom's, FTA32 goniometer (FTA Europe, Cambridge, UK). In this test, the Sessile Drop contact angle technique was utilized and distilled water was used as the probe liquid. Five total measurements at various places on the films were taken for each sample.

2.8. Dynamic Mechanical Analysis

Dynamic mechanical analysis (DMA) was used to measure storage modulus, loss modulus and loss factor (tan delta), were determined using TA Instrument Q800 DMA (TA Instruments, Eschborn Germany). A strain frequency of 1 Hz and 20 µm amplitude was used. The heating ramp from ambient temperature to 120 °C was carried out at a rate of 3 °C/min.

2.9. Statistical Analysis

Statistical analysis of the tensile test results, DSC measurements, and the void content measurements were carried out using General Linear Model (GLM) of two-way ANOVA in Minitab 17 Statistical Software (Minitab Ltd., Coventry, UK). All the values were considered at a 95% confidence interval and p-values are considered significant when $p \leq 0.05$.

3. Results and Discussion

3.1. Processing of PLA and HNT through melt blending

The compounded PLA and PLA/HNT nanocomposite remained transparent in color however the nanocomposite changed in color from transparent to opaque with the blending of HNT at all the different screw speeds. This color change could be attributed to the nucleating effect of HNT in the PLA matrix which was similarly observed by De Silva et al. [27]. This was also observed by Liu et al. with injection moulded composite of PLA and HNT [41] and by Chen et al. with extruded PLA/HNT composite [42].

The screw configuration used is illustrated in Figure 1. It had a feeding zone followed by a mixing section comprising two sets of kneading block elements. The first kneading set had ten paddles, four of which had a forwarding angle of 30°, 60° for the next six, and the remaining paddle at 90°. The second block near the discharge end had six paddles with a 60° forwarding angle. The end of the screw had a metering zone of conveying elements. Processing parameters were varied only in terms of screw speed, which in turn reduces the residence time in general which was in the range of 1-3 mins.

Figure 1.

Twin-screw extrusion is a high shear process, which aids dispersion of different components during melt processing. The main focus of this study was to assess the effect of screw speeds as increases in screw speed during compounding have been shown to increase melt shear and as such homogeneity of the final compounded material. Gamon et. al. hypothesized that a screw speed of 150 rpm was ideal to obtain homogenous properties of fiber-reinforced PLA composites [43]. Normand et.al. demonstrated that when the screw speed is increased from 100 to 600 rpm while compounding polypropylene/clay nanocomposites, the number of the agglomerates decreases and screw speeds higher than 600 rpm did not improve the state of the microscopic dispersion nor had better exfoliation which could be due to the thermal degradation of the clay modifier, mechanical breakage of the clay sheets or degradation of the matrix [44]. Similarly, Domenech et.al. found a reduction in the size of the clay agglomerate as the screw speed increases principally between 100-500 rpm. And more than 500 rpm did not show any changes [45]. Conversely, previous work by Chen et.al. showed that screw speeds of 35 rpm did not give sufficient mixing and necessitated the surface treatment of HNT to improve dispersion [28]. Hence, in this study, the polymer PLA and the PLA/HNT nanocomposites were compounded at three screw speeds of 40, 80, and 140 rpm for comparison. Higher screw speeds could lead to thermal degradation of the nanocomposite. However, the selected screw speeds were not exhaustive and the effects of dispersion at higher screw speeds cannot be assumed based on these findings.

The filler dispersion and melt blending are augmented and intensified by the kneading elements of the screw configuration [36]. Thus using the above-described screw configuration with two kneading elements in the mixing section, three different screw speeds were investigated.

3.2. Differential Scanning Calorimetry

The compounded polymer and the nanocomposites were analyzed for the influence of screw speed on the thermal properties by differential scanning calorimetry. The DSC curves show that the addition of HNT into the PLA matrix with different loadings and compounding at different screw speeds showed no significant difference in the glass transition temperature (Tg) with p=0.42 as shown in Table 1 and Figure 2. A similar result has been reported previously [29].

As seen in Table 1, the cold crystallization temperature (Tcc) decreases compared to PLA. With p=0.00, the statistical analysis confirmed the decrease with an effect of both HNT loading and screw speed. The decrease in the Tcc indicated that HNT has a nucleating effect on the PLA [41,46] and that heterogeneous nucleation was likely to occur where thinner crystalline lamella was formed compared to that of virgin PLA [47]. Hence, the melting temperature of the composite was also lower than that of virgin PLA. A similar decrease in cold crystallization temperature and the melting temperature was observed by Prashanta et.al. Chen et.al, Wu et al., and Guo et al. in their study using surface-treated HNT [28,30,46,48].

A single melting peak was observed for virgin PLA. However, a secondary melting peak was observed for 5 wt. % and becomes clearer for 10 wt. % loading of the HNT when compounded as 140 rpm as seen in Figure 2. This was observed in other studies by Chen et. al. [28], Prashantha et. al. [48] who reported that this was due to the melting of the crystals formed in the cold crystallization stage during heating and followed by recrystallization and further melting processes at higher temperatures [48]. Statistical analysis confirmed the above results with p=0.06 for Tm, the percentage loading of the HNT affected the decrease of Tm.

Figure 2.

Table 1.

3.3. Dynamic Mechanical Analysis

The dynamic mechanical analysis was used to evaluate the viscoelastic properties of the PLA/HNT nanocomposite below and above the glass transition. The temperature at the peak of the Tan δ curve was considered as the Tg of the material. The tan δ peaks as listed in Table 1. show no significant difference in Tg. The glass transition temperature Tg is a measure of rigidity [49] and the Tg does not show any considerable difference from the DSC results. However, the analysis of Tg is more accurately determined by DMA 41]. Hence, the results from the DMA were statistically analyzed to confirm that there is no significant difference in Tg with an increase in screw speed.

3.4 Mechanical Properties

Mechanical testing results found that the Young's Modulus increased significantly (p = 0.02) with the increase in screw speed for both virgin PLA and the nanocomposites as shown in Figure 3. There is a significant increase in Young's modulus for the virgin

PLA at 140 rpm screw speed when compared to 40 and 80 rpm screw speeds separately. The Young's modulus for the composite increases with an increase in screw speed. However, 10 wt. % HNT loaded nanocomposite compounded at 140 rpm screw speed is at maximum. Hence the screw speed and the percentage loadings of the HNT have a significant effect on Young's modulus of the composite.

The tensile strength of the material compounded at 140 rpm screw speed significantly increases with p = 0.039. It should be noted that the highest tensile strength is for 5 wt. % HNT loaded nanocomposite at 140 rpm screw speed. The stiffness of the virgin PLA and the 10 wt. % loaded HNT composite significantly increases when compounded at 140 rpm screw speed. However, the elongation at break is significantly increased for virgin PLA and the 5 wt. % composites at higher screw speed. Statistical analysis confirms both the screw speed and the loadings of HNT had a significant effect with the p-value=0.01 on the stiffness and the elongation at break.

Figure 3.

Compounding at 140 rpm screw speed improved the mechanical properties of the composites. It is noteworthy that the mechanical properties improve significantly for virgin PLA itself as the screw speed increases. This could be attributed to the high shear force at higher screw speed when the polymer structure rearranges during the extrusion process. It is noticed that Young's modulus and the stiffness increase for 10 wt. % HNT loaded composites. Additionally, the tensile strength and the elongation at break increases by 5 wt. % HNT loaded composites for 140 rpm screw speed. The improvement in the tensile strength usually indicates good interfacial bonding resulting in effective stress transfer from the PLA matrix to the reinforcing nanoclay. Guo et.al. reported similar improvements when processed by mini extruder at 50 rpm when utilizing surface-modified HNT [30]. Hence, we can say that melt compounding at 140 rpm or higher screw speed had equivalent results without the modification of HNT.

3.5. Morphology and structural characteristics

Scanning electron microscopy photomicrographs indicated that the structure of the PLA was uniform, and its elemental composition as measured by EDX was recorded with only carbon and oxygen. The incorporation of HNT resulted in the presence of microscale particles, which exhibited an elemental composition consisting of aluminum and silicon which is indicative of the presence of HNT. The heterogeneous structure is observed for 10 wt. % loadings of HNT for all screw speeds. This is due to the presence of agglomerates of HNT with the magnitude of the agglomerates being larger in the 10 wt. % composites. The magnified image of the agglomerate size on the 10 wt. % composite in Figure 4 (D) indicates the cluster of HNT for a wide area. Furthermore, very few agglomerations of small sizes were apparent in 5 wt. % composites compounded at 140 rpm as seen in Figure 4 (B) could indicate a better distribution of HNT in the matrix.

Figure 4.

The elemental composition of the composite as seen in Table 2. indicated the presence of aluminum and silicone from the composition of the HNT, which confirmed the presence of HNT in the polymer matrix. In some, there was an agglomeration of HNT and spaces between the particles and the matrix. From Table 2 and Figure 4 the dispersion of HNT into polymer matrix appears to increase with the increase in screw speed by the increase in the amount of aluminum and silicone present which are elemental in the composition of the HNT.

Table 2.

3.6. Fourier Transfer Infrared (FTIR) Spectroscopy

FTIR spectra for PLA, HNT, and PLA/HNT composites are shown in Figure 5. Virgin PLA exhibited characteristic absorption band at 3571 cm^{-1} corresponding to –OH stretch and absorption bands at 2996 cm^{-1} and 2946 cm^{-1} are attributed to CH stretch and the absorption band at 1750 cm^{-1} corresponding to –C=O carbonyl group [11]. The characteristic absorption band at 1450 cm^{-1} is attributed to the bending vibrations of CH3 and absorption bands at 1384 cm^{-1} and 1364 cm^{-1} are the CH deformation and asymmetric/symmetric bending [~~43~~ 41]. The spectrum of HNT displayed absorption bands at 3695 cm^{-1} and 3621 cm^{-1} that can be assigned to O-H group vibrations and absorption band at 910 cm^{-1} to Al-OH group vibrations.

The spectra of PLA/HNT composites revealed the absorption bands of both PLA and HNT. The overlapping of HNT absorption bands increases the intensity of the PLA absorption band as the screw speed increases in the region between 1300 cm^{-1} - 500 cm^{-1}. For instance, the overlapping of the HNT absorption band 1031 cm^{-1} increases the intensity of the 1043 cm^{-1} absorption band of PLA. This observation is also seen in other studies as well {27,30,41]. The absorption band 1266 cm^{-1} of PLA shifts to 1270 cm^{-1} for 5 wt. % composites and is more intense and sharpens as the screw speed increases. This kind of shift is also seen in the study by Dong et. al. in which the HNT was modified [47]. The observed sharpening, increase in the intensity of the peaks, and shifting to higher frequencies as the screw speed increases are the most for PLA/HNT 5 wt. % nanocomposites at 140 rpm. This can be attributed to the interactions between the PLA and HNT via hydrogen bonding which could have contributed to the increased thermal and mechanical properties of the PLA/HNT composite, which were also confirmed by FTIR in other studies [41].

Figure 5.

3.7. Surface Wettability

Contact angle measurements for PLA were within a range of 60°–65°. The nanocomposite produced by the incorporation of 5 wt. % HNT compounded at different screw speeds did not have a statistically significant effect on the surface wettability of the PLA for p=0.245 and the contact angle remained within the same range as virgin PLA as seen in Figure 6. Hence, they are hydrophilic. However, for 10 wt. % composites the contact angle increased to 99° making it hydrophobic.

(A) (B)

Figure 6.

The contact angle measuring less than 90° corresponds to high wettability and the contact angle more than 90° corresponds to low wettability [50]. The surface of PLA and 5 wt. % composite formed at all screw speeds were found to be hydrophilic, which was also seen in the study by De Silva et al. [27]. The 10 wt. % composites are hydrophobic as the contact angle increases to >90°. Similar findings have been reported by De Silva et.al. which can be attributed to the increase in the surface roughness at higher concentrations. This in turn reduces the surface energy because of more polar groups at higher concentrations of HNT, which makes the material hydrophobic {27].

4. Conclusions

The study of screw speeds during extrusion revealed that compounding at higher screw speed had a significant effect ~~not only~~ on the HNT loaded composite~~,~~ This can be attributed to the high melt shear during compounding which enhanced HNT dispersion. The thermal and mechanical properties along with the morphology of the nanocomposites compounded at higher screw speed had at least equivalent results to those reported in the literature where the HNT were surface treated. Hence, we can say that the high melt shear during compounding assists the better dispersion of the HNT into the polymer matrix which in turn improved the overall properties of the composites without the need for surface treatment of the HNT as desired for various biomedical applications. The main focus of the study was to look at the effect of screw speed as we had observed poor HNT dispersion in previous work when processed at low speed. Nevertheless, the combination of screw elements determining the filling degree, melting degree, residence time distributions (RTDs), or mechanical energy does warrant further investigation.

Funding: Athlone Institute of Technology under the Presidents Seed Fund, Enterprise Ireland funding under the Technology Gateway program, funded this research, grant number TG-2017-0114 and Science Foundation Ireland (SFI) under Grant Number 16/RC/3918

Conflicts of Interest: The authors declare no conflict of interest.

References

1. Lim L.-T., Auras R., Rubino M. Processing technologies for poly(lactic acid). Prog. Polym. Sci. 2008, 33, 820–852.
2. La Mantia F. P., Morreale M. Green composites: a brief review. Compos. Part A Appl. Sci. Manuf. 2011, 42, 579–588.
3. Rasal R. M., Janorkar A. V., Hirt D. E. Poly(lactic acid) modifications. Prog. Polym. Sci. 2010, 35, 338–356.
4. Lasprilla A. J. R., Martinez G. A. R., Lunelli B. H., Jardini A. L., Filho R. M. Poly-lactic acid synthesis for application in biomedical devices – a review. Biotechnol. Adv. 2012, 30, 321–328.
5. Kunduru K. R., Basu A., Domb A. J. Biodegradable polymers: medical applications. Encycl. Polym. Sci. Technol. 2016, 1–22. https://doi.org/10.1002/0471440264.pst027.pub2.
6. Bari S. S., Chatterjee A., Mishra S. Biodegradable polymer nanocomposites: an overview. Polym. Rev. 2016, 56, 287–328.
7. Liu M., Jia Z., Jia D., Zhou C. Recent advance in research on halloysite nanotubes-polymer nanocomposite. Prog. Polym. Sci. 2014, 39, 1498–1525.
8. Anand Narayanan A. G., Babu R., Vasanthakumari R. Studies on halloysite nanotubes (HNT) natural rubber nanocomposites for mechanical thermal and wear properties. Int. J. Eng. Res. Technol. 2016, 5, 152–156.
9. Pollack S., Venkatesh C., Neff M., Healy A. V., Hu G., Fuenmayor E. A., Lyons J. G., Major I., Devine D. M. Polymer-based additive manufacturing: historical developments, process

types, and material considerations. In Polymer-Based Additive Manufacturing; Devine D., Ed.; Springer Nature Switzerland AG: Switzerland, 2019; pp. 1–22.
10. Venkatesh C., Fuenmayor E., Doran P., Major I., Lyons J. G., Devine D. M. Additive manufacturing of PLA/HNT for biomedical applications. Procedia Manuf. 2020, 38,17–24.
11. Garlotta D. A literature review of poly (lactic acid). J. Polym. Environ. 2002, 9,63–84.
12. Chen Y., Geever L. M., Killion J. A., Lyons J. G., Higginbotham C. L., Devine D. M. A review of multifarious applications of poly (lactic acid). Polym. Plast. Technol. Eng. 2016, 2559, 1057–1075.
13. Ramot Y., Haim-Zada M., Domb A. J., Nyska A. Biocompatibility and safety of PLA and its copolymers. Adv. Drug Deliv. Rev. 2016, 107, 153–162.
14. Venkatesh C., Clear O., Major I., Lyons J. G., Devine D. M. Faster release of lumen-loaded drugs than matrix-loaded equivalent in polylactic acid/halloysite nanotubes. Materials 2019, 12, 1830.
15. Dillon B., Doran P., Fuenmayor E., Healy A. V., Gately N. M., Major I., Lyons J. G. Influence of annealing and biaxial expansion on the properties of poly(l-lactic acid) medical tubing. Polymers 2019, 11, 1172.
16. Jia S., Yu D., Zhu Y., Wang Z., Chen L., Fu L. Morphology, crystallization and thermal behaviors of PLA-based composites: wonderful effects of hybrid GO/PEG via dynamic impregnating. Polymers 2017, 9, 528.
17. Sangeetha V. H., Deka H., Varghese T. O., Nayak S. K. State of the art and future prospectives of poly(lactic acid) based blends and composites. Polym. Compos. 2018, 39,81–101.
18. Lazzara G., Massaro M., Milioto S., Riela S. Halloysite-based bionanocomposites. Handb. Compos. Renew. Mater. 2017, 1–8, 557–584.
19. Yang Y. Recent advances on surface modification of halloysite nanotubes for multifunctional applications. Appl. Sci. 2017, 7, 1215.
20. Kamble R., Ghag M., Gaikwad S., Panda B. K. Review article halloysite nanotubes and applications: a review. J. Adv. Sci. Res. 2012, 3,25–29.
21. Lvov Y., Abdullayev E. Functional polymer-clay nanotube composites with sustained release of chemical agents. Prog. Polym. Sci. 2013, 38, 1690–1719.
22. Therias S., Murariu M., Dubois P. Bionanocomposites based on PLA and halloysite nanotubes: from key properties to photooxidative degradation. Polym. Degrad. Stabil. 2017, 145, 1–10.
23. Jock Churchman G., Pasbakhsh P., Hillier S. The rise and rise of halloysite. Clay Miner. 2016, 51, 303–308.
24. Du M., Guo B., Jia D. Newly emerging applications of halloysite nanotubes: a review. Polym. Int. 2010, 59, 574–582.

25. Deepak R., Agrawal Y. K. Study ofnanocomposites with emphasis to halloysite nanotubes. Rev. Adv. Mater. Sci. 2012, 32, 149–157.
26. Dong Y., Marshall J., Haroosh H. J., Mohammadzadehmoghadam S., Liu D., Qi X., Lau K. T. Polylactic acid (PLA)/halloysite nanotube (HNT) composite mats: influence of HNT content and modification. Compos. Part A Appl. Sci. Manuf. 2015, 76,28–36.
27. De Silva R. T., Pasbakhsh P., Goh K. L., Chai S. P., Chen J. Synthesis and characterisation of poly (lactic acid)/halloysite bionanocomposite films. J. Compos. Mater. 2014, 48, 3705–3717.
28. Chen Y., Murphy A., Scholz D., Geever L. M., Lyons J. G., Devine D. M. Surface-modified halloysite nanotubes reinforced poly(lactic acid) for use in biodegradable coronary stents. J. Appl. Polym. Sci. 2018, 135, 46521.
29. Stoclet G., Sclavons M., Lecouvet B., Devaux J., Van Velthem P., Boborodea A., Bourbigota S., Sallem-Idrissi N. Elaboration of poly(lactic acid)/halloysite nanocomposites by means of water assisted extrusion: structure, mechanical properties and fire performance. RSC Adv. 2014, 4, 57553–57563.
30. Guo J., Qiao J., Zhang X. Effect of an alkalized-modified halloysite on PLA crystallization, morphology, mechanical, and thermal properties of PLA/halloysite nanocomposites. J. Appl. Polym. Sci. 2016, 133,1–9.
31. Fuenmayor E., Forde M., Healy A. V., Devine D. M., Lyons J. G., McConville C., Major I. Material considerations for fused-filament fabrication of solid dosage forms. Pharmaceutics 2018, 10,1–27.

32. Pinto V. C., Ramos T., Alves S., Xavier J., Tavares P., Moreira P. M. G. P., Guedes R. M. Comparative failure analysis of PLA, PLA/GNP and PLA/CNT-COOH biodegradable nanocomposites thin films. Procedia Eng. 2015, 114, 635–642.
33. Stanković M., Frijlink H. W., Hinrichs W. L. J. Polymeric formulations for drug release prepared by hot melt extrusion: application and characterization. Drug Discov. Today 2015, 20, 812–823.
34. Lyons J. G., Holehonnur H., Devine D. M., Kennedy J. E., Geever L. M., Blackie P., Higginbotham C. L. The incorporation of an organically modified layered silicate in monolithic polymeric matrices produced using hot melt extrusion. Mater. Chem. Phys. 2007, 103, 419–426.
35. Healy A. V., Waldron C., Geever L. M., Devine D. M. Degradable nanocomposites for fused filament fabrication applications. J. Manuf. Mater. Process. 2018, 2, 29.
36. Li Y., Han C., Zhang X., Xu K., Bian J., Poly D. L. (L-lactide)/ poly(D-lactide)/clay nanocomposites: enhanced dispersion, crystallization, mechanical properties, and hydrolytic degradation. Polym. Eng. Sci. 2014, 54, 914–924.
37.
37. Sasimowski E., Majewski Ł. Effect of the intensive plasticizing zone design on the effectiveness of corotating twin-screw extrusion. Adv. Polym. Technol. 2019, 2019,15–17.
38. Albareeki M. M., Driscoll S. B., Barry C. F. Compounding of polyethylene composites using high speed twin and quad screw extruders. AIP Conf. Proc. 2019, 2139, 020006.
39. Atif R., Inam F. Reasons and remedies for the agglomeration of multilayered graphene and carbon nanotubes in polymers. Beilstein J. Nanotechnol. 2016, 7, 1174–1196.
40. Liu M., Zhang Y., Zhou C. Nanocomposites of halloysite and polylactide. Appl. Clay Sci. 2013, 75–76,52–59.
41. Chen Y., Geever L. M., Killion J. A., Lyons J. G., Higginbotham C. L., Devine D. M. Halloysite nanotube reinforced polylactic acid composite. Polym. Compos. 2017, 38, 2166–2173.
42. Gamon G., Evon P., Rigal L. Twin-screw extrusion impact on natural fibre morphology and material properties in poly(lactic acid) based biocomposites. Ind. Crop. Prod. 2013, 46, 173–185.
43. Normand G., Peuvrel-Disdier E., Vergnes B. Matrix degradation during
during high speed extrusion of polypropylene/clay nanocomposites – influence on filler dispersion. Int. Polym. Process. 2017, 31, 508–516.
44. Domenech T., Peuvrel-Disdier E., Vergnes B. Influence of twin- screw processing conditions on structure and properties of polypropylene – organoclay nanocomposites. Int. Polym. Process. 2012, 27, 517–526.
45. Villmow T., Kretzschmar B., Pötschke P. Influence of screw configuration, residence time, and specific mechanical energy in twin-screw extrusion of polycaprolactone/multi-walled carbon nanotube composites. Compos. Sci. Technol. 2010, 70, 2045–2055.
46. Wu W., Cao X., Zhang Y., He G. Polylactide/halloysite nanotube nanocomposites: thermal, mechanical properties, and foam processing. J. Appl. Polym. Sci. 2013, 130, 443–452.
47. Prashantha K., Lecouvet B., Sclavons M., Lacrampe M. F., Krawczak P. Poly(lactic acid)/halloysite nanotubes nanocomposites: structure, thermal, and mechanical properties as a function of halloysite treatment. J. Appl. Polym. Sci. 2013, 128, 1895–1903.
48. Devine D. M., Hoctor E., Hayes J. S., Sheehan E., Evans C. H. Extended release of proteins following encapsulation in hydroxyapatite/chitosan composite scaffolds for bone tissue engineering applications. Mater. Sci. Eng. C 2017, 84, 281–289.
49. Yuan Y., Lee R., Bracco G., Holst B. Contact angle and wetting properties. In Surface Science Techniques; Springer Series in Surface Sciences, 51, 2013; pp. 3–34.

coatings

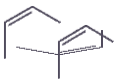

Article

Biodegradation and Antimicrobial Properties of Zinc Oxide–Polymer Composite Materials for Urinary Stent Applications

Chaitra Venkatesh 1,y , Marco Laurenti 2,y , Marina Bandeira 1,3 , Eduardo Lanzagorta 1 ,
Lorenzo Lucherini 2,4, Valentina Cauda 2,* and Declan M. Devine 1

1 Material Research Institute, Athlone Institute of Technology, Athlone, N37 HD68 Co. Westmeath, Ireland;
c.venkatesh@research.ait.ie (C.V.); m.bandeira@research.ait.ie (M.B.); e.lgarcia@research.ait.ie (E.L.); ddevine@ait.ie (D.M.D.)
2 Department of Applied Science and Technology, Politecnico di Torino, C.so Duca degli Abruzzi 24,
10129 Turin, Italy; marco.laurenti@polito.it (M.L.); lucherini.lorenzo@gmail.com (L.L.)
3 Rua Francisco Getúlio Vargas, Universidade de Caxias do Sul, 1130, Caxias do Sul 95070-560, RS, Brazil
4 Soil Mechanics Laboratory (LMS), École Polytechnique Fédérale de Lausanne (EPFL), Station 18,
CH-1015 Lausanne, Switzerland
* Correspondence: valentina.cauda@polito.it; Tel.: +39-11-0907389
y These authors contributed equally to this work.

Received: 5 October 2020; Accepted: 18 October 2020; Published: 20 October 2020

Abstract: Research advancements in the field of urinary stents have mainly been in the selection of materials and coatings to address commonly faced problems of encrustation and bacterial adhesion. In this study, polylactic acid (PLA) and polypropylene (PP) were evaluated with zinc oxide (ZnO) coating to assess its ability to reduce or eliminate the problems of encrustation and bacteria adhesion. PLA and PP films were prepared via twin screw extrusion. ZnO microparticles were prepared using sol-gel hydrothermal synthesis. The as-prepared ZnO microparticles were combined in the form of a functional coating and deposited on both polymer substrates using a doctor blade technique. The ZnO-coated PP and PLA samples as well as their uncoated counterparts were characterized from the physicochemical standpoints, antibacterial and biodegradation properties. The results demonstrated that both the polymers preserved their mechanical and thermal properties after coating with ZnO, which showed a better adhesion on PLA than on PP. Moreover, the ZnO coating successfully enhanced the antibacterial properties with respect to

bare PP/PLA substrates. All the samples were investigated after immersion in simulated body fluid and artificial urine. The ZnO layer was completely degraded following 21 days immersion in artificial urine irrespective of the substrate, with encrustations more evident in PP and ZnO-coated PP films than PLA and ZnO-coated PLA films. Overall, the addition of ZnO coating on PLA displayed better adhesion, antibacterial activity and delayed the deposition of encrustations in comparison to PP substrates.

Keywords: polylactic acid (PLA); polypropylene (PP); zinc oxide; antibacterial coatings; ureteral stents; bacteria biofilm; urine-derived encrustations

1. Introduction

Urinary stents are commonly used to drain retained urine after surgical procedures, in cases of urinary incontinence and in related issues to the urinary tract [1–3]. Although many improvements have been achieved so far, patients still face complications related to the insertion of urinary stents, especially when long-term usage is required. The main problems encountered in commercial urinary stents are friction, the release of substances, encrustation and bacterial adhesion that can cause adverse effects to the patient, such as inflammation [1,4–6]. To date, work is still in progress on the development of a biocompatible, antimicrobial, antifouling and non frictional material potentially used for urinary stents to improve patients' quality of life by reducing the chances of post procedure complications as well as to increase the lifetime of the stent [7–9].

Different materials have been employed to develop urinary stents. However, polymer-based materials are the most used due to their biocompatibility, biological inertness and low cost [7,10]. Moreover, several coatings technologies have been shown to improve biocompatibility, antimicrobial action and prevent encrustation, illustrating the potential of coatings to enhance the functionality of urinary stents [2,8,9,11] and even promoting the sustained delivery of pharmaceutically active compounds [12]. For example, antibiotics coatings were able to prevent biofilm formation and bacterial infections. However, many issues
related to antibiotic resistance have been addressed, showing the loss of antimicrobial action after a few usages [8,13].

In this study, the performance of polylactic acid (PLA) and polypropylene (PP) as a material for urinary stents were evaluated. PLA is the most widely used aliphatic thermoplastic polymer. It is obtained from renewable agricultural resources such as starch from rice, corn, potatoes, beetroot, etc. and is used in various medical applications such as sutures, dermal fillers or stents [14]. PLA has been studied as a coating layer for antimicrobial applications by incorporation of nanoparticles such as silver [15], zinc oxide (ZnO) nanoparticles [16] or ZnO deposition on halloysite nanotubes and further incorporation into PLA [17]. PLA-ZnO nanocomposites have been produced by the method of melt compounding, and the resultant films were found to be amorphous and had antibacterial properties [18,19] and degradation process of the PLA was increased [20].

PP is a polymer from the family of polyolefins that has features such as low density, chemical inertness, and high melting temperature. Due to its high temperature resistance, it is used in various products in clinical environments [21]. It

has been used for stenting in endoscopic dacryocystorhinostomy with successful and higher anatomic and functional efficacy [22,23]. Due to its excellent histocompatibility PP mesh has been studied as suitable stent material for airway strictures [24] and PP-silicone stent has been successfully evaluated for the treatment of benign esophageal strictures [25]. In order to enhance the properties of PP, di_erent methodologies have been tested including reports by Zhao et al. who investigated the photodegradation resistance of PP to UV-irradiation by incorporation of ZnO and found significant improvements [26]. PP has been modified with ZnO to produce hybrid filter material and found to have high filtration e_ciency [27]. Bojarska et al. investigated PP capillary membranes which were modified by ZnO nanowires. The use of plasma was found to improve the adhesion of ZnO nanowires on the PP membrane surface. Moreover, the resulting PP/ZnO membranes exhibited antibacterial properties against Gram-positive and Gram-negative bacteria [28].

This work aims to evaluate the use of ZnO as a novel coating material for the manufacturing of urinary stents. In particular, to achieve a material with superior antimicrobial property, both PLA and PP films were coated with a functional ZnO layer, as zinc oxide is well known for its antimicrobial action against both Gram-positive and Gram-negative bacteria [29,30]. Briefly, the mechanism of antimicrobial action involves the release of zinc ions, production of reactive oxygen species (ROS) and direct contact with the bacteria cell surface causing the rupture of the membrane and changes on the cell metabolism that can lead to cell death [31–34]. Thus, this research focused on the evaluation of the physical and mechanical properties, antimicrobial activity and adhesion of the zinc oxide coatings on PLA and PP substrates for urinary stents application. In particular, we show a different capability of these materials to react to artificial urine solution and another simulated physiological solution, which has a similar inorganic composition of the human plasma. The results indeed show that the behaviour of these ZnO-coated polymers can be efficiently modulated to get highly hydrophilic and biodegradable devices with further antimicrobial properties in the right urinary environment.

2. Materials and Methods

2.1. Preparation of PLA and PP Films

Polylactic acid (PLA) obtained from Corbion, PLALX175 (Total Corbian, Gorinchem, The Netherlands) and polypropylene (PP, Sigma Aldrich Ireland Ltd.,Wicklow, Ireland) were used to produce the polymeric substrates. The PLA had a molecular weight (Mw) of 24,000 g/mol and PP was isostatic with average Mw of ~250,000 g/mol. Both polymers were received in granular form. Twin-screw extrusion was employed to process PLA and PP into films. Extrusion was performed by using an APV (Model MP19TC (35:1) APV Baker, Newcastle-underLyme, UK) twin-screw compounder with 19 mm diameter screws. The temperature profile was maintained (from die to feeder) at 200/190/180/170/160/110/50 _C. PLA was dried in the oven at 80 _C for 4 h. The dried PLA pellets were fed into the hopper of the extruder and extruded at a screw speed of 140 rpm. Extruded strands of the molten composite were then drawn through a three-roll calendar creating continuous films. Similarly, the PP pellets were processed by melt compounding under similar conditions for

comparison. These films were used to punch out ASTM standard tensile test specimens by a physical punching process.

2.2. Synthesis of ZnO Microparticles

Zinc oxide micro particles were prepared via a sol-gel hydrothermal synthesis method as previously reported [35,36], using potassium hydroxide (KOH, Sigma Aldrich, Darmstadt, Germany) and zinc nitrate hexahydrate (Zn(NO3)2_6H2O, Sigma Aldrich) as precursors. All reagents were used as received. First, 5.58 g of potassium hydroxide and 14.8 g of zinc nitrate hexahydrate were dissolved separately in 100 mL of double-distilled water at room temperature. Afterwards, the zinc nitrate solution was added dropwise to the KOH solution under vigorous magnetic stirring conditions. The formed gel was treated at 70 _C for 4 h. Later, the precipitated ZnO powder was filtered from the basic solution and washed several times with demineralized water until pH neutralization and air dried in a muffle furnace at 60 _C overnight.

2.3. Deposition of ZnO Coating on Polymeric Substrates

Different methods were considered to coat PLA and PP substrates. First, a ZnO paste was prepared by adding zinc oxide powders in a 1:2 (w/v) ratio to a solution of acetic acid (1%, Sigma Aldrich), ethanol (67%, Sigma Aldrich) and water (33%). The paste was then stirred and sonicated to obtain a homogeneous dispersion of the particles. The prepared paste was deposited on the surface of both PP and PLA films using the doctor blade technique on a glass slide to obtain a uniform layer. Sodium hydroxide (Sigma Aldrich) and benzophenone (BP) (Sigma Aldrich) were also used for surface activation and grafting of the ZnO coatings to the polymer supports.

In this study three methods were employed:

1. For method 1, the coated PLA was thermally treated at 50 _C for 30 min and 60 _C for 15 min while coated PP films were treated at 70 _C for 15 min.
2. In method 2, ZnO paste was UV grafted onto the PLA substrate using the protocol developed by Shin et al. [37] with adaptations. For this, 20 mL of 10 wt.% acrylic acid aqueous solution was added to 20 mL of benzophenone 0.2 M and stirred under dark conditions. Then, ZnO paste containing 1 g of ZnO was added to the previous solution and stirred for 30 min in the absence of light. The final solution was poured in a glass petri dish containing the PLA films and exposed to UV light for five minutes at 40W. After curing, samples were neutralized by immersion in a sodium bicarbonate (Sigma Aldrich) 0.1 M solution for 10 min, rinsed with distilled water and dried overnight at 40 _C.
3. In method 3, 1 g of ZnO powder was dispersed in 2 mL of ethanol and sonicated for 15 min. Different amounts of benzophenone 0.2 Methanolic solution (0, 0.25 and 0.50 mL) were then added to this solution and stirred until the solution became homogeneous. Then, PP and PLA were coated with ZnO + BP solution and exposed to UV light (0, 5 and 10 min), dried for 1 h at 37 _C and rinsed with water for removing excess reagents. All samples were dried overnight at 37 _C prior to analysis. For this method, PP was previously treated with a 0.1 M sodium hydroxide solution for 18 h for surface activation while PLA did not have any previous treatment.

Only the coatings produced using method 3 with 0.50 mL of BP and 5 min of UV treatment for PLA films and 0.50 mL of BP and no UV treatment for PP films showed good adhesion of the coatings (data not shown). Thus, only these set of samples (named ZnO@PP and ZnO@PLA) were fully characterized in this work.

2.4. Characterization Setup

2.4.1. Physicochemical Characterization

The morphology and chemical composition of the samples were investigated by means of field-emission scanning electron microscopy (FESEM, Merlin Carl Zeiss AG, Oberkochen, Germany) coupled with an energy dispersive x-ray (EDX) detector for chemical composition analyses. Before FESEM imaging, the surface of the samples was coated with a 5 nm-thick Pt coating. The crystalline structure was investigated with X-ray diffraction (XRD) using a Panalytical X'Pert PRO diffractometer (Malvern Panalytical S.r.l., Milan, Italy) in Bragg–Brentano configuration and equipped with a Cu K_ monochromatic radiation (_ = 1.54059 Å) as X-ray source. Fourier transform infrared spectroscopy (FTIR) in attenuated total reflectance (ATR) mode was performed with a Nicolet 5700 FTIR spectrometer (ThermoFisher, Waltham, MA, USA) equipped with diamond crystal. The ATR-IR spectra were background subtracted and acquired with 2 cm◉1 resolution and 64 scans accumulation. Indexing of IR modes have been done according to Socrates [38].

Mechanical properties of the PLA and PP films were characterized by tensile tests, probing each different blend. Tensile testing was carried out on a Lloyd Lr10k tensometer (Ametek ltd,West Sussex, UK) using a 2.5 kN load cell on ASTM standard test specimens at a strain rate of 50 mm/min. Data was recorded using NexygenTMsoftware (Ametek Ltd.). The tensile tests were carried out in adherence to ASTMD 882. Ten individual test specimens were analysed per group and before testing, the thickness of each sample was measured. The percentage strain at maximum load, stress at maximum load, stiffness, and Young's modulus of each sample were recorded.

The surface wettability of the composites was assessed using First Ten Angstroms' FTA32 goniometer (FTA Europe, Cambridge, UK). In this test, the sessile drop contact angle technique was utilized with distilled water as the probe liquid. Five measurements at various places on the films were taken.

Differential scanning calorimetry (DSC) was carried out using a DSC 2920 modulated DSC (TA Instruments, New Castle, DE, USA) with a nitrogen flow rate of 20 mL/min to prevent oxidation. Calibration of the instrument was performed using indium as standard. Test specimens weighing between 8 mg and 12 mg were measured on Sartorius scales (MC 210 P, Sartorius Lab Instruments GmbH & Co. KG, Goettingen, Germany), capable of being read to five decimal places. Samples were crimped in nonperforated aluminium pans, with an empty crimped aluminium pan used as the reference. The thermal history was removed by heating samples from 20 to 220 _C at the rate of 30 _C/min and then held isothermally at 220 _C for 10 min. The samples were then cooled down from 220 to 20 _C at 30 _C/min. Finally, the thermal properties of the samples were recorded by heating the samples from 20 to

220 _C at the rate of 10 _C/min, glass transition temperature, and melting temperature of each sample were recorded.

2.4.2. Biodegradation Essays

Simulated body fluid (SBF) was prepared according to the method described by Kokubo and Takadama [39] with a final pH of 7.45. ZnO-coated PLA and PP films were then placed in the SBF solution in a water bath at 36.5 _ 1 _C. The SBF solution was replaced every two days and the adhesion of the films in SBF solution was monitored for seven days.

The artificial urine was prepared following the protocol described by Sarangapani et al. [40]. The solution was constituted basically by salts, urea (25 g_L◎1) and creatinine (1.10 g_L◎1). The final pH of the solution was 5.7. ZnO-coated films were placed in the artificial urine solution, which was kept at 36.5 _ 1 _C, and monitored for 21 days regarding the adhesion and appearance of encrustation. Uncoated PLA and PP films were also placed in artificial urine for the same soaking time and used as control samples.

2.4.3. Antibacterial Tests

The antimicrobial tests were performed using Staphylococcus aureus ATCC25923 (S. aureus) and Escherichia coli ATCC25922 (E. coli), tryptone soy broth (TSB, Neogen) and resazurin (Sigma Aldrich). S. aureus and E. coli were cultured and grown in an exponential phase in TSB medium at 37 _C. Bacterial cell viability when exposed to di_erent polymer films was analysed in a 12-well plate according to the resazurin cell viability assay. Resazurin indicates cell viability by changing the solution colour from blue to pink when it is chemically reduced to resofurin due to the aerobic respiration that occurs with cell growth. Thus, the reduction of the dye is proportional to the viable cells present in the solution. Overnight cultures of the two bacteria strains were diluted to a concentration of approximately 1.0 _ 104 colony formation unit per millilitre (CFU_mL◎1). Then, 500 _L of TSB and 25 _L of the diluted bacteria were added in each well. After this procedure, coated (10 mm _ 10 mm) and noncoated polymer films were placed in the respective wells. A negative control without bacteria (500 _L of TSB) and positive control with live cells (500 _L of TSB and 25 _L of diluted bacteria solution) were also included in each plate. After overnight incubation at 37 _C, 75 _L of resazurin was added in every well, mixed thoroughly and incubated for 2 h at 37 _C under dark conditions. Then, the colour change of the solution and, consequently, the cell viability was evaluated by absorbance measurement at 600 nm in an ultraviolet-visible (UV-Vis) plate reader (Jenway 6300, Sta_ordshire, UK). The experiment was performed in triplicate and repeated independently three times.

2.4.4. Statistical Analysis

Statistical analysis of the tensile test results, DSC measurements and the surface wettability measurements were carried out using general linear model (GLM) of two-way ANOVA in Minitab 17 Statistical Software (Minitab Ltd., Coventry, UK).

All the values were considered at a 95% confidence interval, and p-values are considered significant when p _ 0.05.

3. Results and Discussion

3.1. Morphological, Structural and Chemical Characterization

Figures 1–3 show the FESEM images and EDX spectra of ZnO-coated PLA and PP substrates (ZnO@PLAand ZnO@PP). It can be observed that ZnO micro particles showing a flower-like morphology (Figure 2) have been successfully deposited atop of both the polymer surface types. Their presence is further corroborated by the detection of Zn traces by EDX analyses. The covering of the PLA substrate is superior with respect to the PP one. This is visible from the comparison of the FESEM images and of the semi quantitative analysis obtained by EDX spectroscopy. Actually, the Zn at.% changes from 31.90% for PLA support to 9.76% for PP, suggesting that ZnO is more abundant on PLA than on PP films.

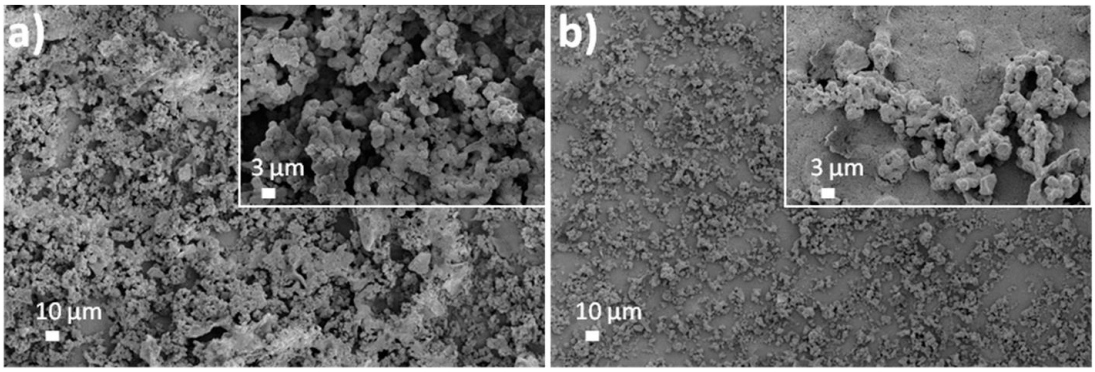

Figure 1. Field-emission scanning electron microscope **(**FESEM) images of ZnO microparticle coatings deposited on (**a**) polylactic acid (PLA) and (**b**) polypropylene (PP) polymeric supports.

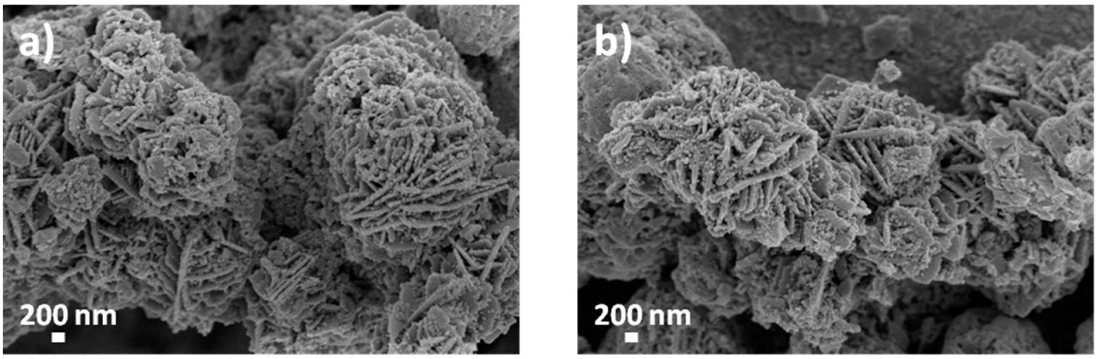

Figure 2. FESEM images showing the flower-like morphology of ZnO microparticle coatings deposited on (**a**) PLA and (**b**) PP polymeric

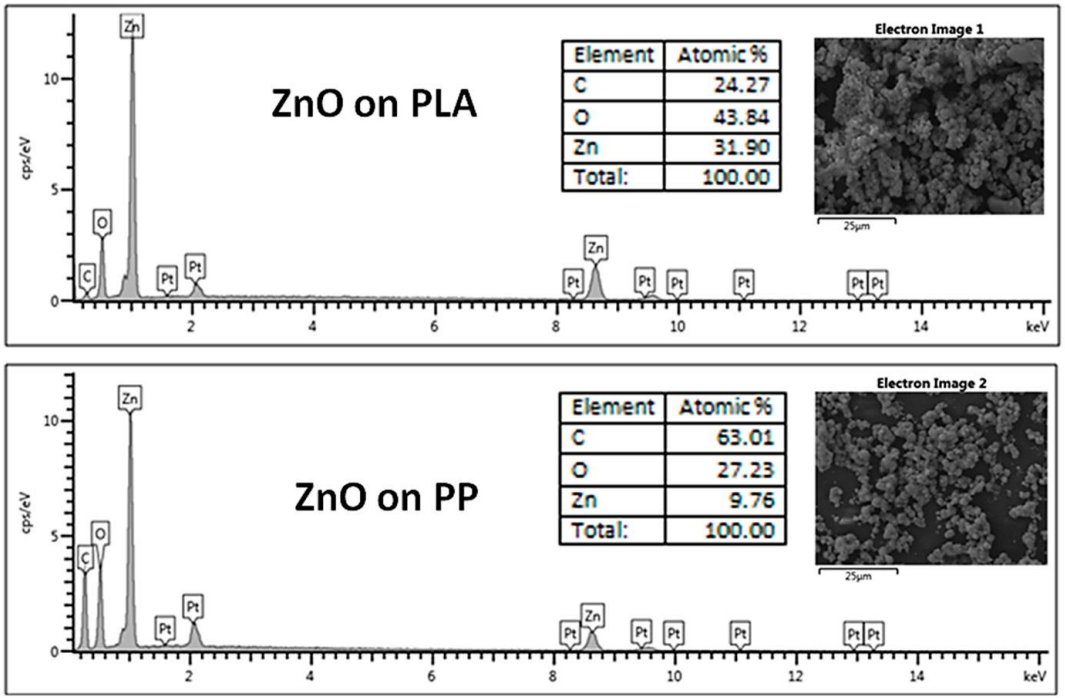

Figure 3. Energy dispersive X-ray (EDX) spectra of ZnO-coated PLA and PP supports

Independently of the polymer, the presence of the ZnO coating after the fabrication process was confirmed also by the detection of the diffraction peaks belonging to wurtzite ZnO phase (Figure 4). The main ones are positioned at 31.8_, 34.4_ and 36.2_, and are ascribed to (100), (002) and (101) crystallographic planes according to the Joint Committee on Powder Diffraction Standards—International Centre for Diffraction Data (JCPDS-ICDD) database (Card No. 89-1397). Other minor reflections coming from additional crystal planes are also visible at higher 2_ angles.

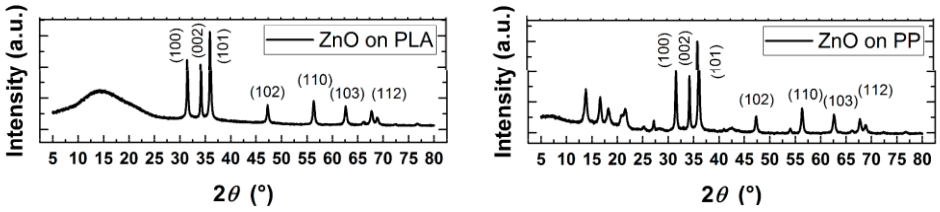

Figure 4. X-ray di_raction (XRD) pattern of sample ZnO@PLA and ZnO@PP

Figure 5 shows the ATR-IR spectra for uncoated PLA and PP substrates as well as from the corresponding samples coated with ZnO microparticle film. The main IR modes are in the range 3000–2900 cm◎1 and near 1450 cm◎1 (both related to the C–H stretching/bending vibrations), at about 1750 cm◎1 (C=O stretching vibration), in the range 1200–1150 cm◎1 (C–O symm. stretch.) and three bands in the range 1130–1040 cm◎1 due to C–O–C symmetric stretching. These prominent modes of the spectrum are the characteristic peaks of PLA and PP [14,26,27]. When the ZnO microparticle coating is present, it is possible to observe a general reduction in intensity of the bands related to the polymeric materials underneath the ZnO materials. This effect is due to the micrometer thickness of the ZnO layer coating

(more or less uniformly) the polymer. An additional broad band corresponding to H–O–H vibration of the ZnO hydrophilic surface is noticed in the range 3500–3000 cm◎1 for both kinds of ZnO-coated polymers. The presence of the ZnO coating is further confirmed by the presence of a broad band in the range 950–850 cm◎1 and due to Zn–OH mode. Similar presence of clear peak in the range 400–700 cm◎1 in PP/ZnO spectrum and absence in PP spectrum was observed in the study of ZnO nanowire growth via plasma activation by Bojarska et al. which could indicate the presence of zinc oxide [28].

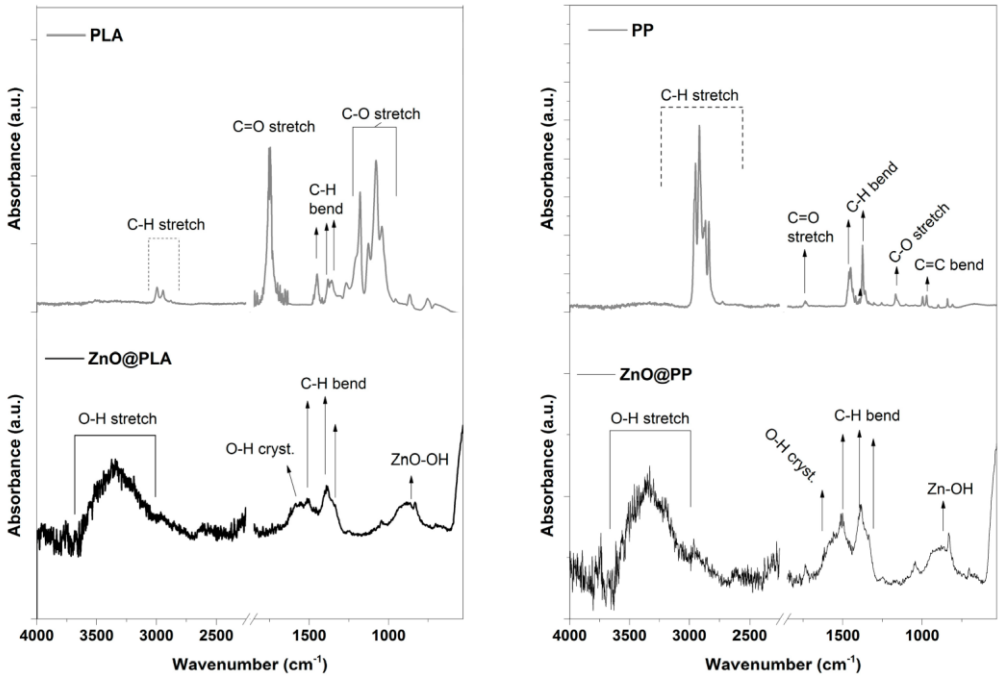

Figure 5. ATR-IR spectra of PLA and PP supports, with or without the presence of the ZnO coating.

3.2. Tensile Testing

The mechanical behaviour of PLA and PP polymers are analysed with and without the presence of the ZnO coating. The graphical representation of the mechanical properties are shown in Figure 6. In case of PLA and ZnO@PLA samples, no significant difference in the tensile strength, elongation at break, stiffness or Young's modulus ($p \geq 0.05$) are observed. Similar results are obtained for PP and ZnO@PP samples. This could be because the ZnO particles film is deposited on the polymer surface, which does not have any impact on the bulk polymer properties. However, various studies have shown a significant difference in mechanical properties when ZnO nanoparticles (NPs) are encapsulated into the polymer matrix [17,18,41–43].

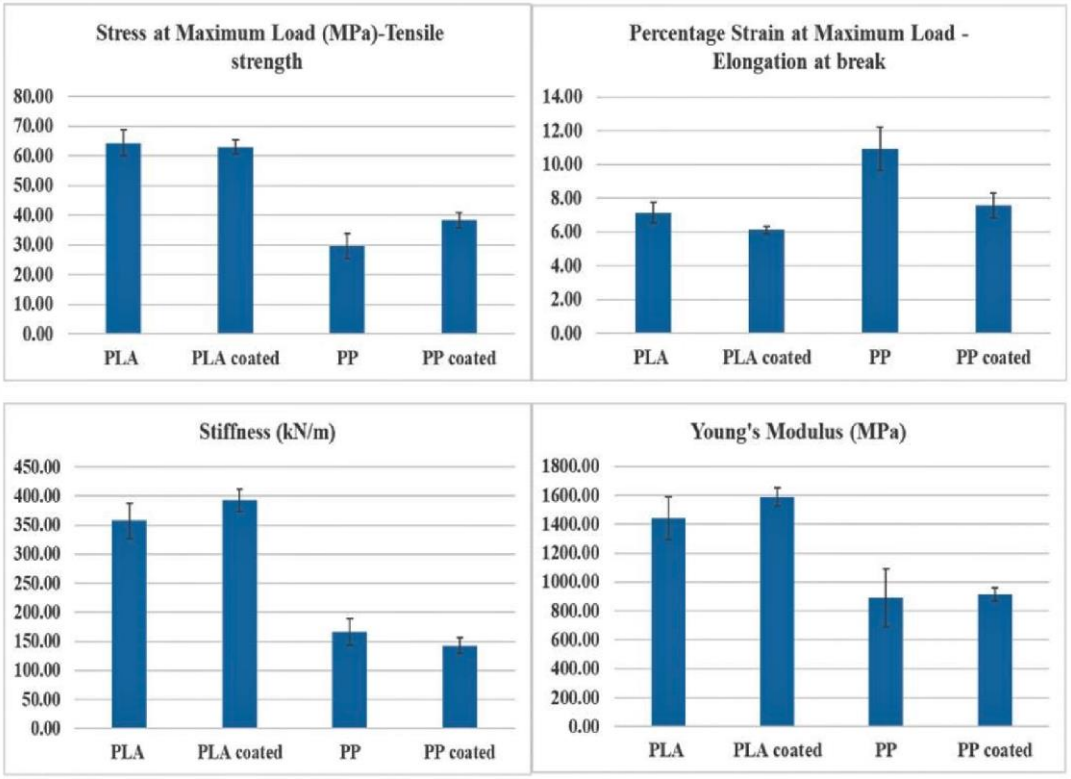

Figure 6. Graphical representation of the mechanical properties of the polymers with and without ZnO coating. There is no significant difference between the coated samples (ZnO@PLA ZnO@PP) and their uncoated counterpart samples.

3.3. Surface Wettability

The surface wettability properties of all the coated and noncoated samples are shown in Figure 7. It was observed that there is a significant decrease in the contact angle of ZnO@PLA and ZnO@PP samples ($p = 1 \times 10^{-3}$) when compared to bare PLA and PP substrates. The photomicrographs of the uncoated PLA surface has a contact angle of 66°, whereas a contact angle of 24.07° is achieved for the sample ZnO@PLA. The images of the uncoated PP has a contact angle of 90.62°, and ZnO@PP has a contact angle of 44.55°. With PP being hydrophobic and PLA being relatively hydrophobic, these results indicate that the presence of the ZnO coating increased the hydrophilicity of the surface. A similar reduction in contact angle values was observed when PLA films were surface-modified and bulk-modified by plasma polymerization/sputtering technique, where glycerol and ethylene glycol were used as additives [15]. In another work, PP film was treated by plasma discharge in order to enhance the surface wettability of PP and improve the adhesion of ZnO NPs [27].

3.4. Differential Scanning Calorimetry (DSC)

The thermal characteristics of the samples were analysed by DSC. The thermographs of the PLA, ZnO@PLA, PP and ZnO@PP samples are as shown in Figure 8. From the analysis of the thermographs, there is no evident difference between the coated and noncoated samples. However, in a study by Pantani et al. [18] the cold crystallization and melting temperature increased as ZnO NPs were incorporated into the PLA matrix by twin screw extrusion [18]. This confirms that the surface ZnO coating of our work did not affect the bulk properties of the considered polymers, corroborating with the tensile test results.

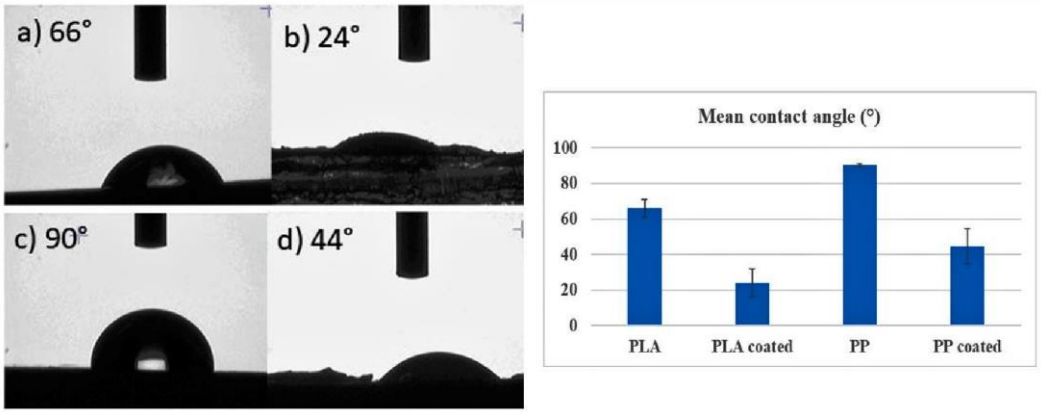

Figure 7. Surface wettability properties of the polymers with and without ZnO coating. With a *p*-value of 0.001, there is a significant decrease in the contact angle of ZnO@PLA and ZnO@PP when compared to the uncoated PLA and PP films. Water droplet on the surface of (**a**) PLA film, (**b**) ZnO@PLA, (**c**) PP film, and (**d**) ZnO@PP.

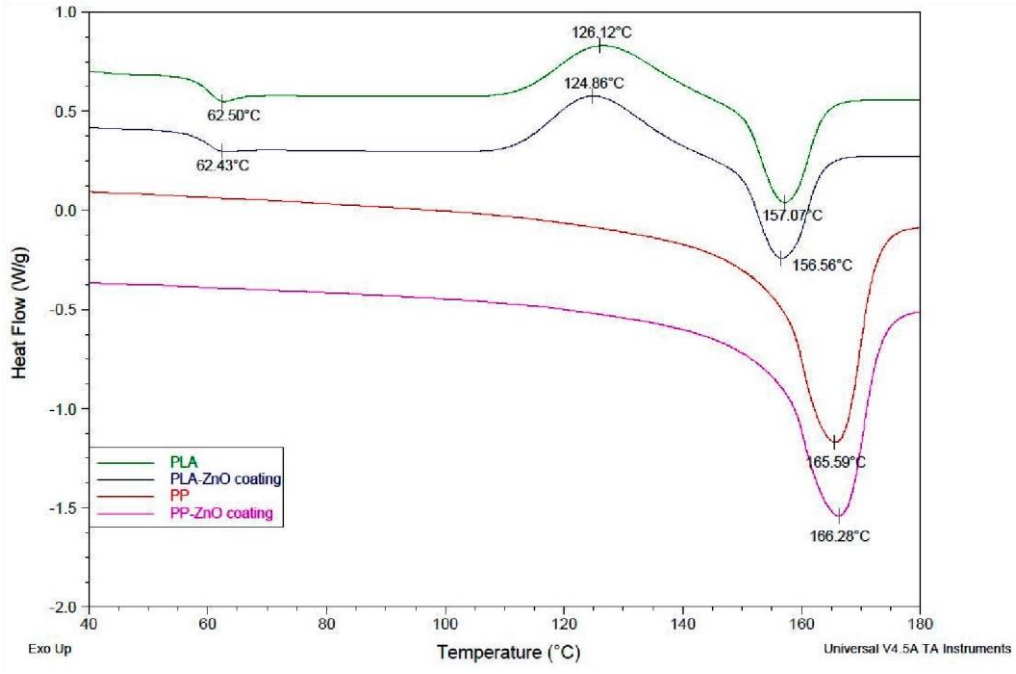

.

Figure 8. DSC thermographs of the PLA, ZnO@PLA, PP and ZnO@PP coated samples. No significant difference was observed between the coated and uncoated samples considering a *p*-value < 0.05.

3.5. Evaluation of the Biodegradation Properties in Biological Fluids

3.5.1. Simulated Body Fluid (SBF)

ZnO@PLA and ZnO@PP samples were immersed in simulated body fluid (SBF) solution to test the adhesion of the ZnO coating to the polymer substrate. Figure 9 shows the pictures of ZnO@PLA and ZnO@PP samples after immersion in this solution for up to seven days. In the case of the PP substrate, the ZnO coating showed a considerable detachment after 2 h in contact with the SBF solution. However, no major changes occurred from 2 h to seven days. Interestingly, no significant alterations were observed for ZnO@PLA samples over time, which indicates a higher adhesion of the ZnO coating to the PLA substrate in comparison to the PP one and well agrees with the results shown in Figure 1.

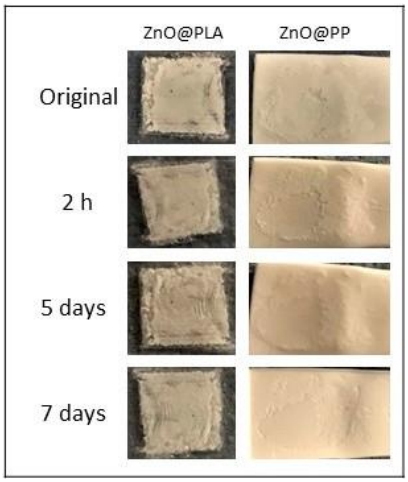

Figure 9. ZnO@PLA and ZnO@PP samples after different time intervals in SBF solution.

FESEM images reported in Figure 10a,c highlights that no visible changes in the morphology of the samples are present. The ZnO coating did not detach completely from the polymer supports and the flower-like ZnO microparticles preserve the original morphology. The presence of the ZnO coating is further confirmed by EDX measurements (Figure 10b,d). The compositional analyses also reveal the presence of P, Ca, Cl and Na, which are due to the prolonged contact of the samples with SBF solution. In particular, the abundance of Ca (around 1.9 at.%) and P (around 2–3 at.%) with respect to the other elements suggests the formation/precipitation of calcium phosphate compounds. This aspect is further supported by the IR spectroscopy results discussed in the following.

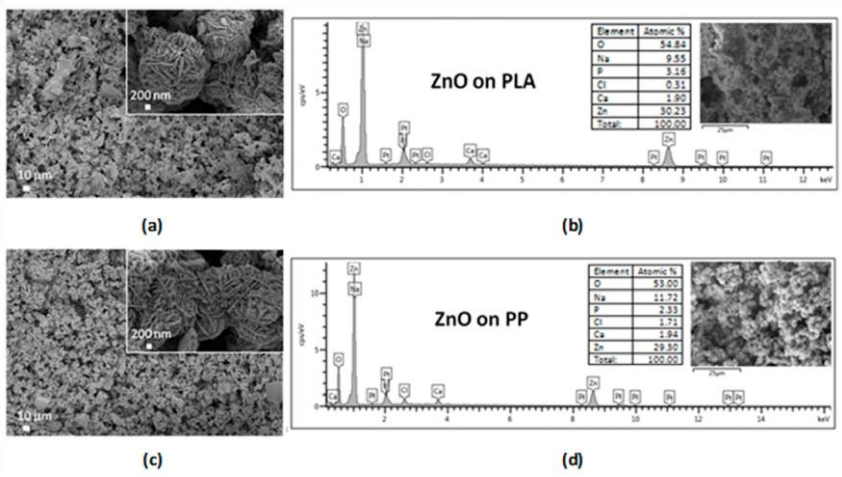

Figure 10. ZnO-coated PLA and PP supports soaked in SBF for 14 days: (**a**,**c**) FESEM images and (**b**,**d**) EDX spectra.

Figure 11 shows the IR spectra acquired after soaking all the sample typologies in SBF for 14 days. Panels a and b refer to the polymer substrates (PP and PLA) while panels c and d show the IR spectra acquired on ZnO@PLA and ZnO@PP samples, respectively. Considering the PLA and PP substrates, no changes are visible when compared to nonsoaked samples. This is likely related to the hydrophobic nature of the uncoated substrates. However, in the presence of the ZnO coating, a relatively intense band in the range 1100–1000 cm^{-1} is observed due to the phosphate (PO_4^{3-}) vibration modes (Figure 11c,d). This is due to the interaction between the ZnO surface and phosphate groups present in SBF solution, which favours the formation of zinc phosphate and calcium phosphate compounds [44,45]. This aspect was also underlined by the corresponding EDX results of Figure 10. This indicates that the presence of the ZnO coating would allow for a more reactive surface able to induce the precipitation of an apatite-like functional layer. In general, an increase of the OH band intensity in the range 3500–3000 cm^{-1} is observed, irrespectively of the presence of ZnO and due to the adsorption of water after the prolonged contact with SBF solution.

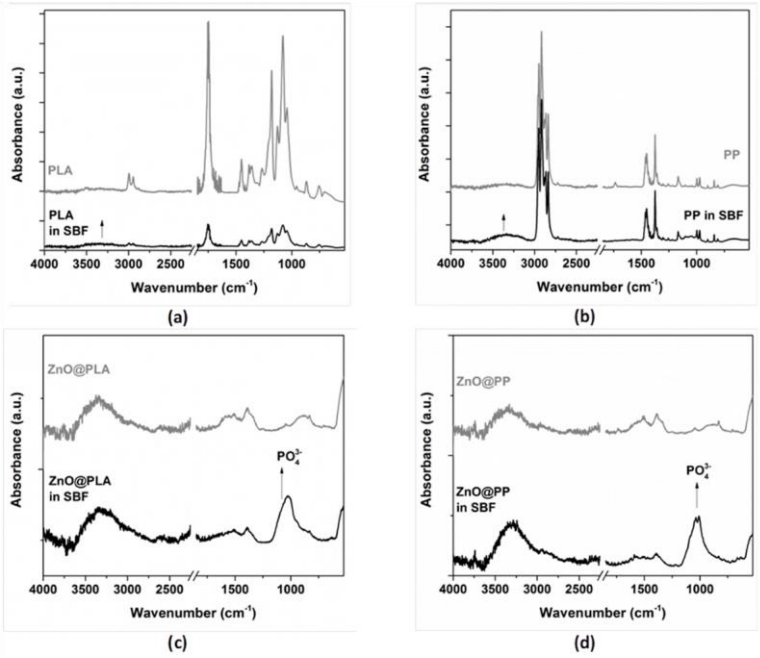

Figure 11. ATR-IR spectra of the samples after soaking in SBF for 14 days: (**a**) only PLA; (**b**) only PP; (**c**) ZnO@PLA; (**d**) ZnO@PP.

The XRD patterns of Figure 12a still show the presence of diffraction peaks belonging to wurtzite ZnO phase (indicated by arrows) and further witness the presence of the ZnO coating at the end of the biodegradation experiment in SBF.

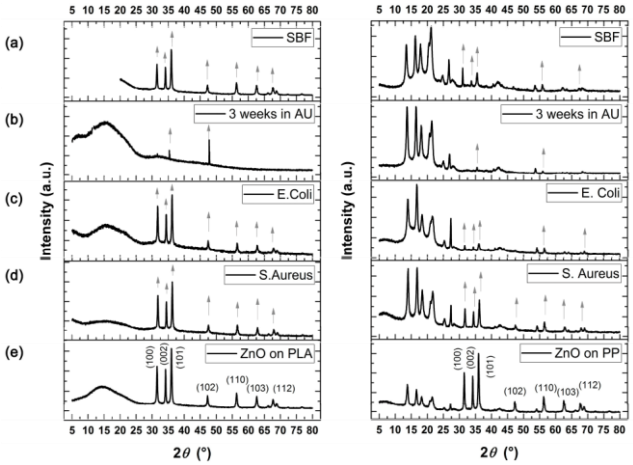

Figure 12. XRD pattern of samples ZnO@PLA and ZnO@PP: (**a**) after soaking in simulated body fluid solution for 14 days; (**b**) after immersion in artificial urine for 21 days; (**c**,**d**) at the end of the antimicrobial tests. XRD pattern of ZnO@PP and ZnO@PLA samples are also shown as reference in panel (**e**). Arrows indicate reflections coming from wurtzite ZnO phase.

3.5.2. Artificial Urine

When testing the coated polymer samples in artificial urine, a strikingly different behaviour was observed if compared to the SBF solution. As seen in Figure 13, ZnO@PLA samples show a considerable detachment of the ZnO layer after two

days of immersion in artificial urine and a complete dissolution was observed after five days. Although the ZnO coatings on the PP supports are less uniform than on PLA, a slower dissolution was noticed when in contact with artificial urine. This might be related to the higher hydrophobicity of PP coated films that interact less with the solution in comparison to PLA films, as seen from the surface wettability analysis discussed in Section 3.3. Independently of the polymeric support, it can be noticed that the ZnO coating dissolved and/or detached faster in artificial urine than in SBF solution. This interesting feature can actually witness the fair tunability of our coated polymers, which selectively react differently upon the medium where they are immersed.

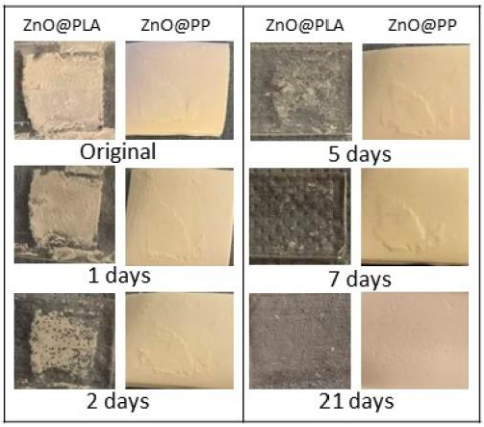

Figure 13. ZnO@PLA and ZnO@PP samples after different time intervals in artificial urine solution.

The biodegradation behaviour of ZnO@PLA and ZnO@PP samples was also evaluated in artificial urine solution for long time periods (21 days). Similarly, uncoated PLA and PP substrates were tested in the same experimental conditions, in order to evaluate any ability of ZnO to prevent the formation of encrustations in an artificial urine environment. If the uncoated PP and PLA supports are considered, the presence of precipitates with different morphologies and shapes can be observed (Figures 14 and 15): tabular-acicular surfaces, sheetlike, globular and spongelike structures are visible. In the case of the PP support (Figure 14), various type of encrustations can be found and in a more abundant way with respect to the PLA support (Figure 15).

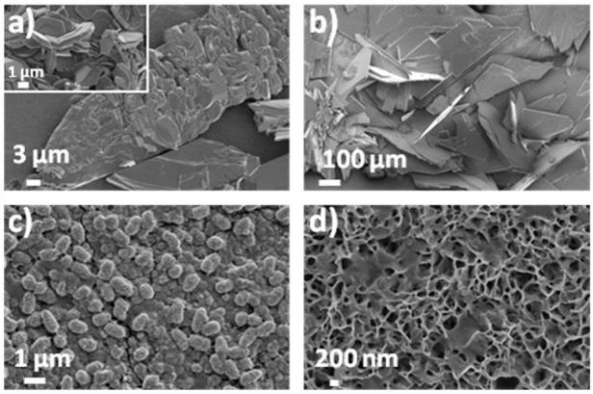

Figure 14. (**a**,**b**) FESEM images showing the formation of calcium phosphates precipitates and encrustations after immersion of PP support into artificial urine for 21 days. (**c**,**d**) Globular-shaped and spongelike morphology of hydroxyapatite precipitates.

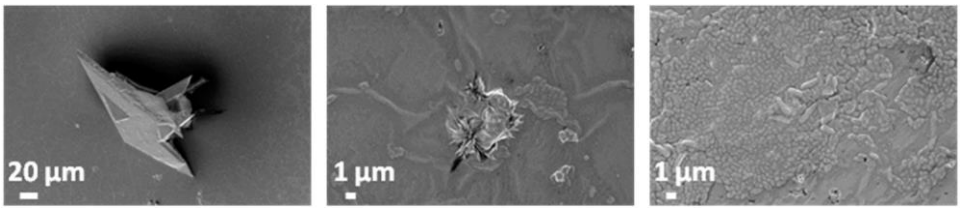

Figure 15. FESEM images of PLA support after immersion in artificial urine for 21 days.

By considering the morphology and the corresponding chemical composition summarized in Figures 16 and 17, calcium phosphate precipitates (Ca/P ratio around 0.9–1) are found for both the samples' types (Figure 14a,b and Figure 15) corresponding to brushite ($CaHPO_4 \cdot 2H_2O$) or hydroxyapatite $Ca_{10}(PO_4)_6(OH)_2$, the latter showing globular-shaped and sponge like morphology (Figure 14c,d) are detected only in the case of the PP support. For both PP and PLA supports, some traces of sodium chloride and potassium chloride are also present and due to the contact of the samples with artificial urine solution, while the presence of struvite $(NH_4)MgPO_4 \cdot 6H_2O$, corresponding to the crystalline prismatic deposits is also recognized (see the central Table in Figure 16). In Figure 15 (left panel), corresponding to the surface of the PLA sample, the typical crystalline structure of calcium oxalate $Ca(COO)_2$ is observed.

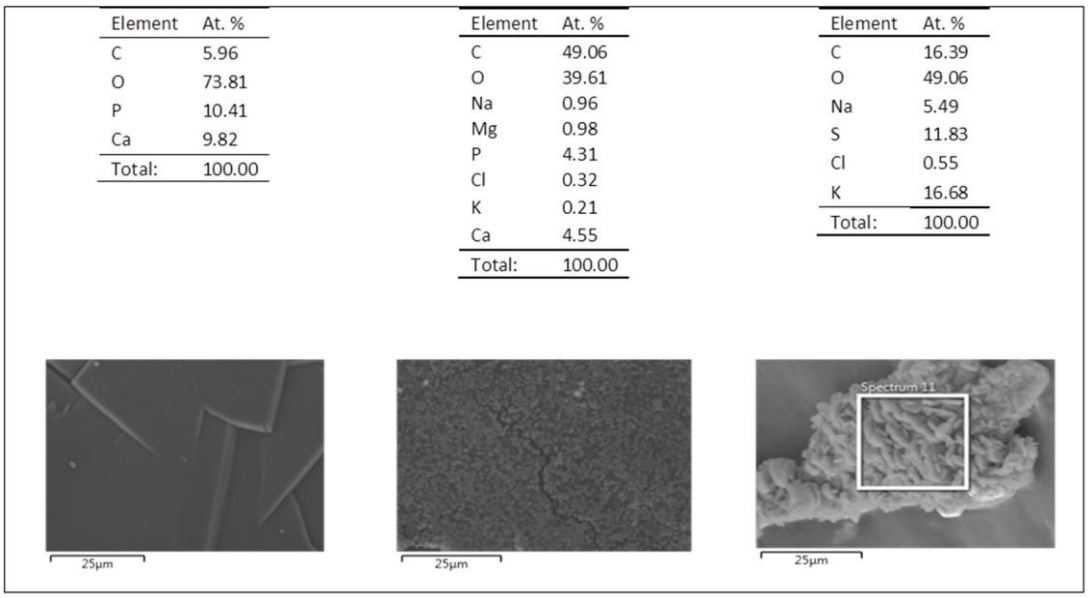

Figure 16. Chemical composition of three different precipitates formed at the surface of PP support after immersion in artificial urine for 21 days.

Differently from the previous case of SBF, the immersion of the ZnO-coated polymer substrates in artificial urine for 21 days negatively affected the ZnO morphology. A strong dissolution of the ZnO coating was observed through the corresponding FESEM images of Figures 18 and 19. There is an absence of the typical flowerlike microparticle morphology previously shown in Figure 1. The ZnO

degradation is further supported by EDX analyses reported in Figures 20 and 21, showing small Zn traces in the case of sample ZnO@PP, while the amount of Zn is negligible for sample ZnO@PLA. Despite the degradation of the ZnO coating, a reduced amount of precipitates is observed for the ZnO@PLA support (Figure 19) with respect to the uncoated PLA counterpart. On the other hand, the presence of ZnO seems to not prevent the formation of encrustations in the case of the PP substrate (Figure 18), which could be related to the low level of ZnO coated onto the surface as observed in EDX. In particular, globular structures (peculiar of hydroxyapatite $Ca_{10}(PO_4)_6(OH)_2$), prismatic crystals of struvite ($(NH_4)MgPO_4 \cdot 6H_2O$) or brushite ($CaHPO_4 \cdot 2H_2O$) and layered sheet like structures are observed on ZnO@PP sample, while similar prismatic needlelike structures of struvite or brushite are found at the surface of sample ZnO@PLA. Furthermore, and similar to the previous case, the presence of sodium chloride (NaCl) and potassium chloride (KCl) is noticed also for the ZnO-coated polymers and due to the prolonged interaction of the samples with artificial urine solution.

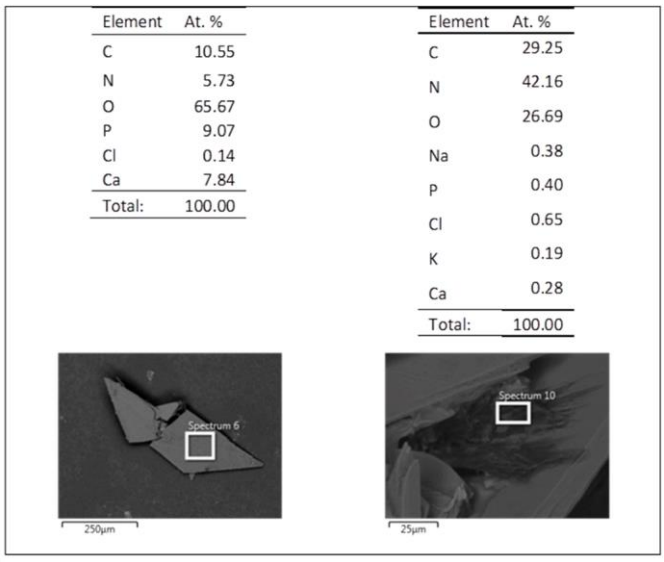

Figure 17. Chemical composition of three different precipitates formed at the surface of PLA support after immersion in artificial urine for 21 days.

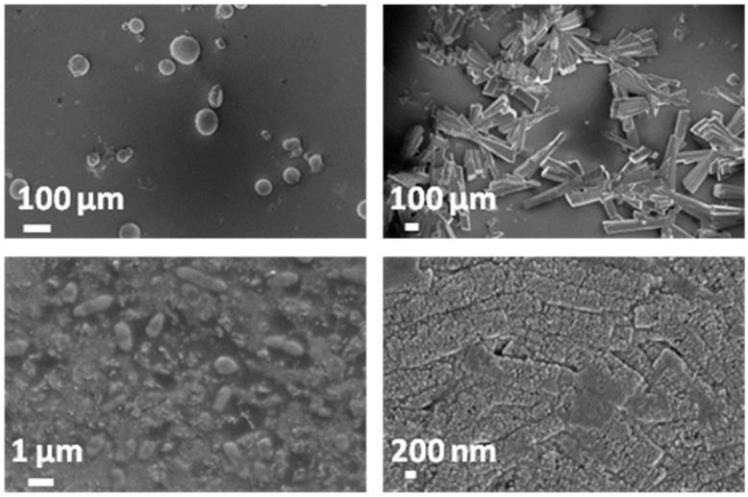

Figure 18. FESEM images of ZnO@PP sample after 21 days in artificial urine.

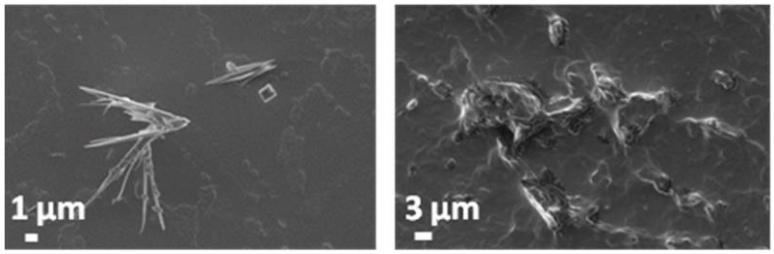

Figure 19. FESEM of ZnO@PLA sample after 21 days in artificial urine.

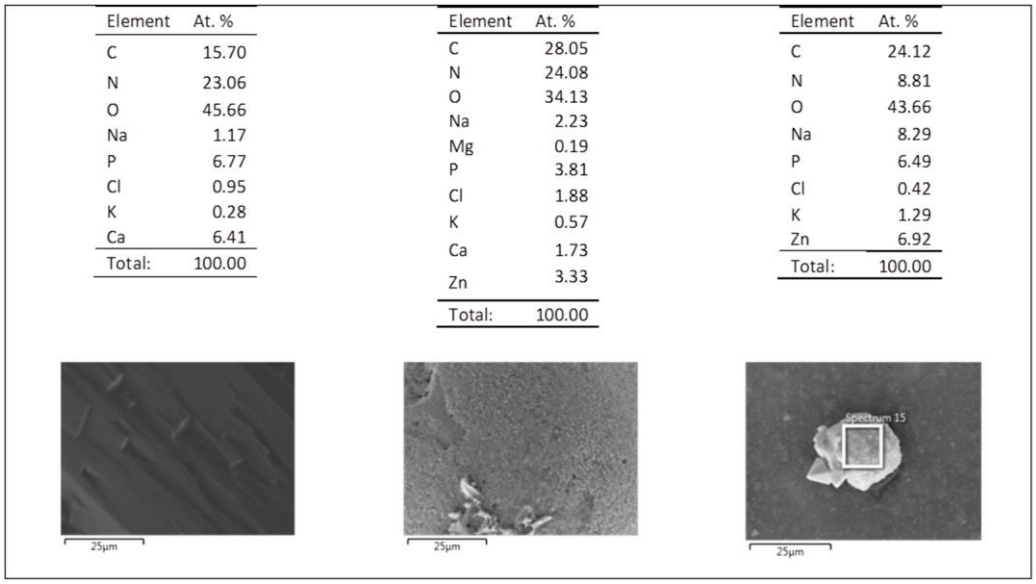

Element	At. %
C	15.70
N	23.06
O	45.66
Na	1.17
P	6.77
Cl	0.95
K	0.28
Ca	6.41
Total:	100.00

Element	At. %
C	28.05
N	24.08
O	34.13
Na	2.23
Mg	0.19
P	3.81
Cl	1.88
K	0.57
Ca	1.73
Zn	3.33
Total:	100.00

Element	At. %
C	24.12
N	8.81
O	43.66
Na	8.29
P	6.49
Cl	0.42
K	1.29
Zn	6.92
Total:	100.00

Figure 20. Chemical composition of three different precipitates formed at the surface of ZnO@PP sample after immersion in artificial urine for 21 days.

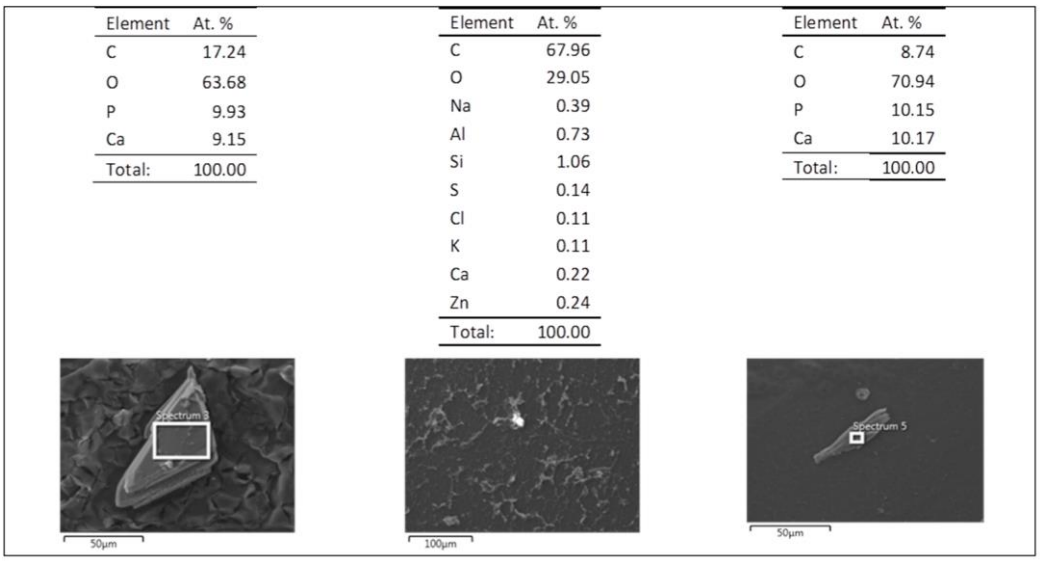

Figure 21. Chemical composition of three different precipitates formed at the surface of ZnO@PLA sample after immersion in artificial urine for 21 days.

Figure 12b shows the XRD pattern of ZnO@PLA and ZnO@PP substrates after the immersion in artificial urine for 21 days. In this case, the diffraction contribution coming from the ZnO microparticle film mostly disappear, with the (101) and (110) diffraction peaks being only slightly detectable. This aspect confirms the partial rather than complete degradation of the ZnO coating at the end of the experiment, as observed from FESEM analyses described previously.

ATR-IR analyses have been performed after soaking the sample in artificial urine for 21 days (Figure 22). Apart from the peaks characteristics of the polymer substrates, a strong change in the shape of the IR absorption band of 3500–3000 cm^{-1} region is visible, and independent of the kind of polymer. In all the samples except ZnO@PLA, the presence of three distinct IR bands at 3218, 3331 and 3440 cm^{-1} is noticed and confirms the formation of precipitates (mainly calcium phosphate compounds), as mentioned previously. These are due to stretching modes of vibration of water of crystallization as also to the N–H secondary stretching mode derived from urea. Additional IR modes due to water of crystallization and N–H bending mode in the range 1670–1610 cm^{-1} are detected as well. Such additional IR bands are barely detectable in sample ZnO@PLA and it confirms a reduced formation of encrustations and precipitates, as previously observed from the corresponding FESEM analyses. On the contrary, sample ZnO@PP shows additional IR bands with respect to the nonsoaked PP sample: the phosphate band in the 1100–1040 cm^{-1} range and at 938 cm^{-1}, carbonate (CO_2^{3-}) bands in the range 1496–1434 cm^{-1} and stretching mode of P–OH at around 866 cm^{-1} [46].

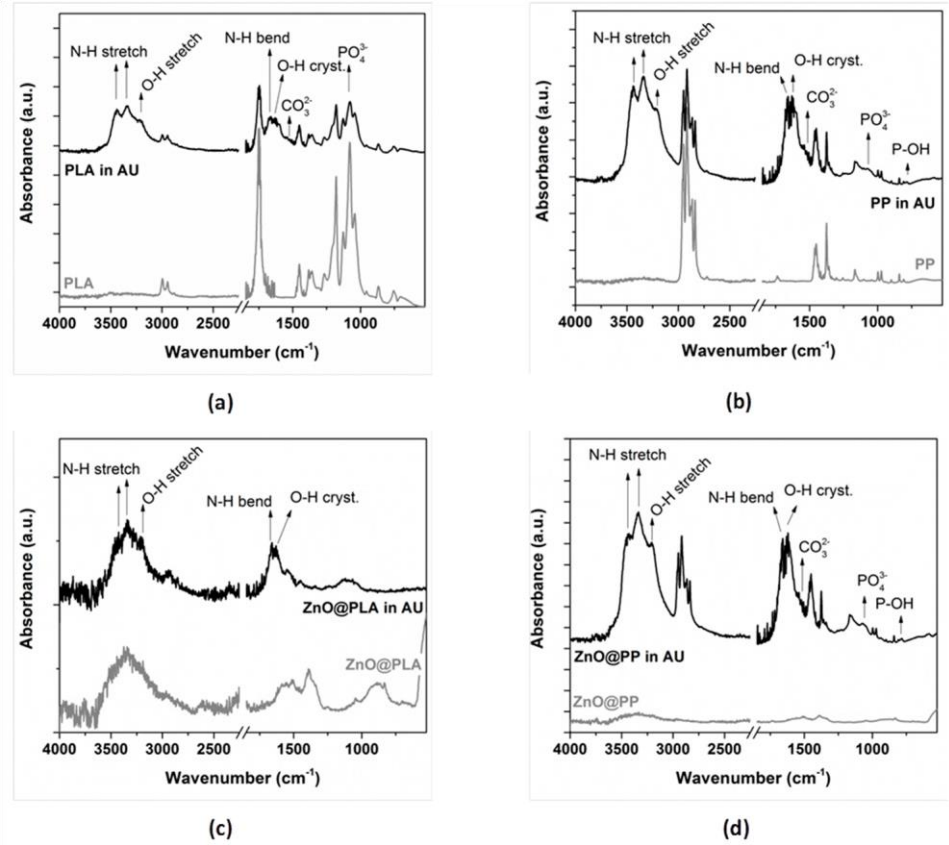

Figure 22. ATR-IR spectra of the samples after immersion in artificial urine for 21 days: (**a**) only PLA; (**b**) only PP; (**c**) ZnO@PLA; (**d**) ZnO@PP.

The strong degradation of the ZnO coating can be due to the acidic environment conditions of artificial urine, which induced ZnO dissolution. Actually, it is known that ZnO becomes more soluble as the pH of the solution decreases and dissolution increases significantly in pH values below 6.0 [47,48]. Thus, the different behaviours of the ZnO coating in both solutions and the faster dissolution of ZnO in artificial urine is probably related to its more acidic nature (pH 5.7) in comparison to the SBF solution (pH 7.45).

Another main issue related to urinary stents is the deposition of salts on the stent surface that can cause the blockage of liquid, inflammation and other complications [2,49]. In this study, encrustation was observed only after three weeks of immersion in artificial urine for ZnO-coated samples and two weeks for noncoated polymer supports. Hence, it can be concluded that the addition of the ZnO coating to both PLA and PP supports can be useful in preventing or at least delaying the deposition of encrustations.

3.6. Antimicrobial Tests

Bacteria cell viability was evaluated on a Gram-negative strain (*E. coli*) and a Gram-positive strain (*S. aureus*). The bacteria strains were incubated in the presence

of noncoated PLA and PP films, and ZnO-coated PLA and PP films. Figure 23 shows the average growth percentages of each strain when incubated with the coated and noncoated films, considering the positive control as the reference for 100% of cell viability, as it was incubated without the presence of any polymer. Cell viability shows a clear reduction when incubated in the presence of ZnO-coated films. In *E. coli*, incubation with noncoated PLA and PP reached 96% viability, while for the incubation with ZnO@PLA and ZnO@PP samples, the viability was reduced to 70% and 71% respectively. Similarly, *S. aureus* achieved 96% and 91% viability with PLA and PP, respectively, but it reached only 67% with ZnO@PLA and 66% with ZnO@PP. With a 95% confidence interval, it was concluded that there is an important difference in cell viability mean values between the ZnO-coated and noncoated samples, implicating successful antimicrobial activity exhibited by the ZnO microparticle film. In the same confidence interval, mean values for cell viability of *E. coli* and *S. aureus* showed no significant difference, suggesting that differences in cell wall structure did not affect the action mechanism of the ZnO particles in this case. Similar results with successful antimicrobial activity of polymer films with ZnO against *E. coli* and *S. aureus* strains were obtained in various studies [50,51].

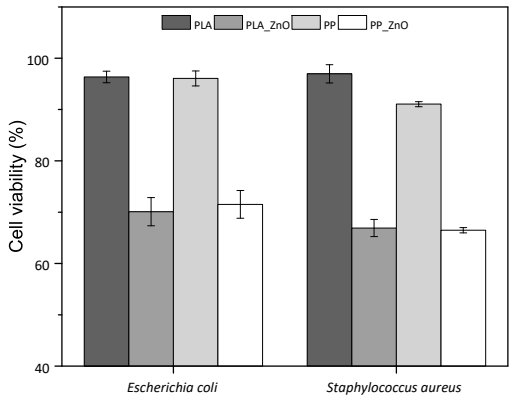

Figure 23. Bacteria cell viability after 24 h treatment with coated and noncoated PLA and PP films. There is no significant difference in the antimicrobial activity between *E. coli* and *S. aureus* ($p < 0.05$).

Figure 24 shows the FESEM images of ZnO@PLA and ZnO@PP supports after the antimicrobial assays performed by culturing *E. coli* and *S. aureus* bacteria on both the samples typologies. In this case, the ZnO coating was still present, as further indicated by the presence of diffraction peaks belonging to ZnO (Figure 12c,d) as well as by the EDX compositional analyses reported in Table 1, which confirm the detection of Zn element in high amounts (around 15 at.%) for both PLA and PP supports. However, the morphology of the microparticles has changed from a flower-like structure to a more compact and round-shaped one. EDX data shown in Table 1 also underline the presence of other elements (Na, Ca, P, etc.) due to the interaction of the considered samples with the medium for bacteria culture.

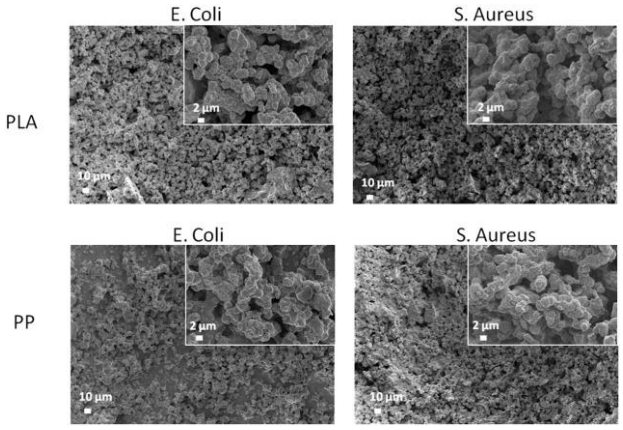

Figure 24. FESEM images of ZnO-coated PLA (top panels) and PP (bottom panels) samples after the antimicrobial assays performed by culturing *E. coli* (left panels) and *S. aureus* bacteria (right panels).

Table1. Chemical composition at the surface of ZnO-coated PLA and PP supports after antimicrobial assays.

Element	*E. coli*		*S. aureus*	
	PLA/ZnO, at.%	**PP/ZnO, at.%**	**PLA/ZnO, at.%**	**PP/ZnO, at.%**
C	28.89	51.08	35.93	29.94
N	4.33	–	–	4.70
O	38.17	30.23	37.49	38.85
Na	7.69	4.97	7.21	7.36
P	3.17	2.12	2.86	2.75
Cl	1.14	0.69	1.26	0.79
K	0.92	0.91	0.92	0.74
S	–	0.13	–	–
Ca	–	0.35	–	–
Zn	15.69	9.52	14.33	14.87
Total.	100.00	100.00	100.00	100.00

4. Conclusions

ZnO coatings were deposited on PLA and PP films by the doctor-blade technique. The ZnO functional layer was obtained starting from high-surface-area, flower-like ZnO microparticles prepared following a simple hydrothermal route. The resulting ZnO@PLA and ZnO@PP samples were studied from the morphological, compositional and structural standpoint. The biodegradation behaviour was investigated by considering the interaction of the considered samples with simulated body fluid and artificial urine solution for prolonged soaking times. Finally, the antimicrobial behaviour was studied as well against *S. aureus* and *E. coli*. It turned

out that adhesion of the ZnO coating was better on PLA supports than on PP. The addition of the ZnO functional layer did not negatively influence the mechanical and thermal properties of both PLA and PP supports. Meanwhile, the surface wetting properties of the polymers changed after ZnO deposition and moved from the hydrophobic to the hydrophilic range. When both the samples typologies were soaked into SBF, ZnO dissolution was only partial and independent of the polymer substrate type. It was also found that both PP and PLA substrates prevent the precipitation/formation of phosphate compounds. The presence of the ZnO coating, in contrast, promoted the formation of phosphate compounds. On the contrary, a strong degradation of the ZnO functional coating was observed when the samples were soaked in artificial urine solution. After 21 days, all characterization results pointed out a complete degradation of the ZnO layer due to the acidic pH conditions of the artificial urine environment. The formation of precipitates/encrustations was observed mostly for PP and ZnO@PP, while it was limited on PLA and ZnO@PLA. The composition of the formed compounds was confirmed by compositional analysis and IR spectroscopy. The antimicrobial tests highlighted a good antibacterial activity against both the considered families of bacteria only in the presence of the functional ZnO coating. It is also worth mentioning that the ZnO coating was not affected by the medium for bacteria culture as it was still present after the bacteria culture.

Author Contributions: Conceptualization, V.C. and D.M.D.; investigation, C.V., M.L., M.B., E.L., and L.L.; data curation, C.V., M.L., and M.B.; writing—original draft preparation, C.V. and M.L.; writing—review and editing, all authors; supervision, M.L., V.C., and D.M.D. All authors have read and agreed to the published version of the manuscript.

Funding: This publication has emanated from research conducted with the financial support of Athlone Institute of Technology under the Presidents Seed Fund, Universidade de Caxias do Sul, grant number CAPES (PDSE -
88881.187620/2018-01) and European Network of Multidisciplinary Research to Improve the Urinary Stents (ENIUS) COST Action CA16217.

Conflicts of Interest: The authors declare no conflict of interest.

References

1. Lam, J.S.; Gupta, M. Update on ureteral stents. *Urology* **2004**, *64*, 9–15. [CrossRef] [PubMed]
2. Yang, L.; Whiteside, S.; Cadieux, P.A.; Denstedt, J.D. Ureteral stent technology: Drug-eluting stents and stent coatings. *Asian J. Urol.* **2015**, *2*, 194–201. [CrossRef] [PubMed]
3. Kim, H.-H.; Kim, K.-W.; Choi, Y.H.; Lee, S.B.; Baba, Y. Numerical analysis of urine flow with multiple sizes of double-j stents. *Appl. Sci.* **2020**, *10*, 4291. [CrossRef]
4. Abdelaziz, A.Y.; Fouda, W.B.; Mosharafa, A.A.; Abelrasoul, M.A.; Fayyad, A.; Fawzi, K. Forgotten ureteral stents: Risk factors, complications and management. *Afr. J. Urol.* **2018**, *24*, 28–33. [CrossRef]
5. Liu, S.; Luo, G.; Sun, B.; Lu, J.; Zu, Q.; Yang, S.; Zhang, X.; Dong, J. Early removal of double-j stents decreases urinary tract infections in living donor renal transplantation: A prospective, randomized clinical trial. *Transplant. Proc.* **2017**, *49*, 297–302. [CrossRef]
6. Ahallal, Y.; Khallouk, A.; Fassi, M.J.E.; Farih, M.H. Risk factor analysis and management of ureteral double-j stent complications. *Rev. Urol.* **2010**, *12*, e147–e151. [CrossRef]
7. Forbes, C.; Scotland, K.B.; Lange, D.; Chew, B.H. Innovations in ureteral stent technology. *Urol. Clin.* **2019**, *46*, 245–255. [CrossRef]

8. Singha, P.; Locklin, J.; Handa, H. A review of the recent advances in antimicrobial coatings for urinary catheters. *Acta Biomater.* **2017**, *50*, 20–40. [CrossRef]
9. Cauda, F.; Cauda, V.; Fiori, C.; Onida, B.; Garrone, E. Heparin coating on ureteral double j stents prevents encrustations: An in vivo case study. *J. Endourol.* **2008**, *22*, 465–472. [CrossRef]
10. Mosayyebi, A.; Vijayakumar, A.; Yue, Q.Y.; Bres-Niewada, E.; Manes, C.; Carugo, D.; Somani, B.K. Engineering solutions to ureteral stents: Material, coating and design. *Cent. Eur. J. Urol.* **2017**, *70*, 270–274. [CrossRef]
11. Cauda, F.; Cauda, V.; Fiori, C. Coated ureteral stent. In *Biomaterials and Tissue Engineering in Urology*; Denstedt, J., Atala, A., Eds.; Woodhead Publishing Ltd.: London, UK, 2009; pp. 134–156.
12. Laurenti, M.; Grochowicz, M.; Dragoni, E.; Carofiglio, M.; Limongi, T.; Cauda, V. Biodegradable and drug-eluting inorganic composites based on mesoporous zinc oxide for urinary stent applications. *Materials* **2020**, *13*, 3821. [CrossRef] [PubMed]
13. Dave, R.N.; Joshi, H.M.; Venugopalan, V.P. Novel biocatalytic polymer-based antimicrobial coatings as potential ureteral biomaterial: Preparation and in vitro performance evaluation. *Antimicrob. Agents Chemother.* **2011**, *55*, 845–853. [CrossRef] [PubMed]
14. Venkatesh, C.; Clear, O.; Major, I.; Lyons, J.G.; Devine, D.M. Faster release of lumen-loaded drugs than matrix-loadedequivalentinpolylacticacid/halloysitenanotube. *Materials***2019**, *12*, 1830. [CrossRef][PubMed]
15. Turalija, M.; Bischof, S.; Budimir, A.; Gaan, S. Antimicrobial PLA films from environment friendly additives. *Compos. Part B Eng.* **2016**, *102*, 94–99. [CrossRef]
16. Zhang, H.; Hortal, M.; Jorda Beneyto, M.; Rosa, E.; Lara, M.; Lorente, I. ZnO-PLA nanocomposite coated paper for antimicrobial packaging application. *LWT-Food Sci. Technol.* **2016**, *78*, 250–257. [CrossRef]
17. De Silva, R.T.; Pasbakhsh, P.; Lee, S.M.; Kit, A.Y. Zno deposited/encapsulated halloysite–poly(lactic acid) (PLA) nanocomposites for high performance packaging films with improved mechanical and antimicrobial properties. *Appl. Clay Sci.* **2015**, *111*, 10–20. [CrossRef]
18. Pantani, R.; Gorrasi, G.; Vigliotta, G.; Murariu, M.; Dubois, P. PLA-ZnO nanocomposite films: Water vapor barrier properties and specific end-use characteristics. *Eur. Polym. J.* **2013**, *49*, 3471–3482. [CrossRef]
19. Marra, A.; Silvestre, C.; Duraccio, D.; Cimmino, S. Polylactic acid/zinc oxide biocomposite films for food packaging application. *Int. J. Biol. Macromol.* **2016**, *88*, 254–262. [CrossRef]
20. Anžlovar, A.; Kržan, A.; Žagar, E. Degradation of PLA/ZnO and PHBV/ZnO composites prepared by melt processing. *Arab. J. Chem.* **2018**, *11*, 343–352. [CrossRef]
21. Maddah, H.A. Polypropylene as a promising plastic: A review. *Am. J. Polym. Sci.* **2016**, *6*, 1–11. [CrossRef]
22. Okuyucu, S.; Gorur, H.; Oksuz, H.; Akoglu, E. Endoscopic dacryocystorhinostomy with silicone, polypropylene, and t-tube stents; randomized controlled trial of efficacy and safety. *Am. J. Rhinol. Allergy* **2015**, *29*, 63–68. [CrossRef] [PubMed]
23. Viswanatha, B.; Vijayashree, M.S. Silicone stenting and polypropylene stenting in endoscopic dacryocystorhinostomy: A prospective comparative study. *Res. Otolaryngol.* **2015**, *4*, 49–53. [CrossRef]
24. Mitsuoka,M.; Hayashi,A.; Takamori,S.; Tayama,K.; Shirouzu,K.Experimentalstudyofthehistocompatibility of covered expandable metallic stents in the trachea. *Chest* **1998**, *114*, 110–114. [CrossRef] [PubMed]

25. Yuan, T.; Zheng, R.; Yu, J.; Edmonds, L.; Wu, W.; Cao, J.; Gao, F.; Zhu, Y.; Cheng, Y.; Cui, W. Fabrication and evaluation of polymer-based esophageal stents for benign esophagus stricture insertion. *RSC Adv.* **2016**, *6*, 16891–16898. [CrossRef]
26. Zhao, H.; Li, R.K.Y. A study on the photo-degradation of zinc oxide (ZnO) filled polypropylene nanocomposites. *Polymer* **2006**, *47*, 3207–3217. [CrossRef]
27. Jakubiak, S.; Tomaszewska, J.; Jackiewicz, A.; Michalski, J.; Kurzydłowski, K.J. Polypropylene–zinc oxide nanorod hybrid material for applications in separation processes. *Chem. Process Eng.* **2016**, *37*, 393–403. [CrossRef]
28. Bojarska, M.; Nowak, B.; Skowron´ski, J.; Pia¸tkiewicz, W.; Gradon´, L. Growth of ZnO nanowires on polypropylene membrane surface—characterization and reactivity. *Appl. Surf. Sci.* **2017**, *391*, 457–467. [CrossRef]
29. Mirzaei, H.; Darroudi, M. Zinc oxide nanoparticles: Biological synthesis and biomedical applications. *Ceram. Int.* **2017**, *43*, 907–914. [CrossRef]
30. Garino, N.; Sanvitale, P.; Dumontel, B.; Laurenti, M.; Colilla, M.; Izquierdo-Barba, I.; Cauda, V.; Vallet-Regì, M. Zinc oxide nanocrystals as a nanoantibiotic and osteoinductive agent. *RSC Adv.* **2019**, *9*, 11312–11321. [CrossRef]
31. Król, A.; Pomastowski, P.; Rafin´ska, K.; Railean-Plugaru, V.; Buszewski, B. Zinc oxide nanoparticles: Synthesis, antiseptic activity and toxicity mechanism. *Adv. Colloid Interface Sci.* **2017**, *249*, 37–52. [CrossRef]
32. Pasquet, J.; Chevalier, Y.; Pelletier, J.; Couval, E.; Bouvier, D.; Bolzinger, M.-A. The contribution of zinc ions to the antimicrobial activity of zinc oxide. *Colloids Surf. A Physicochem. Eng. Asp.* **2014**, *457*, 263–274. [CrossRef]
33. Dimapilis, E.A.S.; Hsu, C.-S.; Mendoza, R.M.O.; Lu, M.-C. Zinc oxide nanoparticles for water disinfection. *Sustain. Environ. Res.* **2018**, *28*, 47–56. [CrossRef]
34. Racca, L.; Canta, M.; Dumontel, B.; Ancona, A.; Limongi, T.; Garino, N.; Laurenti, M.; Canavese, G.; Cauda, V. Zinc oxide nanostructures in biomedicine. In *Smart Nanoparticles for Biomedicine*; Ciofani, G., Ed.; Elsevier: Amsterdam, The Netherlands, 2018; pp. 171–187.
35. Pugliese, D.; Bella, F.; Cauda, V.; Lamberti, A.; Sacco, A.; Tresso, E.; Bianco, S. A chemometric approach for the sensitization procedure of ZnO flowerlike microstructures for dye-sensitized solar cells. *ACS Appl. Mater. Interfaces* **2013**, *5*, 11288–11295. [CrossRef] [PubMed]
36. Cauda, V.; Stassi, S.; Lamberti, A.; Morello, M.; Fabrizio Pirri, C.; Canavese, G. Leveraging ZnO morphologies in piezoelectric composites for mechanical energy harvesting. *Nano Energy* **2015**, *18*, 212–221. [CrossRef]
37. Shin, J.; Liu, X.; Chikthimmah, N.; Lee, Y.S. Polymer surface modification using uv treatment for attachment of natamycin and the potential applications for conventional food cling wrap (ldpe). *Appl. Surf. Sci.* **2016**, *386*, 276–284. [CrossRef]
38. Socrates, G. *Infrared and Raman Characteristic Group Frequencies: Tables and Charts*; John Wiley & Sons: Chichester, UK, 2004.
39. Kokubo, T.; Takadama, H. How useful is SBF in predicting in vivo bone bioactivity? *Biomaterials* **2006**, *27*, 2907–2915. [CrossRef]
40. Sarangapani, S.; Cavedon, K.; Gage, D. An improved model for bacterial encrustation studies. *J. Biomed. Mater. Res.* **1995**, *29*, 1185–1191. [CrossRef]
41. Kruenate, J.; Tongpool, R.; Panyathanmaporn, T.; Kongrat, P. Optical and mechanical properties of polypropylene modified by metal oxides. *Surf. Interface Anal.* **2004**, *36*, 1044–1047. [CrossRef]
42. Jayaramudu, J.; Das, K.; Sonakshi, M.; Siva Mohan Reddy, G.; Aderibigbe, B.; Sadiku, R.; Sinha Ray, S.

Structure and properties of highly toughened biodegradable polylactide/zno biocomposite films. *Int. J. Biol. Macromol.* **2014**, *64*, 428–434. [CrossRef]

43. Tang, Z.; Fan, F.; Chu, Z.; Fan, C.; Qin, Y. Barrier properties and characterizations of poly(lactic acid)/ZnO nanocomposites. *Molecules* **2020**, *25*, 1310. [CrossRef]
44. Laurenti, M.; Lamberti, A.; Genchi, G.G.; Roppolo, I.; Canavese, G.; Vitale-Brovarone, C.; Ciofani, G.;
    Cauda, V. Graphene oxide finely tunes the bioactivity and drug delivery of mesoporous ZnO scaffolds. *ACS Appl. Mater. Interfaces* **2019**, *11*, 449–456. [CrossRef] [PubMed]
45. Laurenti, M.; Cauda, V. Gentamicin-releasing mesoporous ZnO structures. *Materials (Basel)* **2018**, *11*, 314. [CrossRef] [PubMed]
46. Salma, K.; Borodajenko, N.; Plata, A.; Berzina-Cimdina, L.; Stunda, A. Fourier transform infrared spectra of technologically modified calcium phosphates. In Proceedings of the 14th Nordic-Baltic Conference on Biomedical Engineering and Medical Physics, Riga, Latvia, 16–20 June 2008.
47. Richardson, J.J.; Lange, F.F. Controlling low temperature aqueous synthesis of ZnO. 1. Thermodynamic analysis. *Cryst. Growth Des.* **2009**, *9*, 2570–2575. [CrossRef]
48. Sedłak, A.; Janusz, W. Specific adsorption of carbonate ions at the zinc oxide/electrolyte solution interface.
    Physicochem. Probl. Miner. Process. **2008**, *42*, 57–66.
49. Haleblian, G.; Kijvikai, K.; Rosette, J.d.l.; Preminger, G. Ureteral stenting and urinary stone management: A systematic review. *J. Urol.* **2008**, *179*, 424–430. [CrossRef]
50. Mizielin´ska, M.; Kowalska, U.; Jarosz, M.; Sumin´ska, P.; Landercy, N.; Duquesne, E. The effect of UV aging on antimicrobial and mechanical properties of PLA films with incorporated zinc oxide nanoparticles. *Int. J. Environ. Res. Public Health* **2018**, *15*, 794. [CrossRef]
51. Mania, S.; Cies´lik, M.; Konzorski, M.; Swie¸cikowski, P.; Nelson, A.; Banach, A.; Tylingo, R.T. The synergistic´ microbiological effects of industrial produced packaging polyethylene films incorporated with zinc nanoparticles. *Polymers* **2020**, *12*, 1198. [CrossRef]

Polymer-Based Additive Manufacturing

Biomedical Applications

- **Editors**
- Declan M. Devine

Chapter 1. Polymer based Additive Manufacturing: Historical developments, Process Types and Material Considerations

Authors: Steven Pollack[1], Chaitra Venkatesh[2], Martin Neff[3], Andrew V. Healy[2], Guang Hu[2], Evert A Fuenmayor[2], John G Lyons[2], Ian Major[2], Declan M. Devine[2#]

[1] Carbon Inc, Redwood City, California, USA

[2] Athlone Institute of Technology, Co. Westmeath, Ireland

[3] Arburg GmbH + Co KG, Loßburg, Germany

Corresponding Author Declan M Devine. Email: ddevine@ait.ie

Contents

Abstract

3D printing is a manufacturing technique where parts are built in a layer-by-layer fashion. The earliest embodiments were based on generating successive layers of solidified materials at the air liquid interface through exposure with actinic radiation and the lowering of the growing object into a vat of photo-active material. One of the earliest concepts was by Otto Munz in 1956 where he describes "photo-glyph recording". However, many today consider Charles Hull the father of 3D printing as it was his patent that coined the term "stereolithography", and was the first to commercialize a 3D printing apparatus.

Since then, there has being a multitude of technologies developed which fall into the category of 3D printing. While curing of resins remains one of the most widely techniques, other techniques based on the extrusion of polymers, cutting sheets or films and thermally or chemically binding powdered materials have all reached the commercial markets. This chapter aims to give an outline of the most common polymer based 3D printing techniques available today and describes some of the material and processing constraints which should be considered when selecting these systems for 3D printing of biomedical parts.

Keywords

3D Printing, Polymers, Stereolithography, Fused Filament Fabrication, Selective Laser Sintering, PolyJet, InkJet, Freeformer, Laminated Object Manufacturing

Introduction

Three-dimensional (3D) printing, also referred to as additive manufacturing (AM), rapid prototyping (RP), or solid freeform fabrication, is a process which involves the manufacturing of an object or structure by deposition or binding of materials layer-by-layer (Sachs, Cima and Cornie, 1990; Conner *et al.*, 2014; Gross *et al.*, 2014; Prasad and Smyth, 2016). A recent publication by (Norman *et al.*, 2016) indicates that the American Society of Mechanical Engineers (ASTM) favour the term additive manufacturing, however, these terms are routinely used interchangeably as is the case in this body of work.

The origins of 3D printing date back to 1986 when Charles Hull developed, patented and commercialised the first 3D printer. The technique was called Stereolithography Apparatus-1 (SLA-1) and was capable of manufacturing a 3D printed object without the need for moulds or other tooling (Prasad and Smyth, 2016). Further to this work, Hull also developed the .STL (Standard Tessellation Language) file format. Today the STL file format is seen as the gold standard for communication of data between the computer-aided design (CAD) software and 3D printers and it is in this that all the information corresponding to each surface of the 3D model is stored in the form of triangulated sections (Gross *et al.*, 2014)

There has been a multitude of 3D printing methods developed since the patenting of Hull's SLA-1. These methods can be separated depending on the way of layer deposition and the material feedstock. However, regardless of the 3D printing technique employed they all share similarities in the method which they create an object, as the model must be first designed and generated through the use of computer-aided design (CAD) software, e.g., SolidWorks, AutoCAD, Creo Parametric, which is then converted into a STL file and transferred to the specific additive manufacturing device for fabrication. This STL file is cut into "slices" with each of them containing the information required for each layer of the part. A platform is created to support any overhanging structures and the part is built one slice at a time.

Additive manufacturing is a simple, automated process which is fast and inexpensive. (Hiemenz, 2011). The fundamental layer-by-layer manufacturing mechanisms of

additive manufacturing provides a wide range of advantages over conventional manufacturing processes. These include: design freedom and superior levels of design complexity with fewer or single-step manufacturing required; reduced or elimination of post-production finishing; reduced or elimination of tooling and fixtures; shorter cycle times for both designs and processing; multiple material manufacturing; savings in energy and start-up cost (Gao *et al.*, 2015); and reduction or elimination of post-production assembly.

Stereolithography (SLA)

The concept of creating a three-dimensional object from a liquid precursor through photochemistry has a long history (Wohlers, 2005). The earliest embodiments were based on generating successive layers of solidified materials at the air liquid interface through exposure with actinic radiation and the lowering of the growing object into a vat of photo-active material. One of the earliest concept was by Otto Munz in 1956 where he describes "photo-glyph recording"(Munz, 1956). In 1981, Hideo Kodama of Nagoya Municipal Industrial Research Institute described the use of UV exposure controlled by a mask pattern or via a scanning fiber transmitter (Kodama, 1981) to create a 3D object. In 1984, Jean Claude André , Alain Le Mehauté and Olivier de Witte filed their patent application (Andre, Le Mehaute and De Witte, 1984) for this process (their patent was ultimately abandoned). Around the same time, Charles Hull filed his patent (Hull and Arcadia, 1986) , coining the term "stereolithography", and was the first to commercialize a 3D printing apparatus. A variety of photochemically reactive polymers have been used including free-radical, cationic and thiol-ene chemistry (Ligon *et al.*, 2017).

The original commercial SLA consisted of a photopolymer reservoir, or vat, which is underneath a movable platform. At each stage of the "build", the platform, or in latter stages, the most recently created layer is lowered just below the surface of the resin in order to create a thin layer and the laser beam passes back and forth over the liquid solidifying it onto the prior layer as it passes (Fig. 1). More recently, some manufacturers have utilized digital light processors (Hornbeck, 1997) to create an image of the layer in UV light to cure the entire layer at once. This leverages the technology for high-resolution projectors used in the movie industry and developed

by Texas Instruments[2]. Others such as UNIZ, and Photocentric have developed liquid crystal arrays which act as "shutters" create the image of the cross section (sometimes referred to as LCD-SLA).

Frequently, a wiper is drawn across the topmost layer to ensure a uniform liquid film for the next layer. Upon completion of the print, the part is pushed up out of the unreacted resin in the vat, and any sacrificial supports are removed and the parts are post-cured (a final, overall dose of UV) in order to remove any unreacted resin from the printing process. One consequence of this arrangement is that the depth of the resin vat must be at least as deep as the part being built is tall and the vat must be filled. Other companies have developed there own systems SLA including EnvisionTec and RPS. Voit (Voit *et al.*, 2016) has described a concept utilizing a dense "z-fluid" upon which the active photopolymer floats so as to minimize the amount of photopolymer used.

Another approach has been to have the resin reservoir with a UV transparent window with the UV light penetrating from underneath the platform and the build plate moving upwards after each pass (sometimes referred to as inverted-SLA)(Ligon *et al.*, 2017). This greatly reduces the quantity of photoactive resin used during the build. However, a consequence of this geometry is that the resin will cure and span the full gap between the build plate and the window at the bottom of the reservoir. This requires a physical delamination of the growing part from the window at each step. In addition to slowing down the process, there are undesirable mechanical forces on the growing part and the reservoir window. The former can cause decreased accuracy and the latter may require frequent replacement of the reservoir/window. Never the less, companies like Formlabs and EnvisionTec have been very successful in marketing their systems for a variety of applications including dental and medical device applications.

[2] http://www.ti.com/dlp-chip/overview.html retrieved Jan 22nd 2019

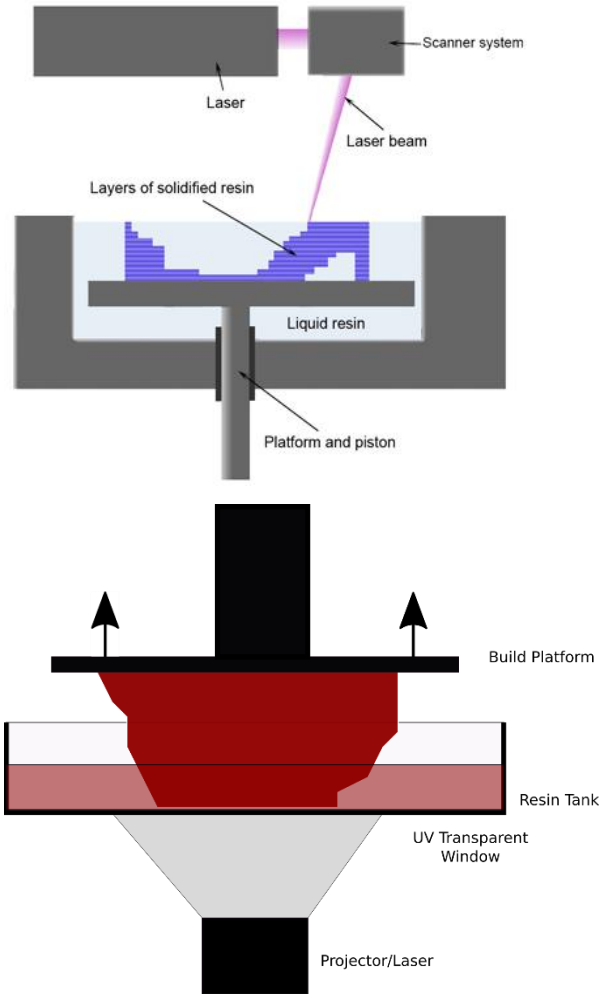

Fig. 1. Left) Conventional SLA utilizes a vat of resin which is lowered as each layer is cured. Right) Inverted SLA utilizes a UV transparent window through which the UV light penetrates from underneath, with the platform and the build plate moving upwards after each pass

In all the above-mentioned systems, there is full solidification of the growing part, either at the liquid/air interface, or at the liquid/window interface, leading to inherently layered internal structures. Recently, DeSimone and co-workers (Tumbleston *et al.*, 2015) described an inverted-SLA system wherein oxygen is introduced at the surface of the window through a transparent, permeable window. The consequence of this oxygen is to deactivate photo-generated free-radicals which initiate the solidification process. Since the oxygen concentration is greatest at the window, there is no reaction and the growing part never attaches to the window. This “dead zone” or continuous liquid interphase (CLIP) allows for the part to be repositioned immediate after an exposure and for fresh resin to flow back in for the next layer’s exposure (Fig. 2). Further, since the oxygen concentration decreases with distance from the window, the extent of solidification increase in proportion to that distance. Thus, there is a gradient

in the degree of solidification moving from the growth front to the already solidified object. Each subsequent layers then interdigitates with the prior layer(s), creating a more monolithic object with substantially less mechanical anisotropy. In theory, other reactive systems could be similarly deactivated by introduction of a suitable agent at the window/resin interface (DeSimone *et al.*, 2015). The company Carbon, Inc. was formed in 2013 based on this technology and the concept of dual cure resins (Rolland, Chen and Poelma, 2016).

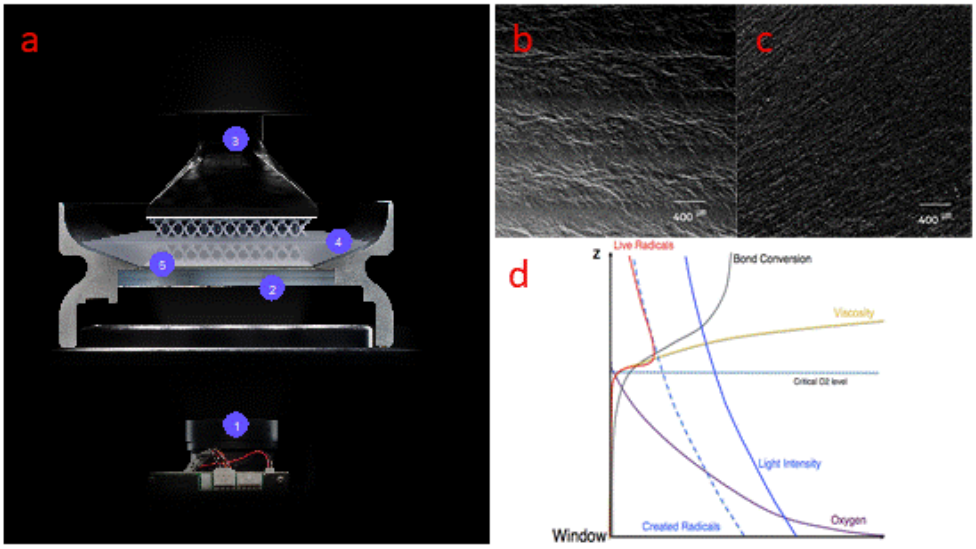

Fig. 2. a) Continuous Liquid Interphase Production (CLIP) where: 1) Light Engine; 2) Oxygen permeable window; 3) Build platform; 4) Resin; 5) Dead zone. b) Conventional SLA fracture surface. c) CLIP based print. d) Lower axis is generalized concentration; vertical axis is distance from the window. Light intensity/radical generation decreases with distance due to molar absorptivity. Oxygen concentration decreases due to diffusivity and reaction with primary radicals. Below the critical oxygen concentration (top of the "dead zone"), polymerization is possible and increases with distance from the window. Graphic courtesy of Matthew Panzer, Carbon, Inc.

As the SLA is the oldest technology it is also the most advanced and is capable of higher spatial resolutions compared to other 3D printing methods. In conventional and inverted-SLA there is a trade-off between xy resolution and build cross section. In laser-based systems, resolution is dictated by the diameter of the focused laser (beam waist) and the angular resolution of the beam steering mirrors (galvanometer). Across various manufacturers and form factors, resolution can range from a 75 to250 micron spot size. The image is "rastered" across the build plane to solidify the desired areas. Alternatively, the entire image can be projected using a large planar UV source and a digital light processors (DLP): an array of micro-mirrors which can illuminate (or suppress) each "pixel" simultaneously. For the commercially available digital light

processors (DLP), these mirrors have a pitch between 8 and 14 microns. The resolution at the image plane (where the layer is solidified) is controlled by the distance of the DLP chip to the window and the imaging optics. Resolution is inversely proportional to build size. Commercial DLP-based SLA systems have resolutions ranging from 35 to 250 microns. Non-commercial systems have been described with pixel sizes down to 10 microns, but with proportionally smaller build cross-sections.

Resolution in the "Z" or build direction is limited by the mechanical stability/reproducibility of the movement of the build platform and control of the photopolymerization process. Unfocussed light can still initiate photopolymerization and cause unwanted solidification, so light absorbing dyes and/or reactive groups in the resin serve to limit polymerization. Build direction resolution can range from 100 microns down to a few microns. Build speed decreases with increase in Z-resolution. For highly specialized applications, micro-stereolithography is now capable of building models with a layer thickness of less than 10 microns which, is limited only by the width of the concentrated ultraviolet (UV) laser or DLP resolution (Melchels, Feijen and Grijpma, 2010).

Part size limitations are related to the particular technology. For conventional SLA, the physical limitations are the volume of the build vat and the optical distortions of the focused laser as it is steered to larger angles, causing the beam waist to take on a more elliptical geometry, which can make resolution vary as a function of xy position. Prodways Technologies has overcome this by utilizing a DLP coupled to an xy stage to move the projected image across the top of the vat. The entire "layer" is projected in sections before moving to the next layer. For inverted-SLA, the mechanical properties of the window become the limiting issue. Hydrodynamic forces between the growing part and the window can cause the window to distort, necessitating slowing down the print process to allow it to mechanically recover after each print step. This problem increases as a function of window cross-section. Also, in inverted SLA, as the window size increases, the overall stiffness of the printer needs to increase to be able to handle the increasing hydrodynamic forces generated between the window and the build plate. Also, for inverted-SLA, maintaining constant resolution with increasing cross-sectional area requires either higher resolution DLPs and/or multiple "tiled" DLPs. In principle, LC shutter based systems are only limited by the technologies for fabricating larger arrays.

One of the limiting factors in the more widespread use of SLA based technologies for medical device fabrication is the limited range of materials properties and biocompatibility. Photopolymerized materials are limited in the range of physical properties they can exhibit, as they are generally non-crystalline and derived from low to moderate molecular weight building blocks. As an approach to this, Carbon has developed "dual-cure resins"(Rolland, Chen and Poelma, 2016). These use photochemistry to generate the initial 3D-dimensional object having low "green" strength. Then, a latent heat-activated thermosetting reaction is initiated by baking the part for 4-12 hours, dependent on the thermosetting chemistry and final part physical properties. Currently, polyurethane, epoxy and cyanate-ester chemistries have been incorporated in Carbon dual cure resins, leading to materials properties equivalent to those from thermoplastic elastomers to high temperature engineering resins.

In all, the polymers used must have suitable biocompatibility (Amato and Ezzell, Jr, 2015) and be able to withstand sterilization. This means at a minimum, they should be able to be tested successfully against the ISO 10993-5 (cytotoxicity) and ISO 10993-10 (irritation and sensitization)(*ISO 10993 - Biological Evaluataion of Medical Devices*, no date), to allow for extended skin contact and short-term (< 24 hours) mucosal contact. For other applications, tests such as systemic toxicity or genotoxicity of leachables will need to be assessed. While this data is not required by most regulatory agencies for the resins themselves, as they are generally interested in the behaviour of the finished device, this affords the end user a degree of security that the final device can safety utilize these materials and pass regulatory scrutiny.

These high resolutions and newer materials enable SLA to be used in biomedical applications (Chua, Leong and Lim, 2003). As such SLA printing has being used for the production of many biomedical parts. Some of the earliest applications of SLA have been in the dental space. Dentists and other oral care practitioners were some of first adopters of 3D SLA printing using the technology for the generation of dental models. While not formally medical devices, they are integral to developing solutions for dental restorations. Align Technologies uses SLA-based 3D printing to generate patient-matched templates for the thermoforming-fabrication of their Invisalign® clear aligners(McLure, 2017). More recently, dentists and oral surgeons are using

specialized software (e.g. 3Shape) and SLA-based 3D printing in the direct fabrication of drill guides to more precisely place dental implants. Lastly, Dentca developed the first FDA-approved resin for the 3D printed fabrication of denture and denture teeth. Other denture resins have since been cleared by the FDA and other regulatory bodies and a number of manufacturers are now using this approach.

Another early adopter of 3D SLA is the hearing aid industry. Most major hearing aid manufactures now fabricate the "in-the-ear" components using 3D printing, transforming a scanned image of a model or direct scan of the outer ear and ear canal. Companies like Starkey state the 98% of their hearing aids are created using 3D printing(Sharma, 2013). Hard components can be fabricated directly using resins from several manufacturers (e.g. Dreve, Pro3Dure, Vertex) or, using sacrificial "egg-shell" or "cocoon" moulds, soft components from thermally-cured silicone resins. A related therapy is the Cerezen™ intra-aural device produced by Renew Healthcare for the treatment of Tempromandibular Disorder (TMD) which places a device in the ear to restrict excessive motion of the joint('Cerezen device provides treatment for temporomandibular joint disorders day and night', 2016).

Medical models are another important area for utilization of SLA. Having models fabricated from clear resins allow for the clinician and patient to visual the relative 3-dimensional positions of organs and lesions. Using design software like Mimics (Materialise) and simple dyes, a colourless transparent resin can have specific organs and structure coloured to mark tumours, vessels and other points of interest[3].

Further uptake by the medical device industry will be driven by greater familiarity with the materials and their acceptance by regulatory agencies. FDA's recent technology guidance for the use of additive manufacture bodes well for this future [4](*FDA's Role in 3D Printing*, no date). However, SLA printing inn continually finding new applications in the biomedical field, as recent case study by students and faculty at UC Berkeley utilizing Carbon's high temperature CE 221 cyanate ester resin for creating patient-matched MRI surface coils for restriction of patient motion and enhanced signal-to-noise ratio (Corea, 2016; Zamarayeva *et al.*, 2018). Looking forward, there are a number of academic laboratories beginning to develop

[3] https://www.materialise.com/en/blog/how-to-3d-print-multicolored-models-formlabs-sla
[4]https://www.fda.gov/MedicalDevices/ProductsandMedicalProcedures/3DPrintingofMedicalDevices/ucm500548.htm

bioresorbable 3D printed devices. A number of groups have demonstrated tissue scaffolds for cartilage regeneration using 3D printed poly(propylene fumarate)(Luo *et al.*, 2016; Parry *et al.*, 2017). In the cardiovascular field, Ameer and Chen (van Lith *et al.*, 2016) have constructed an inverted-SLA printer using Carbon "CLIP" technology and fabricated cardiovascular stents from a novel citrate polyester. Combining novel polymers with these new high resolution SLA print technologies will lead to new therapies and better outcomes for patients.

Fused filament fabrication

Fused filament fabrication (FFF), also known under the trademarked term fused deposition modelling (FDM) is an extrusion based process which is one of the most widely utilised 3D printing technologies today (Fig.). It was developed and patented by Scott Crump of Stratasys Inc. in 1992 (Masood and Song, 2004). FFF is a widely implemented method for 3D printing of solid objects (Skowyra, Pietrzak and Alhnan, 2015). With the invention of FFF it became possible to not only print functional prototypes but also to print concept models and end-user products (McLouth *et al.*, 2017)

The FFF process fabricates 3D models by extruding materials through a heated print head that moves in X and Y directions onto a stage layer by layer (Gross *et al.*, 2014). It uses thermoplastic materials which are produced in the form of a filament and then are extruded from movable head on the FFF machine and deposited in ultra-thin layers onto a substrate, translating the dimensions of digital data into an actual printed parts (Wang *et al.*, 2017). The material is heated slightly above its melting point; this is to ensure it will quickly solidify after being deposited and welds to the former layer or printing bed. Modern domestic FFF printers consist of a heated nozzle which is fed filament by a stepper motor. A chamber before the nozzle melts the material and the filament pushed into this cavity forces out the necessary amount of molten material. Common materials used for FDM include polycarbonate (PC), acrylonitrile butadiene styrene (ABS), polyphenyl sulfone (PPSF), PC-ABS blends, medical-grade polycarbonate, wax, metals and even ceramics (Kruth, Leu and Nakagawa, 1998). It is far from a perfect process as it leaves visible seam lines between layers, overhanging parts need supports to be printed below, build times are long, the resolution is low compared to other techniques. The high relative viscosity of the thermoplastics limits the use of small diameter nozzles for FFF 3D printing with maximum resolution of 40µm (Dermanaki Farahani and Dubé, 2017). This may become a considerable challenge with using fillers/active agent with nozzle clogging occurring due to reduction in flow properties or degradation of one or more components within the filament (Ivanova, Williams and Campbell, 2013).

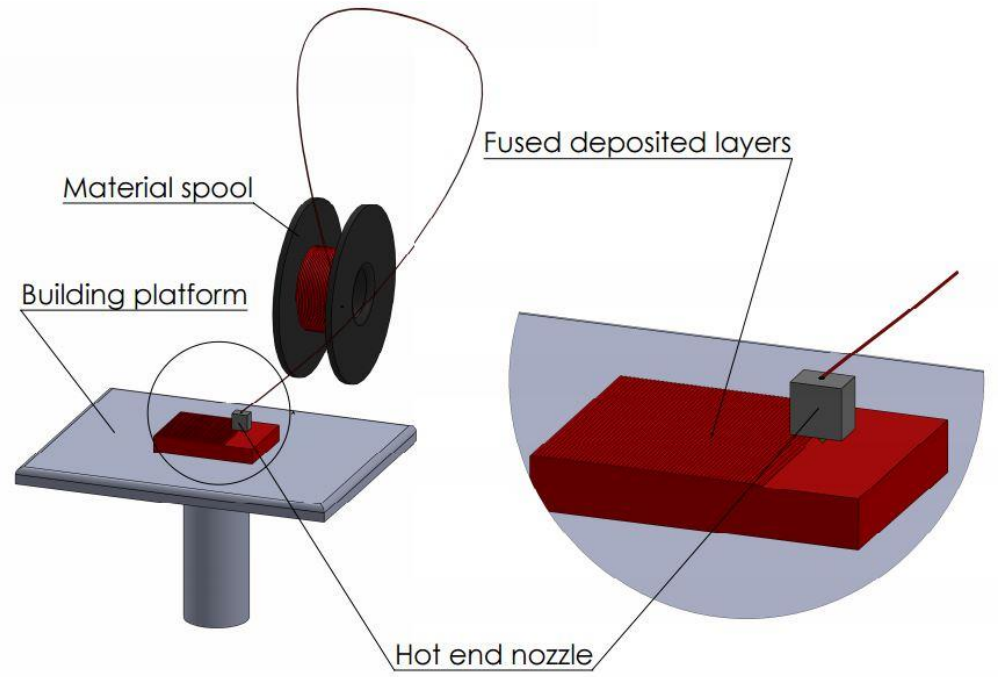

Fig. 3. Schematic of a FFF process. The filament is passed from a roll through a heated nozzle using a stepper motor where it is heated to a temperature just above its melting temperature before placement in ultra-thin layers onto a substrate

However, parts do not require chemical post-processing which is highly desirable for biomedical applications, and the material used are cost-effective and the equipment needed is considered to be simple-to-use and low-cost as compared to other 3D printing techniques (Sood, Ohdar and Mahapatra, 2010) (Bellini and Guceri, 2003).

As FFF is an extrusion based process, it can be highly versatile as in theory any thermoplastic polymer, thermoplastic composite or polymer based drug delivery platform can be used to produce parts using this process (Kokkinis, Schaffner and Studart, 2015)(Fuenmayor *et al.*, 2018). Indeed, HME is a well-established process for the production of pharmaceutical dosage forms, which ensures solvent-free production, low-cost scale-up, and enhanced solubility for poorly water-soluble drugs(Tiwari, Patil and Repka, 2016). It may also be used for the production of parts from high strength polymers such as such as Polyether ether Ketone (PEEK) and polyetherimide. The former is currently approved for use in biomedical applications such as craniomaxillafacial implants and spinal fusion cages. However, although high strength polymers are desirable for use in biomedical application, polymers such as PEEK require processing temperatures of up to 400°C which is above the capabilities of standard FFF machines thereby increasing the cost of the overall system.

In FFF some technical challenges may prevent the production of usable parts. These include low mechanical strength compared to injection moulded parts, long build time and poor surface finish (Zaharin *et al.*, 2018). Other challenges surrounding FFF include poor layer adhesion and layer delamination of the fabricated materials. In addition mechanical properties can also result from the FFF process generating void spaces between deposition lines, which adversely effects properties such as stiffness and strength (Ferreira *et al.*, 2017). These can be addressed by the post processing methods such as microwave treatment, vapour smoothing, metal plating, cold welding, gap filling, polishing, dipping, the use of resin to fill the voids, optimisation of the process parameters and structural optimisation (Dizon *et al.*, 2018)(Yao *et al.*, 2017). Li and researchers demonstrated the improvement in mechanical properties of FFF printed parts following ultrasonic treatment. These results were attributed to ultrasonic vibration causing re- entanglement and deeper interdiffusion, reducing gaps and increasing interfacial area and strength at the raster interface (G. Li *et al.*, 2018).

The infill density and the printing pattern significantly influence the material properties of the printed samples. The effect of these parameters were studied on the tensile, dynamic mechanical and thermoelectric properties of FFF printed conductive acrylonitrile butadiene styrene/zinc oxide (CABS/ZnO) in comparison with (ABS/ZnO) (Yun *et al.*, 2018). CABS is a mixture of acrylonitrile butadiene styrene (ABS) and carbon black residue. There was a positive impact on the electrical conductivity and thermal conductivity. However, no change was observed in tensile strength of the nanocomposite due to infill density. Samples printed in line pattern had better tensile properties with high stiffness and storage modulus while electrical conductivity also improved with line samples when compared to rectilinear samples.(Yun *et al.*, 2018). Additionally, Dul *et al.* demonstrated that the reinforcement effect of the graphene nanoplates in the ABS matrix was optimum at vertical and horizontal orientation when compared to perpendicular orientation (Dul, Fambri and Pegoretti, 2016). Mohamed and researchers developed mathematical models for FFF process parameter optimisation using I-Optimal design. Parameters such as layer thickness, air gap, build orientation show a significant effect on percentage change. This method is proposed to be used for part quality in computer generated optimal design in additive manufacturing (Mohamed, Masood and Bhowmik, 2016)

FFF may be employed in various medical applications to produce 3D parts with complex shapes because of its highly controllable channel size and porosity (Zaharin *et al.*, 2018). A common indication where this could prove advantageous is in the 3D printing of stents. Much work has being carried out in this field with PLA or variations the polymer mostly investigated (Yuanyuan Chen *et al.*, 2016). While Coronary stents remain the holy grail of 3D printed stents, easier success may be found elsewhere where pressures are lower and failure have less catastrophic effects. An example of this was demonstrated by Mills *et al.* who successfully fabricated nasal stents by FFF in porous or mesh form made of multiple polymers in layers (Mills *et al.*, 2017).

One of the most growing area of recent research and development in 3D printing is nanotechnology. Nanotechnology can be seen in various disciplines of science and technology including the areas of polymer based biomaterials, nanoparticle drug delivery, polymer blends, nanofibers and nanocomposites (Bhatt and Anbarasu, 2017).

Nanocomposites are emerging potentially in various industries due to excellent mechanical, electrical and thermal properties. The nanomaterial can be dispersed into the host matrices by 3D printing to produce nanocomposite signifies numerous advantages due to its properties and improves the homogeneity of the product. (Tuan D. Ngo *et al.*, 2018). The high viscosity of the thermoplastics can be further increased by the addition of nanofillers which effects the printability of the nanocomposite filament. This can be addressed by selecting suitable mixing strategies while printing for good dispersion of the nanomaterial into the polymer matrix. Various other methods such as solution mixing by sonication and high shear mixing by extrusion can be employed to reinforce the nanomaterial into the polymer matrix before 3D printing (Dermanaki Farahani and Dubé, 2017).

3D printed nanocomposites can be created using filament which incorporate nanoparticles. Shrinking the scale size to the nano range can change the properties of the materials. A variety of nanomaterials such as carbon nanotubes, graphene, metal nanoparticles are used in 3D printing for various applications (Ivanova, Williams and Campbell, 2013). Several researches have been conducted to study the physical properties of the final printed part when they are blended with nanomaterials. Recent studies show that in FFF the mechanical properties of the filament can be increased by addition of the nanofillers with researchers such as Healy et al. reporting

that halloysite significantly increased Young's modulus 11% and 25% when the loading was two and six percent respectively (Healy et al., 2018).

Nevertheless, it has also being reported that the incorporation of nanofillers can also have adverse effects on the properties of the printed parts. Dorigato *et al.* dispersed multiwalled carbon nanotubes into an ABS matrix and conducted a comparative study of the properties of compression moulded and 3D printed materials. While the stiffness and yield properties increased by the addition nanofillers, the 3D printed samples resulted in loss of ductility and electrical conductivity due to the dependency on the printing direction (Dorigato *et al.*, 2017). Additionally, proper care is necessary during fabrication of the nanocomposite for optimised dispersion of the particles within the matrix as nanoparticles such as carbon nanotubes (CNTs) tend to agglomerate due to their large aspect ratio, chemical structure and small scale (Kim *et al.*, 2018). Functionalisation of the nanoparticles is one of the methods to overcome this issue (Chen *et al.*, 2018). However, processing through screw extrusion using high shear rates may be enough to distribute the nanomaterial without chemical treatment.

Recycling FFF parts has also shown promise. Tian et al. studies recycling of 3D printing of carbon fibre reinforced PLA composites produced by FFF. It was found that the carbon fibre reinforcement enhanced the mechanical properties of PLA (Tian *et al.*, 2016). Additionally, in a subsequent study the recycling and remanufacturing of the carbon fibre reinforced PLA composites from the previously 3D printed carbon fibre filament was assessed. Although aging of the PLA matrix was observed, the recycled composites attained comparatively higher mechanical properties with respect to originally 3D printed composite (Tian *et al.*, 2017).

Selective Laser Sintering (SLS)

SLS was discovered by Carl Deckard and Joe Beaman in 1980s (Gross et al., 2014).. It is a 3D printing technique that uses a high-power power resource such as laser to sinter powered materials (polymer, resin or metal) to build up object (Wang et al., 2017). In contrast to other Additive Manufacturing technologies, laser sintering allows the processing of almost any material that consolidates upon heating, including polymers, metals and even ceramics. High requirements of heat sources during the melting process becomes the biggest barrier to widespread use of this method. However, this challenge is lessened when using polymer based systems as these can

be sintered at temperatures which are lower than those of metals or ceramics. Nonetheless, parts produced by laser sintering can reach material properties that are close to those obtained by other manufacturing processes, such as injection moulding (Verbelen et al., 2016).

A SLS machine usually consists of a powder reserve and a CO2 to sinter the powder. As a first step, the powder bed is filled and preheated to a temperature between the melting and crystallization temperature for semi crystalline polymers and above its glass transition temperature for amorphous (Wudy, Drummer and Drexler, 2014; Shirazi et al., 2015). A layer of powder is spread across the build chamber then the high energy laser can selectively melt and fuse the thin layer of material together. The surrounding powder particles remain loose in the build chamber. As such SLS is not restricted by the need for support materials as overhanging structures can be supported by the unsinkable powder (Wudy, Drummer and Drexler, 2014; Chia and Wu, 2015). Once completed, the printing part moves down to a predefined depth usually 0.1mm and the reserve part moves up to enable a new layer of the power material spread across the build chamber by a blade or a counter rotating roller. This process repeats until the last layer has been printed (Hwa et al., 2017). After production the part is slowly cooled.

The quality of printed part is effected by a multitude of factors from powder composition and morphology, laser energy input, scan spacing and speed and processing (or powder bed) temperature (Dadbakhsh et al., 2016; Macdonald et al., 2017). In terms of powder composition much research has being conducted into the effect of powder size, shape and homogeneity as thousands of polymeric materials could theoretically be frozen below its glass transition temperature and milled either cryogenically or using standard milling processes to create powders for use in SLS. However of these materials there are only a few grades of polymers that are commercially available for use in the SLS process. This includes amorphous, semicrystalline, reinforced or filled polymers. Among these materials, semicrystalline polyamide is the dominant material used (Dadbakhsh et al., 2016). Verbelen *et al.* studied a range of polyamide (PA) grades namely: PA12, PA11 and PA6 to reveal characteristics of these materials that explain it current popularity for laser sintering in an attempt to develop guidelines that can be used for new materials. It was reported that a combination of powder availability, low initial zero-shear viscosity, and the low

tendency to warp due to a large degree of super-cooling coupled with low crystallization shrinkage were deemed to be important factors. Post-condensation behaviour also appeared to play a major role in establishing these properties. However, this behaviour was deemed detrimental for the recyclability of the powder and the consistency of part properties. Moreover, it was concluded that for SLS to become a widespread manufacturing technique, a larger variety of materials that can readily be processed is necessary (Verbelen et al., 2016). To this end the team at KU Leuven investigated cryogenic milling of thermoplastic polyurethane (TPU). The study investigated both coarse powder with rough surfaces and a fine powder which incorporated extremely fine flow modifiers. This work showed that the fine powders were easier to process and while course and fine powders were comparable in shear-punch testing the tensile properties of parts produced using the coarse powder were one third of the fine powders. As the coarse powders were 3x those of the fine powders it is clear that powder size and homogeneity are critical (Dadbakhsh et al., 2016).

Vasquez et al. also examined the characteristics of PA 12 to aid in the selection of materials suitable for SLS. In this work information on the thermal characteristics of the polymer measured by differential scanning calorimetry (DSC) and hot stage microscopy coupled with viscosity data was used to predict the viability of SLS printing of a thermoplastic elastomer (TPE) and a TPU. Thermogravimetric analysis (TGA) was utilized to determine the overall thermal stability region for the polymers. SLS printing of the selected polymer confirmed the viability of this approach for screening the suitability of materials for use in SLS(Vasquez, G.M, Majewski, C.E, Haworth, B. & Hopkinson, 2014).

Freeformer

The main drawback for additive manufacturing in the bomedical sector is that most polymers which have being approved by regularity authoritories for use in the manufacture of medical devices cannot be used without at the least the melt production of a filament. This increases cost, complexity of manufacture and lead times. Additionally, extruding of the polymer into filaments may cause a degree of thermal degradation especially in thermally unstable polymers. To overcome this challenge, the ARBURG Plastic Freeforming (APF) process was developed. This process allows the use of standard polymer granules which are commonly used in conventional

injection moulding to be utilised in the production of 3D printed parts directly, without any other modification or pre-processing steps.

The APF concept of using qualified standard granulate, enables the production of parts at lower costs as there is a wide range of low-cost materials and dyes are available to choose from (Fig. 4). In principle, the APF is suitable for all melt processible resins. Indeed there are opportunities to produce bespoke polymer formulations and composites which can be used for the production of 3D printed parts through standard compounding and granulation processes. With this process there is no critical dimension as is observed with FFF where diameter variations can cause challenges in the production of parts. However, to ensure reproducible parts are produced, material qualification, and individual development work, may be necessary for any new formulation or blend. For this the most important parameters are the processing temperature and temperature resistance. This is supplemented by the layer-by-layer geometrical slicing and automatic preparation of the 3D CAD data according to quality and material-specific criteria to create a system-specific numerical control program. Aspects such as edge, filling and strength strategies as well as the build chamber temperature can also be considered. This results in pre-optimised process data for the individual material types.

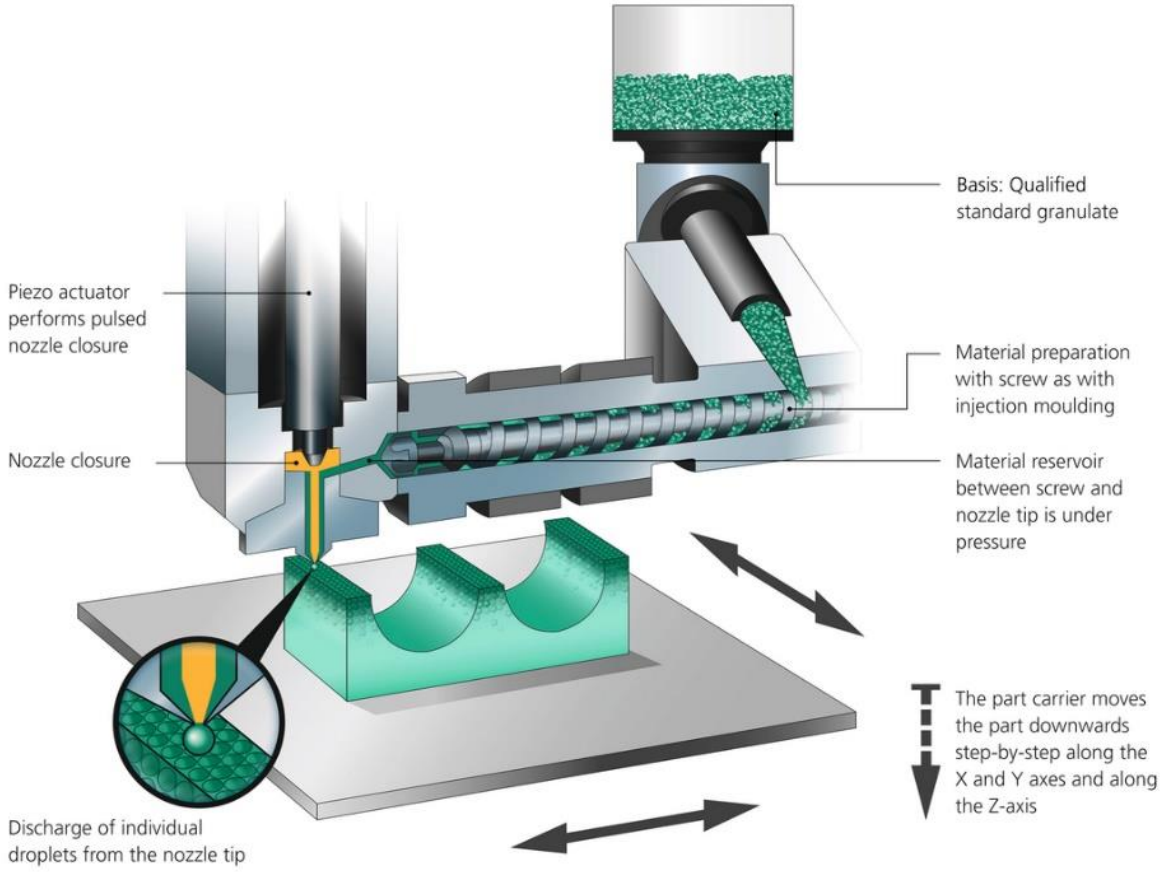

Fig. 4: The APF process principle in detail with (inset) a close-up of the surface of a part produced using the APF process: homogeneous, dense layer build-up

Developed together with the APF process, the “freeformer” is designed as an open production system. Slice and process parameters are freely programmable and can thus be individually optimised at any time. The material database for the APF process is growing continuously and includes process data for a large number of thermoplastics. These include not only the additive standard materials ABS, PC, PA12 (amorphous), but also partially crystalline PP, as well as special plastics such as the high-temperature material PEI, elastic TPU, medical PLA or biopolymers. Taking this as the starting point, modified original materials can also be used quickly and easily. In terms of biomedical implants or devices, this allows the use of polymeric materials which have previously had regularity approval for use in medical devices. The freeformer integrates material preparation with a special plasticising screw and discharge unit. Plasticising is followed by freeforming without the use of a mould where a nozzle closure controlled by high-frequency piezo technology enables extremely rapid opening and closing of the nozzle. Under a material pressure of up to 500 bar, up to 250 plastic droplets are applied per second. Three moving part carriers are positioned

by means of servo motors so that each droplet is placed at the precise point. Solidification of the part is through polymer cooling where the droplets automatically fuse together as they cool in the temperature-controlled build chamber in a layer-by-layer manner.

The surface quality achievable with the APF process features a particularly even and close structure - in all directions (Fig.4). Surface quality, mechanical properties and density are determined by droplet size and process regulation (filling strategy and level). The smaller the plastic droplets and the more closely they are placed next to one another, the finer the structure and the more robust the parts. On the other hand, larger diameters and distances enable shorter build times. Depending on the available nozzle diameters (0.15 mm, 0.2 mm or 0.25 mm), the plastic droplets measure around 0.2 to 0.3 mm. The layer thickness varies between 0.14 and 0.34 mm and the minimum wall thickness is 0.6 to 1.0 mm.

The manufactured products can be used not just as reliable prototypes, but also as fully functional individual parts and small-volume batches. This opens up more efficient processes and new design freedoms when developing and producing products. Prototypes can be subjected to stress tests, for example, and the necessary product adjustments can be identified and implemented at an early stage. In the area of pre-series production, small unit volumes can be achieved using the APF method. The integration of functions by combining part production and assembly in a single process step is a further means of achieving cost efficiency. With this additive process, complete modules can be produced in a fully-assembled state. With regard to lightweight construction and weight reduction, bionically optimised parts can be designed and produced without having to factor in the technical production constraints that apply to injection moulding. In conjunction with the corresponding process regulation, the following component properties can be achieved compared to injection-moulded parts, depending on the material:

- Tensile strength is about 90-98% depending on the resin type (tensile test according to DIN EN ISO 527-02)
- Part density up to 95%
- Surface quality up to Rz = 7.84 µm / Ra = 1.69 µm

In addition the APF process can be combined with injection moulding in conjunction with Industry 4.0 technologies, this makes it economically viable to manufacture single-unit customized batches in a flexible, automated, digitally networked, cyberphysical production system. The individualisation of mass-produced products in terms of 3D geometry and functionality means that plastic parts can be enhanced in such a way as to generate added value for manufacturers. Serial production for specific jobs will commence "on demand" thanks to IT networking. An injection moulding machine and a freeformer can be linked by means of an automation component for this purpose. A digital manufacturing (DM) code applied to the part during the production process turns it into an information carrier and enables it to control its own production steps, this could also be used for part tracking for regularity purposes. The automation of additive manufacturing also reduces unit costs and improves process control. In addition to the automatic opening and closing of the hood and the loading and unloading of the build chamber with loaded parts, automated assembly with base plates or cleaning cycles can also be realised. Loading takes place with in-line measurement and automatic height correction. In addition, data is exchanged and archived at a higher level via an industrial interface. The freeformer is also equipped with several discharge units as standard. This enables functional parts to be produced using several different polymers with combinations of hard and soft polymers possible. As with injection moulding, self-dyeing is possible in master batches. In the case of complex part geometries, the second component can alternatively be used to construct support structures.

In terms of industries and areas of application, the possibilities of the APF process with its wide range of materials are virtually boundless. In the medical technology sector, for example, it can be used for the additive manufacturing of individually adapted implants and orthotics as well as models used in preparation for surgery. Another example of biomedical implants which may benefit from production using the freeformer is the manufacture of customized resorbable polylactide (PLA) based implants, conventionally used as screws or pins for securing bones and tissue. These parts are traditionally produced by injection moulding however production using the freeformer would enable these implants to be tailored precisely to a particular patient. Another opportunity would be in the production of surgical guides through the use of medical imaging to produce 3D CAD data

InkJet techniques

InkJet printing was initially described by Lord Rayleigh in 1878. It was patented by Siemens for 2D printing in 1951, however it was 2001 before InkJet printing was used for 3D printing structures (Gross *et al.*, 2014).

Inkjet technology can be dived into two separate but related 3D printing techniques. The first technology is also referred to as binder jetting, drop-on-demand or powder-liquid 3D printing. This system was developed at Massachusetts Institute of Technology in 1993 (Wang *et al.*, 2017). The system utilises photocurable polymers laid down by an inkjet head to selectively bind powders which are laid down in a similar manner to SLS 3D printing (Shirazi *et al.*, 2015). This process continues with the build bed being lowered and fresh powder spread across the surface until the final part is built. Unbound powder is removed to get the final part (Wang *et al.*, 2017). The key advantage of this technique is the flexibility of the system and processability at room temperatures. As with SLS, theoretically any polymer material in a powder state can printed using this technology. Surface porosity can be high using this technique due to unbound particles which may depending on the application be advantageous(Gross *et al.*, 2014). However, its applicability to biomedical applications may be limited as the binder may incorporate contaminates which are biologically toxic and resolution is limited (Gross *et al.*, 2014; Wang *et al.*, 2017).

Powderless Inkjet technologies such as the Stratasys, PolyJet system which can print 16 µm photopolymer layers. In this system liquid photo-polymer is heated to about 73 °C, jetted onto a surface and instantly cured with UV light. Most commercial printers contain at least two print heads similar to the ones in conventional printing, one for the support material and one for the model material. Additional print heads can be added for higher material throughput or to print multiple materials, which is one major advantage of the process (Mueller, Shea and Daraio, 2015). This system is ideally suited for the production of parts which require two or more distinct properties as combinations of resins can easily be build up within the part due to the number of heads employed. Thin layers of cured material pile up while the build tray moves down until the part is finished. The Stratasys Objet500 Connex3 is one of the most advanced commercially available PolyJet printers it is representative for the current state-of-the-art of inkjet 3D printing (Mueller, Shea and Daraio, 2015). However, as the PolyJet system is relatively new (Wang *et al.*, 2017), the number of resins available is

somewhat limited and to the authors knowledge none are approved for use in implant materials.

Laminated Object Manufacturing

Laminated Object Manufacturing was developed by Helisys (now Cubic Technologies). This system generates a 3D part through stacking layers of polymer sheets. Excess material is removed with a razor or laser which traces the desired shape. Layers are combined using an adhesive or through thermal welding (Gross *et al.*, 2014). Thermal bonding is more desirable than adhesive bonding for biomedical applications as the adhesives may be biologically toxic as was discussed in relation to InkJet printing.

This process is an important automated process used for fabrication of large composite structures in aeronautical industry (Zhang *et al.*, 2015) and in this industry is often referred to as Automated Tape Placement (ATP). Most commonly the ATP system utilises a continuous fibre thermoplastic composite tape to generate high strength composite parts. The tape is laid down in layers with pressure applied with a heated roller during bonding to ensure good contact between layers (Zhang *et al.*, 2015). Engineering materials can be utilised using this process in combination with a heated bed as if the local temperature of the bed or roller is not controlled well enough the part may delaminate due to insufficient bonding between layers or the part may suffer structural damage if the temperatures do not enable good adhesion (Gross *et al.*, 2014).

Summary

As illustrated in this chapter there are a number of additive manufacturing techniques which all have strengths the weaknesses. The type and tolerance of these machines is constantly increasing. This is due in part to the patent lapsing on the earlier techniques which has allowed new entrants into the market. This has coincided with an increase in the development of a lot of new resins for use in 3D printing as many of the new suppliers have moved to an open source resin approach.

While there are many different techniques this chapter has concentrated on the most established processes which are more likely to be used in the production of biomedical parts.

Liquid resin based systems like SLA and PolyJet are capable of the best printing resolutions. However, the resins which are approved for use in biomedical implants are limited. These systems are generally based on thermosetting polymer resins which following curing do not melt on application of heat. Nevertheless, these processes have being used for the production of a variety of products and as the material technology is developed this is set to increase.

Conversely, thermoplastic resin based systems can be used in conjunction with a vast array of regularity approved thermoplastic resins. With FFF, the challenge of delamination between weld lines is a concern however these effects can be lessened with post production processing. The Arburg Freeformer system appears promising in this regard, however again the range of materials which can be processed using this method needs to be expanded.

SLS and Material Jetting are both based on powdered polymers they differ in how the powders are bound. With SLS thermal energy is used which Material Jetting utilises adhesives which may in themselves be toxic. However if this can be overcome both have potential for use in areas where surface roughness is desirable such as in orthopaedic implants. Similar to the previous methods Laminated Object Manufacturing uses sheets of polymers which enables the production of parts from a wide variety of polymer resins. However, these can use thermal or chemical bonding techniques similar to the previous techniques.

With this vast array of processes capable of producing complex parts with complete design freedom from a growing number of materials, it is clear that the application of 3D printing in the biomedical field will continue to grow and find new applications which will improve the lives of countless people now and well into the future.

Acknowledgements

The authors wish to thank Dr. Joe DeSimone and Mr. Ken Sibley, Esq., both of Carbon, Inc. for some of the historical references.

This work was supported in part by financial support from Athlone Institute of Technology under the Presidents Seed Fund, Enterprise Ireland funding under the Technology Gateway program, grant number TG-2017-0114 and Science Foundation Ireland (SFI) under Grant Number 16/RC/3918, co-funded by the European Regional Development Fund.

References

A. Hou (2019) ‘Super-Toughened Poly (lactic Acid) with’, *Polymers*. doi: 10.3390/polym11050771.

A, S. Z. O. (2003) ‘Секція : Matsyutsya Katerina Kiev National University of Technology and Design ASPIRIN – FRIEND OR FOE ? Ahtyamova D . PARAMETERS AFFECTING THE PERFORMANCE OF IMMOBILIZED ENZYME Supervisor : Zvonok O .’ ТНТУ, pp. 150–151.

Abdullayev, E. and Lvov, Y. (2011) ‘Halloysite Clay Nanotubes for Controlled Release of Protective Agents’, *Journal of Nanoscience and Nanotechnology*, 11(5), pp. 10007–10026. doi: 10.1166/jnn.2011.5724.

Abdullayev, E. and Lvov, Y. (2013) ‘Halloysite clay nanotubes as a ceramic “skeleton” for functional biopolymer composites with sustained drug release’, *Journal of Materials Chemistry B*, 1(23), pp. 2894–2903. doi: 10.1039/C3TB20059K.

Abeykoon, C. *et al.* (2014) ‘Investigation of the process energy demand in polymer extrusion: A brief review and an experimental study’, *Applied Energy*. Elsevier Ltd, 136, pp. 726–737. doi: 10.1016/j.apenergy.2014.09.024.

Acharya, P. C. *et al.* (2018) *Discovery and Development, Dosage Form Design Considerations*. Elsevier Inc. doi: 10.1016/B978-0-12-814423-7.00013-7.

Akos, N. I. *et al.* (2013) ‘Preparation , Characterization , and Mechanical Properties of Poly (e - caprolactone)/ Polylactic Acid Blend Composites’, pp. 2–7. doi: 10.1002/pc.

Albareeki, M. M., Driscoll, S. B. and Barry, C. F. (2019) ‘Compounding of polyethylene composites using high speed twin and quad screw extruders’, *AIP Conference Proceedings*, 2139(August). doi: 10.1063/1.5121653.

Alberton, J. *et al.* (2014) ‘Mechanical and moisture barrier properties of titanium dioxide nanoparticles and halloysite nanotubes reinforced polylactic acid (PLA)’, *IOP Conference Series: Materials Science and Engineering*, 64, p. 012010. doi: 10.1088/1757-899X/64/1/012010.

Alexis, F. (2005) ‘Factors affecting the degradation and drug-release mechanism of poly (lactic acid) and poly [(lactic acid) - co - (glycolic acid)]’, 46(June 2004), pp. 36–46. doi: 10.1002/pi.1697.

Alexy, R. D. and Levi, D. S. (2013) ‘Materials and manufacturing technologies available for production of a pediatric bioabsorbable stent’, *BioMed Research International*, 2013. doi: 10.1155/2013/137985.

Ali, Z. A. *et al.* (2017) ‘2-year outcomes with the Absorb bioresorbable scaffold for treatment of coronary artery disease: a systematic review and meta-analysis of seven randomised trials with an individual patient data substudy’, *The Lancet*. Elsevier Ltd, 390(10096), pp. 760–772. doi: 10.1016/S0140-6736(17)31470-8.

Amato, S. and Ezzell, Jr, R. (2015) *Regulatory Affairs for Biomaterials and Medical Devices*. Elsevier. doi: 10.1016/C2013-0-16313-1.

Anand Narayanan, A. G., Babu, R. and Vasanthakumari, R. (2016) ‘Studies on Halloysite Nanotubes (HNT) Natural Rubber Nanocomposites for Mechanical Thermal and Wear Properties’, *International Journal of Engineering Research & Technology*, 5(03), pp. 152–156. doi: 10.17577/IJERTV5IS030167.

Andre, J.-C., Le Mehaute, A. and De Witte, O. (1984) ‘Dispositif pour réaliser un modèle de pièce industrialle (Device for fabrcating an industrial part model)’.

Ang, H. Y., Bulluck, H., *et al.* (2017a) ‘Bioresorbable stents: Current and upcoming bioresorbable technologies’, *International Journal of Cardiology*. Elsevier B.V., 228, pp. 931–939. doi: 10.1016/j.ijcard.2016.11.258.

Ang, H. Y., Bulluck, H., *et al.* (2017b) ‘Bioresorbable stents: Current and upcoming bioresorbable technologies’, *International Journal of Cardiology*. Elsevier B.V., 228, pp. 931–939. doi: 10.1016/j.ijcard.2016.11.258.

Ang, H. Y., Huang, Y. Y., *et al.* (2017) 'Mechanical behavior of polymer-based vs. metallic-based bioresorbable stents', *Journal of Thoracic Disease*, 9(Suppl 9), pp. S923–S934. doi: 10.21037/jtd.2017.06.30.

Ang, H. Y. *et al.* (2018) 'Radiopaque Fully Degradable Nanocomposites for Coronary Stents', *Scientific Reports*, 8(1), pp. 1–14. doi: 10.1038/s41598-018-35663-2.

Anwar, K., Halim, A. and Florida, S. (2012) 'Optimisation of a Twin Screw Extrusion Process for Enhanced Short-term Mechanical Properties of Polyamide 11 nanocompo ....', (June 2014).

ASM International (2004) 'Introduction to Tensile Testing', *Tensile testing*, pp. 1–13. doi: 10.1017/CBO9781107415324.004.

Atif, R. and Inam, F. (2016) 'Reasons and remedies for the agglomeration of multilayered graphene and carbon nanotubes in polymers', *Beilstein Journal of Nanotechnology*, 7(1), pp. 1174–1196. doi: 10.3762/bjnano.7.109.

Azaouzi, M., Makradi, A. and Belouettar, S. (2012) 'Deployment of a self-expanding stent inside an artery: A finite element analysis', *Materials and Design*. Elsevier Ltd, 41, pp. 410–420. doi: 10.1016/j.matdes.2012.05.019.

Balogh, A. *et al.* (2018) 'Supporting Information Continuous End-to-End Production of Solid Drug Dosage Forms : Coupling Flow Synthesis and Formulation by Electrospinning', *Chemical Engineering Journal*. Elsevier, 350(March), pp. 1–23. doi: 10.1016/j.cej.2018.05.188.

Bari, S. S., Chatterjee, A. and Mishra, S. (2016) 'Biodegradable polymer nanocomposites: An overview', *Polymer Reviews*, 56(2), pp. 287–328. doi: 10.1080/15583724.2015.1118123.

Basu, A. *et al.* (2016) 'Poly(lactic acid)-based nanocomposites', *Polymers for Advanced Technologies*, (November). doi: 10.1002/pat.3985.

Bellini, A. and Guceri, S. (2003) 'Mechanical characterization of parts fabricated using fused deposition modeling', *Rapid Prototyping Journal*, 9(4), pp. 252–264. doi: Doi 10.1108/13552540310489631.

Bergström, J. S. and Hayman, D. (2016) 'An Overview of Mechanical Properties and Material Modeling of Polylactide (PLA) for Medical Applications', *Annals of Biomedical Engineering*, 44(2), pp. 330–340. doi: 10.1007/s10439-015-1455-8.

Berretta, S. *et al.* (2017) 'Fused Deposition Modelling of high temperature polymers: Exploring CNT PEEK composites', *Polymer Testing*. Elsevier Ltd, 63, pp. 251–262. doi: 10.1016/j.polymertesting.2017.08.024.

Beshchasna, N. *et al.* (2020) 'Recent Advances in Manufacturing Innovative Stents', *Pharmaceutics*, 12(349), pp. 1–37. doi: 10.3390/pharmaceutics12040349.

Beslikas, T. *et al.* (2011) 'Crystallization Study and Comparative in Vitro – in Vivo Hydrolysis of PLA Reinforcement Ligament', pp. 6597–6618. doi: 10.3390/ijms12106597.

Bezrouk, A. *et al.* (2020) 'Mechanical properties of a biodegradable self-expandable polydioxanone monofilament stent: In vitro force relaxation and its clinical relevance', *PLoS ONE*, 15(7 July), pp. 1–16. doi: 10.1371/journal.pone.0235842.

Bhatia, S. K. (2010a) 'Biomaterials for clinical applications', *Biomaterials for Clinical Applications*, pp. 1–283. doi: 10.1007/978-1-4419-6920-0.

Bhatia, S. K. (2010b) 'Biomaterials for clinical applications', *Biomaterials for Clinical Applications*, pp. 1–283. doi: 10.1007/978-1-4419-6920-0.

Bhatt, A. and Anbarasu, A. (2017) 'Nanoscale Biomaterials for 3D printing', *IOSR Journal of Pharmacy and Biological Sciences*, 12(03), pp. 80–86. doi: 10.9790/3008-1203068086.

Bioabsorbable Stents Global Market Report 2020-30: Covid 19 Growth and Change (2020). Available at: https://www.reportlinker.com/p05948405/Bioabsorbable-Stents-Global-Market-Report-30-Covid-19-Growth-and-Change.html?utm_source=GNW#backAction=2.

von Birgelen, C. *et al.* (2016) 'Very thin strut biodegradable polymer everolimus-eluting and sirolimus-eluting stents versus durable polymer zotarolimus-eluting stents in allcomers with coronary artery disease (BIO-RESORT): a three-arm, randomised, non-inferiority trial', *The Lancet*, 388(10060), pp. 2607–2617. doi: 10.1016/S0140-6736(16)31920-1.

Boland, E. L. *et al.* (2016) 'A Review of Material Degradation Modelling for the Analysis and Design of Bioabsorbable Stents', *Annals of Biomedical Engineering*, 44(2), pp. 341–356. doi: 10.1007/s10439-015-1413-5.

Book, C. (2017) *Zotarolimus properties*. Available at: https://www.chemicalbook.com/ChemicalProductProperty_EN_CB21011766.htm (Accessed: 10 October 2020).

Borhani, S. *et al.* (2018) *Cardiovascular stents: overview, evolution, and next generation*, *Progress in Biomaterials*. Springer Berlin Heidelberg. doi: 10.1007/s40204-018-0097-y.

Botting, R. M. (2000) 'Mechanism of action of acetaminophen: Is there a cyclooxygenase 3?', *Clinical Infectious Diseases*, 31(SUPPL. 5), pp. 202–210. doi: 10.1086/317520.

Bounabi, L. *et al.* (2016) 'Journal of Drug Delivery Science and Technology Development of poly (2-hydroxyethyl methacrylate)/ clay composites as drug delivery systems of paracetamol', *Journal of Drug Delivery Science and Technology*. Elsevier Ltd, 33, pp. 58–65. doi: 10.1016/j.jddst.2016.03.010.

Bracco, G. and Holst, B. (2013) *Surface science techniques*, *Springer Series in Surface Sciences*. doi: 10.1007/978-3-642-34243-1.

Braunersreuther, V., Mach, F. and Montecucco, F. (2012) 'Statins and stent thrombosis', (February), pp. 1–9. doi: 10.4414/smw.2012.13525.

Breitenbach, J. (2002) 'Melt extrusion: from process to drug delivery technology', *European Journal of Pharmaceutics and Biopharmaceutics*, 54(2), pp. 107–117. doi: 10.1016/S0939-6411(02)00061-9.

Brie, D. *et al.* (2016) 'Bioresorbable scaffold — A magic bullet for the treatment of coronary artery disease?', *International Journal of Cardiology*. Elsevier Ireland Ltd, 215(April), pp. 47–59. doi: 10.1016/j.ijcard.2016.04.027.

Bugatti, V. V. G. N. C. G. G. (2017) 'Nanocomposites Based on PCL and Halloysite Nanotubes Filled with Lysozyme: Effect of Draw Ratio on the Physical Properties and Release Analysis', *Nanomaterials*, 7(8), p. 213. doi: 10.3390/nano7080213.

Caiazzo, G. *et al.* (2015) 'Absorb bioresorbable vascular scaffold: What have we learned after 5 years of clinical experience?', *International Journal of Cardiology*, 201, pp. 129–136. doi: 10.1016/j.ijcard.2015.07.101.

Cairns, D. (2003) 'Essentials of Pharmaceutical Chemistry.'

Çakman, G. (2016) 'Preparation and Physical , Thermal Properties of Polycaprolactone / m-Halloysite Nanocomposite', 2(9), pp. 842–848.

Calorimetry, D. S. and Analysis, T. (2010) 'Differential Scanning Calorimetry & Thermo-Gravimetric Analysis , Fleming PTC Differential Scanning Calorimetry & Thermo-Gravimetric Analysis , Fleming PTC', *Scanning*, pp. 1–2.

Campbell, K., Craig, D. Q. M. and Mcnally, T. (2008) 'Poly (ethylene glycol) layered silicate nanocomposites for retarded drug release prepared by hot-melt extrusion', 363, pp. 126–131. doi: 10.1016/j.ijpharm.2008.06.027.

Carazo, E. *et al.* (2019) *Clay minerals in drug delivery systems 6 ´*. doi: 10.1016/B978-0-12-814617-0.00010-4.

Carvalho, J. R. G. *et al.* (2020) 'Biocompatibility and biodegradation of poly (lactic acid) (PLA) and an immiscible PLA / poly (ε -caprolactone) (PCL) blend compatibilized by poly (ε -caprolactone- b -tetrahydrofuran) implanted in horses', *Polymer Journal*. Springer US. doi: 10.1038/s41428-020-0308-y.

Casalini, T. *et al.* (2019) 'A Perspective on Polylactic Acid-Based Polymers Use for Nanoparticles Synthesis and Applications', *Frontiers in Bioengineering and Biotechnology*, 7(October), pp. 1–16. doi: 10.3389/fbioe.2019.00259.

Cassese, S. *et al.* (2016) 'Everolimus-eluting bioresorbable vascular scaffolds versus everolimus-eluting metallic stents: A meta-analysis of randomised controlled trials', *The Lancet*. Elsevier Ltd, 387(10018), pp. 537–544. doi: 10.1016/S0140-6736(15)00979-4.

Castro-aguirre, E. *et al.* (2017) 'Impact of Nanoclays on the Biodegradation of Poly (lactic acid) Nanocomposites', 2, pp. 1–24. doi: 10.3390/polym10020202.

Castro-Aguirre, E. *et al.* (2016) 'Poly(lactic acid)—Mass production, processing, industrial applications, and end of life', *Advanced Drug Delivery Reviews*. Elsevier B.V., 107, pp. 333–366. doi: 10.1016/j.addr.2016.03.010.

Cavallaro, G., Lazzara, G. and Fakhrullin, R. (2018) 'Mesoporous inorganic nanoscale particles for drug adsorption and controlled release'.

'Cerezen device provides treatment for temporomandibular joint disorders day and night' (2016) *Bdj*. Nature Publishing Group, 220, p. 666.

Charifson, P. S. and Walters, W. P. (2014) 'Acidic and basic drugs in medicinal chemistry: A perspective', *Journal of Medicinal Chemistry*, 57(23), pp. 9701–9717. doi: 10.1021/jm501000a.

Charpentier, E. *et al.* (2015) 'Fully bioresorbable drug-eluting coronary scaffolds: A review', *Archives of Cardiovascular Diseases*. Elsevier Masson SAS, 108(6–7), pp. 385–397. doi: 10.1016/j.acvd.2015.03.009.

Chavalitpanya, K. and Phattanarudee, S. (2013) 'Poly (lactic acid)/ Polycaprolactone Blends Compatibilized with Block Copolymer', *Energy Procedia*. Elsevier B.V., 34, pp. 542–548. doi: 10.1016/j.egypro.2013.06.783.

Chellamuthu, Sabarinathan & Muthu, S & Naushad Ali, M. (2012) 'Experimental study on tensile behavior of multi wall carbon nanotube reinforced epoxy composites', (November). doi: 8. 3253-3259.

Chen, C. C. *et al.* (2003) 'Preparation and characterization of biodegradable PLA polymeric blends', *Biomaterials*. Elsevier Ltd, 24(7), pp. 1167–1173. doi: 10.1016/S0142-9612(02)00466-0.

Chen, Y. *et al.* (2014) 'Analysis of the Mechanical Properties of Solvent Cast Blends of PLA/PCL', *https://www.scientific.net/AMM*, 679, pp. 50–56. doi: https://doi.org/10.4028/www.scientific.net/AMM.679.50.

Chen, Y. *et al.* (2016) 'A Review of Multifarious Applications of Poly (Lactic Acid)', *Polymer-Plastics Technology and Engineering*, 2559(March), pp. 1057–1075. doi: 10.1080/03602559.2015.1132465.

Chen, Y. *et al.* (2016) 'Review of Multifarious Applications of Poly (Lactic Acid)', *Polymer - Plastics Technology and Engineering*, 55(10). doi: 10.1080/03602559.2015.1132465.

Chen, Y. *et al.* (2017) 'Halloysite nanotube reinforced polylactic acid composite', *Polymer Composites*, 38(10). doi: 10.1002/pc.23794.

Chen, Y. *et al.* (2018) 'Surface-modified halloysite nanotubes reinforced poly(lactic acid) for use in biodegradable coronary stents', *Journal of Applied Polymer Science*, 135(30), p. 46521. doi: 10.1002/app.46521.

Chia, H. N. and Wu, B. M. (2015) 'Recent advances in 3D printing of biomaterials', *Journal of Biological Engineering*. BioMed Central, 9(1), p. 4. doi: 10.1186/s13036-015-0001-4.

Coates, J. (2000) 'Interpretation of Infrared Spectra , A Practical Approach Interpretation of Infrared Spectra , A Practical Approach', *Encyclopedia of Analytical Chemistry*, pp. 10815–10837. doi: DOI: 10.1002/9780470027318.

Collet, C. *et al.* (2016) 'The Absorb Bioresorbable Vascular Scaffold for the treatment of coronary artery disease', 5247(August). doi: 10.1080/17425247.2016.1227788.

Conijn, M. *et al.* (2018) 'The Y-stenting technique for pulmonary artery bifurcation stenosis: Initial results and mid-term outcomes', *International Journal of Cardiology*. Elsevier B.V., 268, pp. 202–207. doi: 10.1016/j.ijcard.2018.03.100.

Conner, B. P. *et al.* (2014) 'Making sense of 3-D printing: Creating a map of additive manufacturing products and services', *Additive Manufacturing*. Elsevier B.V., 1, pp. 64–76. doi: 10.1016/j.addma.2014.08.005.

Coppola, B. *et al.* (2018) '3D printing of PLA/clay nanocomposites: Influence of printing temperature on printed samples properties', *Materials*, 11(10), pp. 1–17. doi: 10.3390/ma11101947.

Corea, J. R. (2016) *Screen Printed MRI Receive Coils*.

Cui, W. *et al.* (2006) 'Investigation of Drug Release and Matrix Degradation of Electrospun Poly (DL -lactide) Fibers with Paracetanol Inoculation', pp. 1623–1629.

Ćwikła, G. *et al.* (2017) 'The influence of printing parameters on selected mechanical properties of FDM/FFF 3D-printed parts', *IOP Conference Series: Materials Science and Engineering*, 227(1). doi: 10.1088/1757-899X/227/1/012033.

Dadbakhsh, S. *et al.* (2016) 'Effect of powder size and shape on the SLS processability and mechanical properties of a TPU elastomer', *Physics Procedia*, 83, pp. 971–980. doi: 10.1016/j.phpro.2016.08.102.

Dadras, M. *et al.* (2020) 'Biodegradable Nanocomposites Developed from PLA / PCL Blends and Silk Fibroin Nanoparticles : Study on the Microstructure , Thermal Behavior , Crystallinity and Performance', *Journal of Polymers and the Environment*. Springer US, (0123456789). doi: 10.1007/s10924-020-01684-0.

Das, S., Banerjee, R. and Bellare, J. (2005) 'Aspirin loaded albumin nanoparticles by coacervation: Implications in drug delivery', *Trends in Biomaterials and Artificial Organs*, 18(2), pp. 203–212.

Dave, B. (2016) 'Bioresorbable scaffolds: Current evidences in the treatment of coronary artery disease', *Journal of Clinical and Diagnostic Research*, 10(10), pp. 1–7. doi: 10.7860/JCDR/2016/21915.8429.

Dave, R. H., Shah, D. A. and Patel, P. G. (2014) 'Development and Evaluation of High Loading Oral Dissolving Film of Aspirin and Acetaminophen', pp. 112–122. doi: 10.1166/jpsp.2014.1014.

Debra Dunson, Ph.D., E. L. (2017) 'Characterization of Polymers using Dynamic Mechanical Analysis (DMA)'.

Debusschere, N. *et al.* (2015) 'A finite element strategy to investigate the free expansion behaviour of a biodegradable polymeric stent', *Journal of Biomechanics*. Elsevier, 48(10), pp. 2012–2018. doi: 10.1016/j.jbiomech.2015.03.024.

Deepak, R. and Agrawal, Y. K. (2012) 'Study of nanocomposites with emphasis to halloysite nanotubes', *Reviews on Advanced Materials Science*, 32(2), pp. 149–157.

Dermanaki Farahani, R. and Dubé, M. (2017) 'Printing Polymer Nanocomposites and Composites in Three Dimensions', *Advanced Engineering Materials*, 1700539, pp. 1–9. doi: 10.1002/adem.201700539.

DeSimone, J. *et al.* (2015) 'Continuous liquid interphase printing'.

Devine, D. M. *et al.* (2006) 'Multifunctional polyvinylpyrrolidinone-polyacrylic acid copolymer hydrogels for biomedical applications', *International Journal of Pharmaceutics*, 326(1–2), pp. 50–59. doi: 10.1016/j.ijpharm.2006.07.008.

Devine, D. M. *et al.* (2017) 'Extended release of proteins following encapsulation in hydroxyapatite/chitosan composite scaffolds for bone tissue engineering applications', *Materials Science and Engineering C*. doi: 10.1016/j.msec.2017.11.001.

Devine, D. M. *et al.* (2017) 'Extended release of proteins following encapsulation in hydroxyapatite/chitosan composite scaffolds for bone tissue engineering applications', *Materials Science and Engineering C*. Elsevier, 84(November 2016), pp. 281–289. doi:

10.1016/j.msec.2017.11.001.

Devine, D. M., Geever, L. M. and Higginbotham, C. L. (2005) 'Drug release from a N-vinylpyrrolidinone / acrylic acid lubricious hydrophilic coating', 0, pp. 3429–3436.

Dillon, B. *et al.* (2019) 'The influence of low shear microbore extrusion on the properties of high molecular weight poly(l-lactic acid) for medical tubing applications', *Polymers*, 11(4). doi: 10.3390/polym11040710.

Dizon, J. R. C. *et al.* (2018) 'Mechanical characterization of 3D-printed polymers', *Additive Manufacturing*. Elsevier B.V., 20(January), pp. 44–67. doi: 10.1016/j.addma.2017.12.002.

Domenech, T., Peuvrel-Disdier, E. and Vergnes, B. (2012) 'Influence of twin-screw processing conditions on structure and properties of polypropylene - Organoclay nanocomposites', *International Polymer Processing*, 27(5), pp. 517–526. doi: 10.3139/217.2591.

Dong, Y. *et al.* (2015a) 'Polylactic acid (PLA)/halloysite nanotube (HNT) composite mats: Influence of HNT content and modification', *Composites Part A: Applied Science and Manufacturing*, 76(October), pp. 28–36. doi: 10.1016/j.compositesa.2015.05.011.

Dong, Y. *et al.* (2015b) 'Polylactic acid (PLA)/halloysite nanotube (HNT) composite mats: Influence of HNT content and modification', *Composites Part A: Applied Science and Manufacturing*. doi: 10.1016/j.compositesa.2015.05.011.

Dong, Y., Bickford, T. and Haroosh, H. J. (2012) 'Statistical Design of Experiments for Electrospun Poly (lactic acid) (PLA)/ Halloysite Nanotube (HNT) Composites in Response to Fibre Diameter and Thermal Properties', (November), pp. 6–8.

Dorigato, A. *et al.* (2017) 'Electrically conductive nanocomposites for fused deposition modelling', *Synthetic Metals*. Elsevier B.V., 226, pp. 7–14. doi: 10.1016/j.synthmet.2017.01.009.

Dreher, M. L., Nagaraja, S. and Batchelor, B. (2016) 'Effects of fatigue on the chemical and mechanical degradation of model stent sub-units', *Journal of the Mechanical Behavior of Biomedical Materials*. Elsevier, 59, pp. 139–145. doi: 10.1016/j.jmbbm.2015.12.020.

Du, M., Guo, B. and Jia, D. (2010) 'Newly emerging applications of halloysite nanotubes: A review', *Polymer International*, 59(5), pp. 574–582. doi: 10.1002/pi.2754.

Dul, S., Fambri, L. and Pegoretti, A. (2016) 'Fused deposition modelling with ABS-graphene nanocomposites', *Composites Part A: Applied Science and Manufacturing*. Elsevier Ltd, 85, pp. 181–191. doi: 10.1016/j.compositesa.2016.03.013.

Ebube, N. K. *et al.* (1997) 'Sustained Release of Acetaminophen from Heterogeneous Matrix Tablets : Influence of Polymer Ratio , Polymer Loading , and Co-active on Drug Release', 2(2), pp. 161–170.

Ebube, N. K. and Jones, A. B. (2004) 'Sustained release of acetaminophen from a heterogeneous mixture of two hydrophilic non-ionic cellulose ether polymers', 272, pp. 19–27. doi: 10.1016/j.ijpharm.2003.11.020.

Edy Pramono, A., Rebet, I. and Zulfia, A. (2015) 'Tensile and Shear Punch Properties of Bamboo Fibers Reinforced Polymer Composites', *International Journal of Composite Materials*, 5(1), pp. 9–17. doi: 10.5923/j.cmaterials.20150501.02.

Ellis, S. G. *et al.* (2015) 'Everolimus-Eluting Bioresorbable Scaffolds for Coronary Artery Disease', *New England Journal of Medicine*, 373(20), pp. 1905–1915. doi: 10.1056/NEJMoa1509038.

Elsawy, M. A. *et al.* (2017) 'Hydrolytic degradation of polylactic acid (PLA) and its composites', *Renewable and Sustainable Energy Reviews*. Elsevier Ltd, 79(May), pp. 1346–1352. doi: 10.1016/j.rser.2017.05.143.

Englert, C. *et al.* (2018) 'Pharmapolymers in the 21st century: Synthetic polymers in drug delivery applications', *Progress in Polymer Science*. Elsevier B.V., 87, pp. 107–164. doi: 10.1016/j.progpolymsci.2018.07.005.

Farah, S., Anderson, D. G. and Langer, R. (2016) 'Physical and mechanical properties of PLA, and

their functions in widespread applications - A comprehensive review', *Advanced Drug Delivery Reviews*, pp. 367–392. doi: 10.1016/j.addr.2016.06.012.

FDA's Role in 3D Printing (no date).

Ferreira, R. T. L. *et al.* (2017) 'Experimental characterization and micrography of 3D printed PLA and PLA reinforced with short carbon fibers', *Composites Part B: Engineering*. Elsevier Ltd, 124, pp. 88–100. doi: 10.1016/j.compositesb.2017.05.013.

Ferri, J. M. *et al.* (2016) 'Effect of miscibility on mechanical and thermal properties of poly(lactic acid)/ polycaprolactone blends', *Polymer International*, 65(4), pp. 453–463. doi: 10.1002/pi.5079.

Filipovic, N. *et al.* (2018) *Computer Modeling of Stent Deployment in the Coronary Artery Coupled with Plaque Progression*, *Biomaterials in Clinical Practice: Advances in Clinical Research and Medical Devices*. doi: 10.1007/978-3-319-68025-5.

Finotti, P. F. M. *et al.* (2017) 'Journal of the Mechanical Behavior of Biomedical Materials Immiscible poly (lactic acid)/ poly (ε -caprolactone) for temporary implants : Compatibility and cytotoxicity', *Journal of the Mechanical Behavior of Biomedical Materials*. Elsevier Ltd, 68(October 2016), pp. 155–162. doi: 10.1016/j.jmbbm.2017.01.050.

Foerst, J. *et al.* (2013) 'Evolution of Coronary Stents: From Bare-Metal Stents to Fully Biodegradable, Drug-Eluting Stents', *Comb Prod Ther*, (3), pp. 9–24. doi: 10.1007/s13556-013-0005-7.

Fortelny, I. *et al.* (2019) 'Phase Structure, Compatibility, and Toughness of PLA/PCL Blends: A Review', *Frontiers in Materials*, 6(August), pp. 1–13. doi: 10.3389/fmats.2019.00206.

Frank, A., Rath, S. K. and Venkatraman, S. S. (2005) 'Controlled release from bioerodible polymers : effect of drug type and polymer composition', 102, pp. 333–344. doi: 10.1016/j.jconrel.2004.10.019.

Freire, E. (1995) 'Differential Scanning Calorimetry', *Methods in Molecular Biology*, pp. 191–218. doi: 10.1385/0-89603-232-9:125.

Fu, L. *et al.* (2017) 'Engineering a tubular mesoporous silica nanocontainer with well-preserved clay shell from natural halloysite', *Nano Research*, 10(8), pp. 2782–2799. doi: 10.1007/s12274-017-1482-x.

Fuenmayor, E. *et al.* (2018) 'Material considerations for fused-filament fabrication of solid dosage forms', *Pharmaceutics*, 10(2), pp. 1–27. doi: 10.3390/pharmaceutics10020044.

Fujisawa, J. ichi, Eda, T. and Hanaya, M. (2017) 'Facile, quick and selective visible-light sensing of phenol-containing drug molecules acetaminophen and biosol by use of interfacial charge-transfer transitions with TiO2 nanoparticles', *Chemical Physics Letters*. Elsevier B.V., 684, pp. 328–332. doi: 10.1016/j.cplett.2017.07.019.

Fule, R., Paithankar, V. and Amin, P. (2016) 'Hot melt extrusion based solid solution approach: Exploring polymer comparison, physicochemical characterization and in-vivo evaluation', *International Journal of Pharmaceutics*. Elsevier B.V., 499(1–2), pp. 280–294. doi: 10.1016/j.ijpharm.2015.12.062.

Gaaz, T. *et al.* (2017) 'The Impact of Halloysite on the Thermo-Mechanical Properties of Polymer Composites', *Molecules*, 22(6), p. 838. doi: 10.3390/molecules22050838.

Gamon, G., Evon, P. and Rigal, L. (2013) 'Twin-screw extrusion impact on natural fibre morphology and material properties in poly(lactic acid) based biocomposites', *Industrial Crops and Products*. Elsevier B.V., 46, pp. 173–185. doi: 10.1016/j.indcrop.2013.01.026.

Gao, M. *et al.* (2017) 'Preparation of a novel breviscapine-loaded halloysite nanotubes complex for controlled release of breviscapine Preparation of a novel breviscapine-loaded halloysite nanotubes complex for controlled release of breviscapine', *Material Science and Engineering*, 265, pp. 1–8. doi: 10.1088/1757-899X/265/1/012011.

Gao, W. *et al.* (2015) 'The status, challenges, and future of additive manufacturing in engineering', *Computer-Aided Design*. Elsevier Ltd, 69, pp. 65–89. doi: 10.1016/j.cad.2015.04.001.

GaRea, S. A. (2017) *List of Abbreviations*. doi: 10.1016/B978-0-323-46153-5.00014-8.

Garg, S. and Serruys, P. W. (2010a) 'Coronary stents: Current status', *Journal of the American College of Cardiology*. Elsevier Masson SAS, 56(10 SUPPL.), pp. S1–S42. doi: 10.1016/j.jacc.2010.06.007.

Garg, S. and Serruys, P. W. (2010b) 'Coronary stents: Looking forward', *Journal of the American College of Cardiology*. Elsevier Masson SAS, 56(10 SUPPL.), pp. S43–S78. doi: 10.1016/j.jacc.2010.06.008.

Garlotta, D. (2002) 'A Literature Review of Poly (Lactic Acid)', *Journal of Polymers and the Environment*, 9(2), pp. 63–84. doi: 10.1023/A:1020200822435.

Giacchi, G. *et al.* (2016) 'Bioresorbable vascular scaffolds technology: current use and future developments.', *Medical devices (Auckland, N.Z.)*, 9, pp. 185–98. doi: 10.2147/MDER.S90461.

Gill, P., Moghadam, T. T. and Ranjbar, B. (2010) 'Differential scanning calorimetry techniques: applications in biology and nanoscience.', *Journal of biomolecular techniques : JBT*, 21(4), pp. 167–93. Available at: /pmc/articles/PMC2977967/?report=abstract.

Gnanasekaran, K. *et al.* (2017) '3D printing of CNT- and graphene-based conductive polymer nanocomposites by fused deposition modeling', *Applied Materials Today*. Elsevier Ltd, 9, pp. 21–28. doi: 10.1016/j.apmt.2017.04.003.

Gorrasi, G. *et al.* (2014) 'PLA/halloysite nanocomposite films: Water vapor barrier properties and specific key characteristics', *Macromolecular Materials and Engineering*, 299(1), pp. 104–115. doi: 10.1002/mame.201200424.

Gross, B. C. *et al.* (2014) 'Evaluation of 3D printing and its potential impact on biotechnology and the chemical sciences', *Analytical Chemistry*, 86(7), pp. 3240–3253. doi: 10.1021/ac403397r.

Gs, E., Al, K. and Youseffi, M. (2019) 'Effect of screw configuration on the dispersion and properties of polypropylene / multiwalled carbon nanotube composite'.

Gu, L., Zhao, S. and Froemming, S. R. (2012) 'Arterial wall mechanics and clinical implications after coronary stenting: Comparisons of three stent designs', *International Journal of Applied Mechanics*, 4(2). doi: 10.1142/S1758825112500135.

Gu, X. *et al.* (2016) 'Biodegradable, elastomeric coatings with controlled anti-proliferative agent release for magnesium-based cardiovascular stents', *Colloids and Surfaces B: Biointerfaces*. Elsevier B.V., 144, pp. 170–179. doi: 10.1016/j.colsurfb.2016.03.086.

Guerra, A. and Ciurana, J. (2018) '3D-printed bioabsordable polycaprolactone stent: The effect of process parameters on its physical features', *Materials & Design*. Elsevier Ltd, 137, pp. 430–437. doi: 10.1016/J.MATDES.2017.10.045.

Guerra, A. J. *et al.* (2018) '3D-printed PCL/PLA composite stents: Towards a new solution to cardiovascular problems', *Materials*, 11(9), pp. 1–13. doi: 10.3390/ma11091679.

Guerra, A. J., San, J. and Ciurana, J. (2017) 'Fabrication of PCL/PLA Composite Tube for Stent Manufacturing', *Procedia CIRP*. The Author(s), 65, pp. 231–235. doi: 10.1016/j.procir.2017.03.339.

Guerra, A., Roca, A. and de Ciurana, J. (2017) 'A novel 3D additive manufacturing machine to biodegradable stents', *Procedia Manufacturing*. Elsevier B.V., 13, pp. 718–723. doi: 10.1016/j.promfg.2017.09.118.

Guo, J., Qiao, J. and Zhang, X. (2016) 'Effect of an alkalized-modified halloysite on PLA crystallization, morphology, mechanical, and thermal properties of PLA/halloysite nanocomposites', *Journal of Applied Polymer Science*, 133(48), pp. 1–9. doi: 10.1002/app.44272.

Hairaldin, S. Z. *et al.* (2012) 'Effect Addition of Octadecylamine Modified Clay (ODA-MMT) to Polylactide / Polycaprolactone (PLA / PCL) blend', 364, pp. 317–321. doi: 10.4028/www.scientific.net/AMR.364.317.

Hajiali, Z., Dabagh, M. and Jalali, P. (2014) 'A Computational Model to Assess Poststenting Wall Stresses Dependence on Plaque Structure and Stenosis Severity in Coronary Artery', *Mathematical*

Problems in Engineering, 2014. doi: 10.1155/2014/937039.

Hamad, K. *et al.* (2015) 'Properties and medical applications of polylactic acid: A review', *Express Polymer Letters*, 9(5), pp. 435–455. doi: 10.3144/expresspolymlett.2015.42.

Haroosh, H., Chaudhary, Deeptangshu Dong, Y. and Hawkins, B. (2011) 'Electrospun PLA : PCL / halloysite nanotube nanocomposites fibers for drug delivery', *Nineteenth International Conference on Processing and Fabrication of Advanced Materials*, (Pfam Xix), pp. 847–858.

Haroosh, H. J. *et al.* (2013) 'Electrospun PLA: PCL composites embedded with unmodified and 3-aminopropyltriethoxysilane (ASP) modified halloysite nanotubes (HNT)', *Applied Physics A: Materials Science and Processing*, 110(2), pp. 433–442. doi: 10.1007/s00339-012-7233-7.

Healy, A. V *et al.* (2018) 'Degradable Nanocomposites for Fused Filament Fabrication Applications'. doi: 10.3390/jmmp2020029.

Hiemenz, J. (2011) '3D printing jigs , fixtures and other manufacturing tools', *Stratasys,Inc*.

Hoare, D. *et al.* (2019) 'The Future of Cardiovascular Stents : Bioresorbable and Integrated Biosensor Technology', 1900856. doi: 10.1002/advs.201900856.

Holman, H., Kavarana, M. and Rajab, T. K. (2020) 'Smart Materials in Cardiovascular Implants: Shape Memory Alloys and Shape Memory Polymers', *Artificial Organs*, pp. 0–2. doi: 10.1111/aor.13851.

Hornbeck, L. J. (1997) 'Digital Light Processing for high-brightness high-resolution applications', in Wu, M. H. (ed.). International Society for Optics and Photonics, pp. 27–40. doi: 10.1117/12.273880.

Hornsby, P. (2017) 'Compounding of Particulate-Filled Thermoplastics', pp. 95–110. doi: 10.1007/978-3-319-28117-9.

Hou, Z. *et al.* (2008) 'Structural orientation and tensile behavior in the extrusion-stretched sheets of polypropylene/multi-walled carbon nanotubes' composite', *Polymer*, 49(16), pp. 3582–3589. doi: 10.1016/j.polymer.2008.06.008.

Hu, T. *et al.* (2015) 'Controlled Slow-Release Drug-Eluting Stents for the Prevention of Coronary Restenosis: Recent Progress and Future Prospects', *ACS Applied Materials and Interfaces*, 7(22), pp. 11695–11712. doi: 10.1021/acsami.5b01993.

Huang, M. *et al.* (2006) 'Degradation Characteristics of Poly (□ -caprolactone) -Based Copolymers and Blends', pp. 1–7. doi: 10.1002/app.24196.

Hull, C. W. and Arcadia, C. (1986) 'Apparatus for production of three-dimensional objects by stereolithography', *Apparatus for Production of Three-Dimensional Objects by Stereolithography*. doi: 10.1145/634067.634234.

Hwa, L. C. *et al.* (2017) 'Recent advances in 3D printing of porous ceramics: a review', *Current Opinion in Solid State and Materials Science*. Elsevier, pp. 323–347. doi: 10.1016/j.cossms.2017.08.002.

Hyvärinen, M., Jabeen, R. and Kärki, T. (2020) 'The Modelling of Extrusion Processes for'.

Im, S. H., Jung, Y. and Kim, S. H. (2017) 'Current status and future direction of biodegradable metallic and polymeric vascular scaffolds for next-generation stents', *Acta Biomaterialia*, 60, pp. 3–22. doi: 10.1016/j.actbio.2017.07.019.

Innovation, R. (2013) 'MedIcal devIces'.

ISO 10993 - Biological Evaluataion of Medical Devices (no date).

Ivanova, O., Williams, C. and Campbell, T. (2013) 'Additive manufacturing (AM) and nanotechnology: promises and challenges', *Rapid Prototyping Journal*, 19(5), pp. 353–364. doi: 10.1108/RPJ-12-2011-0127.

Jabara, R. *et al.* (2009) 'Bioabsorbable Stents: The Future Is Near, A review of the breakthroughs and challenges of bioabsorbable stents as a potential solution to the risks associated with available drug-

eluting stents', *Cardiac Interventions Today*, June/July(July), pp. 50–53. Available at: http://bmctoday.net/citoday/2009/07/article.asp?f=CIT0709_07.php.

Jaganathan, S. K. *et al.* (2014) 'Biomaterials in Cardiovascular Research: Applications and Clinical Implications', *Biomed Research International*, 2014, p. 11. doi: 10.1155/2014/459465.

Jani, R. and Patel, D. (2014) 'Hot melt extrusion: An industrially feasible approach for casting orodispersible film', *Asian Journal of Pharmaceutical Sciences*. Elsevier Ltd, 10(4), pp. 292–305. doi: 10.1016/j.ajps.2015.03.002.

Jenjob, R. *et al.* (2015) 'Recent trend in applications of polymer materials to stents', pp. 83–88. doi: 10.18528/gii150022.

Jia, S. *et al.* (2017) 'Morphology, crystallization and thermal behaviors of PLA-based composites: Wonderful effects of hybrid GO/PEG via dynamic impregnating', *Polymers*, 9(10). doi: 10.3390/polym9100528.

Jock Churchman, G. *et al.* (2016) 'Unique but diverse: some observations on the formation, structure and morphology of halloysite', *Clay Minerals*, 51(3), pp. 395–416. doi: 10.1180/claymin.2016.051.3.14.

Jock Churchman, G., Pasbakhsh, P. and Hillier, S. (2016) 'The rise and rise of halloysite', *Clay Minerals*, 51(3), pp. 303–308. doi: 10.1180/claymin.2016.051.3.00.

Joussein, E. *et al.* (2005) 'Halloysite clay minerals – a review', *Clay Minerals*, 40(4), pp. 383–426. doi: 10.1180/0009855054040180.

Kalepu, S. and Nekkanti, V. (2015) 'Insoluble drug delivery strategies: Review of recent advances and business prospects', *Acta Pharmaceutica Sinica B*. Elsevier, 5(5), pp. 442–453. doi: 10.1016/j.apsb.2015.07.003.

Kamble, R. *et al.* (2012) 'Review article halloysite nanotubes and applications : A review', *Journal of Advanced Scientific Research*, 3(2), pp. 25–29.

Kandzari, D. E. *et al.* (2020) 'Ultrathin Bioresorbable-Polymer Sirolimus-Eluting Stents Versus Thin Durable-Polymer Everolimus-Eluting Stents for Coronary Revascularization', 13(11). doi: 10.1016/j.jcin.2020.02.019.

Kantesh Balani, Vivek Verma, Arvind Agarwal, R. N. (2015) 'Physical, thermal, and mechanical properties of polymers', in *Biosurfaces: A Materials Science and Engineering Perspective*. First. John Wiley & Sons, Inc, pp. 329–344.

Kawashima, H. *et al.* (2020) 'Expert Opinion on Drug Delivery Drug-eluting bioresorbable scaffolds in cardiovascular disease , peripheral artery and gastrointestinal fields : a clinical update', *Expert Opinion on Drug Delivery*. Taylor & Francis, 00(00), pp. 1–15. doi: 10.1080/17425247.2020.1764932.

Kelnar, I. *et al.* (2016) 'Effect of halloysite on structure and properties of melt-drawn PCL/PLA microfibrillar composites', *Express Polymer Letters*, 10(5), pp. 381–393. doi: 10.3144/expresspolymlett.2016.36.

Kelnar, I. *et al.* (2017) 'Graphite nanoplatelets-modified PLA/PCL: Effect of blend ratio and nanofiller localization on structure and properties', *Journal of the Mechanical Behavior of Biomedical Materials*, 71(March), pp. 271–278. doi: 10.1016/j.jmbbm.2017.03.028.

Khadka, P. *et al.* (2014) 'Pharmaceutical particle technologies: An approach to improve drug solubility, dissolution and bioavailability', *Asian Journal of Pharmaceutical Sciences*. Elsevier Ltd, 9(6), pp. 304–316. doi: 10.1016/j.ajps.2014.05.005.

Khanesar, M. A. (2019) 'Medical Applications of 3D Printing', pp. 3–5. doi: 10.33552/ABEB.2019.02.000531.

Kim, H. *et al.* (2018) 'Enhanced dielectric properties of three phase dielectric MWCNTs/BaTiO 3 /PVDF nanocomposites for energy storage using fused deposition modeling 3D printing', *Ceramics International*. Elsevier Ltd and Techna Group S.r.l. doi: 10.1016/j.ceramint.2018.02.107.

Kimura, T. *et al.* (2015) 'A randomized trial evaluating everolimus-eluting Absorb bioresorbable scaffolds vs. everolimus-eluting metallic stents in patients with coronary artery disease: ABSORB Japan', *European Heart Journal*, 36(47), pp. 3332–3342. doi: 10.1093/eurheartj/ehv435.

King, S. B. and Gogas, B. D. (2017) 'Can the Vanishing Stent Reappear?', *Journal of the American College of Cardiology*, (4), pp. 3–5. doi: 10.1016/j.jacc.2017.10.009.

Klein, L. W. (2006) 'Are drug-eluting stents the preferred treatment for multivessel coronary artery disease?', *Journal of the American College of Cardiology*. Elsevier Masson SAS, 47(1), pp. 22–26. doi: 10.1016/j.jacc.2005.08.057.

Kobo, O. *et al.* (2020) 'Modern stents: Where are we going?', *Rambam Maimonides Medical Journal*, 11(2), pp. 1–9. doi: 10.5041/RMMJ.10403.

Kodama, H. (1981) 'Automatic method for fabricating a three-dimensional plastic model with photo-hardening polymer', *Review of Scientific Instruments*, 52(11), pp. 1770–1773. doi: 10.1063/1.1136492.

Kokkinis, D., Schaffner, M. and Studart, A. R. (2015) 'Multimaterial magnetically assisted 3D printing of composite materials', *Nature Communications*. Nature Publishing Group, 6(1), p. 8643. doi: 10.1038/ncomms9643.

Kokot, G. *et al.* (2018) 'A project of bioresorbable self-expanding vascular stents. the crimping process numerical simulation', *AIP Conference Proceedings*, 1922, pp. 1–7. doi: 10.1063/1.5019071.

Kokubo, T. and Takadama, H. (2006) 'How useful is SBF in predicting in vivo bone bioactivity?', *Biomaterials*, 27(15), pp. 2907–2915. doi: 10.1016/j.biomaterials.2006.01.017.

Krishnaiah, P., Ratnam, C. T. and Manickam, S. (2017) 'Development of silane grafted halloysite nanotube reinforced polylactide nanocomposites for the enhancement of mechanical, thermal and dynamic-mechanical properties', *Applied Clay Science*. Elsevier B.V., 135, pp. 583–595. doi: 10.1016/j.clay.2016.10.046.

Kruth, J.-P., Leu, M. C. and Nakagawa, T. (1998) 'Progress in Additive Manufacturing and Rapid Prototyping', *CIRP Annals - Manufacturing Technology*, 47(2), pp. 525–540. doi: 10.1016/S0007-8506(07)63240-5.

Lamberti, P. *et al.* (2018) 'Evaluation of thermal and electrical conductivity of carbon-based PLA nanocomposites for 3D printing', 020158, p. 020158. doi: 10.1063/1.5046020.

Lawson, G., Ogwu, J. and Tanna, S. (2018) 'Quantitative screening of the pharmaceutical ingredient for the rapid identification of substandard and falsified medicines using reflectance infrared spectroscopy', pp. 1–17.

Lee, J. H. *et al.* (2018) 'Analysis of trends and prospects regarding stents for human blood vessels', *Biomaterials Research*. Biomaterials Research, 22(1), p. 8. doi: 10.1186/s40824-018-0114-1.

Leporatti, S. (2017) 'Halloysite clay nanotubes as nano-bazookas for drug delivery', *Polymer International*, 66(8), pp. 1111–1118. doi: 10.1002/pi.5347.

Li, F. *et al.* (2018) 'Journal of Drug Delivery Science and Technology In vitro release study of sirolimus from a PDLLA matrix on a bioresorbable drug-eluting stent', *Journal of Drug Delivery Science and Technology*. Elsevier, 48(August), pp. 88–95. doi: 10.1016/j.jddst.2018.08.026.

Li, G. *et al.* (2018) 'Effect of ultrasonic vibration on mechanical properties of 3D printing non-crystalline and semi-crystalline polymers', *Materials*, 11(5). doi: 10.3390/ma11050826.

Li, X. *et al.* (2016) 'Chitosan modified halloysite nanotubes as emerging porous microspheres for drug carrier', *Applied Clay Science*. Elsevier B.V., 126, pp. 306–312. doi: 10.1016/j.clay.2016.03.035.

Li, Y. *et al.* (2014) 'Poly(L-lactide)/Poly(D-lactide)/clay nanocomposites: Enhanced dispersion, crystallization, mechanical properties, and hydrolytic degradation', *Polymer Engineering & Science*, 54(4), pp. 914–924. doi: 10.1002/pen.23620.

Ligon, S. C. *et al.* (2017) 'Polymers for 3D Printing and Customized Additive Manufacturing',

Chemical Reviews, 117(15), pp. 10212–10290. doi: 10.1021/acs.chemrev.7b00074.

van Lith, R. *et al.* (2016) '3D-Printing Strong High-Resolution Antioxidant Bioresorbable Vascular Stents', *Advanced Materials Technologies*, 1(9), pp. 1–7. doi: 10.1002/admt.201600138.

Liu, L. *et al.* (2018) 'Comparison of drug-eluting balloon versus drug-eluting stent for treatment of coronary artery disease : a meta-analysis of randomized controlled trials'. BMC Cardiovascular Disorders, pp. 1–16.

Liu, M. *et al.* (2009) 'Halloysite nanotubes as a novel ??-nucleating agent for isotactic polypropylene', *Polymer*. Elsevier Ltd, 50(13), pp. 3022–3030. doi: 10.1016/j.polymer.2009.04.052.

Liu, M. *et al.* (2014) 'Recent advance in research on halloysite nanotubes-polymer nanocomposite', *Progress in Polymer Science*. Elsevier Ltd, 39(8), pp. 1498–1525. doi: 10.1016/j.progpolymsci.2014.04.004.

Liu, M., Zhang, Y. and Zhou, C. (2013) 'Nanocomposites of halloysite and polylactide', *Applied Clay Science*. Elsevier B.V., 75–76, pp. 52–59. doi: 10.1016/j.clay.2013.02.019.

Lun, H., Ouyang, J. and Yang, H. (2014) 'Natural halloysite nanotubes modified as an aspirin carrier', *RSC Adv.* Royal Society of Chemistry, 4(83), pp. 44197–44202. doi: 10.1039/C4RA09006C.

Luo, Y. *et al.* (2016) 'Synthesis and Biological Evaluation of Well-Defined Poly(propylene fumarate) Oligomers and Their Use in 3D Printed Scaffolds', *Biomacromolecules*, 17(2), pp. 690–697. doi: 10.1021/acs.biomac.6b00014.

Luyt, A. S. and Kelnar, I. (2017) 'Effect of halloysite nanotubes on the thermal degradation behaviour of poly(ε-caprolactone)/poly(lactic acid) microfibrillar composites', *Polymer Testing*. Elsevier Ltd, 60, pp. 166–172. doi: 10.1016/j.polymertesting.2017.03.027.

Lvov, Y. and Abdullayev, E. (2013) 'Functional polymer-clay nanotube composites with sustained release of chemical agents', *Progress in Polymer Science*. Elsevier Ltd, 38(10–11), pp. 1690–1719. doi: 10.1016/j.progpolymsci.2013.05.009.

Lvov, Y. M., DeVilliers, M. M. and Fakhrullin, R. F. (2016) 'The application of halloysite tubule nanoclay in drug delivery', *Expert Opinion on Drug Delivery*, 13(7), pp. 977–986. doi: 10.1517/17425247.2016.1169271.

Lyons, J. G. *et al.* (2006) 'The use of Agar as a novel filler for monolithic matrices produced using hot melt extrusion', 64, pp. 75–81. doi: 10.1016/j.ejpb.2006.03.008.

Lyons, J. G., Hallinan, M., *et al.* (2007) 'Preparation of monolithic matrices for oral drug delivery using a supercritical fluid assisted hot melt extrusion process', *International Journal of Pharmaceutics*. Elsevier, 329(1–2), pp. 62–71. doi: 10.1016/J.IJPHARM.2006.08.028.

Lyons, J. G., Holehonnur, H., *et al.* (2007) 'The incorporation of an organically modified layered silicate in monolithic polymeric matrices produced using hot melt extrusion', *Materials Chemistry and Physics*, 103(2–3), pp. 419–426. doi: 10.1016/j.matchemphys.2007.02.080.

Ma, X., Wu, T. and Robich, M. P. (2012) 'Drug-eluting stent coatings', *Interventional Cardiology*, 4(1), pp. 73–83. doi: 10.2217/ica.11.88.

Macdonald, N. P. *et al.* (2017) 'Comparing microfluidic performance of three-dimensional (3D) printing platforms', *Analytical Chemistry*. American Chemical Society, 89(7), pp. 3858–3866. doi: 10.1021/acs.analchem.7b00136.

Majewska, P., Oledzka, E. and Sobczak, M. (2019) 'Biomaterials Science drug-eluting stent technology'. Royal Society of Chemistry. doi: 10.1039/c9bm00468h.

Manallack, D. T. *et al.* (2013) 'The significance of acid/base properties in drug discovery', *Chemical Society Reviews*, 42(2), pp. 485–496. doi: 10.1039/c2cs35348b.

Maniruzzaman, M. *et al.* (2012) 'A review of hot-melt extrusion: process technology to pharmaceutical products.', *ISRN pharmaceutics*, 2012(2), pp. 436763–436769. doi: 10.5402/2012/436763.

Maniruzzaman, M. and Nokhodchi, A. (2017) ‘Continuous manufacturing via hot-melt extrusion and scale up: regulatory matters’, *Drug Discovery Today*. Elsevier Ltd, 22(2), pp. 340–351. doi: 10.1016/j.drudis.2016.11.007.

Manoudis, P. N. and Karapanagiotis, I. (2014) ‘Modification of the wettability of polymer surfaces using nanoparticles’, *Progress in Organic Coatings*. Elsevier B.V., 77(2), pp. 331–338. doi: 10.1016/j.porgcoat.2013.10.007.

Maria, L., Meirelles, A. and Raffin, F. N. (2017) ‘Clay and Polymer-Based Composites Applied to Drug Release : A Scientific and Technological Prospection .’, 1(10), pp. 115–134.

Martinez-Marcos, L. *et al.* (2016) ‘A novel hot-melt extrusion formulation of albendazole for increasing dissolution properties’, *International Journal of Pharmaceutics*. Elsevier B.V., 499(1–2), pp. 175–185. doi: 10.1016/j.ijpharm.2016.01.006.

Masood, S. H. and Song, W. Q. (2004) ‘Development of new metal/polymer materials for rapid tooling using fused deposition modelling’, *Materials and Design*. Elsevier, 25(7), pp. 587–594. doi: 10.1016/j.matdes.2004.02.009.

Matias, E. and Rao, B. (2015) ‘3D printing: On its historical evolution and the implications for business’, *Portland International Conference on Management of Engineering and Technology*. Portland International Conference on Management of, 2015–Septe, pp. 551–558. doi: 10.1109/PICMET.2015.7273052.

Matsuhiro, Y. *et al.* (2020) ‘Difference of vascular healing between bioabsorbable-polymer and durable-polymer new generation drug-eluting stents: an optical coherence tomographic analysis’, *International Journal of Cardiovascular Imaging*. Springer Netherlands, (0123456789). doi: 10.1007/s10554-020-02094-y.

McDowell, G., Slevin, M. and Krupinski, J. (2011) ‘Nanotechnology for the treatment of coronary in stent restenosis: a clinical perspective.’, *Vascular cell*. BioMed Central Ltd, 3(1), p. 8. doi: 10.1186/2045-824X-3-8.

McKittrick, C. M. *et al.* (2020) ‘Development of a Bioactive Polymeric Drug Eluting Coronary Stent Coating Using Electrospraying’, *Annals of Biomedical Engineering*, 48(1), pp. 271–281. doi: 10.1007/s10439-019-02346-6.

McLouth, T. D. *et al.* (2017) ‘The impact of print orientation and raster pattern on fracture toughness in additively manufactured ABS’, *Additive Manufacturing*. Elsevier, 18, pp. 103–109. doi: 10.1016/j.addma.2017.09.003.

McLure, T. (2017) *3D Printing Moves Align Technology Toward $1.3 Billion In Sales*, *Forbes*.

McMahon, S. *et al.* (2018) ‘Bio-resorbable polymer stents: a review of material progress and prospects’, *Progress in Polymer Science*. Elsevier Ltd, 83, pp. 79–96. doi: 10.1016/j.progpolymsci.2018.05.002.

De Mel, A., Cousins, B. G. and Seifalian, A. M. (2012) ‘Surface modification of biomaterials: A quest for blood compatibility’, *International Journal of Biomaterials*, 2012. doi: 10.1155/2012/707863.

Melchels, F. P. W., Feijen, J. and Grijpma, D. W. (2010) ‘A review on stereolithography and its applications in biomedical engineering’, *Biomaterials*. Elsevier Ltd, 31(24), pp. 6121–6130. doi: 10.1016/j.biomaterials.2010.04.050.

Mhlanga, N. and Ray, S. S. (2015) ‘Kinetic models for the release of the anticancer drug doxorubicin from biodegradable polylactide/metal oxide-based hybrids’, *International Journal of Biological Macromolecules*. Elsevier B.V., 72, pp. 1301–1307. doi: 10.1016/j.ijbiomac.2014.10.038.

Mielke, C. H. *et al.* (1976) ‘Hemostasis, Antipyretics, and Mild Analgesics: Acetaminophen vs Aspirin’, *JAMA: The Journal of the American Medical Association*, 235(6), pp. 613–616. doi: 10.1001/jama.1976.03260320021016.

Miguel, C. *et al.* (2017) ‘3D Printing for Biomedical Applications: Where Are We Now?’, *European Medical Journal*, 2(1), pp. 16–22. Available at: http://emjreviews.com/wp-content/uploads/Editor.s-

Pick-3D-Printing-for-Biomedical-Applications-Where-Are-We-Now...pdf.

Mills, D. *et al.* (2017) 'The Use of 3D Printing in the Fabrication of Nasal Stents', *Inventions*, 3(1), p. 1. doi: 10.3390/inventions3010001.

Miyajima, M., Koshika, A., Okada, J., *et al.* (1998) 'Factors influencing the diffusion-controlled release of papaverine from poly (L -lactic acid) matrix', 56, pp. 85–94.

Miyajima, M., Koshika, A., Okada, J., *et al.* (1998) 'The effects of drug physico-chemical properties on release from copoly (lactic/glycolic acid) matrix', *International Journal of Pharmaceutics*, 169(2), pp. 255–263. doi: 10.1016/S0378-5173(98)00133-1.

Miyajima, M. *et al.* (1999a) 'Effect of polymer / basic drug interactions on the two-stage diffusion-controlled release from a poly (L -lactic acid) matrix', 61, pp. 295–304.

Miyajima, M. *et al.* (1999b) 'Mechanism of drug release from poly (L -lactic acid) matrix containing acidic or neutral drugs', 60, pp. 199–209.

Mohamed, O. A., Masood, S. H. and Bhowmik, J. L. (2016) 'Optimization of fused deposition modeling process parameters for dimensional accuracy using I-optimality criterion', *Measurement: Journal of the International Measurement Confederation*. Elsevier Ltd, 81, pp. 174–196. doi: 10.1016/j.measurement.2015.12.011.

Mollace, V. *et al.* (2017) 'Aspirin wears smart', *European Heart Journal - Cardiovascular Pharmacotherapy*, 3(4), pp. 185–188. doi: 10.1093/ehjcvp/pvx017.

Montaseri, H. and Forbes, P. B. C. (2018) 'Trends in Analytical Chemistry Analytical techniques for the determination of acetaminophen : A review', *Trends in Analytical Chemistry*. Elsevier Ltd, 108, pp. 122–134. doi: 10.1016/j.trac.2018.08.023.

Monticelli, O. *et al.* (2014) 'Silsesquioxanes: Novel compatibilizing agents for tuning the microstructure and properties of PLA/PCL immiscible blends', *European Polymer Journal*. Elsevier Ltd, 58, pp. 69–78. doi: 10.1016/j.eurpolymj.2014.06.021.

Moore, S. S., O'Sullivan, K. J. and Verdecchia, F. (2016) 'Shrinking the Supply Chain for Implantable Coronary Stent Devices', *Annals of Biomedical Engineering*, 44(2), pp. 497–507. doi: 10.1007/s10439-015-1471-8.

Moravej, M. and Mantovani, D. (2011) 'Biodegradable metals for cardiovascular stent application: Interests and new opportunities', *International Journal of Molecular Sciences*, 12(7), pp. 4250–4270. doi: 10.3390/ijms12074250.

Moura, N. K. de *et al.* (2019) 'Production and Characterization of Porous Polymeric Membranes of PLA/PCL Blends with the Addition of Hydroxyapatite', *Journal of Composites Science*, 3(2), p. 45. doi: 10.3390/jcs3020045.

Mousa, M. H., Dong, Y. and Davies, I. J. (2016) 'Recent advances in bionanocomposites: Preparation, properties, and applications', *International Journal of Polymeric Materials and Polymeric Biomaterials*, 65(5), pp. 225–254. doi: 10.1080/00914037.2015.1103240.

Mueller, J., Shea, K. and Daraio, C. (2015) 'Mechanical properties of parts fabricated with inkjet 3D printing through efficient experimental design', *Materials and Design*. Elsevier Ltd, 86, pp. 902–912. doi: 10.1016/j.matdes.2015.07.129.

Munz, O. J. (1956) 'Photo-Glyph Recording'.

Murariu, M. *et al.* (2012) 'Polylactide (PLA)-Halloysite Nanocomposites: Production, Morphology and Key-Properties', *Journal of Polymers and the Environment*, 20(4), pp. 932–943. doi: 10.1007/s10924-012-0488-4.

Murariu, M. and Dubois, P. (2016) 'PLA composites: From production to properties', *Advanced Drug Delivery Reviews*. Elsevier B.V., 107, pp. 17–46. doi: 10.1016/j.addr.2016.04.003.

Nagavarma, B. V. N. *et al.* (2012) 'Different Techniques for', *Asian Journal of Pharmaceutical and Clinical Research*, 5, pp. 16–23.

Naseem, R. *et al.* (2017) 'Experimental and computational studies of poly-L-lactic acid for cardiovascular applications: recent progress', *Mechanics of Advanced Materials and Modern Processes*. Mechanics of Advanced Materials and Modern Processes, 3(1), p. 13. doi: 10.1186/s40759-017-0028-y.

Nazila, K. *et al.* (2016) 'Nanoparticles: Mechanisms of Controlling Drug Release', *Chem Rev.*, 116(4), pp. 2602–2663. doi: 10.1021/acs.chemrev.5b00346.Degradable.

Ng, J. *et al.* (2017) 'Local hemodynamic forces after stenting: Implications on restenosis and thrombosis', *Arteriosclerosis, Thrombosis, and Vascular Biology*, 37(12), pp. 2231–2242. doi: 10.1161/ATVBAHA.117.309728.

Ng, J. C. and Yeomans, N. D. (2018) 'Helicobacter pylori infection and the risk of upper gastrointestinal bleeding in low dose aspirin users: systematic review and meta-analysis', *The Medical Journal of Australia*, 209(7), pp. 306–311. doi: 10.5694/mja17.01274.

Ngo, T. D. *et al.* (2018) 'Additive manufacturing (3D printing): A review of materials , methods , applications and challenges', *Composites Part B*. Elsevier, 143(December 2017), pp. 172–196. doi: 10.1016/j.compositesb.2018.02.012.

Ngo, T. D. *et al.* (2018) 'Additive manufacturing (3D printing): A review of materials, methods, applications and challenges', *Composites Part B: Engineering*. Elsevier Ltd. doi: 10.1016/j.compositesb.2018.02.012.

Ni, L. *et al.* (2020) 'Bioresorbable vascular stents and drug- eluting stents in treatment of coronary heart disease : a meta-analysis', 5, pp. 1–7.

Nidhi, K. *et al.* (2011) 'Hydrotropy: A promising tool for solubility enhancement: A review', *International Journal of Drug Development and Research*, 3(2), pp. 26–33. doi: 10.1002/jps.

Norman, J. *et al.* (2016) 'A new chapter in pharmaceutical manufacturing: 3D-printed drug products', *Advanced Drug Delivery Reviews*. Elsevier B.V. doi: 10.1016/j.addr.2016.03.001.

Normand, G. *et al.* (2017) 'Matrix Degradation during High Speed Extrusion of Polypropylene / Clay Nanocomposites – Influence on Filler Dispersion To cite this version : polypropylene / clay nanocomposites – influence on filler dispersion'.

O'Brien, B. and Carroll, W. (2009) 'The evolution of cardiovascular stent materials and surfaces in response to clinical drivers: A review', *Acta Biomaterialia*. Acta Materialia Inc., 5(4), pp. 945–958. doi: 10.1016/j.actbio.2008.11.012.

Okolie, O. *et al.* (2020) '3d printing for hip implant applications: A review', *Polymers*, 12(11), pp. 1–29. doi: 10.3390/polym12112682.

Oliveira, M. and Machado, A. V (2013) 'Preparation of polymer-based nanocomposites by different routes', *Nanocomposites: synthesis, characterization and applications*, pp. 1–22. Available at: http://repositorium.sdum.uminho.pt/handle/1822/26120.

Oliveira, M. and Peter, J. (2003) 'Crystallization and Transformation of Acetaminophen 2003', *Growth (Lakeland)*, pp. 0–4.

Omar, W. A. and Kumbhani, D. J. (2019) 'The Current Literature on Bioabsorbable Stents : a Review'. Current Atherosclerosis Reports.

Onuma, Y. and Serruys, P. W. (2011) 'Bioresorbable scaffold: The advent of a new era in percutaneous coronary and peripheral revascularization?', *Circulation*, 123(7), pp. 779–797. doi: 10.1161/CIRCULATIONAHA.110.971606.

Ostafinska, A. *et al.* (2017) 'Strong synergistic effects in PLA/PCL blends: Impact of PLA matrix viscosity', *Journal of the Mechanical Behavior of Biomedical Materials*, 69(January), pp. 229–241. doi: 10.1016/j.jmbbm.2017.01.015.

Othman, R. *et al.* (2016) 'Fabrication of composite poly (D , L -lactide)/ montmorillonite nanoparticles for controlled delivery of acetaminophen by solvent- displacement method using glass capillary microfluidics', *Colloids and Surfaces B: Biointerfaces*. Elsevier B.V. doi:

10.1016/j.colsurfb.2016.01.042.

Parry, J. A. *et al.* (2017) 'Three-Dimension-Printed Porous Poly(Propylene Fumarate) Scaffolds with Delayed rhBMP-2 Release for Anterior Cruciate Ligament Graft Fixation', *Tissue Engineering Part A*, 23(7–8), pp. 359–365. doi: 10.1089/ten.tea.2016.0343.

Pasbakhsh, P. *et al.* (2016) 'Halloysite nanotubes : Prospects and challenges of their use as additives and carriers – A focussed review', *Clay Minerals*, 51(June), pp. 479–487. doi: 10.1180/claymin.2016.051.3.15.

Patel, S. *et al.* (2015) 'Sustained Release of Antibacterial Agents from Doped Halloysite Nanotubes', *Bioengineering*, 3(1), p. 1. doi: 10.3390/bioengineering3010001.

Patil, H., Tiwari, R. V. and Repka, M. A. (2016) 'Hot-Melt Extrusion: from Theory to Application in Pharmaceutical Formulation', *AAPS PharmSciTech*, 17(1), pp. 20–42. doi: 10.1208/s12249-015-0360-7.

Patrício, T. and Bártolo, P. (2013) 'Thermal stability of PCL/PLA blends produced by physical blending process', *Procedia Engineering*. Elsevier B.V., 59, pp. 292–297. doi: 10.1016/j.proeng.2013.05.124.

Paul, G. M. *et al.* (2018) 'Medical Applications for 3D Printing: Recent Developments.', *Missouri medicine*, 115(1), pp. 75–81. Available at: http://www.ncbi.nlm.nih.gov/pubmed/30228688%0Ahttp://www.pubmedcentral.nih.gov/articlerender.fcgi?artid=PMC6139809.

Pawar, R. P. *et al.* (2014) 'Biomedical Applications of Poly(Lactic Acid)', *PLA Applications*, 4, pp. 40–51. doi: 10.2174/22102965046661404022350 24.

Pearson, H. (1981) 'Comparative Effects of Aspirin and Acetaminophen on Hemostasis', *Archives of Internal Medicine*, 141(3), pp. 305–310. doi: 10.1001/archinte.1981.00340030037008.

Pierchala, M. K. *et al.* (2018) 'Nanotubes in nanofibers: Antibacterial multilayered polylactic acid/halloysite/gentamicin membranes for bone regeneration application', *Applied Clay Science*. Elsevier, 160(November 2017), pp. 95–105. doi: 10.1016/j.clay.2017.12.016.

Pollack, S. *et al.* (2019) 'Polymer-Based Additive Manufacturing: Historical Developments, Process Types and Material Considerations', in Devine, D. (ed.) *Polymer-Based Additive Manufacturing*. file:///C: © Springer Nature Switzerland AG 2019, pp. 1–22. doi: https://doi.org/10.1007/978-3-030-24532-0_1.

Pranzo, D. *et al.* (2018) 'Extrusion-Based 3D Printing of Microfluidic Devices for Chemical and Biomedical Applications: A Topical Review', *Micromachines*, 9(8), p. 374. doi: 10.3390/mi9080374.

Prasad, L. K. and Smyth, H. (2016) '3D Printing technologies for drug delivery: a review', *Drug Development and Industrial Pharmacy*, 42(7), pp. 1019–1031. doi: 10.3109/03639045.2015.1120743.

Prashantha, K. *et al.* (2013) 'Poly(lactic acid)/halloysite nanotubes nanocomposites: Structure, thermal, and mechanical properties as a function of halloysite treatment', *Journal of Applied Polymer Science*, 128(3), pp. 1895–1903. doi: 10.1002/app.38358.

Prete, M. C. and Arnaldo, C. (2016) 'RSC Advances A nanocomposite based on multi-walled carbon nanotubes grafted by molecularly imprinted', pp. 28751–28760. doi: 10.1039/C6RA02150F.

Pretula, J., Slomkowski, S. and Penczek, S. (2016) 'Polylactides—Methods of synthesis and characterization', *Advanced Drug Delivery Reviews*. Elsevier B.V., 107, pp. 3–16. doi: 10.1016/j.addr.2016.05.002.

Puchalski, M. *et al.* (2017) 'Investigation of the influence of PLA molecular structure on the crystalline forms (α'' and α) and Mechanical Properties ofWet Spinning Fibres', *Polymers*, 9(1). doi: 10.3390/polym9010018.

Qi, R. *et al.* (2010) 'Electrospun poly(lactic-co-glycolic acid)/halloysite nanotube composite nanofibers for drug encapsulation and sustained release', *Journal of Materials Chemistry*, 20(47), p. 10622. doi: 10.1039/c0jm01328e.

Qi, R. *et al.* (2013) 'Controlled release and antibacterial activity of antibiotic-loaded electrospun halloysite/poly(lactic-co-glycolic acid) composite nanofibers', *Colloids and Surfaces B: Biointerfaces*. Elsevier B.V., 110, pp. 148–155. doi: 10.1016/j.colsurfb.2013.04.036.

Qiu, T. *et al.* (2020) 'Development of 3D-Printed Sulfated Chitosan Modified Bioresorbable Stents for Coronary Artery Disease', 8(May), pp. 1–12. doi: 10.3389/fbioe.2020.00462.

Qiu, T. and Zhao, L. (2018) 'Research into biodegradable polymeric stents: a review of experimental and modelling work', *Vessel Plus*, 2(6), p. 12. doi: 10.20517/2574-1209.2018.13.

Quiles-Carrillo, L., , Nestor Montanes, Fede Pineiro, A. J.-V. and and Torres-Giner, S. (2018) 'Ductility and Toughness Improvement of Injection-moulded compostable pieces of Polylactide by melt blending with poly(e-caprolactone) and thermoplastic starch', pp. 1–20. doi: 10.3390/ma11112138.

Raleigh, J. V. *et al.* (2018) 'Restenosis, Stent Thrombosis, and Bleeding Complications', 71(15). doi: 10.1016/j.jacc.2018.02.023.

Ramadugu, P. and Latha Alikatte, K. (2016) 'A Review on Biodegradable and Bioabsorbable Stents for Coronary Artery Disease', *Journal of Bioequivalence & Bioavailability*, 08(02), pp. 64–67. doi: 10.4172/jbb.1000269.

Ramot, Y. *et al.* (2016) 'Biocompatibility and safety of PLA and its copolymers', *Advanced Drug Delivery Reviews*. Elsevier B.V., 107, pp. 153–162. doi: 10.1016/j.addr.2016.03.012.

Raquez, J. M. *et al.* (2013) 'Polylactide (PLA)-based nanocomposites', *Progress in Polymer Science*. Elsevier Ltd, 38(10–11), pp. 1504–1542. doi: 10.1016/j.progpolymsci.2013.05.014.

Rebagay, G. and Bangalore, S. (2019) 'Biodegradable Polymers and Stents: the Next Generation?', *Current Cardiovascular Risk Reports*. Current Cardiovascular Risk Reports, 13(8), pp. 2–7. doi: 10.1007/s12170-019-0617-x.

Repka, M. A. *et al.* (2018) 'Melt extrusion with poorly soluble drugs – An integrated review', *International Journal of Pharmaceutics*. Elsevier, 535(1–2), pp. 68–85. doi: 10.1016/j.ijpharm.2017.10.056.

Rolland, J., Chen, K. and Poelma, J. (2016) 'Methods of Producing Polyurethane Three-Dimensional Objects From Materials Having Multiple Mechanisms of Hardening', *US Patent*.

Roy, T. and Chanda, A. (2014) 'Computational Modelling and Analysis of Latest Commercially Available Coronary Stents During Deployment', *Procedia Materials Science*, 5, pp. 2310–2319. doi: 10.1016/j.mspro.2014.07.474.

Rykowska, I. and Nowak, I. (2020) 'Drug-Eluting Stents and Balloons—Materials, Structure Designs, and Coating Techniques: A Review'.

Sachs, E., Cima, M. and Cornie, J. (1990) 'Three-Dimensional Printing: Rapid Tooling and Prototypes Directly from a CAD Model', *CIRP Annals - Manufacturing Technology*. American Society of Mechanical Engineers, 39(1), pp. 201–204. doi: 10.1016/S0007-8506(07)61035-X.

Saerens, L. *et al.* (2014) 'Process monitoring and visualization solutions for hot-melt extrusion: A review', *Journal of Pharmacy and Pharmacology*, 66(2), pp. 180–203. doi: 10.1111/jphp.12123.

Saini, P., Arora, M. and Kumar, M. N. V. R. (2016) 'Poly(lactic acid) blends in biomedical applications', *Advanced Drug Delivery Reviews*. Elsevier B.V., 107, pp. 47–59. doi: 10.1016/j.addr.2016.06.014.

Sakamoto, A. *et al.* (2018) 'Understanding the Impact of Stent and Scaffold Material and Strut Design on Coronary Artery Thrombosis from the Basic and Clinical Points of View', *Bioengineering*, 5(3), p. 71. doi: 10.3390/bioengineering5030071.

Sangeetha, V. H. *et al.* (2018) 'State of the art and future prospectives of poly(lactic acid) based blends and composites', *Polymer Composites*, 39(1), pp. 81–101. doi: 10.1002/pc.23906.

Santos Ana, C. *et al.* (2018) 'Halloysite clay nanotubes for life sciences applications: From drug encapsulation to bioscaffold', *Advances in Colloid and Interface Science*. Elsevier B.V., 257, pp. 58–

70. doi: 10.1016/j.cis.2018.05.007.

Sasimowski, E. and Majewski, Ł. (2019) 'Effect of the intensive plasticizing zone design on the effectiveness of corotating twin-screw extrusion', *Advances in Polymer Technology*, 2019, pp. 15–17. doi: 10.1155/2019/8518341.

Schmitt, R. (2014) *Scanning Electron Microscope*. doi: 10.1007/978-3-642-20617-7.

Semalty, a *et al.* (2010) 'Development and Characterization of Aspirin-Phospholipid Complex for Improved Drug Delivery ABSTRACT ':, *Journal of Pharmaceutical Sciences*, 3(2), pp. 940–947.

Sha, L. *et al.* (2016) 'Polylactic acid based nanocomposites: Promising safe and biodegradable materials in biomedical field', *International Journal of Polymer Science*, 2016. doi: 10.1155/2016/6869154.

Shah, A. K., Wyandt, C. M. and Stodghill, S. P. (2013) 'Physico chemical characterization of a novel anti-cancer agent and its comparison to Taxol ®', 39(July 2011), pp. 89–101. doi: 10.3109/03639045.2012.659187.

Shahi, P. K. *et al.* (2018) 'Silver nanoparticles embedded hybrid organometallic complexes : Structural interactions , photo-induced energy transfer , plasmonic effect and optical thermometry Silver nanoparticles embedded hybrid organometallic complexes : Structural interactions , ph', 065117. doi: 10.1063/1.5020812.

Sharma, R. (2013) 'The 3D Printing Revolution You Have Not Heard About', *Forbes*.

Shi, X. *et al.* (2015) 'Synergistic effects of nucleating agents and plasticizers on the crystallization behavior of Poly(lactic acid)', *Molecules*, 20(1), pp. 1579–1593. doi: 10.3390/molecules20011579.

Shi, Y. *et al.* (2014) 'Experimental and mathematical studies on the drug release properties of aspirin loaded chitosan nanoparticles', *BioMed Research International*, 2014. doi: 10.1155/2014/613619.

Shimura, T. *et al.* (2016) 'Extreme late-phase observation using coronary angioscopy until 7 years after sirolimus-eluting stent implantation', *Coronary Artery Disease*, 27(1), pp. 29–33. doi: 10.1097/MCA.0000000000000315.

Shindo, D. and Oikawa, T. (2002) 'Energy dispersive X-ray spectroscopy', *Analytical electron microscopy for materials science*, pp. 81–102. doi: 10.1007/978-4-431-66988-3.

Shirazi, S. F. S. *et al.* (2015) 'A review on powder-based additive manufacturing for tissue engineering: Selective laser sintering and inkjet 3D printing', *Science and Technology of Advanced Materials*. IOP Publishing, 16(3), pp. 1–20. doi: 10.1088/1468-6996/16/3/033502.

Shoja, M. *et al.* (2015) 'PREPARATION AND CHARACTERIZATION OF POLY (ε -', 10(2), pp. 471–477.

Siegel, S. J. *et al.* (2006) 'Effect of drug type on the degradation rate of PLGA matrices', *European Journal of Pharmaceutics and Biopharmaceutics*, 64(3), pp. 287–293. doi: 10.1016/j.ejpb.2006.06.009.

De Silva, R. T. *et al.* (2014) 'Synthesis and characterisation of poly (lactic acid)/halloysite bionanocomposite films', *Journal of Composite Materials* , 48(30), pp. 3705–3717. doi: 10.1177/0021998313513046.

Simard, T. *et al.* (2014) 'The Evolution of Coronary Stents: A Brief Review', *Canadian Journal of Cardiology*. Canadian Cardiovascular Society, 30(1), pp. 35–45. doi: 10.1016/j.cjca.2013.09.012.

Skjelbred, P., Album, B. and Løkken, P. (1977) 'Acetylsalicylic acid vs paracetamol: Effects on post-operative course', *European Journal of Clinical Pharmacology*, 12(4), pp. 257–264. doi: 10.1007/BF00607424.

Skowyra, J., Pietrzak, K. and Alhnan, M. A. (2015) 'Fabrication of extended-release patient-tailored prednisolone tablets via fused deposition modelling (FDM) 3D printing', *European Journal of Pharmaceutical Sciences*. Elsevier, 68, pp. 11–17. doi: 10.1016/J.EJPS.2014.11.009.

Sood, A. K., Ohdar, R. K. and Mahapatra, S. S. (2010) 'Parametric appraisal of mechanical property

of fused deposition modelling processed parts', *Materials and Design*. Elsevier, 31(1), pp. 287–295. doi: 10.1016/j.matdes.2009.06.016.

Sotoudehbagha, P. *et al.* (2018) 'Novel antibacterial biodegradable Fe-Mn-Ag alloys produced by mechanical alloying', *Materials Science and Engineering: C*. Elsevier B.V, p. #pagerange#. doi: 10.1016/j.msec.2018.03.005.

Stanković, M., Frijlink, H. W. and Hinrichs, W. L. J. (2015) 'Polymeric formulations for drug release prepared by hot melt extrusion: application and characterization', *Drug Discovery Today*, 20(7), pp. 812–823. doi: 10.1016/j.drudis.2015.01.012.

Stephanus, A. and Ivan, L. (2018) 'Effect of blend ratio and nanofiller localization on the thermal degradation of graphite nanoplatelets-modified PLA / PCL', *Journal of Thermal Analysis and Calorimetry*. Springer International Publishing, 0123456789. doi: 10.1007/s10973-018-7870-y.

Stoclet, G. *et al.* (2014) 'Elaboration of poly(lactic acid)/halloysite nanocomposites by means of water assisted extrusion: structure, mechanical properties and fire performance', *RSC Adv.* Royal Society of Chemistry, 4(101), pp. 57553–57563. doi: 10.1039/C4RA06845A.

Strohbach, A. and Busch, R. (2015) 'Polymers for Cardiovascular Stent Coatings', *International Journal of Polymer Science*, 2015. doi: 10.1155/2015/782653.

Surgery, D. and College, S. D. (2017) 'INTERNATIONAL JOURNAL OF SCIENTIFIC RESEARCH DRUG DELIVERY THROUGH DRUG ELUTING STENTS -A REVIEW Pharmacology Bhawani Gupta', (9), pp. 20–22.

Tabraiz Alam, M. S. *et al.* (2019) 'A review based on biodegradable and bioabsorbable stents for coronary artery disease', *Procedia Computer Science*. Elsevier B.V., 152, pp. 354–359. doi: 10.1016/j.procs.2019.05.006.

Tamai, H. *et al.* (2000) 'Initial and 6-month results of biodegradable poly-l-lactic acid coronary stents in humans.', *Circulation*, 102(4), pp. 399–404. doi: 10.1161/01.CIR.102.4.399.

Tang, Y. and Singh, J. (2008) 'Controlled delivery of aspirin: Effect of aspirin on polymer degradation and in vitro release from PLGA based phase sensitive systems', *International Journal of Pharmaceutics*, 357(1–2), pp. 119–125. doi: 10.1016/j.ijpharm.2008.01.053.

Tertis, M. *et al.* (2013) 'Carbon Based Electrodes Modified with Horseradish Peroxidase Immobilized in Conducting Polymers for Acetaminophen Analysis', pp. 4841–4854. doi: 10.3390/s130404841.

Therias, S., Murariu, M. and Dubois, P. (2017) 'Bionanocomposites based on PLA and halloysite nanotubes: From key properties to photooxidative degradation', *Polymer Degradation and Stability*. Elsevier Ltd, pp. 1–10. doi: 10.1016/j.polymdegradstab.2017.06.008.

Tian, X. *et al.* (2016) 'Interface and performance of 3D printed continuous carbon fiber reinforced PLA composites', *Composites Part A: Applied Science and Manufacturing*. Elsevier Ltd, 88, pp. 198–205. doi: 10.1016/j.compositesa.2016.05.032.

Tian, X. *et al.* (2017) 'Recycling and remanufacturing of 3D printed continuous carbon fiber reinforced PLA composites', *Journal of Cleaner Production*. Elsevier Ltd, 142, pp. 1609–1618. doi: 10.1016/j.jclepro.2016.11.139.

Tiwari, R. V., Patil, H. and Repka, M. A. (2016) 'Contribution of hot-melt extrusion technology to advance drug delivery in the 21st century', *Expert Opinion on Drug Delivery*. doi: 10.1517/17425247.2016.1126246.

Torrado, A. R. *et al.* (2015) 'Characterizing the effect of additives to ABS on the mechanical property anisotropy of specimens fabricated by material extrusion 3D printing', *Additive Manufacturing*. Elsevier B.V., 6, pp. 16–29. doi: 10.1016/j.addma.2015.02.001.

Trabert, B. *et al.* (2014) 'Aspirin, Nonaspirin Nonsteroidal Anti-inflammatory Drug, and Acetaminophen Use and Risk of Invasive Epithelial Ovarian Cancer: A Pooled Analysis in the Ovarian Cancer Association Consortium', *JNCI Journal of the National Cancer Institute*, 106(2), pp. djt431-djt431. doi: 10.1093/jnci/djt431.

Tumbleston, J. R. *et al.* (2015) 'Additive manufacturing. Continuous liquid interface production of 3D objects.', *Science (New York, N.Y.)*. American Association for the Advancement of Science, 347(6228), pp. 1349–52. doi: 10.1126/science.aaa2397.

Tyler, B. *et al.* (2016) 'Polylactic acid (PLA) controlled delivery carriers for biomedical applications', *Advanced Drug Delivery Reviews*. Elsevier B.V., 107, pp. 163–175. doi: 10.1016/j.addr.2016.06.018.

U. S. Food and Drug Administration (2017) 'Class 1 Device Recall Absorb Bioresorbable Vascular Scaffold (BVS) System'. Available at: https://www.accessdata.fda.gov.

Urquijo, J., Guerrica-Echevarría, G. and Eguiazábal, J. I. (2015) 'Melt processed PLA/PCL blends: Effect of processing method on phase structure, morphology, and mechanical properties', *Journal of Applied Polymer Science*, 132(41), pp. 1–9. doi: 10.1002/app.42641.

Valapa, R., Pugazhenthi, G. and Katiyar, V. (2016) *Hydrolytic Degradation Behaviour of Sucrose Palmitate Reinforced Poly(lactic acid) Nanocomposites*, *International Journal of Biological Macromolecules*. Elsevier B.V. doi: 10.1016/j.ijbiomac.2016.04.040.

Vasquez, G.M, Majewski, C.E, Haworth, B. & Hopkinson, N. (2014) '2014_A targeted material selection process for polymers in laser sintering', 1–4(2014), pp. 127–138. doi: http://dx.doi.org/10.1016/j.addma.2014.09.003.

Verbelen, L. *et al.* (2016) 'Characterization of polyamide powders for determination of laser sintering processability', *European Polymer Journal*. doi: 10.1016/j.eurpolymj.2015.12.014.

Vieira, A. C. *et al.* (2010) 'Degradation and Viscoelastic Properties of PLA-PCL, PGA-PCL, PDO and PGA Fibres', *Materials Science Forum*, 636–637(January 2014), pp. 825–832. doi: 10.4028/www.scientific.net/msf.636-637.825.

Vieira, A. C. *et al.* (2011) 'Mechanical study of PLA-PCL fibers during in vitro degradation', *Journal of the Mechanical Behavior of Biomedical Materials*. Elsevier Ltd, 4(3), pp. 451–460. doi: 10.1016/j.jmbbm.2010.12.006.

Villmow, T., Kretzschmar, B. and Pötschke, P. (2010) 'Influence of screw configuration, residence time, and specific mechanical energy in twin-screw extrusion of polycaprolactone/multi-walled carbon nanotube composites', *Composites Science and Technology*. Elsevier Ltd, 70(14), pp. 2045–2055. doi: 10.1016/j.compscitech.2010.07.021.

Virmani, R., Jinnouchi, H. and Finn, A. V. (2017) 'Discontinuity', *Journal of the American College of Cardiology*, 70(19), pp. 2345–2348. doi: 10.1016/j.jacc.2017.09.029.

Voit, W. *et al.* (2016) 'Cartridge-Based 3D Printing System'.

Wachirahuttapong, S., Thongpin, C. and Sombatsompop, N. (2016) 'Effect of PCL and Compatibility Contents on the Morphology, Crystallization and Mechanical Properties of PLA/PCL Blends', *Energy Procedia*. The Author(s), 89, pp. 198–206. doi: 10.1016/j.egypro.2016.05.026.

Wang, C. *et al.* (2020) 'Design , Characterization , and 3D Printing of Cardiovascular Stents with Zero Poisson ' s Ratio in Longitudinal Deformation', *Engineering*. THE AUTHORS, (xxxx), pp. 0–11. doi: 10.1016/j.eng.2020.02.013.

Wang, P.-J. *et al.* (2018) 'Strain-induced accelerated asymmetric spatial degradation of polymeric vascular scaffolds', *Proceedings of the National Academy of Sciences*, p. 201716420. doi: 10.1073/pnas.1716420115.

Wang, Q. *et al.* (2014) 'Colloids and Surfaces B : Biointerfaces Adsorption and release of ofloxacin from acid- and heat-treated halloysite', *Colloids and Surfaces B: Biointerfaces*. Elsevier B.V., 113, pp. 51–58. doi: 10.1016/j.colsurfb.2013.08.036.

Wang, X. *et al.* (2017) '3D printing of polymer matrix composites: A review and prospective', *Composites Part B: Engineering*. Elsevier Ltd, 110, pp. 442–458. doi: 10.1016/j.compositesb.2016.11.034.

Waterbeemd, H. Van De and Rose, S. (2008) 'Quantitative Approaches to Structure – Activity Relationships', pp. 491–513.

Wee, D. *et al.* (2020) 'Bioresorbable Polymeric Sca ff old in Cardiovascular Applications', *Int. J. Mol. Sci*, (Cvd), pp. 1–35. doi: doi:10.3390/ijms21103444.

Wei, Z. *et al.* (2019) 'Simultaneous Determination of Acetaminophen and Tyrosine Using Screen-printed Electrochemical Sensor Based on MWCNTs-doped Poly (glycine)/ Poly (acrylic acid) Conducting Polymers', 14, pp. 6748–6758. doi: 10.20964/2019.07.26.

Wenger, R. and Giraud, M.-N. (2018) '3D Printing Applied to Tissue Engineered Vascular Grafts', *Applied Sciences*, 8(12), p. 2631. doi: 10.3390/app8122631.

Wiebe, J., Nef, H. M. and Hamm, C. W. (2014) 'Current status of bioresorbable scaffolds in the treatment of coronary artery disease', *Journal of the American College of Cardiology*, 64(23), pp. 2541–2551. doi: 10.1016/j.jacc.2014.09.041.

Wilson, W. M. and Cruden, N. L. M. (2013) 'Advances in coronary stent technology: current expectations and new developments', *Research Reports in Clinical Cardiology*, 4, pp. 85–96. doi: 10.2147/RRCC.S34408.

Wishart DS, E. a. (2017) *DrugBank 5.0: a major update to the DrugBank database for 2018.* doi: doi: 10.1093/nar/gkx1037.

Wohlers, T. T. (2005) *Early Research & Development, Wohlers Report 2005: rapid prototyping, tooling and manufacturing state of the industry worldwide progress report*.

Woodruff, M. A. and Hutmacher, D. W. (2010) 'The return of a forgotten polymer - Polycaprolactone in the 21st century', *Progress in Polymer Science (Oxford)*, 35(10), pp. 1217–1256. doi: 10.1016/j.progpolymsci.2010.04.002.

Wu, D. *et al.* (2009) 'Selective Localization of Multiwalled Carbon Nanotubes in Poly (ε - caprolactone)/ Polylactide Blend', pp. 417–424.

Wu, F. *et al.* (2019) 'Halloysite nanotubes coated 3D printed PLA pattern for guiding human mesenchymal stem cells (hMSCs) orientation', *Chemical Engineering Journal*. Elsevier, 359(October 2018), pp. 672–683. doi: 10.1016/j.cej.2018.11.145.

Wu, W. *et al.* (2013) 'Polylactide/halloysite nanotube nanocomposites: Thermal, mechanical properties, and foam processing', *Journal of Applied Polymer Science*, 130(1), pp. 443–452. doi: 10.1002/app.39179.

Wu, Y. *et al.* (2012) 'Comparison of acute recoil between bioabsorbable poly-L-lactic acid XINSORB stent and metallic stent in porcine model', *Journal of Biomedicine and Biotechnology*, 2012. doi: 10.1155/2012/413956.

Wudy, K., Drummer, D. and Drexler, M. (2014) 'Characterization of polymer materials and powders for selective laser melting', *AIP Conference Proceedings*, 1593(May), pp. 702–707. doi: 10.1063/1.4873875.

Yang, H., Zhang, Y. and Ouyang, J. (2016) *Physicochemical Properties of Halloysite*. 1st edn, *Developments in Clay Science*. 1st edn. Elsevier Ltd. doi: 10.1016/B978-0-08-100293-3.00004-2.

Yang, K. *et al.* (2018) 'Bio-functional design, application and trends in metallic biomaterials', *International Journal of Molecular Sciences*, 19(1). doi: 10.3390/ijms19010024.

Yao, X. *et al.* (2017) 'Evaluation of carbon fiber-embedded 3D printed structures for strengthening and structural-health monitoring', *Materials and Design*. Elsevier Ltd, 114, pp. 424–432. doi: 10.1016/j.matdes.2016.10.078.

Yin, R., Yang, D. and Wu, J. (2014) 'T h e r a n o s t i c s Nanoparticle Drug- and Gene-eluting Stents for the Prevention and Treatment of Coronary Restenosis', 4(2). doi: 10.7150/thno.7210.

Youssef, R. F. *et al.* (2015) 'Applications of three-dimensional printing technology in urological practice', *BJU International*, 116(5), pp. 697–702. doi: 10.1111/bju.13183.

Yuan, P., Tan, D. and Annabi-Bergaya, F. (2015) 'Properties and applications of halloysite nanotubes: recent research advances and future prospects', *Applied Clay Science*. Elsevier B.V., 112–113, pp. 75–93. doi: 10.1016/j.clay.2015.05.001.

Yun, Y. *et al.* (2018) 'Effect of Printing Parameters on Tensile, Dynamic Mechanical, and Thermoelectric Properties of FDM 3D Printed CABS/ZnO Composites', *Materials*, 11(4), p. 466. doi: 10.3390/ma11040466.

Zaharin, H. A. *et al.* (2018) 'Additive Manufacturing Technology for Biomedical Components: A review', *IOP Conference Series: Materials Science and Engineering*, 328, p. 012003. doi: 10.1088/1757-899X/328/1/012003.

Zaki, H. (2011) 'Spectroscopy Surface Analysis of Paracetamol and Paracetamol and Excipient Systems', pp. 1–256.

Zamarayeva, A. (EECS/UC B. *et al.* (2018) 'Custom, 3D Sprayed MRI receive coils', in *International Society for Magnetic Resonance in Medicine*. Paris.

Zhang, A., Zhang, Y. and Zhu, Z. (2019) 'Thermal properties of Halloysite nanotubes (HNTs) intercalation complexes-A review', 01055.

Zhang, J., Ma, S. and Gene, H. (2017) 'Guided bone regeneration with asymmetric collagen-chitosan membranes containing aspirin- loaded chitosan nanoparticles', *International Journal of Nanomedicine*, 12, pp. 8855–8866.

Zhang, K. *et al.* (2014) 'Surface modification of implanted cardiovascular metal stents: From antithrombosis and antirestenosis to endothelialization', *Journal of Biomedical Materials Research - Part A*, 102(2), pp. 588–609. doi: 10.1002/jbm.a.34714.

Zhang, P. *et al.* (2015) 'Placement suitability criteria of composite tape for mould surface in automated tape placement', *Chinese Journal of Aeronautics*, 28(5), pp. 1574–1581. doi: 10.1016/j.cja.2015.06.002.

Zhang, W. *et al.* (2019) 'Biosensors and Bioelectronics An electrochemical sensor based on electro-polymerization of ca ff eic acid and Zn / Ni-ZIF-8 – 800 on glassy carbon electrode for the sensitive detection of acetaminophen', *Biosensors and Bioelectronic*. Elsevier B.V., 131(February), pp. 200–206. doi: 10.1016/j.bios.2019.01.069.

Zhao, J. *et al.* (2016) 'Drug loaded nanoparticle coating on totally bioresorbable PLLA stents to prevent in-stent restenosis', pp. 1–8. doi: 10.1002/jbm.b.33794.

Zivic, F. *et al.* (2018) *Biodegradable Metals as Biomaterials for Clinical Practice : Iron-Based Materials*.

Abstracts
Published: 28 October 2020

ENIUS. European Network of multidisciplinary research to Improve the Urinary Stents. COSTS Actions. CA16217. European Cooperation in Science & Technology

Urolithiasis volume 48, pages553–559 (2020) Cite this article

548 Accesses Metrics

Selected Abstracts from the "***Advances in Urinary Stents. Biomaterials, Coatings and Drug Eluting Stents***". Training School Meeting. Name of Meeting Organizer. European Network of multidisciplinary research to Improve the Urinary Stents (ENIUS). COSTS Actions. CA16217. European Cooperation in Science & Technology. University of Lublin (Poland), 26th–27th September, 2019.

17. Development of high-strength drug-eluting biodegradable stents by additive manufacturing

Chaitra Venkatesh[1*], Ian Major[1], John G. Lyons[2], Declan M. Devine[1]
[1]Material Research Institute, Athlone Institute of Technology, Ireland; [2]Faculty of Engineering and Informatics, Athlone Institute of Technology, Ireland

Biodegradable polymer nanocomposites are considered to be good alternatives in urology which provide support before they are absorbed by the body over a period of time. In this study, an innovative biodegradable nanocomposite is developed by using polylactic acid (PLA) as the base polymer, and is reinforced with non-toxic nanoclay, halloysite nanotubes (HNTs) by the extrusion process. These materials are selected as they are widely used in the biomedical field due to their biodegradability, natural availability and high mechanical properties.

Thus far, the effect of screw-speed during extrusion, drug-loading and drug-release kinetics, and 3D printing of the nanocomposite into model medical implants has been examined. The increase in screw speeds during extrusion resulted in significant increase in strength, toughness and thermal properties by better dispersion of the nanoclay in the polymer matrix as hydrogen-bonding interactions occur between the materials.

Further, for the drug release study, HNTs were first encapsulated with a model drug Aspirin. Then, the drug loaded HNTs of both ratios were blended into PLA matrix via melt-extrusion to form drug-loaded nanocomposite films. For comparison, the HNTs, PLA and Aspirin were tumble-mixed and processed as a separate batch. The results indicate the improved mechanical durability, drug-loading efficiency and sustained drug-release profile.

The nanocomposite was successfully extruded into filaments of 1.75 ± 0.10 mm diameter in-house using twin screw extruder with a specialized die fixed to the extruder for the manufacture of production grade 3D printing filament. This resultant filament was utilized for Fused Filament Fabrication (FFF) into standard tensile test bars and 25 mm model medical implants using a standard FFF printing machine. The nanocomposite was successfully 3D printed into model medical implants.

ENIUS training school “Ureteral stents: from modelling to commercialisation”

Swiss Institute for Translational and Entrepreneurial Medicine (SITEM) in Bern (Switzerland)

Best Poster Award 2019: Category: “Ureteral Stent Innovation”

THE TIMES THE SUNDAY TIMES GOOD UNIVERSITY GUIDE 2018 INSTITUTE OF TECHNOLOGY OF THE YEAR

AIT Research

DEVELOPMENT OF HIGH STRENGTH DRUG-ELUTING BIODEGRADABLE STENT BY ADDITIVE MANUFACTURING

Chaitra Venkatesh[1], Ian Major[1], John G Lyons[2], Declan M Devine[1]

[1] *Materials Research Institute, Athlone Institute of Technology, Athlone, Co. Westmeath, Ireland*

[2] *Faculty of Engineering and Informatics, Athlone Institute of Technology, Athlone, Co. Westmeath, Ireland*

INTRODUCTION

The use of biodegradable polymer materials are considered to be good alternatives in urology, cardiovascular and tracheal airway stenosis which provide support before it is absorbed by the body over a period of time and also in oesophageal and gastroenterology fields. In this study, an innovative biodegradable nanocomposite is developed by using polylactic acid (PLA) as the base polymer, and is reinforced with non-toxic nanoclay, halloysite nanotubes (HNTs) by the extrusion process. These materials are selected as they are widely used in the biomedical field due to their biodegradability, natural availability and high mechanical properties. Thus far, the effect of screw speed during extrusion, drug loading and drug release kinetics, and 3D printing of the nanocomposite into model medical implants has been examined.

EXPERIMENTAL DETAILS

MATERIALS

PLA was obtained from Corbion, PLA LX 175. HNT was supplied by Applied Minerals; DRAGONITE-HP. Acetyl Salicylic acid (Aspirin) was obtained from Sigma-Aldrich Ireland Ltd.

METHODS

To determine the effect of screw speed on PLA/HNT nanocomposites, 5% and 10% of HNTs were blended into the PLA matrix through compounding at screw speeds of 40, 80 and 140 rpm. In similar condition virgin PLA was compounded for comparison. The resultant polymer melt was quench cooled onto a calendar system to produce composite films for testing.

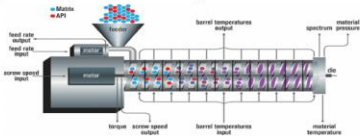

Fig 1. Twin screw extrusion (Researchgate.net)

To study the drug loading and release kinetics, the model drug aspirin is encapsulated into the nanocomposites by two different methods for comparison. The drug release mechanism was studied by placing the samples in SBF pH 7.4 in dissolution apparatus at 36°C.

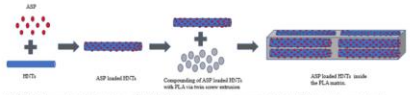

Fig 2. Schematic illustration PLA/(HNTs/ASP) nanocomposite by Preloading method

Fig 3. Schematic illustration of PLA/HNTs/ASP nanocomposite by Matrix loading method.

The 3D printable filament from the nanocomposite was produced in house using a high precision filament production line of diameter size 1.75±0.10 mm. These filaments were printed into tensile test specimen and implant using a Fused Filament Fabrication 3D printer MakerGear M2, US.

Fig 4. Photographs of the (a) in-house high precision filament production line (b) MakerGear M2 3D printer.

RESULTS

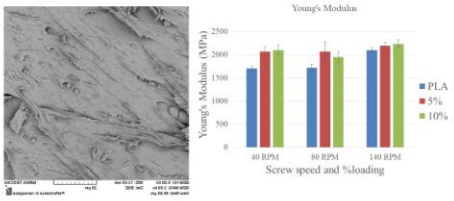

Fig. 5. (a) Photomicrograph of PLA/HNT 5% nanocomposite at 140 rpm shows good dispersion. (b) The increase in screw speed and the HNT loadings had significant effect (with p-value = 0.01 for both) on the increase in Young's modulus of the virgin PLA and the PLA/HNT nanocomposites.

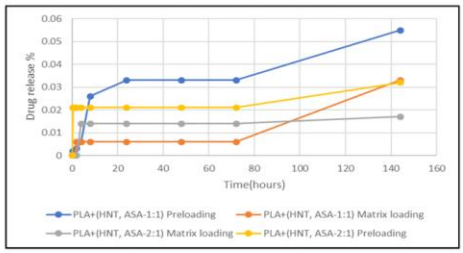

Fig 6. Drug release profiles of lumen loaded PLA/HNT nanocomposite shows more increase in initial drug release percentage than matrix loaded with sustained release over 9 days for both lumen and matrix loaded nanocomposites. And the drug loading efficiency was 66.6%.

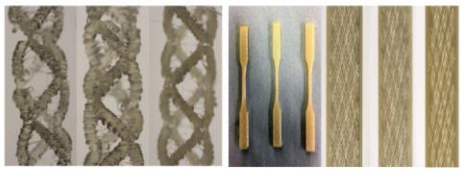

Fig 7. Photographs from optical microscope of 3D printed implants of (a) PLA, (b) PLA/HNT 3% and (c) PLA/HNT 5% nanocomposites. 3D printed tensile bars (a) (L-R) PLA, PLA/HNT 3% and PLA/HNT 5% nanocomposites. (b) Zoomed in photograph of PLA (c) zoomed in photograph of PLA/HNT 3% and (d) zoomed in photograph of PLA/HNT 5% nanocomposite indicates the infill pattern becomes denser with increase in the nanoclay percentage along with change in colour.

CONCLUSION

A high strength nanocomposite was manufactured by studying the different screw speed parameters during the extrusion process. This nanocomposite was successfully loaded with API and there was sustained release. Further, it was possible to develop 3D printing filament of a diameter 1.75±0.10 mm in-house for use in FFF 3D printing. The 3D printed model implants were successfully fabricated.

ACKNOWLEDGEMENTS

This work is emanated from research conducted with the financial support of Athlone Institute of Technology under the Presidents Seed Fund.

THE TIMES THE SUNDAY TIMES GOOD UNIVERSITY GUIDE 2018 INSTITUTE OF TECHNOLOGY OF THE YEAR

AIT Research

AIT Research Day 2019

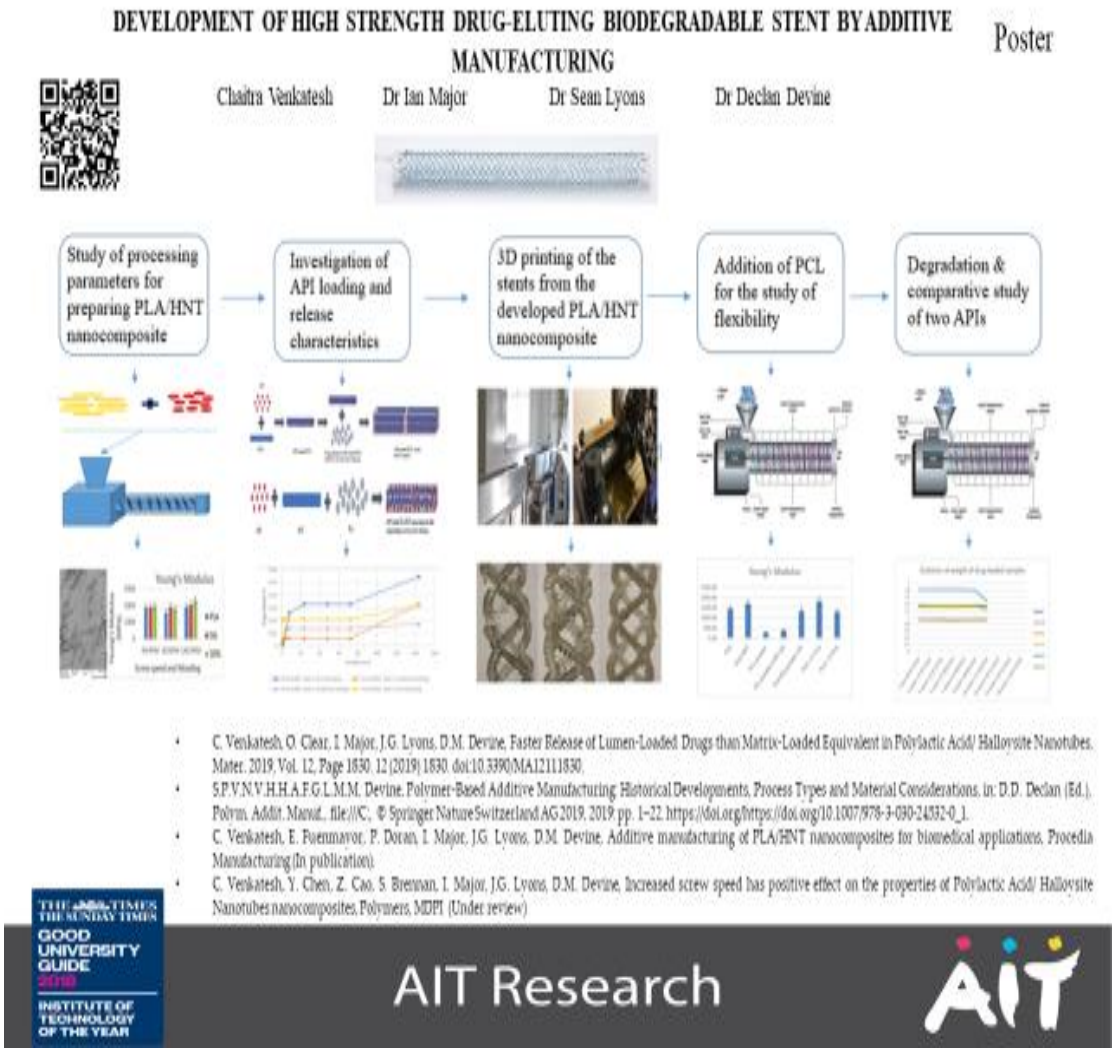

STUDY OF DRUG RELEASE MECHANISM ON THE NANOCOMPOSITE FOR DRUG-ELUTING BIODEGRADABLE STENTS

Chaitra Venkatesh[1], Oran Clear[2], Ian Major[1], John G. Lyons[2], Declan M. Devine[1]

[1]*Materials Research Institute, Athlone Institute of Technology, Dublin Road, Athlone, Co. Westmeath, Ireland*

[2]*Faculty of Engineering and Informatics, Athlone Institute of Technology, Dublin Road, Athlone, Co. Westmeath, Ireland*

INTRODUCTION

The use of biodegradable polymer materials are considered to be good alternatives in urology (1), cardiovascular (2) and tracheal airway stenosis which provide support before it is absorbed by the body over a period of time and also in oesophageal and gastroenterology fields (3). However, polymer on its own do not possess all the required properties for use in high strain environment. Hence, in this study Polylactic acid (PLA) is blended with Halloysite nanotubes (HNTs) through extrusion.There are several studies on polymer nanocomposites used as drug delivery systems [4]. In this research Polylactic acid (PLA)/Halloysite nanotubes (HNTs) nanocomposite were prepared as drug delivery systems for model drug aspirin. It was hypothesised that preloading HNT with Aspirin would result in sustained drug release compared to loading the drug into the polymer matrix.

EXPERIMENTAL DETAILS

MATERIALS

PLA was obtained from Corbion, PLA LX 175. The density of the PLA is 1.24 g/cm³. HNT was supplied by Applied Minerals; DRAGONITE-HP and has a density of 2.56 g/cm³. Acetyl Salicylic acid (Aspirin) was obtained from Sigma-Aldrich Ireland Ltd.

METHODS

The model drug aspirin is encapsulated into the HNTs. The drug loaded HNTs are reinforced into the PLA matrix by twin screw extrusion at the screw speed of 140 rpm. The PLA and the drug loaded HNTs were in the ratio of 95:5. The 5% of HNTs were loaded with aspirin in the ratios of 2:1 and 1:1. These are referred here as preloading. For comparison, the same ratios of HNTs, Aspirin and the PLA are premixed and processed similarly which are referred as matrix loading. The drug release mechanism was studied by placing the samples in SBF pH 7.4 in dissolution apparatus at 36°C.

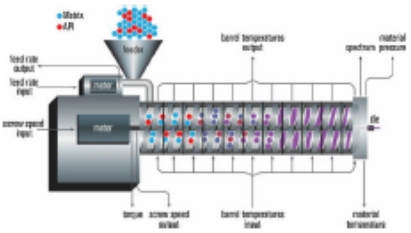

Fig 1. Twin screw extrusion (Researchgate.net)

RESULTS

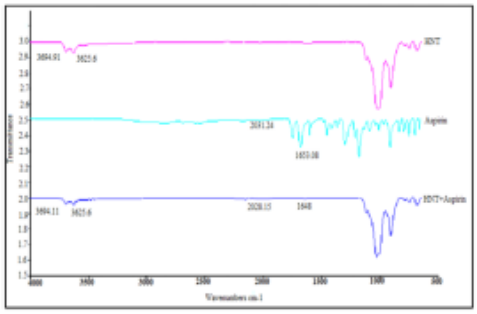

Fig 2. FTIR spectra of HNT, aspirin and aspirin loaded HNT samples. The peak of aspirin at 2031.24 cm-1 and 1653.08 cm-1 corresponds with the peak of Aspirin loaded HNT at 2028.15cm-1 and 1648 cm-1. This indicates the drug is loaded in the HNT.

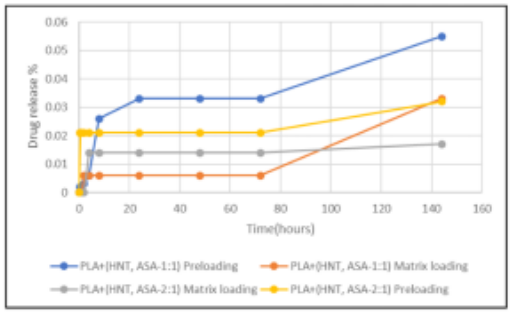

Fig 3. Drug release profiles of PLA/HNT nanocomposite loaded with aspirin in 1:1 and 2:1 ratio by preloading of HNT with drug and matrix loaded nanocomposite shows more increase in drug release percentage for 1:1 ratio nanocomposite than 2:1 ratio nanocomposites.

CONCLUSION

The pre-loading of the aspirin into HNTs was analysed with the peak of aspirin as observed at 2028.15 cm-1 and 1648 cm-1 indicating the successful loading of aspirin into the HNT. The drug elution chart shows that aspirin could be loaded in the nanocomposite and the release is extending. The drug release mechanism study is continuing for the above graph.

REFERENCES

1. Ryan P. Donahue, Andrew W. Stamm, Robert P. Gibbons, Christopher R. Porter, Kathleen C. Kobashi, John M. Corman, Una J. Lee, Evolution of the Ureteral Stent: the Pivotal Role of the Gibbons Ureteral Catheter, Urology (2018), https://doi.org/10.1016/j.urology.2018.02.007.
2. D. Ibric et al. / International Journal of Cardiology 215 (2016) 47–59
3. Zhu et. al. Ther Adv Gastroenterol 2017, Vol. 10(1) 11-19DOI: 10.1177/1756283X16671670
4. Hemlata Patil, Roshan V. Tiwari and Michael A. Repka/AAPS PharmSciTech, Vol. 17, No. 1, February 2016 (# 2015) DOI: 10.1208/s12249-015-0360-7

ACKNOWLEDGEMENTS

This work is emanated from research conducted with the financial support of Athlone Institute of Technology under the Presidents Seed Fund, Enterprise Ireland funding under the Technology Gateway programme grant number TG-2017-0114 and Science Foundation Ireland (SFI) under Grant Number 16/RC/3918..

Young Researcher Meeting (YRM) 2018

Royal College of Surgeons in Ireland (RCSI) in Dublin

SUSTAINED RELEASE OF API THROUGH DRUG LOADING INTO NANOPARTICLE COMPONENT OF NANOCOMPOSITE

Chaitra Venkatesh[1], Oran Clear[2], Ian Major[1], John G.Lyons[2], Declan M. Devine[1]

[1]*Materials Research Institute, Athlone Institute of Technology, Dublin Road, Athlone, Co. Westmeath, Ireland*

[2]*Faculty of Engineering and Informatics, Athlone Institute of Technology, Dublin Road, Athlone, Co. Westmeath, Ireland*

INTRODUCTION

Hot Melt Extrusion (HME) has emerged to be an attractive process in manufacturing of drug delivery systems [1]. There are several studies on polymer nanocomposites used as drug delivery systems [2]. In this research Polylactic acid (PLA)/Halloysite nanotubes (HNTs) nanocomposite were prepared as drug delivery systems by extrusion. The model drug aspirin is encapsulated into the HNTs. The drug loaded HNTs are reinforced into the PLA matrix by twin screw extrusion. For comparison, the HNTs, Aspirin and the PLA are premixed and processed similarly.

EXPERIMENTAL DETAILS

MATERIALS

PLA was obtained from Corbion, PLA LX 175. The density of the PLA is 1.24 g/cm³. HNT was supplied by Applied Minerals; DRAGONITE-HP and has a density of 2.56 g/cm³. Acetyl Salicylic acid was obtained from Sigma-Aldrich Ireland Ltd.

METHODS

The model drug aspirin is encapsulated into the HNTs. The drug loaded HNTs are reinforced into the PLA matrix by twin screw extrusion at the screw speed of 140 rpm. The PLA and the drug loaded HNTs were in the ratio of 95:5. The 5% of HNTs were loaded with aspirin in the ratios of 2:1 and 1:1. These are referred here as direct loading. For comparison, the same ratios of HNTs, Aspirin and the PLA are premixed and processed similarly which are referred as indirect loading. The drug release mechanism was studied by placing the samples in SBF pH 7.4 in dissolution apparatus at 36°C, 100rpm.

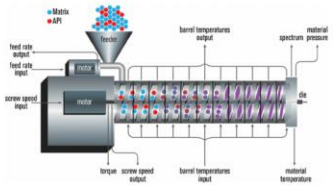

Fig 1. Twin screw extrusion (Researchgate.net)

RESULTS

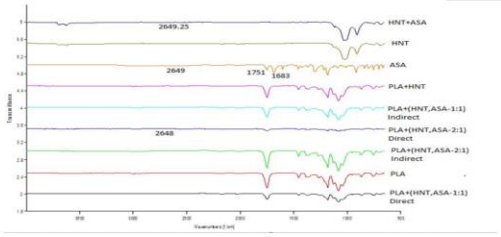

Fig 2. FTIR spectra of all samples shows the characteristic peaks of PLA, HNT, PLA/HNT nanocomposite and Aspirin respectively.

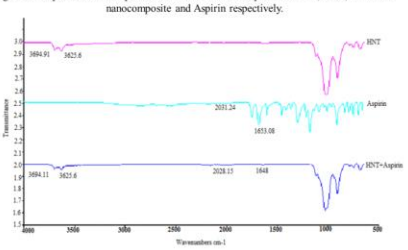

Fig 3. FTIR spectra of HNT, Aspirin and Aspirin loaded HNT samples. The peak of aspirin at 2031.24 cm-1 and 1653.08 cm-1 corresponds with the peak of Aspirin loaded HNT at 2028.15cm-1 and 1648 cm-1. This indicates the drug is loaded in the HNT.

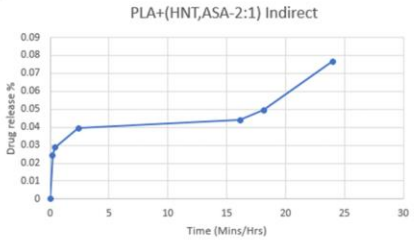

Fig 4. Drug release profiles of indirectly loaded 2:1 sample. The release burst occurs within first hour and gradual increase in the release is continued,

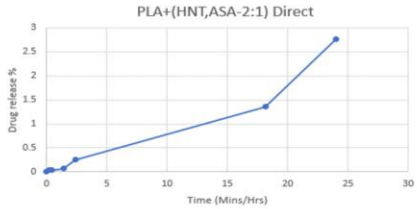

Fig 5. Drug release profiles of directly loaded 2:1 sample. The initial release is gradually increasing and continues.

CONCLUSION

The loading of the aspirin on the HNT was analysed with the peak of aspirin at 2028.15 cm-1 and 1648 cm-1 in the aspirin loaded HNT sample. The drug elution over a period of 2 days shows that aspirin could be loaded well in the nanocomposite and the release is extending. The drug release mechanism study is continuing. Hence, future work will be to assess further the control of drug release rate.

REFERENCES

- Hemlata Patil, Roshan V. Tiwari and Michael A. Repka/AAPS PharmSciTech, Vol. 17, No. 1, February 2016 (# 2015) DOI: 10.1208/s12249-015-0360-7
- Xiazhi Zhang, Rui Guo, Jiqing Xu, Yong Lan, Yanpeng Jiao, Changren Zhou and Yaowu Zhao Journal of Biomaterials Applications 0(0) 1–14 2015 DOI:10.1177/0885328215593837

ACKNOWLEDGEMENTS

Funding of this project was provided by the Athlone Institute of Technology President Seed fund.

APPENDICES

Chapter 4

Mechanical properties

Young's modulus (Mpa)

40 RPM

Sl. No.	PLA	5%	10%
1	1916.82	2132.08	2118.28
2	1766.32	1702.44	2072.65
3	1986.17	2041.19	1865.07
4	1781.09	2034.28	2258.27
5	1649.34	1721.48	2207.32
6	2149.75	1942.44	2004.43
7	1855.82	1831.08	1893.17
8	1674.63	1828.90	1811.65
9	1831.05	2198.63	1983.17
10	2177.03	1684.64	1575.26
MEAN	1707.031	2069.724	2096.663
SD	49.06103	98.46001	104.0105

80 RPM

Sl. No.	PLA	5%	10%
1	1798.30	1747.77	2028.47
2	1786.83	1740.02	2075.75
3	1546.60	2135.19	1846.84
4	1289.15	1909.87	1654.56
5	1326.45	2454.01	1758.08
6	1639.03	1981.30	1752.23
7	1382.15	2060.05	1810.27
8	1738.51	1749.11	1987.42
9	1641.70	1885.54	1624.58
10	1705.47	1572.75	1545.23
MEAN	1718.30	2070.99	1949.75
SD	69.02	209.45	115.69

140 RPM

Sl. No.	PLA	5%	10%
1	2068.33	2256.18	2147.37
2	1829.71	2057.74	2270.04
3	2137.64	1985.36	2296.34
4	1637.71	1809.46	2349.50
5	2193.18	1724.94	2301.22
6	1674.97	2203.33	2847.59
7	1751.14	1851.81	2507.05
8	1994.38	2191.00	2214.28
9	2094.46	2250.18	2123.44
10	2112.66	2200.64	2172.55
MEAN	2095.87	2193.18	2234.34
SD	62.18	71.73	81.88

Stiffness (N/m)

40 RPM

Sl. No.	PLA	5%	10%
1	262.47	243.29	241.71
2	260.18	211.92	236.51
3	292.57	232.92	212.82
4	240.19	232.13	248.32
5	215.58	214.29	242.71
6	321.12	221.65	237.04
7	257.97	208.94	216.03
8	243.20	223.87	214.24
9	273.52	260.00	234.52
10	311.65	192.23	186.29
MEAN	235.83	186.40	362.37
SD	15.03	12.10	16.61

80 RPM

Sl. No.	PLA	5%	10%
1	169.48	186.29	269.34
2	190.36	169.76	213.45
3	192.97	219.01	189.09
4	150.45	195.90	204.96
5	172.38	263.47	175.33
6	166.62	190.06	236.30
7	130.26	216.75	240.37
8	180.34	184.04	201.06
9	177.11	184.45	229.19
10	205.22	169.32	202.86
MEAN	235.64	205.00	250.00
SD	14.19	27.44	11.38

140 RPM

Sl. No.	PLA	5%	10%
1	317.54	257.45	245.03
2	296.09	239.07	259.03
3	372.53	230.66	276.32
4	295.60	217.74	268.10
5	377.66	196.83	272.14
6	316.23	255.99	336.75
7	308.81	211.31	286.07
8	347.57	263.65	266.45
9	382.39	252.09	242.30
10	337.50	251.11	256.92
MEAN	362.37	250.00	284.30
SD	16.61	11.38	26.63

Stress at max load

40 RPM

Sl. No.	PLA	5%	10%
1	58.46	54.61	49.19
2	56.81	47.31	54.83
3	61.20	55.86	24.01

80 RPM

Sl. No.	PLA	5%	10%
1	55.44	55.76	50.61
2	57.94	58.82	43.80
3	46.66	59.63	53.28

4	56.07	59.54	51.97
5	53.37	51.62	50.85
6	55.62	52.90	45.76
7	60.05	49.54	22.94
8	64.00	48.31	22.70
9	52.23	53.86	49.68
10	66.91	48.64	40.41
MEAN	51.52	50.85	50.13
SD	3.78	2.77	3.04

4	45.64	45.76	53.61
5	49.36	64.54	45.61
6	52.96	67.97	53.70
7	52.56	52.33	47.00
8	68.31	56.81	49.39
9	65.13	56.43	48.81
10	60.87	60.77	39.21
MEAN	52.49	53.42	48.50
SD	4.06	4.63	4.72

140 RPM

Sl. No.	PLA	5%	10%
1	57.69	47.12	46.40
2	57.39	60.95	51.70
3	54.47	58.95	52.62
4	56.80	54.35	49.14
5	61.43	51.23	48.27
6	58.22	57.63	57.88
7	61.25	44.59	52.04
8	56.35	60.87	50.57
9	57.31	57.89	50.49
10	49.49	53.97	49.27
MEAN	58.88	59.26	50.84
SD	1.93	1.59	1.35

% Strain at max load

40 RPM

Sl. No.	PLA	5%	10%
1	4.03	4.84	4.51
2	4.54	4.03	5.07
3	4.51	4.29	1.55
4	4.26	4.50	4.43
5	5.02	5.65	3.99
6	4.47	5.06	4.32
7	4.45	4.73	1.77
8	5.27	4.90	2.06
9	4.84	4.93	4.83
10	4.90	5.95	5.47
15	4.69		
MEAN	4.85	4.95	4.75
SD	0.33	0.36	0.37

80 RPM

Sl. No.	PLA	5%	10%
1	4.76	4.91	4.82
2	5.13	5.09	5.45
3	4.79	5.20	5.01
4	4.72	4.71	5.80
5	6.22	5.36	4.26
6	5.01	5.33	5.86
7	6.41	4.57	4.97
8	5.59	5.27	4.76
9	5.61	5.70	5.06
10	5.25	6.31	3.83
MEAN	4.94	4.90	4.81
SD	0.22	0.26	0.29

140
RPM

Sl. No.	PLA	5%	10%
1	5.10	4.40	4.31
2	5.89	5.05	4.48
3	4.40	5.33	4.32
4	5.93	5.01	4.37
5	5.89	5.07	4.15
6	5.69	4.38	4.98
7	5.33	4.51	4.10
8	5.13	5.77	4.76
9	5.02	4.52	5.28
10	4.37	4.85	4.26
MEAN	5.66	5.25	4.50
SD	0.31	0.32	0.27

EDX

PLA/HNT5_40

Spectrum	In stats.	C	O	Al	Si	Au	Total
Spectrum 1	Yes	48.83	42.53	0.47	0.51	7.65	100.00
Spectrum 2	Yes	50.76	48.49	0.39	0.36		100.00
Max.		50.76	48.49	0.43	0.43	7.65	
Min.		48.83	42.53	0.39	0.36	7.65	

PLA/HNT5_80

Spectrum	In stats.	C	O	Al	Si	Total
Spectrum 1	Yes	49.90	48.80	0.64	0.66	100.00
Mean		49.90	48.80	0.64	0.66	100.00

Std. deviation		0.00	0.00	0.00	0.00	
Max.		49.90	48.80	0.64	0.66	
Min.		49.90	48.80	0.64	0.66	

PLA/HNT5_140

Spectrum	In stats.	C	O	Al	Si	Total
Spectrum 1	Yes	50.58	47.85	0.87	0.70	100.00
Mean		50.58	47.85	0.87	0.70	100.00
Std. deviation		0.00	0.00	0.00	0.00	
Max.		50.58	47.85	0.87	0.70	
Min.		50.58	47.85	0.87	0.70	

PLA/HNT10_40

Spectrum	In stats.	C	O	Al	Si	Total
Spectrum 1	Yes	48.44	48.88	1.32	1.35	100.00
Mean		48.44	48.88	1.32	1.35	100.00
Std. deviation		0.00	0.00	0.00	0.00	
Max.		48.44	48.88	1.32	1.35	
Min.		48.44	48.88	1.32	1.35	

PLA/HNT10_80

Spectrum	In stats.	C	O	Al	Si	Total
Spectrum 1	Yes	49.99	46.26	1.82	1.93	100.00
Mean		49.99	46.26	1.82	1.93	100.00
Std. deviation		0.00	0.00	0.00	0.00	
Max.		49.99	46.26	1.82	1.93	
Min.		49.99	46.26	1.82	1.93	

PLA/HNT10_140

Spectrum	In stats.	C	O	Al	Si	Cl	K	Total
Spectrum 1	Yes	42.95	52.70	1.92	1.98	0.18	0.26	100.00
Mean		42.95	52.70	1.92	1.98	0.18	0.26	100.00
Std. deviation		0.00	0.00	0.00	0.00	0.00	0.00	
Max.		42.95	52.70	1.92	1.98	0.18	0.26	
Min.		42.95	52.70	1.92	1.98	0.18	0.26	

Chapter 5
Mechanical properties

Young's Modulus (MPa)						
	B1	**B2**	**B3**	**B4**	**B5**	**B6**
	1741.78	1804.96	1574.56	1658.98	1401.03	1717.35
	1707.02	1773.82	1528.52	1308.31	1372.84	1705.18
	1558.89	1690.74	1445.18	1281.82	1874.31	1699.19
	1500.75	1610.88	1369.11	1268.19	1272.06	1507.44
	1431.24	1608.00	1295.59	1252.93	1762.38	1461.86
	1431.11	1600.36	1279.14	1240.35	1726.72	1454.00
	1430.06	1549.59	1265.95	1129.59	1705.56	1413.01
	1299.11	1477.36	1232.48	1111.39	1682.88	1368.74
	1261.18	1471.64	1146.89	1024.97	1663.57	1348.37
	1241.09	1400.94	1124.83	932.22	1578.33	1331.02
	1165.24	1398.22		932.17	1518.45	1250.47
Average	1433.41	1551.93	1326.23	1194.63	1599.40	1477.88
SD	177.57	157.93	143.83	196.50	229.01	155.47
Average	1470.41	1483.02	1383.51	1234.58	1686.57	1396.17
SD	51.88	73.36	93.44	54.32	57.70	50.37

% Strain - Elongation at break						
	B1	**B2**	**B3**	**B4**	**B5**	**B6**
	6.04	6.73	7.36	6.98	9.35	7.01
	5.25	6.28	6.51	6.88	7.15	6.95
	4.98	6.26	6.08	6.64	6.97	6.90
	4.69	6.25	6.01	6.49	6.55	6.46
	4.32	6.20	5.08	6.39	6.50	6.30
	4.30	5.99	5.06	6.05	6.40	6.22
	4.07	5.90	5.06	5.95	6.30	6.16

	4.07	5.89	5.02	5.93	6.29	6.14
	4.02	5.81	4.90	5.63	6.28	5.64
	3.98	5.68	3.94	5.24	6.23	5.53
	3.70	5.57		4.99	6.13	5.33
Average	4.49	6.01	5.50	6.11	6.28	6.24
SD	0.66	0.33	0.93	0.61	0.89	0.55
Average	4.60	6.28	6.02	6.57	6.50	6.64
SD	0.41	0.22	0.80	0.31	0.23	0.32

Stiffness (kN/m)						
	B1	**B2**	**B3**	**B4**	**B5**	**B6**
	199.13	225.61	276.62	248.89	270.80	210.48
	198.92	222.33	265.86	230.89	212.99	198.20
	193.79	218.63	251.95	226.84	177.57	187.20
	186.50	202.26	248.46	215.59	219.88	186.75
	179.43	195.50	236.43	215.58	188.19	186.00
	174.44	192.12	228.06	210.98	224.28	185.43
	173.67	192.10	218.44	198.11	209.98	184.85
	173.30	186.30	211.51	198.00	147.97	178.82
	166.94	185.66	189.86	194.47	184.73	176.97
	145.83	185.20	168.80	188.03	166.14	169.25
	144.14	176.20		154.73	145.38	145.85
Average	176.01	196.48	229.60	207.46	186.45	182.71
SD	17.89	16.49	31.87	23.91	30.57	15.55
Average	191.56	212.87	255.87	227.56	213.89	193.73
SD	7.61	11.82	13.99	12.27	32.42	9.51

	Stress (MPa) - Tensile strength					
	B1	**B2**	**B3**	**B4**	**B5**	**B6**
	57.94	65.26	58.64	59.86	75.39	63.31
	53.41	63.89	55.43	59.74	44.03	58.77
	49.57	62.61	50.56	49.60	63.99	58.52
	48.24	61.40	48.31	48.33	62.75	58.40
	46.44	58.64	47.77	48.10	60.98	58.17
	46.27	54.95	47.11	44.06	60.94	53.51
	44.54	52.87	42.07	42.82	59.85	53.02
	44.50	48.64	41.98	42.75	59.41	51.31
	42.57	47.62	41.78	41.27	45.83	50.63
	40.91	47.53	27.41	36.14	58.90	48.30
	31.39	46.79		30.48	56.89	45.97
Average	45.98	54.74	46.11	45.74	56.21	54.54
SD	6.54	7.00	8.21	8.46	9.25	5.05
Average	50.31	61.13	51.30	51.62	66.22	58.45

SD	4.16	3.45	4.29	6.03	5.86	2.83

Drug dissolution study

Standard curve for aspirin

Concentration (g/L)	**Absorbance 270 nm**	**A*K 270 nm**
1	2.639	739
0.5	1.49	417.31
0.2	0.615	172.34
0.05	0.148	41.49
0.02	0.059	16.46

Drug release for 216 hours

Hours	b1	b2	b3	b5
0	0	0	0	0
0.5	0.002	0	0	0.021
1	0.002	0	0	0.021
2	0.003	0.006	0	0.021
4	0.006	0.006	0.014	0.021
8	0.026	0.006	0.014	0.021
24	0.033	0.006	0.014	0.021
48	0.033	0.006	0.014	0.021
72	0.033	0.006	0.014	0.021
144	0.055	0.033	0.017	0.032
216	0.051	0.02	0.017	0.023

Chapter 6

Standard curve for aspirin

Concentration (g/L)	**Absorbance 270 nm**	**A*K 270 nm**
1	2.639	739
0.5	1.49	417.31
0.2	0.615	172.34
0.05	0.148	41.49
0.02	0.059	16.46

Standard curve for paracetamol

Concentration (g/L)	**Absorbance 275 nm**	**A*K 275 nm**
1	2.903	812.73
0.5	2.882	806.93
0.2	2.6	728.08
0.1	1.512	423.22
0.05	0.758	212.38
0.02	0.291	81.396

0.01	0.159	44.408

Degradation study

Wight loss measurement

Weeks		**0**	**2**	**4**	**6**	**8**	**14**	**20**	**26**	**32**
PLA+(HNT+Asp)		0	1.06	1.06	1.06	1.06	1.06	1.06	1.06	5.32
PLA+(HNT+PAR)		0	0	0	0	0	9.63	26	41	49
PLA+ASP		0	0	0	0	1.1	18.6	34.06	84	87.3
PLA+PAR		0	0	0	0.758	0.758	0.758	7.57	16.6	39.4
PLA		0	0	0	0	0	1.2	1.5	2.2	4.7
PLA+HNT		0	0	0	0.4	0.62	0.83	1.62	3.56	8.1

20^{th} week

Batch Reference	**Stress at Maximum Load (MPa)**	**Percentage Strain at Maximum Load**	**Stiffness (kN/m)**	**Young's Modulus (MPa)**
PLA	3.69	6.80	2820.0	542.30
PLA	13.38	1.95	3143.0	1208.86
PLA	20.27	2.29	2852.3	1240.13
PLA	31.57	2.84	3073.0	1302.12
Mean	17.23	3.47	2972.08	1073.4
Std deviation	11.73	2.25	160.10	356.15
Batch Reference	**Stress at Maximum Load (MPa)**	**Percentage Strain at Maximum Load**	**Stiffness (kN/m)**	**Young's Modulus (MPa)**
PLA-HNT	44.55	5.28	3117.4	1309.84
PLA-HNT	44.59	4.04	3105.8	1568.60
PLA-HNT	44.32	4.38	3626.0	1812.98
PLA-HNT	45.81	4.22	3457.9	1516.64
PLA-HNT	38.89	3.82	3139.8	1330.43
PLA-HNT	47.50	4.09	3346.1	1493.77
Mean	44.28	4.31	3298.83	1505.38
Std deviation	2.90	0.51	214.48	183.1

32^{nd} week

Batch Reference	**Stress at Maximum Load (MPa)**	**Percentage Strain at Maximum Load**	**Stiffness (kN/m)**	**Young's Modulus (MPa)**
P+APAP+H	4.62	0.76	326.78	933.66
P+APAP+H	7.82	1.09	354.17	1017.73
Mean	6.22	0.93	340.47	975.69

Std deviation	2.27	0.23	19.37	59.45
Batch Reference	**Stress at Maximum Load (MPa)**	**Percentage Strain at Maximum Load**	**Stiffness (kN/m)**	**Young's Modulus (MPa)**
PLA+APAP	0.40	0.90	56.77	149.39
Batch Reference	**Stress at Maximum Load (MPa)**	**Percentage Strain at Maximum Load**	**Stiffness (kN/m)**	**Young's Modulus (MPa)**
PLA+ASP	0.31	0.64	16.66	59.49
Batch Reference	**Stress at Maximum Load (MPa)**	**Percentage Strain at Maximum Load**	**Stiffness (kN/m)**	**Young's Modulus (MPa)**
P+ASP+H	0.18	0.52	23.75	59.96
P+ASP+H	0.91	0.33	176.00	470.58
Mean	0.54	0.43	99.87	265.27
Std deviation	0.51	0.14	107.66	290.35

Chapter 7

Mechanical properties

Batch	Young's Modulus	Stiffness	Stress at maximum load	% Strain
PLA 1	355.97	218031.03	31.89	11.81
PLA 2	429.59	233913.36	36.43	11.42
PLA 3	362.67	241535.46	31.83	21.53
PLA 4	415.06	272384.45	32.81	11.58
PLA 5	392.81	237160.81	33.88	17.20
Mean	391.22	240605.02	33.37	14.71
SD	32.02	19855.88	1.90	4.52
P3% 1	445.62	264698.87	39.04	13.68
P3% 2	483.63	282923.73	41.55	17.61
P3% 3	401.48	259708.54	31.72	12.82
Mean	443.58	269110.38	37.44	14.70
SD	41.11	12220.16	5.11	2.55
P5% 2	279.83	175768.17	25.37	12.99

P5%4	413.51	259738.88	34.45	12.40
P5%5	377.94	237396.47	30.11	12.86
Mean	357.10	224301.17	29.97	12.75
SD	69.24	43490.06	4.54	0.31

Chapter 8

Invitro degradation
Weight loss measurement

Weeks	**0**	**2**	**4**	**6**	**8**	**14**	**20**	**26**	**32**
PLA	0	0	0	0	0	1.2	1.5	2.2	4.7
PLA + HNT	0	0	0	0.4	0.4	0.83	1.62	3.56	8.1
PLA + A 5%	0	0	0	0.6	1.4	6.8	9.9	15.14	18.56

0week

Batch Reference	**Stress at Maximum Load (MPa)**	**Percentage Strain at Maximum Load**	**Stiffness (kN/m)**	**Young's Modulus (MPa)**
PLA	69.08	8.68	337.53	1298.2
PLA	64.80	6.13	345.93	1330.5
PLA	70.61	7.21	390.06	1560.2
PLA	62.02	6.87	280.26	1086.3
PLA	73.10	6.75	359.27	1392.5
PLA	64.04	6.95	360.63	1567.9
PLA	59.09	7.46	385.29	1579.1
PLA	60.86	6.84	369.90	1528.5
PLA	61.18	7.02	353.83	1474.3
PLA	62.61	7.26	382.85	1495.5
PLA	64.24	7.05	385.72	1542.9
PLA	61.48	7.62	338.93	1448.4
Mean	64.43	7.15	357.52	1442.0
Std deviation	4.32	0.61	30.59	145.33
Batch Reference	**Stress at Maximum Load (MPa)**	**Percentage Strain at Maximum Load**	**Stiffness (kN/m)**	**Young's Modulus (MPa)**
PLA+HNT	54.98	6.99	345.31	1569.6
PLA+HNT	58.38	7.04	363.97	1582.5
PLA+HNT	60.19	8.12	416.59	1735.8
PLA+HNT	62.04	7.22	385.46	1633.3
PLA+HNT	54.48	6.65	369.73	1621.6
PLA+HNT	63.25	7.50	427.65	1859.4
PLA+HNT	57.32	6.93	440.35	1881.8
PLA+HNT	59.52	7.19	389.02	1691.4

PLA+HNT	59.67	7.28	400.88	1698.7
PLA+HNT	55.33	7.17	401.80	1931.7
PLA+HNT	60.93	7.34	385.99	1678.2
PLA+HNT	56.76	7.54	354.51	1672.2
Mean	58.57	7.25	390.10	1713.0
Std deviation	2.85	0.37	29.08	118.37
Batch Reference	**Stress at Maximum Load (MPa)**	**Percentage Strain at Maximum Load**	**Stiffness (kN/m)**	**Young's Modulus (MPa)**
PLA + A5%	48.88	6.42	200.31	2003.1
PLA + A5%	45.71	6.69	192.55	1481.1
PLA + A5%	54.05	6.78	232.87	1687.5
PLA + A5%	52.25	6.38	224.96	1906.4
PLA + A5%	51.01	6.61	209.55	1563.8
PLA + A5%	55.10	6.85	257.57	1764.2
PLA + A5%	55.97	6.57	196.00	2130.5
PLA + A5%	57.96	7.35	243.06	1787.2
PLA + A5%	48.39	6.52	238.20	1701.4
PLA + A5%	49.43	6.30	231.21	1864.6
PLA + A5%	49.12	7.42	375.06	1465.1
PLA + A5%	48.03	6.47	287.46	1774.4
PLA + A5%	54.63	5.91	175.38	1992.9
PLA + A5%	48.65	6.47	214.44	1817.3
Mean	51.37	6.62	234.19	1781.4
Std deviation	3.63	0.39	49.78	194.69

8th week

Batch Reference	**Stress at Maximum Load (MPa)**	**Percentage Strain at Maximum Load**	**Stiffness (kN/m)**	**Young's Modulus (MPa)**
PLA	48.5	3.47	421.2	1815.5
PLA	61.7	5.8	412.5	1718.9
PLA	65.4	6.26	380.2	1728.3
PLA	64	6.04	375.4	1770.8
PLA	56.2	5.23	364.1	1556
PLA	56.4	5.15	426.3	1761.4

Mean	58.7	5.325	396.62	1725.2
Std deviation	6.29	1.01	26.51	89.69
Batch Reference	**Stress at Maximum Load (MPa)**	**Percentage Strain at Maximum Load**	**Stiffness (kN/m)**	**Young's Modulus (MPa)**
PLA-HNT	36.4	2.81	386.8	1934
PLA-HNT	56	5.4	378.4	1801.8
PLA-HNT	53.4	5	335.8	1679
PLA-HNT	56.6	5.28	375.6	1976.8
PLA-HNT	53.1	5.4	392.7	1722.3
PLA-HNT	50.4	5.3	407	1849.9
Mean	50.98	4.865	379.38	1827.3
Std deviation	7.48	1.02	24.12	116.5
Batch Reference	**Stress at Maximum Load (MPa)**	**Percentage Strain at Maximum Load**	**Stiffness (kN/m)**	**Young's Modulus (MPa)**
PLA+A5%	59.4	5.18	195.4	2171.3
PLA+A5%	63.8	5.2	285.4	2339.7
PLA+A5%	70.7	4.63	257.8	2929.6
PLA+A5%	61	4.74	228	2650.9
PLA+A5%	50.8	4.59	241.02	2191.1
PLA+A5%	59.1	4.81	218.1	2478.2
Mean	60.8	4.86	237.62	2460.1
Std deviation	6.51	0.269	31.49	292.4

20th week

Batch Reference	**Stress at Maximum Load (MPa)**	**Percentage Strain at Maximum Load**	**Stiffness (kN/m)**	**Young's Modulus (MPa)**
PLA	3.69	6.80	2820.0	542.30
PLA	13.38	1.95	3143.0	1208.86
PLA	20.27	2.29	2852.3	1240.13
PLA	31.57	2.84	3073.0	1302.12
Mean	17.23	3.47	2972.08	1073.4
Std deviation	11.73	2.25	160.10	356.15
Batch Reference	**Stress at Maximum Load (MPa)**	**Percentage Strain at Maximum Load**	**Stiffness (kN/m)**	**Young's Modulus (MPa)**
PLA-HNT	44.55	5.28	3117.4	1309.84
PLA-HNT	44.59	4.04	3105.8	1568.60
PLA-HNT	44.32	4.38	3626.0	1812.98
PLA-HNT	45.81	4.22	3457.9	1516.64
PLA-HNT	38.89	3.82	3139.8	1330.43
PLA-HNT	47.50	4.09	3346.1	1493.77
Mean	44.28	4.31	3298.83	1505.38

Std deviation	2.90	0.51	214.48	183.1
Batch Reference	**Stress at Maximum Load (MPa)**	**Percentage Strain at Maximum Load**	**Stiffness (kN/m)**	**Young's Modulus (MPa)**
PLA+A5%	31.36	2.96	1756.8	1597.09
PLA+A(15 g)	35.55	2.79	2189.3	1824.40
PLA+A(15 g)	31.28	2.22	1616.1	1795.66
PLA+A(15 g)	42.59	2.63	1683.9	2104.93
PLA+A(15 g)	34.90	2.93	2038.8	1698.97
PLA+A(15 g)	48.06	3.54	2047.6	1706.34
Mean	37.29	2.84	1888.75	1787.9
Std deviation	6.70	0.435	233.13	174.9

32nd week

Batch Reference	**Stress at Maximum Load (MPa)**	**Percentage Strain at Maximum Load**	**Stiffness (kN/m)**	**Young's Modulus (MPa)**
PLA+HNT	11.68	2.04	316.46	1180.8
PLA+HNT	0.67	5.34	75.44	281.5
PLA+HNT	1.70	0.52	187.18	698.4
PLA+HNT	5.24	2.55	235.35	878.2
PLA+HNT	9.89	1.72	277.07	1033.8
PLA+HNT	8.11	1.83	271.04	1011.3
PLA+HNT	0.51	0.11	146.23	545.6
Mean	5.40	2.01	215.54	804.3
Std deviation	4.60	1.70	84.34	314.70

Batch Reference	**Stress at Maximum Load (MPa)**	**Percentage Strain at Maximum Load**	**Stiffness (kN/m)**	**Young's Modulus (MPa)**
PLA+A5%	15.05	2.67	451.60	1117.8
PLA+A5%	9.83	1.49	445.29	1341.2
PLA+A5%	2.39	0.20	314.40	1218.6

PLA+A5 %	3.29	0.33	376.99	1461.2
PLA+A5 %	10.33	1.31	379.19	1289.8
PLA+A5 %	3.42	0.90	174.87	705.1
PLA+A5 %	1.57	0.27	193.81	781.5
PLA+A5 %	7.21	0.80	439.48	1399.6
Mean	6.64	1.00	346.95	1164.4
Std deviation	4.78	0.83	110.36	281.09